

UNCLASSIFIED

AD NUMBER

ADB013005

LIMITATION CHANGES

TO:

Approved for public release; distribution is unlimited.

FROM:

Distribution authorized to U.S. Gov't. agencies only; Test and Evaluation; DEC 1975. Other requests shall be referred to Air Force Avionics Laboratory, AFAL/WRP, Wright-Patterson AFB, OH 45433.

AUTHORITY

afal ltr, 23 mar 1979

THIS PAGE IS UNCLASSIFIED

THIS REPORT HAS BEEN DELIMITED  
AND CLEARED FOR PUBLIC RELEASE  
UNDER DOD DIRECTIVE 5200.20 AND  
NO RESTRICTIONS ARE IMPOSED UPON  
ITS USE AND DISCLOSURE.

DISTRIBUTION STATEMENT A

APPROVED FOR PUBLIC RELEASE;  
DISTRIBUTION UNLIMITED.



AFAL-TR-75-219

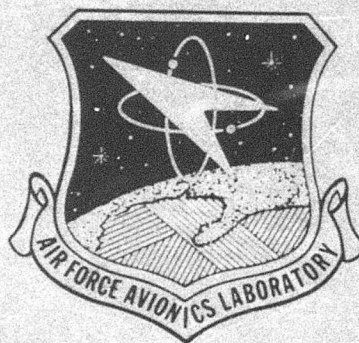
ADB013005

AD No. \_\_\_\_\_  
DDC FILE COPY

ADVANCED RADAR REFLECTOR STUDIES

The ElectroScience Laboratory  
The Ohio State University

December 1975

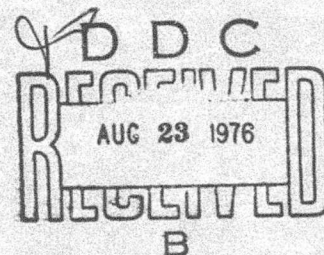


Copy available to DDC does not  
permit fully legible reproduction.

TECHNICAL REPORT AFAL-TR-75-219

Distribution limited to U.S. Gov't agencies only (test and evaluation); statement applied December 1975. Other requests for this document must be referred to Air Force Avionics Laboratory (AFAL/WRP), WPAFB 45433.

AIR FORCE AVIONICS LABORATORY  
AIR FORCE WRIGHT AERONAUTICAL LABORATORIES  
AIR FORCE SYSTEMS COMMAND  
WRIGHT-PATTERSON AIR FORCE BASE, OHIO 45433



# NOTICE

When Government drawings, specifications, or other data are used for any purpose other than in connection with a definitely related Government procurement operation, the United States Government thereby incurs no responsibility nor obligation whatsoever; and the fact that the government may have formulated, furnished, or in any way supplied the said drawings, specifications, or other data, is not to be regarded by implication or otherwise as in any manner licensing the holder or any other person or corporation, or conveying any rights or permission to manufacture, use, or sell any patented invention that may in any way be related thereto.

This technical report has been reviewed and is approved for publication.

*Vittal P. Pyati*

VITTAL P. PYATI, Ph.D.  
Program Monitor

*William F. Bahret*

WILLIAM F. BAHRET  
Actg Chief, Passive ECM Branch  
Electronic Warfare Division

FOR THE DIRECTOR

*Ollie H. Edwards*

OLLIE H. EDWARDS, Colonel, USAF  
Chief, Electronic Warfare Division

ACCESSION for		
NTIS	White Section	<input type="checkbox"/>
DDC	Buff Section	<input checked="" type="checkbox"/>
UNANNOUNCED		<input type="checkbox"/>
JUSTIFICATION		
BY		
DISTRIBUTION/AVAILABILITY CODES		
Dist.	ADIRL	and/or SPECIAL
B		



SECURITY CLASSIFICATION OF THIS PAGE (When Data Entered)

DD FORM 1 JAN 73 1473 EDITION OF 1 NOV 65 IS OBSOLETE

SECURITY CLASSIFICATION OF THIS PAGE (When Data Entered)


UNCLASSIFIED

SECURITY CLASSIFICATION OF THIS PAGE(When Data Entered)

20.

programmed for larger numbers of wires. All programs are documented in this report.

Data generated during the course of the effort are also presented in this report, including curves of the reduction (due to coupling) in average scattering cross section as a function of number density of chaff elements.



UNCLASSIFIED

SECURITY CLASSIFICATION OF THIS PAGE(When Data Entered)

## FOREWORD

This report was prepared and submitted August, 1975 by The Ohio State University ElectroScience Laboratory, Department of Electrical Engineering, 2015 Neil Avenue, Columbus, Ohio 43210 under Contract F33615-72-C-1435, Project No. 62204F, Task No. 76331333, extending from April 1972 to June 1975. Dr. V. P. Pyati, AFAL/WRP, was the Program Monitor.

The authors of this report wish to acknowledge the many conversations they had with the immediate sponsors, Dr. V. Pyati, Mr. R. Puskar, and Ms. M. Gauvey, during the entire course of the contract. They also express thanks to Professor J. Richmond who showed a lively interest in the work and who helped in many of its phases.

REPORTS AND PUBLICATIONS UNDER CONTRACT F 33615-72-C-1435

- 3401-1 Annual Summary Report, June 1974
- 3401-2 "Application of Linear Iteration to Electromagnetic Scattering by Random Arrays of Wires," V. P. Cable, August 1975
- 3401-3 Final Summary Report, "Advanced Radar Reflector Studies," R.J. Garbacz, V. Cable, R. Wickliff, R. Caldecott, J. Buk, D. Lam, K. Demarest, A. Yee

Wickliff, R.G. and Garbacz, R.J., "The Average Backscattering Cross Section of Clouds of Randomized Resonant Dipoles," IEEE Trans. on Antennas and Propagation, Vol. AP-22, No. 3, pp. 503-505.

Cable, V.P., "Application of Linear Iteration to Electromagnetic Scattering by Random Arrays of Wires," Ph.D. Dissertation, The Ohio State University, August 1975.

	Page
I. INTRODUCTION	1
II. TECHNICAL DISCUSSION AND RESULTS	5
A. The Frozen Chaff Cloud Model	5
B. Representative Cloud Characteristics	6
C. Computer-Generation of Scattering Data	7
(1) Introductory Remarks	7
(2) Direct Methods	9
(a) Theoretical Considerations	9
(b) Calculated Results for Chaff Clouds	12
(3) Sparse Matrix Methods	24
(a) Theoretical Considerations	24
(b) Calculated Results for Chaff Clouds	34
(4) Indirect (Iterative) Methods	71
(a) Theoretical Considerations	71
Linear First Degree Methods	
(J,G-S,SOR)	72
Convergence Criteria	76
A Physical Interpretation of the	
J,G-S, and SOR Methods	81
Sphere of Influence (SOI) Iteration	83
(b) Calculated Results for Chaff Clouds	87
A Check Case	88
SOR Solutions for Scattering by Large	
Clouds of Chaff Elements	94
SOI Solution for Scattering by Small	
Clouds of Chaff Elements	118
Comments on the Application of SOR,	
Surface Patch, and Wire Grid Models	121
D. The Question of Closer Spacings	121
E. The Question of Mixed Dipole Lengths	148
F. Additional Experimental Results	149
(1) Experimental Verification	154
(2) Extinction Measurements through an	
Artificial Chaff Cloud	154
(3) Scattering from Touching Chaff Elements	166
G. The Aircraft-Chaff-Tracker	
Interaction Problem	166
III. DISCUSSION	174
IV. RECOMMENDATIONS FOR FUTURE EFFORT	177

APPENDIX A	STATISTICAL ANALYSIS EMPLOYED IN THIS REPORT	179
	A. Definitions	179
	B. Statistical Analysis of Backscattering Data	185
APPENDIX B	REACTION MATCHING IN ELECTROMAGNETICS PROBLEMS	196
	A. Scattering Properties of Obstacles	196
	B. Scattering by Perfectly Conducting Bodies	198
	C. Numerical Solutions	202
	D. Examples of Bases for Surface Patch and Wire-Grid Modelling	205
	E. Chaff Clouds	210
	F. A Convenient Change in Notation	211
APPENDIX C	CLOUD GEOMETRY	214
	A. The Radially Inhomogeneous Cloud	214
	B. The Homogeneous Cloud	221
APPENDIX D	FULL MATRIX COMPUTER PROGRAM FOR MULTIPLE LENGTHS	223
APPENDIX E	SPARSE MATRIX COMPUTER PROGRAM	241
APPENDIX F	ITERATION COMPUTER PROGRAM (SOR)	273
	A. Far Zone Mutual Impedance Between Moderate and Distantly Separated Sinusoidal Dipoles	273
	B. Computer Programs	280
APPENDIX G	SPLIT-GATE AND LEADING EDGE TRACKER PERFORMANCE ON SHORT PULSE ECHOES	313
	A. Introduction	313
	B. Discussion of Tracker Performance	313
	C. Simulation	315
	D. Typical Results	317
	E. Conclusions	318
REFERENCES		341



# LIST OF ILLUSTRATIONS

Figure		Page
1	Calculated average backscattering cross sections for ensembles of clouds containing $N \leq 30$ dipoles with an average spacing $d/\lambda = 2$ .	14
2	Calculated average backscattering cross sections for ensembles of clouds containing $N \leq 30$ dipoles with an average spacing $d/\lambda = 1.5$ .	15
3	Calculated average backscattering cross sections for ensembles of clouds containing $N \leq 30$ dipoles with an average spacing $d/\lambda = 1.0$ .	16
4	Calculated average backscattering cross sections for ensembles of clouds containing $N \leq 30$ dipoles with an average spacing $d/\lambda = 0.5$ .	17
5	Calculated ensemble averages of the spatial averages shown in Fig. 1. Straight line	18
6	Calculated ensemble averages of the spatial averages shown in Fig. 2.	19
7	Calculated ensemble averages of the spatial averages shown in Fig. 3.	20
8	Calculated ensemble averages of the spatial averages shown in Fig. 4.	21
9	Calculated spatial average backscattering cross sections for ensembles of clouds containing $50 < N < 200$ dipoles with an average spacing $d/\lambda = 2$ .	22
10	Calculated spatial average backscattering cross sections for ensembles of clouds containing $50 < N < 200$ dipoles with an average spacing $d/\lambda = 0.5$ .	23
11	Measured and calculated values of the spatial average cross sections of ensembles of clouds containing $50 < N < 800$ dipoles with average spacings $d/\lambda \approx 0.5-0.6$ . Bistatic angle $\beta=0^\circ$ .	26

Figure		Page
12	Measured values of the spatial average cross sections of ensembles of clouds containing $50 < N < 800$ dipoles with average spacings $d/\lambda \approx 0.5-0.6$ . Bistatic angle $\beta=45^\circ$ .	27
13	Measured and calculated values of the spatial average cross sections of ensembles of clouds containing $50 < N < 800$ dipoles with average spacings $d/\lambda \approx 0.5-0.6$ . Bistatic angle $\beta=90^\circ$ .	28
14	Measured and calculated values of the spatial average cross sections of ensembles of clouds containing $50 < N < 800$ dipoles with average spacings $d/\lambda \approx 0.5-0.6$ . Bistatic angle $\beta=135^\circ$ .	29
15	Average backscatter as a function of frequency of four random clouds.	30
16	The structure of an $11 \times 11$ matrix and its auxiliary before renumbering.	33
17	The structure of the $11 \times 11$ renumbered matrix of Fig. 16 and its auxiliary.	33
18	The structure of a $28 \times 28$ matrix and its auxiliary.	35
19	The structure of the $28 \times 28$ renumbered matrix of Fig. 18 and its auxiliary.	36
20	Average number of non-zero terms in the upper triangle of the sparse matrix using 10% rule.	38
21	Average number of non-zero terms in the upper triangle of the sparse matrix using 10% rule.	39
22	Radius of "sphere of influence" vs average dipole spacing.	43
23	$\theta$ - $\theta$ backscattering patterns as calculated using the full and sparse matrix, cloud #1, $d/\lambda=0.5$ .	44
24	$\phi$ - $\phi$ backscattering patterns as calculated using the full and sparse matrix, cloud #1, $d/\lambda=0.5$ .	45
25	$\theta$ - $\theta$ backscattering patterns as calculated using the full and sparse matrix, cloud #2, $d/\lambda=2.0$ .	46
26	$\phi$ - $\phi$ backscattering patterns as calculated using the full and sparse matrix, cloud #2, $d/\lambda=2.0$ .	47

Figure		Page
27	$\theta$ - $\theta$ backscattering patterns as calculated using the full and sparse matrix, cloud #1, $N = 200$ .	48
28	$\phi$ - $\phi$ backscattering patterns as calculated using the full and sparse matrix, cloud #1, $N = 200$ .	49
29	$\theta$ - $\phi$ backscattering patterns as calculated using the full and sparse matrix, cloud #1, $N = 200$ .	50
30	$\theta$ - $\theta$ backscattering patterns as calculated using the full matrix, cloud #2, $N=200$ , $d/\lambda=2.0$ .	51
31	$\theta$ - $\theta$ backscattering patterns as calculated using the sparse matrix, cloud #2, $N=200$ , $d/\lambda=2.0$ .	52
32	$\phi$ - $\phi$ backscattering patterns as calculated using the full matrix, cloud #2, $N=200$ , $d/\lambda=2.0$ .	53
33	$\phi$ - $\phi$ backscattering patterns as calculated using the sparse matrix, cloud #2, $N=200$ , $d/\lambda=2.0$ .	54
34	$\theta$ - $\phi$ backscattering patterns as calculated using the full matrix, cloud #2, $N=200$ , $d/\lambda=2.0$ .	55
35	$\theta$ - $\phi$ backscattering patterns as calculated using the sparse matrix, cloud #2, $N=200$ , $d/\lambda=2.0$ .	56
36	$\theta$ - $\theta$ backscattering patterns as calculated using the full matrix, cloud #3, $N=200$ , $d/\lambda=2.0$ .	57
37	$\theta$ - $\theta$ backscattering patterns as calculated using the sparse matrix, cloud #3, $N=200$ , $d/\lambda=2.0$ .	58
38	$\phi$ - $\phi$ backscattering patterns as calculated using the full matrix, cloud #3, $N=200$ , $d/\lambda=2.0$ .	59
39	$\phi$ - $\phi$ backscattering patterns as calculated using the sparse matrix, cloud #3, $N=200$ , $d/\lambda=2.0$ .	60
40	$\theta$ - $\phi$ backscattering patterns as calculated using the full matrix, cloud #3, $N=200$ , $d/\lambda=2.0$ .	61
41	$\theta$ - $\phi$ backscattering patterns as calculated using the sparse matrix, cloud #3, $N=200$ , $d/\lambda=2.0$ .	62
42	Spatial average backscatter from ten different clouds using full and sparse matrices.	63
43	Cumulative probability function of backscattering cross section, cloud #1.	64

Figure		Page
44	Cumulative probability function of backscattering cross section, cloud #2.	65
45	Cumulative probability function of backscattering cross section, cloud #3.	66
46	Time saving and element error vs sphere of influence radius using sphere of influence model plus 10% rule over the 10% rule alone.	68
47	Time saving vs number of dipoles using sphere of influence model plus 10% rule over the 10% rule alone.	69
48	Sample random array for Jacobi and Gauss-Seidel iteration method.	82
49	Sample random array for Sphere of Influence iteration method.	87
50	A planar array of resonant wires used as a check case.	89
51	Broadside backscatter and comparison of convergence norms (I), $\epsilon(k)$ and (IV) versus iteration k for the periodic array of Fig. 50 using SOR with $\omega = 0.4$ .	90
52	Specular bistatic cross section ( $\beta = 60^\circ$ ) and $\epsilon(k)$ versus iteration k for periodic array of Fig. 50 using SOR with $\omega = 0.4$ .	91
53	Specular bistatic cross section ( $\beta = 120^\circ$ ) and $\epsilon(k)$ versus iteration k for periodic array of Fig. 50 using SOR with $\omega = 0.4$	92
54	Backscatter cross section and convergence norms (I), (II), $\epsilon(k)$ and (IV) versus iteration k for 199 dipole random array using SOR with $\omega = 0.6$	95
55	Backscatter cross section and $\epsilon(k)$ versus iteration k for 500 dipole random array ( $8 \text{ dip}/\lambda^3$ ) using SOR with $\omega = 0.4$ and $\omega = 0.5$ .	96

Figure		Page
56	Bistatic cross section pattern for 500 dipole random array for $k=10, 29$ and $36$ using SOR with $\omega=0.4$	97
57	Backscatter cross section and convergence norms (I) and $\epsilon^{(k)}$ versus iteration $k$ for 1000 dipole random array #1 ( $\theta_0=90^\circ, \phi_0=0^\circ$ ) using SOR with $\omega=0.4$ .	100
58	Bistatic cross section pattern for 1000 dipole random array #1 ( $\theta_0=90^\circ, \phi_0=0^\circ$ ) at $k=5, 15$ and $29$ using SOR with $\omega=0.4$ .	101
59	Backscatter cross section and $\epsilon^{(k)}$ versus iteration $k$ for 1000 dipole random array #1 ( $\theta_0=90^\circ, \phi_0=10^\circ$ ) using SOR with $\omega = 0.4$ .	102
60	Bistatic cross section pattern for 1000 dipole random array #1 ( $\theta_0=90^\circ, \phi_0=10^\circ$ ) at $k = 6, 15, 30$ and $42$ using SOR with $\omega=0.4$ .	103
61	Backscatter cross section and $\epsilon^{(k)}$ versus iteration $k$ for 1000 dipole random array #1 ( $\theta_0=90^\circ, \phi_0=20^\circ$ ) using SOR with $\omega=0.4$ .	104
62	Bistatic cross section pattern for 1000 dipole random array #1 ( $\theta_0=90^\circ, \phi_0=20^\circ$ ) at $k = 15, 25$ and $35$ using SOR with $\omega=0.4$ .	105
63	Backscatter cross section and $\epsilon^{(k)}$ versus iteration $k$ for 1000 dipole random array #1 ( $\theta_0=90^\circ, \phi_0=30^\circ$ ) using SOR with $\omega=0.4$ .	106
64	Bistatic cross section pattern for 1000 dipole random array #1 ( $\theta_0=90^\circ, \phi_0=30^\circ$ ) at $k = 15, 30$ and $41$ using SOR with $\omega=0.4$ .	107
65	Backscatter cross section and convergence norms (I), $\epsilon^{(k)}$ and (IV) versus iteration $k$ for 1000 dipole random array #1 ( $\theta_0=90^\circ, \phi_0=40^\circ$ ) using SOR with $\omega=0.4$ .	108
66	Bistatic cross section pattern for 1000 dipole random array #1 ( $\theta_0=90^\circ, \phi_0=40^\circ$ ) at $k = 25, 35$ and $45$ using SOR with $\omega = 0.4$ .	109

Figure		Page
67	Backscatter cross section and $\epsilon^{(k)}$ versus iteration $k$ for 100 dipole random array #2 ( $\theta_0=90^\circ$ , $\phi_0=0^\circ$ ) using SOR with $\omega = 0.25, 0.3, 0.35$ and $0.4$ .	110
68	Bistatic cross section pattern for 1000 dipole random array #2 ( $\theta_0=90^\circ$ , $\phi_0=0^\circ$ ) at $k = 15, 30, 45$ and $61$ using SOR with $\omega = 0.3$ and $0.25$ .	111
69	Backscatter cross section and $\epsilon^{(k)}$ versus iteration $k$ for 100 dipole random array #2 ( $\theta_0=90^\circ$ , $\phi_0=10^\circ$ ) using SOR with $\omega = 0.2, 0.25$ and $0.3$ .	
70	Bistatic cross section pattern for 1000 dipole random array #2 ( $\theta_0=90^\circ$ , $\phi_0=10^\circ$ ) at $k = 20, 30$ and $36$ using SOR with $\omega = 0.2$ .	113
71	Backscatter, total and average bistatic cross sections versus iteration $k$ for random array #1 (Fig. 57).	114
72	Backscatter, total and average bistatic cross sections versus iteration $k$ for random array #1 (Fig. 59).	115
73	Backscatter, total and average bistatic cross sections versus iteration $k$ for random array #2 (Fig. 69).	116
74	Backscatter cross section and $\epsilon^{(k)}$ versus iteration $k$ for 100 dipole random array using SOI with $c = 0.2$ ( $M=14$ ) and $c = 0.1$ ( $M=44$ ).	119
75	Backscatter cross section and $\epsilon^{(k)}$ versus iteration $k$ for 100 dipole random array using SOR with $\omega = 0.7, 0.6$ and $0.5$ .	120
76	$\theta$ - $\theta$ backscattering pattern, $N=50$ dipoles, $P=2$ segments, $d/\lambda=0.25$ , 12-point integration.	125
77	$\theta$ - $\theta$ backscattering pattern, $N=50$ dipoles, $P=2$ segments, $d/\lambda=0.25$ , exact integration.	126
78	$\theta$ - $\theta$ backscattering pattern, $N=50$ dipoles, $P=4$ segments, $d/\lambda=0.25$ , exact integration.	127



Figure		Page
79	$\phi$ - $\phi$ backscattering pattern, N=50 dipoles, P=2 segments, $d/\lambda=0.25$ , 12 point integration.	128
80	$\phi$ - $\phi$ backscattering pattern, N=50 dipoles, P=2 segments, $d/\lambda=0.25$ , exact integration.	129
81	$\phi$ - $\phi$ backscattering pattern, N=50 dipoles, P=4 segments, $d/\lambda=0.25$ , exact integration.	130
82	$\theta$ - $\phi$ backscattering pattern, N=50 dipoles, P=2 segments, $d/\lambda=0.25$ , 12 point integration.	131
83	$\theta$ - $\phi$ backscattering pattern, N=50 dipoles, P=2 segments, $d/\lambda=0.25$ , exact integration.	132
84	$\theta$ - $\phi$ backscattering pattern, N=50 dipoles, P=4 segments, $d/\lambda=0.25$ , exact integration.	133
85	$\theta$ - $\theta$ backscattering pattern, N=50 dipoles, P=2 segments, $d/\lambda=0.125$ , 12 point integration.	134
86	$\theta$ - $\theta$ backscattering pattern, N=50 dipoles, P=2 segments, $d/\lambda=0.125$ , exact integration.	135
87	$\theta$ - $\theta$ backscattering pattern, N=50 dipoles, P=4 segments, $d/\lambda=0.125$ , exact integration.	136
88	$\phi$ - $\phi$ backscattering pattern, N=50 dipoles, P=2 segments, $d/\lambda=0.125$ , 12 point integration.	137
89	$\phi$ - $\phi$ backscattering pattern, N=50 dipoles, P=2 segments, $d/\lambda=0.125$ , exact integration.	138
90	$\phi$ - $\phi$ backscattering pattern, N=50 dipoles, P=4 segments, $d/\lambda=0.125$ , exact integration.	139
91	$\theta$ - $\phi$ backscattering pattern, N=50 dipoles, P=2 segments, $d/\lambda=0.125$ , 12 point integration.	140
92	$\theta$ - $\phi$ backscattering pattern, N=50 dipoles, P=2 segments, $d/\lambda=0.125$ , exact integration.	141
93	$\theta$ - $\phi$ backscattering pattern, N=50 dipoles, P=4 segments, $d/\lambda=0.125$ , exact integration.	142
94	Histogram of the center-to-center distances of random two-dipole clouds. Average spacing $d/\lambda \simeq 1/43$ .	143

Figure		Page
95	Histograms of the spatially averaged radar cross sections of the clouds generated for Fig. 94.	144
96	Histograms of the radar cross sections (single aspect of the clouds generated for Fig. 94.	145
97	Histograms of the center-to-center distance of random two-dipole clouds.	146
98	Histograms of the spatially averaged radar cross sections of the clouds generated for Fig. 97.	147
99	Average cross section of random two-dipole clouds as a function of average center-to-center spacing between dipoles.	148
100	Calculated average backscattering cross sections for ensembles of clouds containing equal numbers of two wire lengths, $\ell_1/\lambda = 0.495$ , $\ell_2/\lambda = 0.703$ , with average spacing $d/\lambda = 4.0$ .	150
101	Calculated average backscattering cross sections for ensembles of clouds containing equal numbers of two wire lengths, $\ell_1/\lambda = 0.495$ , $\ell_2/\lambda = 0.703$ , with average spacing $d/\lambda = 1.0$ .	151
102	Calculated average backscattering cross sections for ensembles of clouds containing equal numbers of two wire lengths, $\ell_1/\lambda = 0.495$ , $\ell_2/\lambda = 0.703$ , with average spacing $d/\lambda = 0.5$ .	152
103	Calculated average backscattering cross sections for ensembles of clouds containing equal numbers of two wire lengths, $\ell_1/\lambda = 0.495$ , $\ell_2/\lambda = 0.703$ , with average spacing $d/\lambda = 0.25$ .	153
104	A typical styrofoam 2" cube, dipole, and jig for accurately inserting the dipole.	155
105	Styrofoam cubes in styrofoam box for creating a cloud of dipoles.	156



Figure		Page
106	Measured and calculated E-plane backscattering cross-section patterns for a 3 x 3 x 3 array of 27 parallel dipoles spaced about $0.53\lambda$ apart.	157
107	Measured and calculated E-plane backscattering cross-section patterns for a 5 x 5 x 5 array of 125 parallel resonant dipoles spaced about $0.53\lambda$ apart.	158
108	Measured and calculated E-plane backscattering cross-section patterns for a cloud of 27 dipoles randomly oriented in styrofoam cubes. Average dipole spacing was $0.53\lambda$ .	159
109	Measured insertion loss of same-sense and cross-sense polarizations for 1000 resonant dipoles encapsulated in 2.38" foam spheres.	161
110	Measured insertion loss of same-sense and cross-sense polarizations for 1000 resonant dipoles encapsulated in 2" foam spheres.	162
111	Measured insertion loss of same-sense and cross-sense polarizations for ~3200 resonant dipoles encapsulated in 1-1/2" foam spheres.	163
112	Measured insertion loss of same-sense and cross-sense polarizations for ~7200 resonant dipoles encapsulated in 1" foam spheres.	164
113	Radar cross section vs $360^\circ$ of rotation of 1.5 cm Al chaff on 4" foam sphere.	168
114	Radar cross section vs $360^\circ$ of rotation of 1.5 cm Al chaff on 4" foam sphere.	169
115	Radar cross section vs $360^\circ$ of rotation of 1.5 cm Al chaff on 4" foam sphere.	170
116	Radar cross section vs $360^\circ$ of rotation of 1.5 cm Al chaff on 4" foam sphere.	171
117	Radar cross section vs $360^\circ$ of rotation of 1.75 cm glass chaff on 4" foam sphere.	172
118	Radar cross section vs $360^\circ$ of rotation of 1.75 cm glass A chaff on 4" foam sphere.	173

Figure		Page
I-9	The decrease in average backscattering cross section due to coupling for a range of average dipole spacings (Gaussian density distribution assumed).	175
I-1	Sketches of the exponential probability density function and corresponding cumulative probability function for the backscattering cross section of a chaff cloud.	180
I-2	Sketches of a histogram and associated Gaussian probability distribution of spatial average cross sections of frozen chaff clouds.	182
I-3	Sketch of a typical spatial frequency spectrum of a frozen chaff cloud.	185
I-4	The highest spatial frequency $W_n$ in the spectrum of a frozen chaff cloud, as function of $N$ and $d/\lambda$ .	186
I-5	The histogram and associated Gaussian probability distribution of the spatial averages of 80 frozen chaff clouds containing 30 dipoles each.	188
I-6	Ensemble average backscatter $\overline{\langle \sigma \rangle}$ over 80 frozen chaff clouds with average spacing $d/\lambda = 2$ .	194
I-7	Ensemble average backscatter $\overline{\langle \sigma \rangle}$ over 80 frozen chaff clouds with average spacing $d/\lambda = 0.5$ .	195
II-1	Scattering cross-section configurations.	197
II-2	Arbitrary metallic scatterer in presence of primary sources.	199
II-3	Equivalent problem.	200
II-4	Subsectionalization of $S$ and $S'$ and convenient surface coordinate system $(\xi, \zeta)$ .	204
II-5	Examples of subsectional basis functions for surface scatterer.	206

Figure		Page
II-6	Mode structure for computing backscatter cross section from thin square flat plate (perfect conductor) using overlapping cosine mode.	207
II-7	Nonoverlapping dipole segments and overlapping dipole segments.	208
II-8	Equivalence of reactions between colinear axial test source and tubular surface current and equivalent parallel filamentary cases.	209
II-9	Sample mode structure on wire-grid model of conducting surface.	210
II-10	a) Thin cylindrical wires. b) Approximate filamentary model using piecewise sinusoidal expansions $\Phi_n$ on surface and $\Phi_m$ on axis.	212
VI-1	Bistatic scatter cross section for 100 dipole array ( $8 \text{ dip}/\lambda^3$ ) comparing exact and far zone A matrix calculations.	274
VI-2	Bistatic scatter cross section for 100 dipole array ( $8 \text{ dip}/\lambda^3$ ) comparing full (exact) A matrix and sparse A matrix using 10% sparsing rule.	276
VI-3	Sinusoidal dipoles and far zone approximations.	277
G-1	An extended target echo.	313
G-2	A differential target echo.	314
G-3	$v = 140 \text{ m/s}$ . Leading edge tracker.	320
G-4	$v = 180 \text{ m/s}$ . Leading edge tracker.	321
G-5	$v = 220 \text{ m/s}$ . Leading edge tracker.	322
G-6	$v = 260 \text{ m/s}$ . Leading edge tracker.	323
G-7	$v = 300 \text{ m/s}$ . Leading edge tracker.	324
G-8	$v = 100 \text{ m/s}$ . Slit-gate tracker.	325

Figure		Page
G-9	$v = 180$ m/s. Slit-gate tracker.	326
G-10	$v = 200$ m/s. Slit-gate tracker.	327
G-11	$v = 200$ m/s. Slit-gate tracker.	328
G-12	$v = 260$ m/s. Slit-gate tracker.	329
G-13	$v = 340$ m/s. Slit-gate tracker.	330
G-14	$v = 380$ m/s. Slit-gate tracker.	331
G-15	$v = 410$ m/s. Slit-gate tracker.	332

# LIST OF TABLES

Table		Page
I	Percent Error in Bistatic Averages Caused by Setting Mutual Impedances Below (0.1) ( $Z_{11}$ ) to Zero	31
2	Number on Non-zero Terms in Upper Triangle	40
3	% of Non-zero Terms in Sparse Matrix Upper Triangle	40
4	m, the Number of elements in a "Sphere of Influence"	40
5	Clock Times of Three Parts of Spare Matrix Routine	70
6	Convergence Norm Definitions	93
7		124
8	Experimentally Determined Extinction Rates	165
I	Highest Spectral Frequencies	191
II	Spatial Averages of 80 Clouds	192
III	The Data of Table II Classified into Relative Frequencies of Occurrence	193
IV	Cumulative Probability Values	193
VI-1	Data Comparison for Different Mutual Impedance Calculations for 100 Dipole Array	275

# LIST OF SYMBOLS

$N$	- number of dipoles in a cloud, Gaussianly distributed in the radial direction
$\delta$	- standard deviation of the Gaussian dipole distribution
$d/\lambda$	- average spacing between dipoles
$M$	- number of clouds in an ensemble of clouds
$\lambda$	- wavelength
$\beta$	- bistatic angle
$\sigma_m(\theta)$ or $\sigma(\theta)$	- backscattering cross section of $m$ th cloud as a function of angle $\theta$ around great circle cut
$\langle \sigma_m \rangle$ or $\langle \sigma \rangle$	- spatial average or mean value of $\sigma_m(\theta)$ over $360^\circ$ of the angle $\theta$
$\overline{\langle \sigma_m \rangle}$ or $\overline{\langle \sigma \rangle}$	- ensemble average of $\langle \sigma_m \rangle$ values over $1 \leq m \leq M$ clouds forming an ensemble
$\sigma_m 1/5$ or $\sigma_{1/5}$	- first quintile of $\sigma_m$
$\sigma_m 1/2$ or $\sigma_{1/2}$	- median of $\sigma_m$
$\sigma_m 4/5$ or $\sigma_{4/5}$	- fourth quintile of $\sigma_m$
$\overline{\sigma}_{1/5}$	- ensemble average of $\sigma_m 1/5$
$\overline{\sigma}_{1/2}$	- ensemble average of $\sigma_m 1/2$
$\overline{\sigma}_{4/5}$	- ensemble average of $\sigma_{4/5}$
$p_m(\sigma_m)$ or $p(\sigma)$	- probability density function of $\sigma_m$
$P_m(\sigma_m)$ or $P(\sigma)$	- cumulative probability function of $\sigma_m$
$s_m$	- standard deviation of $\sigma_m$
$q_{\text{mean}}(\langle \sigma \rangle)$	- (Gaussian) probability density function of the mean, $\langle \sigma \rangle$
$s_{\text{mean}}$	- standard deviation of $\langle \sigma \rangle$
$q_{1/5}(\sigma_{1/5})$	- (Gaussian) probability density function of the first quintile $\sigma_{1/5}$

$s_{1/5}$	- standard deviation of $\sigma_{1/5}$
$q_{1/2}(\sigma_{1/2})$	- (Gaussian) probability density function of the median $\sigma_{1/2}$
$s_{1/2}$	- standard deviation of $\sigma_{1/2}$
$q_{4/5}(\sigma_{4/5})$	- (Gaussian) probability density function of the fourth quintile $\sigma_{4/5}$
$s_{4/5}$	- standard deviation of $\sigma_{1/2}$
$F_m(\omega)$	- spatial frequency spectrum of $\sigma_m$
$W_m$	- highest spatial frequency of $F_m(\omega)$
$W$	- average of $W_m$ for all M clouds in an ensemble
$W'$	- average highest spatial frequency as calculated using a two-dipole interference model
$Z \equiv A$	- impedance matrix of cloud
$I \equiv x$	- vector of dipole currents
$V, b$	- plane wave excitation voltage vector
$H$	- iteration or error reducing matrix
$H_J$	- iteration or error reducing matrix for Jacobi
$H_{GS}$	- iteration or error reducing matrix for Gauss-Seidel
$H_\omega$	- iteration or error reducing matrix for successive overrelaxation
$\omega$	- relaxation factor
$\epsilon^{(k)}$	- convergence norm

Other symbols are defined in context as necessary.



## I. INTRODUCTION

Since World War II, chaff, which is a code name for a collection of thousands of linear resonant dipoles, has been used as an effective passive ECM against pertinent threat radar systems. One generally recognizes at least two significant roles for chaff; first, self-protection as in the case of aircraft against fire control radars, and second, in situations where initially sown dipole corridors saturate radar receivers and the corridors are subsequently utilized as penetration aids. Heretofore, the echoing area or the radar cross section of a chaff cloud has been calculated by multiplying the number of dipoles by the so-called "tumble average radar cross-section" of a single dipole. Estimates based on this simple model have been poor. Experimental measurements are between 2-50% of the theoretical value, depending upon the situation. Furthermore, once certain dipole densities have been reached doubling or even quadrupling the number of dipoles show very little increase in echo area. The significance of these discrepancies is that the simple tumble average model is not satisfactory and it is high time one undertakes a more realistic study of the electromagnetic scattering and attenuation properties of chaff clouds. To fulfill the requirements, the ElectroScience Laboratory under sponsorship of the Air Force Avionics Laboratory has undertaken a comprehensive study of the electromagnetic behavior of chaff clouds. The effort has been conveniently divided into three phases of increasing complexity. These are

1. Scattering behavior of single length, i.e., one frequency, dipoles with moderate mutual coupling between the elements.
2. Same as above but with close coupling, even touching.
3. Clouds of different dipole lengths, i.e., multiple frequency clouds

The work performed under this contract emphasized (1), with some effort devoted to (2) and (3).

The scattering and extinction behavior of large ensembles of particles has long been a subject of study in such diverse disciplines as acoustics, quantum mechanics and electromagnetics [1]. Most work is based upon certain assumptions which make the problem analytically tractable, such as very small particle size, large spacing, no coupling or forward-neighbor coupling only, etc. In their domains of validity, mathematical models based on such



assumptions have indeed been useful in treating particulate media. In the case of a chaff cloud, however, two features complicate the problem: the particles are linear dipoles of lengths  $\lambda/2$  (resonant) or greater and therefore cannot be considered small; and during the early history of the cloud, before it fully blooms, these dipoles are closely spaced and strongly coupled electromagnetically. Furthermore, blooming implies non-stationary cloud statistics, and packaging configuration, dispensing technique and atmospheric conditions all influence the electromagnetic behavior of the cloud in time. These and many other problems face the investigator who wishes to answer such questions as, "How many dipoles is optimum for a cloud in a given tactical situation." "Is there a particular shape or density or density distribution of a cloud that is preferred?" "What are the expected scintillation rates?" "Can one make a cloud bloom faster electromagnetically?" These questions cannot be answered until we understand how a medium composed of many strongly resonant scatterers, which may be closely coupled, interacts with a radar wave, that is, until we can answer the basic question, "How does a chaff cloud scatter?"

Many attempts have been made in the past to answer the above question, usually to obtain the spatial average backscatter at resonance for a cloud of dipoles "frozen" in time [2,3]. Extensions were made to include nonresonant dipoles and dipoles with preferred orientations [4] as well as the dynamics of the dipoles [5,6,7,8]. In all instances, however, the effects of coupling among elements were not included in the analysis due to ensuing computational difficulties. Only recently has it become possible to account for coupling, at least on a limited basis, by use of large digital computer techniques [9,10,11]. Although we shall never be able (or ever wish) to account for all interactions among the millions of dipoles in a typical chaff cloud, the present capability of handling 250 resonant dipoles gives hope of accounting for sufficient numbers of interactions to obtain an accurate statistical description of the behavior of any cloud.

The purpose of our work was to bring the computer to bear on the chaff cloud problem in order to investigate the limits of simplifying approximations, to support, refine, or replace simple models, to obtain and interpret statistical data, and, basically, to better understand the scattering mechanism. This final report describes results developed over the three year time span of the contract. Because the effort extended over such a long period, many of the earlier methods for generating scattering data were superceded by improved methods, but the results still remain valid and valuable for the inferences that can be made from them. Thus, many of these early results, reported in Reference 12, are presented here as well to provide a complete and integrated overview of the effort.

The main chapter of this report, entitled, Technical Discussion and Results, is divided into several sections. In Section A we discuss the concept of a frozen cloud as a useful chaff model in the absence of realistic time varying data; in Section B (and Appendix A) are discussed the statistical quantities we have used to describe the radar cross section of a chaff cloud. Section C is a lengthy one which itself is divided into several parts: Introductory Remarks, which is intended to provide a very brief and general discussion of the method of moments (more details appear in Appendix B) by which the integral equation describing the electromagnetic chaff interaction problem is reduced to a set of simultaneous algebraic (matrix) equations suitable for processing by digital computer; Direct Methods, which describes the most commonly applied techniques for solving the above-mentioned matrix equations, such as the method of Crout; Sparse Matrix Methods, which describes special algorithms which are useful if the matrix is large and is sparse, i.e., has many zeros in it; i.e., weak coupling between chaff elements, and Indirect, or Iterative, Methods, which appear to be useful for large matrices, i.e., large numbers of chaff elements, without the assumption of sparsity. Typical results, as derived by each method, are presented in appropriate sections, together with a discussion and conclusions inferred from those results. In some instances verifying experimental data are also given to support the computations. Computer programs used to generate the results, either by the direct, sparse or iterative methods, are documented in Appendices D, E and F, respectively.

The primary emphasis during the contract was the investigation of clouds of resonant (half-wave) dipoles which were not "too closely" spaced. Some effort was expended to better define what "too closely" means in terms of the computer models used in our work, and this is discussed in Section D of Chapter II. Section E is addressed to chaff clouds containing multi-length elements for purposes of broadbanding the chaff echo to meet threats over a range of frequencies. Section F is devoted to experimental results. Although the bulk effort was primarily computational, some experimental data were recorded to verify the computed results and to observe certain scattering and extinction behaviors of moving dipoles in numbers much greater than can be handled by computer (~8000). These and other experimental efforts are reported in this section.

Section G of Chapter II is on a topic somewhat divorced from that of chaff cloud scattering characteristics. In it we present an initial effort to investigate the aircraft-chaff cloud-tracking missile intercept problem. Many of the parameters of this problem are unknown, such as location and motion of scattering centers from a particular aircraft as a function of its maneuvers, the precise aerodynamic and electromagnetic behavior of chaff clouds spawned by the aircraft, and the range and tracking behavior of

the missile radars under such complex returns. Although these quantities were assumed in this study, it is anticipated that the approaches suggested here will become very useful for computerized simulation studies when more accurate input data become available through diverse research programs. More detail is given in Appendix G.

Chapter III concludes the body of the report with an overall discussion of our findings and suggestions for future effort.

Six appendixes were already alluded to. One additional appendix (C) describes the Gaussianly distributed density of dipoles employed throughout most of the contract. In the late stages of our work uniformly dense clouds were preferred and their generation is briefly described as well.

## II. TECHNICAL DISCUSSION AND RESULTS

### A. The Frozen Chaff Cloud Model

It is appropriate to discuss the first fundamental assumption upon which all our work, be it by computer or by laboratory experiment, rests. This is the assumption of the "frozen" chaff cloud model.

Scattering by a real chaff cloud is a stochastic process in the independent variable, time. At any given instant not only do we find the dipoles randomly positioned and oriented, but over a short interval of time they move and give rise to random fluctuations in the cross section (be it monostatic, bistatic, or forward). Moreover, with the passage of time, the cloud evolves from a dense to a tenuous conglomerate of dipoles so that, viewed over a long interval, the stochastic scattering process appears nonstationary, i.e., its statistics change with time.

In order to approximate the lower order statistics associated with a certain instant of time, one might consider an ensemble of similarly evolving clouds and take averages over this ensemble at the time of interest. This viewpoint leads us to the so called ensemble model, in which time is stopped at regular intervals, a "snapshot" taken of each cloud in the ensemble of clouds, and the ensemble average of backscatter calculated for each time sample. As time progresses and the cloud blooms, we assume the ensemble averages from each successive set of "snapshots" change and faithfully characterize the time average's behavior of a random cloud in evolution.

The generation of a large ensemble of clouds and the computation of ensemble average backscatter, for example, as the clouds evolve in time is an expensive process, especially if the clouds contain many dipoles. Thus there arises the proposition, instead of generating many different clouds (requiring the calculation of mutual impedances among dipoles for each new cloud) to form an ensemble over which to average, can we more efficiently obtain an equivalent ensemble average by viewing the same cloud (requiring the calculation of mutual impedances among dipoles only once) at many different aspects, then spatially averaging the back scattering cross section over all these aspect angles? As will be seen, the answer appears to be a qualified affirmative in that the spatial average backscattering cross sections for similar (i.e., same number of dipoles with same average spacing) but different clouds do differ in general, so that it is not sufficient to spatially average only one cloud return and accept that as a good equivalent ensemble average. One must generate an ensemble of clouds, obtain a spatial average backscattering cross section for each and then obtain an ensemble average of these spatial

averages. The point being that this latter ensemble is smaller than the former, thereby demanding fewer calculations of mutual impedances, etc. with resulting enhanced efficiency of computation (at least for large clouds). In all our work we obtain ensemble averages using this modified ensemble model, which we call the frozen model.

Going one step further in the search for computational efficiency, there arises the proposition, can we illuminate one or a few similar clouds from one aspect (requiring the calculation of induced currents only once for each cloud generated) and average the bistatic scattering cross section over a range of bistatic angles and expect this average to be simply related to the ensemble average of backscattering cross section? Or further, can one relate the average of total scattering cross section to the ensemble average of backscattering cross section? The answer to both these propositions appears to be negative, or at least the relationships are not clear to us from the data we have generated.

#### B. Representative Cloud Characteristics

In the previous section, we discussed the frozen model of a chaff cloud as a substitute for the more complex time-varying model, under the assumption that the scattering characteristics derived from each model agree. The characteristics which we have in mind are, of course, statistical in nature and should be discussed more fully so that the reader understands the results presented later.

Viewed in time, the monostatic or bistatic echo from a cloud consists of an average return plus a scintillation term. The average is expected to change as the cloud blooms - a symptom of non-stationarity - but if its rate of change is slow with respect to the scintillation rate, the scattering process might be considered stationary over small time intervals. With each such time interval, therefore, are associated a mean value, i.e., the time average radar cross section, a variance, i.e., the mean square of the time-varying component of the radar cross section, and a frequency spectrum of the cross section. The totality of all such sets of quantities taken during selected time intervals constitute a partial statistical description of the cloud behavior.

By assuming a frozen model, appropriate to one of the above-mentioned intervals of time (i.e., with average dipole spacing appropriate to the time interval in the evolution of a blooming cloud), we substitute viewing angle for time as the independent variable and obtain a spatial average radar cross section. As mentioned earlier, it turns out that this spatial average radar cross section differs from cloud-to-cloud, so in the frozen cloud



model we assume an ensemble of clouds and obtain a distribution of spatial average radar cross sections. The ensemble average of this distribution of spatial averages is assumed to be equivalent to the time average radar cross section for the time interval of interest. From this distribution we also obtain a variance of the spatial average, a quantity which has no obvious meaning in the time-averaging process, but is useful for estimating a confidence level for the ensemble average cross section obtained from the frozen model. It may be that the variance of the spatial average is simply related to the variance of the random time process, but at present we have no supporting evidence since no time-varying clouds have been generated.

The frequency spectrum of the frozen model is not expected to equal that of the time-varying cloud; it is useful, however, for estimating the minimum number of aspect angles at which to view the clouds in the frozen model, since a number smaller than this causes obvious aliasing of the spectrum.

A more quantitative discussion of the statistical notions and notation employed in later sections of this report are presented in Appendix A.

### C. Computer-Generation of Scattering Data

#### 1. Introductory Remarks

The second fundamental assumption underlying this work is that the generation of volumes of scattering data necessary for a statistical study of frozen models ultimately is more efficient, convenient and inexpensive by means of a computer than by laboratory experiment. Experimental data were considered essential to the contract, but primarily as verification of corresponding computed data. We leave discussion of the experimental aspects to a later section and here elaborate on the computer-generation of scattering data.

The computer-solution of scattering by a cloud of coupled resonant dipoles is based on the reaction matching technique of Richmond [9]. This is a moment method of the Galerkin type, i.e., in which the testing functions and basis functions are identical. It assumes that each dipole is divided into  $P$  segments ( $P = 2$  has been found to be satisfactory for the configurations discussed in this report), and a piecewise sinusoidal current of unknown amplitude and phase is assumed to flow on each segment. The coupling (i.e., mutual impedance) between each such segment of current and any other segment (or itself) can be expressed in the form of a reaction integral (i.e., an inner product integral) from which the method takes its name. The significant fact which makes the reaction matching technique particularly attractive is that all

these reaction integrals may be evaluated in closed form, thereby permitting the rapid determination of all the elements of a  $N \times N$  impedance matrix  $[Z]$  (representing all self-and-mutual impedances among the  $N$  dipoles in a cloud) whose inversion yields the desired dipole currents ( $I$ ) induced by a plane wave ( $E$ ) incident from any angle. This technique is well established and has been used to obtain scattering data for many wire obstacles. A more detailed description of the reaction matching technique is given in Appendix B.

With the assurance that the computer-generated scattering data are within the tolerance of experimental data, we turn our attention to the simulation of chaff clouds by the frozen model. Early in the program the  $N$  dipoles in a typical cloud were assumed to be resonant in free space, randomly oriented according to a spherical probability density function (i.e., all orientations equally likely) and randomly located according to a Gaussian radial density with average spacing  $d/\lambda$  between dipoles. This average spacing was obtained by considering 76% of the  $N$  dipoles to be located within a sphere of radius  $2.05\delta$ , where  $\delta$  is the standard deviation of the aforementioned Gaussian radial distribution. The volume of this sphere is equated to the volume of a cube which itself is subdivided into  $0.76N$  equal cubes, each of which is size  $d/\lambda$  on an edge and is considered to contain one dipole, yielding  $d/\lambda = 3.62 N^{-1/3} \delta/\lambda$ . Appendix C contains the details of this inhomogeneous cloud generation.

The foregoing choice of a cloud tapering from a dense central region to tenuous edge blending with free space seemed logical in the beginning. An actual chaff cloud might be expected to display such an inhomogeneity; furthermore, a uniformly dense cloud, for high densities, might be expected to exhibit a coherent scatter from the abrupt free space-cloud interface as well as an incoherent part. Our choice of a tapered density reduces the coherent part, which is desirable since this part would be dependent upon the exact shape of the cloud, which in the actual case is unknown and changing with time. At the same time, however, the tapered density suffers drawbacks. The parameter which we used to describe the tightness of the dipoles,  $d/\lambda$ , or "average spacing", is an average over a substantial part of the cloud. The average spacings are much smaller than this number near the cloud center and much larger closer to its edge. As the program progressed, it became clear that it would be better to assume clouds with uniform densities so that trends in the various methods, such as the sparse matrix and the iterative, could be correlated with respect to a more uniquely defined average spacing (or density) parameter. The details of the homogeneous cloud generation are contained in Appendix C.

We state here once and for all that, except where noted, all results appearing in this report are based on the Gaussian radial distribution for the cloud. The reader will find uniformly dense clouds assumed only in the section describing indirect methods.

## 2. Direct Methods

### (a) Theoretical Considerations

As discussed above, and in more detail in Appendix II, the electromagnetic scattering problem can be transformed via the method of moments into an  $N \times N$  matrix equation of the form

$$(1) \quad ZI = V$$

where the right hand vector  $V$  is known from the direction, polarization, and strength of the known incident plane wave and the elements of the  $Z$  matrix can all be calculated using reaction matching. The problem is to determine the current vector  $I$ , each component of which is the current  $I_n$  induced on the  $n$ th chaff dipole.

A direct solution for nonsingular  $Z$  can be expressed in terms of the inverse matrix  $Z^{-1}$ ; i.e.,

$$(2) \quad I = Z^{-1}V$$

However, the solution process may or may not include actual computation of the inverse. Practical examples of solutions expressible in the form of Eq. (2) are Gaussian elimination and LU decomposition. Both of these methods are based on triangularization of  $Z$ ; Gaussian elimination yields one solution per triangularization whereas, LU decomposition yields any number of solutions for different right hand side vectors. LU decomposition represents a class of compact methods including the Crout, Doolittle and Choleskey methods [37] which do not require storage of intermediate matrices during triangularization as does Gaussian elimination. Final elements of the triangular form are obtained by accumulation and when done in double precision arithmetic and rounded to single precision before storage, solutions by any of these methods will contain a minimum of roundoff error. Solutions to certain electromagnetic problems require repeated responses to variety of excitations. LU decomposition methods are well suited to this requirement and are probably the most widely used in electromagnetic computations.



Successful decomposition or factorization of a matrix is based on the LU theorem. The theorem is stated as follows: Let  $Z_k$  represent the  $k$ th principal submatrix of  $Z$ , formed by eliminating  $n-k$  rows and columns from  $Z$ . If

$$(3) \quad \det Z_k \neq 0, \quad k = 1, 2, \dots, n-1,$$

then there exist two unique triangular matrices  $L = [l_{ij}]$  and  $U = [u_{ij}]$ , with  $L$  the unit lower triangular (i.e., ones on the main diagonal and zeros above the diagonal) such that

$$(4) \quad Z = LU$$

and

$$(5) \quad \det Z = \prod_{i=1}^n u_{ii}.$$

The  $U$  matrix in this case is the same upper triangular matrix obtained by performing Gaussian elimination and  $L$  is related to the sequence of matrices  $M_k$ ,  $k=1, 2, \dots, n-1$ , which accomplished this triangularization. Details of computing elements of  $L$  and  $U$  are left to Appendix I of Reference 38. Equation (1) can now be restated in factored form as

$$(6) \quad LU I = V$$

and the solution is computed by setting

$$(7) \quad UI = I$$

in Eq. (6) and solving the resulting triangular system for  $I$  by forward substitution. This solution is then substituted back into Eq. (7) and the final triangular system is solved by backward substitution. These forward and backward substitutions are the only calculations needed for other solutions to the same system with different  $E$  (excitation) vectors. The factored form of  $Z$  defined by Eqs. (4) and (5) is referred to by Westlake [39] as Doolittle decomposition. The familiar Crout decomposition as described by Westlake performs lower triangularization on  $Z$  and

U becomes unit upper triangular. Choleskey's method, or the square-root method, requires Z to be at least symmetric. Factorization in this case leads to the form

$$(8) \quad Z = GG^T$$

(T denotes transpose) with the determinant given by

$$(9) \quad \det Z = \prod_{i=1}^N (g_{ii})^2 .$$

Gaussian elimination along with the Crout and Doolittle methods generally gives better results when a column reordering strategy is used on  $Z(k)$  to position the element of largest absolute magnitude in the  $k$ th row in the pivotal position (diagonal) at the  $k$ th step of the triangularization process. Choleskey's method, on the other hand, does not require this repositioning strategy when applied to positive definite matrices. The EM problems treated in this study result in complex symmetric (nonhermitian) matrices and in general this partial positioning process should be included. Experience has shown, however, that for most EM problems solved in this manner, sufficient accuracy is obtained without pivoting in spite of the indefiniteness of the coefficient matrix. Elements along the main diagonal generally are larger in magnitude than the off diagonal elements which no doubt contributes to this characteristic.

The size of a particular computer's fast access memory along with growth of roundoff accumulation are inherent limitations of these methods. The size problem can be overcome to a certain extent. However, unless precision is also improved, roundoff must eventually obscure acceptable solutions. One method for studying conditions which affect solution errors is to compute a relative error bound for the solution algorithm being used. Relative error is expressed in the form

$$(10) \quad \text{Relative Error} = \frac{\|I - \bar{I}\|}{\|I\|} ,$$

where  $I$  and  $\bar{I}$  represent the exact and computed solutions, respectively, to Eq. (1) and  $\|\cdot\|$  signifies an appropriate vector norm. Definitions of useful vector and matrix norms are given in Appendix C of Ref. [38].

Error bounds naturally tend to be conservative and are often considered useless for this reason. Nevertheless, bounds considered in proper perspective can yield information otherwise unavailable to the user. Computation of a bound based on the number of unknowns ( $N$ ), the algorithm, and the precision, may reveal trends which can bring confidence or a note of caution into play and is justified if only to indicate such a trend is possible when pushing the limits of a particular machine's size and accuracy. More discussion of condition numbers and error bounds appears in Ref. [38].

#### (b) Calculated Results for Chaff Clouds

Using the computer routines based upon the method of Crout and documented in Appendix II of Reference 12, clouds with  $N = 10, 15, 20, 25, 30, 50, 100, 150, 200$  dipoles were considered for average spacings,  $d/\lambda = 0.5, 1.0, 1.5, 2.0$ . Not all combinations of ( $N, d/\lambda$ ) were investigated equally intensively since computations for larger  $N$  values are time-consuming and certain trends could be discerned without them. Most work concentrated on clouds with  $N < 30$ , and on the backscattering cross section. Figures 1-4 show the average backscattering cross section  $\langle \sigma_m \rangle$  of the  $m$ th cloud in an ensemble of  $M = 29$  clouds in the frozen model, where  $1 \leq m \leq M$ . These figures give data for clouds containing up to  $N = 30$  dipoles and average spacings  $d/\lambda = 0.5, 1.0, 1.5, 2.0$ . As expected, the values of  $\langle \sigma_m \rangle$  distribute themselves over a range (note that where the density of dots in Figs. 1-4 is high, they are plotted aside one another), so it is appropriate to present an average value of the  $\langle \sigma_m \rangle$ , which we denote by  $\langle \bar{\sigma} \rangle$ . This has been done in Figs. 5-8, where  $\langle \bar{\sigma} \rangle$  is represented by a point. For the cases,  $N = 10, 30$ , which were investigated more extensively, the ranges which enclose 95.45% of all the values of  $\langle \sigma_m \rangle$  can be represented by a vertical line (extending from  $\langle \bar{\sigma} \rangle - 2 S_{\text{mean}}$  to  $\langle \bar{\sigma} \rangle + 2 S_{\text{mean}}$ ), where  $S_{\text{mean}}$  is the standard deviation of the distribution of  $\langle \sigma_m \rangle$ . The details of the distributions of  $\langle \sigma_m \rangle$  are discussed more fully in Appendix I; here, it suffices to say that these curves give some idea of the expected cross section from a cloud of chaff with coupling as a function of number of dipoles and average dipole spacing (i.e., dipole density). In Figs. 1-8, each straight line represents the ideal case of no coupling, in which case the average cross section of  $N$  dipoles is expected to be simply  $N$  times  $\langle \sigma_0 \rangle$ , the average cross section of a single resonant dipole.\* If the average cross section of a single resonant dipole is defined to be the cross section of that dipole averaged over all possible tumble angles, equally weighted (spherical

---

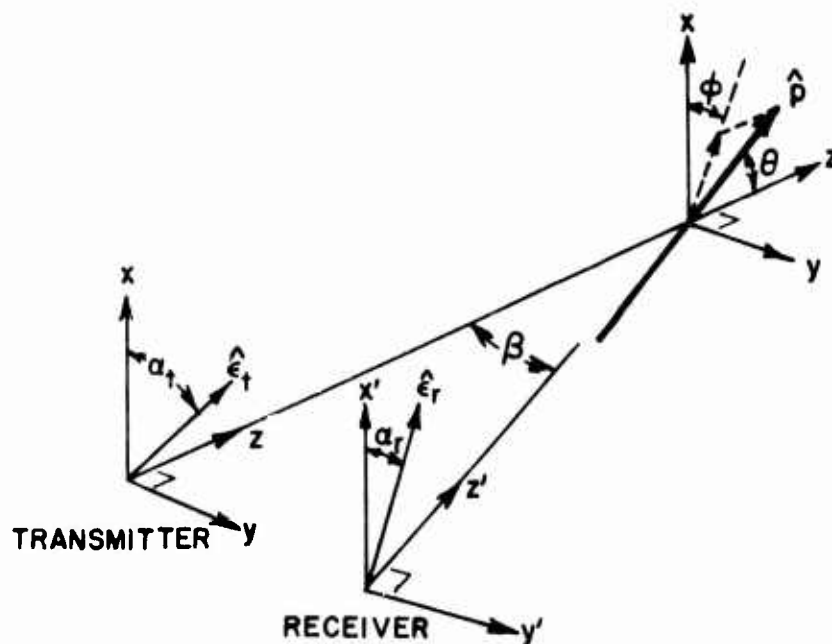
\*Actually, this straight line is an approximation strictly valid for uniform density clouds. However, for the non-uniform clouds considered here, it is an extremely good approximation.

probability density function for orientation), then  $\langle \sigma_0 \rangle$  is equal to about  $1/5$  times the maximum cross section of the dipole, or  $\langle \sigma_0 \rangle \approx 0.15\lambda^2$ . From these curves it is evident that with an average spacing of  $d/\lambda = 2.0$ , the curve  $N\langle \sigma_0 \rangle$  fairly well predicts the values of  $\langle \sigma \rangle$ , implying that coupling effects are weak and decoupled theory may as well be applied. But as  $d/\lambda$  decreases below 2.0 the values of  $\langle \sigma \rangle$  drops below those predicted by the curve  $N\langle \sigma_0 \rangle$  for the decoupled dipoles. Although fewer clouds were investigated for  $N > 30$ , the same trends persist, as indicated by Figs. 9 and 10.

Although most data generated were of backscattering cross section, some bistatic scattering cross sections were investigated as well. Figures 11-14 present results for rather dense clouds ( $d/\lambda \approx 0.59$ ) and bistatic angles  $\beta = 0^\circ$  (monostatic),  $45^\circ$ ,  $90^\circ$ ,  $135^\circ$  for vertical-to-vertical and vertical-to-horizontal polarizations. Computed data appear as circles and measured data appear as solid dots. (The methods used to obtain the experimental data are described below). Again, the straight lines  $N\langle \sigma_0(\beta) \rangle$  represent the ideal case of uncoupled elements, where  $\langle \sigma_0(\beta) \rangle$  is the tumble average bistatic cross section a single resonant dipole, calculated according to the formula,

$$(11) \langle \sigma_0(\beta) \rangle = 0.05\lambda^2 [1 + 2 (\cos \alpha_t \cos \alpha_r + \cos \beta \sin \alpha_t \sin \alpha_r)^2]$$

where  $\alpha_t$  and  $\alpha_r$  are the angles of the polarization vectors as shown in the accompanying sketch. In every case, we observe the same phenomenon - coupling effects a decrease in average cross section for both polarization combinations and all bistatic angles.



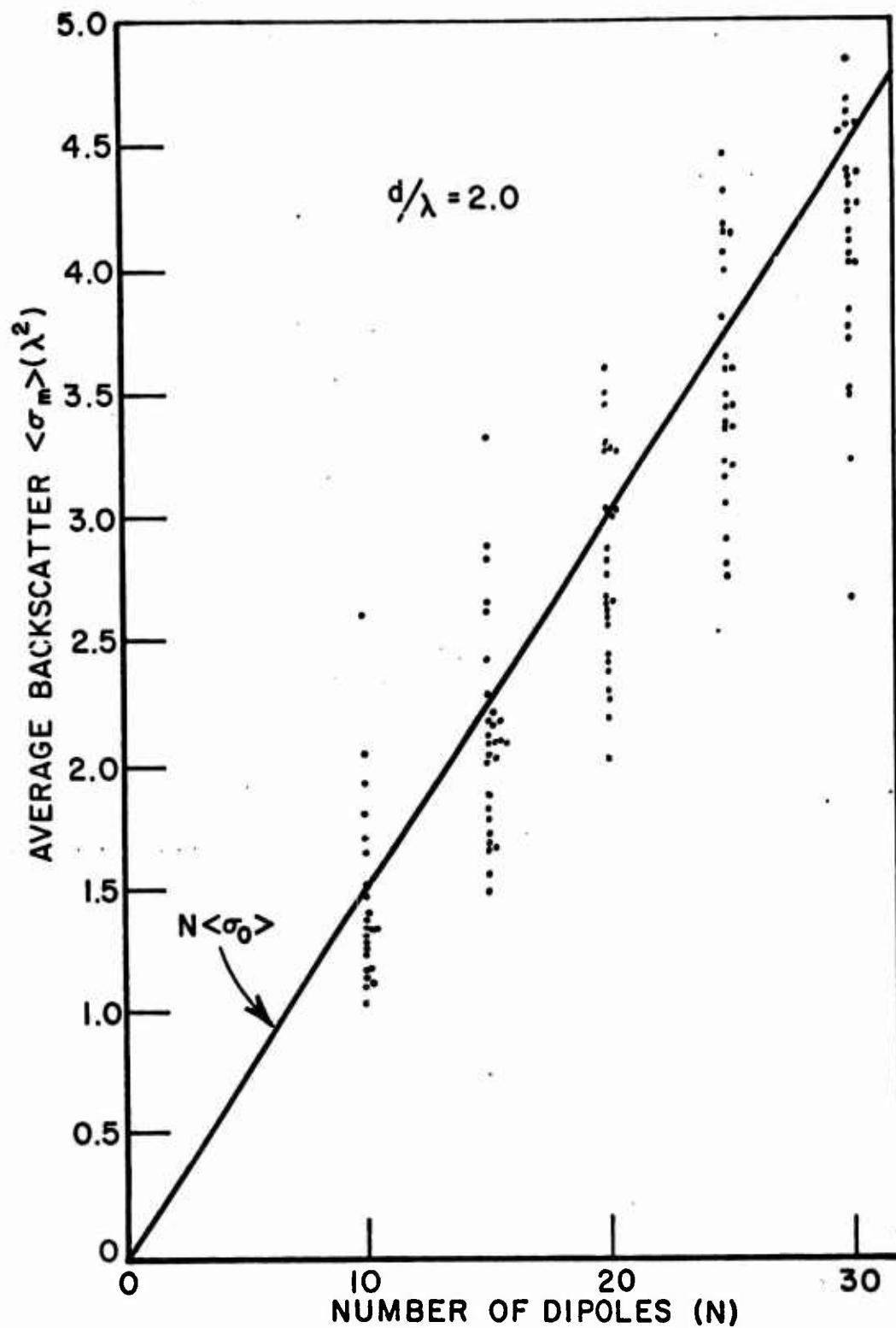


Figure 1. Calculated average backscattering cross sections for ensembles of clouds containing  $N \leq 30$  dipoles with an average spacing  $d/\lambda = 2$ . Straight line represents decoupled dipoles.

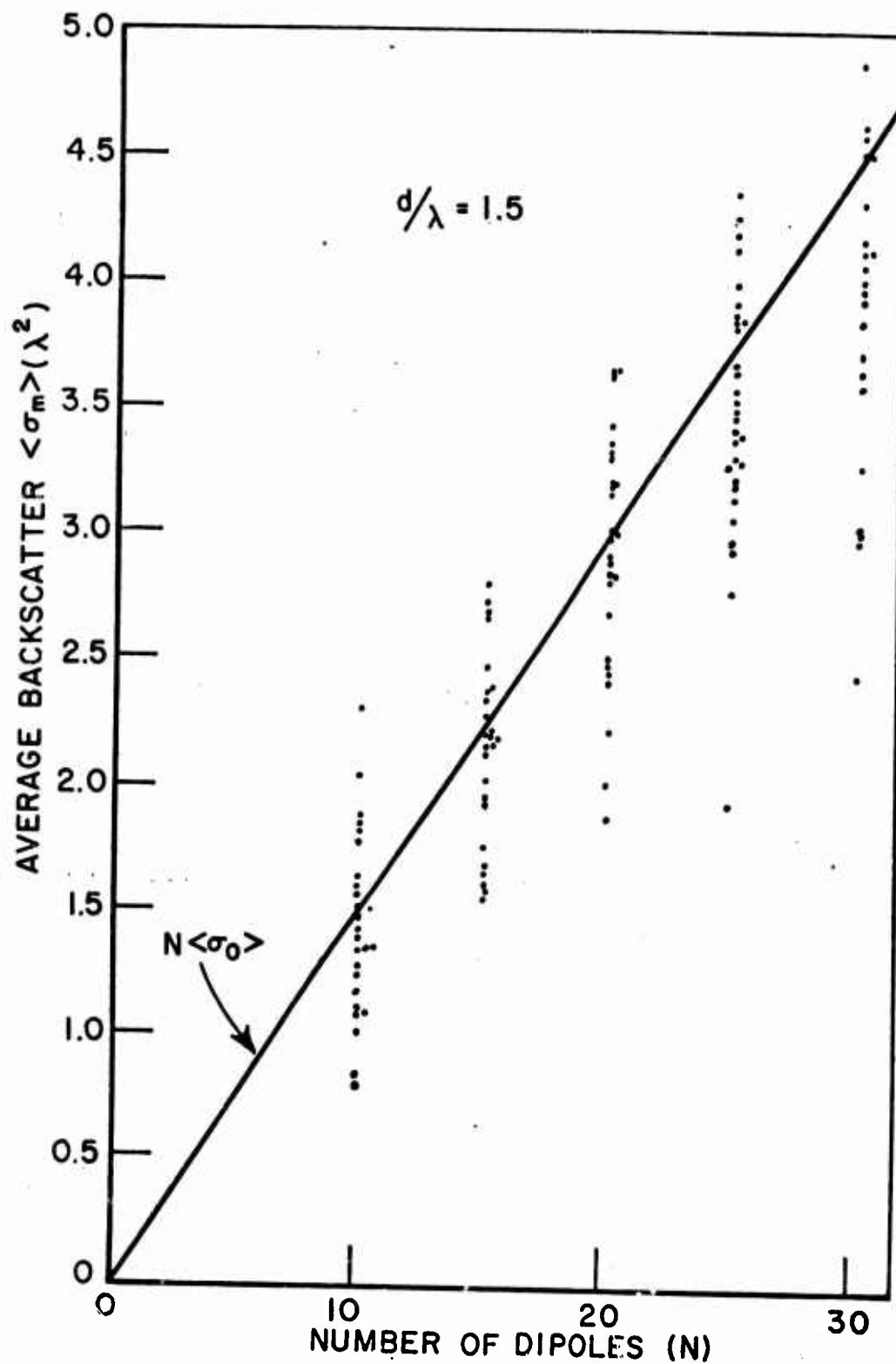


Figure 2. Calculated average backscattering cross sections for ensembles of clouds containing  $N < 30$  dipoles with an average spacing  $d/\lambda = 1.5$ . Straight line represents decoupled dipoles.



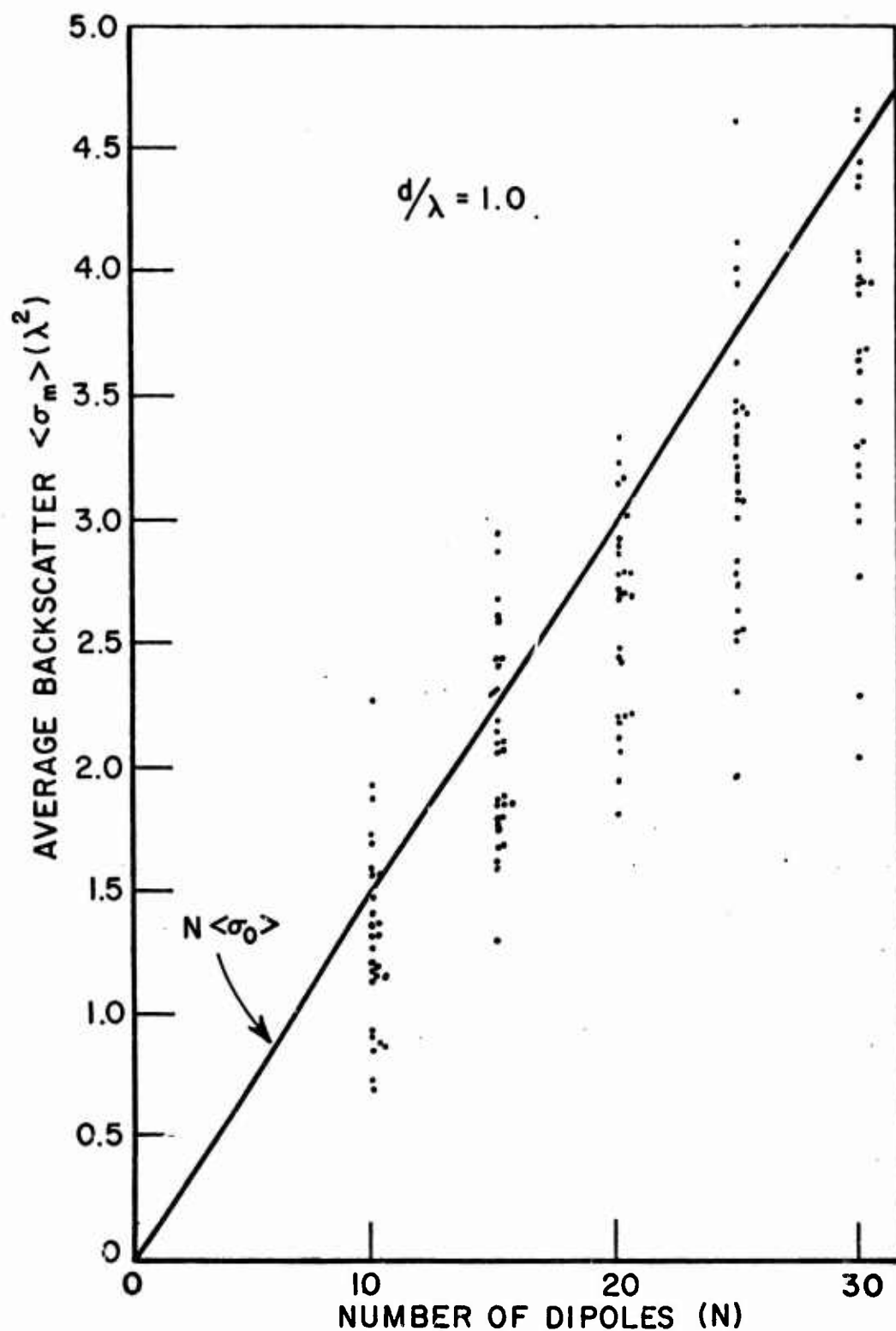


Figure 3. Calculated average backscattering cross sections for ensembles of clouds containing  $N \leq 30$  dipoles with an average spacing  $d/\lambda = 1.0$ . Straight line represents decoupled dipoles.

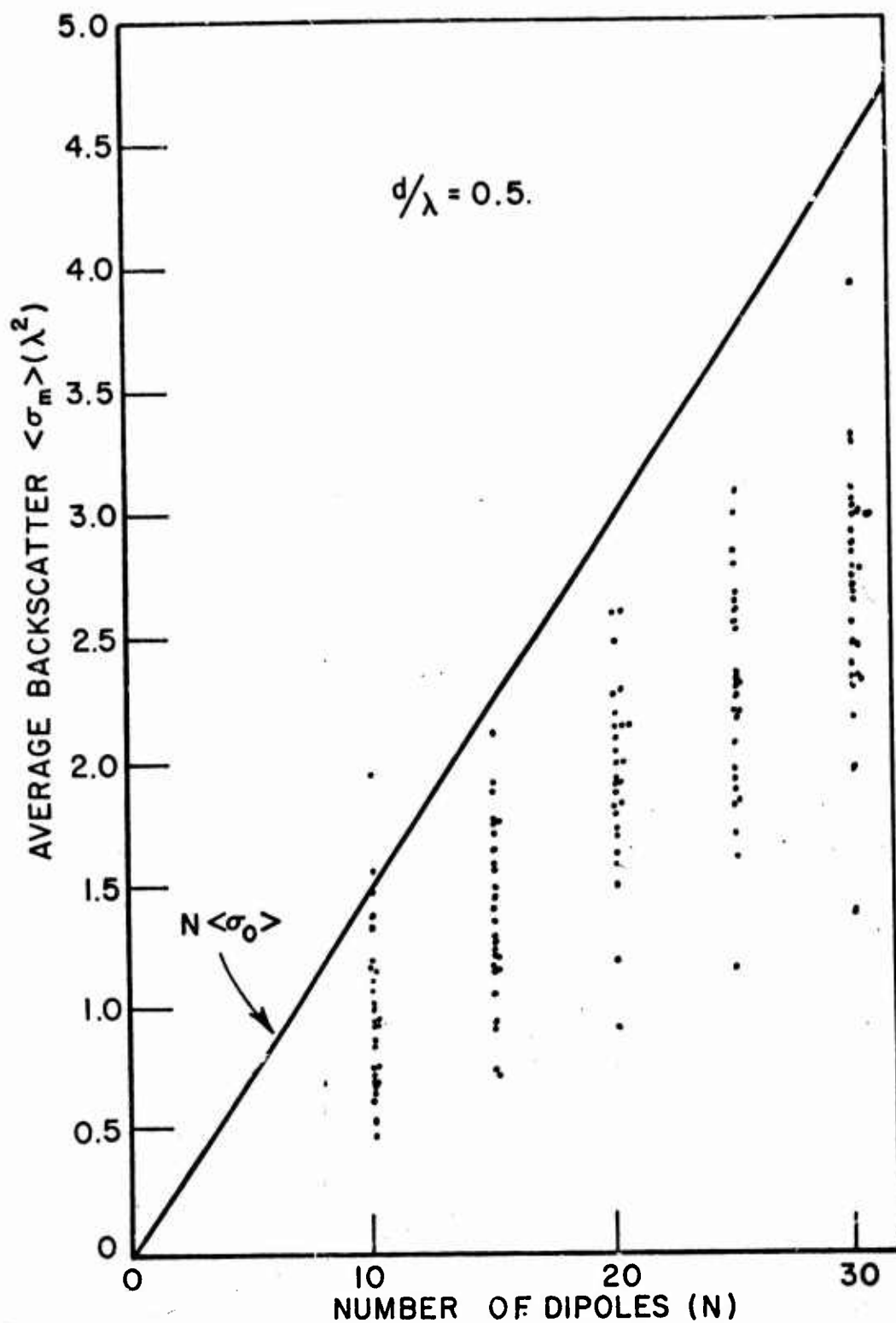


Figure 4. Calculated average backscattering cross sections for ensembles of clouds containing  $N \leq 30$  dipoles with an average spacing  $d/\lambda = 0.5$ . Straight line represents decoupled dipoles.

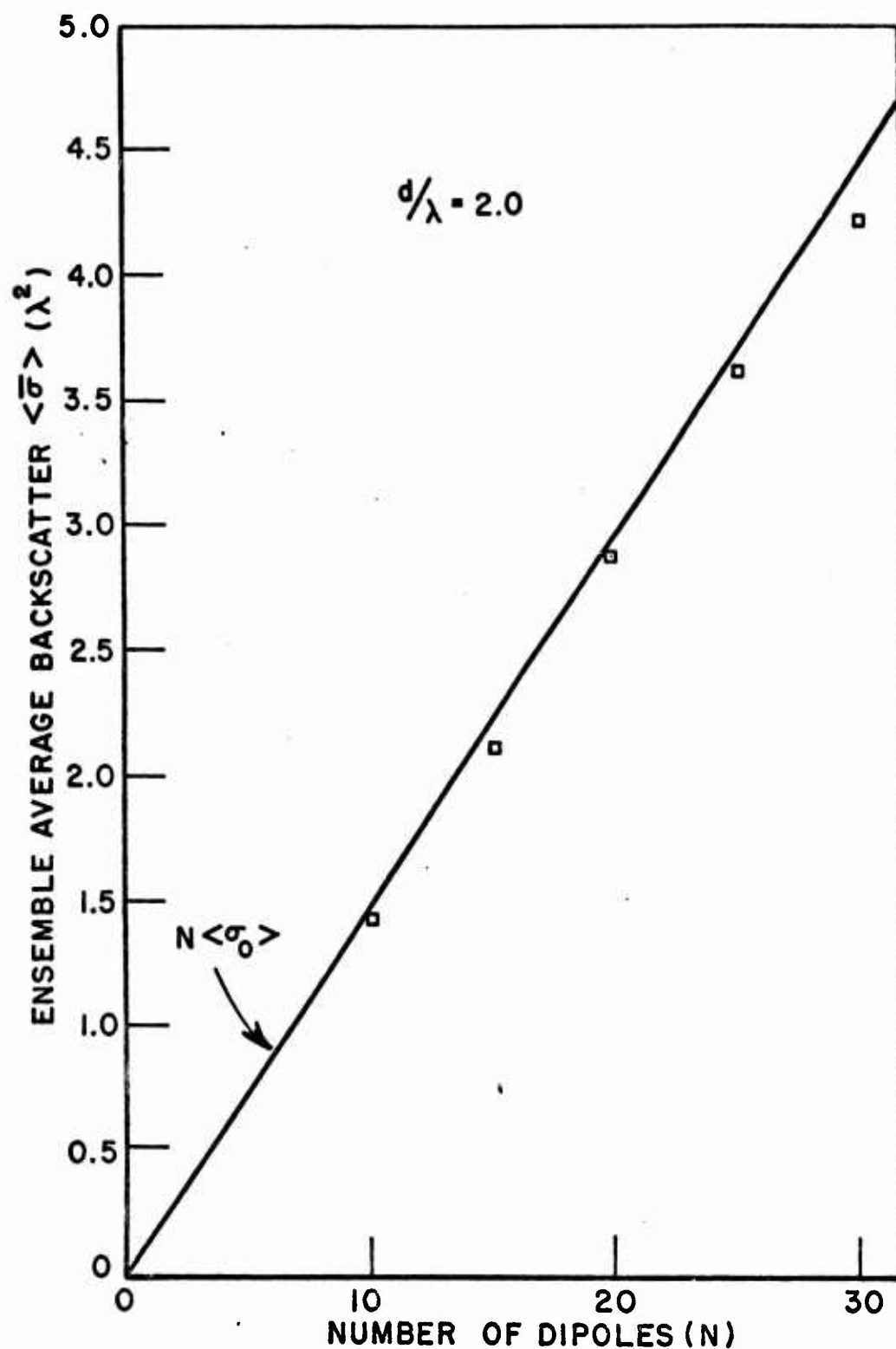


Figure 5. Calculated ensemble averages of the spatial averages shown in Fig. 1. Straight line represents decoupled dipoles.

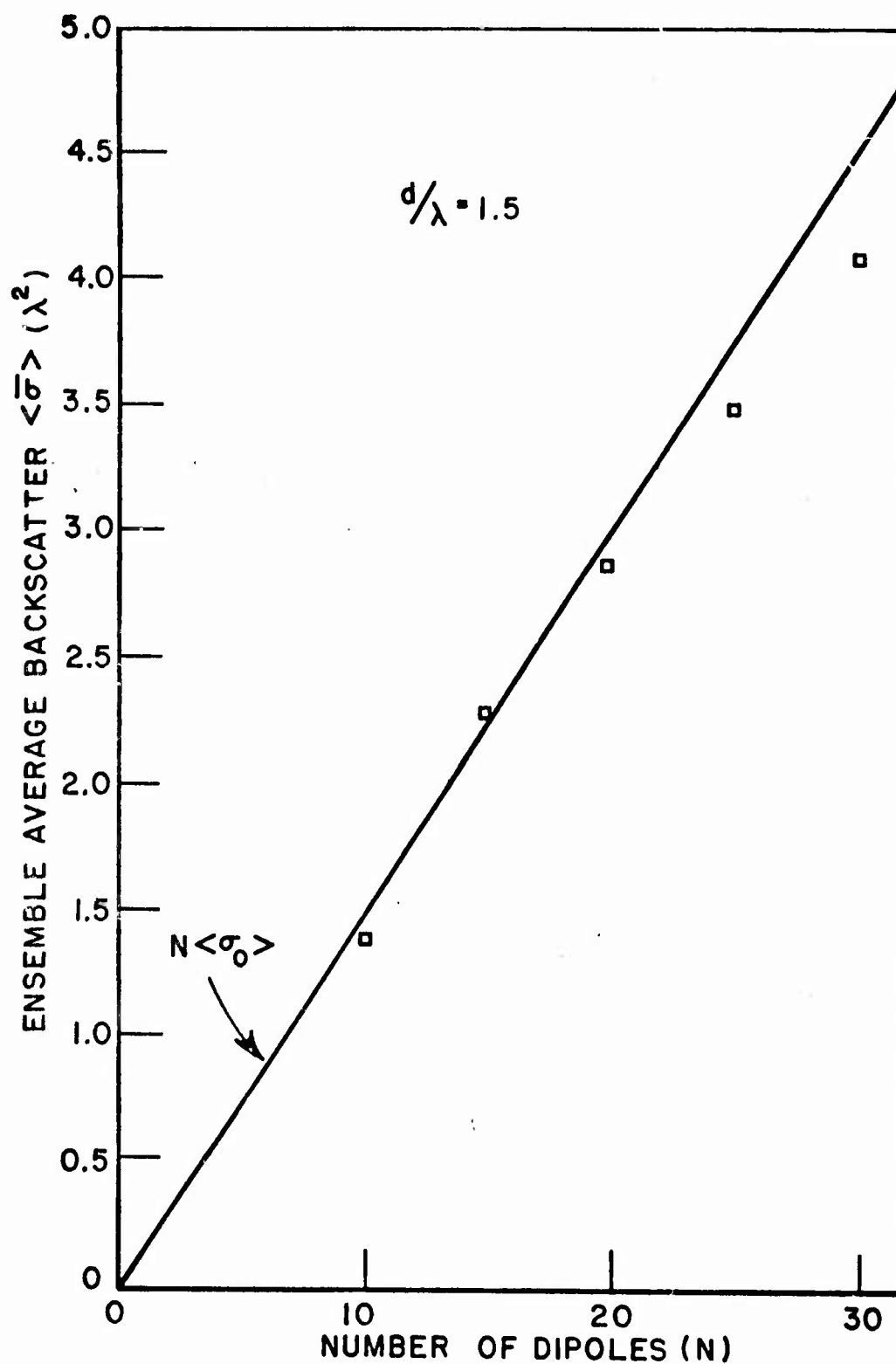


Figure 6. Calculated ensemble averages of the spatial averages shown in Fig. 2. Straight line represents decoupled dipoles.

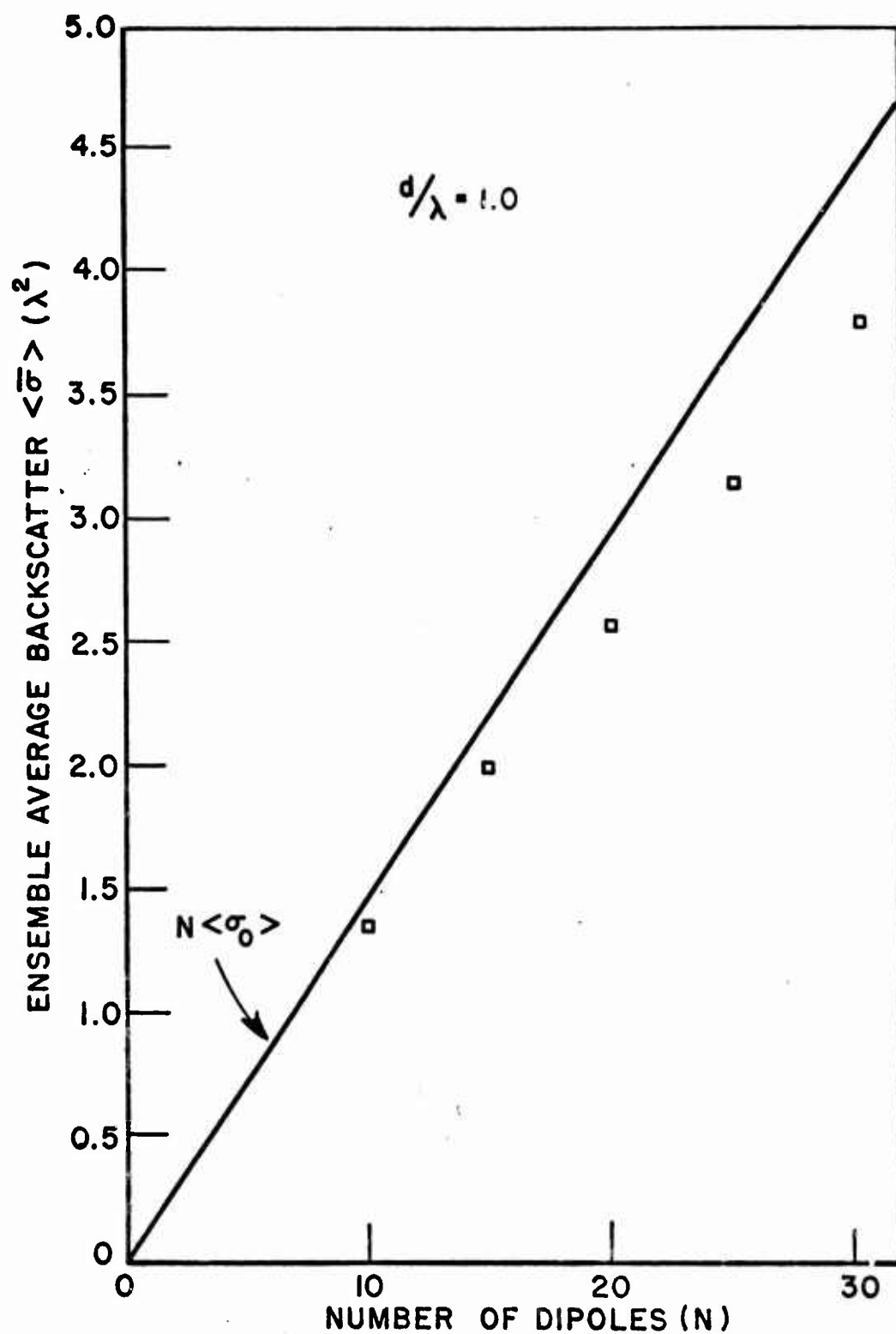


Figure 7. Calculated ensemble averages of the spatial averages shown in Fig. 3. Straight line represents decoupled dipoles.

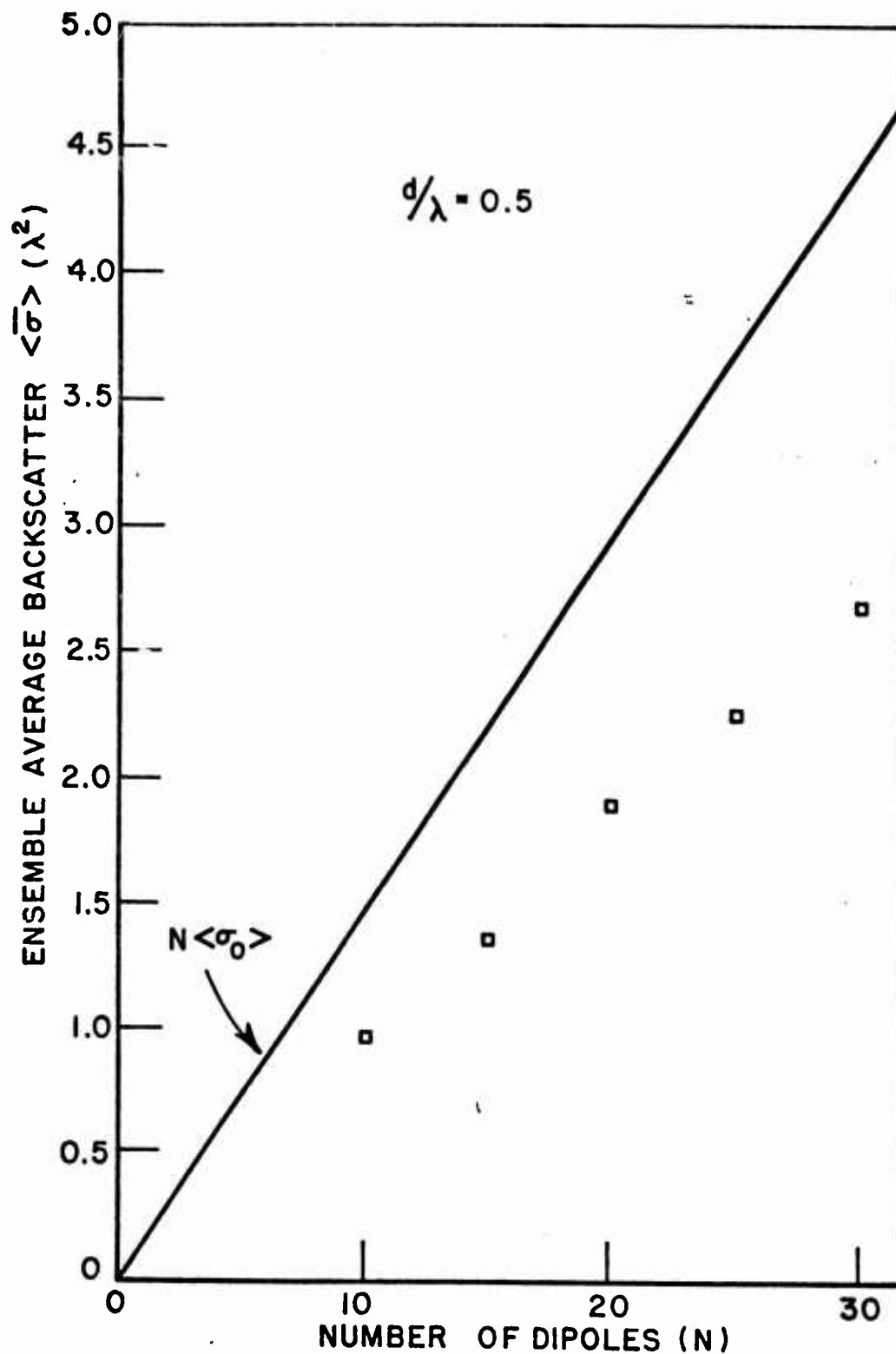


Figure 8. Calculated ensemble averages of the spatial averages shown in Fig. 4. Straight line represents decoupled dipoles.



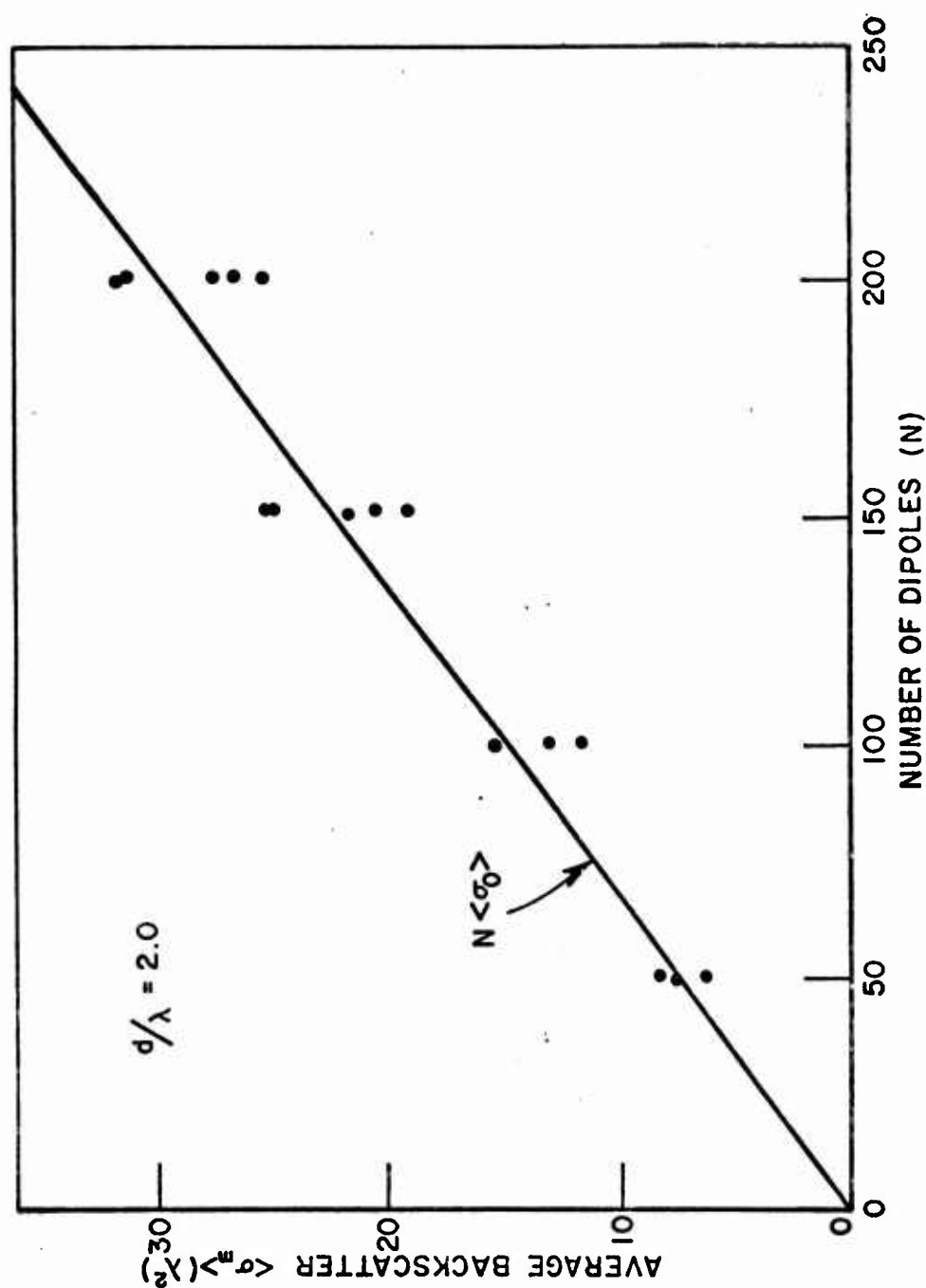


Figure 9. Calculated spatial average backscattering cross sections for ensembles of clouds containing  $50 < N < 200$  dipoles with an average spacing  $d/\lambda = 2$ . Straight line represents decoupled dipoles.

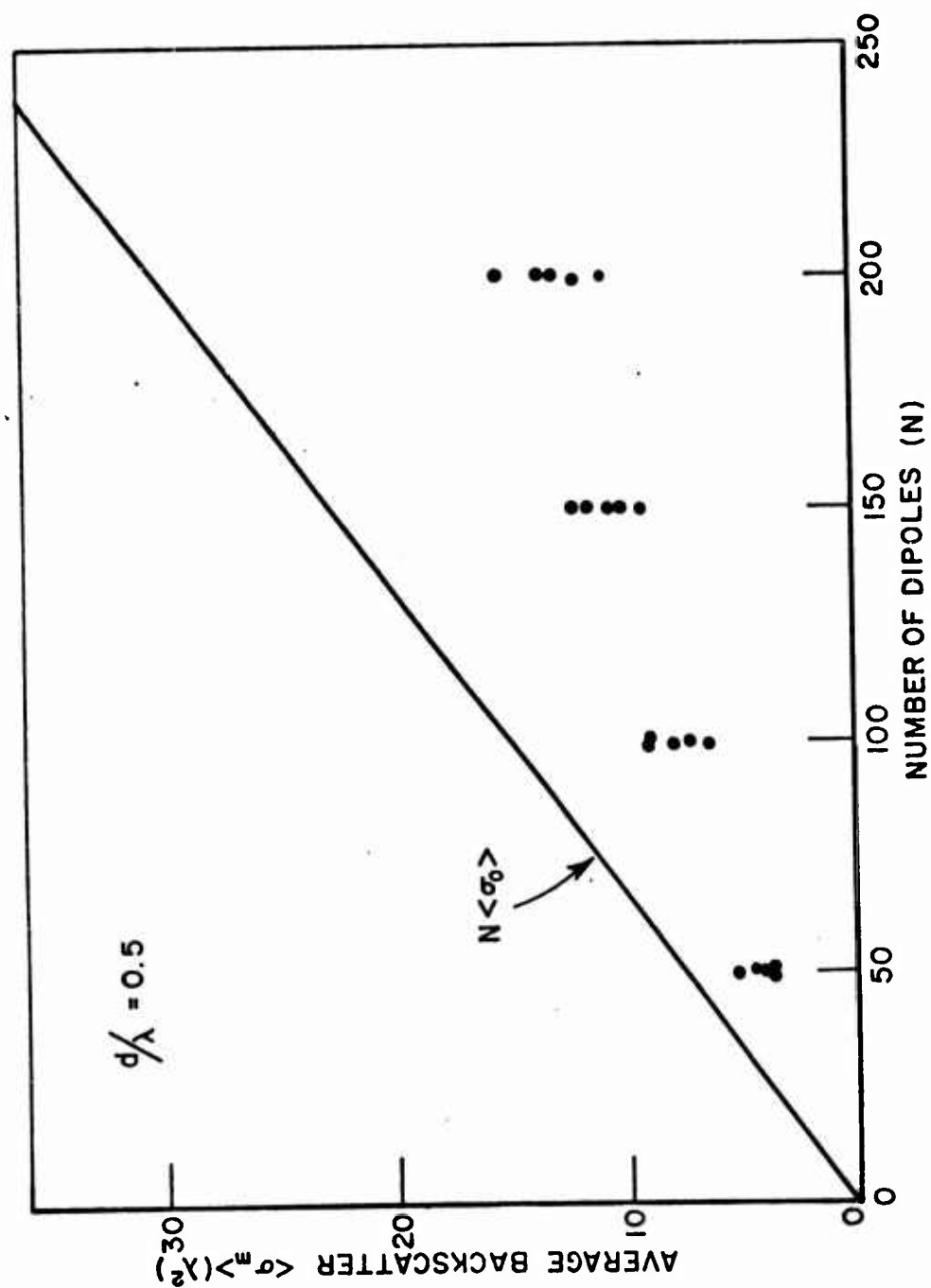


Figure 10. Calculated spatial average backscattering cross sections for ensembles of clouds containing  $50 < N < 200$  dipoles with an average spacing  $d/\lambda = 0.5$ . Straight line represents decoupled dipoles.

To obtain the bistatic scattering data of Figs. 11-14 up to 800 polyfoam spheres, each containing a dipole, were enclosed in a polyethylene bag which was rotated by means of strings. Horizontal polarization was transmitted to minimize string reflections and as the bag was rotated a cross section pattern was recorded and automatically averaged. Between runs, the bag was jostled to form a new cloud so that a variance could be observed for the average return.

Figure 15 shows the calculated spatial average backscatter as a function of frequency of four particular random clouds of  $N = 30$  dipoles each. In this figure, vertical-to-vertical polarization is assumed and  $l/\lambda$  is the electrical length of each dipole which is varied through the resonance region. The curves marked  $N < \sigma_0 >$  is for the ideally decoupled case and the other curves are for average spacings for each cloud of  $d/\lambda = 2.0$  and  $0.5$ . As expected, the closer spacing reduced the backscatter, but it does not significantly change the frequency of resonance. This result leads us to conclude that it is fruitless to seek a chaff cloud which blooms to a higher value of radar cross section than expected early in its evolutionary history by cutting the dipoles to any length other than the free space resonant length.

### 3. Sparse Matrix Methods

#### (a) Theoretical Considerations

In addition to the gathering of computed and measured data to obtain averages of backscattering cross sections, some effort has been directed at alternative methods for solving large matrix equations. The reaction method of Richmond leads to kernel matrices of the order  $N \times N$  which effectively must be inverted by one method or another. Using Crout-type methods just discussed and a large scale computer limit  $N$  to about 250; if more dipoles than this are of interest other methods must be sought to overcome the storage and time problems. In this and the following section we discuss two methods which we investigated - sparse matrix and iterative techniques.

Before launching into a discussion of these techniques, it is appropriate to enquire why one is interested in larger numbers of dipoles, especially since information concerning far scattered data are more easily derived from smaller clouds. The answer lies in the intent to characterize a chaff cloud by more than its average cross section, in particular, to calculate the fields inside a cloud as a function of depth of penetration and obtain some insight to the extinction and phase shift incurred. In order to obtain a substantial depth, it may be necessary to account for more than 250 dipoles, in which case new computer methods are

necessary. Such information would be useful for estimating the thickness of a layer of dipoles beyond which additional dipoles add very little to the average backscatter.

The solution to the problem of scattering from a cloud of  $N$  dipoles involves a system of  $N$  equations in  $N$  unknowns. Each of these equations contains  $N$  terms. Since all  $N^2$  terms must be stored, even large computer systems run out of fast-access memory for relatively few ( $N < 300$ ) dipoles. In order to study larger clouds, some means of reducing the number of stored elements is required.

The terms in the equations relate to the interaction (mutual impedance) between pairs of dipoles in the cloud. For dipoles that are widely separated or nearly perpendicular to each other, the associated mutual impedance can become quite small. If some threshold level is chosen for the magnitude of the mutual impedance and all mutual impedances below this threshold are ignored (i.e., set to zero), an approximate solution to the scattering problem may be obtained. The often-used assumption of completely independent dipoles is an extreme example of this type of approximation. Systems of linear equations of this type (i.e., where each equation contains only a few terms) may be solved by what are known as sparse matrix methods.

Sparse matrix methods are similar to other techniques (e.g., Crout, Gauss reduction), except that only non-zero terms are stored and only operations involving non-zero terms are performed. Thus they are faster and require less storage when applicable.

In order to determine whether such an approximate solution can be used for studying chaff clouds, a few tests were run using standard solution techniques (i.e., without implementing the time- and storage-saving algorithms) for several values of the threshold mentioned earlier. In this way the applicability of sparse matrix techniques could be determined before effort was expended to develop specialized computer programs.

Setting the threshold to a value equal to 10% of the magnitude of the dipole self-impedance resulted in a satisfactory percentage of zeros (nearly 80%) in the impedance matrix for several test clouds. The bistatic scattering patterns of twenty thirty-dipole clouds (with  $d/\lambda = 0.5$ ) were calculated using both the full impedance matrix and the sparse matrix obtained with the 10% threshold described above. Each pattern was averaged over  $360^\circ$  of bistatic angle and for each cloud the average obtained using the full matrix solution was compared with the average obtained using the sparse matrix solution. The percentage error for each of the twenty clouds is listed in Table I (where a + error means the sparse matrix yielded an average higher than did the full matrix).

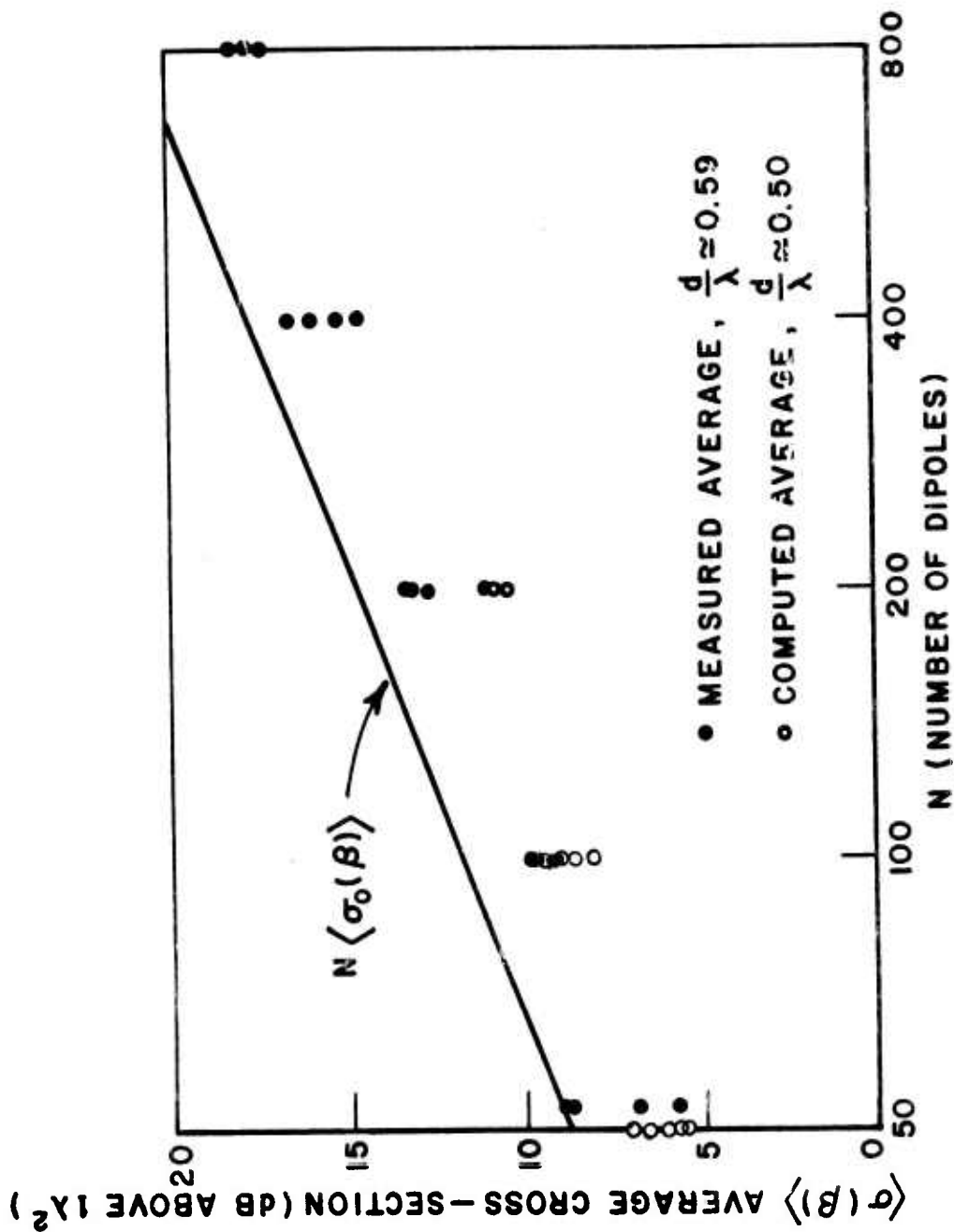


Figure 11. Measured and calculated values of the spatial average cross sections of ensembles of clouds containing  $50 < N < 800$  dipoles with average spacings  $d/\lambda \sim 0.5-0.6$ . Bistatic angle  $\beta = 0^\circ$  (monostatic case). Straight line represents decoupled dipoles.

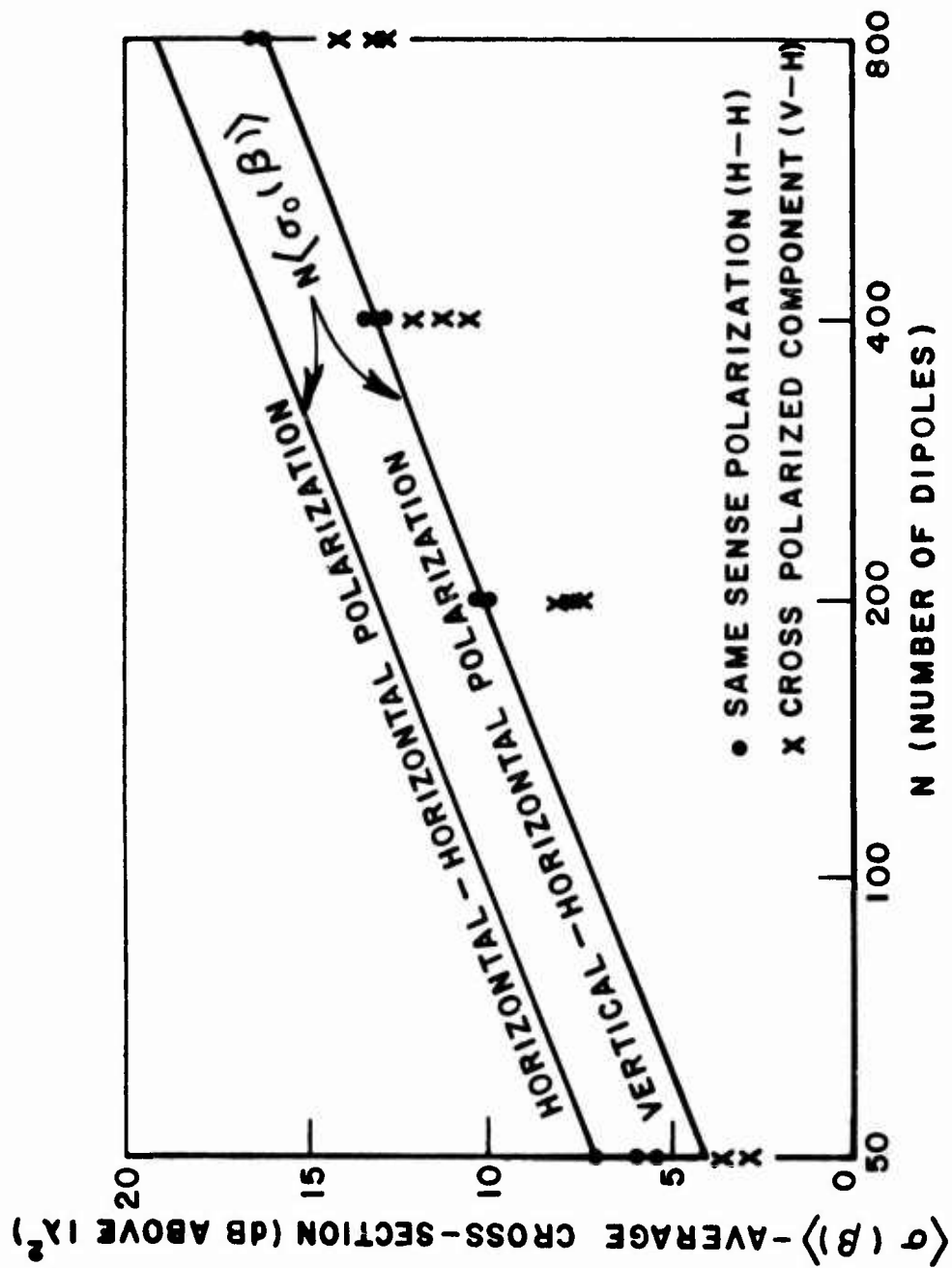


Figure 12. Measured values of the spatial average cross sections of ensembles of clouds containing  $50 < N < 800$  dipoles with average spacings  $d/\lambda \approx 0.5-0.6$ . Bistatic angle  $\beta=45^\circ$ . Straight line represents decoupled dipoles.



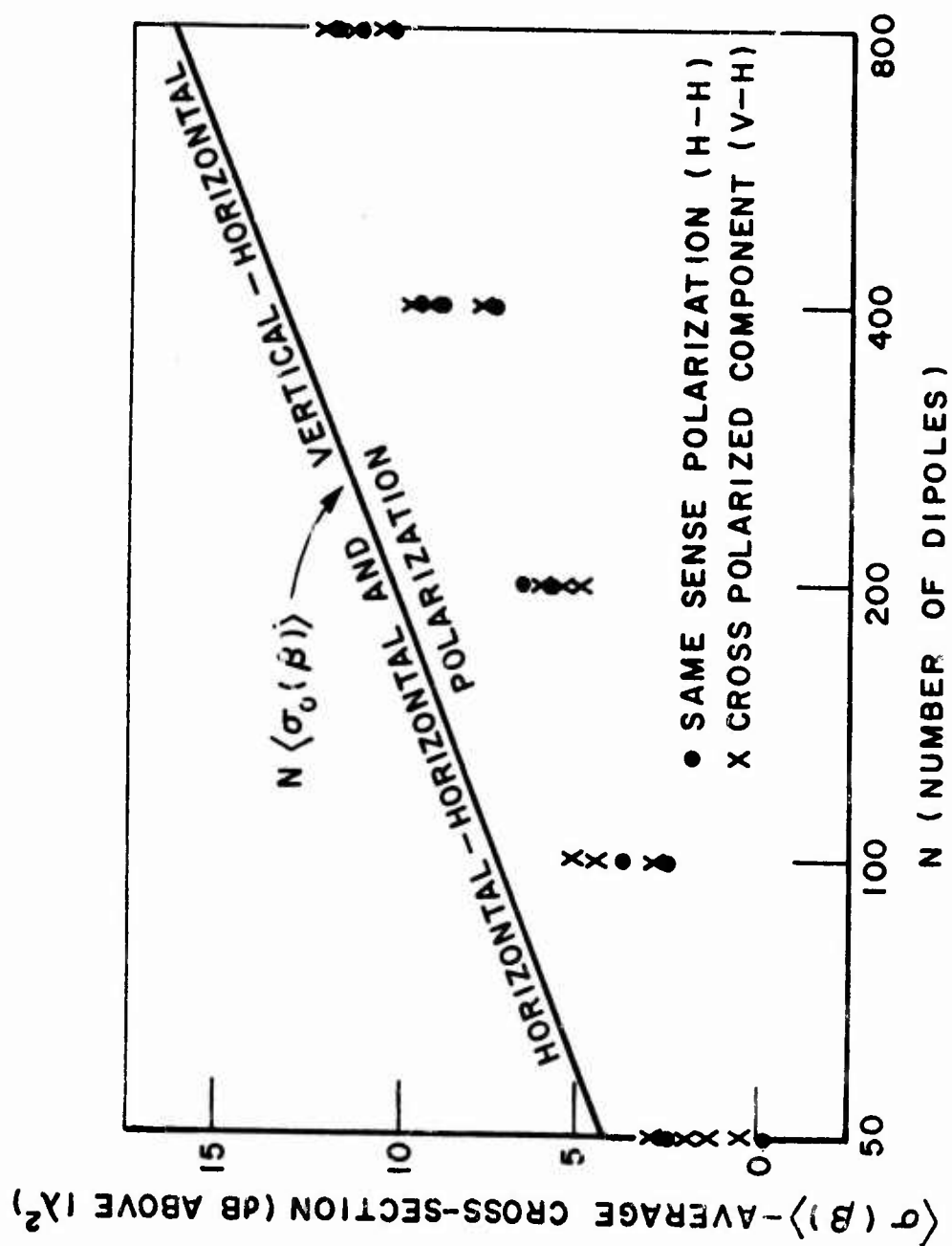


Figure 13. Measured and calculated values of the spatial average cross sections of ensembles of clouds containing  $50 < N < 800$  dipoles with average spacings  $d/\lambda \approx 0.5-0.6$ . Bistatic angle  $\alpha=90^\circ$ . Straight line represents decoupled dipoles.

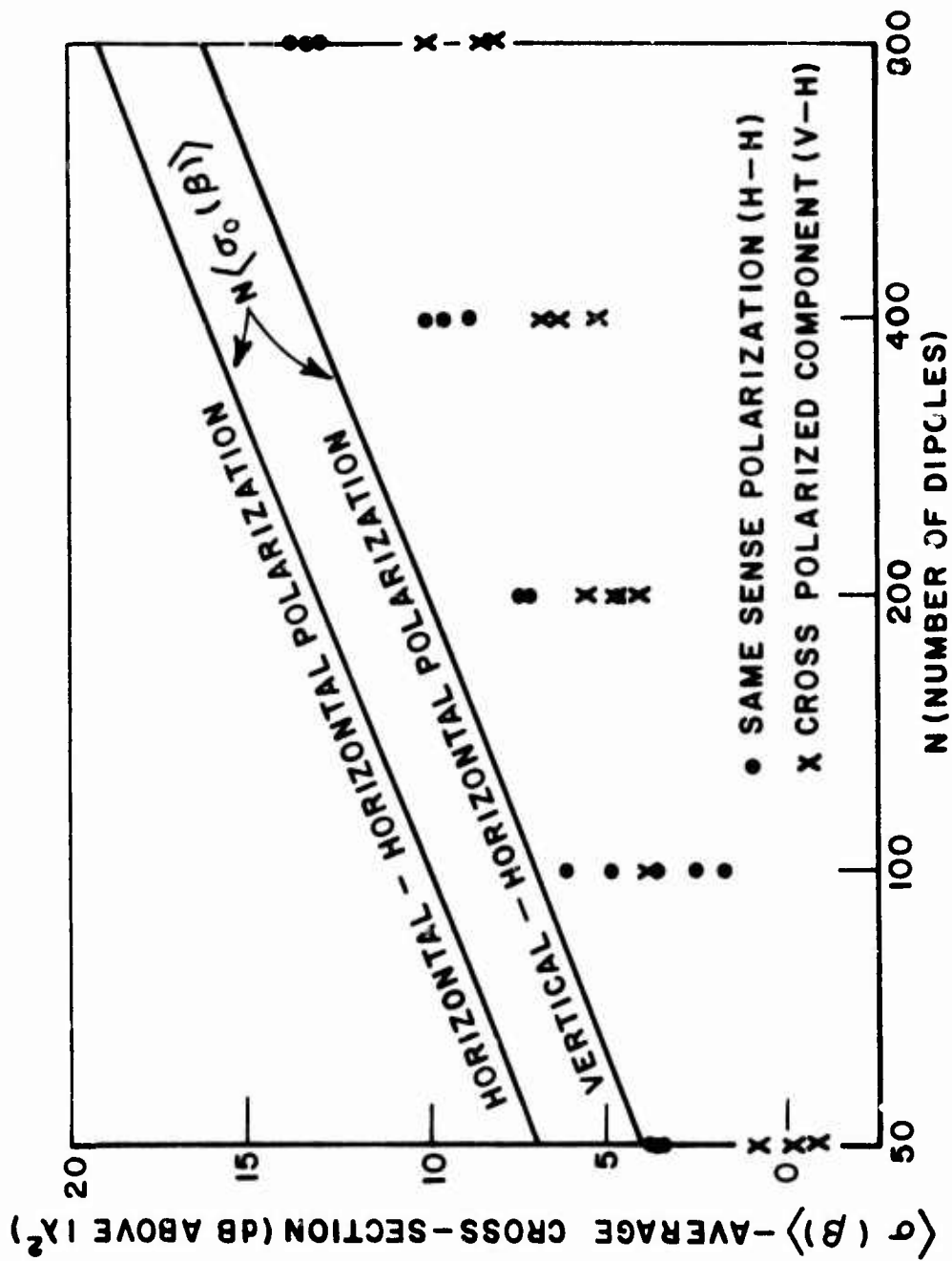


Figure 14. Measured and calculated values of the spatial average cross sections of ensembles of clouds containing  $50 < N < 800$  dipoles with average spacings  $d/\lambda \approx 0.5-0.6$ . Bistatic angle  $\beta=135^\circ$ . Straight line represents decoupled dipoles.

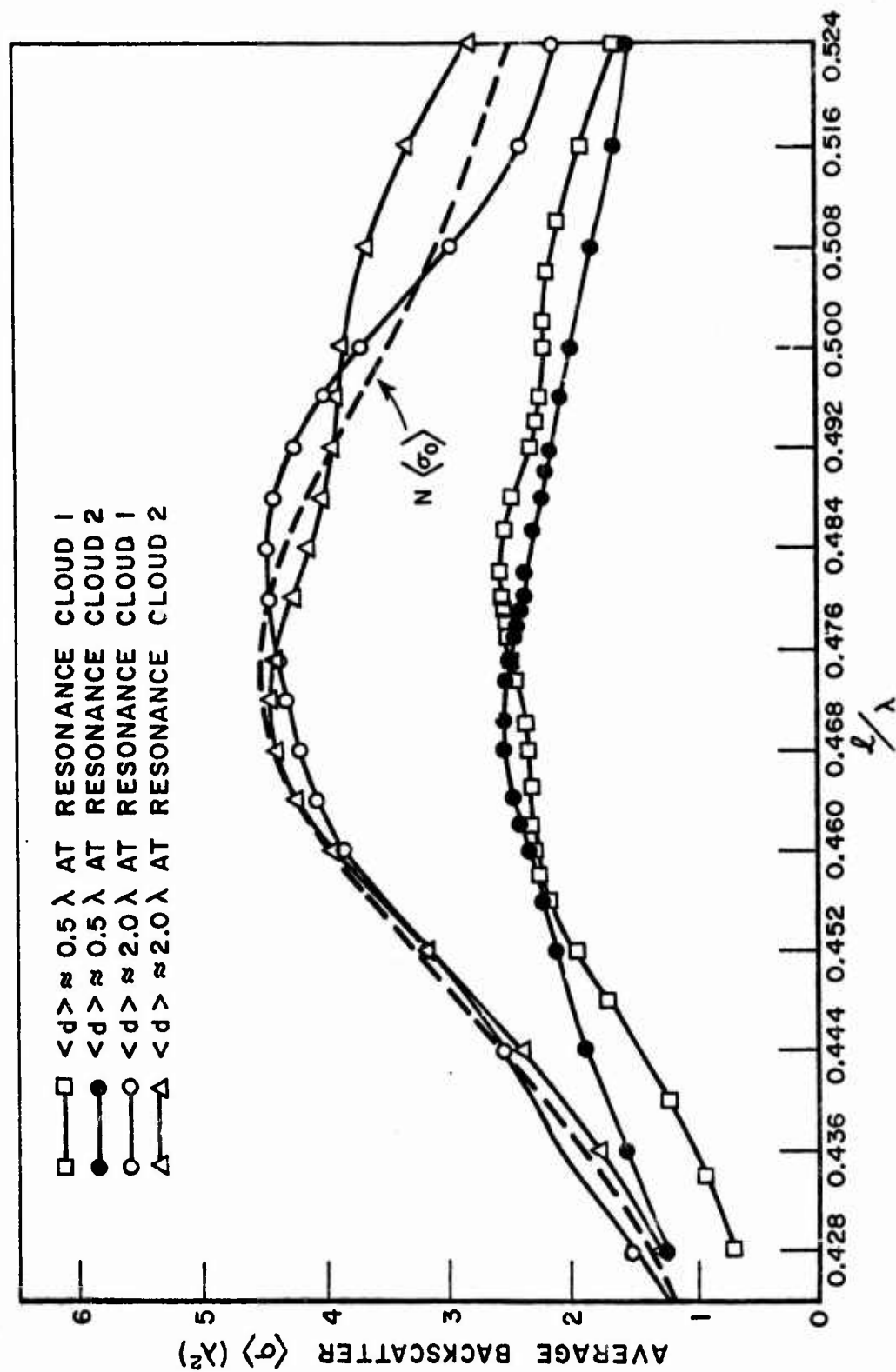


Figure 15. Average backscatter as a function of frequency of four random clouds.

The average error was 5.3% and the average absolute error was 6.8%, well within tolerance levels of practical measurements.

From these calculations it appeared feasible to further develop sparse matrix programs for use on chaff cloud scatter calculations.

TABLE I  
PERCENT ERROR IN BISTATIC AVERAGES CAUSED BY SETTING MUTUAL IMPEDANCES BELOW (0.1) ( $Z_{11}$ ) TO ZERO.

-4.2	+5.3	+ 2.9	+11.9	+8.7	-3.2
-7.7	+6.7	+10.0	+13.3	+13.8	+2.6
+10.2	+5.5	+ 4.8	+ 3.5	+ 4.3	

Sparse matrix methods require that a special scheme be used to index the stored elements of the matrix. Also most direct methods of solving systems of linear equations operate on the matrix to produce a new matrix which in general is not sparse even though the original matrix was sparse. Sparse matrix methods require that this new matrix be sparse as well. These two requirements have been approached and formulated in a variety of ways [40-45].

The approach used here is that given by Berry [44]. The off-diagonal non-zero elements of the upper triangular portion of the matrix are stored consecutively in linear array U. The diagonal elements (which are all non-zero) are stored in a linear array D. Two pointer arrays II and J are used to index the array U. II(K) contains the starting location of row K in U and J contains the column indices of the elements in the same order as the elements as contained in U. An example given by Berry [44] should help clarify this scheme. For the matrix Y given below, the arrays would be as follows:

$$Y = \begin{bmatrix} y_{11} & 0 & y_{13} & 0 & y_{15} \\ 0 & y_{22} & y_{23} & y_{24} & 0 \\ y_{31} & y_{32} & y_{33} & y_{34} & 0 \\ 0 & y_{42} & y_{43} & y_{44} & 0 \\ y_{51} & 0 & 0 & 0 & y_{55} \end{bmatrix}$$

$$\begin{array}{llll}
II(1) = 1 & J(1) = 3 & U(1) = y_{13} & D(1) = y_{11} \\
II(2) = 3 & J(2) = 5 & U(2) = y_{15} & D(2) = y_{22} \\
II(3) = 5 & J(3) = 3 & U(3) = y_{23} & D(3) = y_{33} \\
II(4) = 6 & J(4) = 4 & U(4) = y_{24} & D(4) = y_{44} \\
II(5) = 6 & J(5) = 4 & U(5) = y_{34} & D(5) = y_{55}
\end{array}$$

A specialized matrix decomposition known as the "square root method" [46] is used to solve the system of equations. This method is similar to those associated with the names Gauss, Crout, Doolittle, Cholesky, Banachiewicz, etc. [47].

Before decomposition, the algorithm given by Barry is used to determine a renumbering of the unknown (pivoting on the diagonal) such that the number of non-zero elements in the auxiliary matrix produced by the decomposition is reduced. The advantage of this renumbering is easily seen in a couple of examples. Figure 16 shows the structure of an 11 by 11 matrix and its auxiliary before renumbering. Crosses represent non-zero elements occurring in both the original matrix and its auxiliary. Zeros represent non-zero elements occurring only in the auxiliary matrix, i.e., non-zero elements that were introduced by the decomposition. Blanks represent zero elements occurring in both the original matrix and its auxiliary. Figure 17 shows the structure of the matrix after renumbering and the structure of the auxiliary of this new matrix in the same way. The renumbering used was as follows:

original unknown no.	1	2	3	4	5	6	7	8	9	10	11
new unknown no.	1	9	7	6	5	2	3	8	4	10	11

The structure of Fig. 17 may be obtained from that of Fig. 16 and the above table. For example: to generate the seventh row of Fig. 17, first note that the seventh unknown in the renumbered system was the third unknown in the original system. This means that the third row of the original matrix is the seventh row of the new matrix. Columns have also been interchanged according to this same renumbering so that  $Z_{33} \rightarrow Z_{77}$ . To find the other elements in the new seventh row, note in Fig. 16 that the off-diagonal elements in row 3 are  $Z_{34}$ ,  $Z_{36}$ , and  $Z_{38}$  and convert both subscripts as given in the table to obtain

	1	2	3	4	5	6	7	8	9	10	11
1	X						X		X		
2		X								X	X
3			X	X		X		X			
4			X	X		X		X			
5					X		X		X	X	
6			X	X		X		0			
7	X				X		X		X	0	
8			X	X		0		X		X	X
9	X				X		X		X	0	
10		X			X		0	X	0	X	0
11		X						X		0	X

Fig. 16. The structure of an 11 x 11 matrix and its auxiliary before renumbering. Crosses are non-zero elements occurring in both matrices; zeros are non-zero elements occurring only in the auxiliary; blanks are zero elements in both matrices.

	1	2	3	4	5	6	7	8	9	10	11
1	X		X	X							
2		X				X	X				
3	X		X	X	X						
4	X		X	X	X						
5			X	X	X					X	
6		X				X	X	X			
7		X				X	X	X			
8						X	X	X		X	X
9									X	X	X
10					X			X	X	X	0
11								X	X	0	X

Fig. 17. The structure of the 11 x 11 renumbered matrix of Fig. 16 and its auxiliary. Symbols are the same as in Fig. 16.



$Z_{34} \rightarrow Z_{76}$ ,  $Z_{36} \rightarrow Z_{72}$ , and  $Z_{38} \rightarrow Z_{78}$  which is the structure shown in Fig. 17.

Figures 18 and 19 show the structure of a 28 by 28 matrix before and after renumbering in the same way.

The renumbering used in this case was as follows:

original	1	2	3	4	5	6	7	8	9	10	11	12	13	14
new	9	18	24	22	8	20	14	21	27	15	19	16	13	17
original	15	16	17	18	19	20	21	22	23	24	25	26	27	28
new	25	28	7	5	4	3	2	1	26	23	10	6	11	12

The number of non-zero elements occurring in the auxiliary matrix is substantially reduced by the renumbering as may be seen by comparing the number of zeros in Figs. 16 and 18 with the number of zeros in Figs. 17 and 19.

#### (b) Calculated results for Chaff Clouds

In order to estimate the savings in time and computer storage requirements resulting from use of the sparse matrix algorithm, a study was made of these parameters using the ElectroScience Laboratory Datacraft 6024 computer and the Wright-Patterson Air Force Base CDC 6600 computer.

In particular, it would be useful to obtain some estimate of the number of non-zero elements which are regarded as significant enough to retain and store. If we regard as zero any elements in the impedance matrix whose magnitude is less than 10% of the magnitude of the self impedance (diagonal) elements, and we calculate the number of non-zero elements remaining in the upper triangle matrix (Table 2), we can obtain the percent of non-zero elements in the upper triangle (Table 3). The numbers presented in these tables are averages of values obtained from 10 randomly generated clouds for each combination of average spacing  $d/\lambda$  and number of dipoles  $N$ .

	1	2	3	4	5	6	7	8	9	10	11	12	13	14	15	16	17	18	19	20	21	22	23	24	25	26	27	28
1	X	X	X																									
2	X	X	X				X	X	X																			
3	X	X	X				0	0	0					X									X					
4				X	X	X	X		X		X																	
5				X	X	X	0		0		0																	
6				X	X	X	0		0		0				X								X					
7		X	0	X	0	0	X	0	0		0			0	0								0					
8		X	0				0	X	X	X	0	X		0	0								0				X	
9		X	0	X	0	0	0	X	X	0	X	0		0	0								0	X			0	
10								X	0	X	X	0		0	0								0	0			0	
11				X	0	0	0	0	X	X	X	0	X	0	0		X						0	0			0	
12								X	0	0	0	X	0	X	0		0						0	0			X	
13											X	0	X	0	X		X						0	0			0	
14			X				0	0	0	0	0	X	0	X	0	X	0						0	0			0	
15						X	0	0	0	0	0	0	X	0	X	X	0						0	0			0	
16														X	X	X	0						0	X			X	0
17											X	0	X	0	0	0	X	X					0	0			0	0
18																	X	X	X				0	0			0	0
19																		X	X	X			0	0			0	0
20																			X	X	X		0	0			0	0
21																				X	X	X	0	0			0	0
22																					X	X	0	0			0	0
23			X			X	0	0	0	0	0	0	0	0	0	0	0	0	0	0	0	0	0	X	X	X		0
24									X	0	0	0	0	0	0	X	0	0	0	0	0	0	0	X	X	X	X	X
25																							X	X	X	0	0	0
26																								X	0	X	0	0
27																X	0	0	0	0	0	0	0	X	0	0	X	0
28								X	0	0	0	X	0	0	0	0	0	0	0	0	0	0	0	0	0	0	0	X

Fig. 18. The structure of a 28 x 28 matrix and its auxiliary. Symbols are the same as in Fig. 16.

	1	2	3	4	5	6	7	8	9	10	11	12	13	14	15	16	17	18	19	20	21	22	23	24	25	26	27	28
1	X	X																										
2	X	X	X																									
3		X	X	X																								
4			X	X	X																							
5				X	X		X																					
6						X																	X					
7				X			X					X						X										
8								X											X		X							
9									X									X						X				
10										X														X		X		
11											X													X				X
12												X				X						X						
13							X						X						X						X			
14														X				X				X						
15															X				X			X						
16												X				X	X					X						
17															X	X					0			X				X
18								X						X				X			X	0		X			X	
19							X						X		X				X		0	X			0		X	
20								X												X		X			X	X		
21											X				X	X	0	X	0		X	0		0	0		X	0
22								X						X				0	X	X	0	X		0	0	0	X	0
23						X				X	X													X		X	X	X
24								X								X	X				0	0		X	0	X	0	0
25													X						0	X	0	0		0	X	0	0	X
26											X									X		0	X	X	0	X	0	0
27													X					X	X		X	X	X	0	0	0	X	0
28											X						X				0	0	X	0	X	0	0	X

Fig. 19. The structure of the 28 x 28 renumbered matrix of Fig. 18 and its auxiliary. Symbols are the same as in Fig. 16.

The average numbers presented in Table 2 are plotted vs  $N$  with  $d/\lambda$  as a parameter in Figs. 20 and 21. They all show a remarkably linear character, indicating that significant coupling (non zero elements) exists between an arbitrary dipole and only its neighbors inside a surrounding "volume of influence". Thus, with  $d/\lambda$  fixed and  $N$  increasing, we expect, and do observe, the number of non-zero elements to increase proportionally to  $N$ , not  $N^2$ . Consequently, the percent of non-zero elements for a fixed  $d/\lambda$  decreases as  $1/N$  with increase in  $N$ . Recalling the rule of thumb that this percent should not exceed about 20% if sparse matrix techniques are to be effective, we see that this condition is satisfied for all  $d/\lambda > 0.5$  for  $n > 200$ , a fortiori for the larger  $d/\lambda$  values. The absolute number of non-zero elements, (Table 2) or course, determines the memory required of the computer. Extrapolating the linear curves of Figs. 20 and 21, it appears that a capability of storing 20,000 non-zero elements (about the number of elements in the upper triangle of the full matrix associated with a cloud of 200 fully coupled elements - an entirely feasible problem of the W-P computer) permits the sparse matrix solution of clouds containing approximately 1100, 5300, 15,300, and 32,000 dipoles if the average spacings  $d/\lambda$  are 0.5, 1.0, 1.5, and 2.0, respectively. Investigations involving time savings, described later, lead us to less optimistic estimates.

The variation of the number of non-zero elements in the upper triangle with  $d/\lambda$ ,  $N$  fixed, is not as clearly explainable in physical terms as is the variation with  $N$ ,  $d/\lambda$  fixed. If we consider each dipole to be coupled only to  $m$  neighbors within a surrounding "volume of influence", then the number  $m$  should be equal to the number of non-zero elements in the upper triangle divided by  $N$ . Performing this operation on Table 2, we obtain Table 4, and observe that, except for the smallest spacing  $d/\lambda = 0.5$ , the values of  $m$  (i.e., the number of elements in a "volume of influence") are approximately independent of  $N$ , as one would expect. For  $d/\lambda = 0.5$ , clouds with lesser values of  $N$  probably are too small to obtain fair values for  $m$ , so we presume those values of  $m$  obtained for the largest clouds ( $N = 200$ ) are most accurate. Accepting these latter numbers, one recognizes, of course, that they are only symbolic of the influence of coupling; they only give some indication of the (integer) number of neighbors which are effectively coupled to a given element in some average sense. We can venture one step further and assume that each "volume of influence" is a "sphere of influence", with volume  $V_{d/\lambda} = (d/\lambda)^3 m$  (where the subscript recognizes that the "sphere of influence" has a size which is probably dependent on the cloud density, i.e.,  $d/\lambda$ ). Doing this for  $N = 200$ , the radii in wavelengths  $R_{d/\lambda}/\lambda$  of the "spheres of

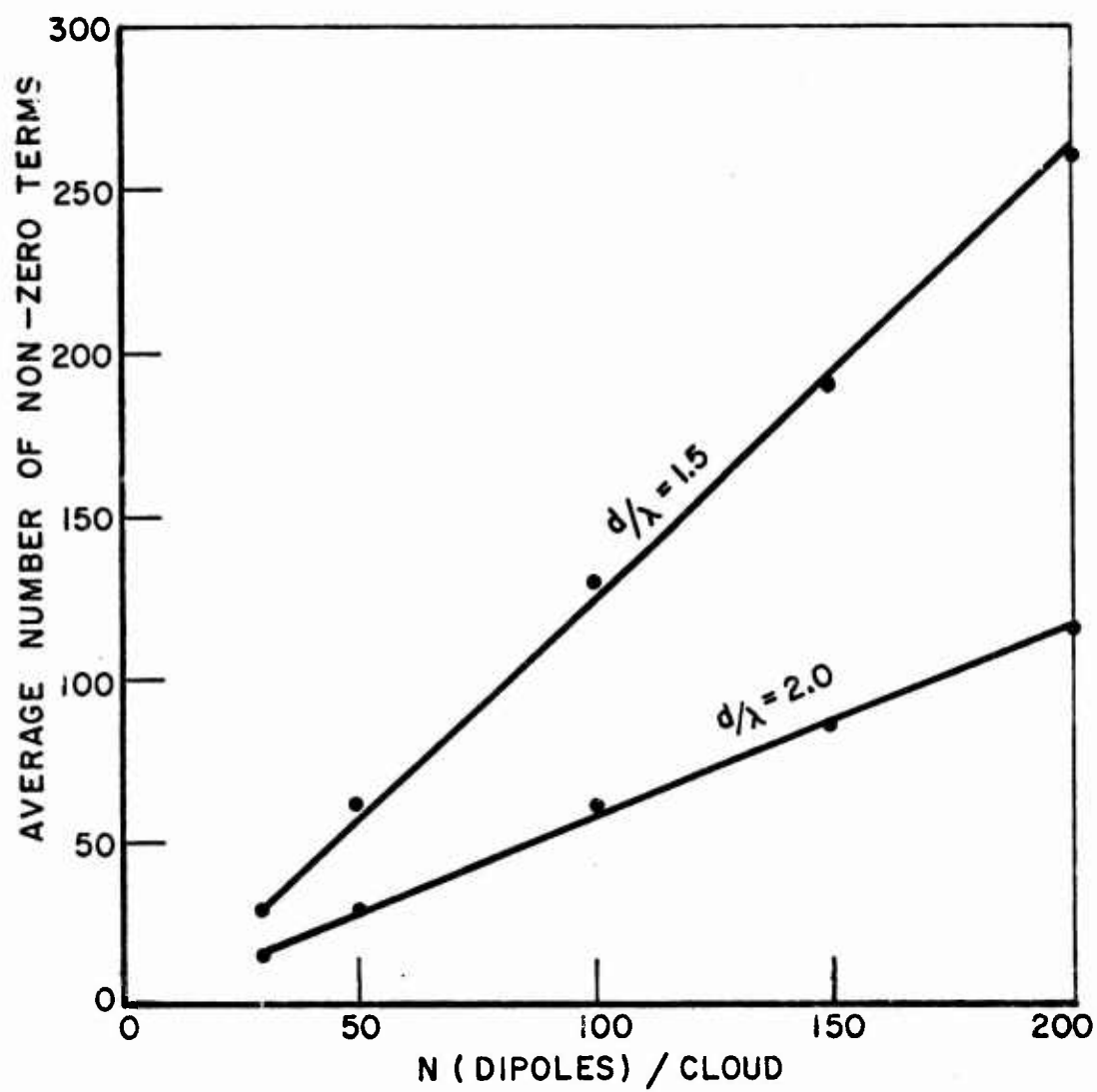


Figure 20. Average number of non-zero terms in the upper triangle of the sparse matrix using 10% rule.

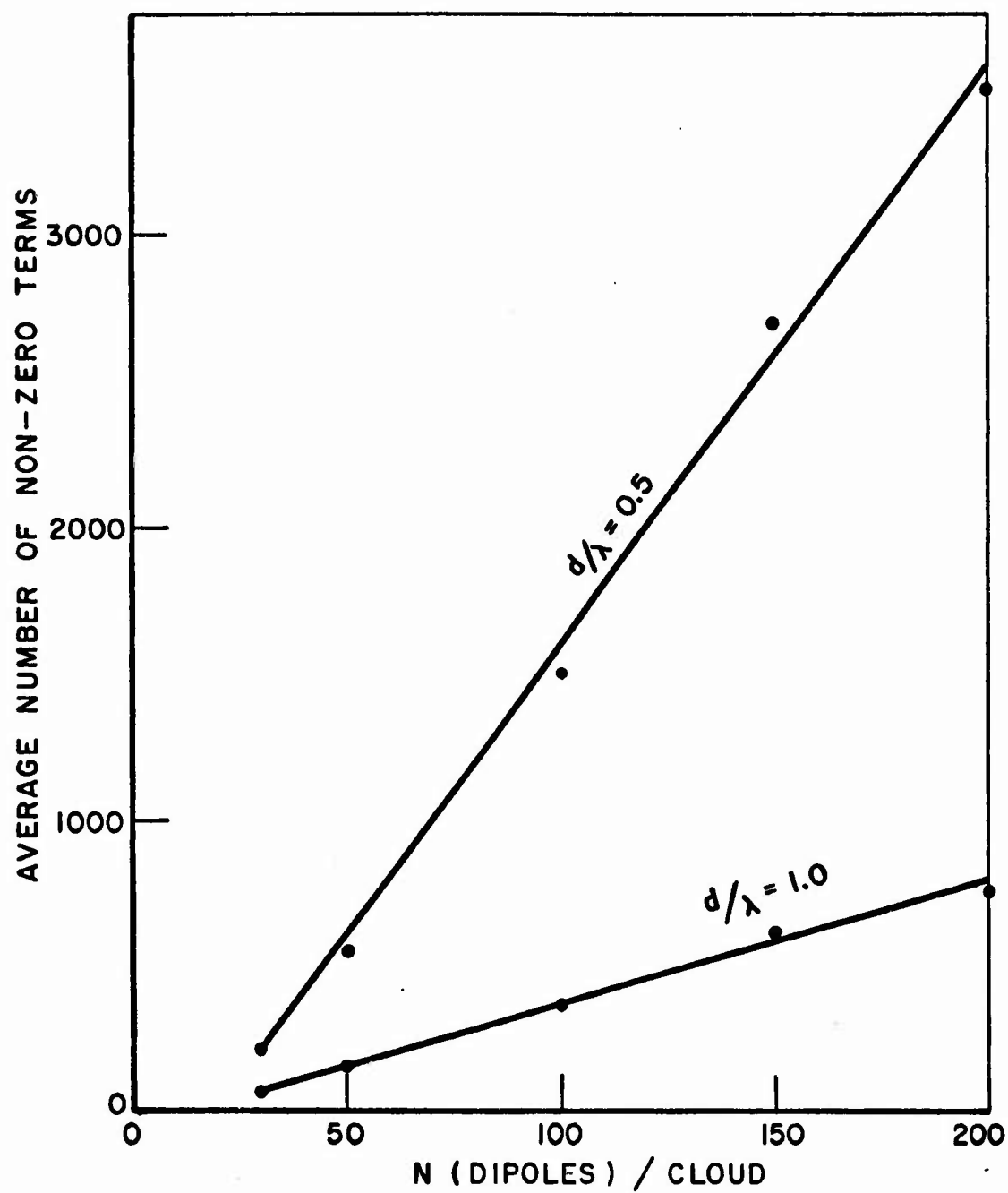


Figure 21. Average number of non-zero terms in the upper triangle of the sparse matrix using 10% rule.



TABLE 2

NUMBER OF NON-ZERO TERMS IN UPPER TRIANGLE

	$\frac{N}{d/\lambda}$	50	100	150	200
Sparse Matrix	2.0	30	62	86	125
	1.5	62	130	190	260
	1.0	160	360	600	750
	0.5	550	1500	2800	3500

TABLE 3

% OF NON-ZERO TERMS IN SPARSE MATRIX UPPER TRIANGLE

$\frac{N}{d/\lambda}$	50	100	150	200
2.0	2.45%	1.25%	0.77%	0.63%
1.5	5.06%	2.62%	1.70%	1.30%
1.0	13.06%	7.27%	5.37%	3.75%
0.5	44.90%	30.30%	25.05%	17.58%

TABLE 4

m, THE NUMBER OF ELEMENTS IN A "SPHERE OF INFLUENCE"

$\frac{N}{d/\lambda}$	50	100	150	200
2.0	0.6	0.62	0.573	0.625
1.5	1.24	1.3	1.26	1.3
1.0	3.2	3.6	4.0	3.75
0.5	11.0	15.0	18.7	17.5

influence" are found to be 2.35, 2.18, 2.07, and 1.73 for spacings  $d/\lambda$  of 2.0, 1.5, 1.0 and 0.5, respectively. Although more data would be necessary to substantiate it, this variation in  $R_{d/\lambda}/\lambda$  appears to be a linear increase with  $d/\lambda$ , as shown in Fig. 22. The fact that the "radius of influence",  $R_{d/\lambda}/\lambda$ , decreases as the cloud becomes more dense, i.e., as  $d/\lambda$  decreases, could be explained by the increased shielding effect of the outermost elements from the center dipole of interest by those elements in-between. And the fact that the values of  $R_{d/\lambda}/\lambda$  exceed 2.0 for the larger spacings lends credence to our present analysis because previous data showed the dipoles to be essentially decoupled for these larger spacings.

All the foregoing work is based upon the 10% threshold level below which a matrix element is regarded as zero. The question arises, how severely does this change the scattering cross section and, in particular, the spatial average backscatter from that which would be obtained using the full matrix? To show the effect of sparsing the impedance matrix we present in Figs. 23-26 backscattering patterns (same sense polarizations of transmitter and receiver for clouds containing  $N = 30$  dipoles with two different average spacings,  $d/\lambda = 0.5$  and  $2.0$ , calculated on the ElectroScience Laboratory computer using the full matrix and the sparse matrix (with 10% sparsing rule). We expect that the sparsed matrices for these clouds contain about 95% zeros when  $d/\lambda = 2.0$  and about 50% zeros when  $d/\lambda = 0.5$ . Of course, as  $N$  increases, these percentages will increase. A similar set of calculations were performed on the Wright-Patterson Air Force Base CDC-6600 computer for three different clouds containing  $N=200$  dipoles, each  $0.475$  wavelengths long, and with average spacing,  $d/\lambda=2.0$ . Figures 27-29 compare superimposed backscattering patterns (same sense polarizations and cross polarizations of transmitter and receiver) using the full matrix and sparse matrix (with 10% sparsing rule). Figures 30-41 show similar patterns for two other clouds with  $N = 200$ ,  $d/\lambda = 2.0$ . We expect that the sparsed matrices for these clouds contain about 99.4% zeros (see Table 3).

All these patterns, particularly those for the  $N = 200$  clouds, are interesting because they display three features worth mentioning. First, the patterns show differences in fine structure but are very similar in gross structure in all cases. Second, Figs. 25-41, all for average spacings  $d/\lambda = 2.0$ , show a recognizable repetition of the pattern every  $180^\circ$ , i.e., the backscattering pattern behaves about the same when the cloud is viewed from a selected direction or from the opposite to that direction. Furthermore, the patterns corresponding to the sparsed matrix show this symmetry even more than do those for the full matrix. This behavior is expected because in all these

cases, the clouds are tenuous enough (i.e., dipoles are weakly coupled) and do not contain sufficient numbers of dipoles to exhibit significant extinction of energy from front to back of the clouds. If all dipoles were of resonant length and were perfectly decoupled, we would observe perfect symmetry of the patterns; our dipoles are of resonant length (making each one essentially a single mode structure with a  $180^\circ$  phase shift upon reflection from it, i.e., all diagonal elements of the  $Z$  matrix are essentially pure real), but they are not decoupled, upsetting the symmetry somewhat. Sparsing artificially decouples many elements (95%, 99.4% as mentioned earlier), so we expect the sparsed results to closer approach the ideal, i.e., display more symmetric patterns than do the full matrix patterns. Notice that for the denser clouds, Figs. 23 and 24, where  $d/\lambda = 0.5$ , pattern symmetry disappears for full or sparse matrix solutions. Here, the strong coupling definitely upsets the symmetry and even the artifice of decoupling with a 10% rule does not decouple enough elements (only about 50% as mentioned above) to regain symmetry. A third feature, not directly observable from Figs. 25-41 but derivable from them, is the effect of sparsing upon the spatial average backscatter. Figure 42 presents bar graphs of average backscatter obtained from each of 10 different clouds with  $N = 30$ ,  $d/\lambda = 2.0$ , each calculated using full matrices and matrices sparsed by the 10% rule. Clearly, the average backscatter, even with the full matrix, varies from cloud to cloud, as expected from results presented earlier, but the error incurred by using the sparse matrix is less than this variance, and results in a value for average backscatter which is slightly too high in most cases by a few percent. That it is too high and not too low is expected because sparsing results in a cloud which closer approaches the ideal decoupled cloud and our results have shown that coupling lowers the average echo below that for the ideal. Another mode of presenting the same effect of sparsing on spatial average backscatter is shown in Figs. 43-45. For the three clouds containing  $N = 200$  dipoles, the cumulative probabilities  $P(\sigma/\lambda^2)$  of backscattering cross section were calculated. The solid line in each figure is associated with the sparse matrix, the dots with the full matrix, and the crosses with the ideal decoupled case (calculated from  $P(\sigma/\lambda^2) = 1 - e^{-\sigma/30}$ ; see Appendix I). The spatial averages associated with the three algorithms are indicated by the vertical lines. Notice that all three mathematical algorithms infer that the backscattering cross section exceeds the average cross section approximately 40% of the time.

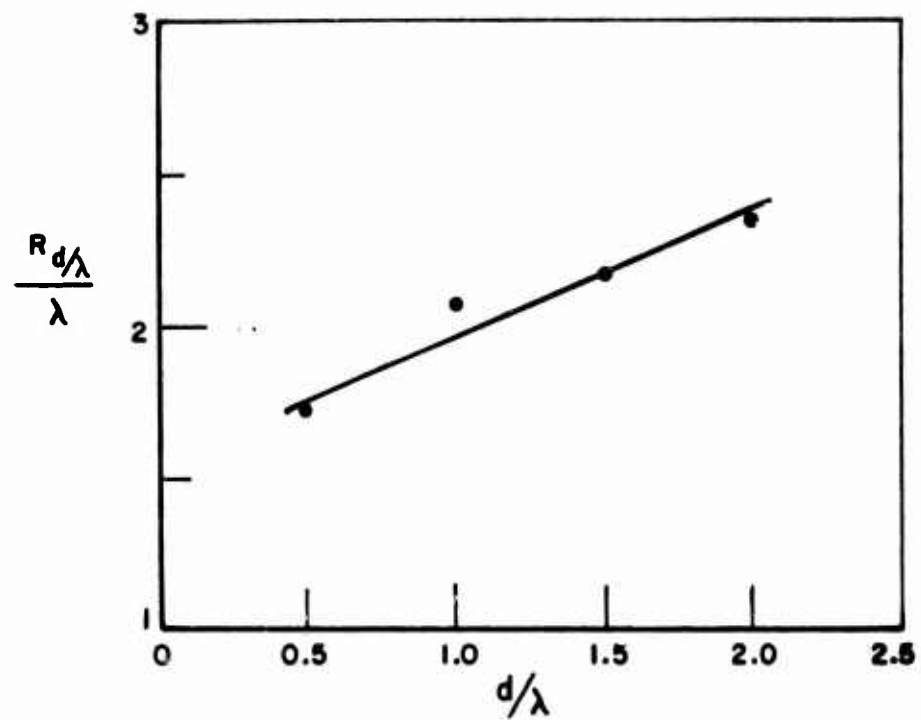


Figure 22. Radius of "sphere of influence" vs average dipole spacing.

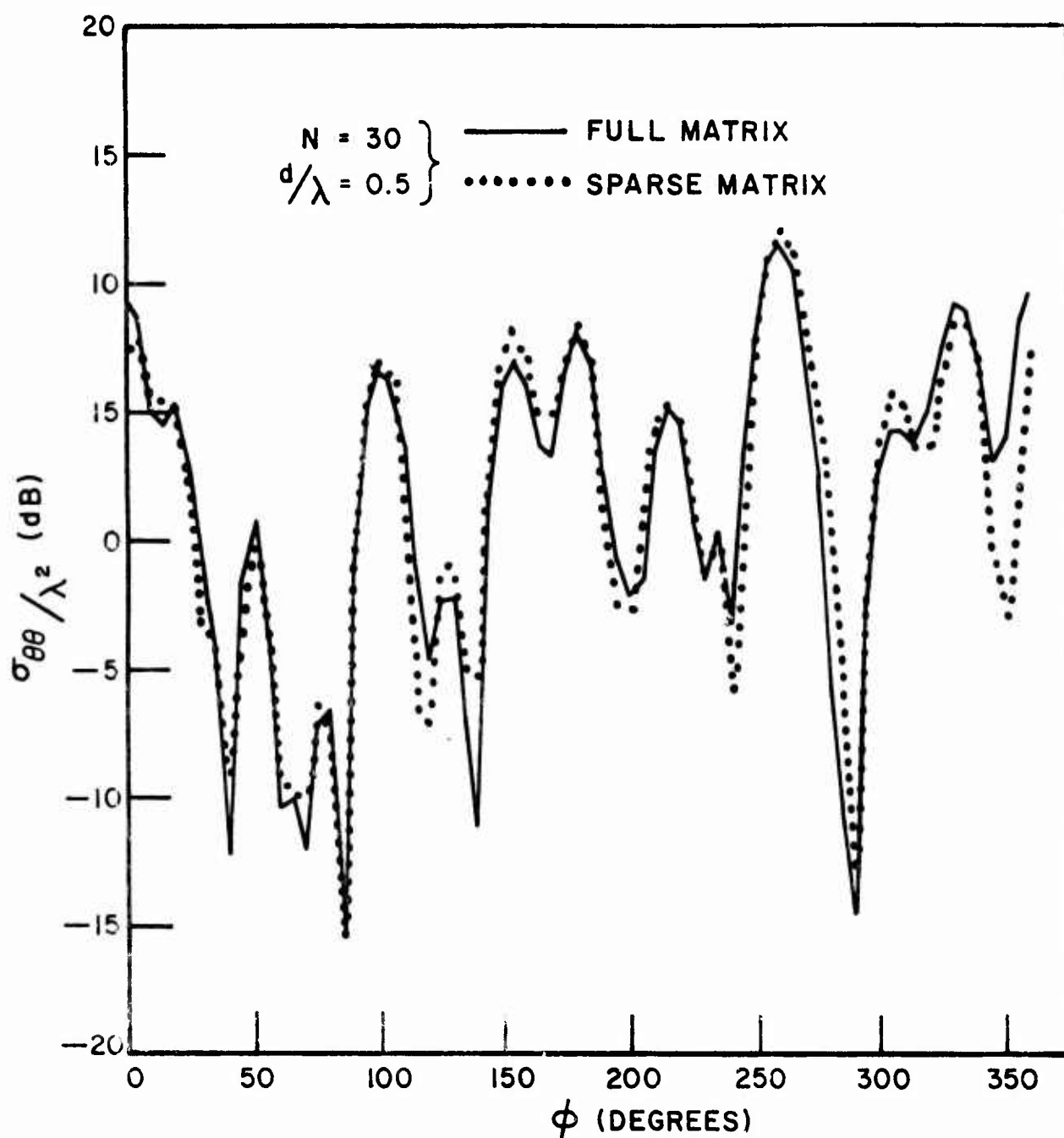


Figure 23.  $\theta - \theta$  backscattering patterns as calculated using the full and sparse matrix, cloud #1,  $d/\lambda = 0.5$ .

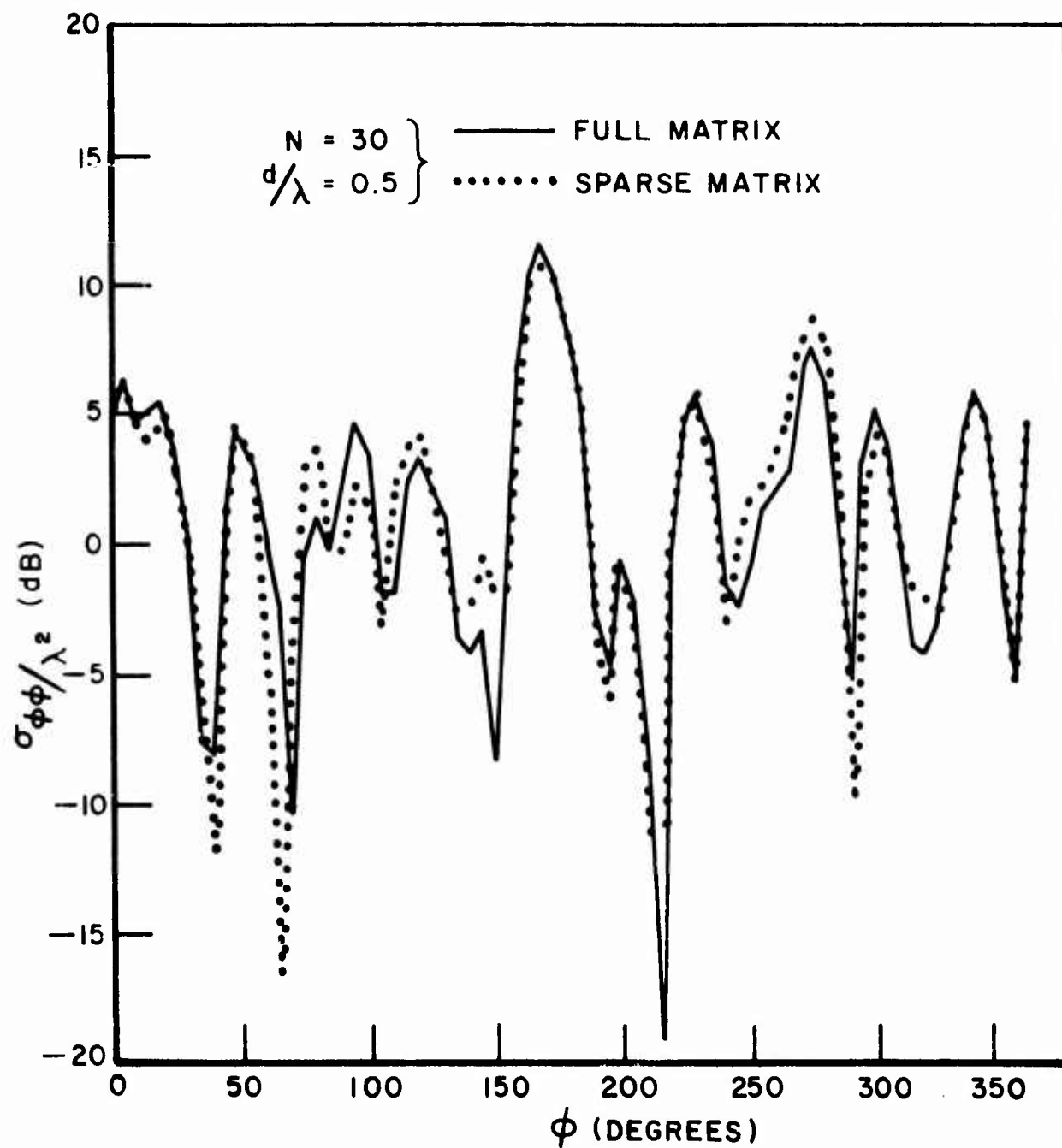


Figure 24.  $\phi$ - $\phi$  backscattering patterns as calculated using the full and sparse matrix, cloud #1,  $d/\lambda = 0.5$ .



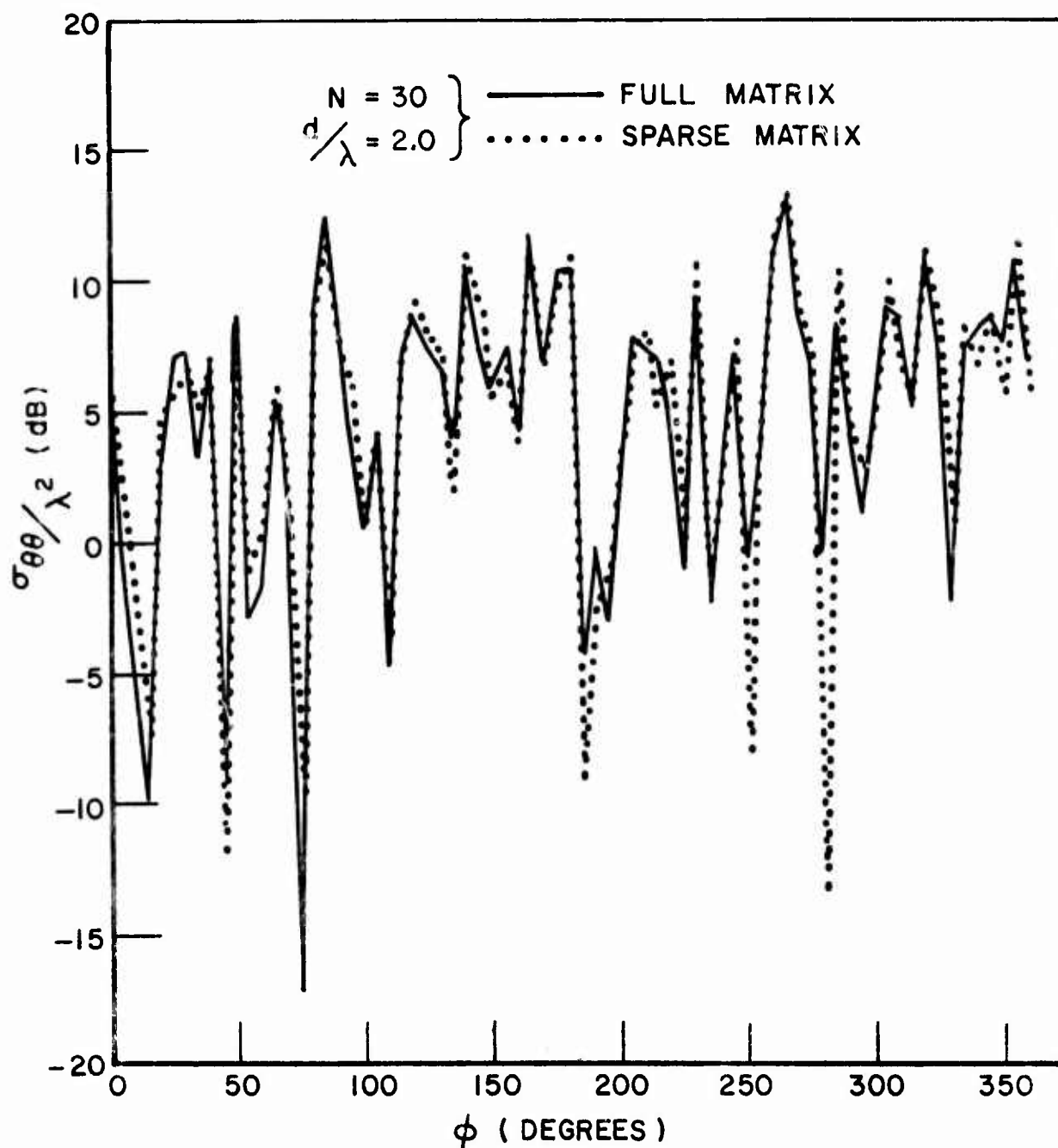


Figure 25.  $\theta$ - $\theta$  backscattering patterns as calculated using the full and sparse matrix, cloud #2,  $d/\lambda = 2.0$ .

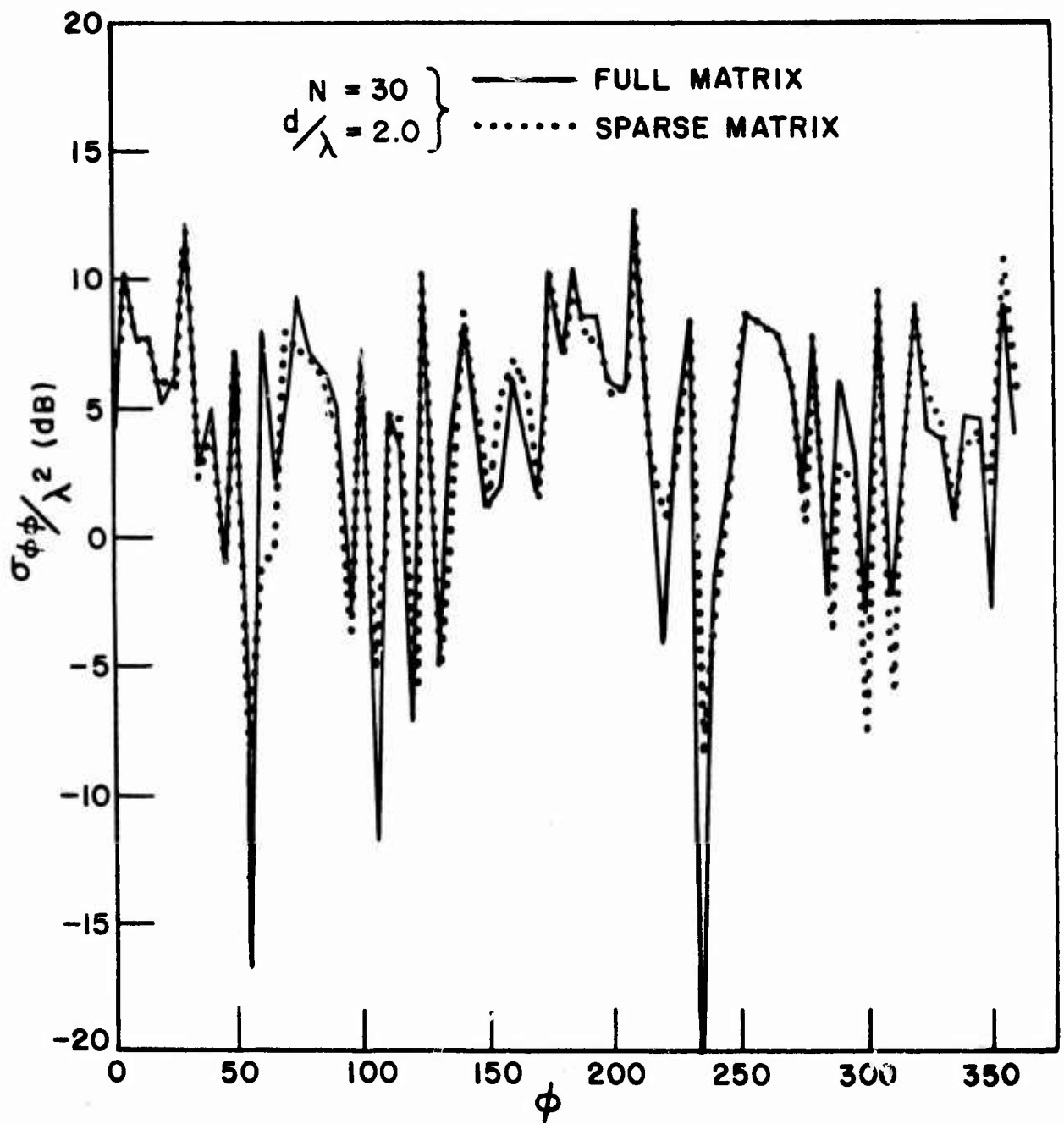


Figure 26,  $\phi$ - $\phi$  backscattering patterns as calculated using the full and sparse matrix, cloud #2,  $d/\lambda = 2.0$ ,

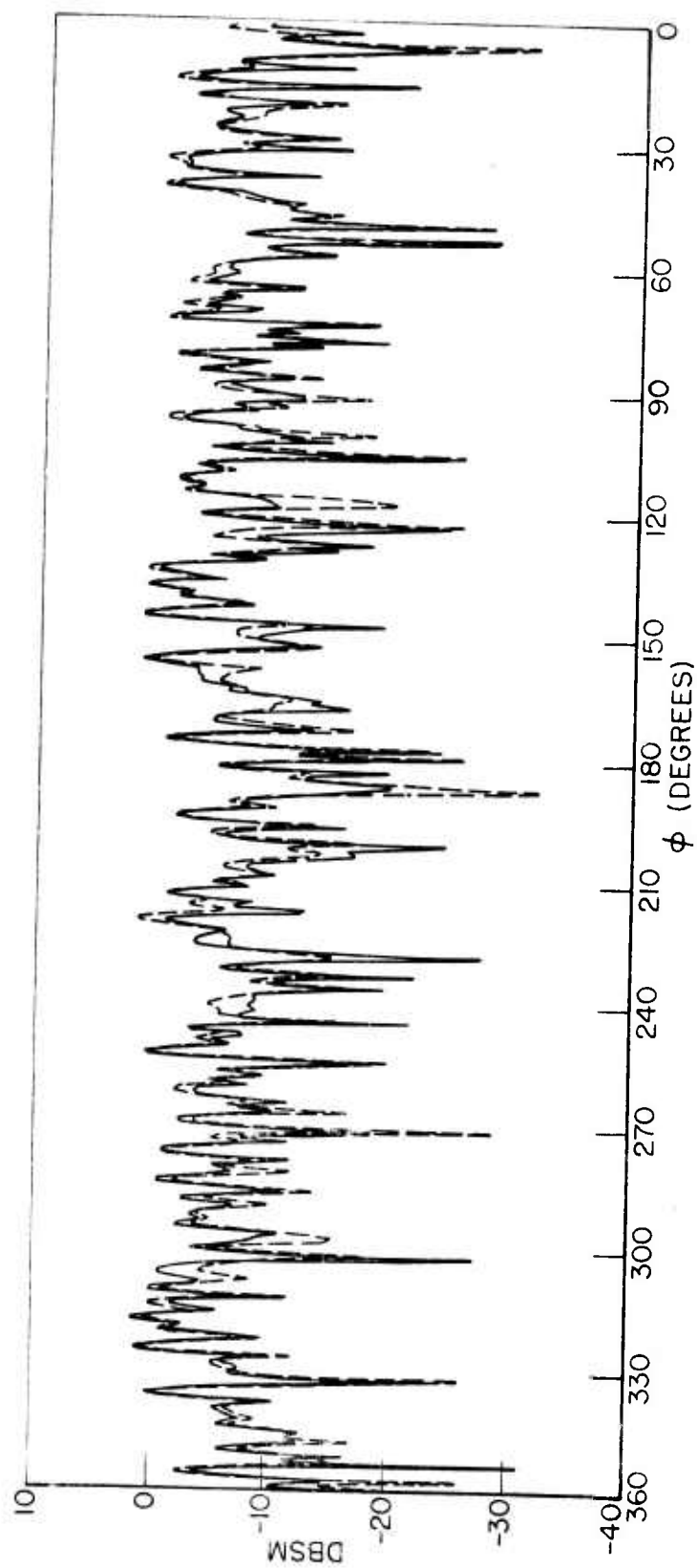


Figure 27.  $\theta-\theta$  backscattering patterns as calculated using the full and sparse matrix, cloud #1,  $N = 200$ .

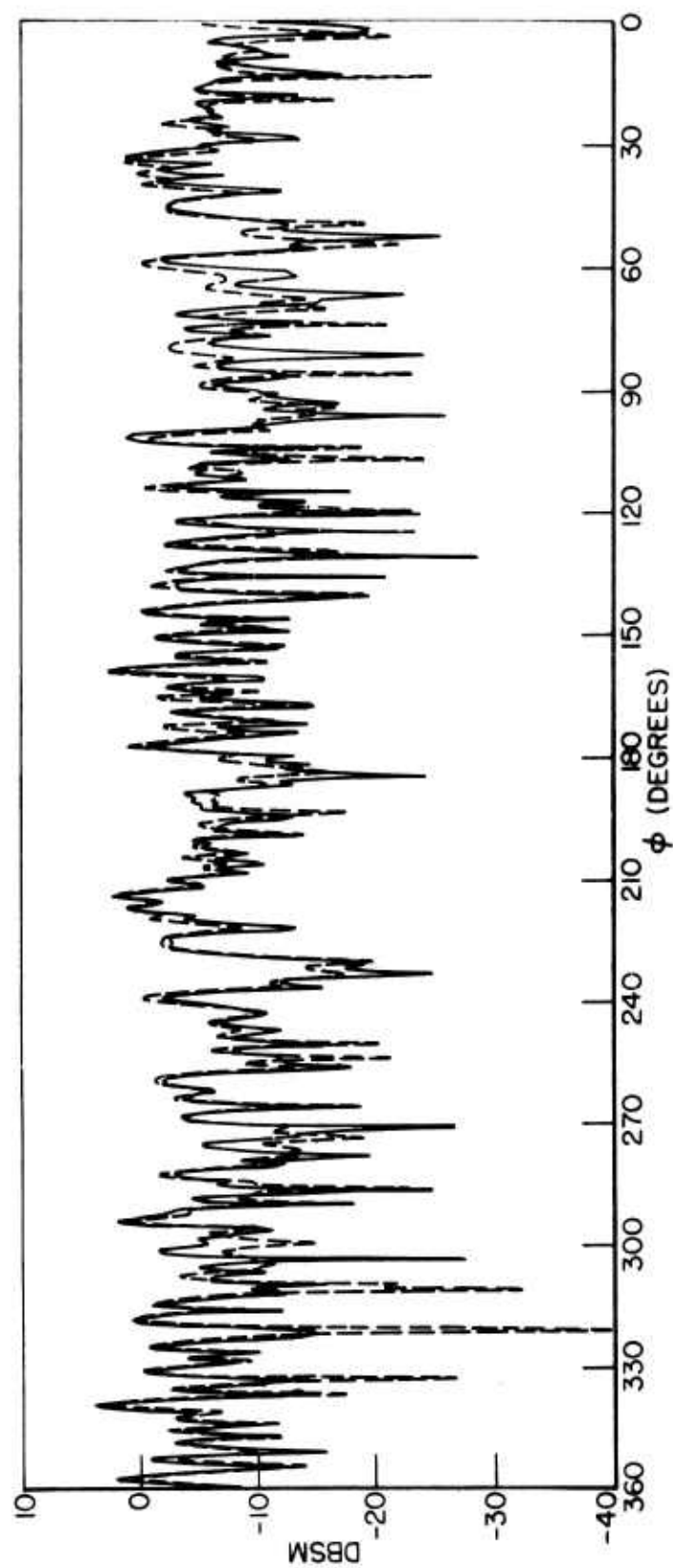


Figure 28.  $\phi$ - $\phi$  backscattering patterns as calculated using the full and sparse matrix, cloud #1,  $N = 200$ .

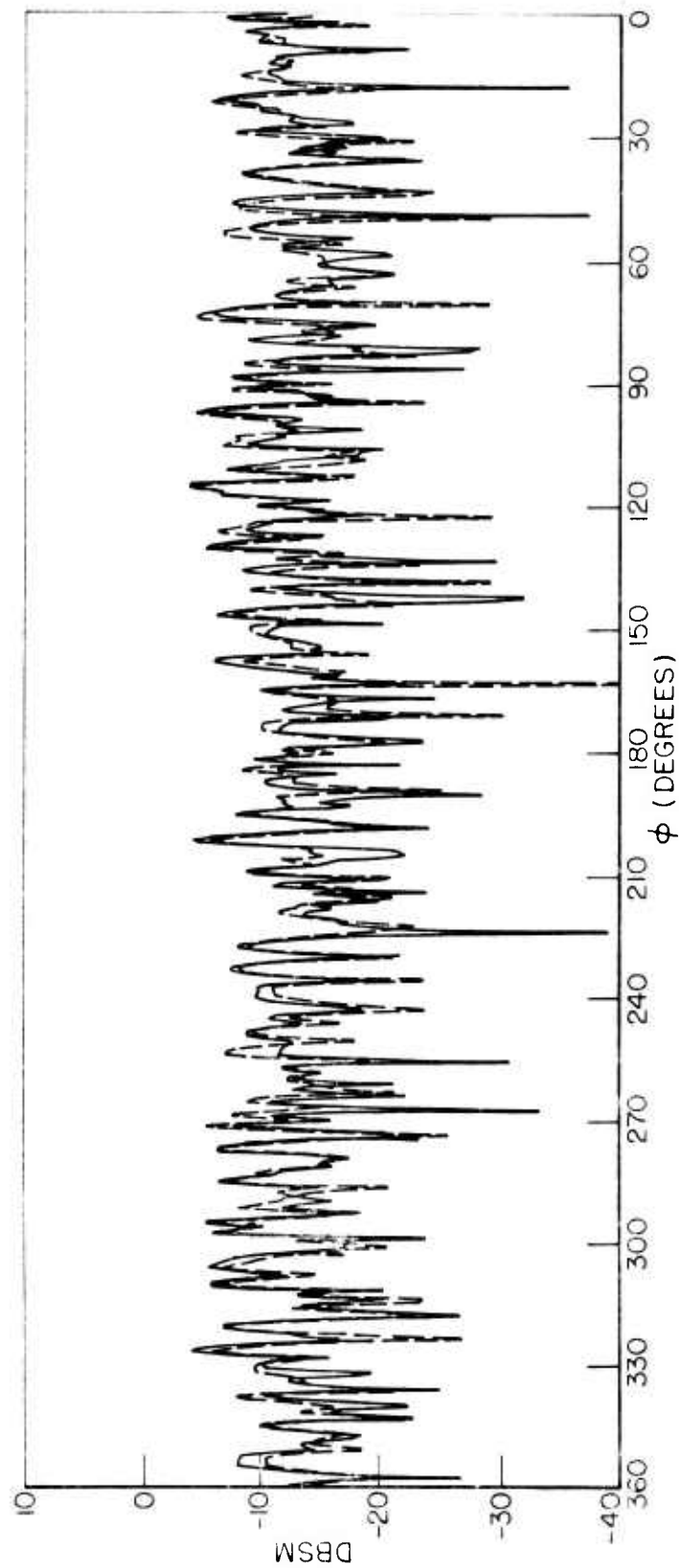


Figure 29.  $\theta$ - $\phi$  backscattering patterns as calculated using the full and sparse matrix, cloud #1,  $N = 200$ .

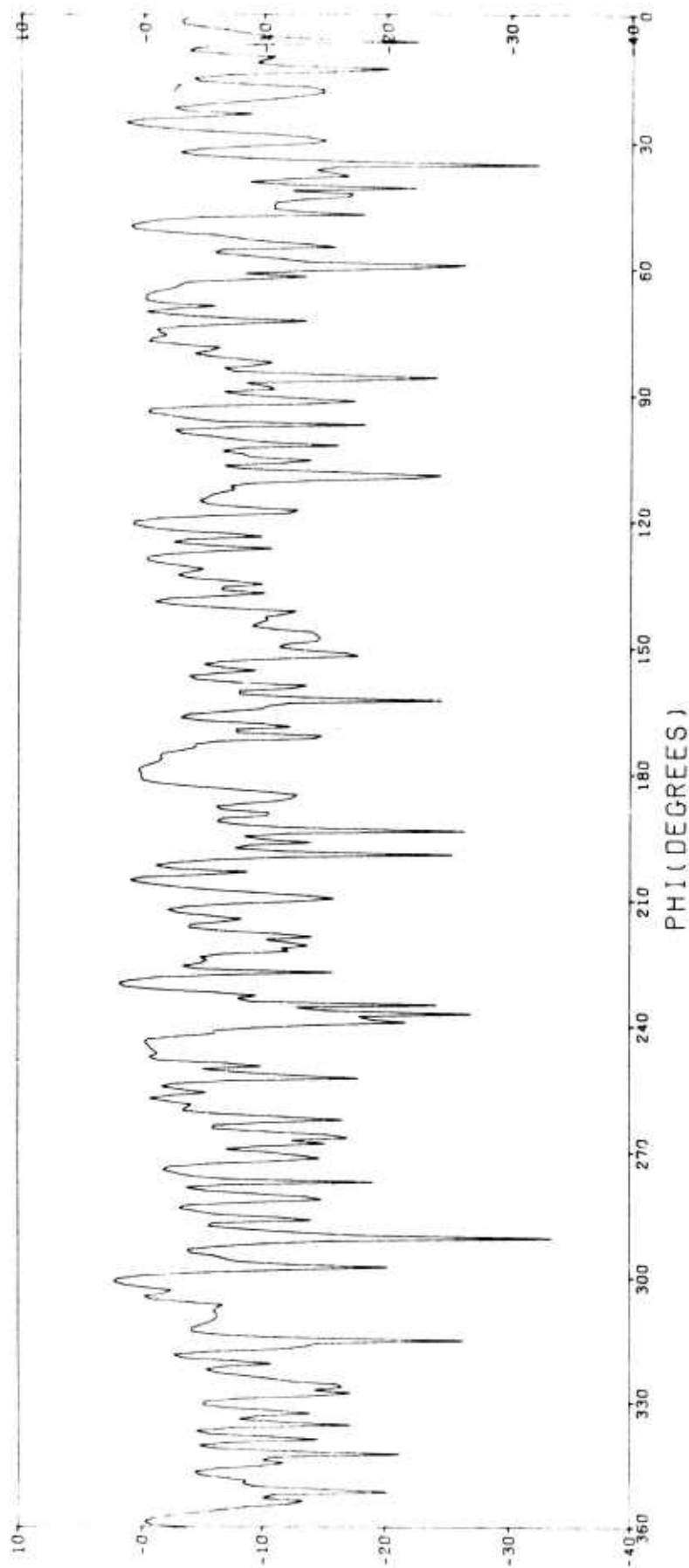


Figure 30.  $\theta = 0$  backscattering patterns as calculated using the full matrix, cloud #2,  $N = 200$ ,  $d/\lambda = 2.0$ .



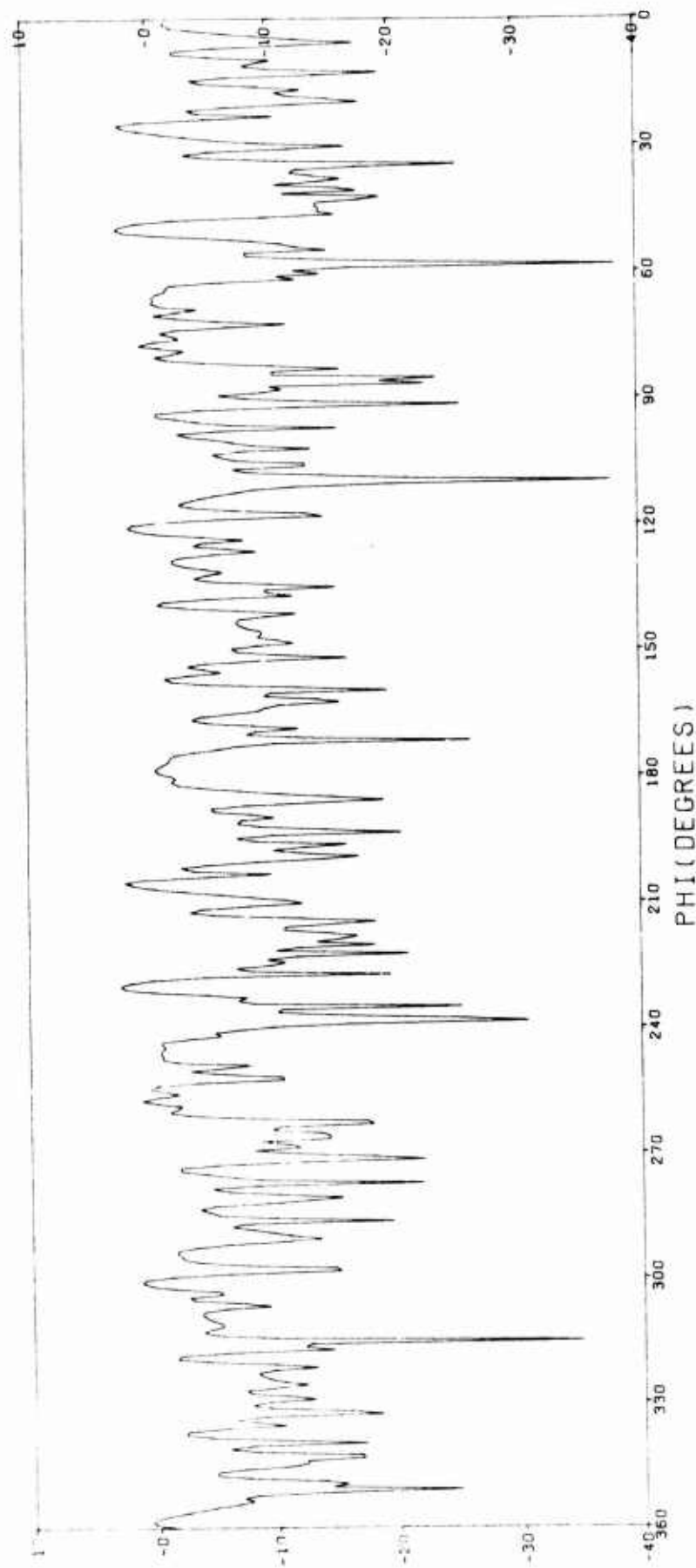


Figure 31.  $\theta$ - $\theta$  backscattering patterns as calculated using the sparse matrix, cloud #2,  $N = 200$ ,  $d/\lambda = 2.0$ .

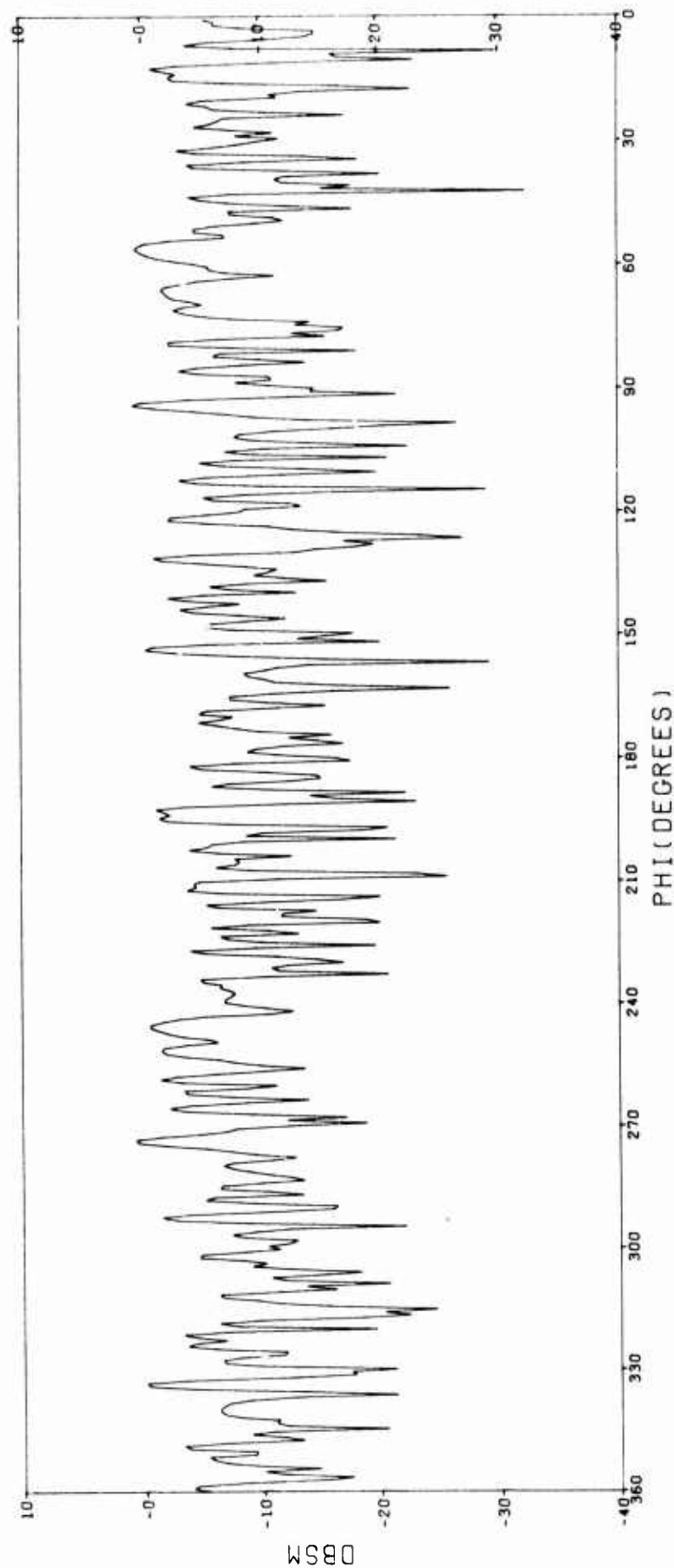


Figure 32.  $\phi$ - $\phi$  backscattering patterns as calculated using the full matrix, cloud #2,  $N = 200$ ,  $c/\lambda = 2.0$ .

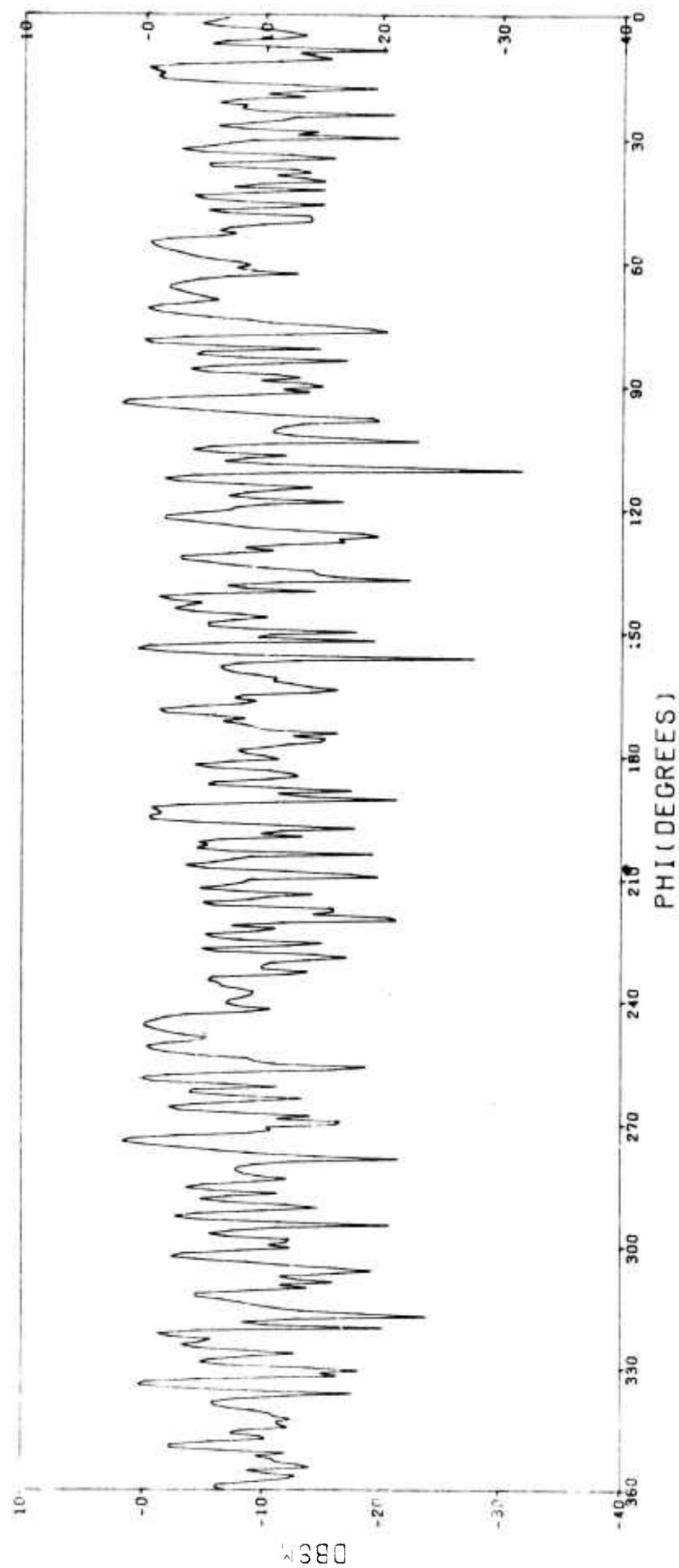


Figure 33.  $\phi$ - $\phi$  backscattering patterns as calculated using the sparse matrix, cloud #2,  $N = 200$ ,  $d/\lambda = 2.0$ .

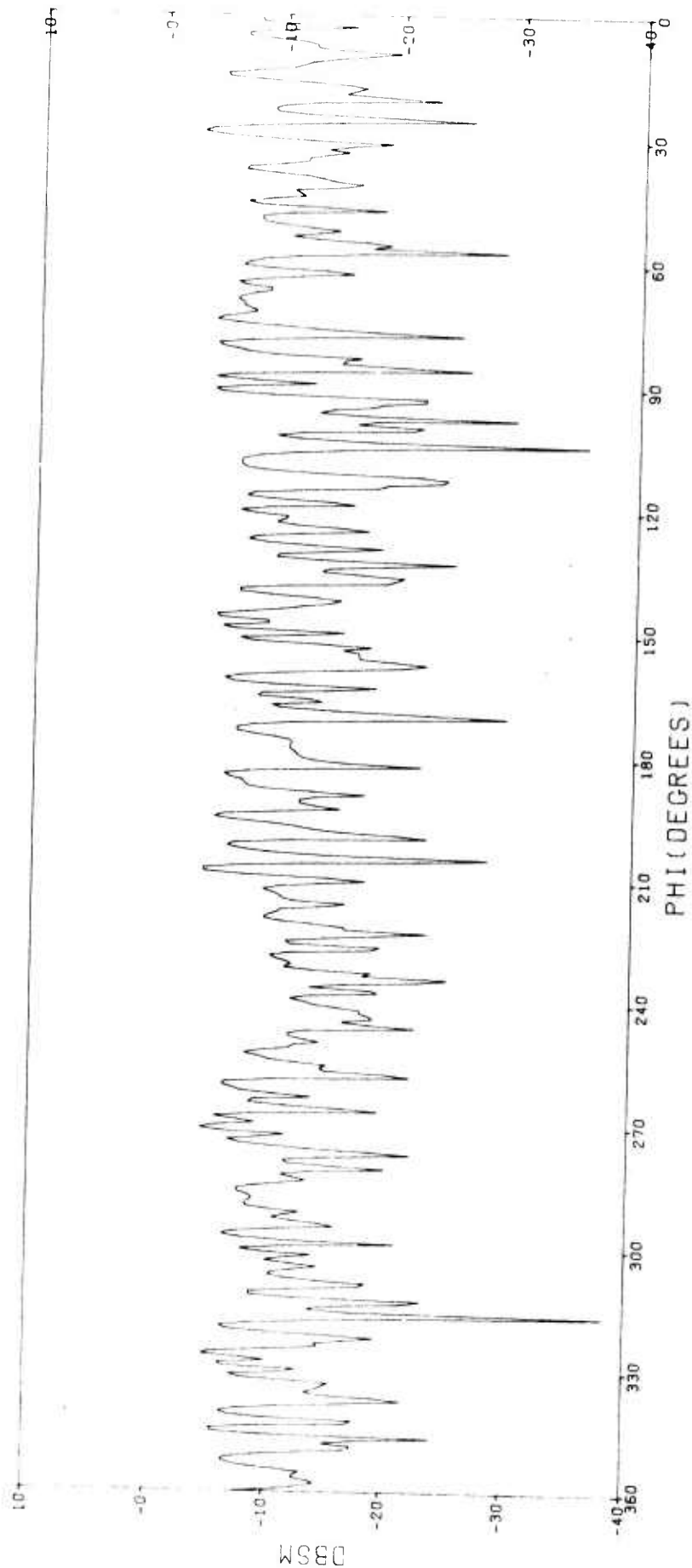


Figure 34.  $\theta$ - $\phi$  backscattering patterns as calculated using the full matrix, cloud #2,  $N = 200$ ,  $d/\lambda = 2.0$ .

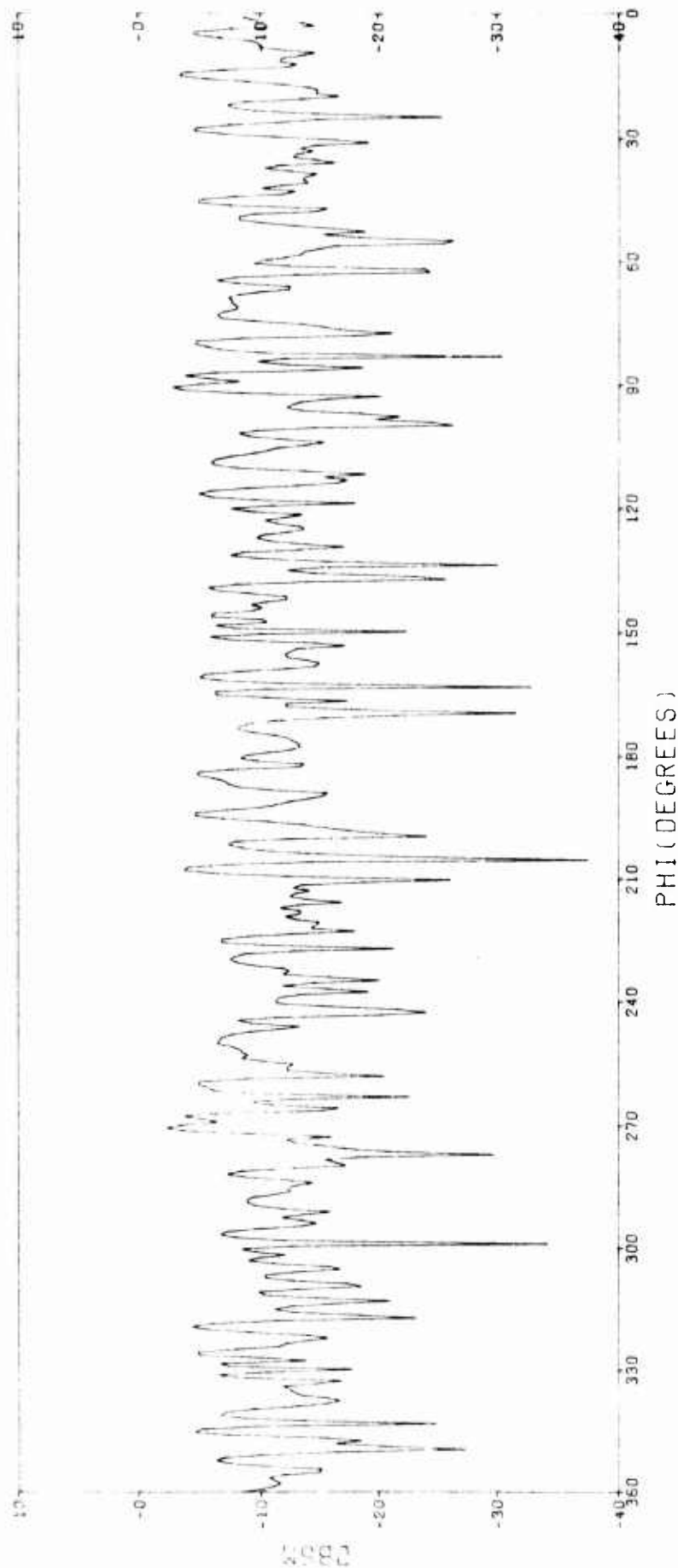


Figure 35.  $\theta$ - $\phi$  backscattering patterns as calculated using the sparse matrix, cloud #2,  $N = 200$ ,  $d/\lambda = 2.0$ .

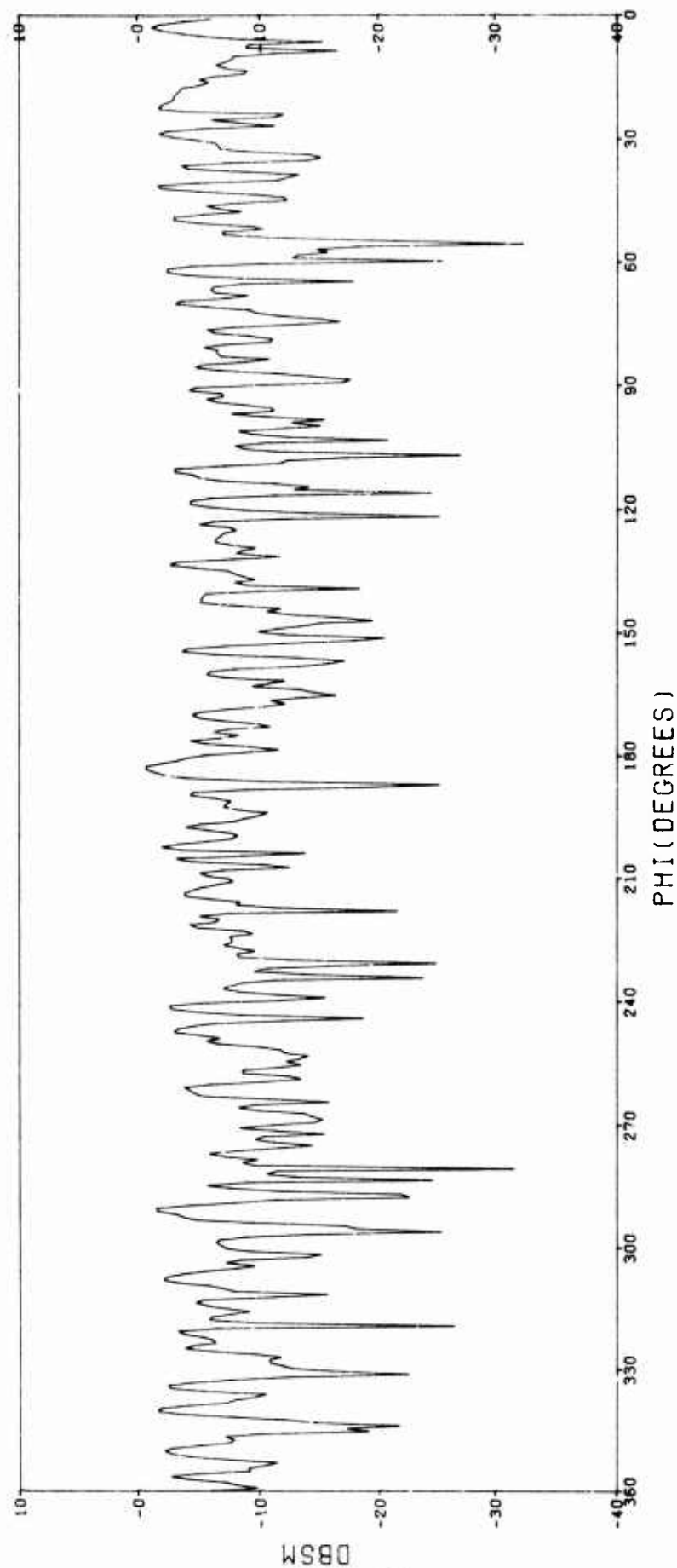


Figure 36. 0-0 backscattering patterns as calculated using the full matrix, cloud #3, N = 200,  $d/\lambda = 2.0$ .



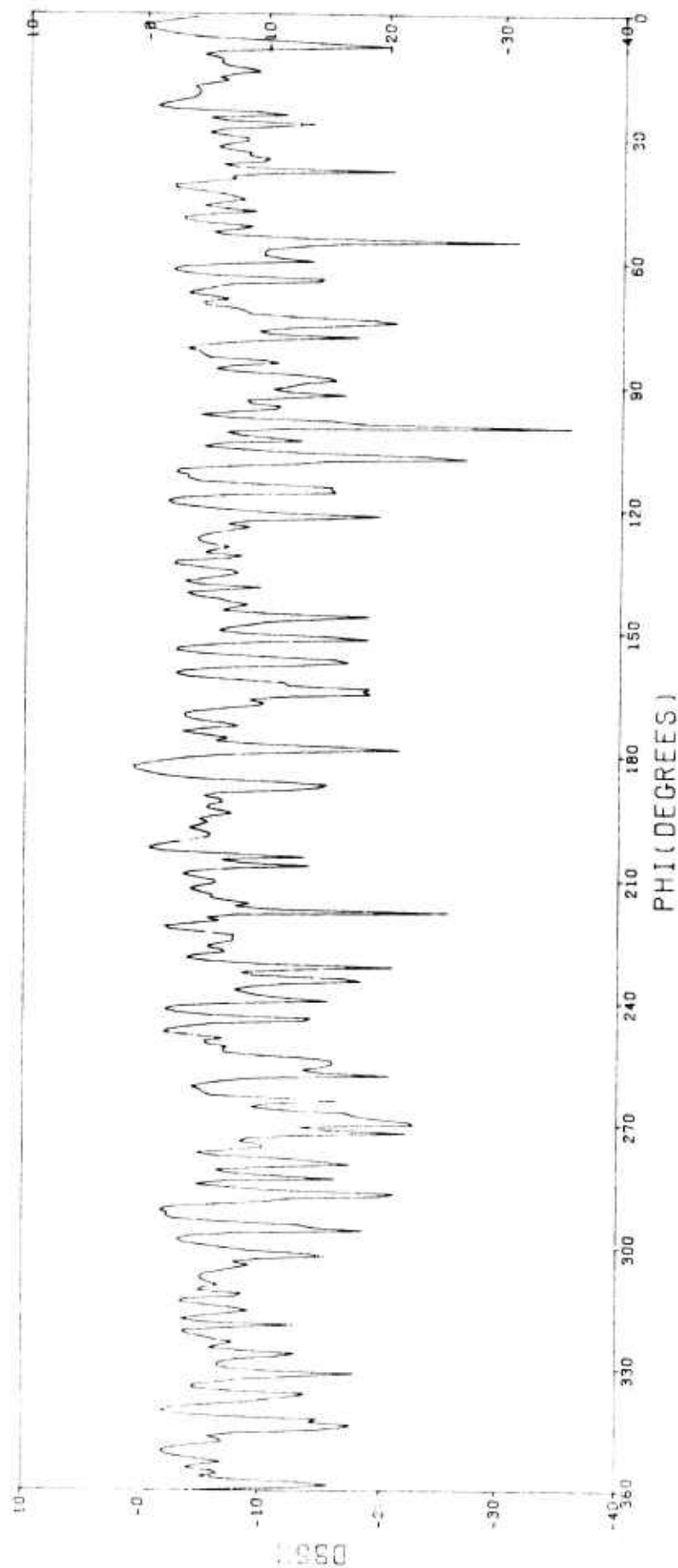


Figure 37.  $\theta-\theta$  backscattering patterns as calculated using the sparse matrix, cloud #3,  $N = 200$ ,  $d/\lambda = 2.0$ .

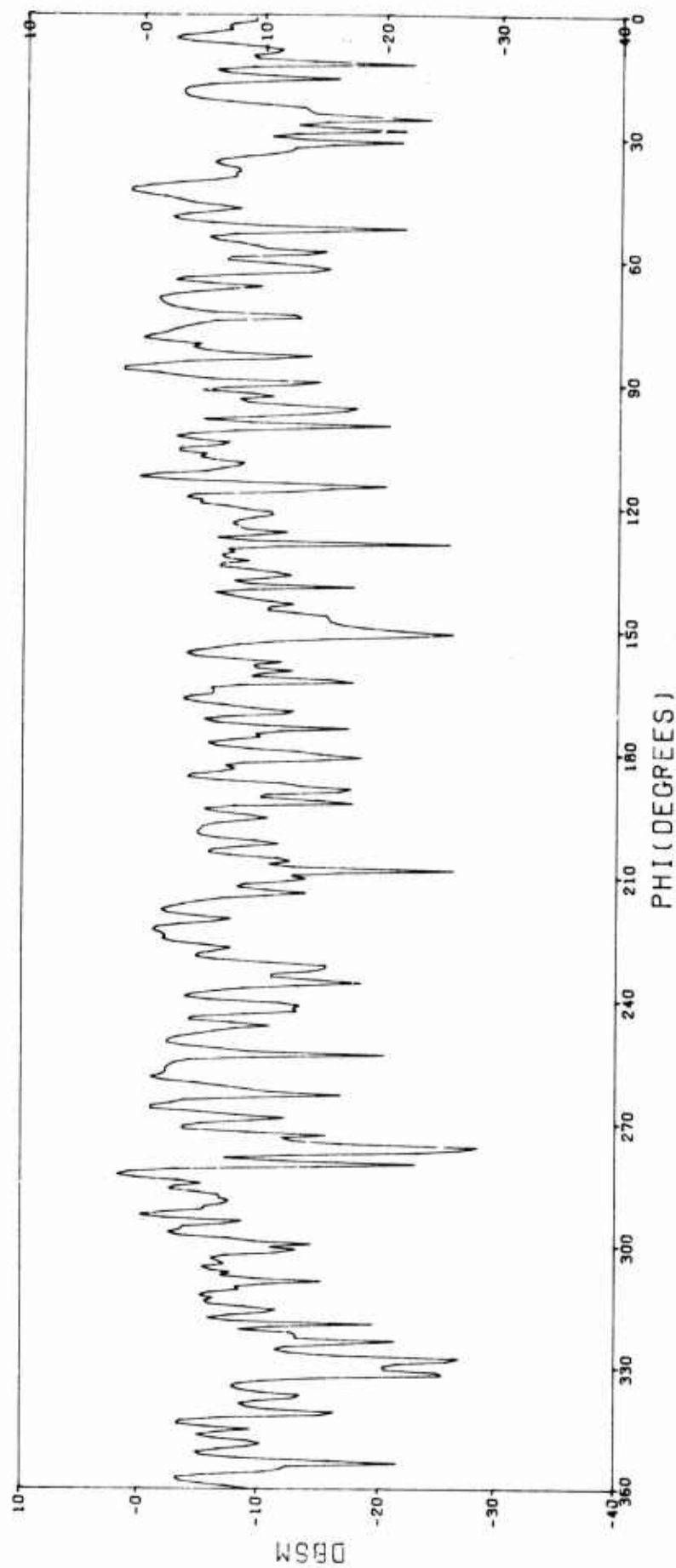


Figure 38.  $\phi$ - $\phi$  backscattering patterns as calculated using the full matrix, cloud #3,  $N = 200$ ,  $d/\lambda = 2.0$ .

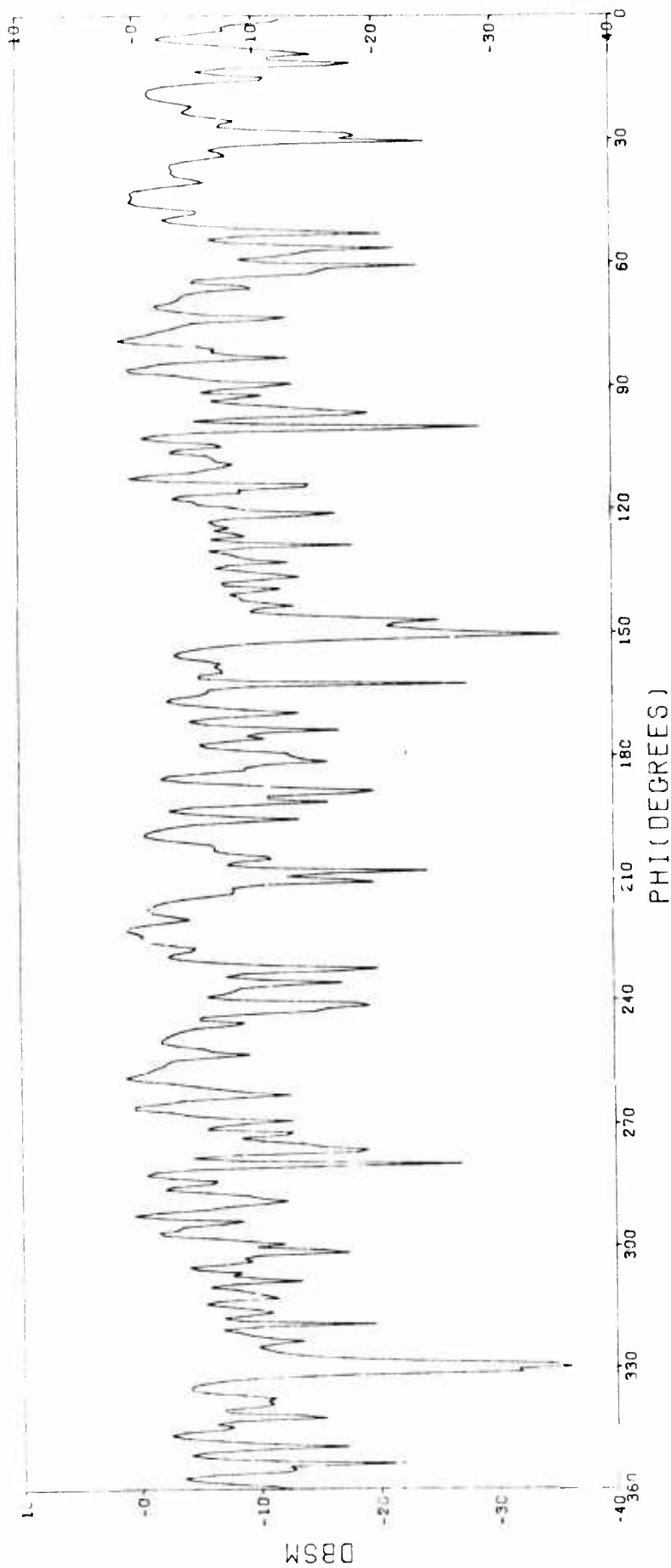


Figure 39.  $\phi$ - $\phi$  backscattering patterns as calculated using the sparse matrix, cloud #3,  $N = 200$ ,  $d/\lambda = 2.0$ .

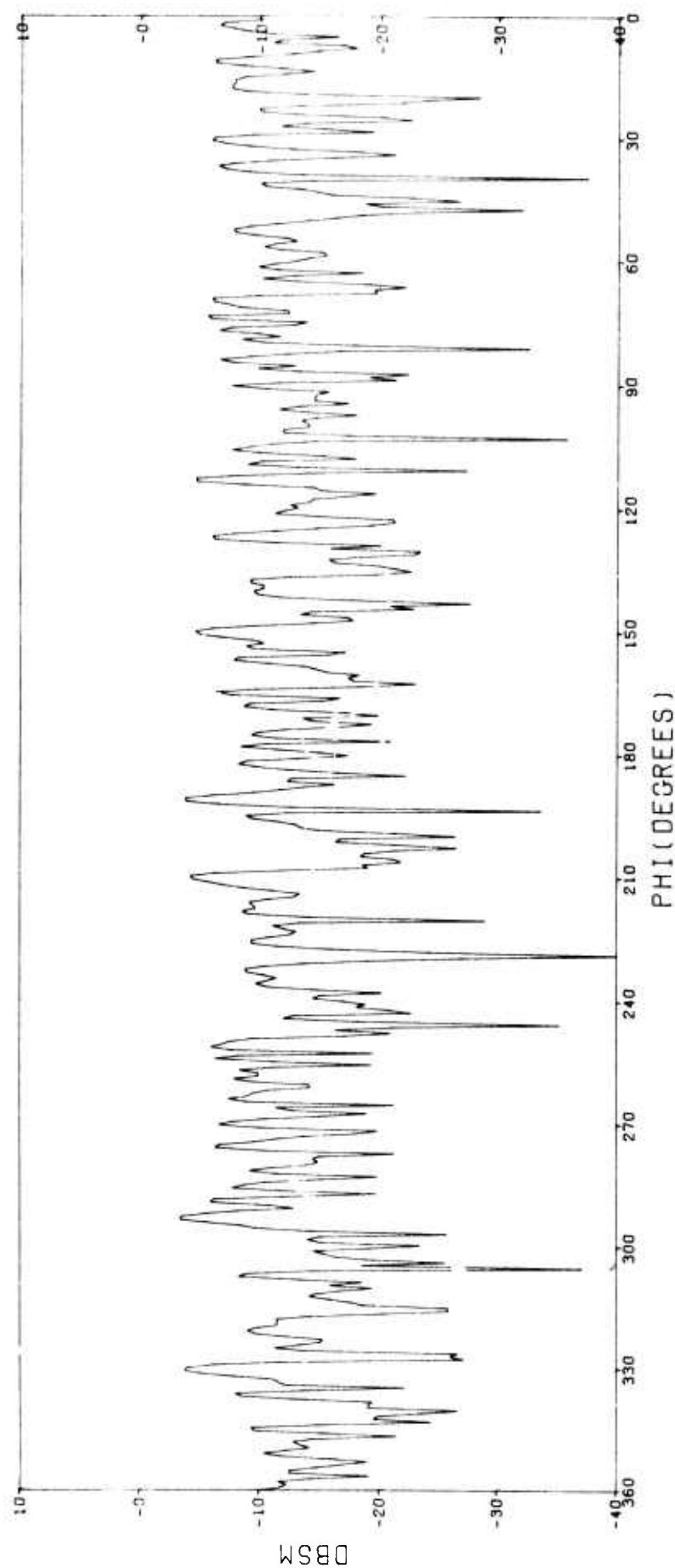


Figure 40.  $\theta$ - $\phi$  backscattering patterns as calculated using the full matrix, cloud #3,  $N = 200$ ,  $d/\lambda = 2.0$ .

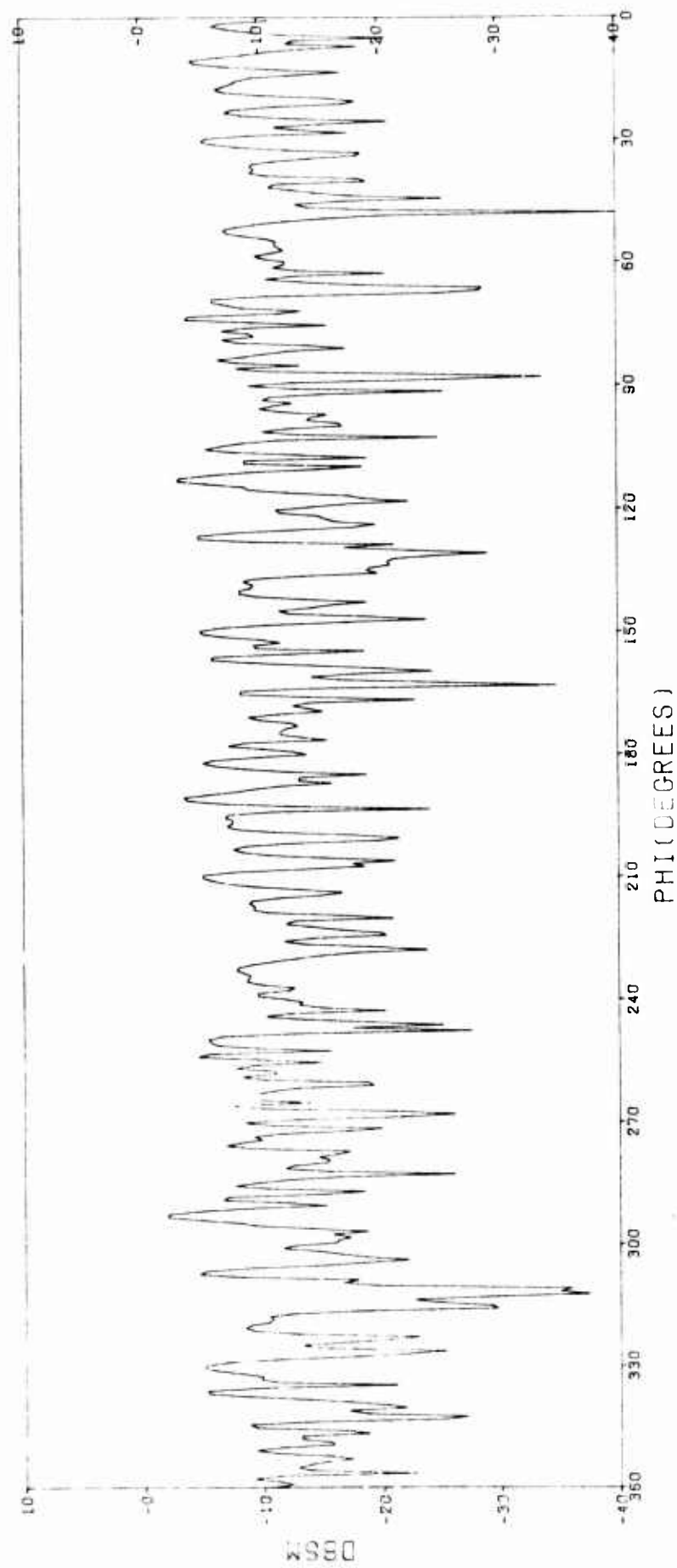


Figure 41.  $\sigma \cdot \psi$  backscattering patterns as calculated using the sparse matrix, cloud #3,  $N = 200$ ,  $d/\lambda = 2.0$ .

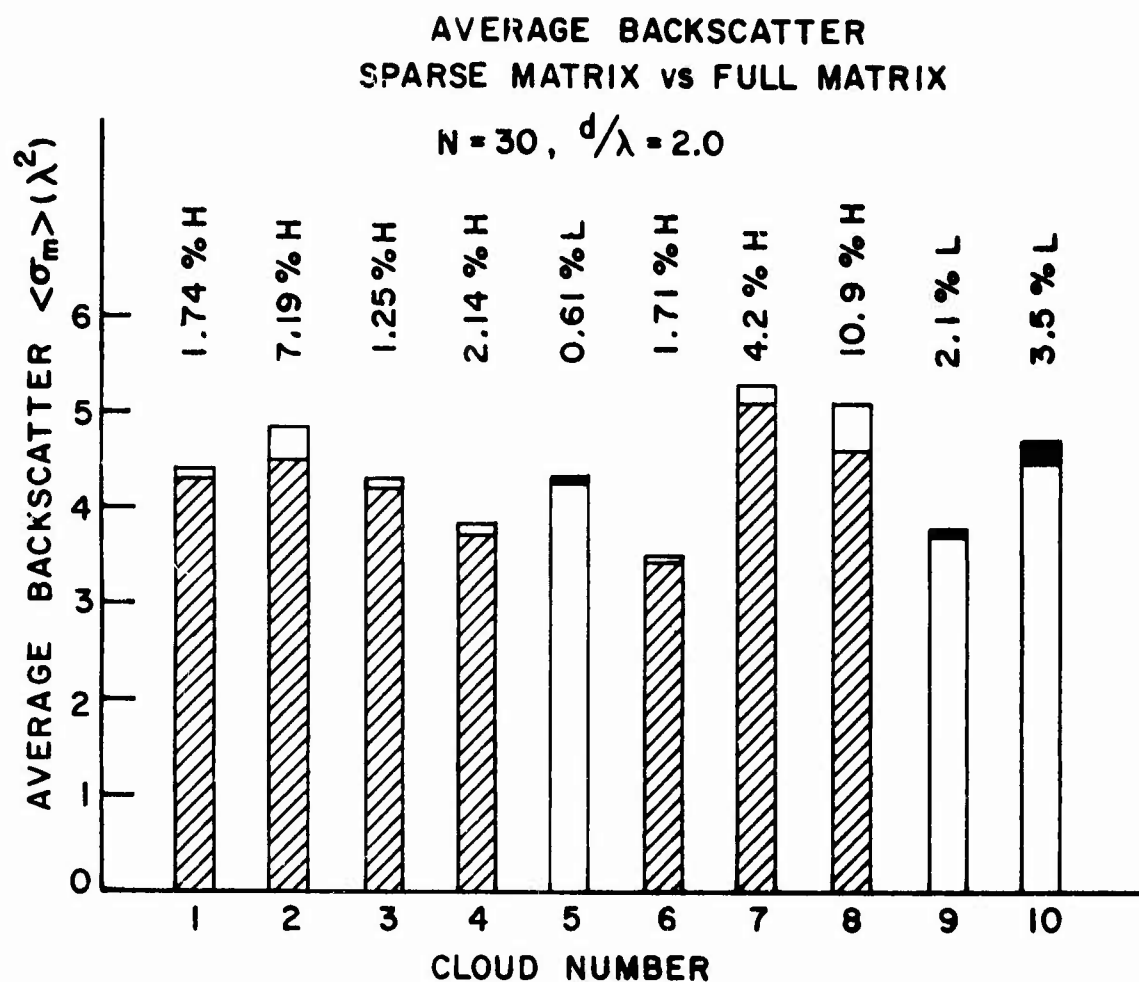


Figure 42. Spatial average backscatter from ten different clouds using full and sparse matrices; the symbolism L or H indicates that the sparse matrix result was lower or higher, respectively, than the full matrix result by the indicated percentage.



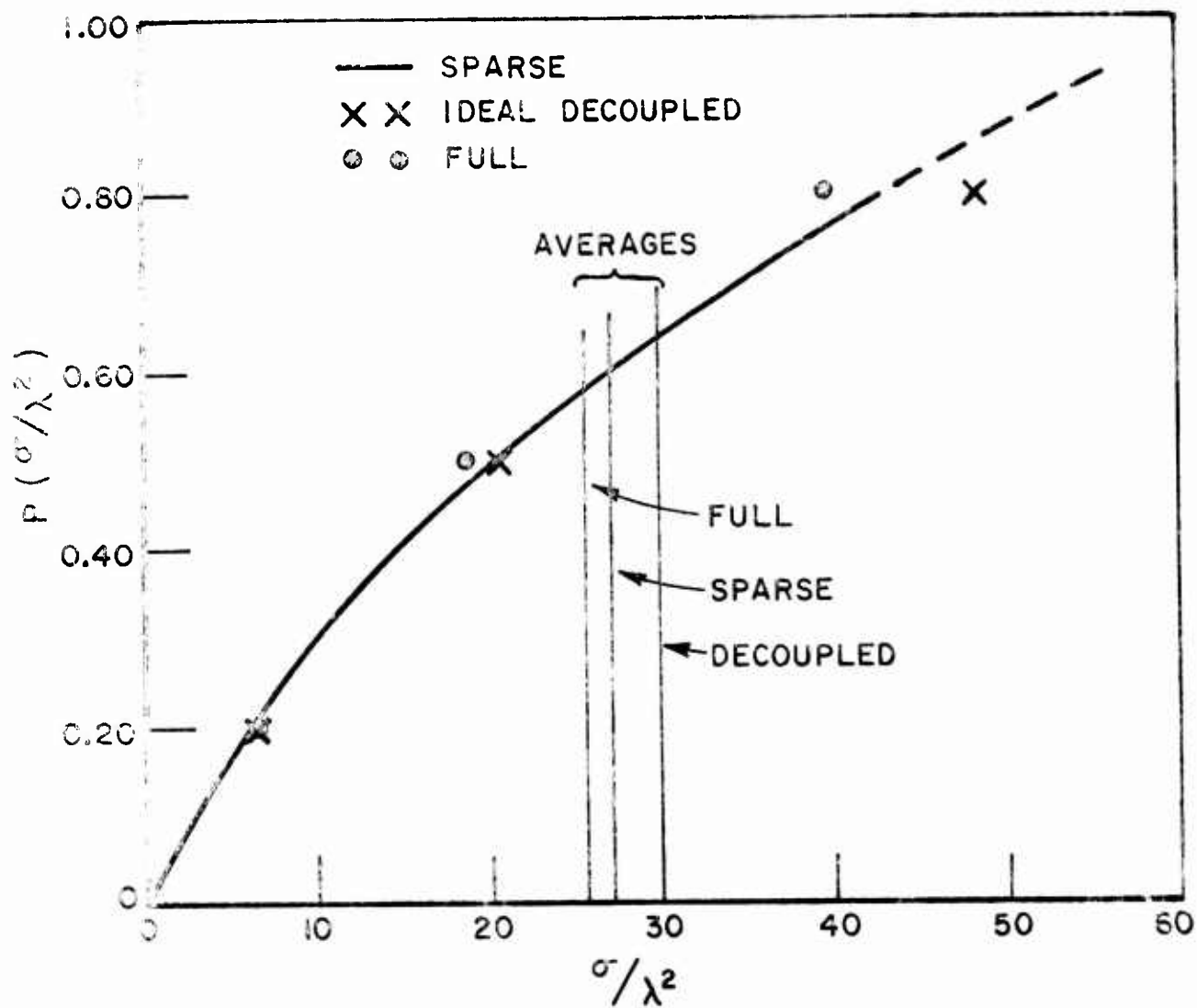


Figure 43. Cumulative probability function of backscattering cross section, cloud #1.

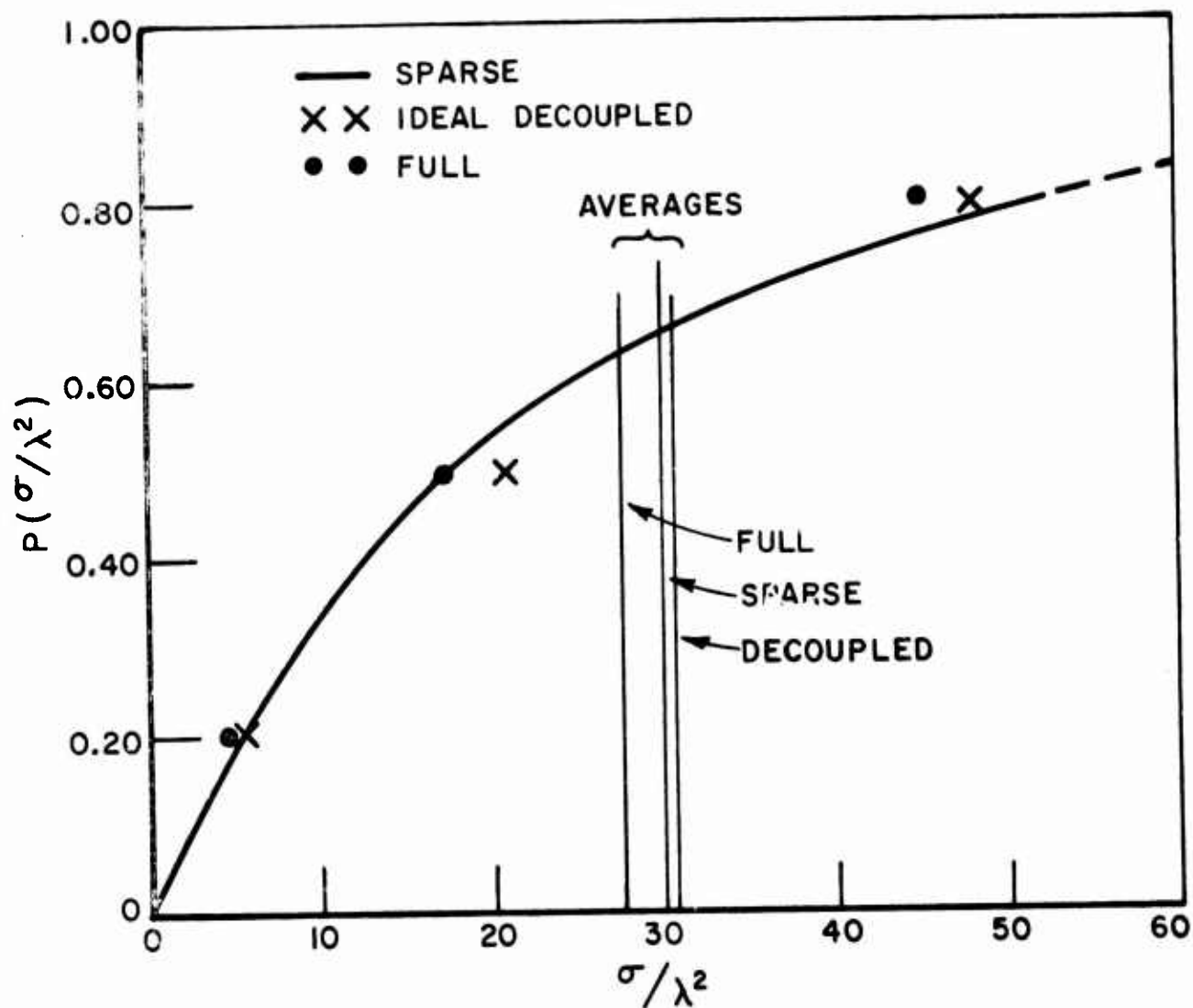


Figure 44. Cumulative probability function of backscattering cross section, cloud #2.

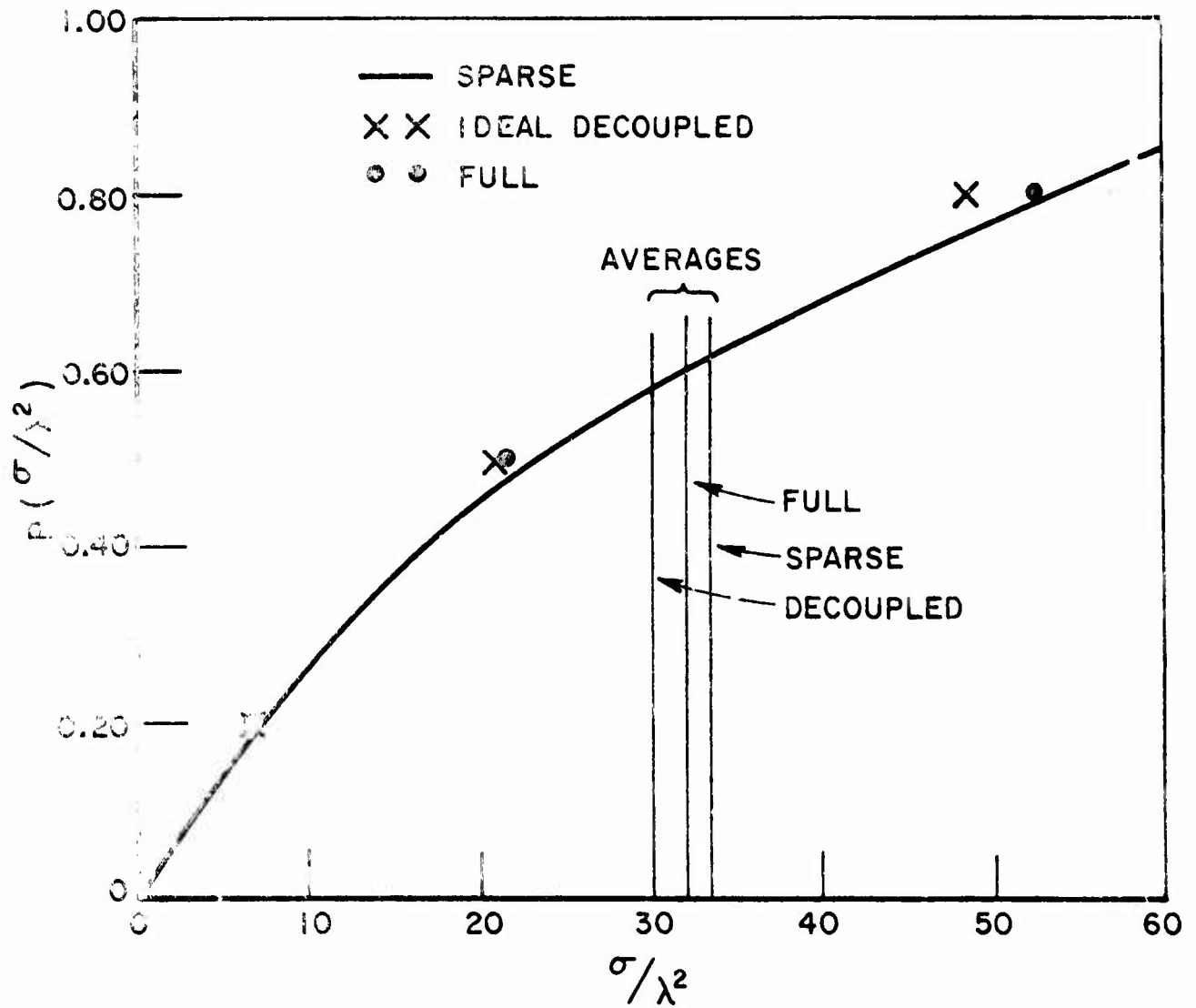


Figure 45. Cumulative probability function of backscattering cross section, cloud #3.

It is clear from what has been said previously that the sparse matrix incurs substantial savings in computer memory. But how about time saved? We may consider the time consumed (on the ElectroScience Laboratory Datacraft computer) by three separate operations: matrix setup time, i.e., the time taken to generate the Z matrix elements; reordering, i.e., the time taken to reorder the Z matrix so that its auxiliary matrix will also be sparse; and backscattering, i.e., the time taken to calculate the backscattering cross section at one look angle.

The number of elements in large matrices rapidly becomes exorbitant, even taking into consideration the identity of all the diagonal elements and symmetry about the diagonal. Applying the 10% rule permits us to store only a few or less percent of these elements, but to apply the rule, all of them must be calculated. This takes a great deal of time. In order to reduce this matrix setup time, we appealed to the evidence of Fig. 22 to create what we call a "sphere-of-influence" model. In this model we avoid the calculation of the vast majority of the matrix elements by superimposing on the 10% rule, a sphere-of-influence rule, whereby one calculates only those matrix elements representing the coupling of the dipole of interest to its neighbors lying within a specified spherical volume centered at the dipole, all other couplings being assumed zero. Figure 46 shows the computer time saved by applying the sphere of influence rule as well as the 10% rule over the time taken by applying the 10% rule only. It is based upon averages of 20 clouds of 100 dipoles each, and shows the time saved for assumed sphere of influence radii from  $2.07\lambda$  to  $2.5\lambda$ . The larger the sphere-of-influence, the smaller the time savings, of course. But the larger the sphere of influence, the more identical become the matrices sparsened by the two different rules. The number of elements which differ in the two matrices so sparsened, are presented in Fig. 46 as the percentage of the  $N^2$  elements in each matrix. Clearly, at about a radius of  $2.4$ , the two become identical, implying that the sphere-of-influence sparse model should yield backscattering patterns equally as good as those obtained from the 10% sparse model. Note that our average spacing of  $d/\lambda = 1.0$  is assumed for the clouds. Denser clouds would exhibit less time saving. Figure 47, also for fixed  $d/\lambda = 1.0$ , indicates the time saving for a variety of choices of  $N$ , using  $2.07\lambda$  and  $2.5\lambda$  radii for the sphere of influence. As expected, the time saving rises as  $N$  increases.

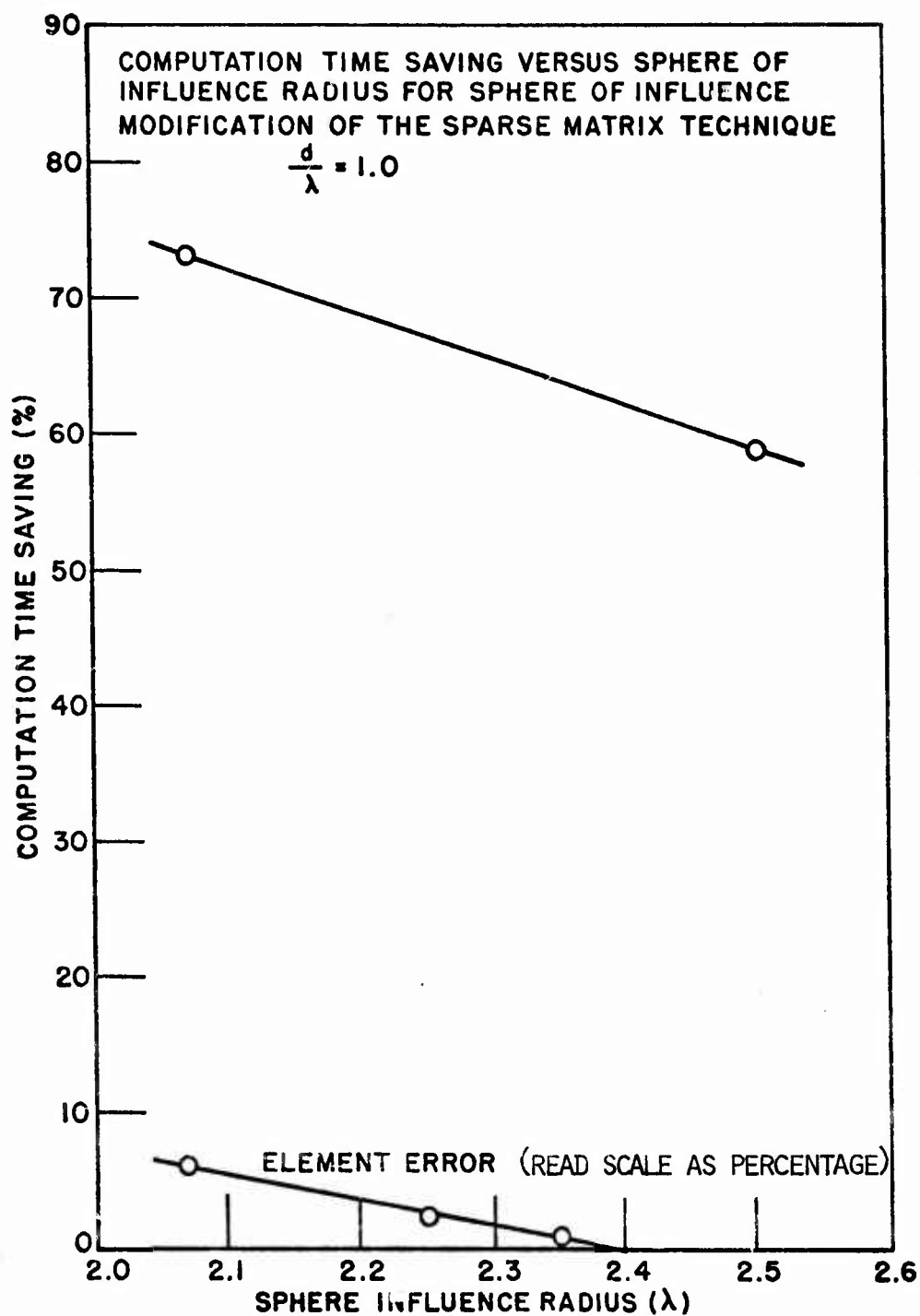


Figure 46. Time saving and element error vs sphere of influence radius using sphere of influence model plus 10% rule over the 10% rule alone

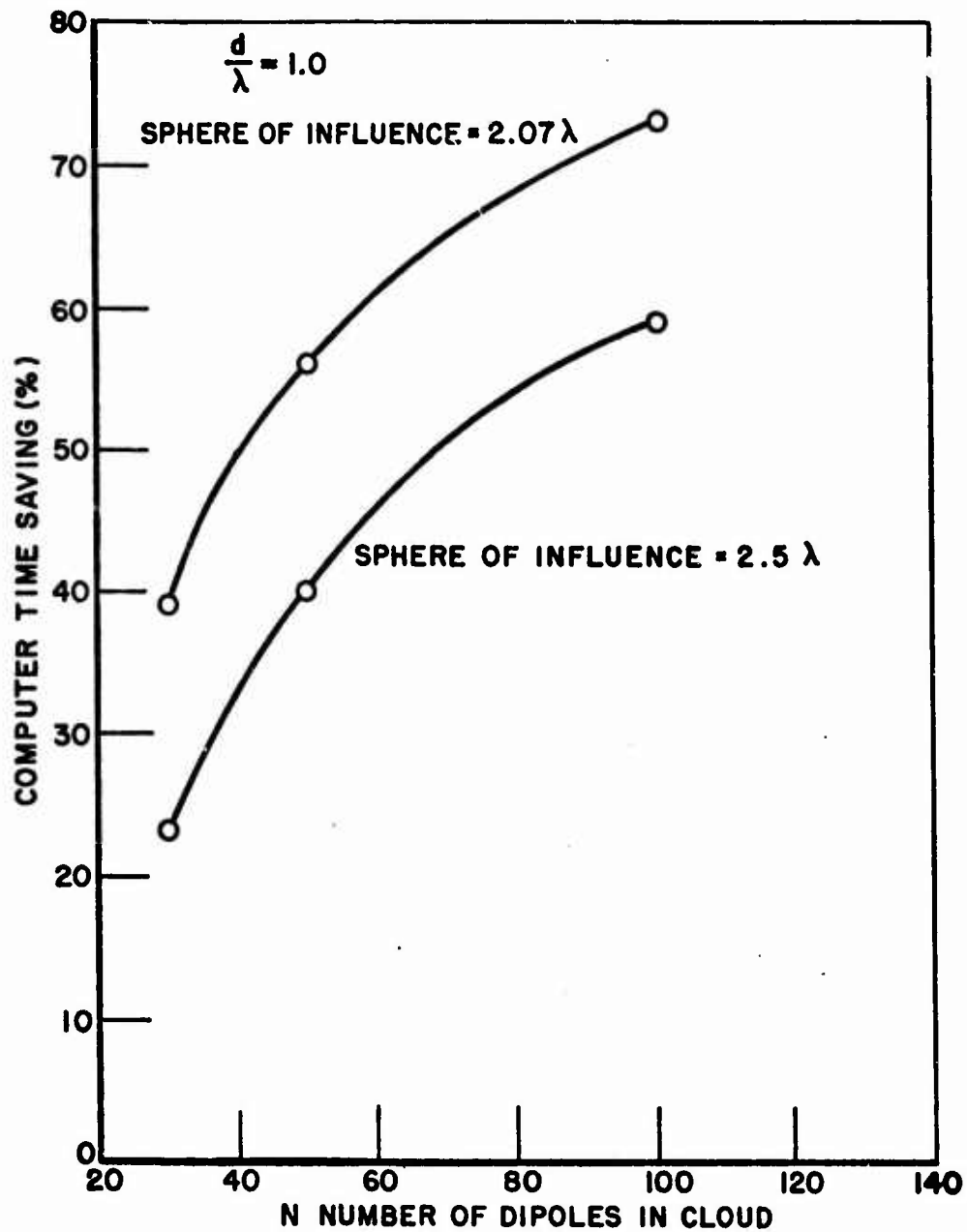


Figure 47. Time saving vs number of dipoles using sphere of influence model plus 10% rule over the 10% rule alone.



The foregoing data reflect a very substantial time saving in matrix setup time with little penalty in echo area. Evidence did exist, however, that the sparse matrix algorithm, even with the sphere-of-influence rule built in, was time consuming. This evidence was verified when a computation of an  $N = 500$  dipole cloud with  $d/\lambda = 1.0$  the Wright-Patterson Air Force Base CDC 6600 computer overran its allotted time of 5000 seconds. In order to investigate this time consumption more carefully on our own machine, a set of backscatter data were accumulated for one look angle with clouds of 30, 50, and 100 dipoles, each with average spacings of  $d/\lambda = 0.5$  and  $1.0$ . Twenty such clouds were considered for each case and average times obtained for the three parts of the sparse matrix program. The sphere-of-influence plus 10% rules were applied to sparse each matrix and the results tabulated in Table E. The numbers do not represent real times but clock times on the ESL machine. Time ratios are of importance here.

TABLE 5  
CLOCK TIMES OF THREE PARTS OF SPARSE MATRIX ROUTINE

$d/\lambda$	N	No. of non-zero elements	Matrix Setup	Reordering	1 look angle	Total time
1.0	30	76	842	475	17	1,350
1.0	50	148	1,863	1,884	31	3,743
1.0	100	343	5,033	17,410	76	22,534
0.5	30	220	1,117	2,807	30	3,968
0.5	50	500	3,069	21,277	66	24,449
0.5	100	1,462	11,311	414,121	219	425,667

In this table total time is the sum of the previous three operations plus some small amount for inherent operations. The average number of nonzero elements in the upper right triangle of the Z matrix are also given. Clearly, with the sphere-of-influence rule applied, it is the reordering time which is preponderant and causes the sparse matrix algorithm to be so time consuming. In an effort to reduce this reordering, an attempt was made to partially reorder. The results, however, were not encouraging and the effort was terminated.

The sparse matrix computer program used to obtain the foregoing results is documented in Appendix E.

Before turning to another topic we should point out one facet of the sparse matrix approximation as arrived at by the 10% and sphere-of-influence rule. That is, these sparsing techniques are determined by the Z matrix alone; they do not take into consideration the currents induced on the dipoles. For example, the influence of the  $i$ th dipole current upon the voltage induced in the  $j$ th dipole is proportional to  $z_{ij}I_i$ , the product of the  $ij$ th matrix element and the  $i$ th current. Simply setting  $z_{ij}$  to zero if it is smaller than 10% of  $z_{ij}$  may not be rigorously appropriate if  $I_i$  is large. However, the 10% rule appears to do a satisfactory job for obtaining the average backscatter. If, however, one is interested in extinction of current through the cloud, the 10% rule or, even worse, the sphere-of-influence model, cannot be expected to yield good results for, by their nature, these approximations modify the coherent forward scattered wave as it proceeds through the cloud. Since this is an important phenomenon dictating the extinction rate in the first few wavelengths into the cloud, a better model would have to be devised if one is interested in extinction. The indirect methods described below might serve such a purpose.

#### 4. Indirect (Iterative) Methods

##### a. Theoretical Considerations

Sections 2 and 3 have discussed direct and sparse matrix methods for solving the equation,

$$(12a) \quad ZI = V.$$

In this section we discuss indirect methods, of which linear iteration forms a special class and which we will emphasize. In order to avoid ambiguity in notation, in this section we will rewrite Eq. (12a) as

$$(12b) \quad Ax = b$$

and develop all pertinent equations in terms of  $A$ ,  $x$ , and  $b$  rather than  $Z$ ,  $I$ , and  $V$ .

All indirect methods of solving Eq. (12b) for  $x$  can be viewed from the implicit formulation given by

$$(13) \quad x = f(A, b, x),$$

implicitness being characterized by the appearance of unknown vector  $x$  on both sides. The symbol  $f$  in the above expression represents a function or set of rules (algorithm) with the minimal property that the exact  $x$  satisfies Eq. (13) identically. One additional condition on  $f$  needed here is that it be able to transform an approximation to  $x$  into an improved approximation. It would be too much to ask that one application of Eq. (13) yield the exact solution. However, repeated applications might be expected to give successively better approximations and this is precisely the essence of iteration. Notation can be added to the implicit form of Eq. (13) to give a general formula for iteration, i.e.,

$$(14) \quad x^{(k)} = f^{(k)}(A, b, x^{(k-1)}, x^{(k-2)}, \dots, x^{(k-m)}),$$

where  $x^{(k)}$  represents the  $k^{\text{th}}$  iterate or approximation of  $x$ . Note, in this form,  $x^{(k)}$  is considered to be related to  $m$  previous iterates, in which case the iteration is of  $m^{\text{th}}$  degree. Also note that, in general, the function  $f^{(k)}$  can change from step to step. If  $f^{(k)}$  remains invariant throughout the iteration process ( $k = 1, 2, \dots$ ), then the iteration is called stationary and if not, it is called non-stationary. The iteration process is referred to as linear for  $f^{(k)}$ 's which are linear functions of  $x^{(k-1)}, x^{(k-2)}, \dots, x^{(k-m)}$  and nonlinear otherwise. Iterative methods subdivide still further into point-step and group or block-step methods and these categories depend on the choice of  $f^{(k)}$ . More specifically, the point-step methods proceed to improve the individual components of solution vector  $x^{(k)}$  one-at-a-time, independently of the other elements, while block-step methods normally improve blocks of elements of  $x^{(k)}$ , independently of other blocks. A rather unique block type iterative method will be introduced later which will allow "overlap" of these blocks based on the physical scattering problem. Discussed in this section are three classical linear stationary methods of first degree; the Point-Jacobi (J) method, the Gauss-Seidal (GS) method and the method of Successive Over-relaxation (SOR) together with their physical interpretation from the scattering viewpoint. Also included is a discussion of convergence criteria for these methods and finally a presentation of results, mostly calculated using SOR.

#### Linear First Degree Methods (J, GS, SOR)

The basic equation underlying many linear indirect methods is derived from Eq. (12b) by adding  $x$  to both sides and rearranging to give

$$(15) \quad x = (I-A) x + b,$$

which, in terms of a sequence of iterates can be written as

$$(16) \quad x^{(k)} = Hx^{(k-1)} + b,$$

where

$$(17) \quad H \equiv I - A.$$

H is usually referred to as the iteration or error reducing matrix and is related to the functions  $f^{(k)}$  described in the previous section. Iteration via Eq. (16) is linear, stationary and of first degree. This expression yields a number of classical techniques which differ by the "splitting" of matrix A. Consider the splitting defined by

$$(18) \quad A = D - E - F$$

where  $D = [a_{ii}]$ ,  $i = 1, \dots, N$ , is a diagonal matrix and  $E = [-a_{ij}]$ ,  $i > j$ , is strictly lower triangular and  $F = [-a_{ij}]$ ,  $i < j$ , is strictly upper triangular. The iteration of Eq. (16) then becomes

$$(19) \quad x^{(k)} = D^{-1}(E+F)x^{(k-1)} + D^{-1}b,$$

where the iteration matrix is identified as

$$(20) \quad H_J = D^{-1}(E+F).$$

Equation (19) describes the well known Point-Jacobi (J) method [48] or method of "simultaneous displacements" [49]. Here, new components of  $x^{(k)}$  are computed as functions of components of  $x^{(k-1)}$  as follows:

$$(21) \quad x_i^{(k)} = -\frac{1}{a_{ii}} \sum_{\substack{j=1 \\ j \neq i}}^N a_{ij} x_j^{(k-1)} + \frac{1}{a_{ii}} b_i$$

Note however, that by carefully considering the ordering of improvements in  $x^{(k)}$  Eq. (21) can be modified to incorporate the latest improvements in  $x^{(k)}$  at intermediate steps; i.e.,

$$(22) \quad x_i^{(k)} = -\frac{1}{a_{ii}} \left( \sum_{j=1}^{i-1} a_{ij} x_j^{(k)} + \sum_{j=i+1}^N a_{ij} x_j^{(k-1)} \right) + \frac{1}{a_{ii}} b_i$$

or, in matrix notation,

$$(23) \quad x^{(k)} = (D-E)^{-1} F x^{(k)} + (D-E)^{-1} b.$$

Here, the iteration matrix is given by

$$(24) \quad H_{GS} = (D-E)^{-1} F.$$

Equation (23) is the familiar Gauss-Seidel (GS) method [50], also known as the method of "successive displacements".

Both the J and the GS techniques can be considered special cases of a larger class of computer oriented "relaxation" methods often referred to as Over-relaxation (OR) methods [51]. A basic equation governing these methods is given by

$$(25) \quad \bar{x}^{(k)} = \bar{x}^{(k-1)} + \omega (x^{(k)} - \bar{x}^{(k-1)})$$

where the "relaxation factor" is usually chosen to be a real constant in the range  $0 < \omega < 2$  and  $x^{(k)}$  is computed by either the J or the GS method [52]. The technique for computing  $x^{(k)}$  is clearly not restricted to the above two methods; here, however, only the GS method will be assumed. This assumption leads to the defining equation for the familiar Successive Over-relaxation (SOR) method [53]; namely,

$$(26) \quad x^{(k)} = (I - \omega D^{-1} E)^{-1} [(1 - \omega) I - \omega D^{-1} F] x^{(k-1)} + (I - \omega D^{-1} E)^{-1} \omega D^{-1} b,$$

where the iteration or error reducing matrix  $H$  is given by

$$(27) \quad H_{\omega} = (I - \omega D^{-1} E)^{-1} [(1 - \omega) I - \omega D^{-1} F].$$

The computational procedure for SOR is given by Eqs. (22) and (25) and therefore, for  $\omega=1$ , SOR reduces identically to the GS

method. Incidentally, when the solution  $x^{(k)}$  in Eq. (25) is computed by the J method, the resulting technique is called the method of "simultaneous over-relaxation" (JOR) [54] and reduces directly to the J method for  $\omega=1$ .

The SOR method of Eq. (26) is obviously a stationary linear method of first degree. Nevertheless, SOR can be made non-stationary by not restricting  $\omega$  to being a constant for all iterations. It is not, on the other hand, clear how  $\omega$  should be varied to improve the speed of the iteration procedure (convergence) for the general case. More will be said of this subject in a later discussion on convergence.

An alternative form for these same iteration procedures can be derived in terms of an approximate or psuedo inverse to matrix A. Let  $\tilde{A}^{-1}$  represent an approximation to the inverse  $A^{-1}$  of Eq. (13). Then, the kth iterate  $x^{(k)}$  can be written as  $x^{(k-1)}$  plus a correction term  $d^{(k-1)}$  given by

$$(28) \quad d^{(k-1)} = \tilde{A}^{-1} r^{(k-1)},$$

where the residual vector  $r^{(k-1)}$  is defined by

$$(29) \quad r^{(k-1)} = b - Ax^{(k-1)}.$$

Equations (28) and (29) can be combined to give

$$(30) \quad d^{(k-1)} = -\tilde{A}^{-1}A x^{(k-1)} + \tilde{A}^{-1}b,$$

whereupon, the kth iterate may be written as

$$(31) \quad x^{(k)} = (I - \tilde{A}^{-1}A)x^{(k-1)} + \tilde{A}^{-1}b.$$

The H matrix here has the form

$$(32) \quad H = (I - \tilde{A}^{-1}A)$$

and it is easily shown that the following choices for A lead to the previously derived H matrices; i.e.,



$$(33) \quad \tilde{A} = D \rightarrow \text{Eq. 20 (J)}$$

$$(34) \quad \tilde{A} = D-E \rightarrow \text{Eq. 24 (GS)}$$

$$(35) \quad \tilde{A} = \frac{1}{\omega} D-E \rightarrow \text{Eq. 27 (SOR)}.$$

An additional point to be noted in this latest discussion is that  $\tilde{A}$  need not be identified with a rigorous matrix form such as those given in Eqs. (33) to (35).  $\tilde{A}$  can merely be representative of a special algorithm for computing the approximations to  $x$ . Equation (31) in this case will no longer represent a rigorous matrix equation. This is in line with the previous comment that  $f$  in Eq. (13) may in fact represent only a set of rules or algorithm for computation. More will be said later concerning a less-than-rigorous notation.

#### Convergence Criteria

Success or failure of any iterative method is measured in terms of the limit of the sequence  $\langle x^{(k)} \rangle$  as  $k \rightarrow \infty$ ; i.e., if  $x^{(k)}$  reaches the exact solution  $x$  in the limit, then the method is obviously successful and if not, the method fails. Although seemingly straightforward, certain questions remain unanswered. Namely, is information available to indicate, a priori, when a particular method will converge and, if so, what quantitative measures can be counted on to indicate sufficient convergence since the exact solution is never known? The first question is answered rather easily which the following paragraphs will show. The second question however turns out to be the more practical yet difficult question to answer. Reasons for this will be made clearer in the final portions of this section.

The normed vector space defined in Appendix C of Ref. 38 can be reintroduced here in terms of the limit of the sequence  $\langle x^{(k)} \rangle$  in the following way,

$$(36) \quad \lim_{k \rightarrow \infty} \|x - x^{(k)}\| = 0,$$

where  $x$  is the exact solution satisfying Eq. (16) identically; i.e.,

$$(37) \quad x = Hx + b.$$

The following result is obtained by considering the difference between Eqs. (37) and (16),

$$(38) \quad (x-x^{(k)}) = H(x-x^{(k-1)})$$

and can be taken recursively to yield

$$(39) \quad (x-x^{(k)}) = H^k(x-x^{(0)}).$$

Note here that  $x^{(0)}$  is the initial "guess" corresponding to  $k=0$ , hence,  $(x-x^{(0)})$  is a constant vector. Compatible norms (see Appendix C of Ref. 38) are needed on both sides of Eq. (39) to give

$$(40) \quad ||x-x^{(k)}|| \leq ||H||^k ||x-x^{(0)}||,$$

where the inequality  $||H^k|| \leq ||H||^k$  has been included in bringing this expression to the form of Eq. (40). Recall, Eq. (36) defines the unique condition for convergence of  $\langle x(k) \rangle$  in the established normed space and by applying this condition to Eq. (40), the necessary and sufficient condition for convergence of Eq. (16) becomes

$$(41) \quad \lim_{k \rightarrow \infty} ||H||^k = 0,$$

and this condition can only be satisfied if

$$(42) \quad ||H|| < 1$$

Hence, the properties of  $H$  determine convergence characteristics of Eq. (16) for any starting vector  $x^{(0)}$ . The natural norm of Eq. (42) remains as yet unspecified but has a lower bound (see Appendix F of Ref. 38) in the spectral radius given by

$$(43) \quad ||H|| \geq \rho\{H\}$$

where the spectral radius of  $H$ ,  $\rho\{H\}$ , is defined by

$$(44) \quad \rho\{H\} \equiv \max_i |\lambda_i|$$

and the  $\lambda_i$ 's are solutions to the determinantal eigenequation,

$$(45) \quad \det(H - \lambda I) = 0.$$

Therefore, the necessary and sufficient condition for convergence of Eq. (16) to the solution  $x$  (see Appendix G of Ref. 38 for this proof) is given by

$$(46) \quad \rho\{H\} < 1.$$

Convergence properties for the iterative methods outlined earlier can be predetermined as the above procedure indicates; however, for certain special cases, calculation of eigenvalues can be avoided. This would certainly be an advantage, especially for those cases when the order of matrix  $H$  is large (e.g.,  $N > 100$ ). These special cases can be recognized in terms of the following properties [55] of the original matrix  $A$  and the splitting of  $A$  defined in Eq. (18):

1. If  $E + F \geq 0$ ,

$$D > 0,$$

and

$$\rho\{D^{-1}(E + F)\} < 1$$

then  $A$  is an M-matrix.

2. If

$$\|D^{-1}(E + F)\|_{\infty} < 1$$

then  $A$  is strictly diagonally dominant.

3. If no  $N \times N$  permutation matrix  $P$  which permutes rows and columns of an  $N \times N$  matrix exists such that

$$PAP^T = \begin{bmatrix} D_1 & G \\ 0 & D_2 \end{bmatrix}, \quad (T \text{ denotes transpose})$$

where  $D_1, D_2$  are square matrices and

$$\|D^{-1}(E + F)\|_{\infty} \leq 1,$$

then A is irreducibly diagonally dominant.

4. A has the following properties;  
A is hermitian ( $A = A^*$ ) and (\* denotes complex conjugate transpose)

A is positive definite (eigenvalues of A are

$\lambda_i$ ,  $i = 1, 2, \dots, N$  and satisfy  $\lambda_i > 0$ , for all  $i$ .)

The convergence of the J and GS methods is assured for any matrices satisfying 1, 2 or 3 above and the SOR method necessarily converges for  $0 < \omega < 2$  when condition 4 is met. Proofs of these sufficient conditions for convergence are given in Varga [56]. If, in addition to condition 4, A has "property A" as originally defined by Young [57], then an optimum relaxation factor  $\omega_{opt}$  can be computed for the SOR method. This optimum factor is given by

$$(47) \quad \omega_{opt} = \frac{2}{1 + \sqrt{1 - \nu^2}},$$

where

$$(48) \quad \nu = \rho\{H_J\}$$

and  $H_J$  is computed from Eq. (20). If, on the other hand, A does not satisfy "property A", then  $\omega_{opt}$  can only be determined empirically.

The discussion of convergence, so far, has centered on finding the spectral radii of appropriate iteration matrices or on the special properties of the original matrix A. Consider, however, the more general matrices which appear in the EM problems studied here. The A matrices in these cases are complex symmetric (nonhermitian) and not diagonally dominant in all but the most trivial cases. They are positive definite, or at least positive semi-definite, in the sense that

$$(49) \quad \operatorname{Re}\{x^*Ax\} \geq 0 \quad (*\text{denotes complex conjugate transpose}),$$

where this quantity is related to real power dissipated (radiated) by the system represented by impedance matrix  $A$ . These basic characteristics of the EM problem eliminate any possibility of satisfying conditions 1-4 above. Therefore, the only rigorous technique is to compute the appropriate spectral radius, but some difficulty in computing  $\rho\{H\}$  is likely to be encountered for many practical EM problems due to the size of  $N$ . General sub-routines are available [58] for calculating complex eigenvalues of complex matrices; however, when  $N$  becomes large ( $>250$ ), these routines will require more fast-access memory than available on most computing machines. Even if these computations are possible, the authors suggest that the time and effort used in searching for a "largest" eigenvalue would better be used trying the iterative technique.

A suitable measure of convergence characteristics usually must be determined empirically. One natural choice is a measure based on the vector of residuals defined by Eq. (29), or

$$(50) \quad r^{(k)} = b - Ax^{(k)}$$

This expression can be misleading since it states that if  $r^{(k)}=0$ , the  $x^{(k)}$  is the exact solution and this is correct. However, to assume that  $x^{(k)}$  is near the exact solution when  $r^{(k)}$  is small (but not zero) may be a gross overassumption. A hint of this specious behavior is given by the following bound on the relative error in  $x^{(k)}$ ,

$$(51) \quad \frac{\|x - x^{(k)}\|}{\|x\|} \leq \frac{\|r^{(k)}\|}{\|b\|} \text{Cond}\{A\} .$$

Clearly, the ratio  $\|r^{(k)}\|/\|b\|$  must be considered in light of the condition number of  $A$  and the possible effects it may have on the upper bound of Eq. (51). It is also important to point out that all norms of residuals defined by Eq. (50) do not necessarily decrease monotonically when the iteration process is convergent; i.e., they sometimes oscillate or increase. Even then, Eq. (51) implies that if a monotonically decreasing norm is found, it may still be mere speculation to assume  $x^{(k)}$  is in some sense approaching the correct solution. Still another measure of convergence is to consider a norm of the change in  $x^{(k)}$ , from one iteration to the next. Consider the following normed difference,

$$(52) \quad ||\delta x^{(k)}|| \equiv ||x^{(k)} - x^{(k-1)}||$$

and ask the following question:

Does there exist a value of  $k$ , say  $k_\infty$ , and some  $\epsilon > 0$  such that for  $k > k_\infty$ ,  $||\delta x^{(k)}|| < \epsilon$ ?

If so, the process can be said to converge. The particular choice of  $\epsilon$  used to indicate sufficient convergence, however, is critical since the normed difference given by Eq. (52) is not necessarily a monotonically decreasing measure, even if the solution is convergent.

A last comment is in order before proceeding. Certainly, the most reassuring indication of convergence would be to compare solutions obtained by different techniques and possibly even by a physical measurement and find that they agree. This type of comparison should obviously be sought wherever possible and this was indeed the case in this study. In a following section we present certain confirmed iterative results and these results are used to justify the choice of error measure used for reliably indicating convergence.

#### Physical Interpretation of the Jacobi and Gauss-Seidel Methods

A physical interpretation of the J and GS methods is presented here with the aid of Fig. 48. The A matrix of previous equations here represents the 5 x 5 impedance matrix corresponding to the 5 dipoles shown in the figure. Consider the initial excitation on each dipole to be the incident field and the initial current vector to be  $x^{(0)} = 0$ .

The J method in general computes  $x^{(k)}$  by considering the incident field and the scattered fields produced by  $x^{(k-1)}$ . The latter contribution is zero for  $k = 1$ , hence the J method calculates  $x^{(1)}$  corresponding to the "uncoupled" array. The J method improves the solution for  $k > 1$  by accounting for the incident field and the scattered fields at each dipole where the scattered fields are produced by "old" currents. This interpretation of the J method in terms of multiple scattering within the array was first described by Tai [59]. All elements of the solution vector are updated simultaneously at the end of each iteration, hence the name "method of simultaneous displacements".



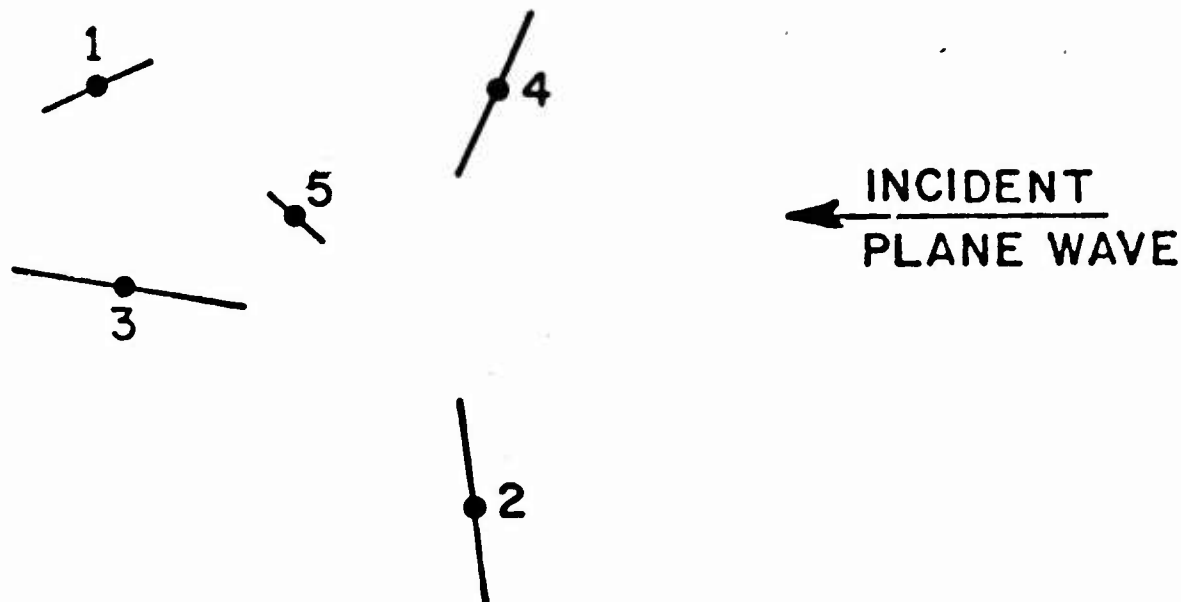


Figure 48. Sample random array for Jacobi and Gauss-Seidel iteration methods.

The GS method uses the "latest" currents whenever possible, i.e., the initial current on element #1 due to the incident field is

$$(53) \quad x_1^{(0)} = \frac{b_1}{a_{11}},$$

the initial current on element #2 due to the incident field plus the scattered field from element #1 is

$$(54) \quad x_2^{(0)} = (b_2 + a_{21}x_1^{(0)})/a_{22},$$

the initial current on element #3 is due to the incident field plus the scattered fields from elements #1 and #2

$$(55) \quad x_3^{(0)} = (b_3 + a_{31}x_1^{(0)} + a_{32}x_2^{(0)})/a_{33},$$

etc. The name "method of successive displacements" clearly applies to the above description and, as we might expect, the GS method has superior convergence properties since it accounts for

$$\sum_{i=1}^n i$$

interactions per iteration whereas the J method only accounts for  $n$  interactions per iteration.

The SOR method operates on the GS iterates by "relaxing" the latest correction through a weighted averaging process. Note that, even though SOR degenerates to GS for  $\omega=1$ , convergence of SOR ( $\omega \neq 1$ ) can be relatively good while GS may not converge at all. Physical interpretation of SOR in terms of scattering is more difficult than for J or GS. Weighted averaging of currents seems to be a purely mathematical concept. However, by assuming the array to be immersed in a medium which modifies the multiply scattered fields either by introducing "loss" or "gain", this would cause corresponding reductions or increases in interactions between dipoles. The application of an iterative procedure (e.g., GS) under these "relaxation" conditions could also be termed a form of SOR. The loss or gain in this case could either be reduced as the iteration converged or left in if the convergence required it. The solution to a "lossy" problem might be of considerable value in certain cases, especially if the "lossless" case could be deduced from such a solution.

#### Sphere of Influence (SOI) Method

The SOI technique is an empirically derived concept based on the electromagnetic scattering viewpoint. The approach stems directly from the array problem where the overall scatterer is so large and intricately detailed that it produces a matrix problem too large to handle by direct methods. Hence, the larger problem is broken up into a reasonable number of smaller problems each of which can be solved directly. The heart of the method lies in the hope that the solution to the large case can be obtained by interacting these smaller solutions with one another through an iterative process. The idea of "influence" manifests itself as a mutual impedance or coupling criterion between dipoles as in the case of the random array. Distance between dipoles provides a natural means for determining gross effects between dipoles and relative orientation is another. When these criteria fail to give a precise decision rule, a comparison of the mutual impedance to a preset level can be made. The level or threshold used here is defined to be a prescribed fraction of the diagonal or self impedance term. This criterion is also similar to that used in the

sparse matrix approximation for the scattering problem. Recall, the sparse matrix approach attempts to "thin" the matrix by deciding which elements are less important (i.e., below a certain magnitude) and a special algorithm is used to solve the thinned matrix problem exactly. This, however, is not the solution to the original problem and it is for this reason that iteration may provide the only means for finding the exact solution to the original problem for these large cases.

The basic SOI method computes groups of closest coupled neighbors and uses these "overlapping" groups to form a sequence of  $N$  reduced iteration submatrices. Closeness is measured by the relative influence between dipoles using the a priori criterion mentioned above. The  $N$  iteration submatrices will in general be distinct and the  $j$ th submatrix will be used to compute only the current on the  $j$ th dipole (point-step). The  $N$  subsystems formed by these submatrices are each solved by a direct technique and the scattered tangential electric fields are computed after each iteration and compared to the incident tangential electric fields as a check on the zero tangential electric field boundary condition along each dipole. The same residual mode voltage column  $r^{(k)}$  of Eq. (50) is proportional to the total tangential electric fields and is used as the excitation column for the next iteration if boundary conditions are not sufficiently met. The process is continued until  $\|r^{(k)}\|$  is reduced to an acceptable level.

One possible formulation for SOI is given in the following equations with the understanding that the overall technique cannot be simply described by a single matrix equation as with the other methods mentioned thus far. Let  $A(m_j|m_j)$  represent the  $m_j \times m_j$  iteration submatrix containing self and mutual impedances for the  $j$ th dipole and its  $m_j-1$  most closely coupled neighbors. The members of this  $j$ th subsystem (submatrix) are obtained by applying the following condition to the  $j$ th row of  $A$ ,

$$(56) \quad c|a_{jj}| < |a_{jp}|, \quad \begin{matrix} p = 1, 2, \dots, N \\ p \neq j \end{matrix}$$

where  $c$  is a prescribed (empirical) real constant in the range  $0 < c < 1$ . The  $j$ th subsystem at the  $k$ th step of the iteration process is then given by

$$(57) \quad A(m_j|m_j) d^{(k)}(m_j) = r^{(k-1)}(m_j)$$

when  $r^{(k-1)}(m_j)$  is the  $m_j \times 1$  "subvector" of residuals on the  $j$ th group of dipoles and  $d^{(k)}(m_j)$  is a  $m_j \times 1$  subvector which includes the  $k$ th correction to the current on dipole  $j$ , i.e.,

$$(58) \quad x_j^{(k)} = x_j^{(k-1)} + d_j^{(k)}.$$

The  $k$ th iteration is complete after  $N$  subsystems of the form Eq. (57) ( $j=1,2,\dots,N$ ) have been solved and all corrections ( $j=1,2,\dots,N$ ) of the form E. (58) have been made. A new residual is obtained again by including the original  $A$  matrix and  $b$  vector in Eq. (50).

Consider a simple application of SOI to the 5 dipole array illustrated in Fig. 49. The region ("sphere") of influence around dipole #1 ( $j=1$ ) is shown figuratively as a circle about dipole #1. Recall, this circle actually represents the region of influence for which Eq. (56) is satisfied for  $j=1$  for the given value for  $c$ . The matrix equation for this subset will be of order  $m_1=3$  and for the  $k$ th iteration this equation takes the form

$$(59) \quad \begin{bmatrix} a_{11} & a_{13} & a_{15} \\ a_{31} & a_{33} & a_{35} \\ a_{51} & a_{53} & a_{55} \end{bmatrix} \begin{bmatrix} d_1^{(k)} \\ d_3^{(k)} \\ d_5^{(k)} \end{bmatrix} = \begin{bmatrix} r_1^{(k-1)} \\ r_3^{(k-1)} \\ r_5^{(k-1)} \end{bmatrix}$$

Direct solution of this subsystem yields subvector  $d_3^{(k)}$  from which the  $k$ th correction to  $x_1^{(k-1)}$  is obtained, i.e.,

$$(60) \quad x_1^{(k)} = x_1^{(k-1)} + d_1^{(k)}.$$

Some experience is necessary in choosing constant  $c$  in order that the maximum of  $m_j$  defined by

$$(61) \quad \max_j m_j = M$$

remains within the capacity of the machine and yet still yields a convergent solution. The two extreme choices for  $c$  are  $c = 0$  and  $c = 1$ . All submatrices corresponding to the choice  $c=0$  are identically equal to the original  $A$  matrix and the first subsystem therefore yields a total solution for  $x$  with one application of the direct method, assuming of course the computer can do this.

The  $c=1$  choice causes SOI to degenerate to the J method since only the diagonal terms are inverted in this case.

A potentially important modification to the SOI method is the inclusion of a "forward scatter" (FS) model. Consider the dipoles which are located on the far side of a very large and dense array. These dipoles are very likely to be shadowed by those located on the directly illuminated side of the array. Hence, an improved "region of influence" for dipoles deep inside the array (or on the back side) could be obtained by taking into account the well known coherent forward scatter phenomenon which occurs along the line-of-sight. The reasoning here is that as the incident wave passes over these resonant dipoles (up front), the rescattered fields in the forward direction are nearly of opposite phase to the progressing incident wave and as this incident wave moves farther into the array, these coherently rescattered fields begin to "buck out" the incident wave. This eventually produces a shadowing effect on dipoles in the deep interior and far side regions of the array.

The above concepts of FS are rather simple to grasp; however, implementation of FS into the SOI algorithm is relatively messy. The FS process entails checking all  $a_{ij}x_j^{(k)}$  products which occur on or near the line-of-sight aspect through the array to the  $i$ th dipole. The "up stream"  $j$ th dipoles with scatter products which satisfy

$$(62) \quad \pi/2 < \arg\{a_{ij}x_j^{(k)}\} < 3\pi/2$$

are then chosen to be included in the next  $(k+1)$  subsystem (submatrix) for calculating the current on dipole  $i$ . The newly modified SOI-FS method is nonstationary since the  $N$  submatrices will no longer be constants for the whole process. They will of course become more constant as  $x^{(k)}$  nears a constant solution; however, in general, these submatrices will be quite changeable in the early stages of the iteration. Also note that, the resulting subsystems will be larger than for SOI alone for a given constant  $c$  and hence, implementing FS into SOI will generally require different values for  $c$  in order to maintain  $M$  in the viable range for direct solutions. The addition of FS should, however, improve convergence of SOI and thereby allow an increase in  $c$  in order to make room for the new dipoles added in by FS.

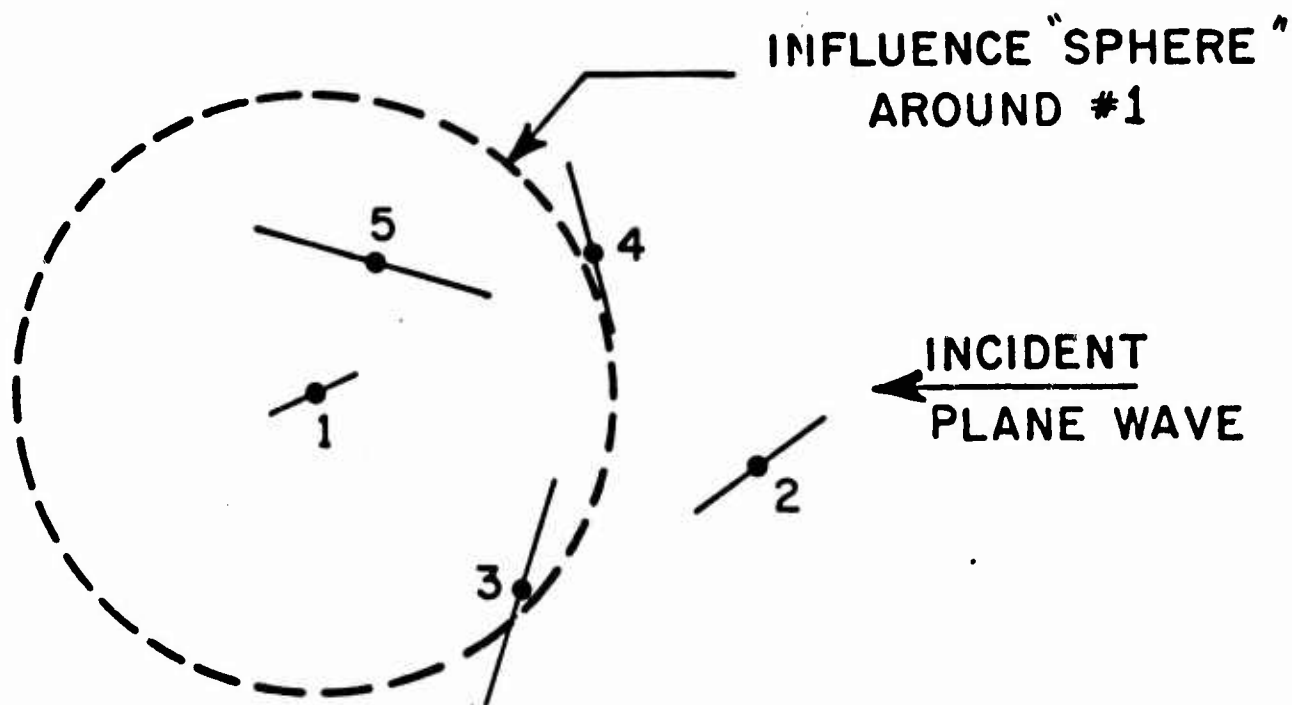


Figure 49. Sample random array for Sphere of Influence iteration method.

(b) Calculated results for chaff clouds

In Chapter VI of Ref. [38] there appear a set of curves of error bounds and condition norms for a few typical impedance matrices arising from chaff clouds. In general, these bounds rise with increase in dipole density and numbers, a trend which eventually must be reckoned with if direct solutions to larger order systems are sought. In light of this the iterative schemes are attractive and are used here to solve for the scattering from clouds of up to 1000 dipoles.

Numerical results presented in this section are divided into four areas: a check case; applications of SOR iteration to the solution of electromagnetic scattering by large clouds of thin resonant dipoles; application of SOI iteration to the solution of electromagnetic scattering by a small cloud of thin resonant dipoles; comments on applications of SOR to surface patch and wire-grid models. The appropriate equations from the preceding sections



have been translated into FORTRAN and documented listings of these programs appear in Appendix VI. All calculations were performed with 11 digit precision on a Datacraft Model 6024 computer having approximately 32k of real fast-access memory and 32k of virtual (disk) memory. Cycle time for this computer is approximately 1 microsecond. Certain special programming techniques, unique to this machine, are incorporated in the FORTRAN programs to allow psuedo-random access to approximately 6-1/2 million (24 bit) additional words of disk memory. Three and one-fourth million complex numbers can be computed, then stored in a special truncated form (6 digits) and retrieved using this technique. Also, a special subprogram is included which computes mutual impedances between "distant" dipoles; description and verification of this subprogram are also given in Appendix VI. This subprogram uses a special simplified calculation of the mutual impedance when dipoles are spaced greater than  $1\lambda$  and inclusion of this simplified calculation resulted in a computation time for the approximately one-tenth that of the original estimate for the  $N = 1000$  case; estimate  $\sim 10 - 12$  hours, actual time  $\sim 1$  hour.

It is important to note that all the results up to this point have assumed radially inhomogeneous densities for the clouds; in this section, however, all the results assume randomized clouds of uniform density.

#### A Check Case

Because some of the clouds treated here by iterative methods are so large, it is difficult to verify that the methods are actually giving correct values for echo, since no other reliable independent methods exist for comparison checks. Yet such checks are imperative if one is to have some confidence in the results. To this end we chose as a check case the planar array sketched in Fig. 50. It contains 841 resonant dipoles interlaced into a periodic structure with average spacings between nearest neighbors of approximately  $0.57\lambda$ . By the technique developed by Munk [60] scattering from such an array can be readily obtained under the assumption of no edge effects, i.e., the array is considered to be a section of an infinite array. Using Munk's technique and SOR (with  $\omega = 0.4$ ) we have calculated the bistatic cross section at the specular angle ( $\theta_r = 180^\circ - \theta_i$ ) for three different incidence angles ( $\theta_i = 90^\circ, 60^\circ, 30^\circ$ ) in the y-z plane. The resulting values of the cross section  $\sigma$  vs iteration order are shown for the three angles, respectively, in Figs. 51-53. In all cases these values obtained by SOR agree very well with Munk's results, the greatest discrepancy ( $-0.45$  dB) appearing at the  $\theta_i = 30^\circ$  incidence angle. This disagreement is thought to be inherent in the Munk solution for angles close to grazing.

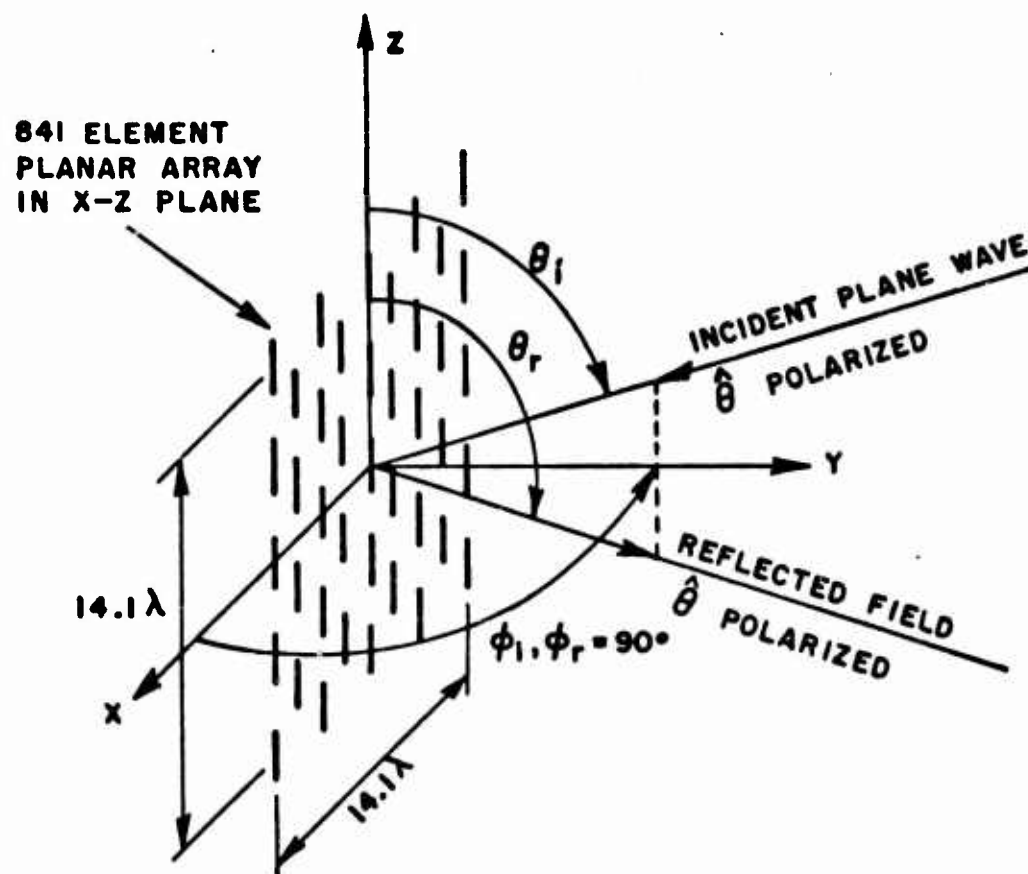


Figure 50. A planar array of resonant wires used as a check case.

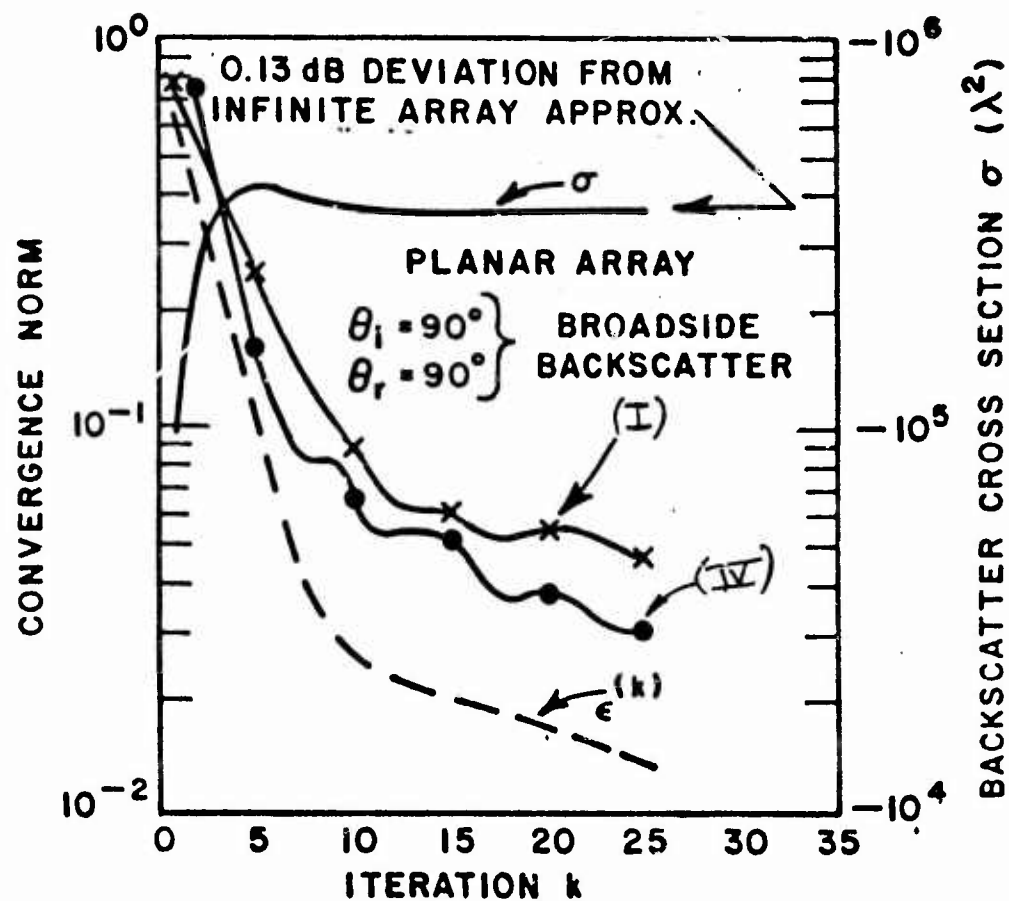


Figure 51. Broadside backscatter and comparison of convergence norms (I),  $\epsilon^{(k)}$  and (IV) versus iteration  $k$  for the periodic array of Fig. 50 using SOR with  $\omega = 0.4$ .

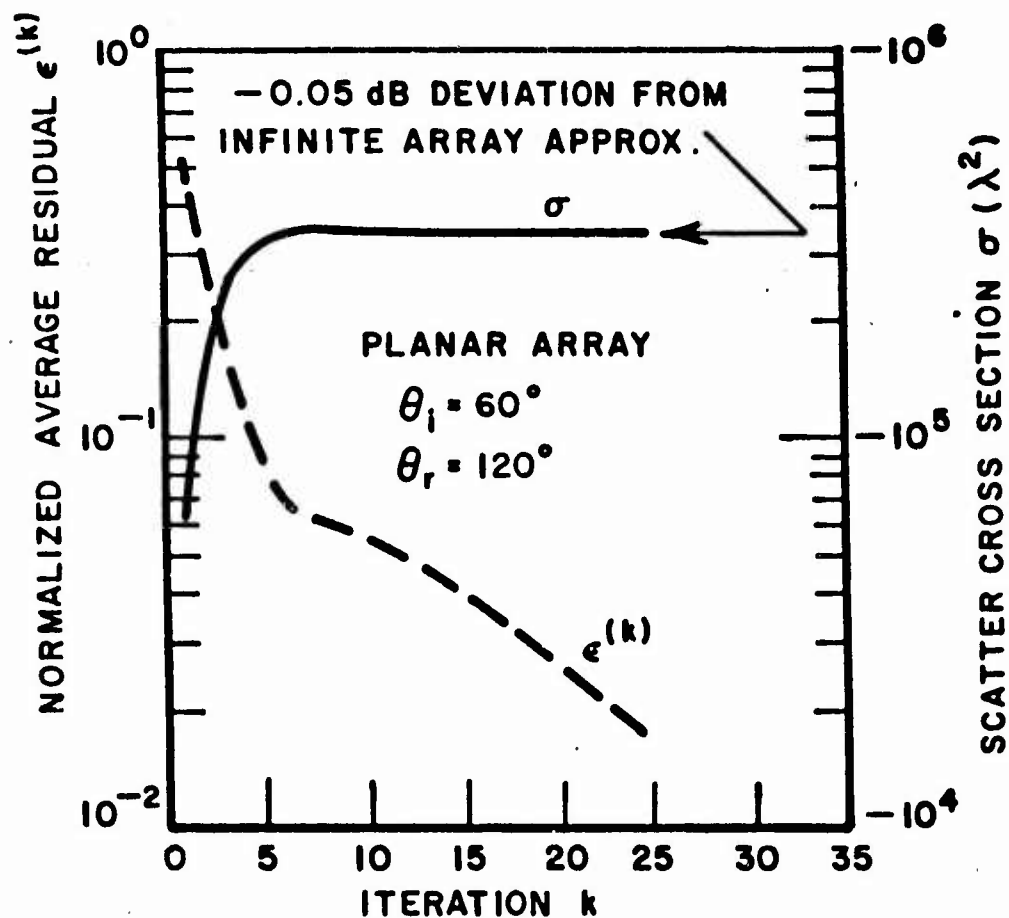


Figure 52. Specular bistatic cross section ( $\beta = 60^\circ$ ) and  $\epsilon(k)$  versus iteration  $k$  for periodic array of Fig. 50 using SOR with  $\omega = 0.4$ .

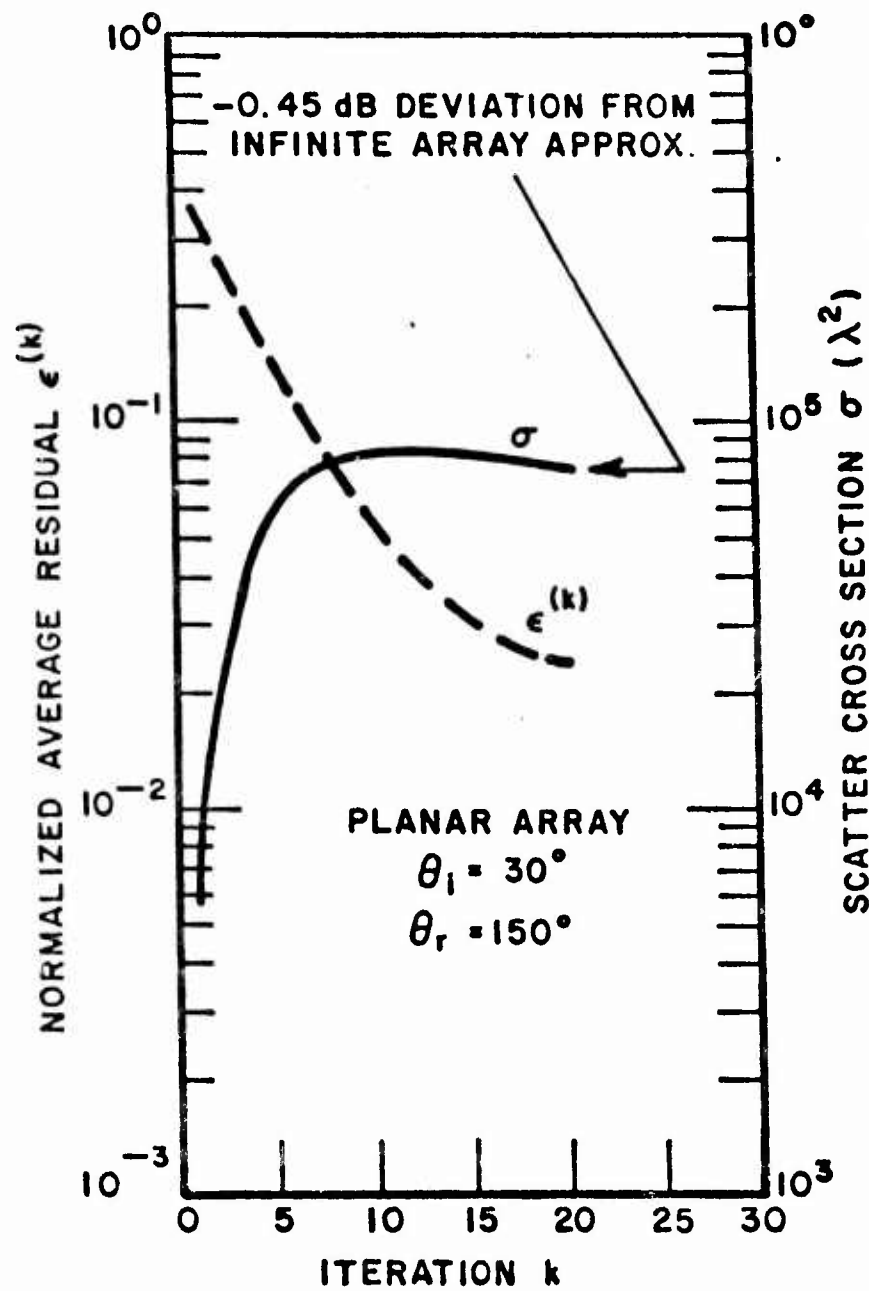


Figure 53. Specular bistatic cross section ( $\beta = 120^\circ$ ) and  $\epsilon(k)$  versus iteration  $k$  for periodic array of Fig. 50 using SOR with  $\omega = 0.4$ .

In Figs. 51-53 certain "convergence norms" are also computed for each iterate  $k$  and displayed for comparison as quantitative measures of convergence. Four different norms appear in various figures of this section; three are based on the residuals  $r^{(k)}$  defined by Eq. (50) and one is based on normed changes in solution  $x^{(k)}$  similar to that defined by Eq. (52). A summary of these convergence norms is presented in the following table.

TABLE 6  
CONVERGENCE NORM DEFINITIONS

Norms* based on $r^{(x)}$			Norm based on $x^{(k)}$
(I)	(II)	(III)	(IV)
$\frac{\ r^{(k)}\ _{\infty}}{\ b\ _{\infty}}$	$\text{Max}_i \frac{ r_i^{(k)} }{ b_i }$	$\frac{\ r^{(k)}\ _1}{N\ b\ _{\infty}} \equiv \epsilon^{(k)}$	$\text{Max}_i \frac{ x_i^{(k)} - x_i^{(k-1)} }{\min\{ x_i^{(k)} ,  x_i^{(k-1)} \}}$

\*See Appendix C of Ref. 38 for definitions of vector norms used.

The (I) and (IV) norms in this table were chosen strictly as representatives of the quantities appearing in Eqs. (51) and (52) while the (II) and (III) norms were defined with the physical problem in mind, i.e., (II) is a normalized measure of the residual indicating the boundary condition ( $E_{\text{TAN}} = 0$ ) mismatch on one dipole in the array and (III) is a normalized average of all residuals for the whole array. The (III) norm will be denoted by  $\epsilon^{(k)}$  in all data presented in this section. Two points should be made here. One is that the  $\epsilon^{(k)}$  norm appears in all cases we have calculated to be the best balanced and most trustworthy; the other is that the behavior of  $\epsilon^{(k)}$  appears no different for random arrays of dipoles than it does for the periodic array. Since the results in cross section were very satisfactory for the periodic array, we infer that the similar behavior of  $\epsilon^{(k)}$  implies satisfactory results in cross section for the random arrays.

Very little information is found in the literature on suitable choices for SOR convergence measures for large complex system of equations such as those treated here. The convergence norm calculations are presented for the purpose of empirically determining just such a measure for these types of problems, e.g., one which might eventually be included in the computer programs to indicate a reliable stopping point in the iterative process. The normalized average residual  $\epsilon^{(k)}$  appears to possess



the uniform characteristics needed for this job. It also has the interpretation of being a measure of the "average" boundary condition  $E_{TAN} = 0$  over the whole array. Other norms considered do not appear to indicate this same overall condition of the iterated solution but, tend to pin-point specific residuals or changes in the solution which, to a great extent, do not seriously affect the array scattering properties in the far field. Other "averaging" norms might do as well or better than  $\epsilon(k)$ ; however, this study has concentrated on isolating only this one case which seems to be well suited for these types of problems.

No attempts were made in this study to determine optimum relaxation factors for SOR. An initial choice of  $\omega$  was made at the outset of each new problem and if convergence was indicated, no changes were made; the exception is Fig. 67, where changes were made during the same iteration run with little observable effect.

#### SOR Solutions for Scattering by Large Clouds of Chaff Elements

The SOR iteration technique is used to solve Eq. (12b) for the currents induced in arrays of dipoles by plane wave fields of Eqs. (II-2) and (II-3). The  $\hat{\theta}$  polarized backscatter  $\sigma$  and bistatic cross section for certain bistatic angles ( $\beta = \pm 10^\circ$  range) are calculated from these currents at each step  $k$  of the iteration.

Figure 54 considers an initial case of 100 dipoles in the random array configuration. The SOR technique ( $\omega = 0.6$ ) can be compared to solution by a direct method (Cholesky); resulting solutions from both methods agree quite well ( $< 0.1$  dB). This figure also includes calculated values for the four norms appearing in Table 6. The (II) and (IV) norms vary erratically, although both show overall decreases over the range of  $k$ . The (I) norm and  $\epsilon(k)$  both show a consistent decrease, but only  $\epsilon(k)$  is "monotonic" over the whole range.

Convergence characteristics of  $\sigma$  for a 500 dipole random array are indicated in Fig. 55 for SOR iteration using two values of relaxation factor,  $\omega=0.5$  and  $\omega=0.4$ . Only  $\epsilon(k)$  was calculated in this case. The  $\omega=0.5$  case appears to converge faster (steeper slope on  $\epsilon(k)$ ) in the early stages ( $k = 1$  to  $k \approx 20$ ), however better overall convergence was obtained for  $\omega=0.4$ . Figure 56 shows a sample of the bistatic cross section pattern for  $k = 10, 20$  and  $36$ . This figure indicates the degree of convergence obtained in this  $\beta = \pm 10^\circ$  sector at the corresponding stage in the iteration. The convergence of the

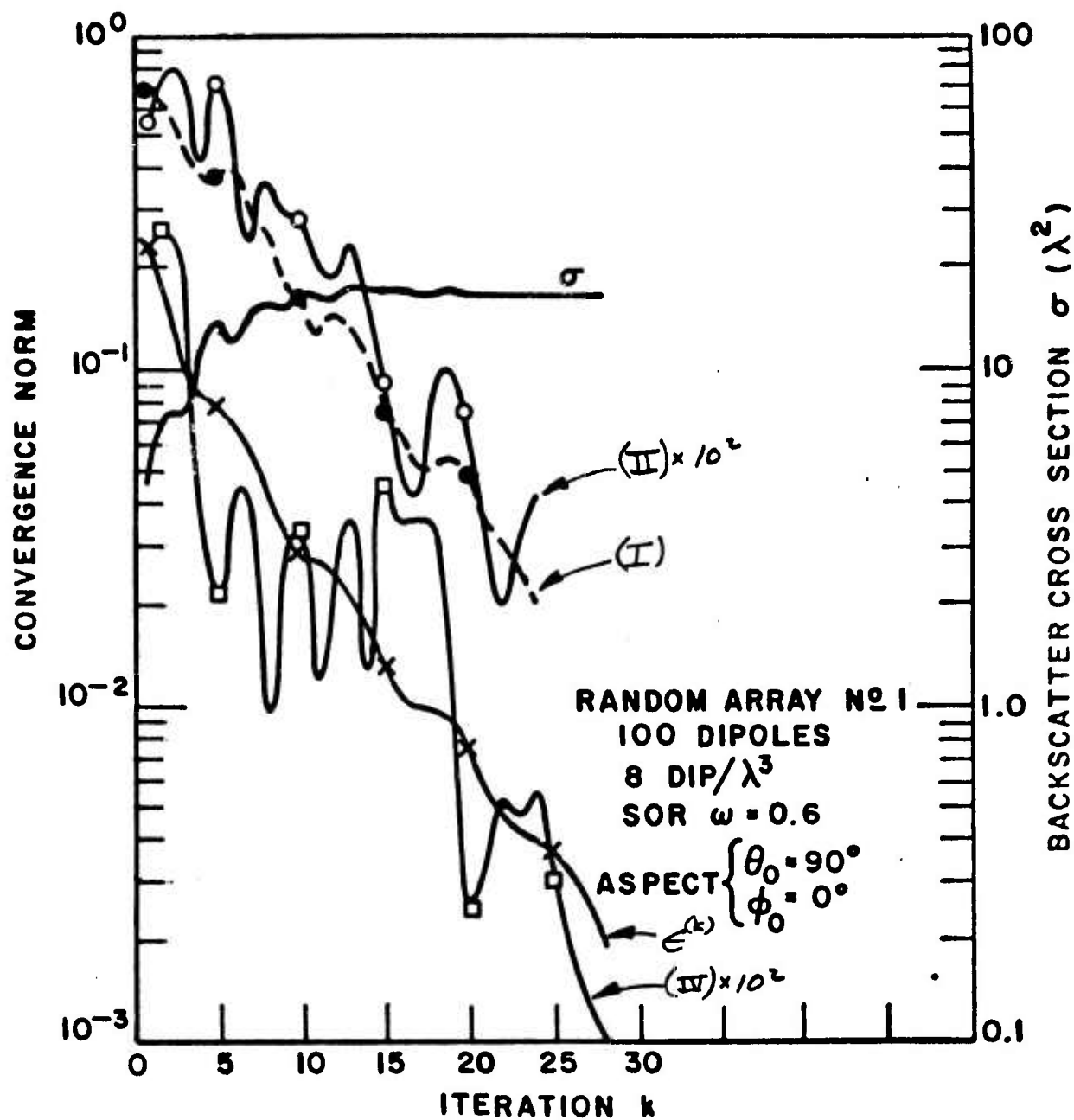


Figure 54. Backscatter cross section and convergence norms (I), (II),  $\epsilon^{(k)}$  and (IV) versus iteration  $k$  for 100 dipole random array using SOR with  $\omega = 0.6$ .

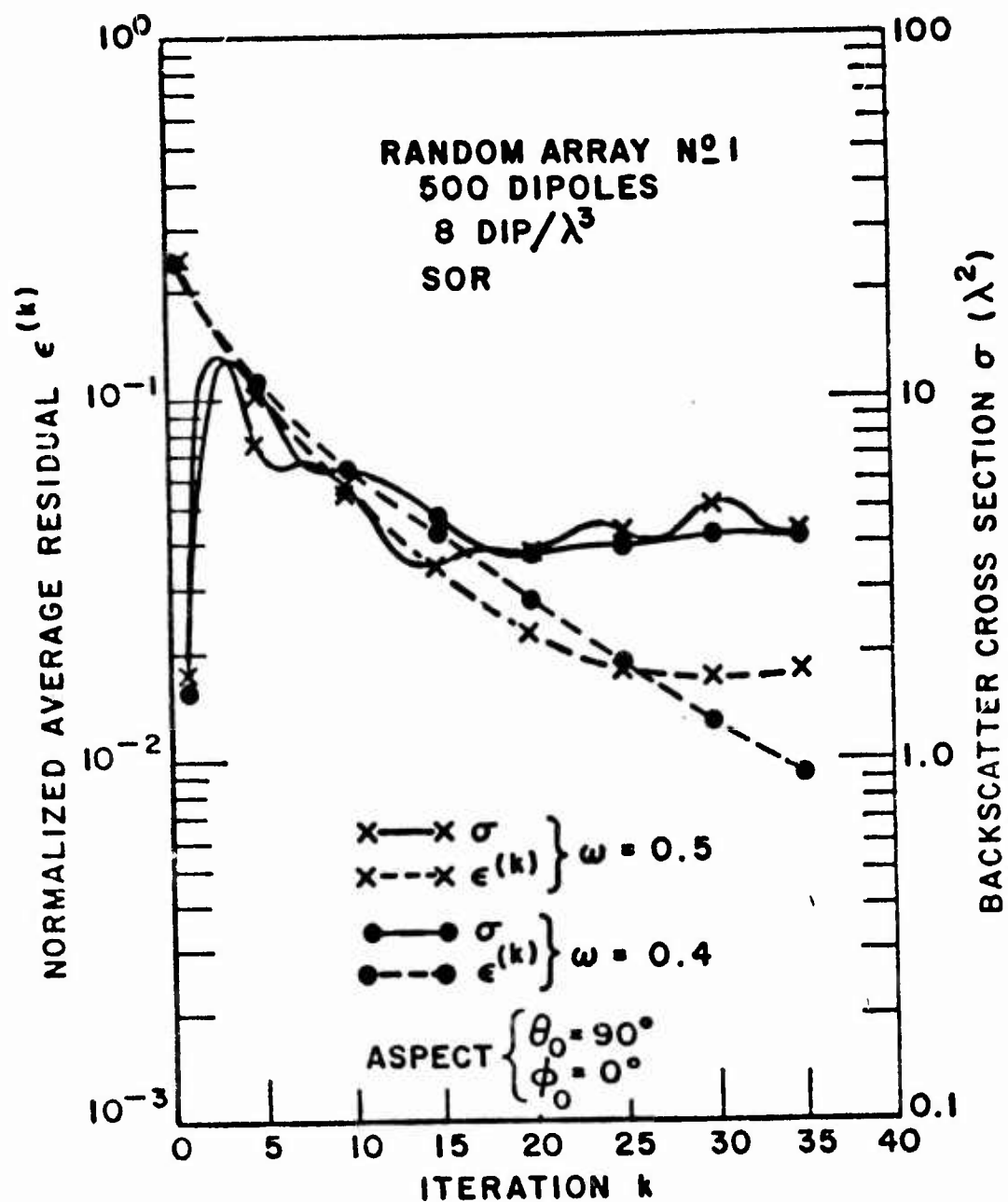


Figure 55. Backscatter cross section and  $\epsilon(k)$  versus iteration  $k$  for 500 dipole random array (8 dip/ $\lambda^3$ ) using SOR with  $\omega = 0.4$  and  $\omega = 0.5$ .

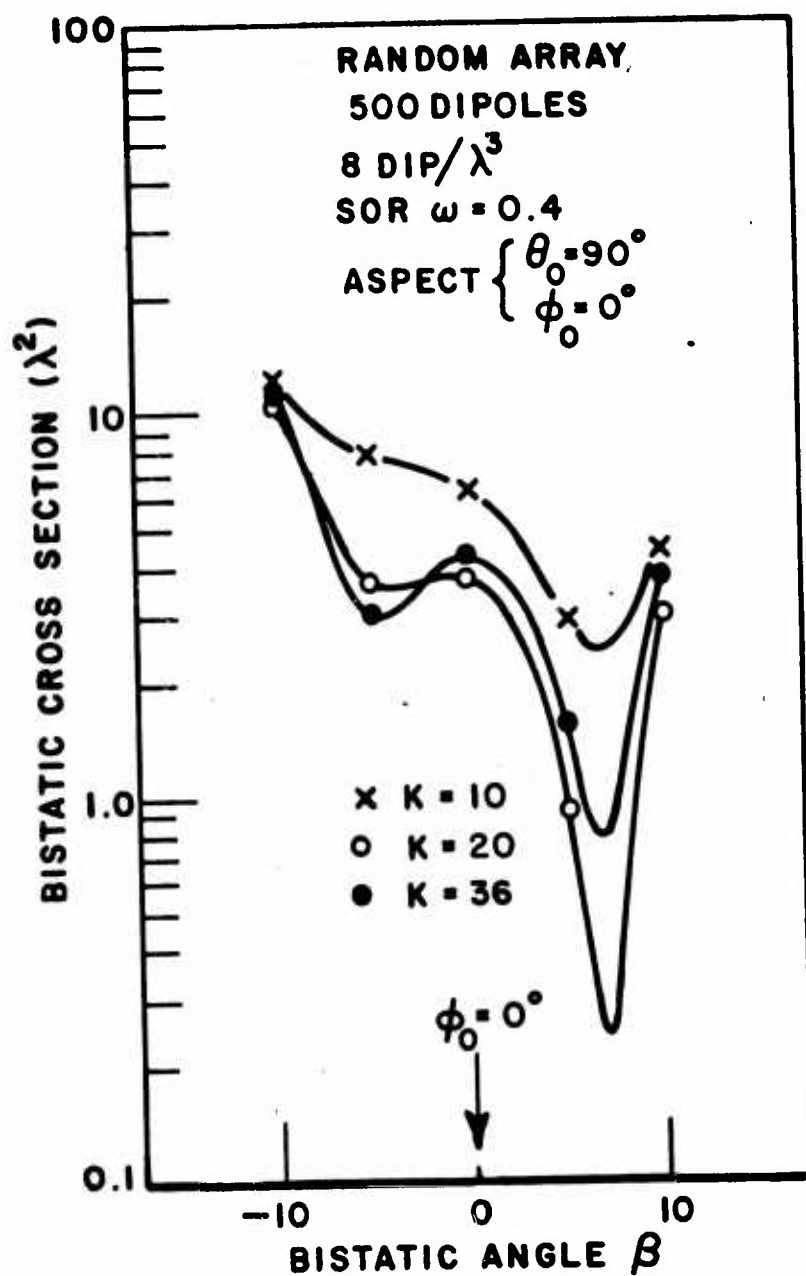


Figure 56. Bistatic cross section pattern for 500 dipole random array for  $k = 10, 20$  and  $36$  using SOR with  $\omega = 0.4$ .

bistatic pattern seems to be best in the larger amplitudes and for  $k > 20$ , major changes occur only in the null regions.

Figure 57 is the first of a series of 10 figures showing five SOR iterated solutions ( $\omega=0.4$ ) for a single 1000 dipole random array (#1). These figures alternately show  $\sigma$  backscatter and bistatic cross section for five aspect angles of the incident wave. Each of these cases corresponds to a new "b" vector for the right hand side of Eq. (12b).

Figure 57 indicates convergence of  $\sigma$  backscatter and shows a comparison of the (I) norm and  $\epsilon(k)$  for  $\theta_0 = 90^\circ$ ,  $\phi_0 = 0^\circ$ . The (I) norm in this case has lost all resemblance of being a monotonically decreasing norm while  $\epsilon(k)$  continues to show a smooth decrease with increasing  $k$ . The curve for  $\sigma$  backscatter in this case converges smoothly to the value  $\sigma \approx 90\lambda^2$ , a rather high value for these random arrays. Figure 58 displays a portion of the bistatic pattern ( $\beta=\pm 10^\circ$ ). Here, the amplitude changes on the peak are less than 1 dB for  $k > 5$ , while the null depth changes are more than 10 dB over this same interval.

Figure 59 considers a new aspect angle ( $\theta_0=90^\circ$ ,  $\phi_0 = 10^\circ$ ) for the same random array. Here,  $\sigma$  backscatter shows somewhat irregular convergence as compared to the previous aspect; however, the same smooth decrease in  $\epsilon(k)$  is omnipresent. The bistatic patterns for  $k = 6, 15, 30$  and  $42$  of Fig. 60 indicate considerable change is taking place over this range. The largest changes, however, occur in the null regions and peak amplitude regions show the lesser changes.

Figures 61 and 62 indicate  $\sigma$  and bistatic patterns for  $\theta_0 = 90^\circ$ ,  $\phi_0 = 20^\circ$ . The  $\epsilon(k)$  norm in Fig. 61 again shows monotonic improvement in average residuals and Fig. 62 indicates essentially converged bistatic patterns for  $k > 15$  with changes less than 2 dB in peak amplitude and less than 3 dB in the null region. Oscillations of  $\sigma$  in Fig. 61 are less than plus or minus 1 dB and decreasing for  $k > 25$ .

Figures 63 and 64 show  $\sigma$ ,  $\epsilon(k)$  and bistatic cross section for  $\theta_0 = 90^\circ$ ,  $\phi_0 = 30^\circ$ . Fluctuations in  $\sigma$  for  $k > 16$  are less than 2 dB and  $\epsilon(k)$  is again smoothly decreasing. Bistatic patterns appear to change very little for  $k > 30$ .

Figures 65 and 66 are the last figures showing data for large random array #1 ( $\theta_0 = 90^\circ$ ,  $\phi_0 = 40^\circ$ ). Convergence norms (I) and (IV) are included in Fig. 65 with  $\epsilon(k)$ . Although, norms (I) and (IV) do not have the smooth decrease shown by  $\epsilon(k)$ , it appears that an average curve of (IV) over this range of  $k$  would repeat the trend indicated by  $\epsilon(k)$ . The oscillatory nature of  $\sigma$  backscatter is confirmed in the bistatic pattern curves of

Fig. 66. The final bistatic curve ( $k = 45$ ) is bounded by the  $k = 25$  and  $k = 35$  patterns and again, largest changes occur in the null region.

Data in the following four figures (Figs. 67-70) were calculated for a second large random array (#2) with the same average density ( $8 \text{ dip}/\lambda^3$ ) and number of dipoles ( $N = 1000$ ) as in the previous case. The new array was generated with a new initialization of the random positioning programs. The two cases considered for this new array correspond to aspect angles  $\theta_0 = 90^\circ$ ,  $\phi_0 = 0^\circ$  and  $10^\circ$ .

Figure 67 shows  $\sigma$  and  $\epsilon^{(k)}$  data calculated for  $\theta_0 = 90^\circ$ ,  $\phi_0 = 0^\circ$  case and Fig. 68 presents the corresponding bistatic patterns. Four values of relaxation factor ( $\omega = 0.4, 0.35, 0.3$  and  $0.25$ ) were used in this case with the initial iteration performed with  $\omega = 0.4$ . The results for  $\omega = 0.4$  are indicated in Fig. 67 by the marginally convergent curve. The iteration was then restarted ( $k = 1$ ) with  $\omega = 0.35$  and continued through  $k = 12$ ; at which time,  $\omega$  was changed and the iteration carried out to  $k = 30$  for  $\omega = 0.3$ ; then  $\omega$  was again changed this time to  $\omega = 0.25$  and the process carried out to the final iteration  $k = 61$ . The reason for changing  $\omega$  during the same iteration run was an attempt to isolate variations, if any, in  $\epsilon^{(k)}$  which might correspond to different values of  $\omega$ . No recognizable changes were noted; in fact, the iteration appeared to be converged for all  $k > 30$  ( $\omega = 0.3, 0.25$ ) and the bistatic patterns in Fig. 68 confirm this to a great extent.

A second aspect angle ( $\theta_0 = 90^\circ$ ,  $\phi_0 = 10^\circ$ ) is considered in Figs. 69 and 70. Here, SOR was restarted three times for random array #2 with  $\omega = 0.3, 0.25$  and  $0.2$ . The two cases  $\omega = 0.3$  and  $0.25$  were not convergent as Fig. 69 shows and  $\omega$  had to be reduced to  $\omega = 0.2$  to obtain the one convergent case indicated in the figure. Figure 70 shows bistatic patterns for  $k = 20, 30$  and  $36$  for the converging case. The largest changes in these patterns again occur in the null regions.

Three additional figures are included in this section (Figs. 71, 72, and 73) comparing convergence characteristics of  $\sigma$  backscatter,  $\langle \sigma \rangle$  (the bistatic cross section average over  $\beta = \pm 10^\circ$ ) and  $\sigma_T$  (total scatter cross section from the forward scattering theorem reviewed in Appendix K). Figure 71 presents  $\sigma_T$  and  $\langle \sigma \rangle$  with the  $\sigma$  curve previously calculated in Fig. 57. The bistatic average  $\langle \sigma \rangle$  in this case shows little, if any, improvement over the original  $\sigma$  curve; however,  $\sigma_T$  is converged as early as  $k = 5$ . The rapid convergence of  $\sigma_T$  indicates that apparently the total power scattered in all directions by the random array is insensitive to the computed currents, compared to either  $\sigma$  or  $\langle \sigma \rangle$ .



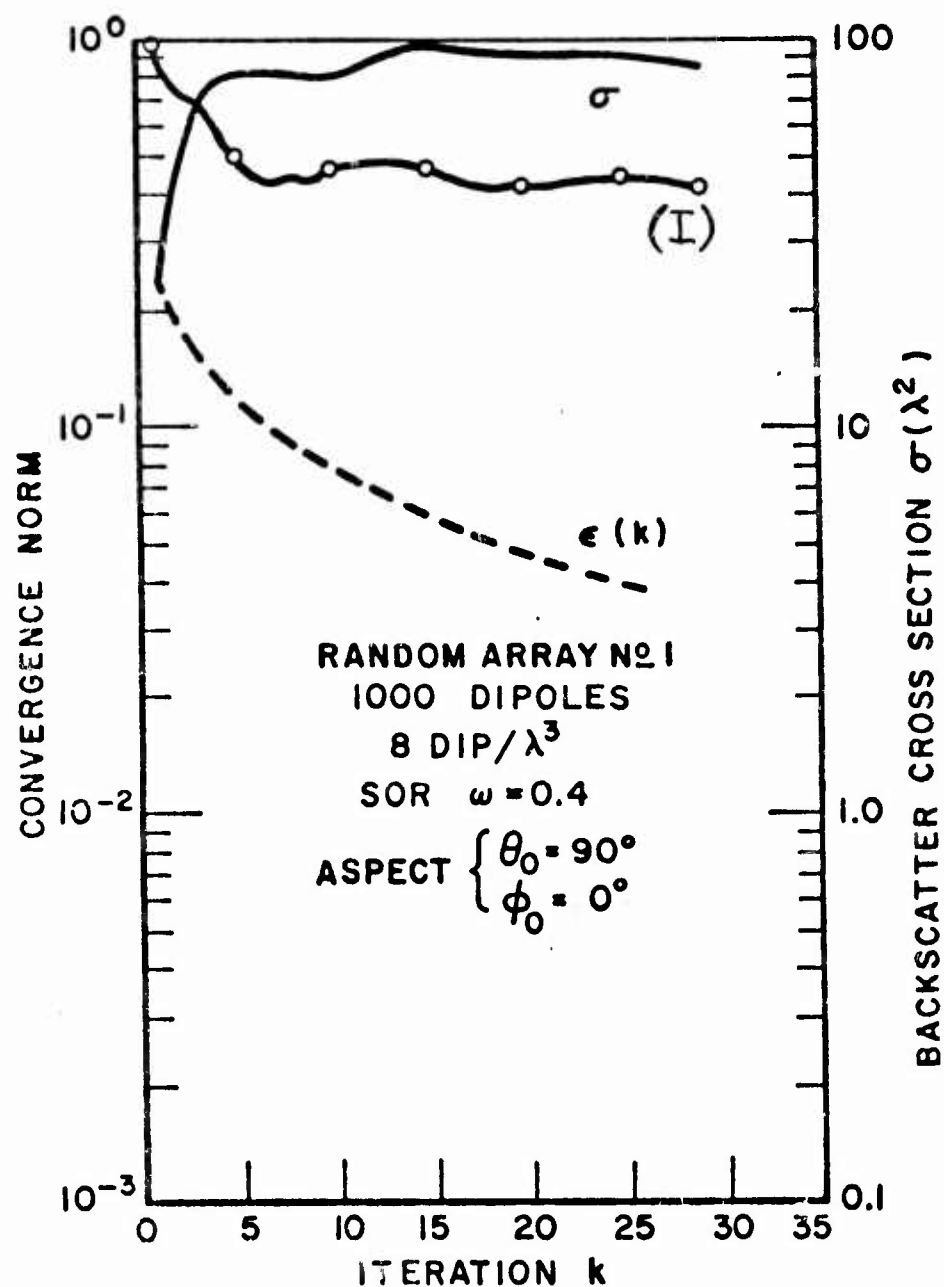


Figure 57, Backscatter cross section and convergence norms (I) and  $\epsilon(k)$  versus iteration  $k$  for 1000 dipole random array #1 ( $\theta_0=90^\circ$ ,  $\phi_0=0^\circ$ ) using SOR with  $\omega = 0.4$ .

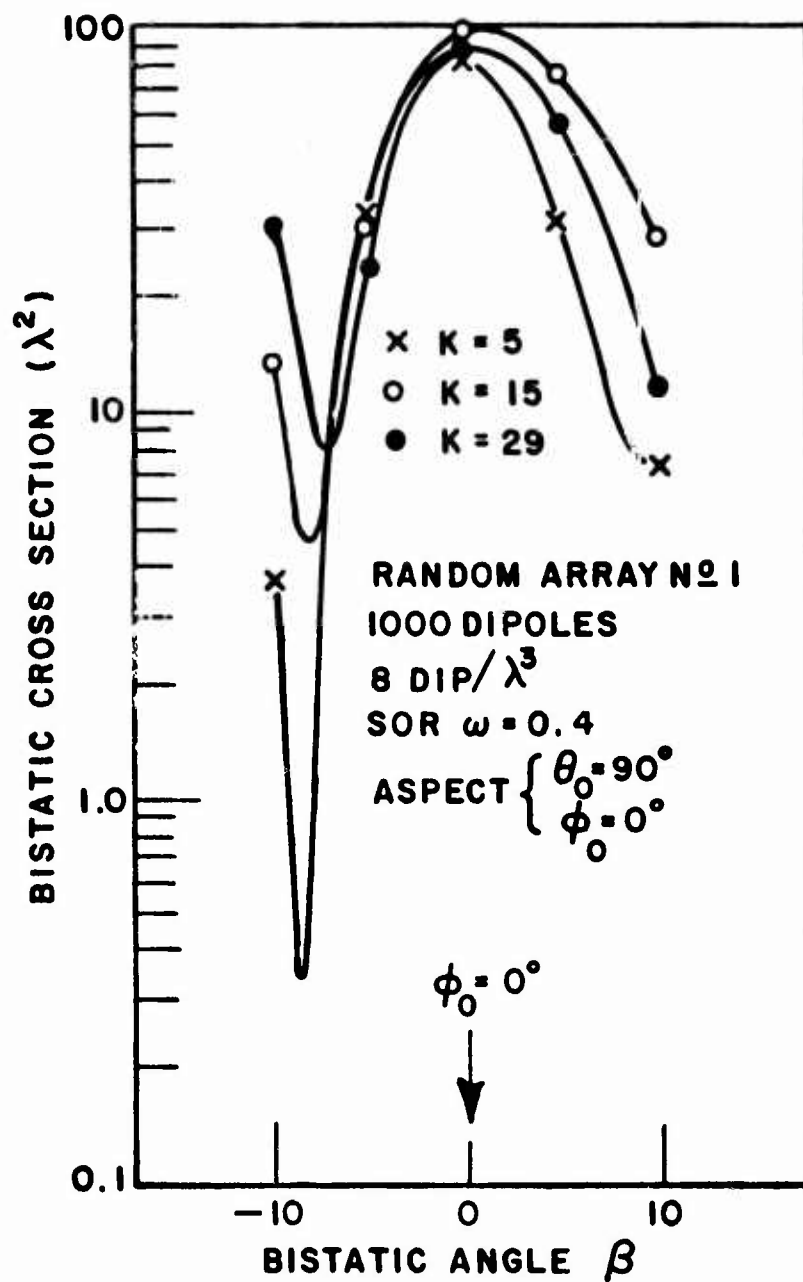


Figure 58. Bistatic cross section pattern for 1000 dipole random array #1 ( $\theta_0 = 90^\circ$ ,  $\phi_0 = 0^\circ$ ) at  $k = 5, 15$  and  $29$  using SOR with  $\omega = 0.4$ .

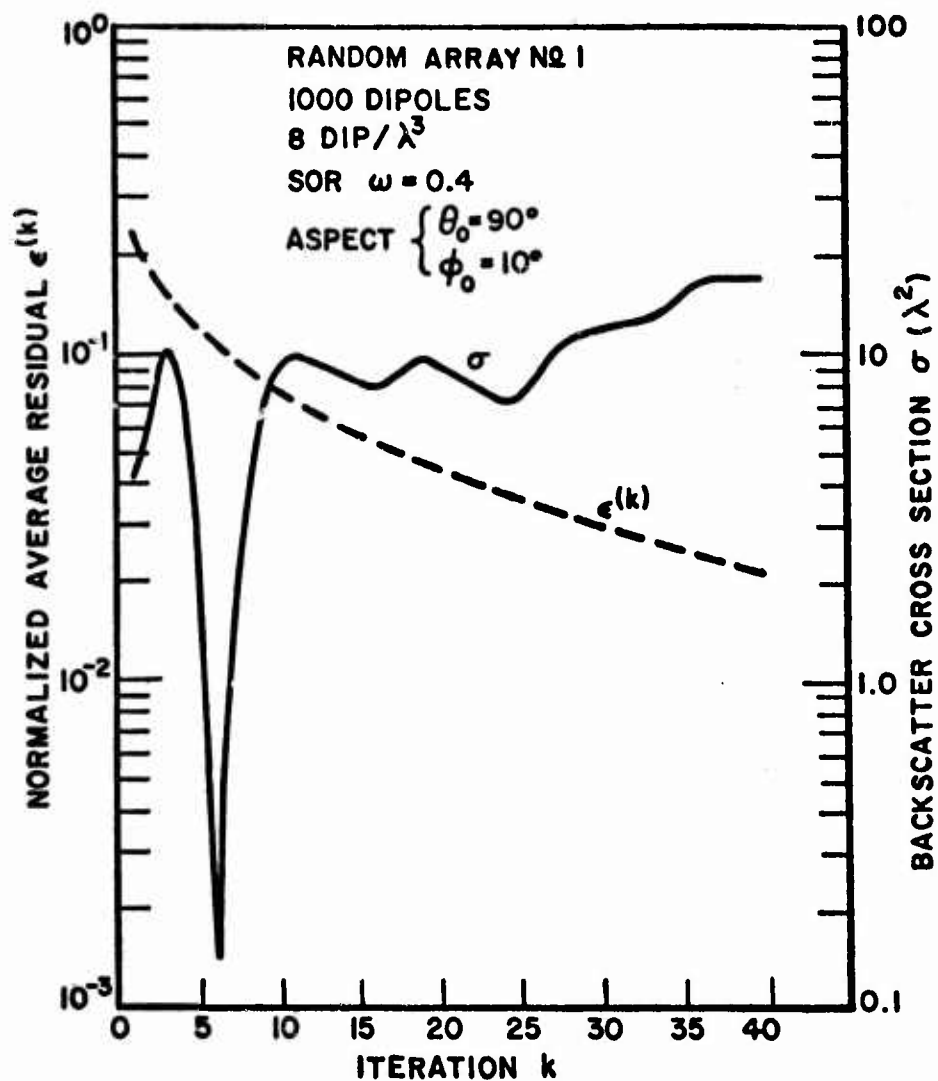


Figure 59, Backscatter cross section and  $\epsilon(k)$  versus iteration k for 1000 dipole random array #1 ( $\theta_0 = 90^\circ$ ,  $\phi_0 = 10^\circ$ ) using SOR with  $\omega = 0.4$ .

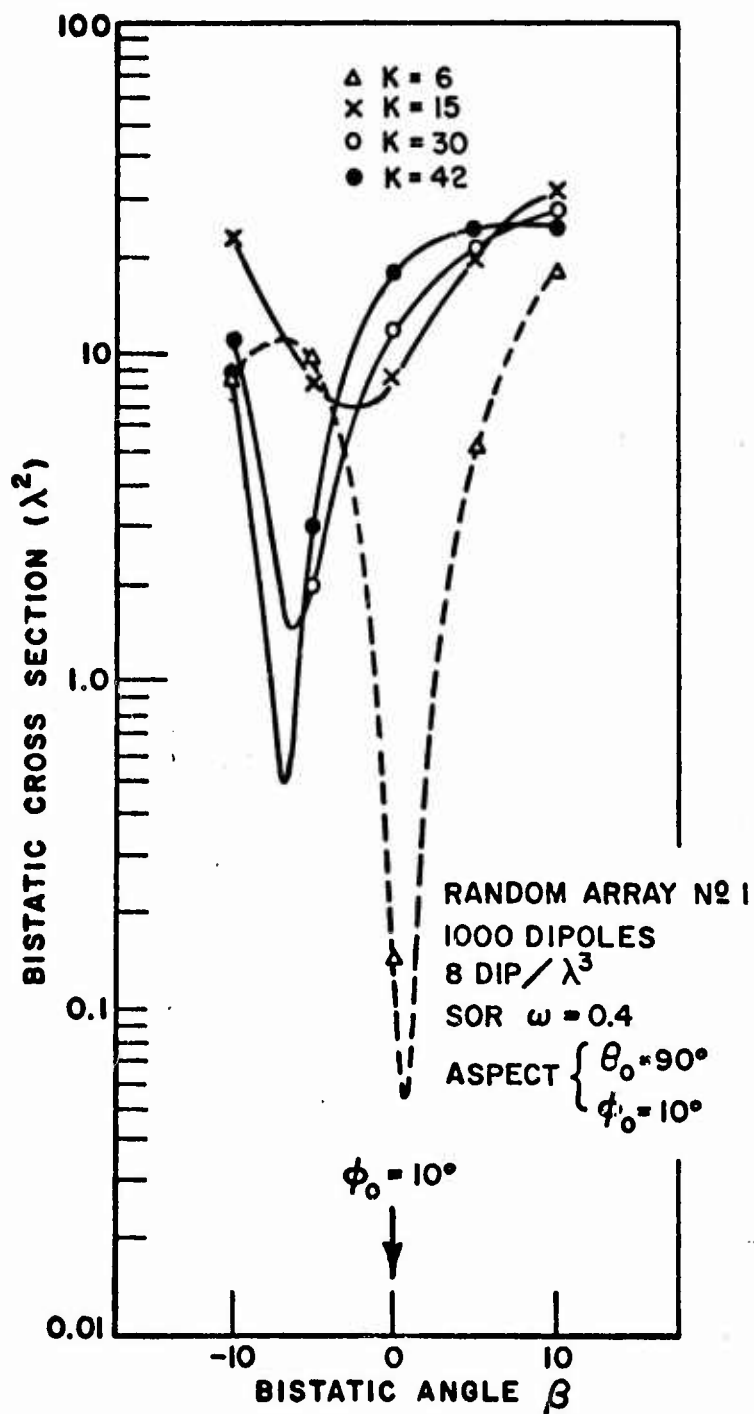


Figure 60. Bistatic cross section pattern for 1000 dipole random array #1 ( $\theta_0 = 90^\circ$ ,  $\phi_0 = 10^\circ$ ) at  $k = 6, 15, 30$  and  $42$  using SOR with  $\omega = 0.4$ .

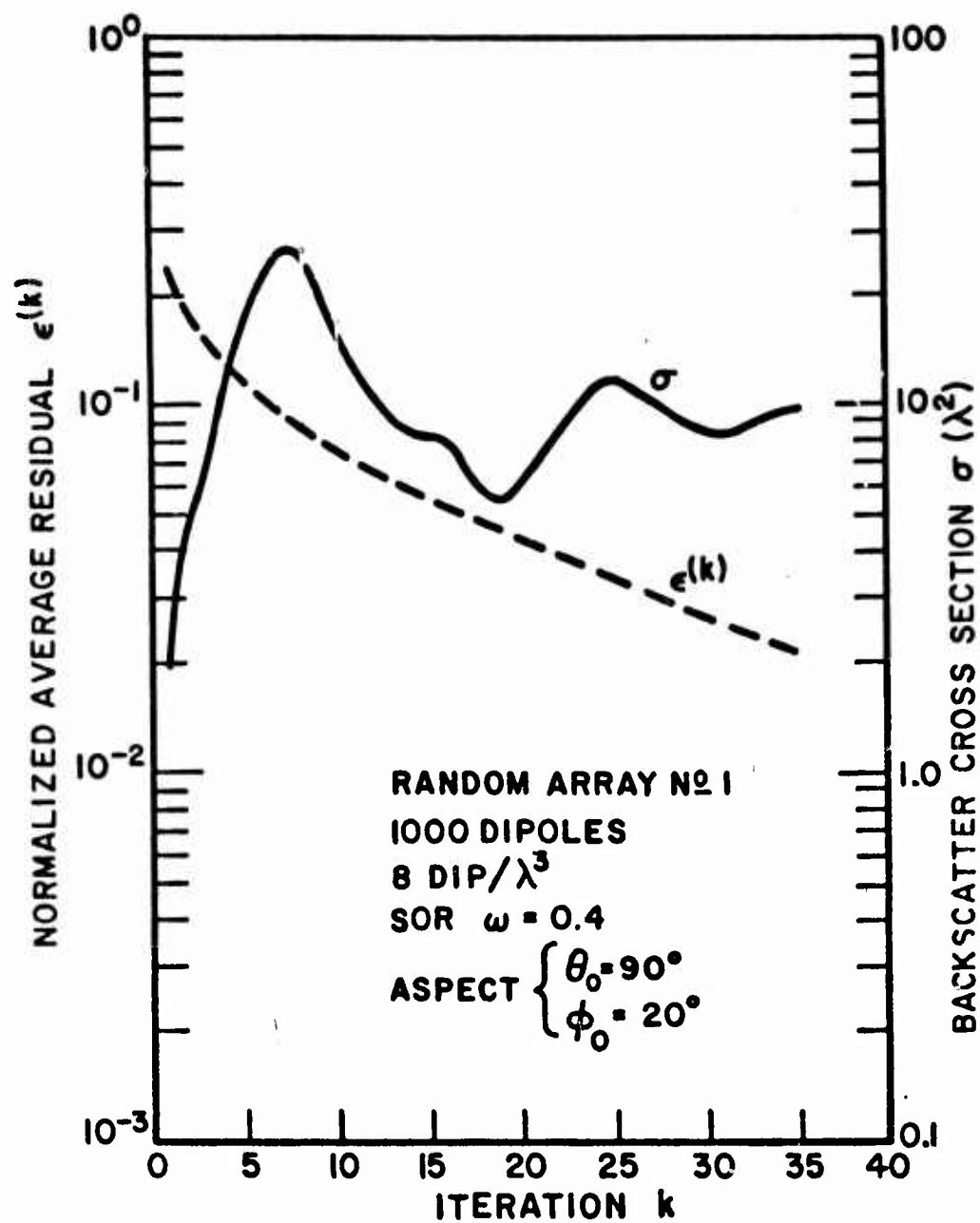


Figure 61. Backscatter cross section and  $\epsilon^{(k)}$  versus iteration  $k$  for 1000 dipole random array #1 ( $\theta_0 = 90^\circ$ ,  $\phi_0 = 20^\circ$ ) using SOR with  $\omega = 0.4$ .

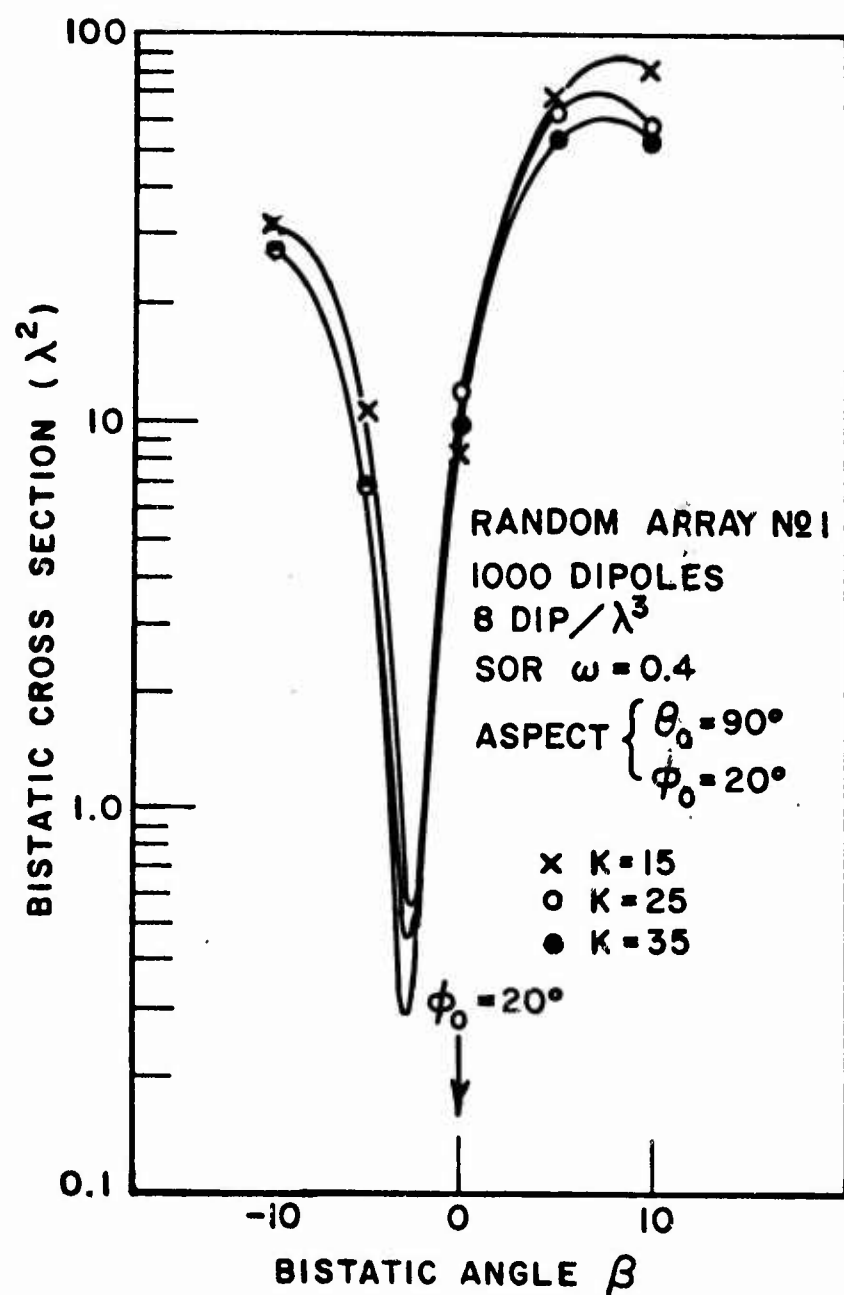


Figure 62. Bistatic cross section pattern for 1000 dipole random array #1 ( $\theta_0 = 90^\circ$ ,  $\phi_0 = 20^\circ$ ) at  $k = 15$ , 25 and 35 using SOR with  $\omega = 0.4$ .



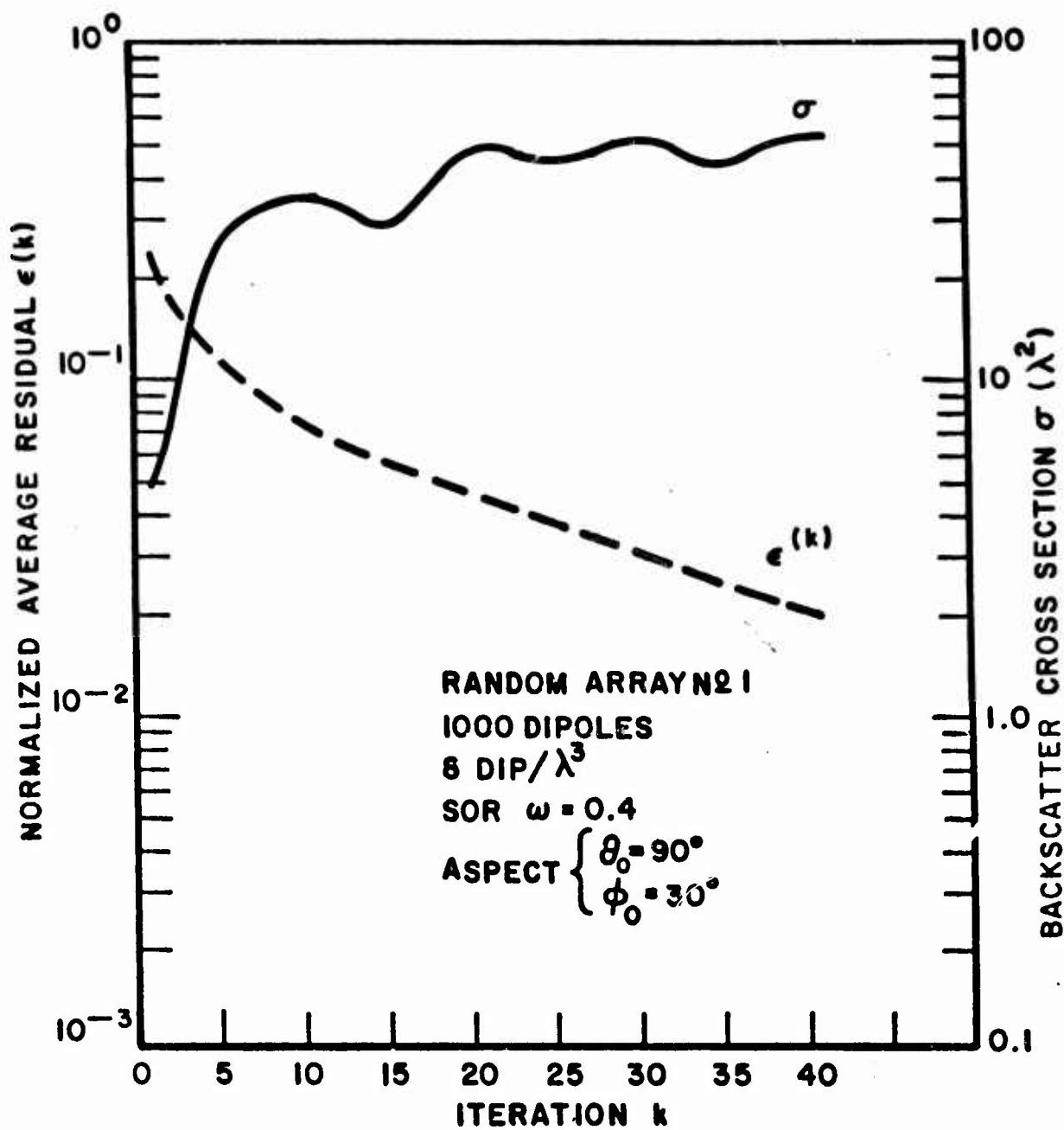


Figure 63. Backscatter cross section and  $\epsilon(k)$  versus iteration  $k$  for 1000 dipole random array #1 ( $\theta_0 = 90^\circ$ ,  $\phi_0 = 30^\circ$ ) using SOR with  $\omega = 0.4$ .

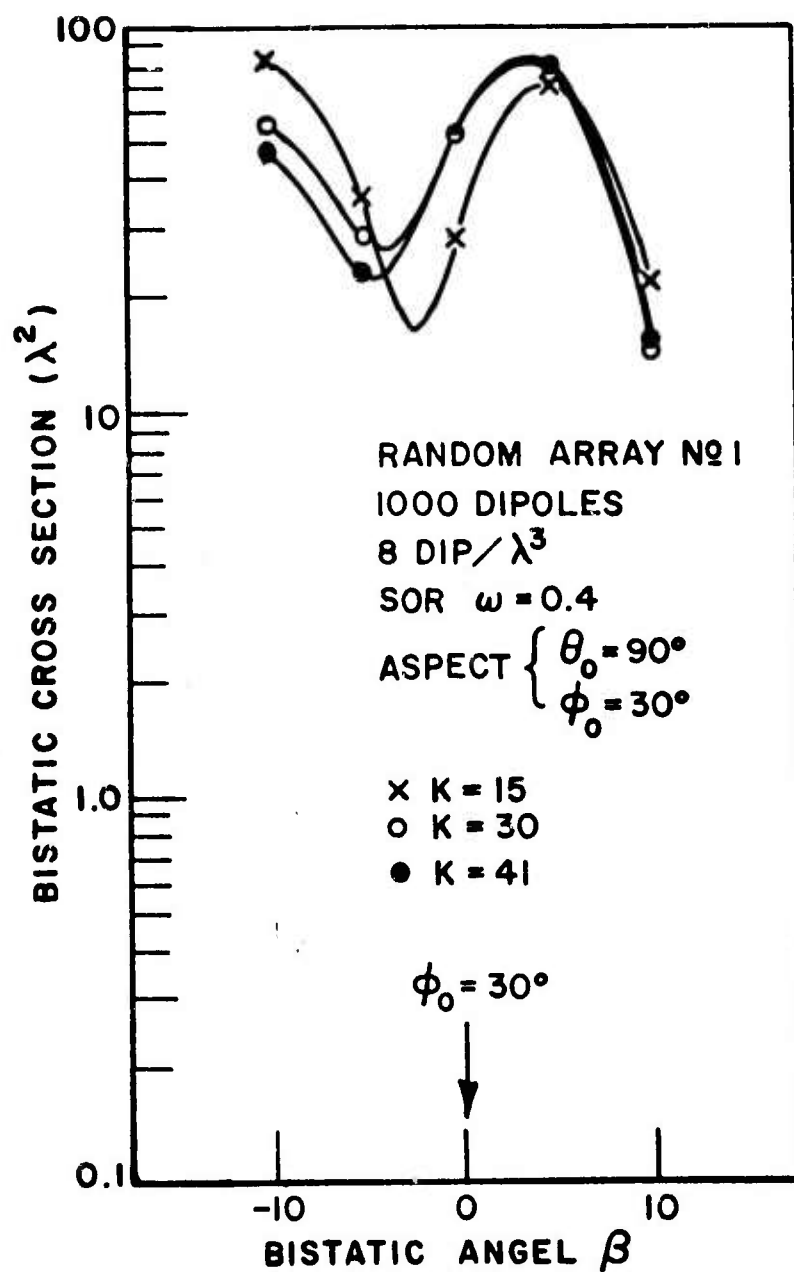


Figure 64. Bistatic cross section pattern for 1000 dipole random array #1 ( $\theta_0 = 90^\circ$ ,  $\phi_0 = 30^\circ$ ) at  $k = 15$ , 30 and 41 using SOR with  $\omega = 0.4$ .

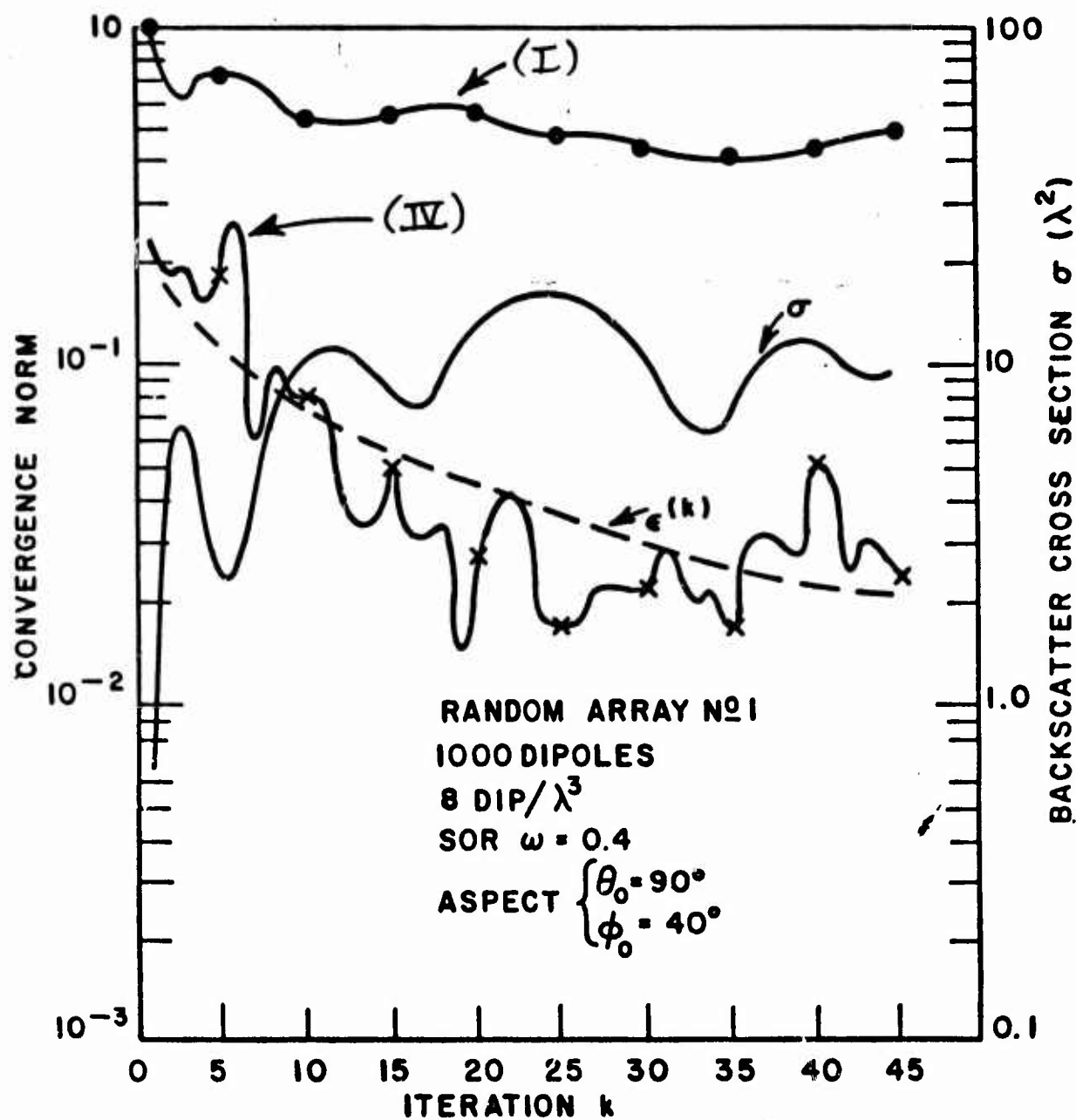


Figure 65. Backscatter cross section and convergence norms (I),  $\epsilon(k)$  and (IV) versus iteration  $k$  for 1000 dipole random array #1 ( $\theta_0=90^\circ$ ,  $\phi_0=40^\circ$ ) using SOR with  $\omega=0.4$ .

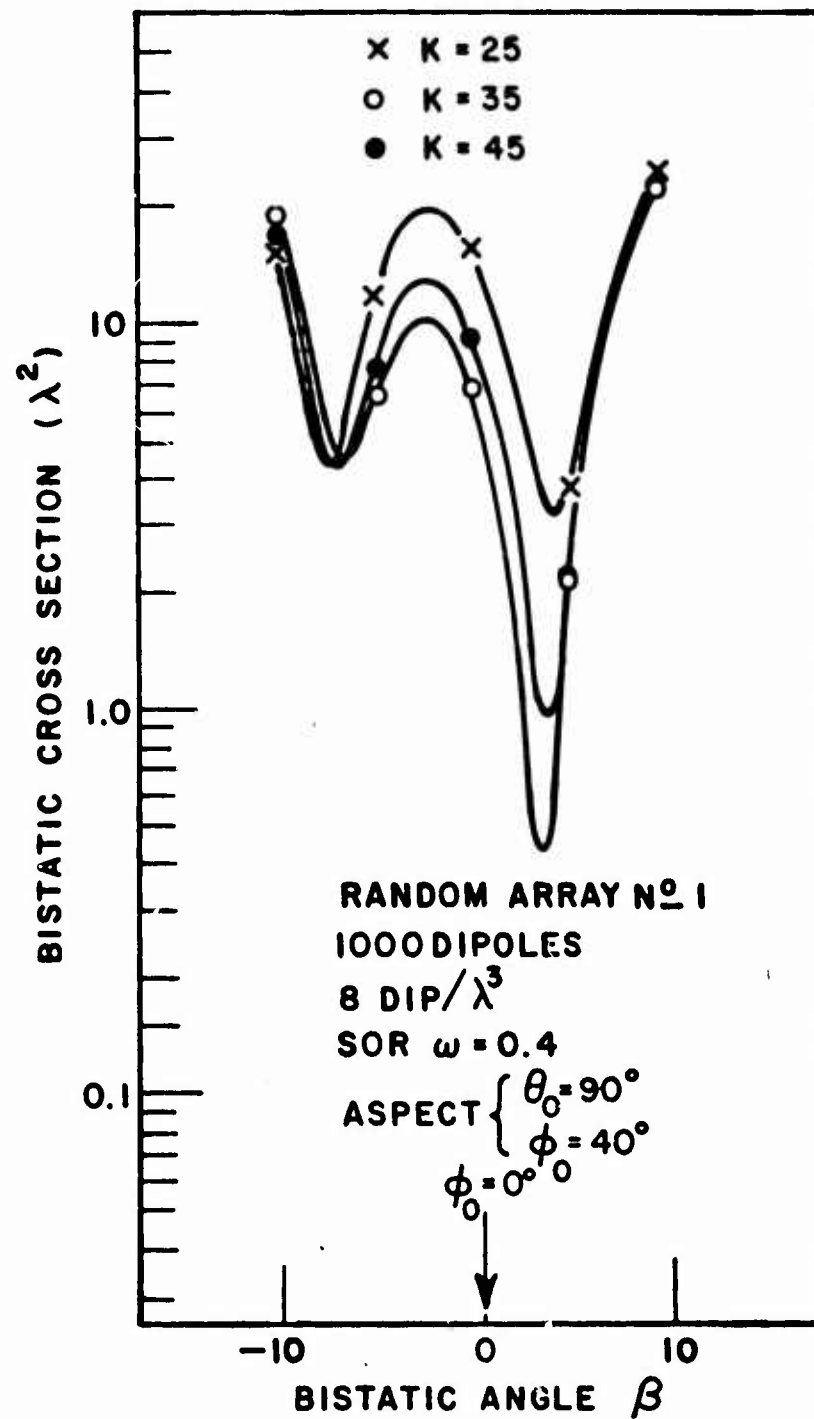


Figure 66. Bistatic cross section pattern for 1000 dipole random array #1 ( $\theta_0 = 90^\circ$ ,  $\phi_0 = 40^\circ$ ) at  $k = 25, 35$  and  $45$  using SOR with  $\omega = 0.4$ .

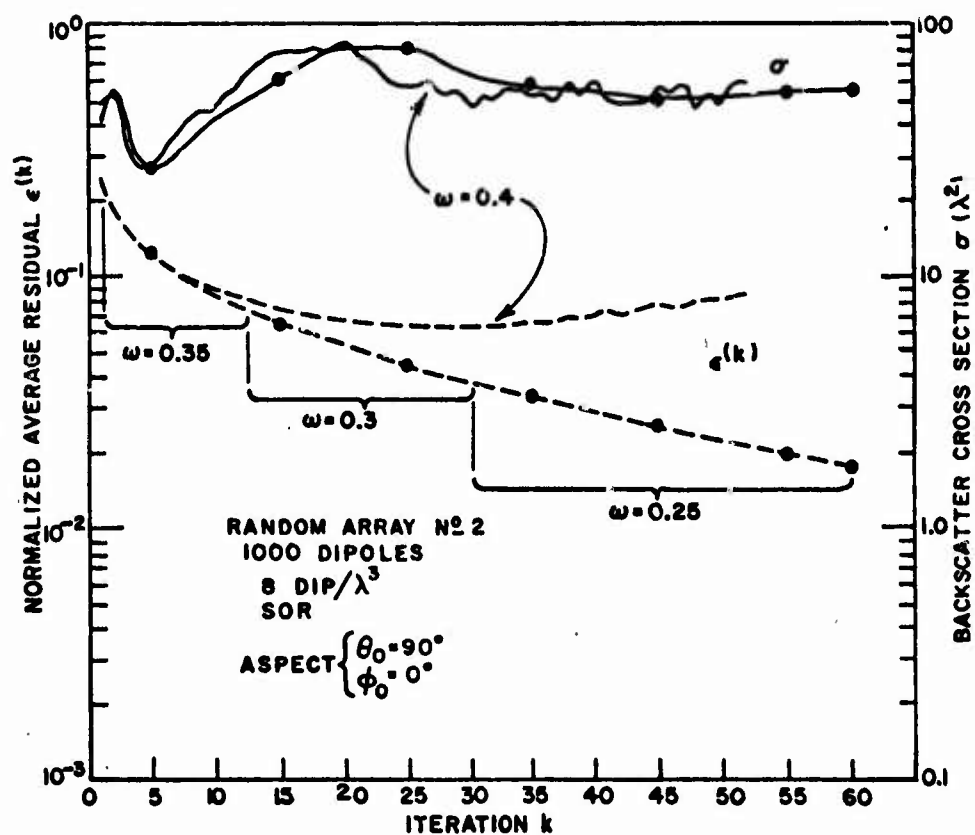


Figure 67. Backscatter cross section and  $\epsilon(k)$  versus iteration  $k$  for 1000 dipole random array #2 ( $\theta_0 = 90^\circ$ ,  $\phi_0 = 0^\circ$ ) using SOR with  $\omega = 0.25, 0.3, 0.35$  and  $0.4$ .

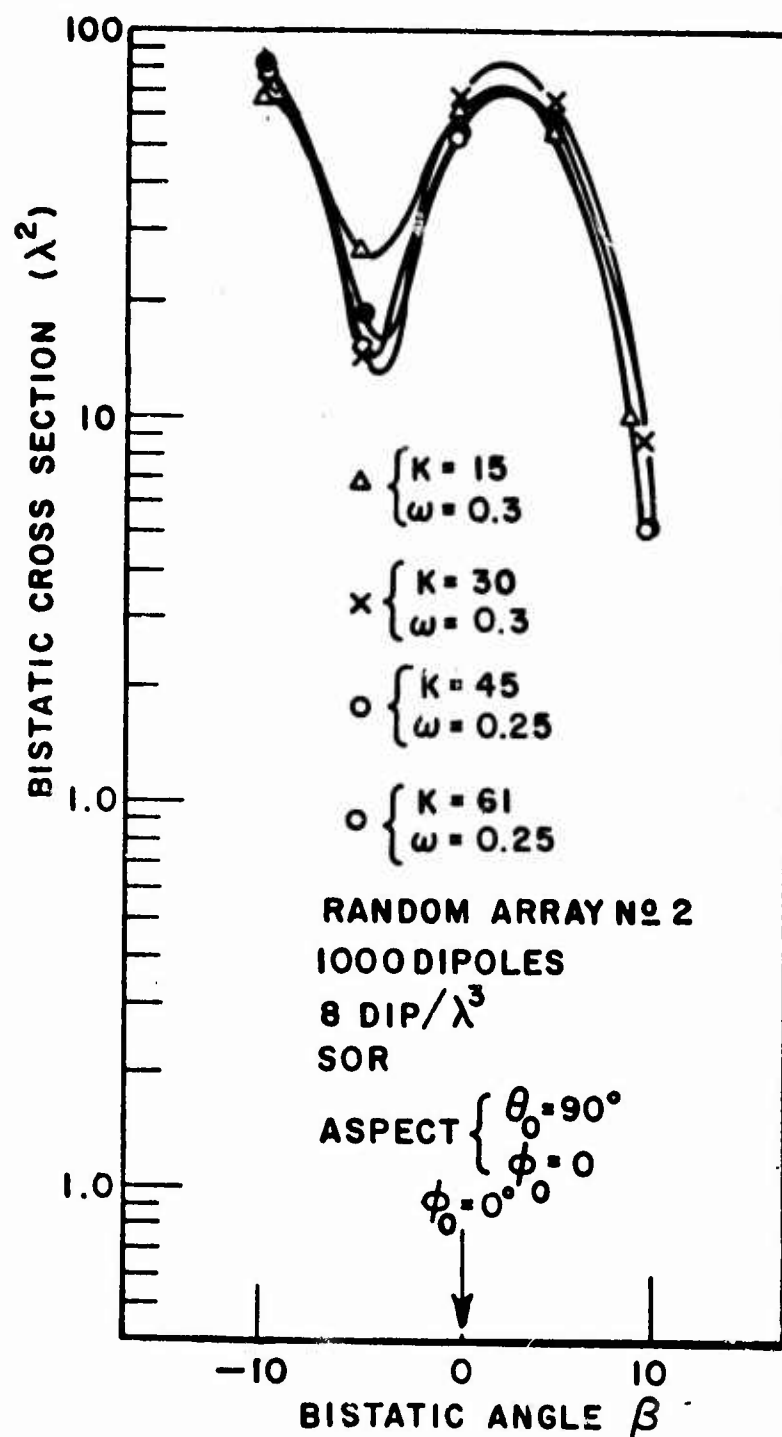


Figure 68. Bistatic cross section pattern for 1000 dipole random array #2 ( $\theta_0 = 90^\circ$ ,  $\phi_0 = 0^\circ$ ) at  $k = 15, 30, 45$  and  $61$  using SOR with  $\omega = 0.3$  and  $0.25$ .



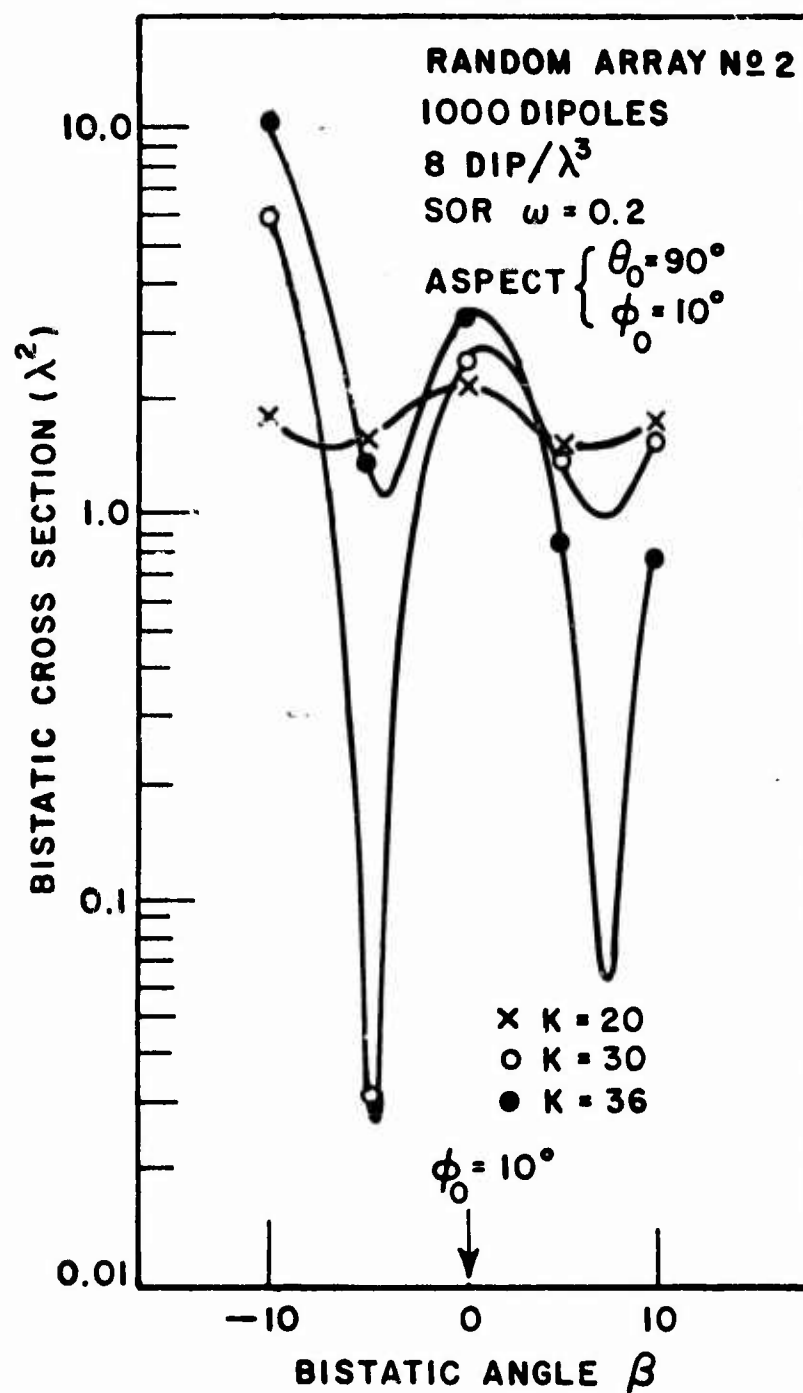


Figure 70. Bistatic cross section pattern for 1000 dipole random array #2 ( $\theta_0 = 90^\circ$ ,  $\phi_0 = 10^\circ$ ) at  $k = 20, 30$  and  $36$  using SOR with  $\omega = 0.2$ .

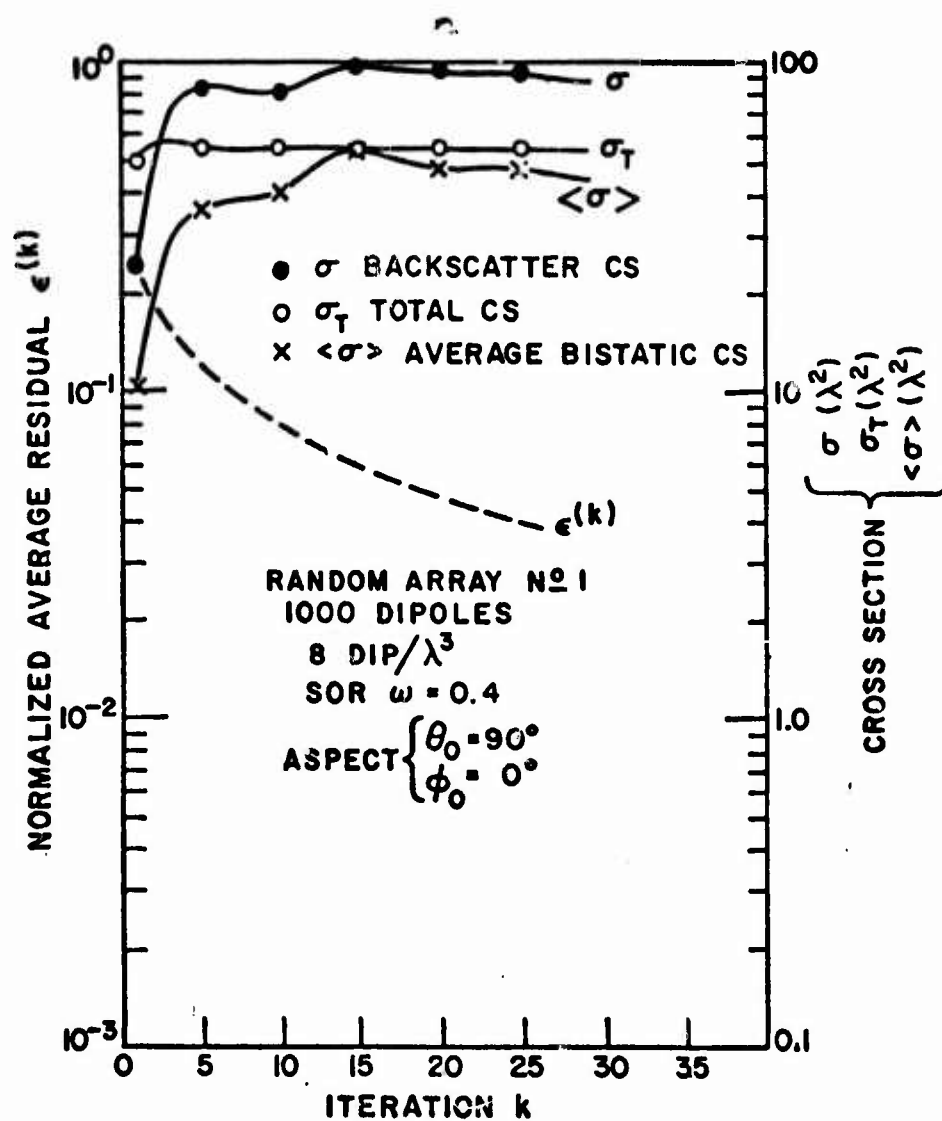


Figure 71. Backscatter, total and average bistatic cross sections versus iteration  $k$  for random array #1 (Fig. 57).

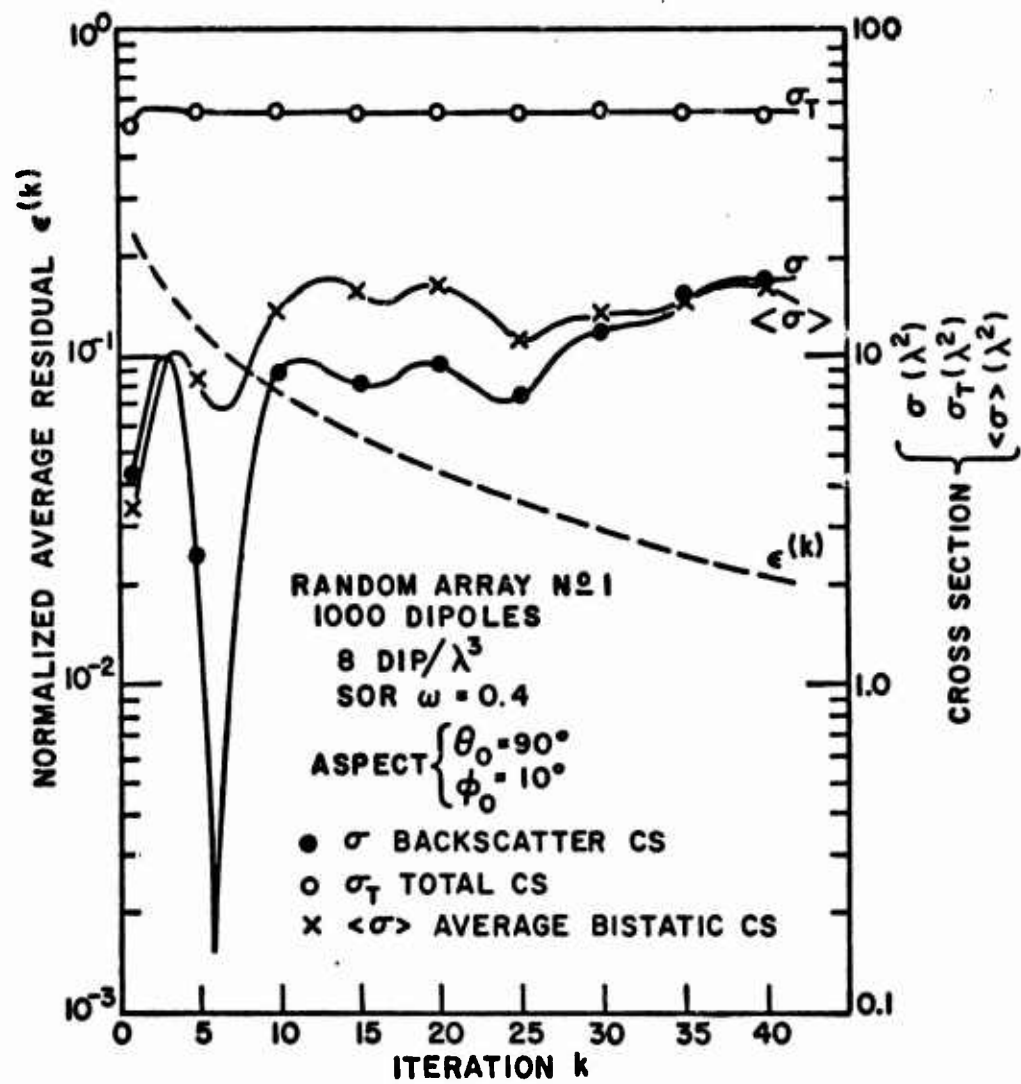


Figure 12. Backscatter, total and average bistatic cross sections versus iteration  $k$  for random array #1 (Fig. 59).

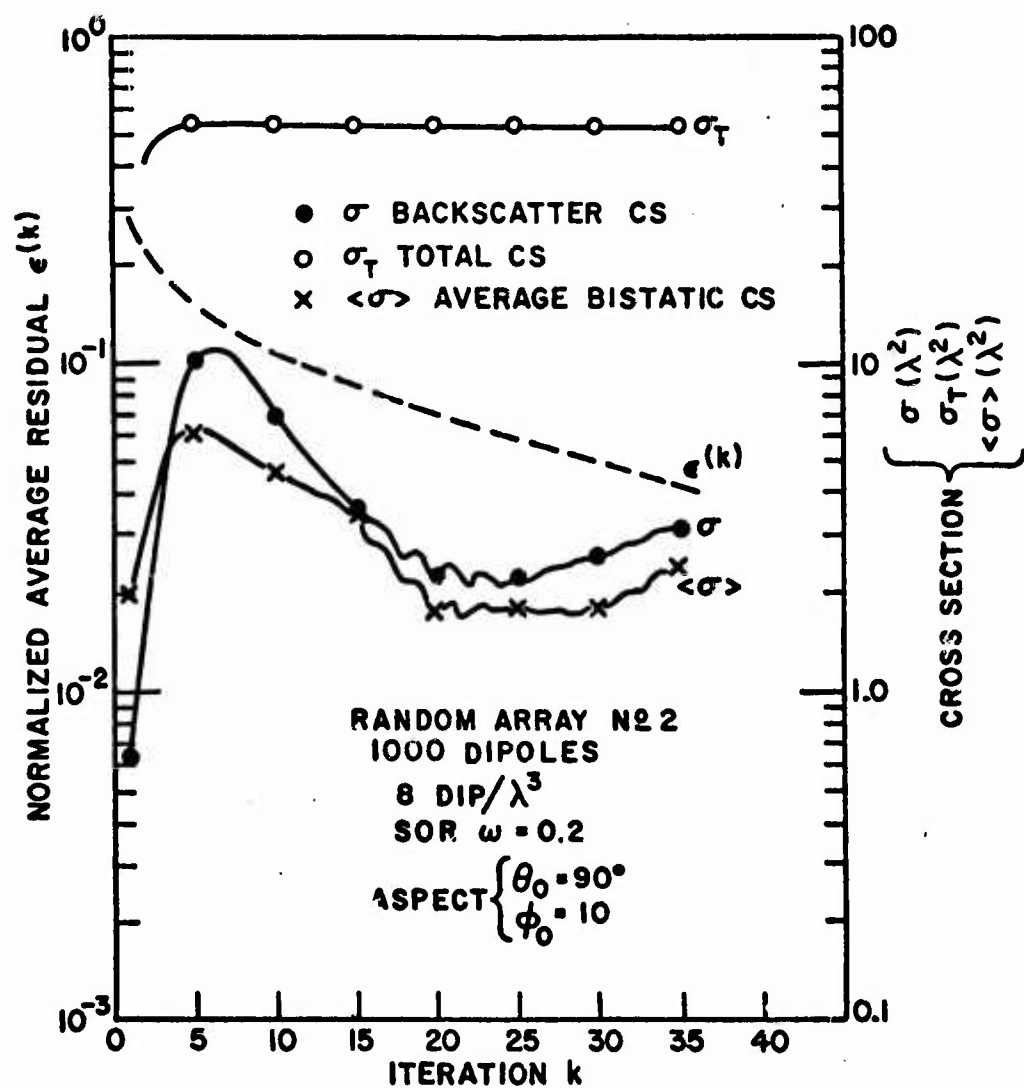


Figure 73, Backscatter, total and average bistatic cross sections versus iteration  $k$  for random array #2 (Fig. 69).

Figure 72 illustrates  $\sigma_T$ ,  $\langle\sigma\rangle$ , and the previously computed  $\sigma$  data from Fig. 59. The average  $\langle\sigma\rangle$  in this case does smooth out the large dip in the vicinity of  $k = 6$ , however, its overall convergence characteristics are no improvement over  $\sigma$  (unaveraged). Total cross section  $\sigma_T$  for  $k > 5$  has converged to very nearly the same final  $\sigma_T$  value in the previous figure (same array).

Values of  $\sigma_T$  and  $\langle\sigma\rangle$  are compared in Fig. 73 with  $\sigma$  from Fig. 69 for random array #2. Both  $\sigma$  and  $\langle\sigma\rangle$  in this case have similar characteristics, however, neither one shows significant improvement in convergence rate over the other. Note, the converged  $\sigma_T$  for this new case (array #2) is essentially the same as that obtained for random array #1).

An important result brought out by all these data is that convergence rates for many cases appear to be functions of excitation; i.e., given matrix A (e.g., random array #1),  $\omega_{opt}$  will vary with "b". This is even more apparent for random array #2 where one value of  $\omega$  gave convergence for the first angle ( $\omega = 0.25$ ), but was not sufficient to give convergence at the second aspect angle. This particular characteristic of SOR solutions to these EM problems merit further investigation.

Much of the  $\sigma$  backscatter data presented in these figures indicates a rather wide range of convergence rates for  $\sigma$ ; yet, many of these same cases have very similar characteristics in  $\epsilon(k)$ . These same cases often have apparently well converged bistatic patterns with most readjustments occurring in the "null" amplitudes beyond certain values for  $k$ . However, the  $\sigma$  backscatter curves sometimes still exhibit considerable instability in spite of the above signs. A probable cause for this wide range in convergence rates for  $\sigma$  is the slope of the  $\sigma$  backscatter pattern at the desired aspect angle; e.g., if the aspect corresponds to a relatively flat amplitude portion of the  $\sigma$  pattern, then convergence of  $\sigma$  will more than likely appear in fewer iterations. (A major exception to this viewpoint is the rapid convergence of  $\sigma$  for the large periodic array. Here, the reason for fast convergence is probably not due so much to the flatness of the pattern as to the generally reduced magnitudes of the off-diagonal elements of matrix A. Convergence rates of  $\sigma$  for random arrays having lesser volume densities of dipoles would certainly be faster for this same reason.) The chosen aspect angle for random arrays can often unknowingly correspond to a steep skirt or be near a null (cusp) in the  $\sigma$  backscatter pattern and the slightest changes in calculated currents will cause pronounced changes in the iterated  $\sigma$  curves. If, however, these same  $\sigma$  curves are accompanied by smooth monotonically decreasing  $\epsilon(k)$ 's, then these iterated solutions can still in some average sense be assumed to be nearing

the true solution. This implies that averages of  $\sigma$ , over many seemingly converged cases, might actually be good approximations of the true averages if  $\sigma$  were known exactly. A great deal more data is obviously needed to confirm or deny this relationship. However, if this should be the case, many of the statistics of for these large rather dense random arrays could be calculated without requiring rigorous convergence of the iterative technique to the exact solution.

There are certain distinct characteristics which keep re-appearing in these iterated solutions for the 1000 dipole random arrays: namely, rapid convergence of  $\sigma_T$  and the relative stability of angular positions of peaks and nulls in the bistatic patterns. A sample calculation of the half power beam width for a uniformly excited circular aperture with the same projected area as the 1000 dipole array ( $\sim 120\lambda^2$ ) results in an approximate  $9^\circ$  beam width. The half power beam widths of peaks appearing in the bistatic patterns interestingly enough consistently fall in the  $6^\circ - 10^\circ$  range. These characteristics are undoubtedly related to the fundamental size and density of these arrays. Further investigations of these relationships and of overall  $\sigma$  backscatter statistics appears to be warranted.

#### SOI Iteration Solution for Scattering by a Small Cloud of Chaff Elements

The newly derived SOI technique introduced previously is used here to solve Eq. (12b) for a 100 dipole ( $8 \text{ dip}/\lambda^3$ ) random array. The results are shown in Fig. 74 where the two sets of curves correspond to two values of influence coefficient  $C$ . The direct solution obtained by Cholesky's method is also indicated. Computations corresponding to  $C = 0.2$  required approximately 30 seconds per iteration and used a  $14 \times 14$  maximum submatrix size. Convergence of  $\sigma$  in this case was irregular and  $\epsilon(k)$  increased for  $k > 16$ . Computations for  $C = 0.1$  required a maximum  $44 \times 44$  submatrix and 150 sec/iteration and convergence in this case took fewer iterations ( $k \sim 7$ ) and  $\epsilon(k)$  exhibited a pronounced decrease over this same range.

Figure 75 is included here for comparison of SOI with SOR. The SOR iteration is used in this case to solve the same system of equations as for the above SOI method. The  $\sigma$  and  $\epsilon(k)$  data for three relaxation factors are shown;  $\omega = 0.7$  was a divergent case,  $\omega = 0.6$  converged in the fewest number of steps and  $\omega = 0.5$  converged, but required more iterations than  $\omega = 0.6$ . Iteration time for SOR ( $N = 100$ ) was approximately nine seconds per iteration - a considerable improvement in time over SOI. The SOI algorithm is extremely inefficient compared to the simple form of SOR and for comparable rates of convergence, SOR is estimated to be approximately 15 times faster.



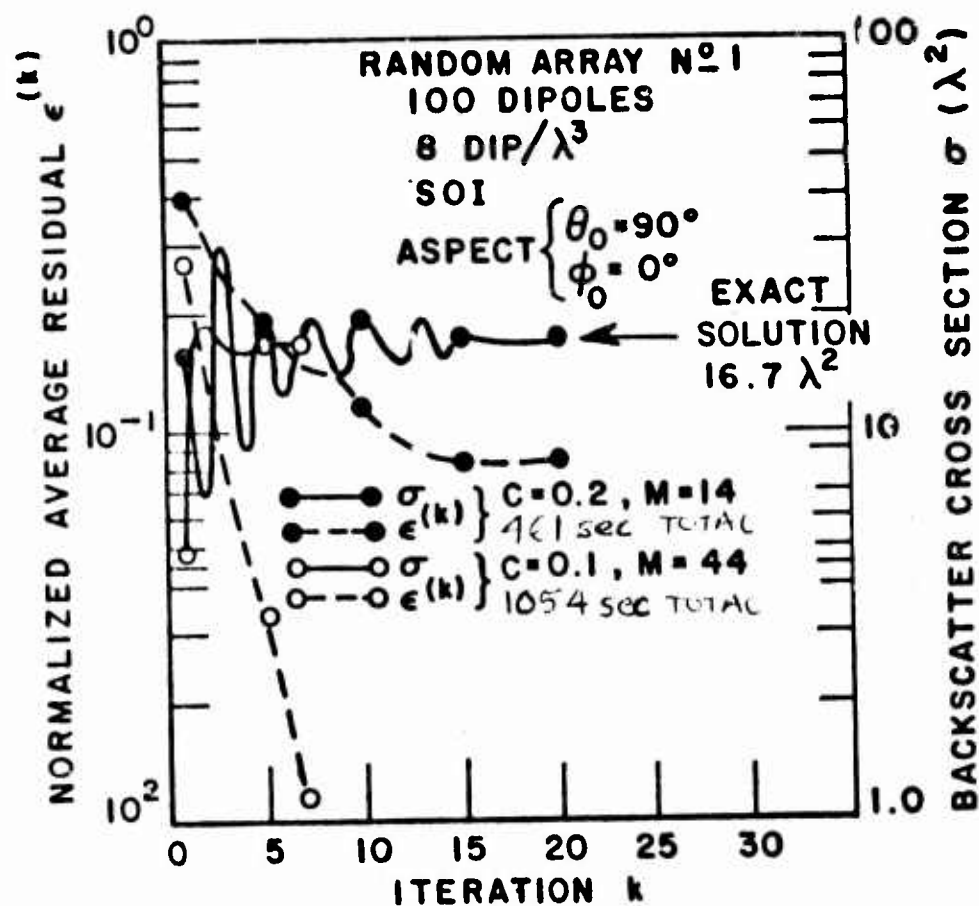


Figure 74. Backscatter cross section and  $\epsilon^{(k)}$  versus iteration  $k$  for 100 dipole random array using SOI with  $c = 0.2$  ( $M=14$ ) and  $c = 0.1$  ( $M=44$ ).

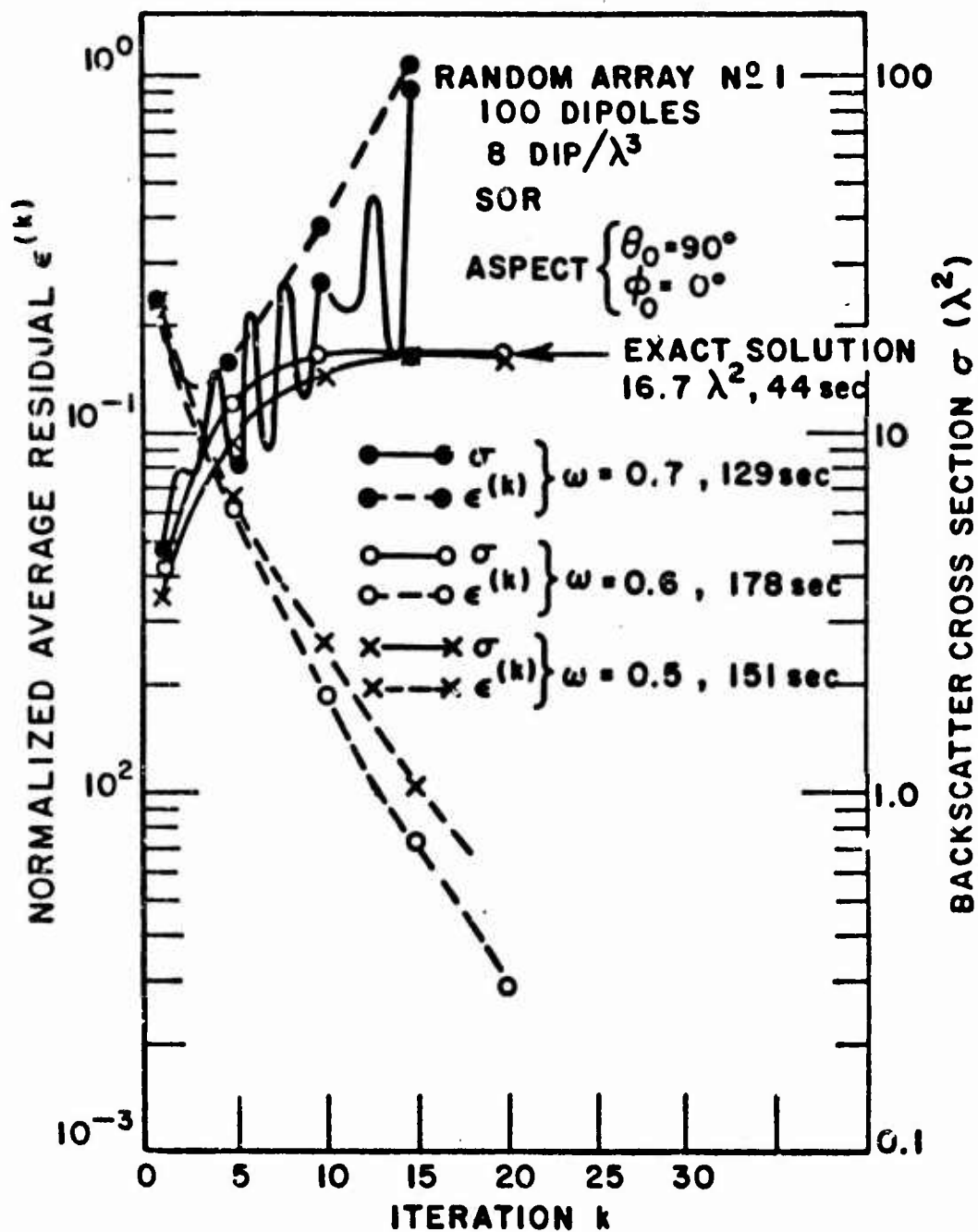


Figure 75. Backscatter cross section and  $\epsilon^{(k)}$  versus iteration  $k$  for 100 dipole random array using SOR with  $\omega = 0.7, 0.6$  and  $0.5$ .

The direct solution to the above case required approximately 44 seconds while SOR took 90 seconds ( $k = 10$ ,  $\omega = 0.6$ ) to solve the same system. Recall, however, that the number of computations (multiplications) in Cholesky's direct method goes up as  $\sim 1/6 N^3$ , while SOR used  $\sim N^2$  computations per iteration; therefore, if the number of iterations required to achieve the desired accuracy is  $< 1/6 N$ , then the SOR iteration will have a time advantage, even over the direct method.

#### Comments on the Applications of SOR to Surface Patch and Wire-Grid Models

Calculations using the SOR technique to solve Eq. (12b) for a surface patch-modeled flat plate and wire-grid modeled circular loop (polygon loop) have been unsuccessful, even for trivially small cases using a 12-mode surface patch-modeled square plate ( $\lambda \times \lambda$ ) and a 10-mode wire-grid modeled loop ( $0.3\lambda$  radius). Both types of modeling used the overlapping type modes, cosines for the plate and piecewise sinusoids for the loop. The apparent numerical difficulty arises in the large magnitudes of the overlapping mutual impedances; these mutuals are, in fact, almost as large in magnitude as the self impedances positioned on the main diagonal of  $A$ . Hence, it appears that if off-diagonal terms in rows of  $A$  are almost as large in magnitude as the self term, then the SOR method fails to converge for all  $\omega$ . A modified approach which may be worth investigating is a hybrid iteration technique probably combining SOI with SOR. The method would again be based on solving small systems of equations directly (SOI) but then using these current solutions to up-date other currents in the the corresponding "Sphere of Influence". This could be considered another form of "overlapping" block iteration.

#### D. The Question of Closer Spacings

In all the work described so far, the reader will notice that we have not discussed clouds with average spacings,  $d/\lambda$ , less than 0.5, or in other words, clouds with average dipole densities greater than  $8/\lambda^3$ . Here we mean "average density" in the sense of Appendix III, which implies that, for the kind of radially inhomogeneous clouds we assumed in the majority of cases, the actual dipole densities in the center of the cloud can be as high as  $24/\lambda^3$ . (For the uniform clouds discussed in the previous section, of course, the average dipole densities apply throughout the cloud.) Considering that each dipole is almost  $\lambda/2$  in length these numbers should convey the impression of a rather tightly packed cloud with many elements very close at their closest points. It was this proximity which led us to be cautious and question the validity of our algorithm for obtaining the currents on dipoles in clouds with  $d/\lambda < 0.5$  on the average. In our algorithm we assume that

each wire is divided into two ( $P=2$ ) equal segments which support one ( $P-1$ ) piecewise sinusoidal current mode. This assumption forces the effects of coupling from nearby wires to reside only in the complex amplitude of the current mode - coupling cannot change the shape of this single current mode. For two wires which approach each other very closely, except in very special relative orientations, we suspect that the true situation demands a change in the shape of the current distribution as well, meaning that the wires should be divided into more segments ( $P>2$ ), thereby supporting more than one piecewise sinusoidal mode thereby allowing flexibility in current shape. This is easily done and is provided for in our computer programs; however, doing so has the undesirable effect of reducing the number of wires allowed in a cloud, the impedance matrix size being fixed. We investigated the validity of our two-segment model with increasing cloud densities in the hope that it would hold up for denser clouds than those represented by  $d/\lambda = 0.5$ . This section presents some of our findings.

In order to investigate the question of closer spacings we calculated spatial average backscattering cross sections using three variants of the Richmond reaction matching technique:

- (1) Two-segment model with 12 point numerical integration. This variant is the one used for essentially all the results produced under this contract. In it, each dipole is divided into two segments supporting piecewise-sinusoidal currents whose reaction integrals are performed approximately using a 12 point numerical integration routine.
- (2) Two-segment model with exact integration. This variant is similar to (1) but the reaction integrals are expressed analytically in closed form and are evaluated exactly. This method is superior to (1) in precision, is equivalent to (1) in required computer memory, but takes more time (about 60% more time, it turns out).
- (3) Four-segment model with exact integration. This variant models each dipole with four segments, thereby allowing a more precise resolution of the induced current on the dipole than is possible with the two-segment model. The currents on each segment are integrated exactly. This method is the most precise of the three, but it requires nine times the computer memory required by the two-segment models and a great deal more computer time. Thus, whereas we can solve for 200 dipole clouds with two segment models we could solve for only 22 dipole clouds using a four-segment model.

We assumed inhomogeneous clouds containing  $N=10$  dipoles and calculated the average backscattering cross section of each (averaged over the usual 512 different aspect angles around a great circle in V-V and H-H polarizations). Twenty clouds were randomly generated for each spacing  $d/\lambda = 0.5$  and  $0.25$  and results for each were calculated using the three variants discussed above. Typical results of these calculations are presented in Table 7.

The conclusions derived from Table 7 may be summarized as follows:

- (1) For  $d/\lambda = 0.5$ , all three methods give results in close agreement. Thus, we have some assurance that the model we have been using heretofore (the two-segment model with numerical integration) is sufficiently accurate.
- (2) For  $d/\lambda = 0.25$ , the two-segment model with exact integration appears to correlate better with the four-segment model, although the model with numerical integration really does not perform badly at all. To be safe, however, we suggest use of the two-segment model with exact integration for average spacings less than  $0.5$  at the expense of 60% more computation time.

The three reaction matching variants described above were also used to generate (using the Wright-Patterson Air Force Base computer) pattern functions of six inhomogeneous, 50 dipole clouds - three with  $d/\lambda = 0.25$  and three with  $d/\lambda = 0.125$ . The results are plotted in Figs. 76-93. From these patterns it appears that for the larger average spacing, a two segment, exact integration model is adequate to obtain good scattering patterns, but for the smaller average spacing, even the four segment, exact integration model has not clearly converged in its pattern function. We feel that for average spacings less than  $0.25\lambda$  (i.e.,  $64/\lambda^2$  density) in the inhomogeneous clouds assumed here, the algorithms presented in this report are not reliable.

One additional study which was made involved the statistics of the echo from 200 clouds, each composed of only two dipoles randomly spaced and oriented in the usual manner. From these clouds we generated histograms of the backscattering cross section at one look-angle and the backscattering cross section averaged over 512 look angles. For the case where the average spacing was  $d/\lambda = 1.43$  (Fig. 94 gives the statistical distribution of the spacing), the relative frequencies of the cross sections averaged over 512 look angles, with and without coupling, are given in Figs. 95a,b, respectively. Relative frequencies based on 1 look angle are given in Figs. 96a,b. Note that, although the averages derived in Figs. 95 and 96 are consistent, the distributions are different, the data for 1 look angle being more spread out. For



the 512 look angle case, the appearance of an exponential distribution is clearer. In both cases, the coupled and uncoupled dipoles exhibit similar histograms, as expected with an average spacing as large as  $1.43\lambda$ .

TABLE 7

N = 10 dipoles  
d =  $0.5\lambda$

Cloud Number	Two-Segment Model		Four-Segment Model
	Numerical Integration	Exact Integration	Exact Integration
1	1.080880	1.080899	1.068370
2	1.139636	1.243639	1.277114
3	1.124152	1.131229	1.130523
4	1.789712	1.789627	1.745001
5	0.861137	0.861061	0.893994
6	1.293543	1.444584	1.442656
7	0.489466	0.469868	0.460119
8	1.070567	1.070436	1.070025
9	0.902232	0.901733	0.904238
10	0.649599	0.620836	0.617651

N = 10 dipoles  
d =  $0.25\lambda$

1	0.657790	0.651528	0.647247
2	0.680643	0.741439	0.745068
3	0.680060	0.686915	0.669449
4	0.575100	0.53224	0.536879
5	0.468432	0.476924	0.477237
6	0.835393	0.989235	1.001033
7	0.337658	0.298744	0.294067
8	0.566090	0.565526	0.537847
9	0.681039	0.872147	0.851511
10	0.306615	0.314593	0.311840



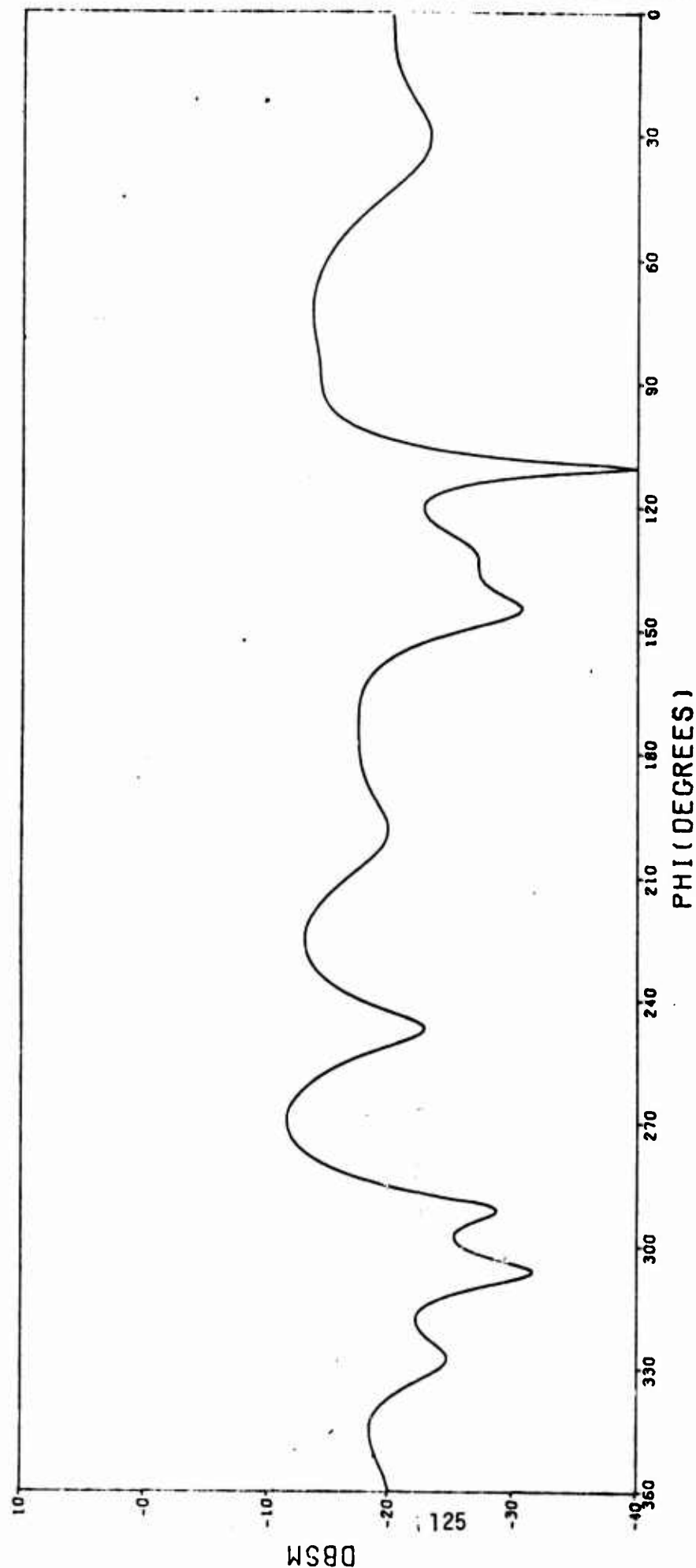


Figure 76.  $\theta-\theta$  backscattering pattern,  $N=50$  dipoles,  $d/\lambda=0.25$ ,  $P=2$  segments, 12-point integration.

50 DIPOLE RANDOM CLOUD, D=0.25 LAMDA, INT=0, NOS=2, THETA-THETA RCS

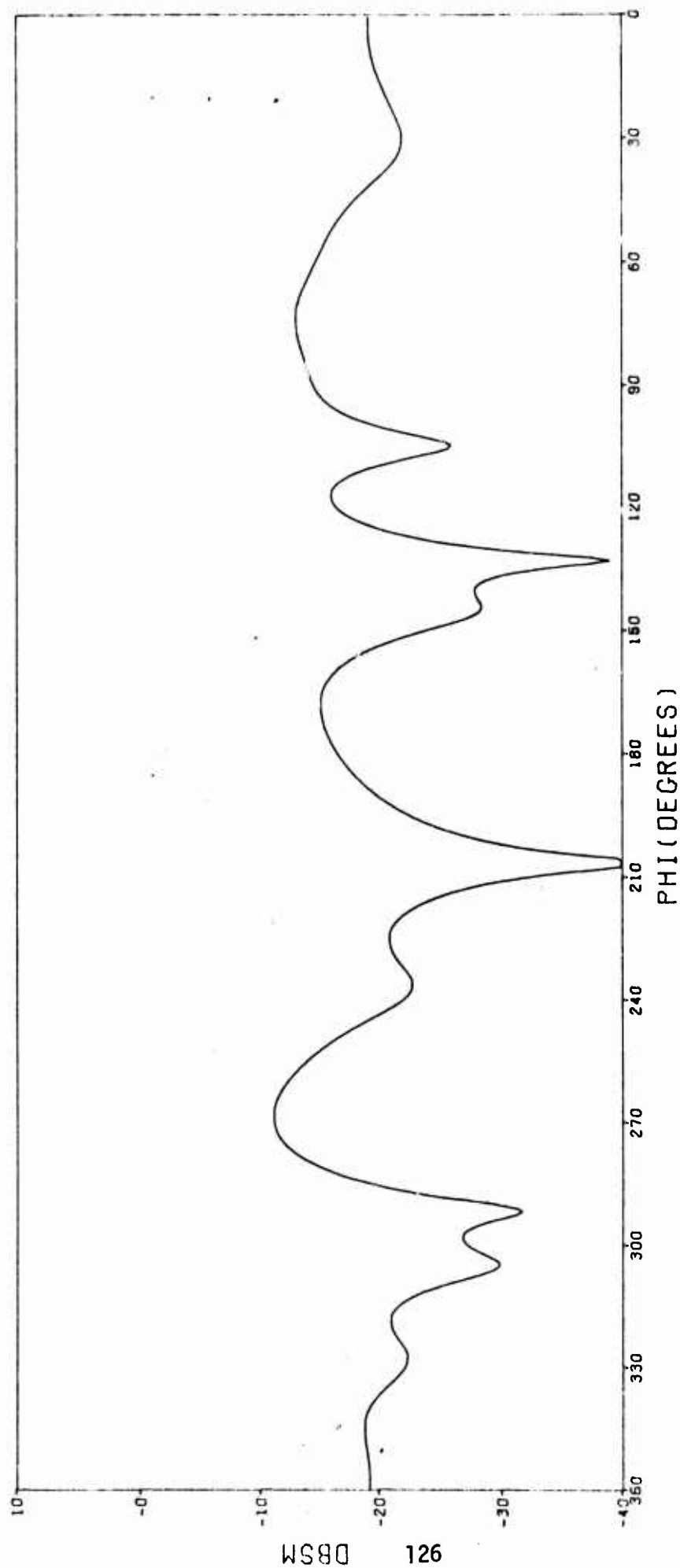


Figure 77.  $\theta-\theta$  backscattering pattern,  $N=50$  dipoles,  $P=2$  segments,  $d/\lambda=0.25$ , exact integration.

50 DIPOLE RANDOM CLOUD. D=0.25 LAMDA. INT=0. NOS=4, THETA-THETA RCS

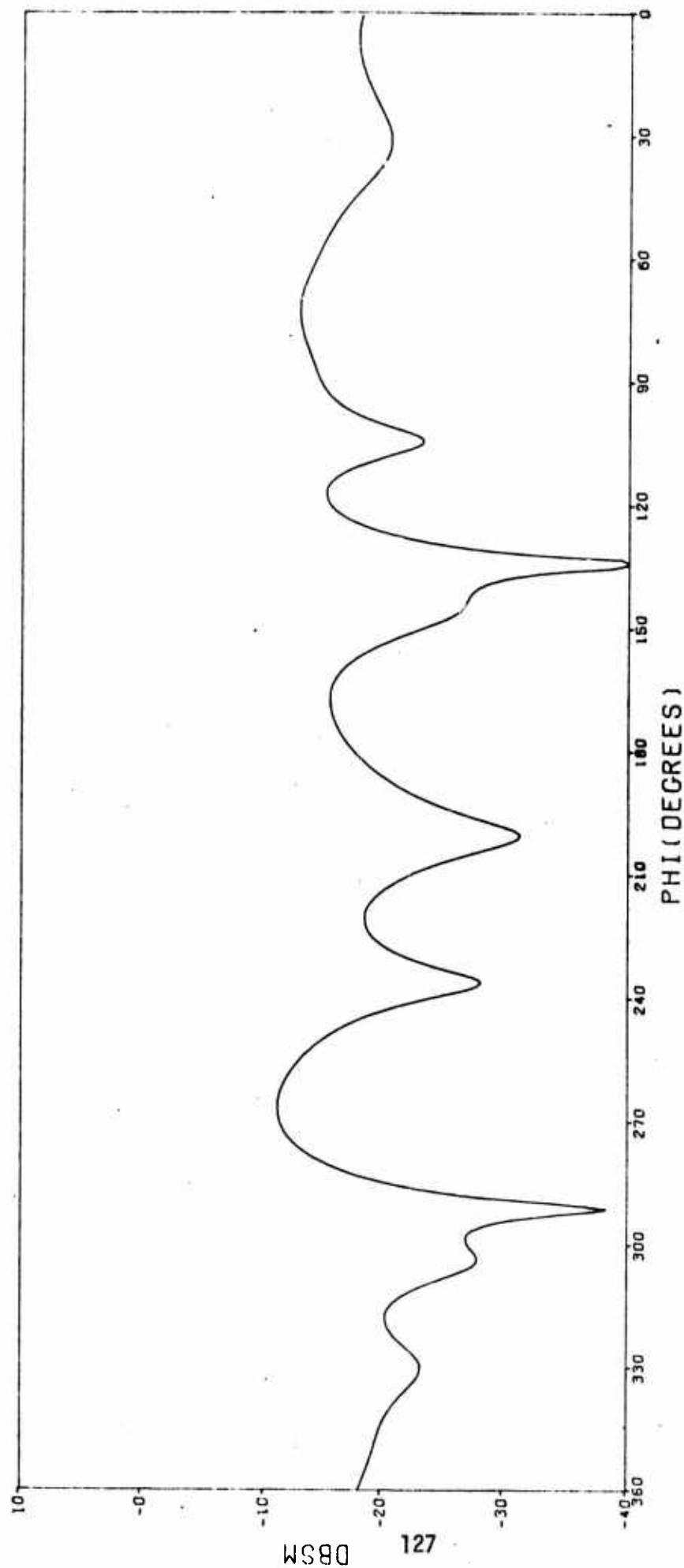


Figure 78.  $\theta-\theta$  backscattering pattern,  $N=50$  dipoles,  $P=4$  segments,  $d/\lambda=0.25$ , exact integration.

50 DIPOLE RANDOM CLOUD.  $D=0.25 \lambda$ .  $N=50$  dipoles,  $P=2$  segments,  $\phi-\phi$  backscattering pattern,  $N=50$  dipoles,  $P=2$  segments,  $d/\lambda=0.25$ , 12 point integration.

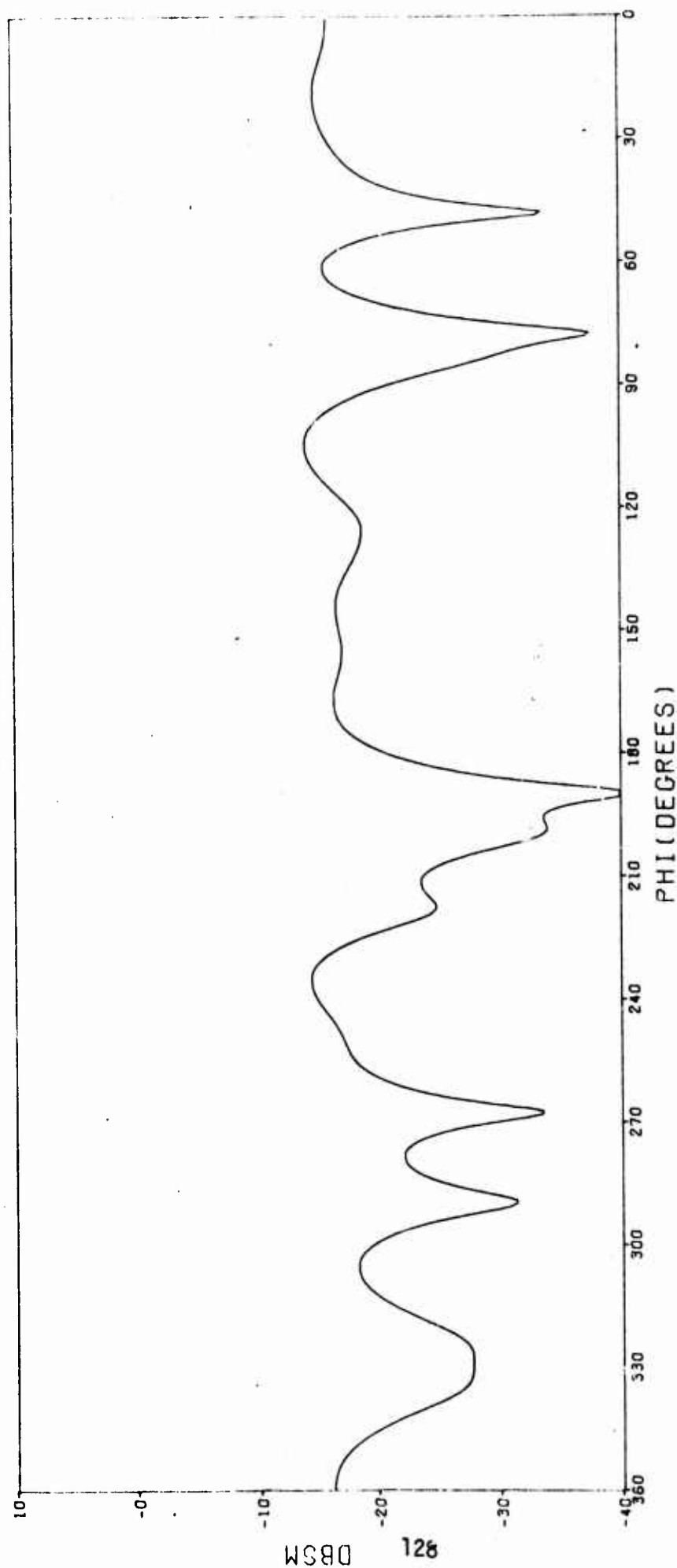


Figure 79.  $\phi-\phi$  backscattering pattern,  $N=50$  dipoles,  $P=2$  segments,  $d/\lambda=0.25$ , 12 point integration.

50 DIPOLE RANDOM CLOUD.  $D=0.25$  LAMDA.  $\text{INT}=0$ .  $\text{NOS}=2$ .  $\text{PHI}-\text{PHI}-\text{RCS}$

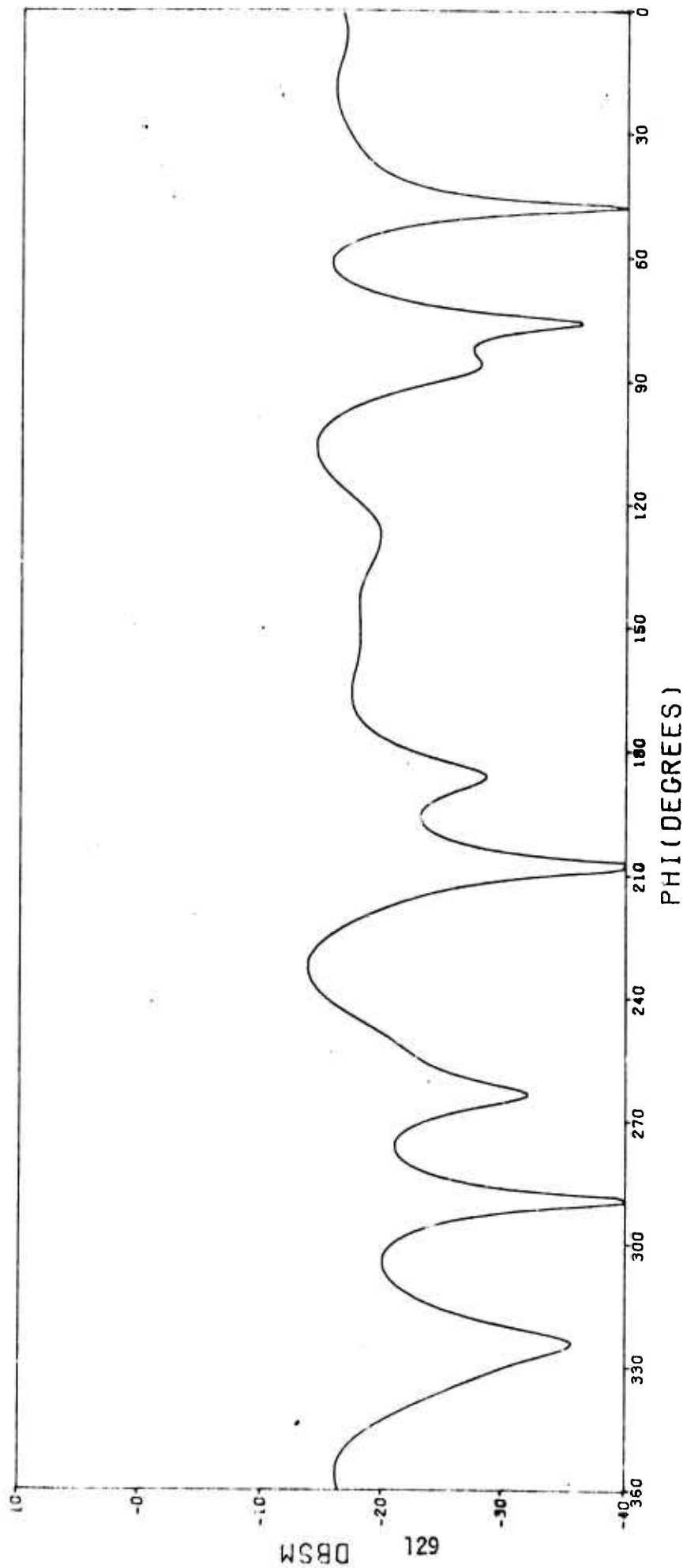


Figure 80.  $\phi-\phi$  backscattering pattern,  $N=50$  dipoles,  $P=2$  segments,  $d/\lambda=0.25$ , exact integration.

50 DIPOLE RANDOM CLOUD.  $D=0.25$  LAMDA.  $INT=0$ .  $NOS=4$ .  $\phi-\phi$  PHI-PHI-RCS

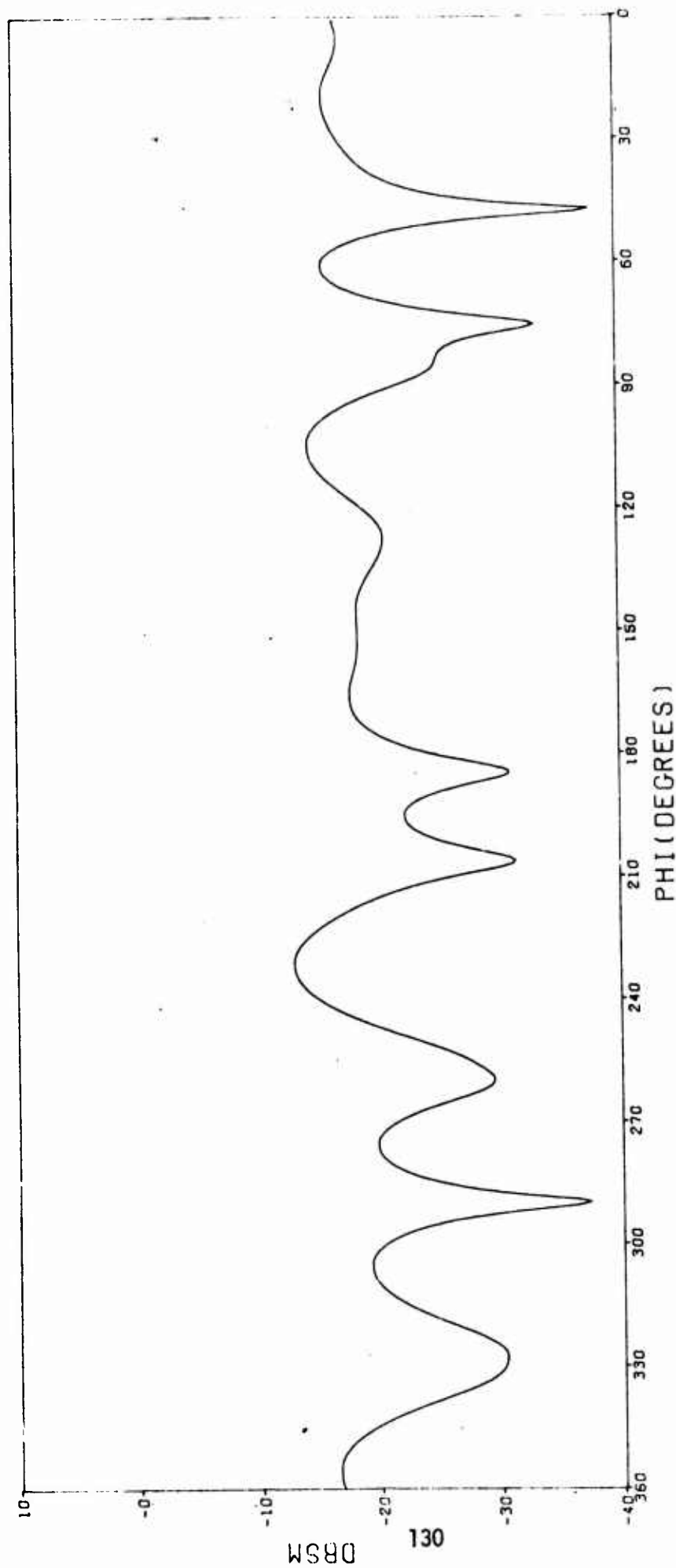


Figure 81.  $\phi-\phi$  backscattering pattern,  $N=50$  dipoles,  $P=4$  segments,  $d/\lambda=0.25$ , exact integration.



50 DIPOLE RANDOM CLOUD. D=0.25 LAMDA. INT=1, NOS=2, THETA-PHI RCS

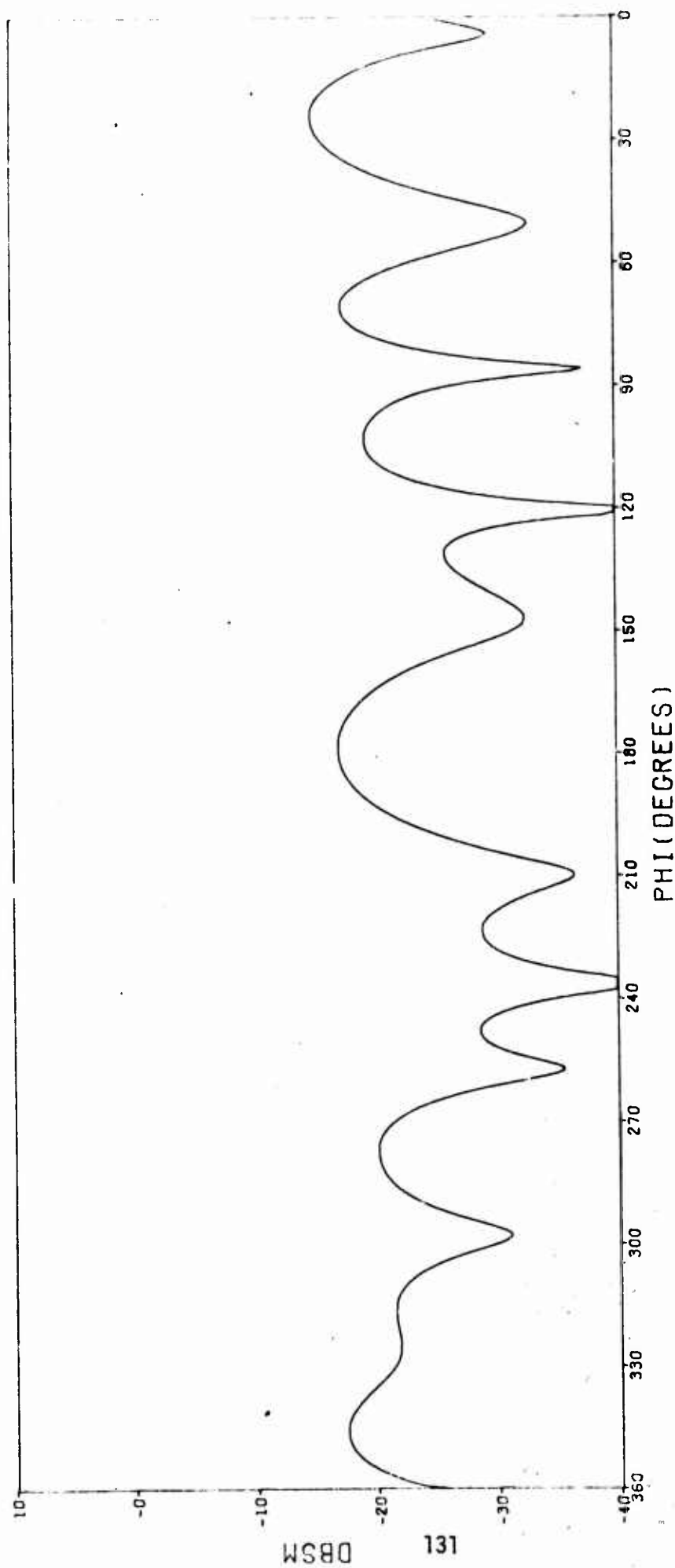


Figure 82.  $\theta$ - $\phi$  backscattering pattern, N=50 dipoles, P=2 segments,  $d/\lambda=0.25$ , 12-point integration.

50 DIPOLE RANDOM CLOUD. D=0.25 LAMDA. INT=0. NOS=2. THETA-PHI RCS

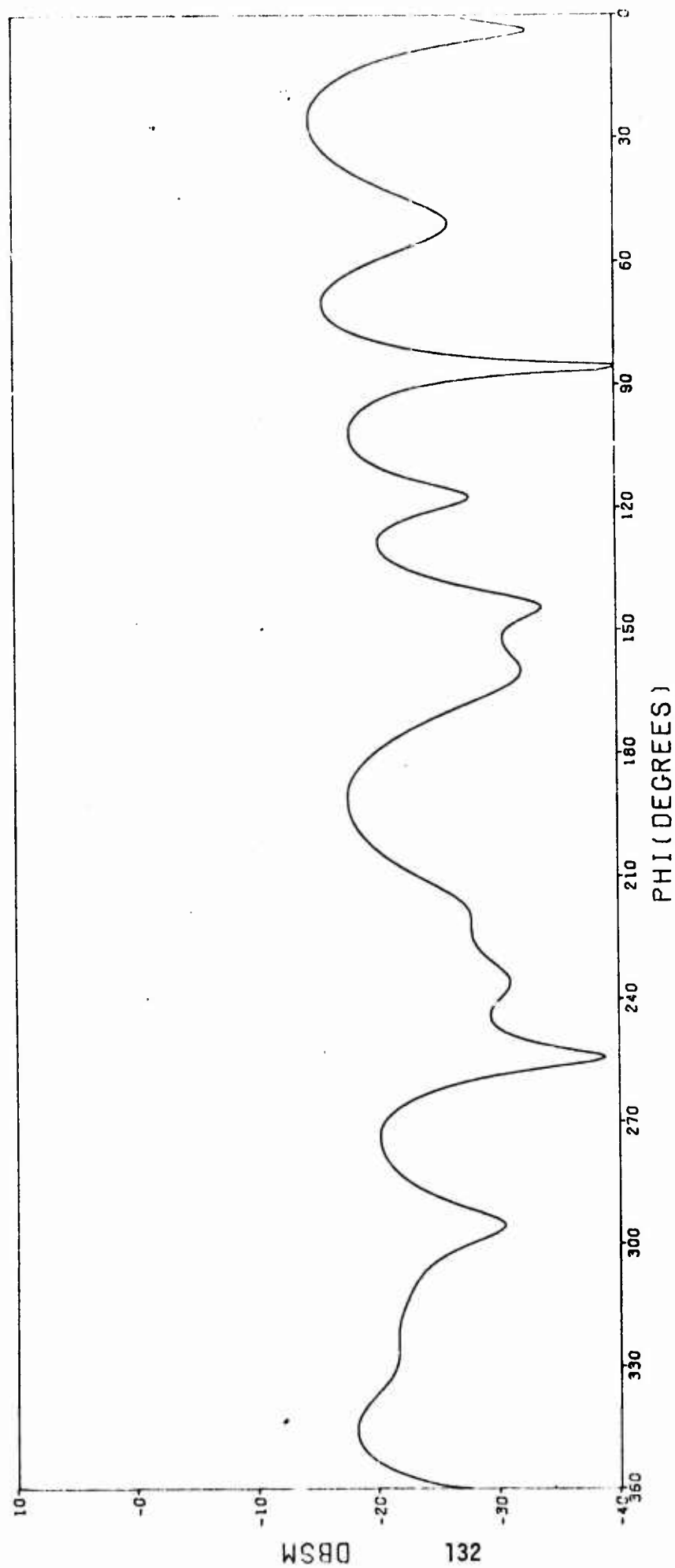


Figure 83.  $\theta-\phi$  backscattering pattern,  $N=50$  dipoles,  $P=2$  segments,  $d/\lambda=0.25$ , exact integration.

50 DIPOLE RANDOM CLOUD, D=0.25 LAMDA, INT=0, NOS=4, THETA-PHI RCS

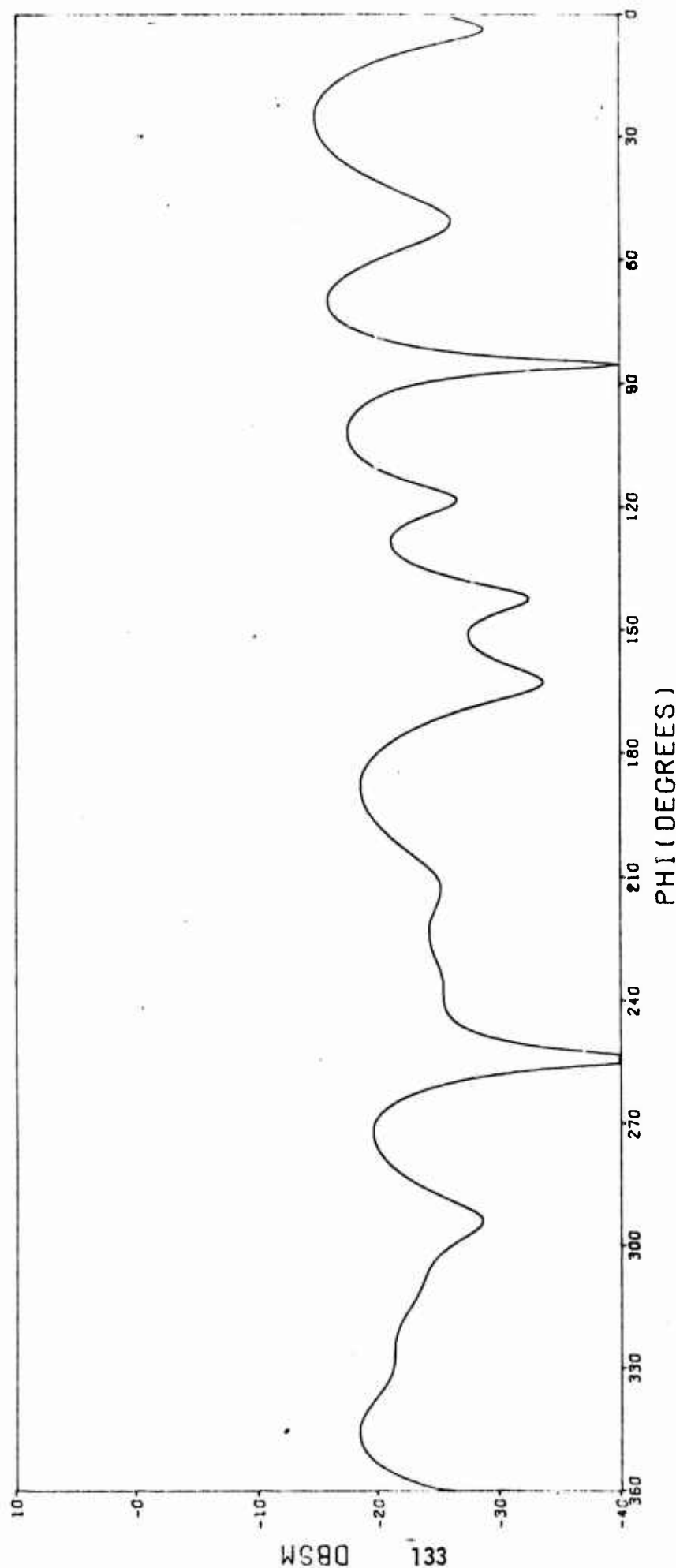


Figure 84.  $\theta$ - $\phi$  backscattering pattern, N=50 dipoles, P=4 segments,  $d/\lambda=0.25$ , exact integration.

50 DIPOLE RANDOM CLOUD. D=0.125 LAMDA. INT=1. NOS=2. THETA-THETA RCS

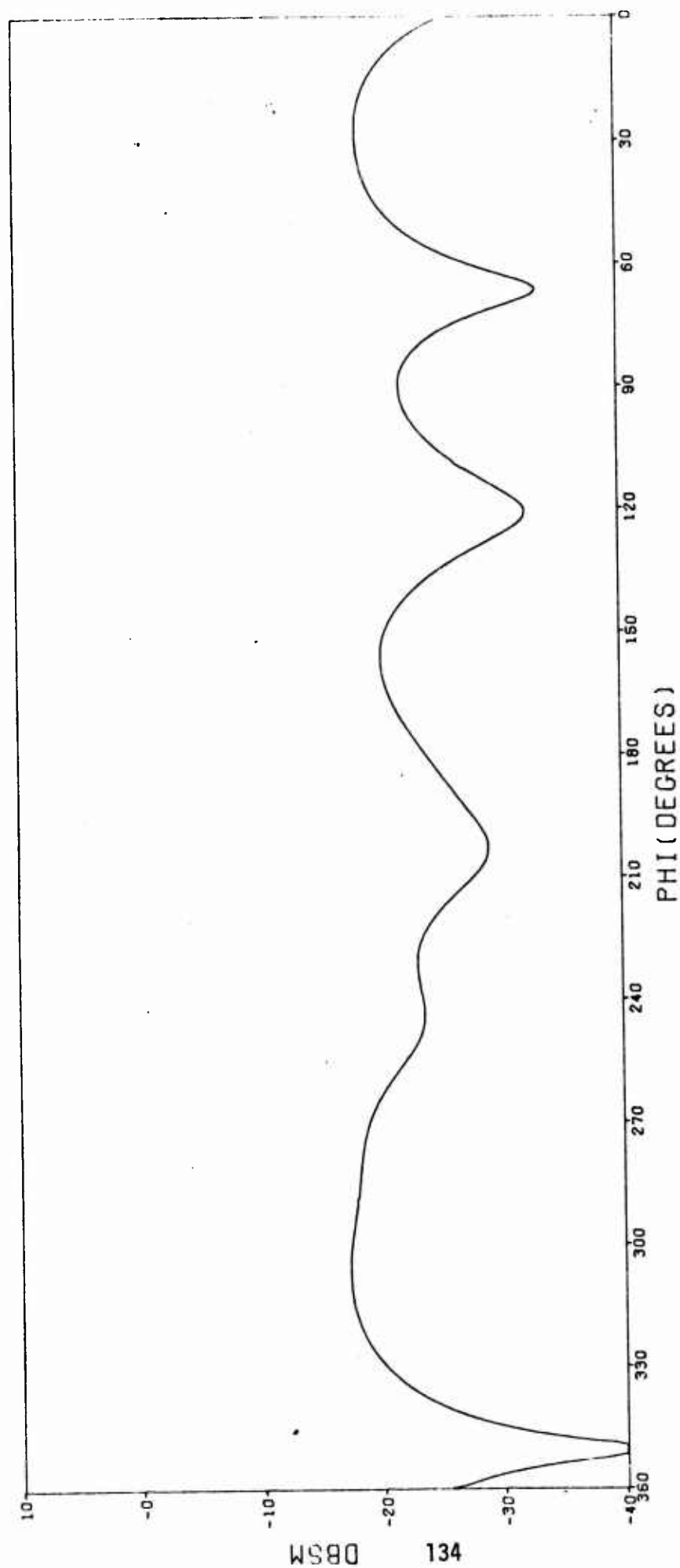


Figure 85.  $\theta-\theta$  backscattering pattern,  $N=50$  dipoles,  $P=2$  segments,  $d/\lambda=0.125$ , 12-point integration.

50 DIPOLE RANDOM CLOUD.  $D=0.125$  LAMDA.  $INT=0$ ,  $NOS=2$ .  $\theta=\theta$ .  $\theta=\theta$

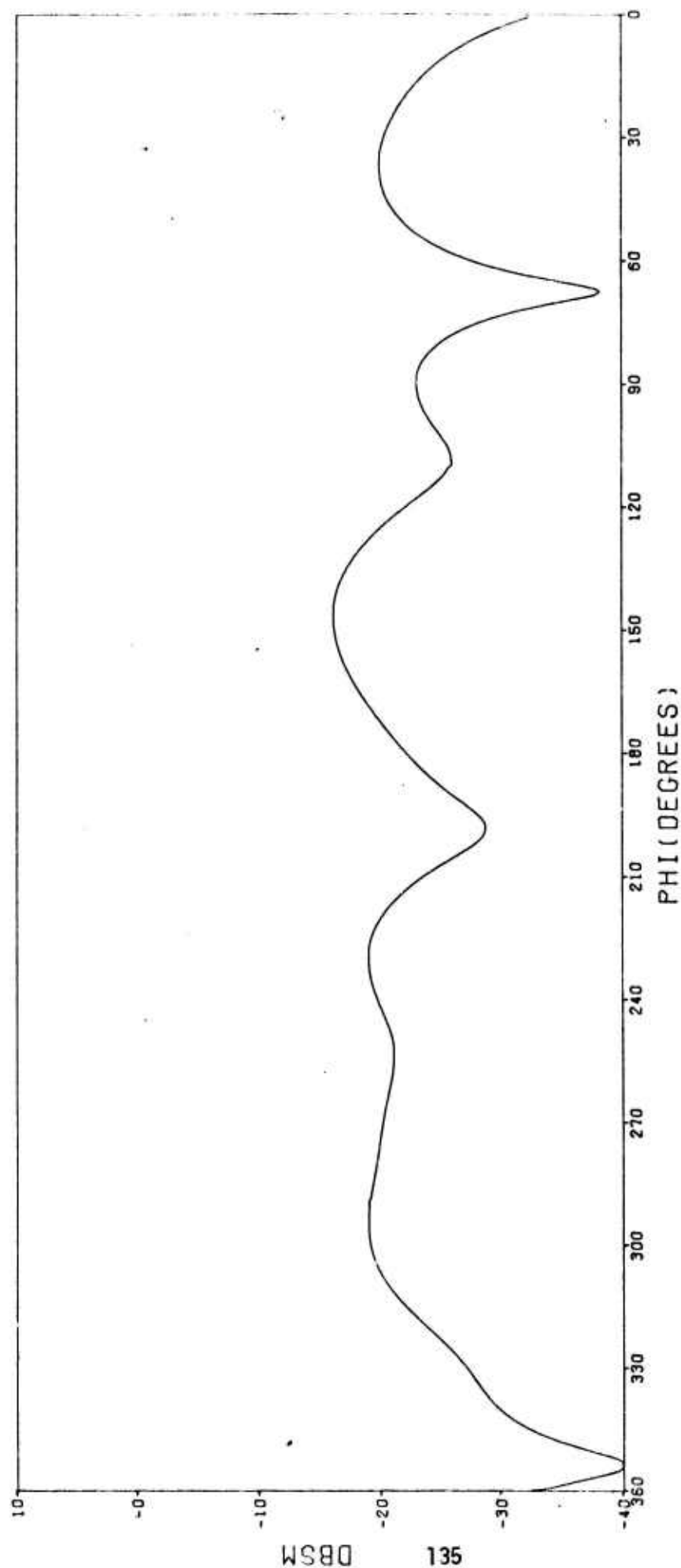


Figure 86.  $\theta=\theta$  backscattering pattern,  $N=50$  dipoles,  $P=2$  segments,  $d/\lambda=0.125$ , exact integration.

50 DIPOLE RANDOM CLOUD. D=0.125 LAMDA. INT=0. NOS=4. THETA-THETA RCS

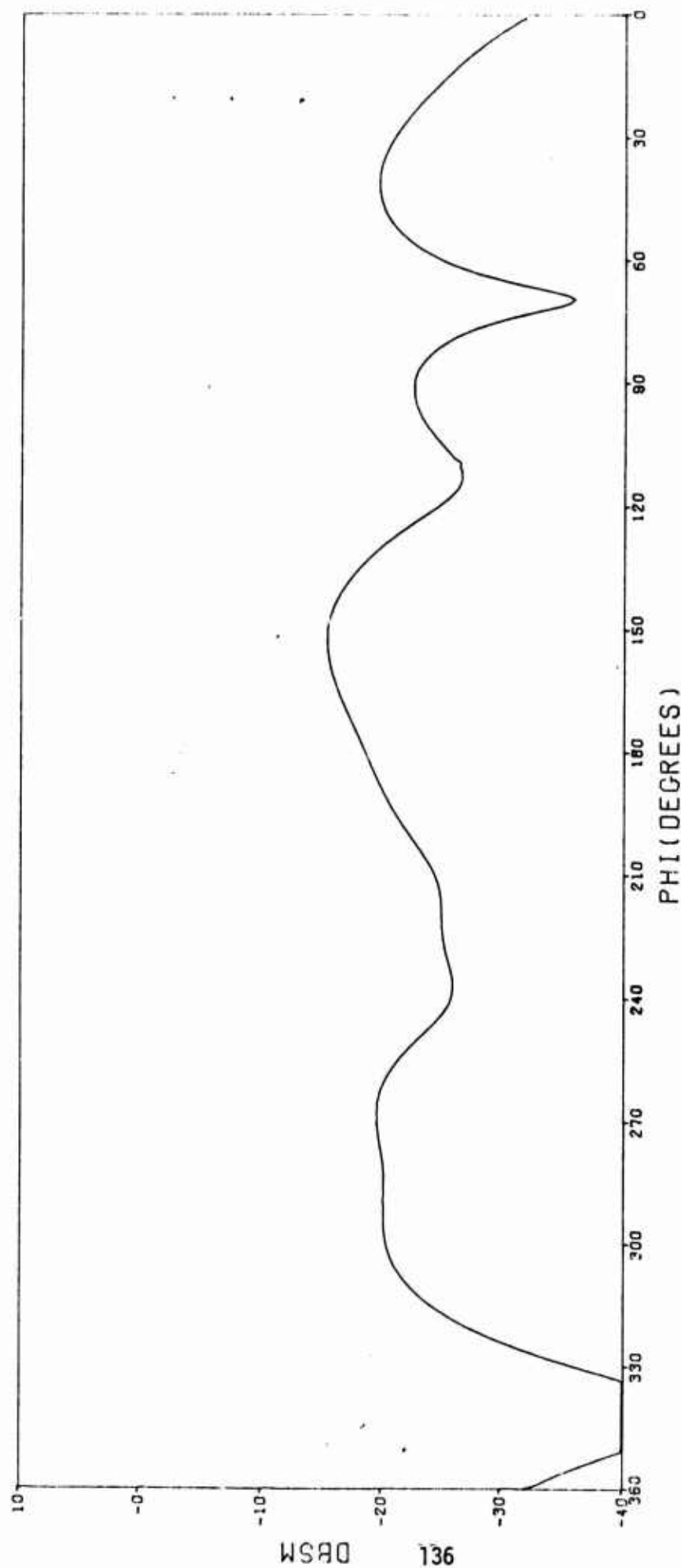


Figure 87.  $\theta-\theta$  backscattering pattern,  $N=50$  dipoles,  $P=4$  segments,  $d/\lambda=0.125$ , exact integration.



50 DIPOLE RANDOM CLOUD. D=0.125 LAMDA. INT=1. NOS=2. PHI-PHI-RCS

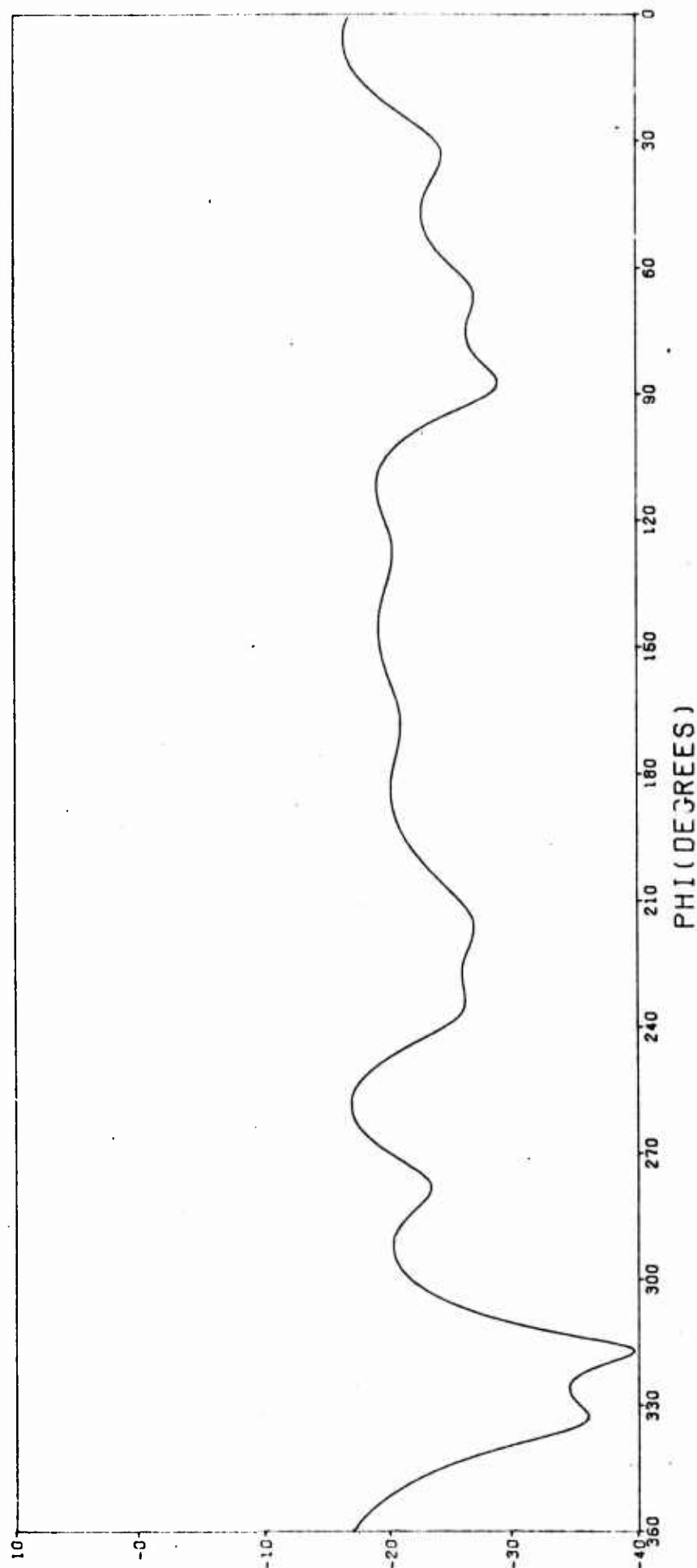


Figure 88.  $\phi$ - $\phi$  backscattering pattern, N=50 dipoles, P=2 segments,  $d/\lambda=0.125$ , 12-point integration.

50 DIPOLE RANDOM CLOUD. D=0.125 LAMDA, INT=0. NOS=2. PHI-PHI-RCS

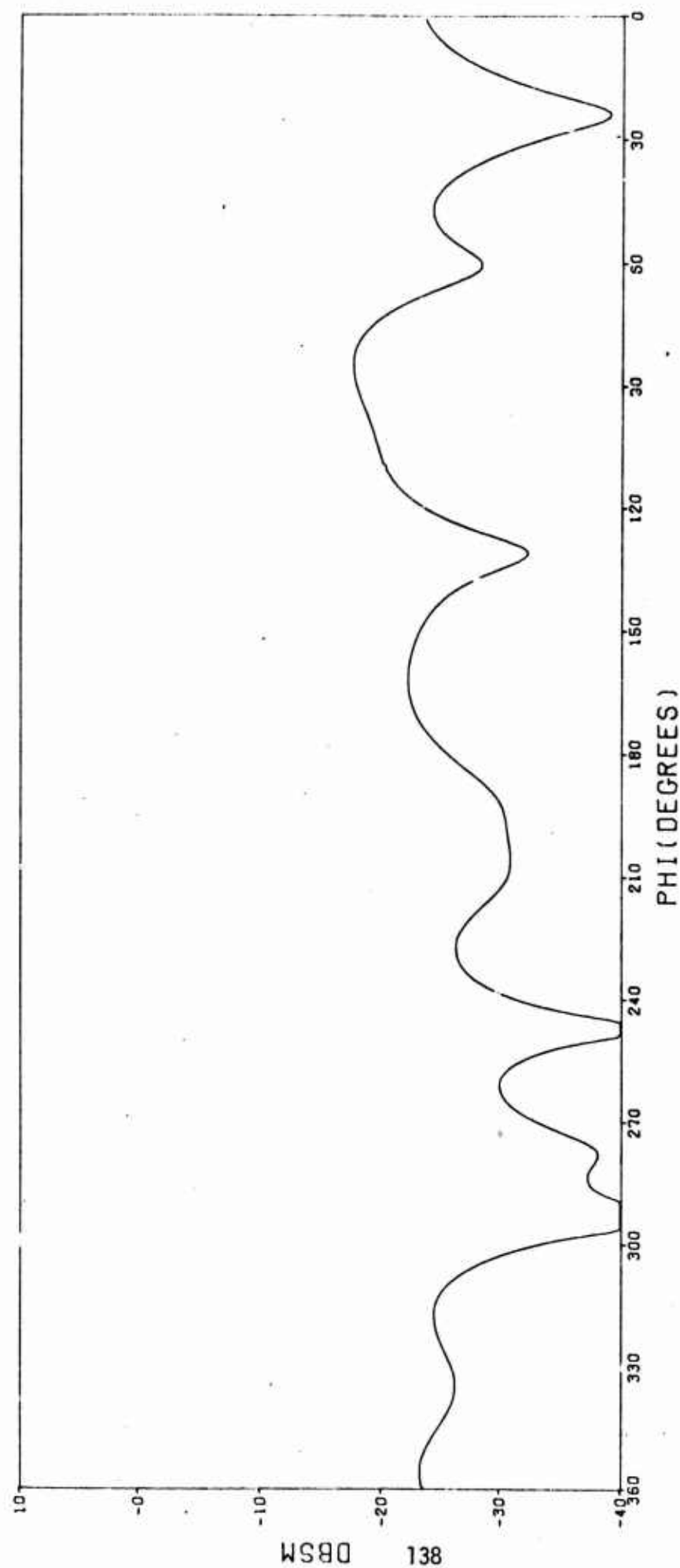


Figure 89.  $\phi$ - $\phi$  backscattering pattern,  $N=50$  dipoles,  $P=2$  segments,  $d/\lambda=0.125$ , exact integration.

50 DIPOLE RANDOM CLOUD, D=0.125 LAMDA, INT=0, NOS=4, PHI-PHI-RCS

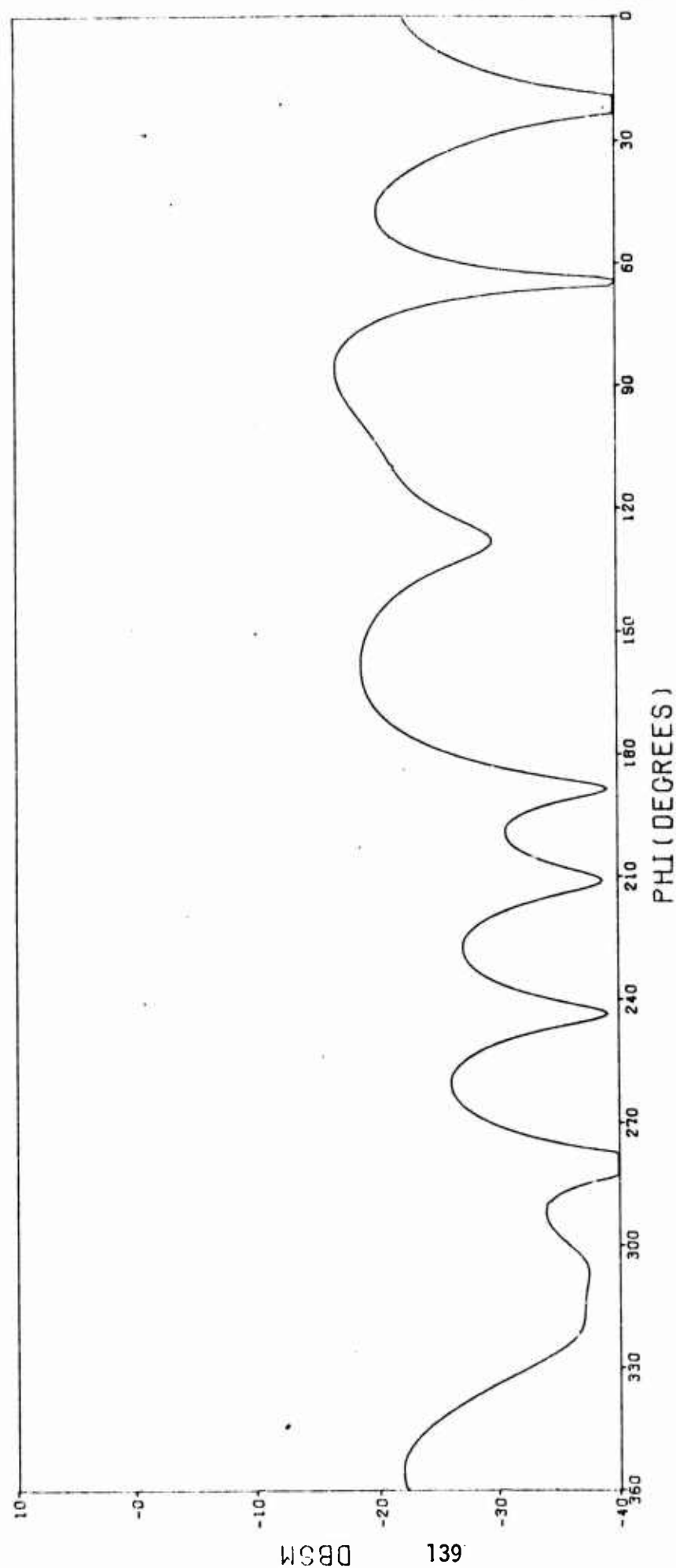


Figure 90.  $\phi$ - $\phi$  backscattering pattern, N=50 dipoles, P=4 segments,  $d/\lambda=0.125$ , exact integration.

50 DIPOLE RANDOM CLOUD. D=0.125 LAMDA. INT=1. NOS=2. THETA-PHI RCS

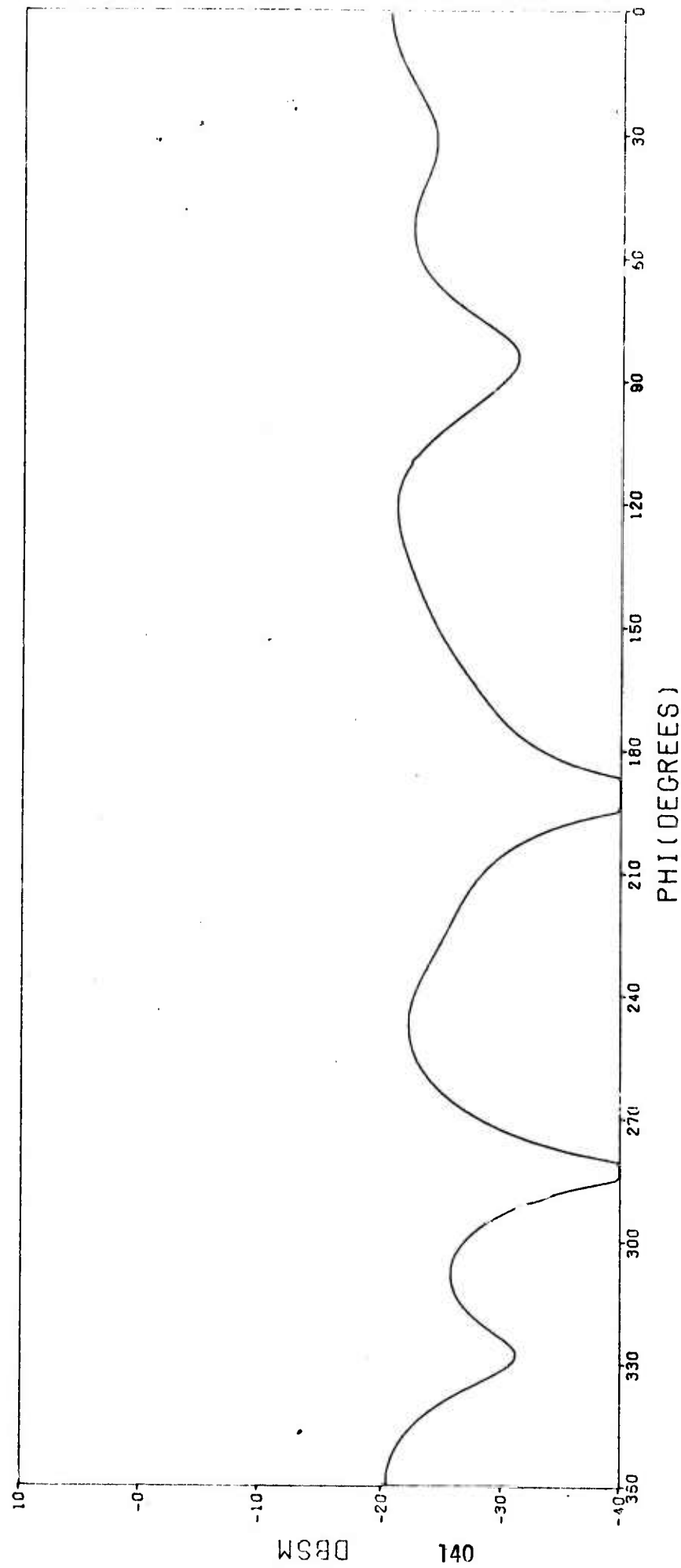


Figure 91.  $\theta$ - $\phi$  backscattering pattern, N=50 dipoles, P=2 segments,  $d/\lambda=0.125$ , 12-point integration.

50 DIPOLE RANDOM CLOUD. D=0.125 LAMDA. INT=0. NOS=2. THETA-PHI RCS

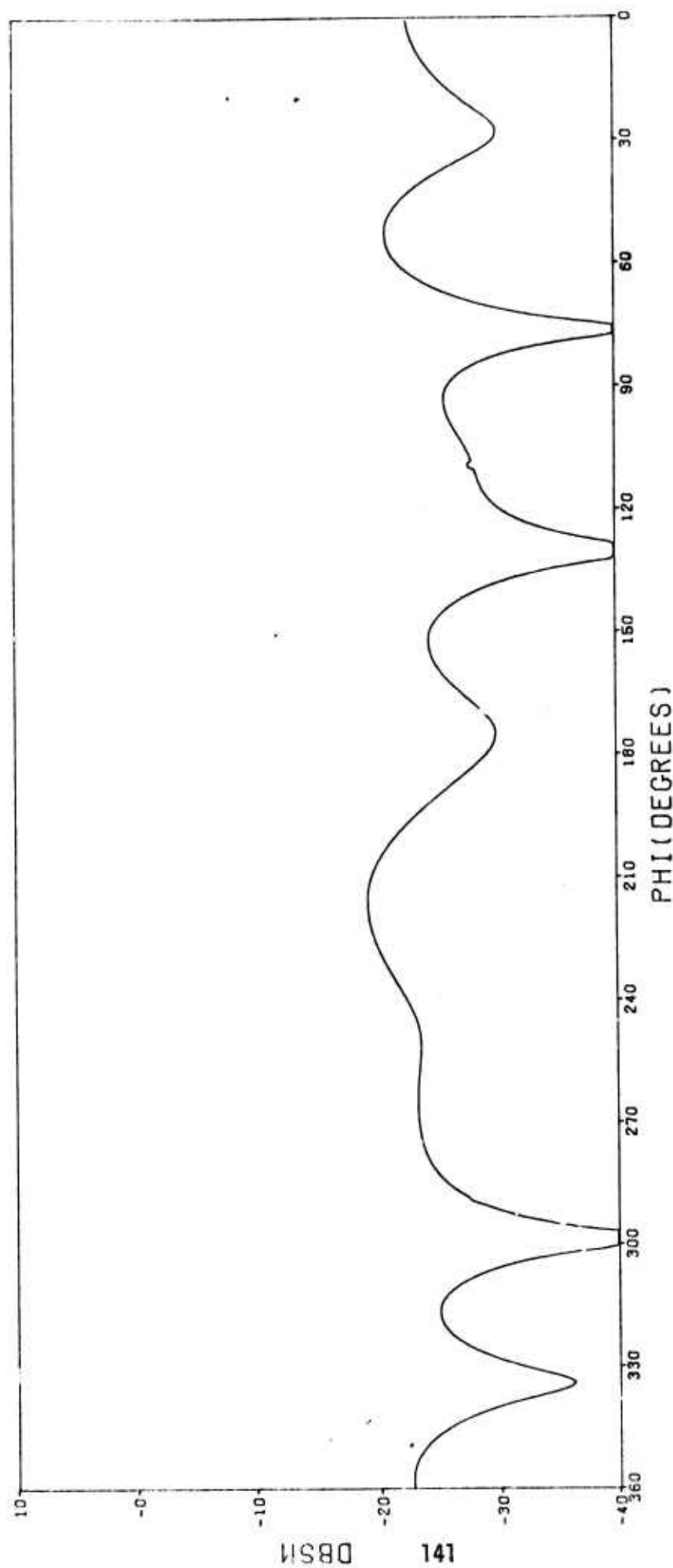


Figure 92.  $\theta$ - $\phi$  backscattering pattern,  $N=50$  dipoles,  $P=2$  segments,  $d/\lambda=0.125$ , exact integration.

50 DIPOLE RANDOM CLOUD. D=0.125 LAMDA. INT=0. NOS=4. THETA-PHI RCS

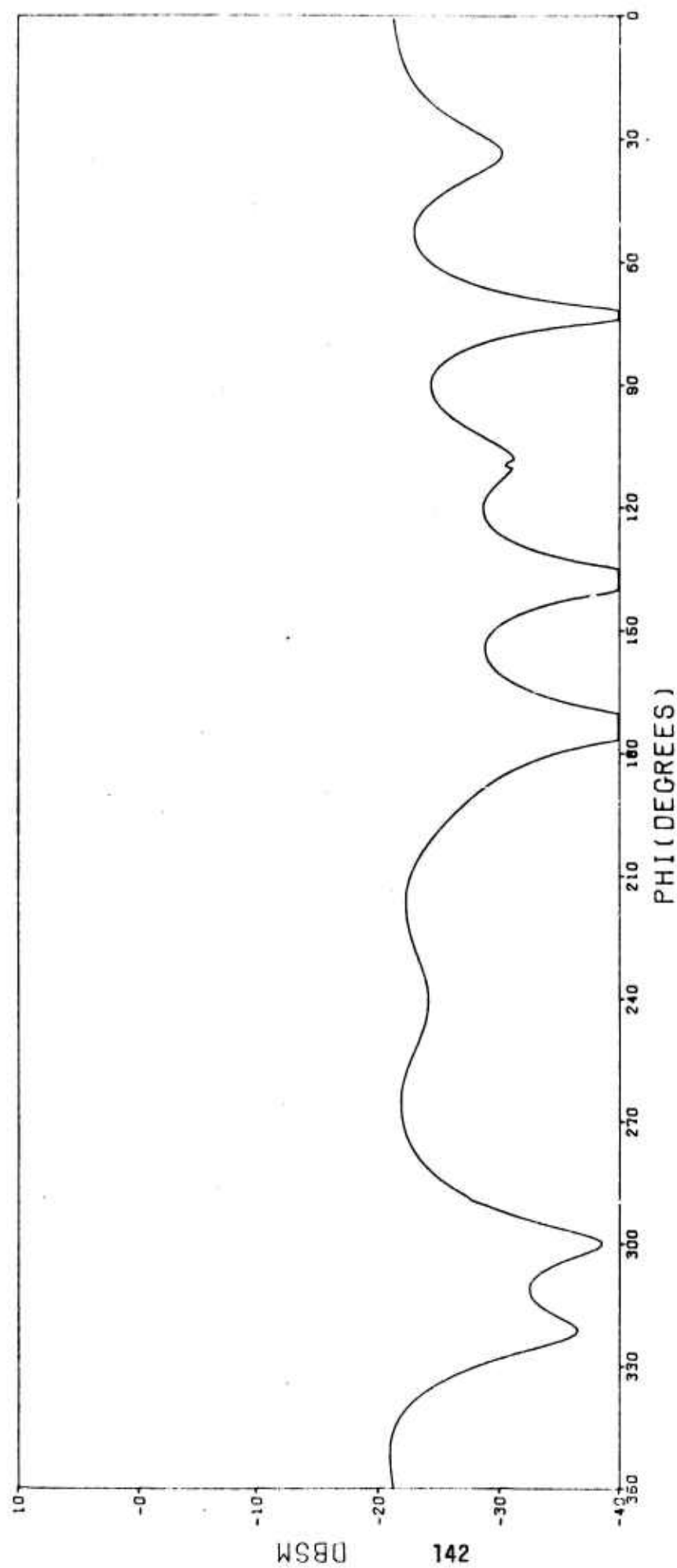


Figure 93.  $\theta-\phi$  backscattering pattern, N=50 dipoles, P=4 segments,  $d/\lambda=0.125$ , exact integration.



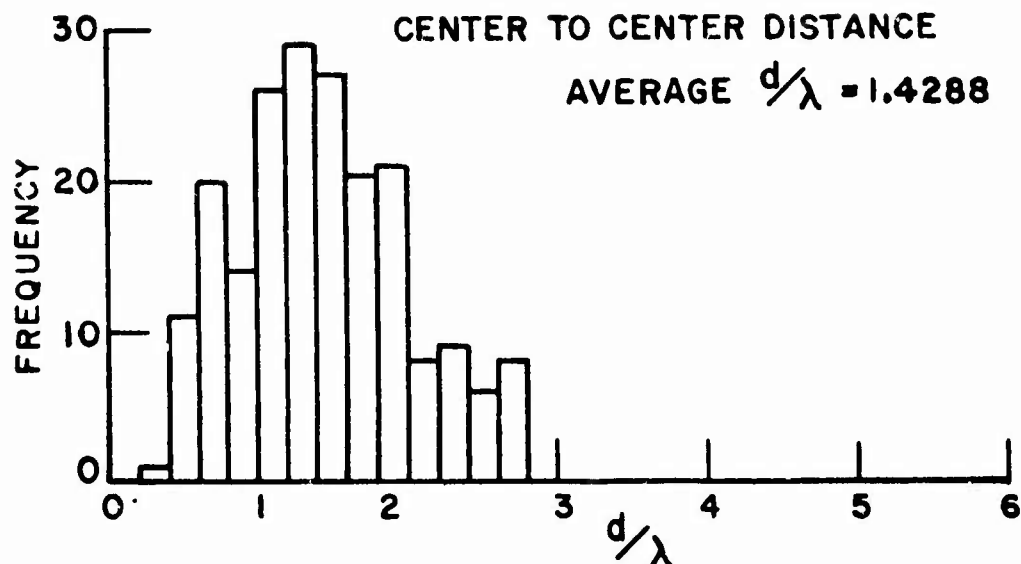


Figure 94. Histogram of the center-to-center distances of random two-dipole clouds. Average spacing  $d/\lambda \approx 1.43$ .

If a very small average spacing is assumed, and accordingly, a 4-segment model with exact integration is used for each dipole, the curves of Figs. 97-98 result. Figure 97 is the distribution of the spacing, with the rather small value of average spacing  $d/\lambda = 0.286$ . Figures 98a,b present the relative frequencies of the cross sections averages over 512 look angles with and without coupling. Again, the exponential trend of the histograms is evident.

From Figs. 95b and 98b, for the two dipoles uncoupled, we note that for far spacings, the average echo is about  $2\langle\sigma_0\rangle$  or about  $0.35\lambda^2$ , whereas for close spacing the average echo exceeds this ( $\sim 0.47\lambda^2$ ). This is expected because for such a close average spacing the two dipoles cannot be excited incoherently and their echo therefore lies above that for totally incoherent scatterers. This effect for two dipoles variously spaced is shown in Fig. 99. The  $2\langle\sigma_0\rangle$  law does not appear to be reached until  $d/\lambda \sim 1.4$ . For clouds containing larger numbers of uncoupled dipoles, the limit  $N\langle\sigma_0\rangle$  is expected to be reached for smaller spacings due to the larger overall extent of the clouds.

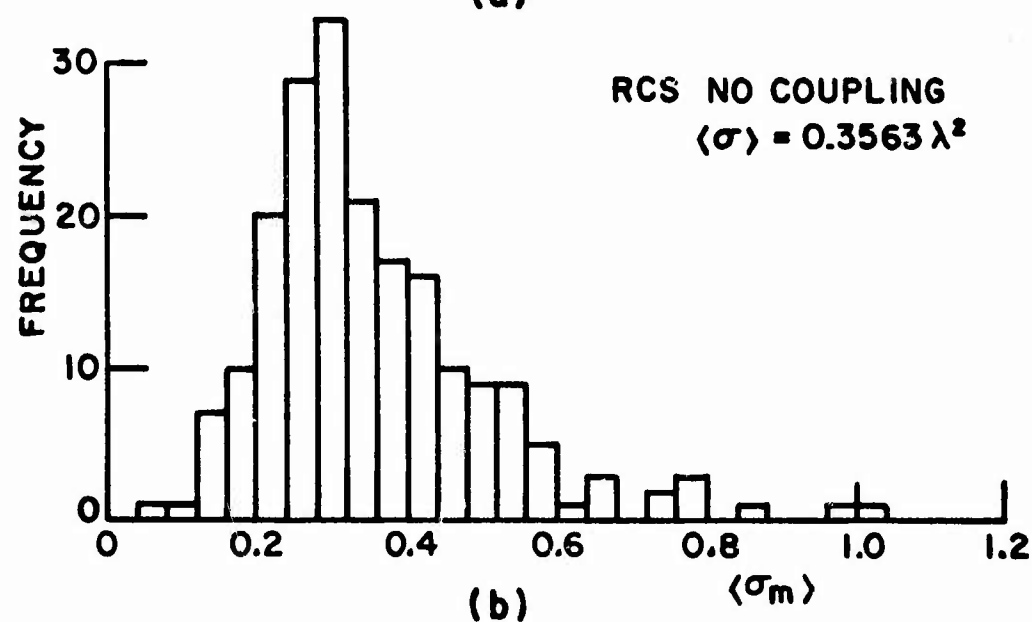
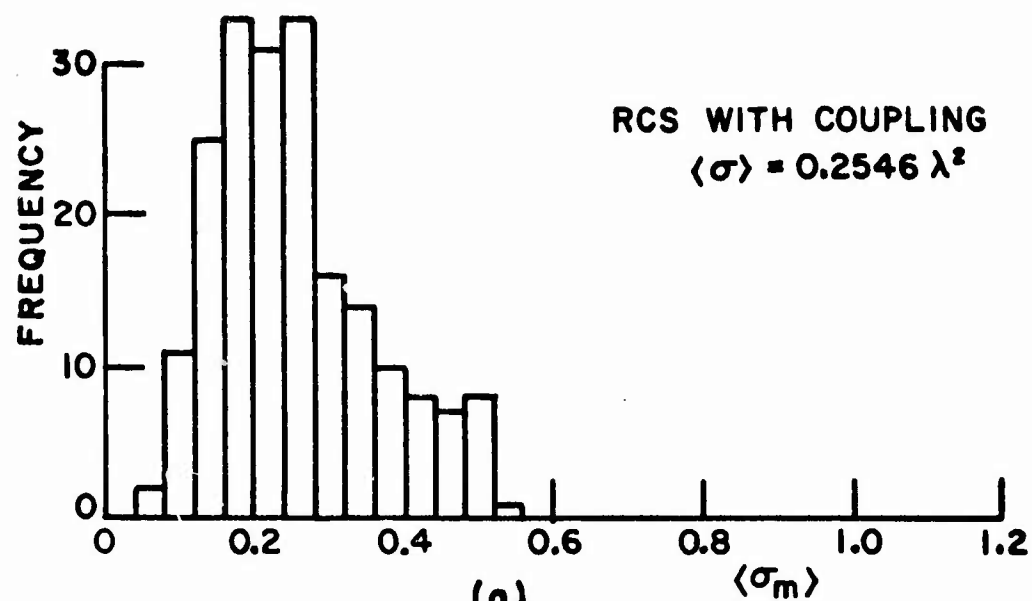


Figure 95. Histograms of the spatially averaged radar cross sections of the clouds generated for Fig. 94: (a) with coupling (b) with no coupling.

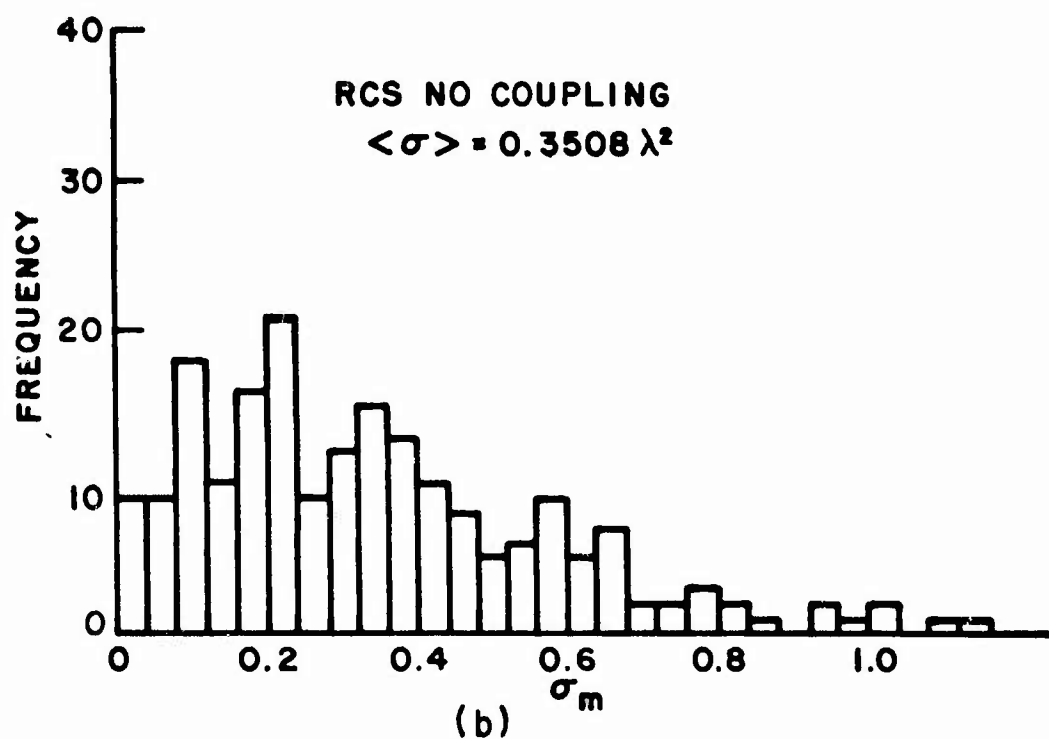
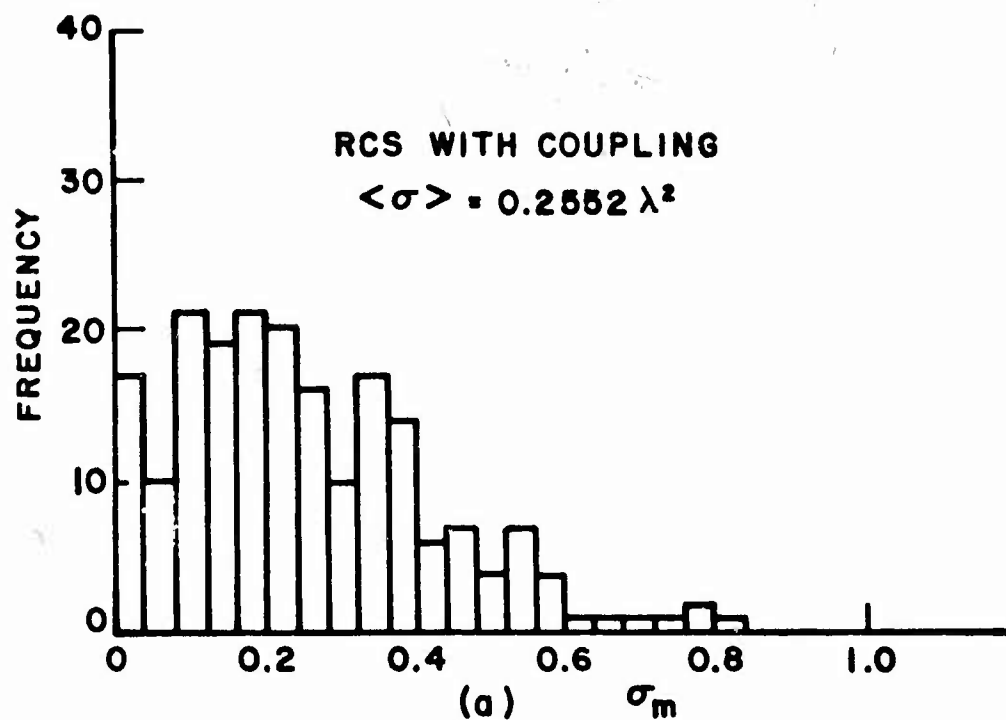


Figure 96. Histograms of the radar cross sections (single aspect) of the clouds generated for Fig. 94.  
 (a) with coupling (b) with no coupling.

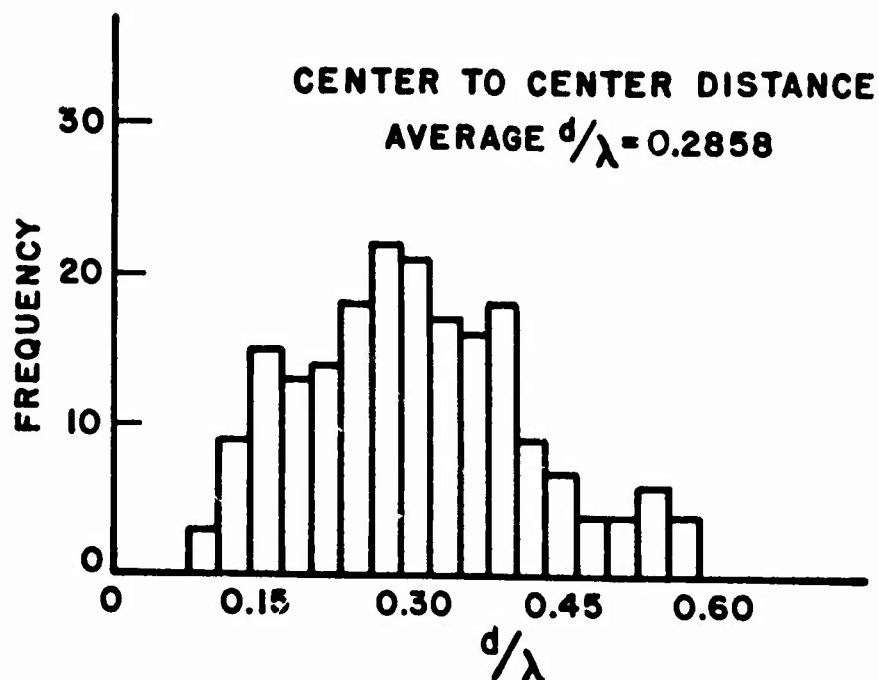


Figure 97. Histogram of the center-to-center distance of random two-dipole clouds. Average spacing  $d/\lambda \approx 0.29$ .

From Figs. 95a and 98a, for the two dipoles coupled, we see a trend consistent with what has been said in the above paragraph. These figures show an average cross section of  $\sim 0.25\lambda^2$  for both the far-spaced and the near-spaced dipoles, seemingly violating the earlier conclusion that the near-spaced dipoles, because they are more strongly coupled, should present a smaller average cross section than do the far-spaced dipoles. What we are seeing however is the effect of coherent excitation due to the close proximity of the wires, an effect which increases the average cross section. It is not increased as high as the uncoupled wires, however, due to the coupling which tends to reduce the average cross section, and so ends up with a value which in our example happens to about equal that for the coupled wires with larger spacing.

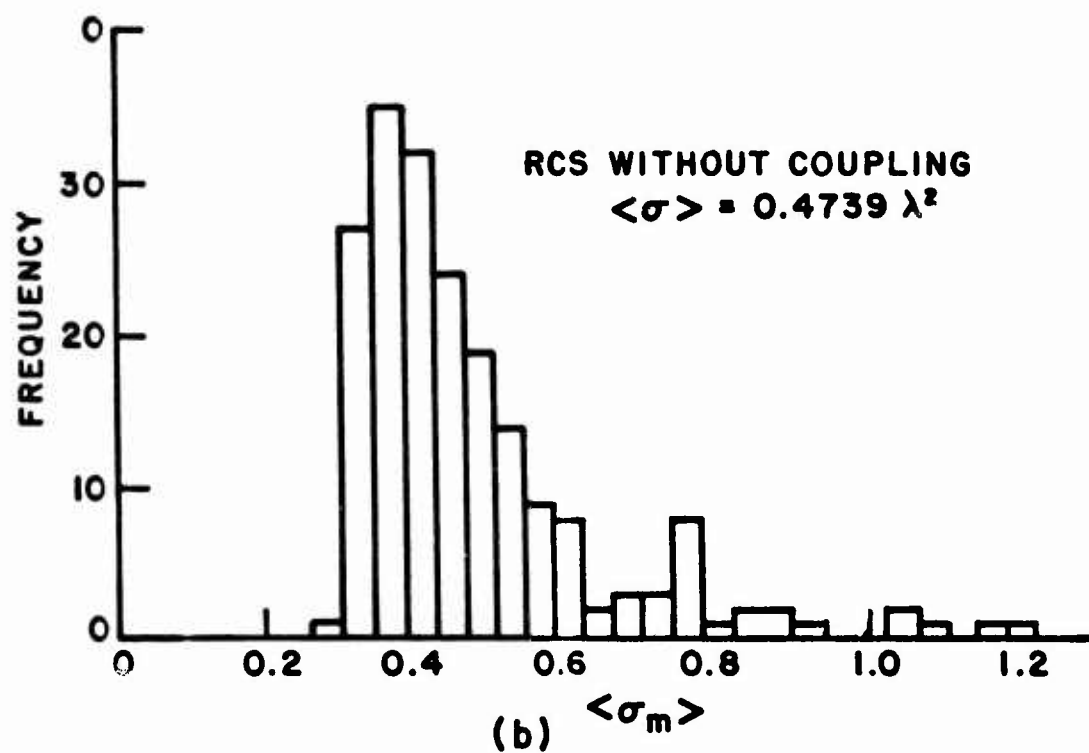
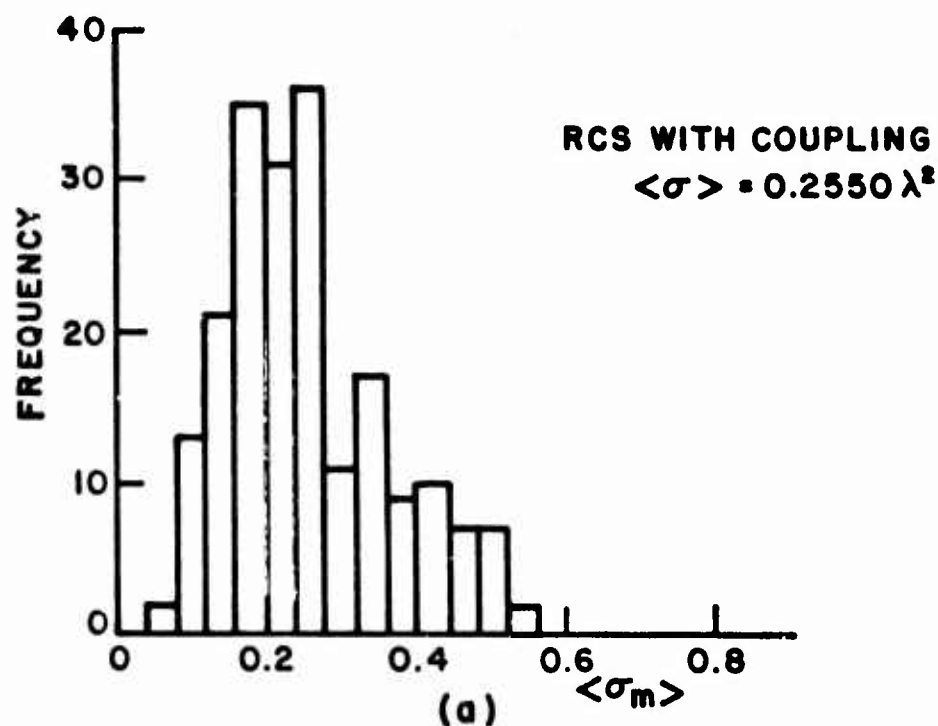


Figure 98. Histograms of the spatially averaged radar cross sections of the clouds generated for Fig. 97. (a) with coupling (b) with no coupling.

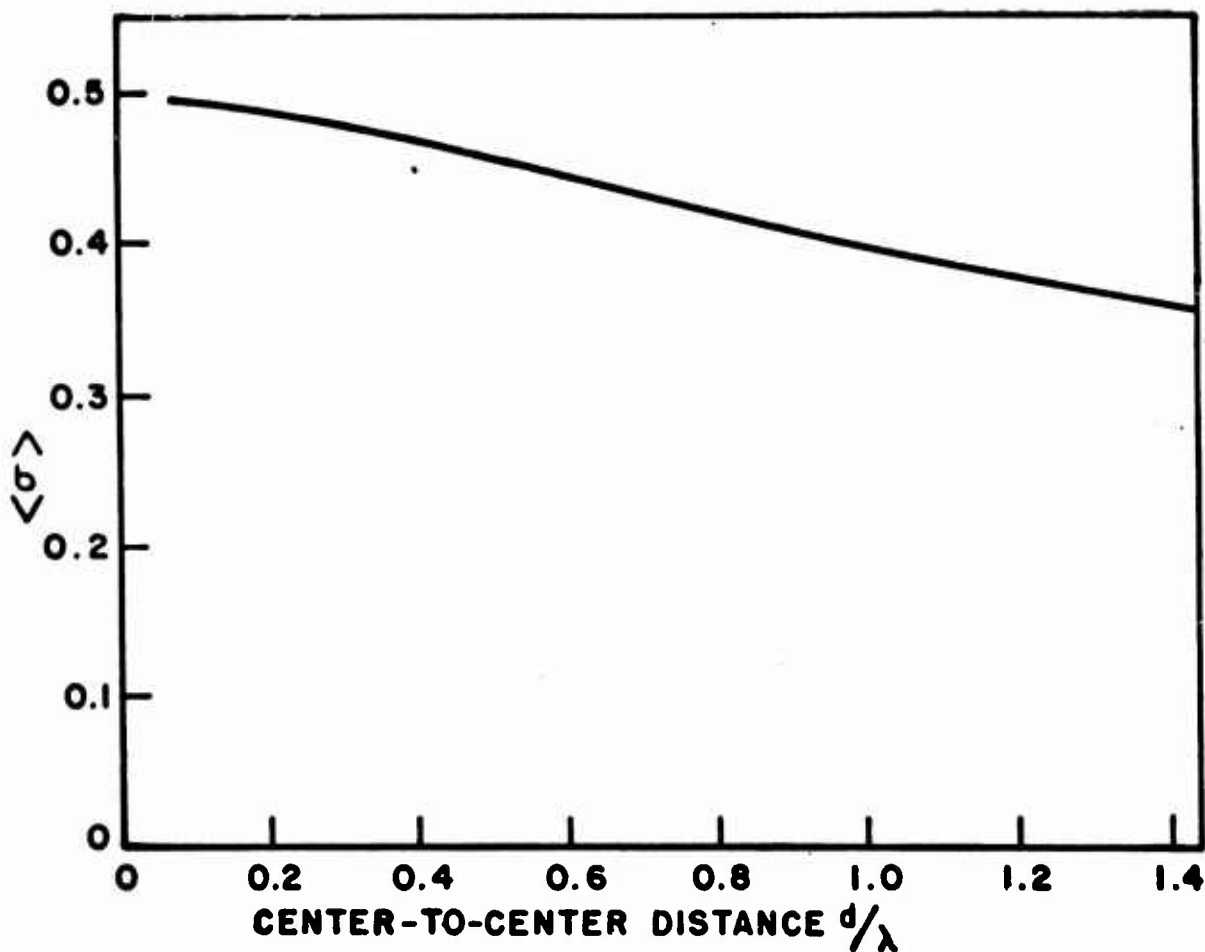


Figure 99. Average cross section of random two-dipole clouds as a function of average center-to-center spacing between dipoles.

#### E. The Question of Mixed Lengths

Tenuous chaff clouds consisting of wires of identical length resonating at about a half wavelength display a bandwidth of about 20%, or somewhat greater for denser clouds (see Fig. 15). Threats which are expected over a greater bandwidth than this demand the use of a variety of wire lengths within the same chaff cloud. This poses the question, what is the influence of coupling on chaff elements of mixed lengths? If the bandwidth ratio of interest is 10 to 1 for example, at the low end of the spectrum some wires will be  $0.05\lambda$  long and others will be  $0.5\lambda$  long. At the high end of the spectrum, some wires will be  $0.5\lambda$  long and others will be  $5\lambda$  long. The first case presents little difficulty - the shorter



wires are very ineffective scatterers, coupled only weakly to nearby neighbors and their presence can be ignored to a very good approximation. The second case does present problems, however, because the larger wires require a large number of segments to model them accurately. This has the undesirable effect of reducing the total number of wires permitted in a cloud, assuming a fixed matrix size.

During the period of this contract, we made a brief investigation of small clouds containing wires of two lengths,  $0.475\lambda$  and  $0.703\lambda$  long. The shorter wires were resonant, each one in isolation having a maximum tumble average cross section of about  $\langle\sigma_1\rangle \simeq 0.15\lambda^2$ ; the longer wires were antiresonant, each one in isolation having a minimum tumble average cross section of about  $\langle\sigma_2\rangle \simeq 0.038\lambda^2$  [61]. These two lengths were purposely chosen to take advantage of their maximum disparity in tumble average echo. Four curves, shown in Figs. 100-103, were generated, each showing the calculated averaged backscattering cross section  $\langle\sigma_m\rangle$  of clouds containing  $N = 2, 4, 6$ , and  $8$  wires, averaging being over 512 look angles in the  $\theta-\theta$  and  $\phi-\phi$  polarizations of transmitter and receiver. Ten clouds, each with these numbers of wires, were calculated and the  $\langle\sigma_m\rangle$  of each are plotted as a dot. The ensemble average of these ten values are plotted as a cross. Four different values of average spacing,  $d/\lambda = 4.0, 1.0, 0.5, 0.25$ , as defined for inhomogeneous clouds, were assumed, and in all cases equal numbers  $N_1=N_2=N/2$  of wires of the two lengths were assumed. On each of the curves, the straight line  $N_1\langle\sigma_1\rangle+N_2\langle\sigma_2\rangle$  vs  $N$  appears in order to give the reader an estimate for the average echo in the absence of coupling. The trends are the same as those observed in previous work treating clouds of identical resonant wires. Average echo is reduced by coupling but not by as large a percentage as in the case where all wires are resonant. For example, for  $d/\lambda = 0.5$ , if all  $N$  wires are resonant, one expects the average echo of  $N$  wires with coupling to be about 60% of that with these same wires uncoupled. If, however, the  $N$  wires are half resonant and half antiresonant, one can expect the average echo of the  $N$  wire mixture to be about 78% of that with the same wires uncoupled. Evidently, the antiresonant dipoles, whose tumble average echo is naturally low, are not so severely influenced by coupling.

The computer program used to generate data for multiple length chaff is given in Appendix D.

#### F. Additional Experimental Results

During the earlier phases of this program a few experiments were performed to gather data, to check, or to complement calculated data. Some of the results of these experiments have already been presented where appropriate; in this section we document whatever other experimental data were recorded.

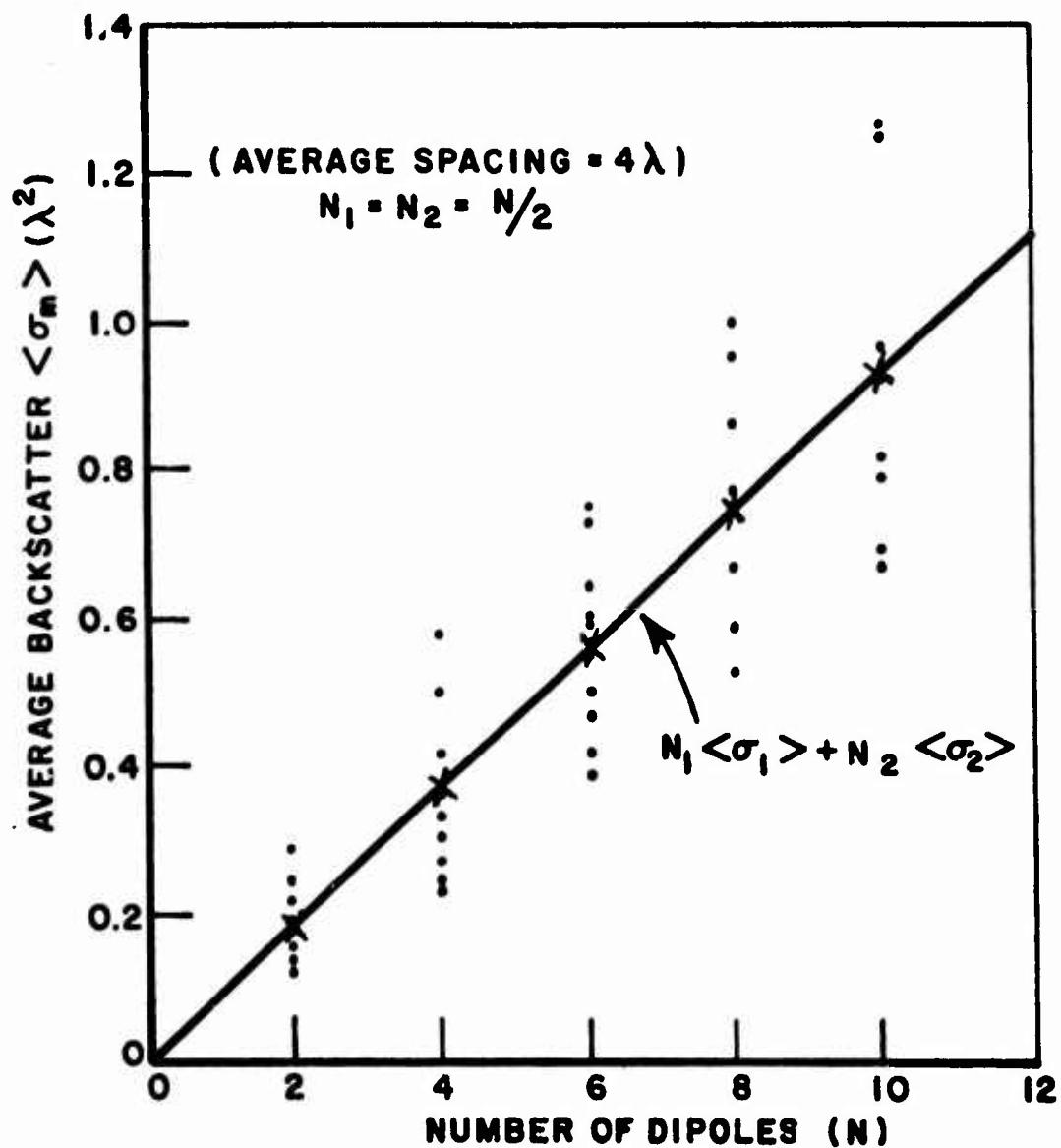


Figure 100. Calculated average backscattering cross sections for ensembles of clouds containing equal numbers of two wire lengths,  $\ell_1/\lambda = 0.495$ ,  $\ell_2/\lambda = 0.703$ , with average spacing  $d/\lambda = 4.0$ . Straight line represents decoupled dipoles, crosses are averages of the data.

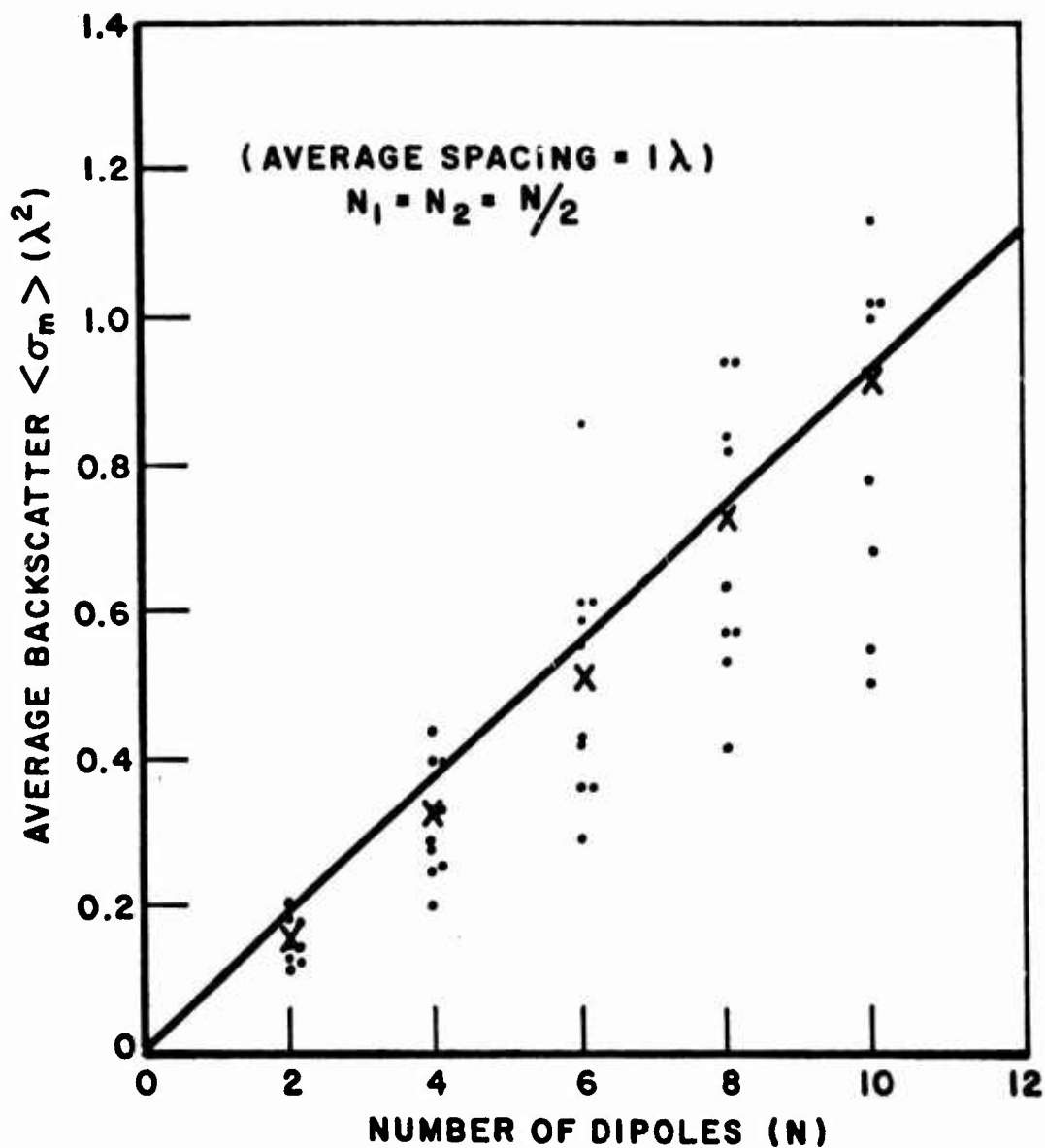


Figure 101. Calculated average backscattering cross sections for ensembles of clouds containing equal numbers of two wire lengths,  $\ell_1/\lambda = 0.495$ ,  $\ell_2/\lambda = 0.703$ , with average spacing  $d/\lambda = 1.0$ . Straight line represents decoupled dipoles, crosses are averages of the data.

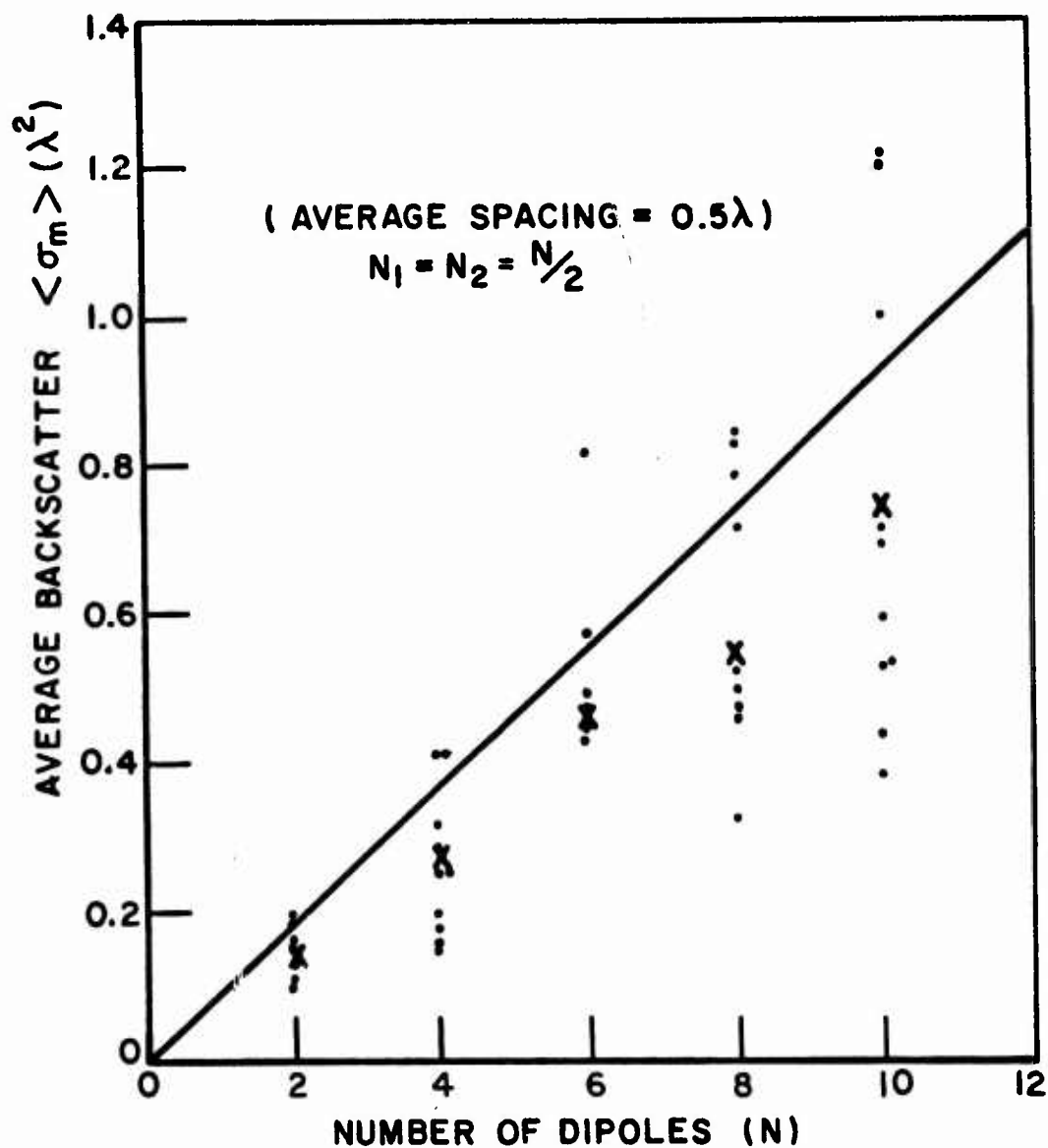


Figure 102. Calculated average backscattering cross sections for ensembles of clouds containing equal numbers of two wire lengths,  $l_1/\lambda = 0.495$ ,  $l_2/\lambda = 0.703$ , with average spacing  $d/\lambda = 0.5$ . Straight line represents decoupled dipoles, crosses are averages of the data.

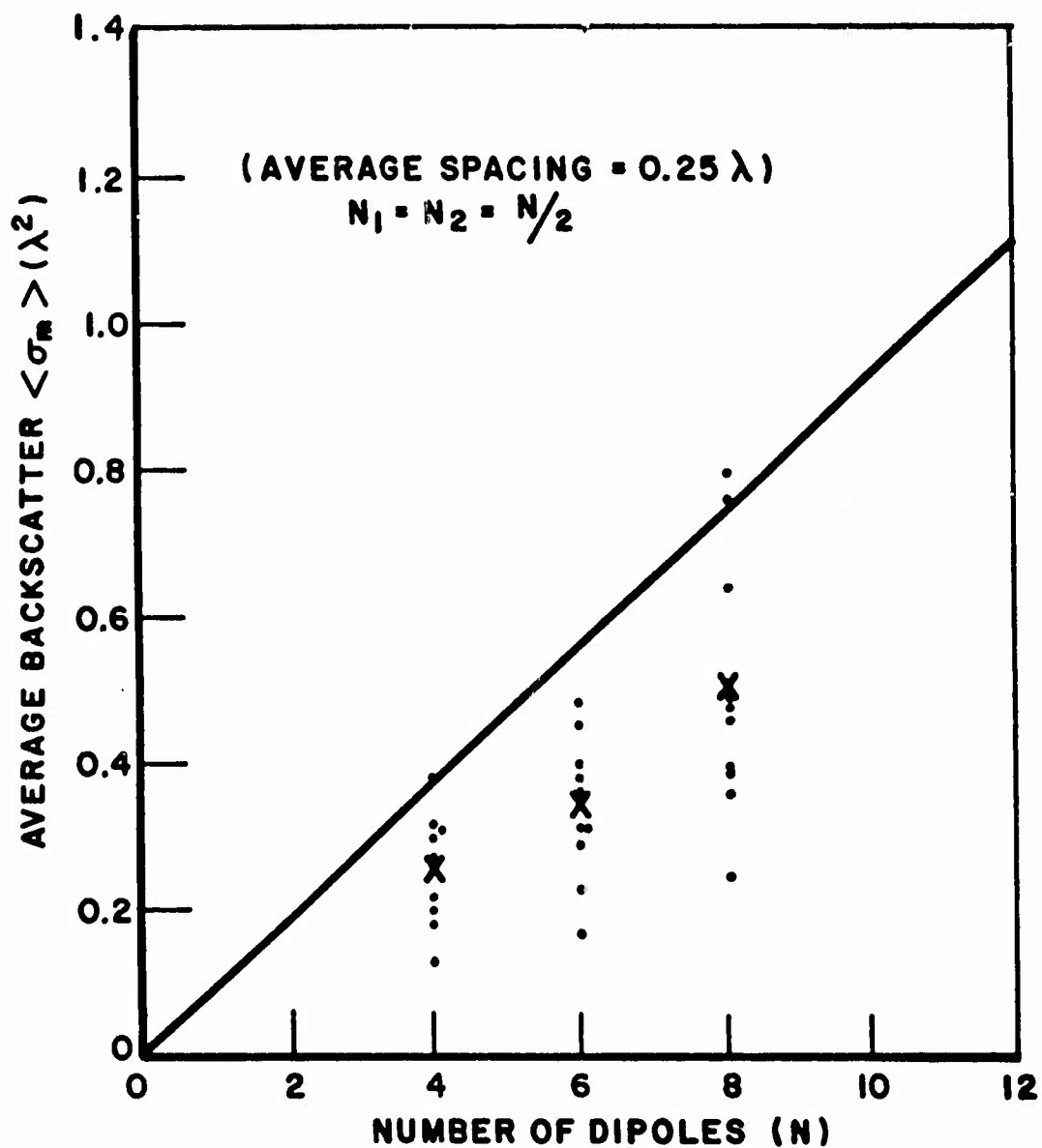


Figure 103. Calculated average backscattering cross sections for ensembles of clouds containing equal numbers of two wire lengths,  $\lambda_1/\lambda = 0.495$ ,  $\lambda_2/\lambda = 0.703$ , with average spacing  $d/\lambda = 0.25$ . Straight line represents decoupled dipoles, crosses are averages of the data.

## (1) Experimental Verification

It is important to verify that the data calculated by computer are indeed good approximations to what would be measured in controlled laboratory experiments. Such experiments were performed on selected frozen models which were considered to be severe tests of the computer predictions. Figures 104 and 105 show photographs of a matrix of 125 carefully dimensional 2.0" x 2.0" styrofoam cubes. Each cube can have embedded in it (by means of an accurately machined jig) a rod, located near one edge. By orienting each cube in one of 12 different possible positions and placing it in a styrofoam box, a cloud of 125 dipoles can be built up. Although this scheme does not allow all possible orientations of the dipoles, there is a sufficient variety of orientations and spacings to create a rather aperiodic structure.

The most severe test of the accuracy of the computer routines is to compare experimental and calculated backscattering patterns (using full matrix Scroust) when all dipoles are oriented parallel in a regular periodic array and closely spaced. Results for two such cases are presented in Figs. 106 and 107 for 27 dipoles and 125 dipoles, respectively. In both cases all dipoles were horizontal and the backscattering cross sections for horizontal polarizations of transmitter and receiver were recorded in a horizontal 360° cut around the cloud. A frequency of 3.13 GHz was chosen to bring each dipole to its free space resonance, and caused a spacing between adjacent dipoles of  $d/\lambda = 0.53$ . Typical disparities of about 2 dB are evident, but the overall pattern is well predicted. Some of the disparity is due to imperfections in the mathematical model and round off error, but most of the error is caused by errors in measurement. We made several experimental runs, tearing the cloud apart and reconstructing it as identically as possible between each run, and found that the experimental data had a variance which enclosed the calculated curves. This convinced us that the computer routines are accurate and the data based on them are as valid as if measured. Another 27-dipole cloud was constructed with the dipoles randomly oriented with an average spacing of  $d/\lambda = 0.53$ . Calculated and measured results are shown in Fig. 108 and again they compare very well.

In the above experiments, the 125-cube styrofoam matrix without dipoles had an echo below the internal noise level of the measuring system.

## (2) Extinction Measurements Through an Artificial Chaff Cloud

A beam proceeding through a random medium such as a chaff cloud suffers energy loss through scattering by each particle into directions other than forward and into polarizations other than incident. This



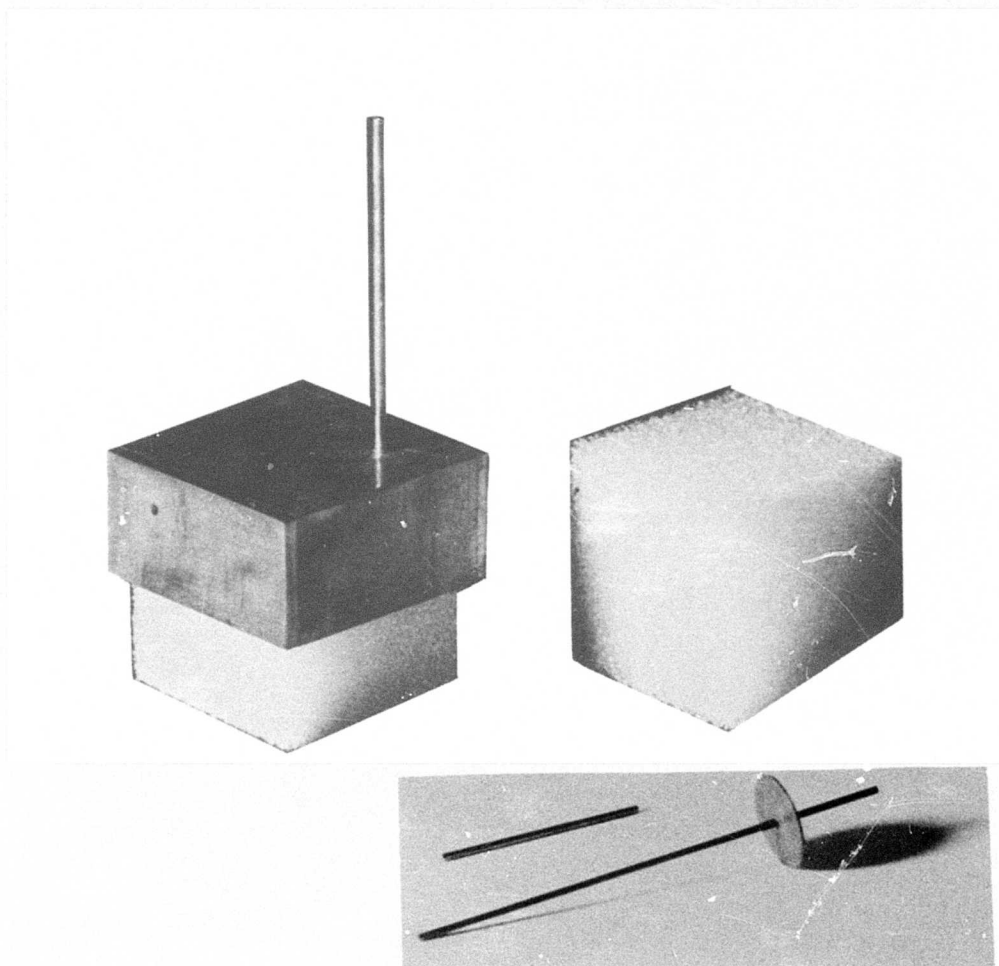


Figure 104. A typical styrofoam 2" cube, dipole, and jig for accurately inserting the dipole.

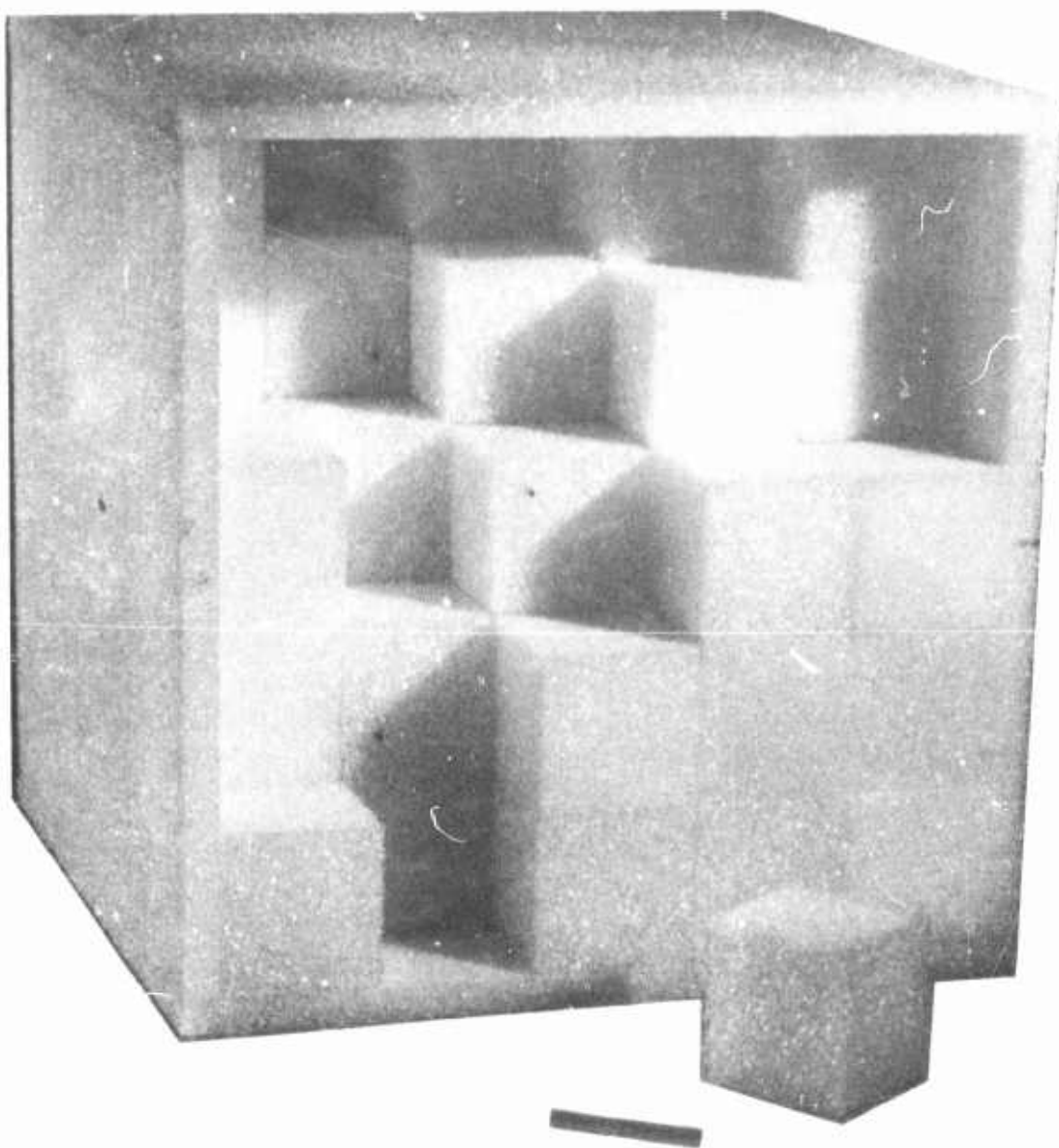


Figure 105. Styrofoam cubes in styrofoam box for creating a cloud of dipoles.

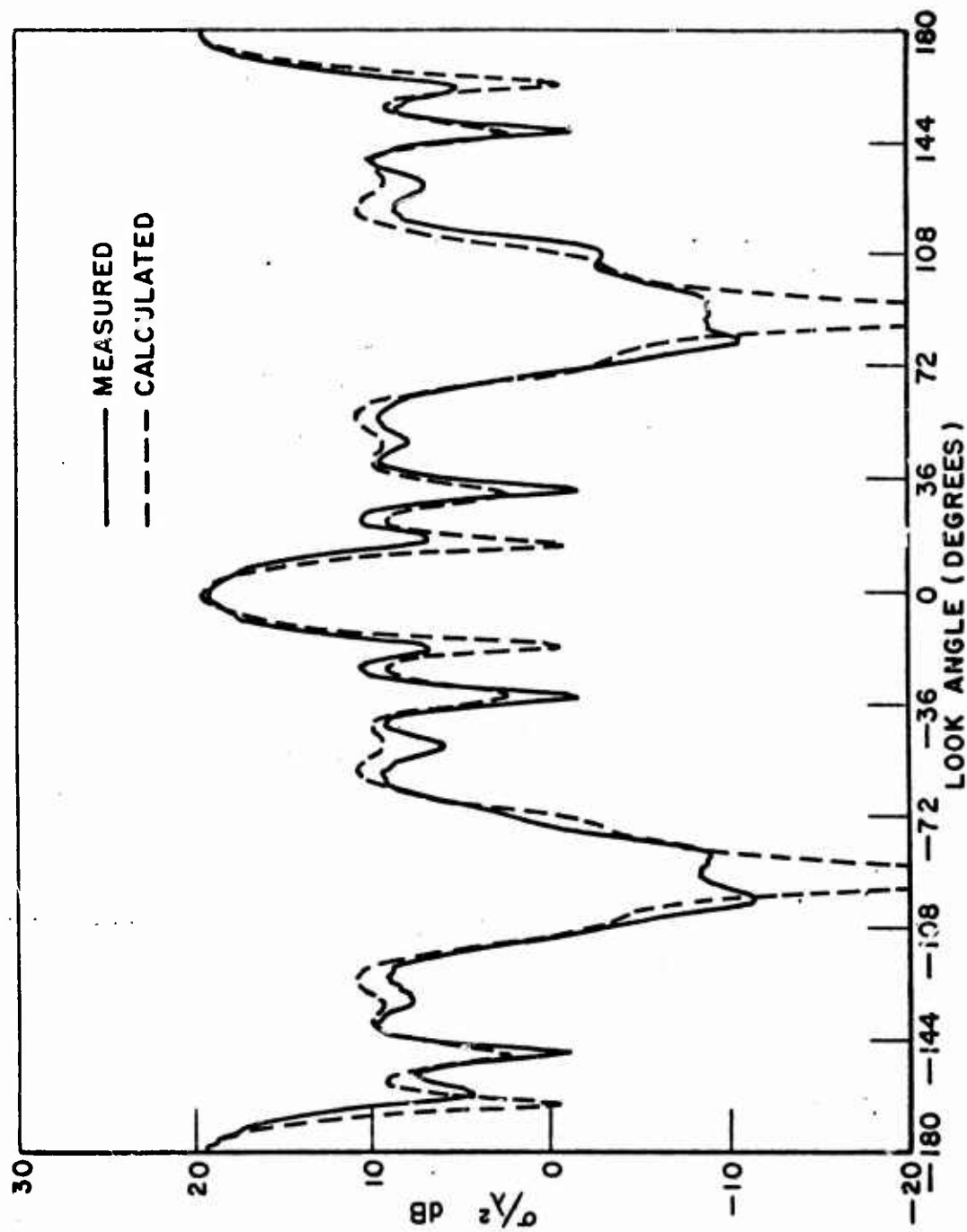


Figure 106. Measured and calculated E-plane backscattering cross-section patterns for a 3 x 3 x 3 array of 27 parallel dipoles spaced about 0.53λ apart.

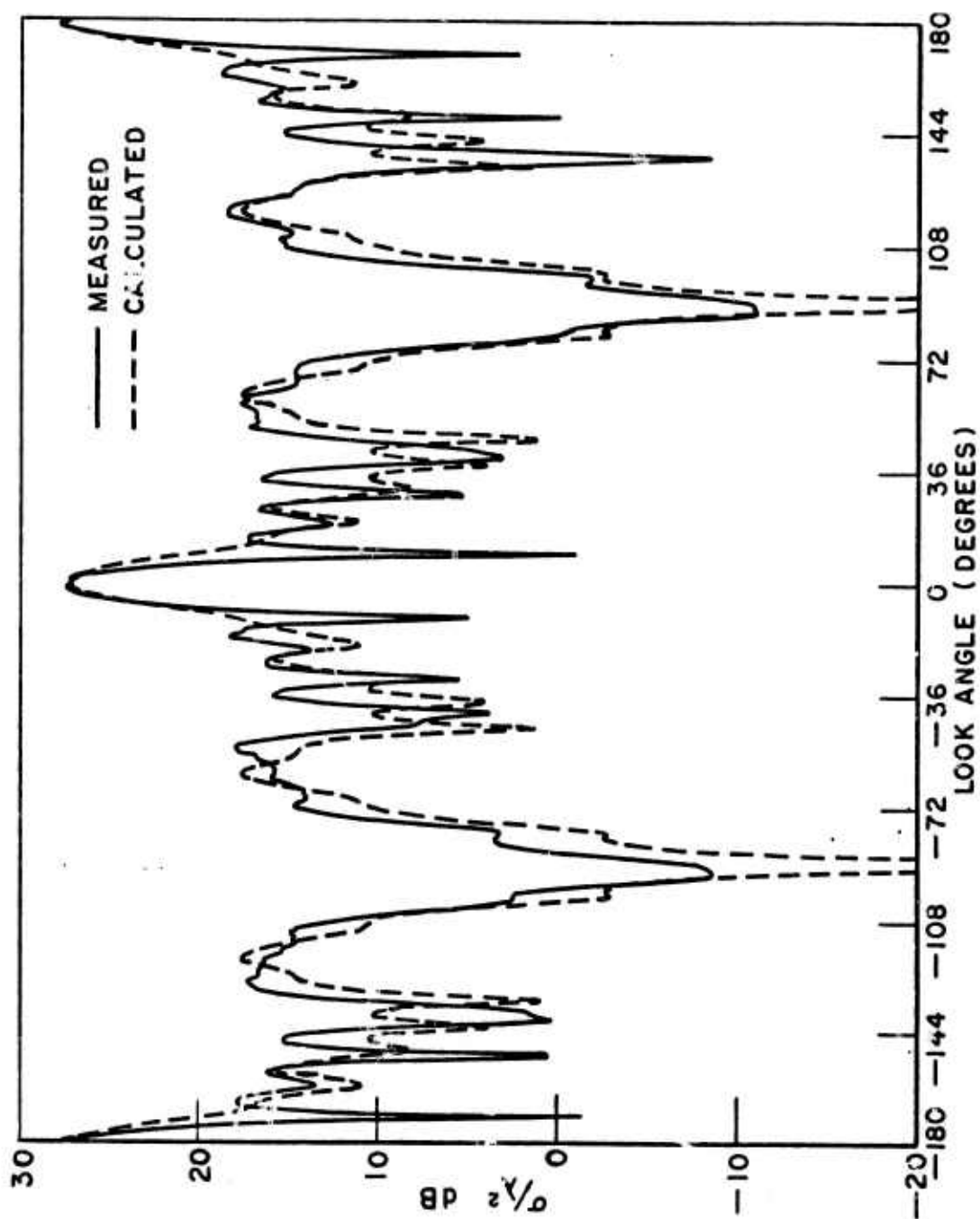


Figure 107. Measured and calculated E-plane backscattering cross-section patterns for a 5 x 5 x 5 array of 125 parallel resonant dipoles spaced about  $0.53\lambda$  apart.

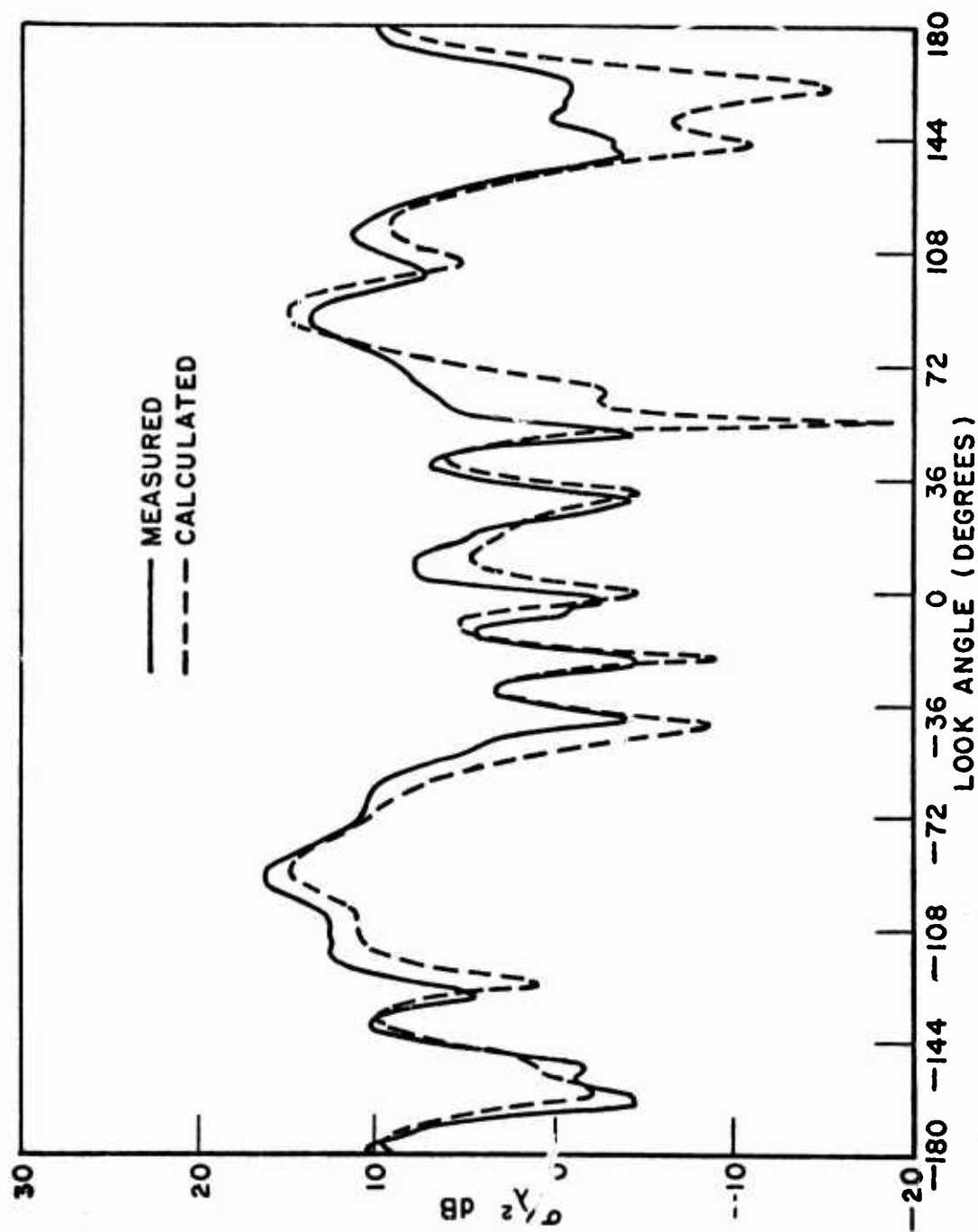


Figure 108. Measured and calculated E-plane backscattering cross-section patterns for a cloud of 27 dipoles randomly oriented in styrofoam cubes. Average dipole spacing was  $0.53\lambda$ .



extinction of the beam is important to chaff cloud investigations because, clearly, if it causes a significant diminution of energy toward the rear of the cloud, chaff elements there will be relatively ineffective contributors to backscatter and might be better used elsewhere. To observe extinction and extinction rate through a chaff cloud as functions of dipole density is therefore of interest to us. However, to obtain significant extinction requires a sizeable cloud containing thousands of dipoles, and considering that the problem is a statistical one in which many similar clouds must be generated to obtain averages, the computer generation of extinction data becomes a formidable task. Moreover, in the early part of this program we did not have the capability of generating such large clouds, so we turned to a few experiments to observe the extinction through artificial chaff clouds. In this section we document some of the results of these experiments.

Figures 109-112 show the average insertion loss observed between a horn antenna and a receiving dipole probe situated in various line-of-sight positions within a medium of tumbling resonant dipoles. The dipoles were enclosed in a wooden "box", 30" long in the direction of propagation and having a 24" square cross section, with foam "windows" at both ends and hairflex absorber (or aluminum foil) lining on the other four walls. The box was supported on circular rims such that it could be rotated continuously about the line-of-sight axis, thereby tumbling its contents in a random manner. The dipole probe, encapsulated in a protective foam sphere, was drawn along the line-of-sight from the front window to the rear one along a slender dielectric-tube containing the coaxial line exiting through the rear window and feeding the receiver. A horn antenna disposed about 33" from the front window served as the illuminating source. The signal received from the probe was measured for several minutes duration of tumbling and averaged over this time period for selected probe positions between the windows.

The curves shown in Figs. 109-112 show the averaged difference (in dB) between the received signals without and with dipoles in the box, i.e., insertion loss, for polarization of the probe parallel to and orthogonal to the incident linearly polarized wave. Ideally, this differencing scheme should remove the effect of range on energy decrease and leave only the extinction due to particle scattering. All data were taken at about 2.9 GHz. Figure 109 shows results for 1000 resonant dipoles (nails), each one encapsulated completely in a 2.38" foam sphere. Figure 110 shows results for 1000 resonant dipoles (copper wire), each one encapsulated completely in a 2" diameter foam sphere, tumbled together with 850 free dipoles. Figure 111 shows results for ~3200 resonant dipoles (nails) in 1-1/2" foam spheres while Fig. 112 shows results for ~7200 resonant dipoles (nails) in 1" foam spheres. (In these latter two cases the dipoles protruded outside the spheres.) The effects of progressively higher dipole densities is evident in the progressively increasing



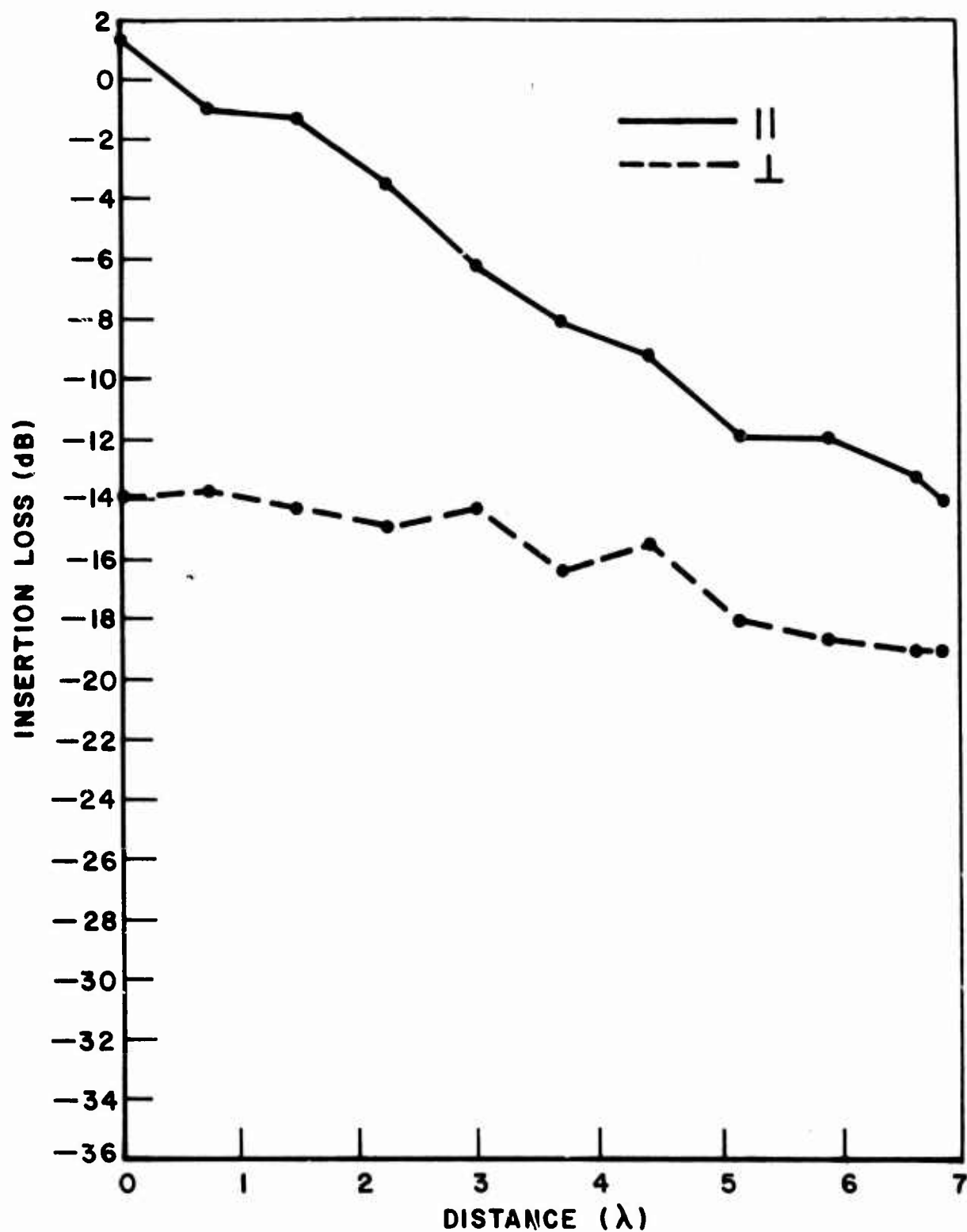


Figure 109. Measured insertion loss of same-sense and cross-sense polarizations for 1000 resonant dipoles encapsulated in 2.38" foam spheres,  $f \approx 2.9$  GHz.

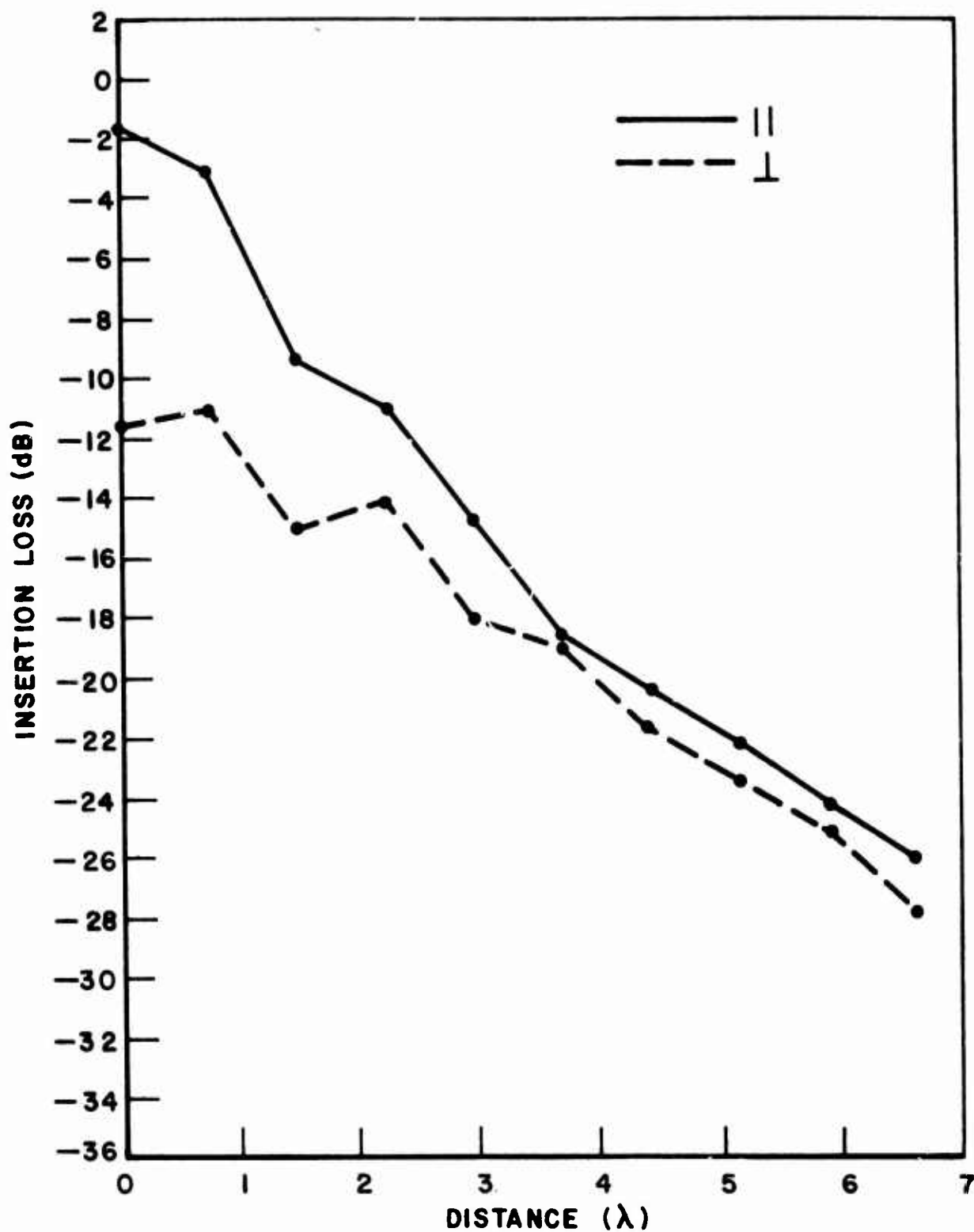


Figure 110. Measured insertion loss of same-sense and cross-sense polarizations for 1000 resonant dipoles encapsulated in 2" foam spheres, plus 250 free dipoles.  $f \approx 2.9$  GHz.

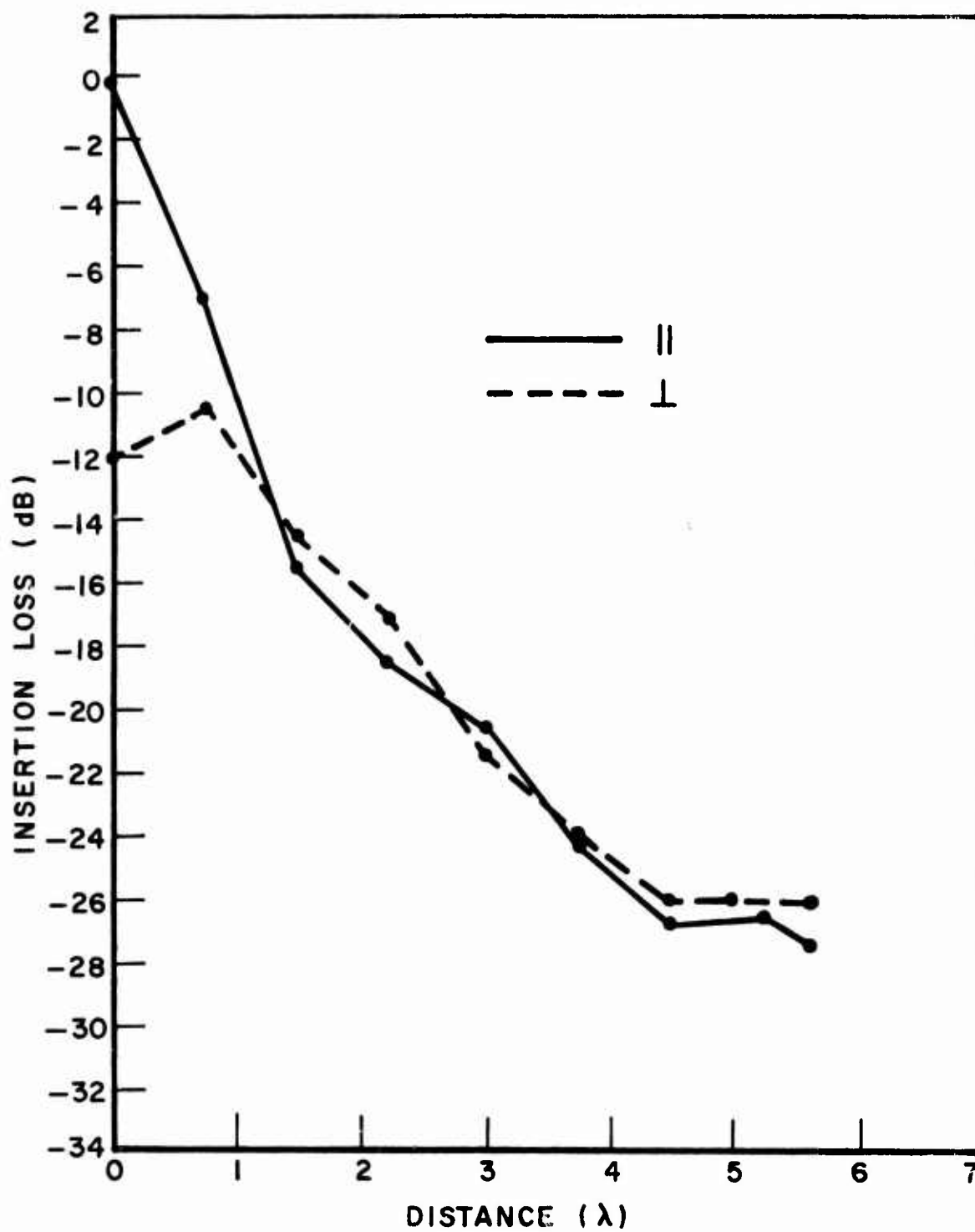


Figure 111. Measured insertion loss of same-sense and cross-sense polarizations for  $\sim 3200$  resonant dipoles encapsulated in 1-1/2" foam spheres.  $f \approx 2.9$  GHz.

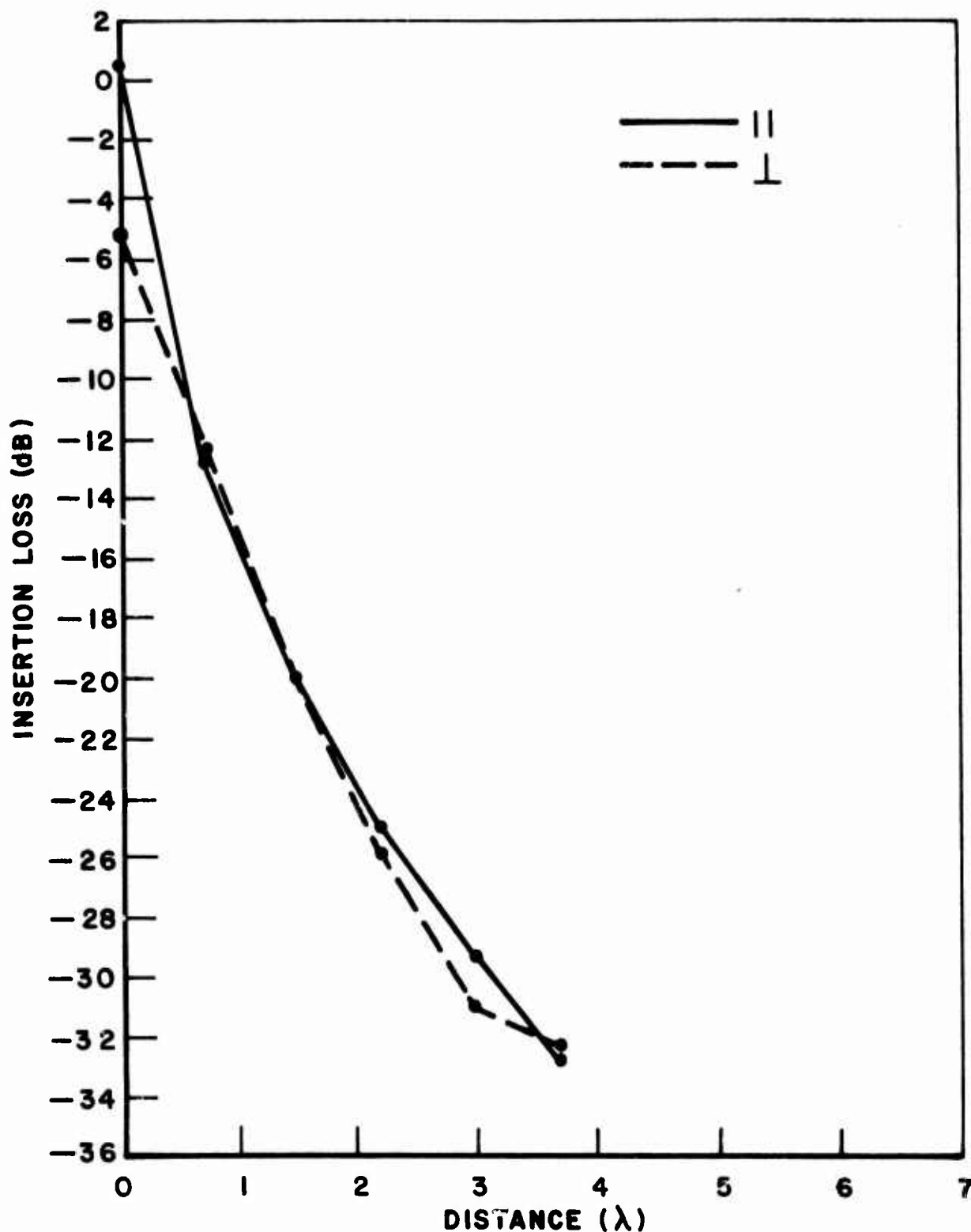


Figure 112. Measured insertion loss of same-sense and cross-sense polarizations for  $\sim 7200$  resonant dipoles encapsulated in 1" foam spheres.  $f \approx 2.9$  GHz.

extinction rates shown in this sequence of figures. Some standing wave effects between the windows are also evident in the non-monotonically decreasing character of the curves. Averaging this undesired effect out, one observes extinction rates which are higher in the region within 3 or 4 wavelengths of the front interface than they are deeper in the cloud. Deep in the cloud the parallel and orthogonally polarized components exhibit the same extinction rates as well as the same extinction. This is to be expected because deep in the cloud the incident wave has been so severely depolarized by the many random scattering interactions that no polarization preference exists. Table 8 lists the approximate extinction rates deep in the cloud.

TABLE 8  
EXPERIMENTALLY DETERMINED EXTINCTION RATES

Fig. No.	Density ( $\text{dip}/\lambda^3$ )	Extinction rate ( $\text{dB}/\lambda$ )
109	$\sim 5$	$\sim 2.9$
110	$\sim 7$	$\sim 3$
111	$\sim 9$	$\sim 3.6$
112	$\sim 12$	$\sim 6$

The dipole densities listed here are rough estimates.

Some additional tests were performed with metal sheets covering two and then four of the hairflex-coated walls. Energy scattered by the particles out of the incident beam into the walls is absorbed there if all walls are hairflex. This would simulate a cloud smaller in transverse extent than the incident beamwidth, any energy exiting the sides of the cloud being lost to space. Energy scattered by the particles out of the incident beam into the walls is reflected back into the beam if all the walls are metal. This would simulate a very large cloud illuminated by a plane wave. As expected, the extinction rate was reduced in this latter case; for example, in one set of tests the observed rates deep in the clouds were  $4.1 \text{ dB}/\lambda$ ,  $3 \text{ dB}/\lambda$ , and  $1.8 \text{ dB}/\lambda$  with 0, 2, and 4 walls covered with metal, respectively.

### (3) Scattering from Touching Chaff Elements

A series of measurements were made of the radar backscatter from 4" foam spheres sprinkled with aluminum strip chaff and aluminized glass chaff provided by the Avionics Laboratory. Figures 113-116 relate to the aluminum strip chaff and Figs. 117 and 118 relate to the glass chaff. In all figures, the solid curves represent the echo of a 4" foam sphere silver-painted (its imperfect surface explaining the echo fluctuations with  $360^\circ$  of rotation). The other curves represent foam spheres coated with the chaff elements. Each figure presents two such curves, for two  $360^\circ$  cuts about the sphere, each labelled with the curve average in  $\lambda^2$ .

The chaff elements were applied by sprinkling them randomly upon a sphere made tacky with a spray solvent. The aluminum strip chaff density was quite low - on the order of a 100 elements distributed over the whole surface. (A surface density of about  $0.5 \text{ dipole}/\lambda^2$ .) They were 1.5 cm long, implying resonance of an individual dipole at about 9.5 GHz. Because so few elements touched, the sequence of curves (Figs. 113-116) show a resonance effect about this same frequency. The average echo at resonance (9.53 GHz) was on the order of  $6.6\lambda^2$ , about equal to the cross section of a solid metal sphere. It's also about equal to 50 (i.e., one half the total number of dipoles) times the tumble average cross section of a single dipole at resonance, giving the impression that the front hemisphere looks almost like a solid metal hemisphere, shielding the elements on the back hemisphere. A short effort (described in a monthly letter to the sponsor) was devoted to investigating this shielding effect, but results were inconclusive.

#### G. The Aircraft-Chaff-Tracker Interaction Problem

During the last month of the contract, the sponsor supported an effort to computer-simulate the interaction of a combined aircraft-chaff cloud target with a split-gate missile tracking radar. Because the research effort is concurrent with the writing of this final report, only its general outline is described here. Details are presented in Appendix G.

A computer software routine has been developed which presents on a CRT the simulated aircraft radar plot of both the PPI indicator and a height finding indicator. Relative orientation of both aircraft and missile are displayed as a visual aid. Evasive aircraft maneuvers in all three dimensions and in time incorporating preselected aircraft response characteristics (due to inertia and stress limitations) can be controlled by the operator. Chaff clouds are deployed at will by action of the operator. The missile radar, incorporating either a split-gate range tracker or a leading edge range tracker with selected gate width and time response, dictates the trajectory of the missile under selected time response.



characteristics of the angle tracker and missile inertial system. (This program includes a missile velocity increase with time and variable maneuverability with altitude and shift of its center of gravity with burn.) Presently, the aircraft presents to the radar an echo composed of three Gaussian pulses of selected durations and amplitudes. Also, deployed chaff clouds remain fixed in space (but fall behind the aircraft as the aircraft moves ahead) and present to the tracker an echo which remains constant in time and aspect. The integrated radar signal returned from the aircraft and chaff clouds, if any are present, is calculated as a function of time and relative missile position and compared with an assumed thermal noise signal. If the resulting signal-to-noise ratio dips below a selected threshold, break-lock conditions apply and the missile continues on a ballistic flight. Presently, a numerical printout is made of the time-space-S/N history of assumed tactical maneuvers. This is difficult to interpret at a glance, so some consideration is being given to a graphical plot of the same data so that successful tactics can be discerned and modified easily and quickly. Also the data will be taped for later retrieval and analysis. A sketch of this work is given in Appendix G.

Ultimately, the success of the effort described to simulate the radar interaction problem depends upon the validity of the input data, i.e., good radar echo from aircraft and chaff clouds as functions of aspect and time, accurate dynamic response characteristics of the aircraft and missile and of the radar, and realistic tactical maneuvers. It is toward this goal that the present chaff contract and complementary ones are directed.

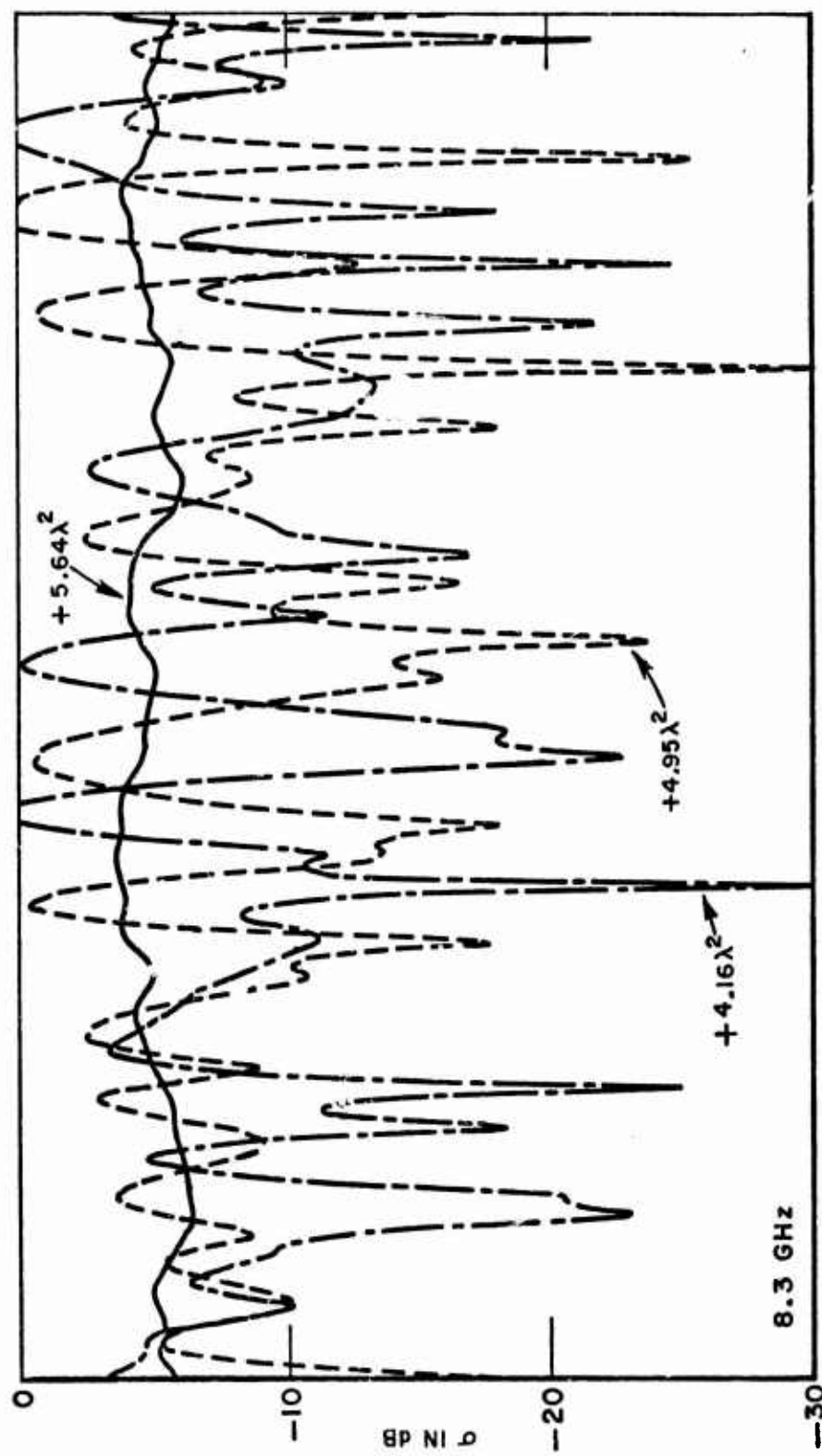


Figure '113. Radar cross section vs 360° of rotation of 1.5 cm Al chaff on 4" foam sphere.

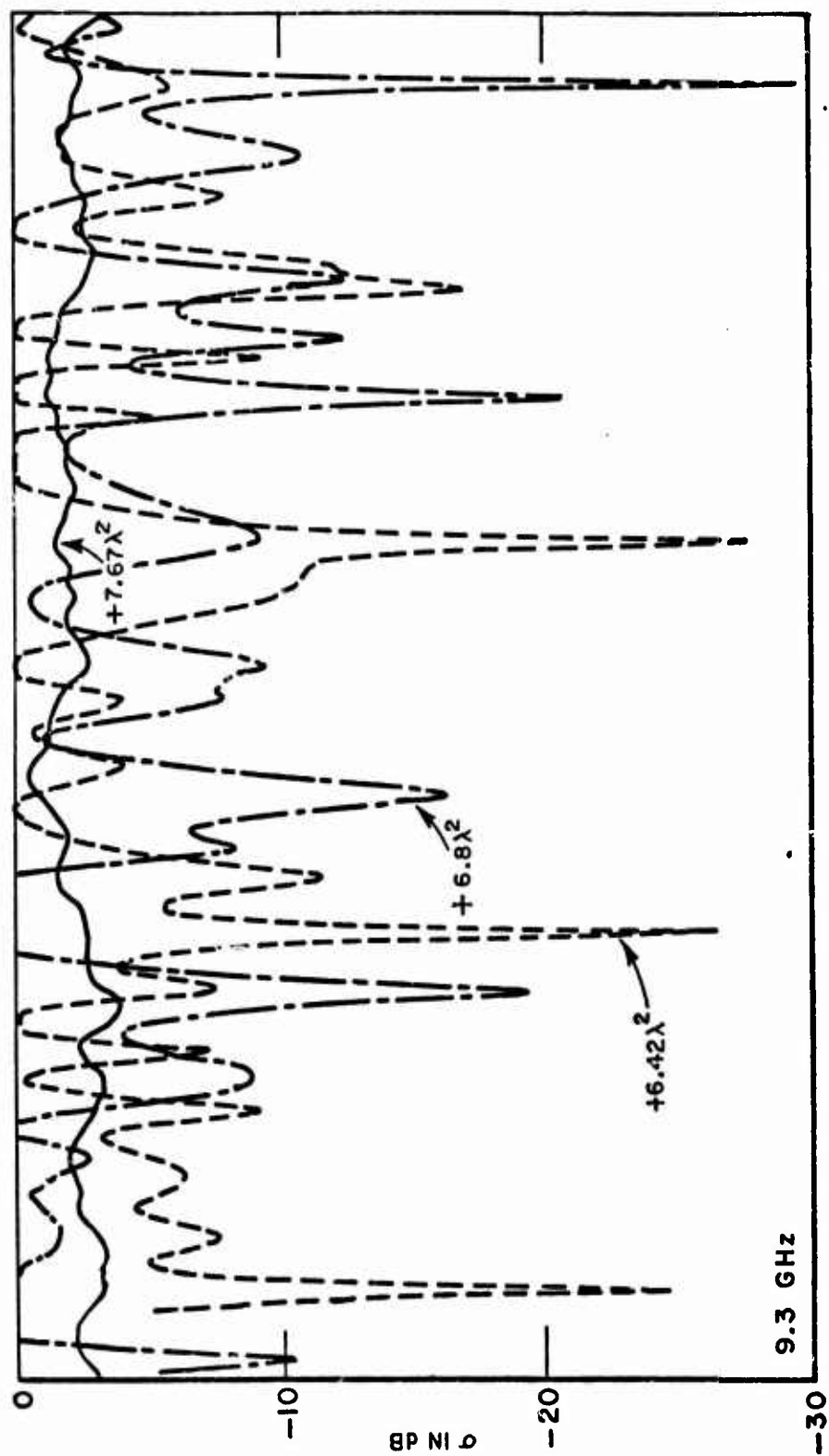


Figure 114. Radar cross section vs 360° of rotation of 1.5 cm Al chaff on 4" foam sphere.

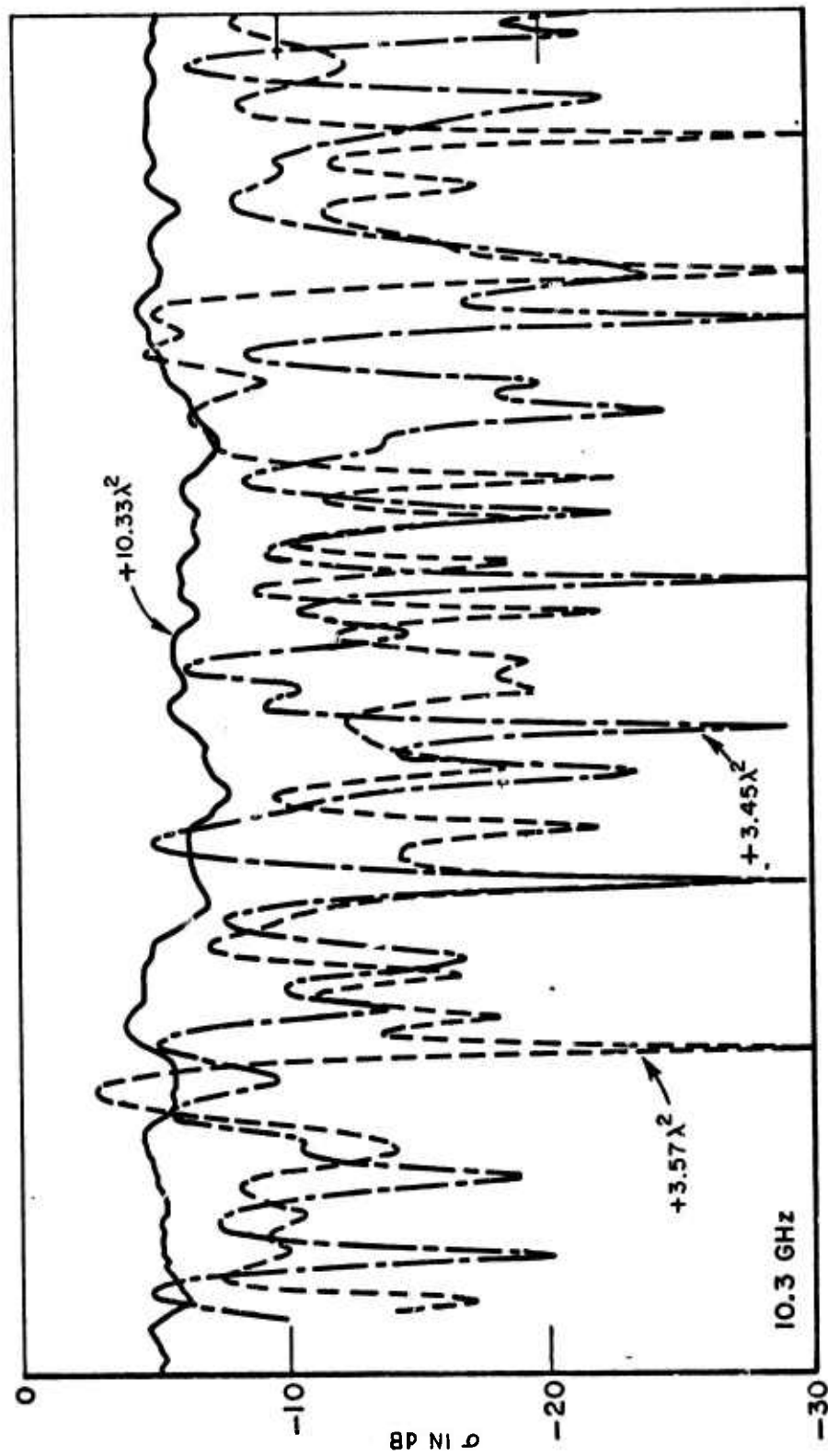


Figure 115. Radar cross section vs  $360^\circ$  of rotation of 1.5 cm Al chaff on 4" foam sphere.

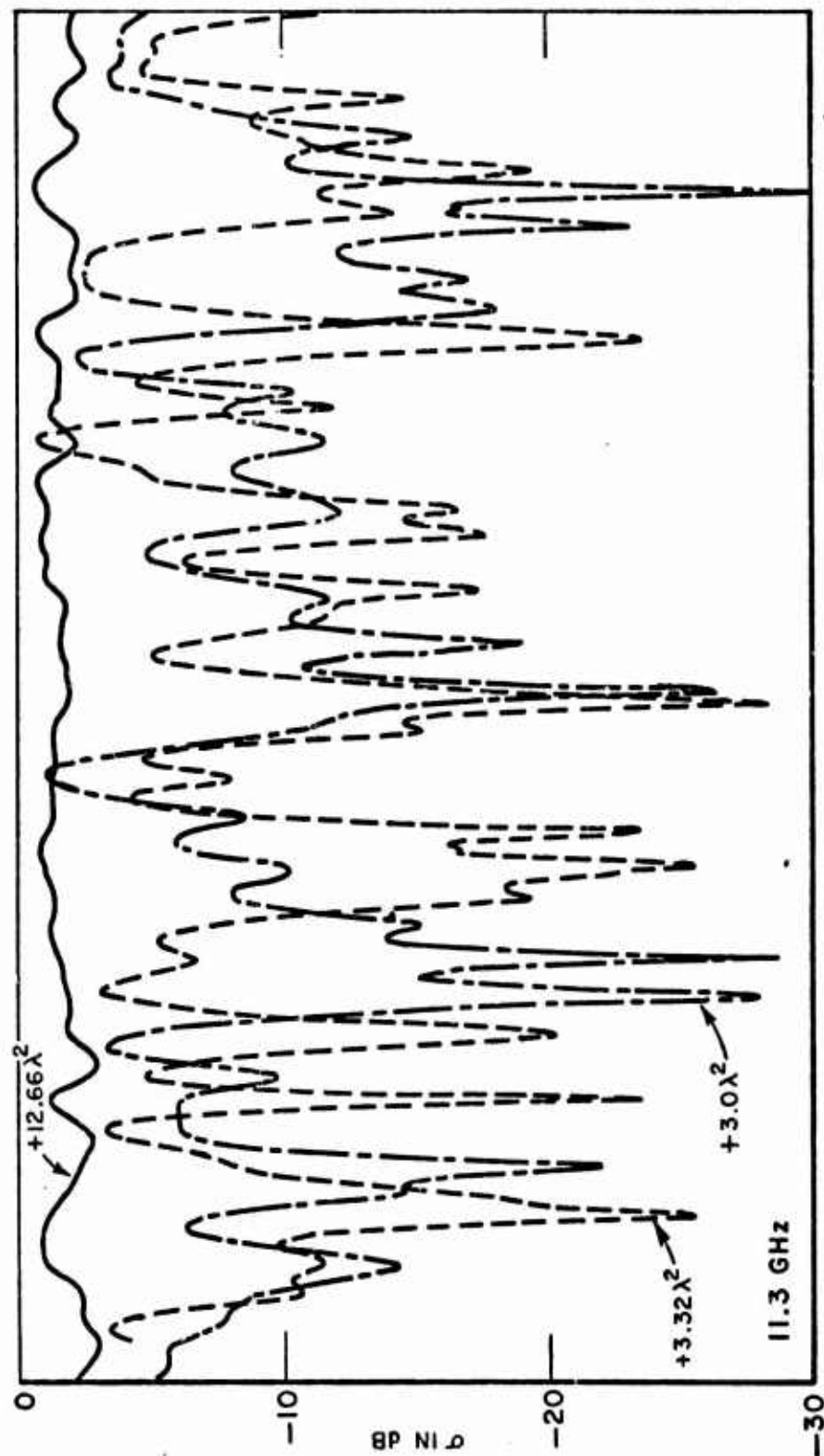


Figure 116. Radar cross section vs 360° of rotation of 1.5 cm Al chaff on 4" foam sphere.

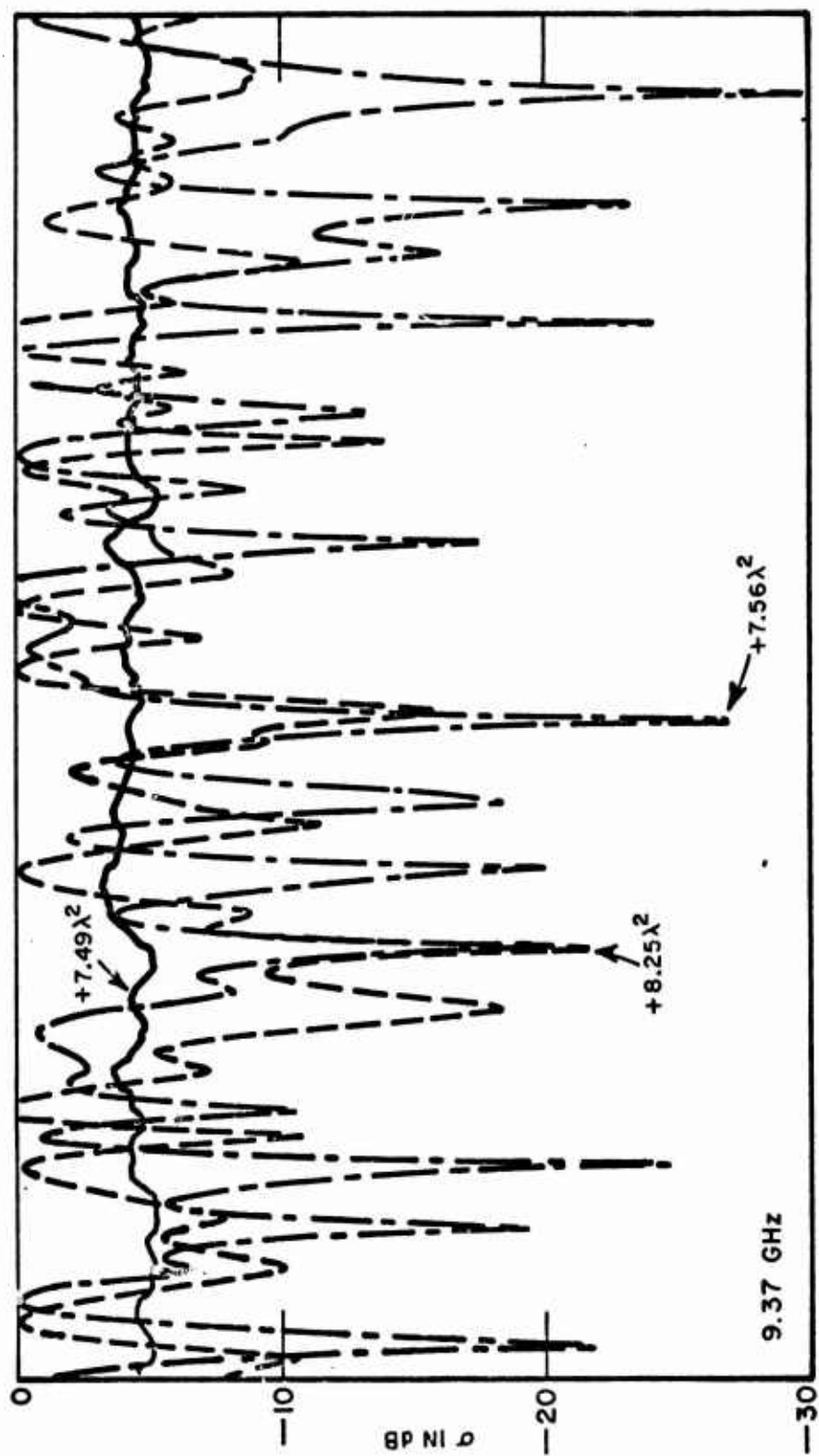


Figure 117. Radar cross section vs  $360^\circ$  of rotation of 1.75 cm glass chaff on 4" foam sphere.



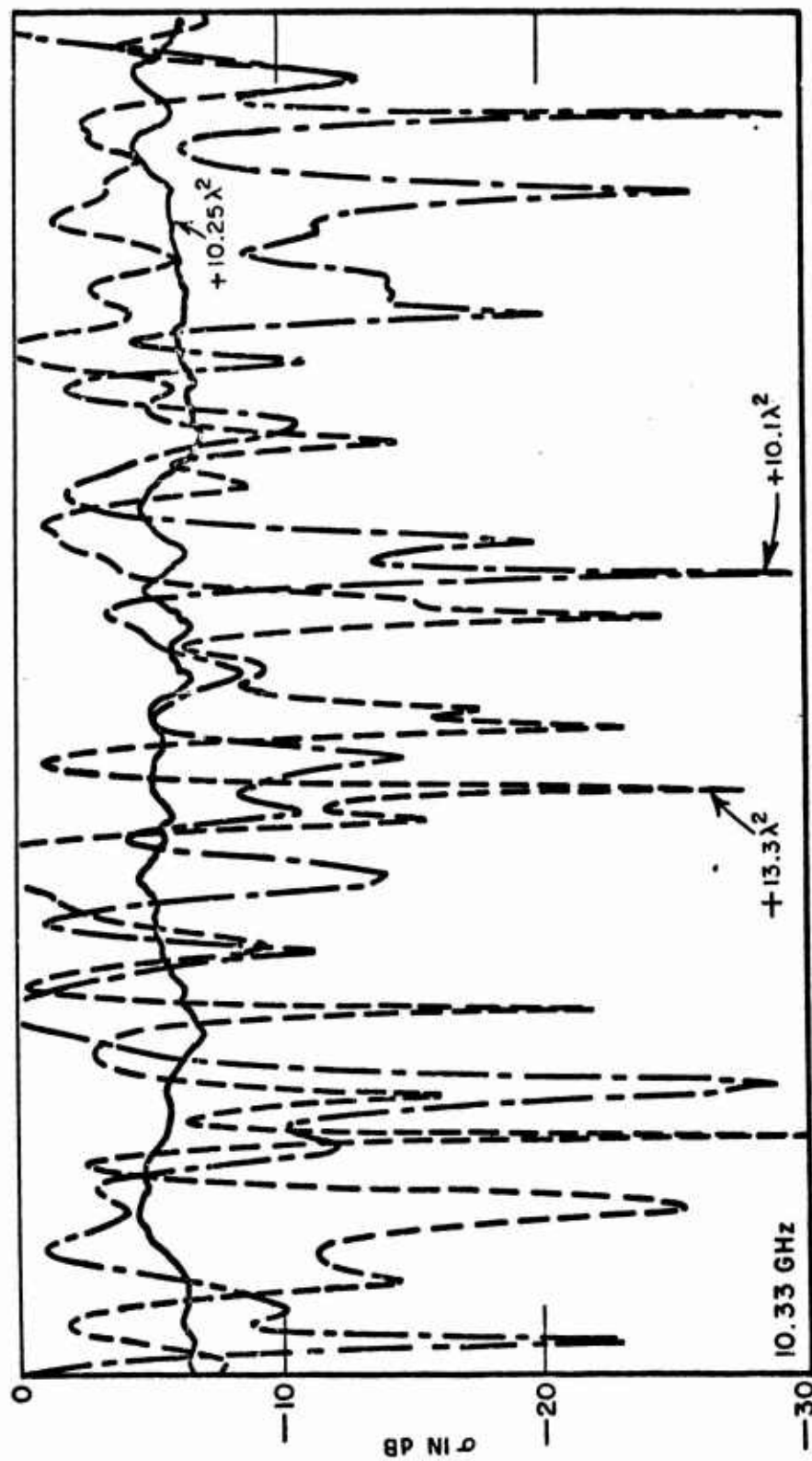


Figure 118. Radar cross section vs 360° of rotation of 1.75 cm glass chaff on 4" foam sphere.

### III. DISCUSSION

Using the frozen model of a chaff cloud together with an experimentally verified computer routine we conclude that for clouds of up to 200 coupled resonant dipoles, the backscattering cross section is, on the average, reduced from that predicted by uncoupled theory when the average dipole spacing falls below 2 wavelengths. It is important to remind the reader that these conclusions are based upon data calculated for inhomogeneous clouds, i.e., spherical clouds whose dipole number density varied along the radial direction according to a Gaussian function. The array dipole spacings were maximum at the center of the cloud and equal to about 1/3 those of the average dipole spacings defined and used here. Dipole orientations were always assumed equally likely. Using data gathered for all such clouds containing up to 30 dipoles, the ratios of the average backscattering cross section calculated with coupling to that calculated without coupling are summarized in Fig. 119 for average dipole spacings down to 0.5 wavelengths. It appears that at an average spacing of about 0.4 wavelengths the average radar return can be expected to be reduced about 3 dB by coupling effects. We have not included spacings smaller than 0.5 because approximations concerning the coupling terms in the computer routine come into question beyond this point. More exact relations are available if needed and are discussed in this report (see below), but they require more time and expense to implement on the computer. Moreover, closer spacings increase the probability that more and more dipoles touch, a feature which can be incorporated into the computer but not without some encumbrance.

Although less data were gathered for bistatic angles up to  $135^\circ$  (all of it experimental), both same-sense and crossed-sense linear polarizations showed trends similar to backscatter - closer average spacings effected reduced cross sections. In addition, several frequency runs by computer showed that even at the smallest average spacing of 0.5 wavelength the dipole resonance frequency remains essentially unchanged from the free space resonance frequency. For the spacings investigated, apparently the loading effects on a typical dipole in the cloud due to all of its neighbors essentially influence only the amplitude of the current and not its shape, thereby causing reduced scatter but maintaining about the same resonance frequency. Thus, we conclude that for average spacings down to  $0.5\lambda$  ( $\sim 8$  dipoles/ $\lambda^3$ ) each chaff element should be cut to its free-space resonant length to achieve best performance from the cloud.

In additional scattering measurements, some effect was devoted to an experimental evaluation of the extinction through a cloud of dipoles, averaged over time as the dipoles were set into motion. In this report curves are presented of the insertion loss incurred by the presence of the dipoles as functions of depth and for several densities.

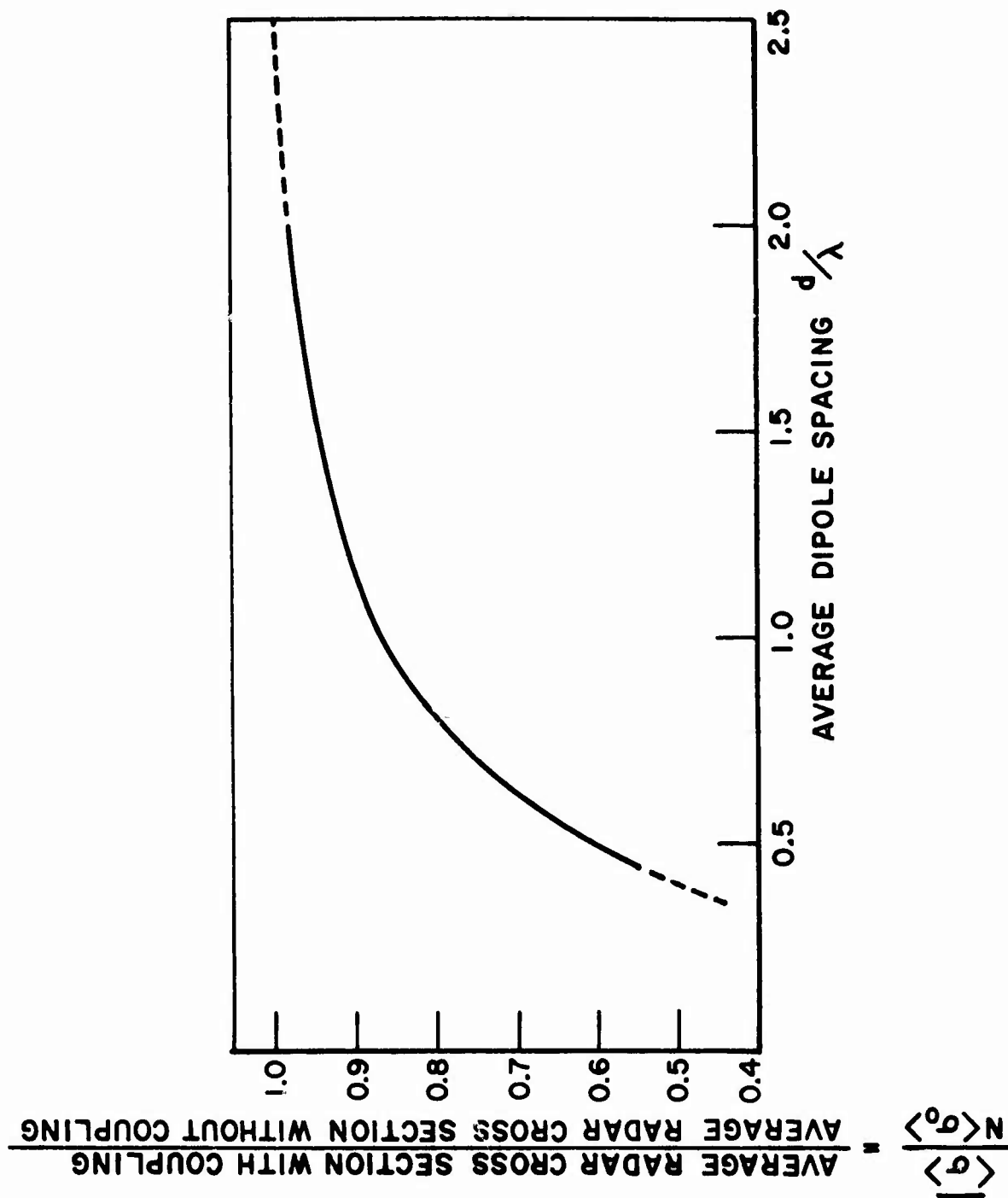


Figure 119. The decrease in average backscattering cross section due to coupling for a range of average dipole spacings (Gaussian density distribution assumed).

A table summarizing the extinction rates is given on page 165. These rates indicate a rather rapid extinction of energy as the wave proceeds into the cloud, even for rather tenuous clouds. Thus, if one is to design efficient chaff clouds, i.e., place the chaff dipoles where they will create the most effective echo, it is important to account for the effect of extinction and to predict it. Other experiments were performed to obtain backscattering patterns for a range of frequencies of foam spheres covered with aluminum and glass-chaff. The patterns show that at the resonance frequency of the individual dipoles, the sphere displays an average cross section essentially the same as that of conducting sphere of the same size, even when the dipoles are rather sparsely distributed over the sphere surface.

A study was made of clouds with dipoles spaced on the average less than  $0.5\lambda$  - down to  $0.125\lambda$  - to investigate the accuracy of the two-segment model employed in almost all the cases discussed here. It was found that the 2-segment model appeared satisfactory down to average spacings of  $0.25\lambda$  if an exact (rather than a 12-point Gaussian) integration was employed to find the mutual impedances. A penalty of a 60% increase in calculation time was incurred, however. For average spacings as small as  $0.125\lambda$ , even a four segment model with exact integration did not yield sufficiently stable results. Thus, the programs presented in this report are not considered reliable for inhomogeneous clouds with average spacings less than  $0.25\lambda$ . Of course, the programs can easily be modified to increase segmentation but the resulting consumption of rapid-access memory becomes intolerable.

A small amount of data were calculated for clouds containing two chaff lengths and the results show the same effect of coupling as was observed with single length chaff. It appears though that the elements which have a lower tumble average cross section (because they are anti-resonant) are less influenced by mutual coupling. Not enough data were accumulated to give an empirical mixture rule to estimate the average cross section of any combination of any two element lengths.

In order to extend our capability to calculate radar cross sections of clouds with more than 200 dipoles without exceeding the fast access memory capabilities of even the largest computers two investigations were initiated. One of the use of the sparse matrix technique. This method takes into account the physical fact that dipoles which are electrically far apart in the cloud are only weakly coupled; this in turn implies that many elements of the impedance matrix relating the fields and currents are almost null. If such elements are arbitrarily set to zero and their number exceeds about 80% of the total number of matrix elements, sparse matrix algorithms may be applied which effect large savings in computer memory - so much so that matrices of much larger order than normally possible can be inverted. This method has been applied to the chaff scattering problem with some success, but it was found to be more time consuming than expected, particularly in the matrix reordering portion of the algorithm. Also, the arbitrary



sparsing of the impedance matrix causes approximations which make a study of the extinction through the cloud impossible using this technique. A second method which does not suffer from this latter disadvantage is the iterative scatter technique which assumes initial currents on the dipoles as if they were uncoupled and updates all these currents in successive steps corresponding to what might be thought of as successive orders of inter-dipole scatter. We have found the successive overrelaxation (SOR) method together with the Gauss-Seidel algorithm to be the most successful iterative method we have used on clouds of resonant wires. (It was found to be less successful on solid obstacles.) Details will be found in a separate technical report [38]; in this report we show scattering results for clouds containing 1000 dipoles calculated using SOR. Some check cases are also presented to validate the method. Although, like the sparse matrix technique, the iterative method is time consuming, it does permit calculation of scattering data for much larger clouds than can be conveniently handled any other way, and should yield accurate extinction data.

One other topic which was investigated briefly during this contract period was the analysis of the aircraft-tracker radar interaction in the presence of chaff. Detailed results will be found in a separate technical report [62].

Computer programs used to calculate the data generated for this contract are given in appendices.

#### IV. RECOMMENDATIONS FOR FUTURE EFFORT

(1) We have observed that as closer and closer spacings between dipoles are assumed, the current distribution on each dipole is not only changed in amplitude, but also in shape along the length of the dipole. To represent this distorted shape requires more than a two-segment model of the dipole if a piecewise sinusoidal basis is used. We suggest the use of two basis functions, each defined over the entire length of the dipole, one being even, the other odd with respect to the dipole center. The even function appears as a cosine function blunted at the ends while the odd function appears as a sine function whose peaks are shifted toward the dipole extremities. We feel that such basis functions should be sufficient to account for the current distortions due to the influence of nearby neighbors without

increasing the order of the matrix equations. How much more dense this technique will allow the clouds to become beyond the  $8 \text{ dipoles}/\lambda^3$  number is not known.

(2) We know that for extremely dense clouds where many dipoles are touching, the method of moments is not a viable technique. The cloud appears in some sense as a solid body of conducting material, whose surface is almost fur-like and changing with time. We suggest that such a surface be modelled as a random surface with only incoherent scatter and for chosen cloud shapes, the calculated echo patterns be compared with experimentally derived patterns.

(3) Beyond the problem of dense clouds is the fact that most chaff clouds contain dipoles of various lengths to meet threats over a range of frequencies. The low frequencies present no new problems, but at the higher frequencies, those dipoles resonant at low frequencies become electrically long and require many segments (or modes) to adequately describe the currents induced on them. This enlarges the matrix to sizes which cannot be handled by computers. Thus, we suggest the use of basis functions which are travelling waves rather than standing waves and thereby reduce the number needed. The longer wires would of necessity be assumed straight, uncoupled to each other and to the short elements.

(4) The computer simulation of an aircraft-missile intercept problem in the presence of chaff should be continued. Better models should be developed for the echo return from a typical aircraft as a function of its aspect with respect to the incident wave. Realistic radar models, including effects of doppler and angle tracking should be incorporated. And, probably most difficult, more accurate chaff cloud returns should be simulated.



# APPENDIX A STATISTICAL ANALYSIS EMPLOYED IN THIS REPORT

## A. Definitions

We assume a frozen model for a chaff cloud and shall denote the back-scattering cross section of the  $m$ th cloud in the ensemble illuminated from an angle  $\theta$ , by  $\sigma_m(\theta)$  often leaving the  $\theta$ -dependence implicit for convenience. Averages with respect to angle  $\theta$  (here called spatial averages) will be denoted by Poisson brackets,  $\langle \rangle$ , while ensemble averages over a set of clouds will be denoted by the overbar,  $\bar{\phantom{x}}$ .

It can be shown<sup>13,14</sup> that the backscattering cross section  $\sigma_m(\theta)$  of the  $m$ th cloud in the ensemble of clouds forming the frozen model, under the assumption of no coupling among dipoles, follows an exponential probability density function,\* sketched in Fig. I-1a,

$$(I-1) \quad p_m(\sigma_m) = \begin{cases} \frac{1}{\langle \sigma_m \rangle} e^{-\frac{\sigma_m}{\langle \sigma_m \rangle}} & , \sigma_m \geq 0 \\ 0 & , \sigma_m < 0 \end{cases}$$

where  $\langle \sigma_m \rangle$  is the spatial average of  $\sigma_m(\theta)$  over all  $\theta$  given by

$$(I-2) \quad \langle \sigma_m \rangle = \int \sigma_m(\theta) d\theta .$$

Evidence that indeed Eq. (I-1) is valid is presented in Ref. 11 for clouds of up to 30 dipoles spaced on the average by two wavelengths (negligible coupling case). There also exist some actual radar chaff measurements which indicate an exponential distribution of back-scattering cross section.<sup>15</sup>

The standard deviation<sup>16</sup> of  $\sigma_m(\theta)$  is by definition

$$(I-3) \quad s_m = \sqrt{\langle (\sigma_m - \langle \sigma_m \rangle)^2 \rangle} = \left[ \int (\sigma_m(\theta) - \langle \sigma_m \rangle)^2 d\theta \right]^{1/2} = \langle \sigma_m \rangle$$

and the variance of  $\sigma_m(\theta)$  is equal to  $s_m^2$ .

The cumulative probability function associated with  $\sigma_m$  is of interest and sketched in Fig. I-1b, is

\*It can be shown that the exponential probability density function is strictly applicable only if the cloud density is uniform, which in the present case is not true. However, for the clouds considered here, it is a very good approximation.

$$(I-4) \quad P_m(\sigma_m) = \int_{-\infty}^{\sigma_m} p_m(x) dx = \begin{cases} 1 - e^{-\frac{\sigma_m}{\langle \sigma_m \rangle}}, & \sigma_m \geq 0 \\ 0, & \sigma_m < 0 \end{cases}$$

This function, evaluated at, say  $\sigma_m = \sigma_m'$ , gives the fraction of all possible values of  $\sigma_m$  which lie in the range,  $0 \leq \sigma_m \leq \sigma_m'$ . Special values of  $\sigma_m'$  are given names which we will refer to later. For example if  $P_m(\sigma_m') = 1/5$ ,  $\sigma_m' = \sigma_m 1/5$  is called the 20% or first quintile; if  $P_m(\sigma_m') = 1/2$ ,  $\sigma_m' = \sigma_m 1/2$  is called the 50% or median (as distinct from the mean or average value we have symbolized by  $\langle \sigma_m \rangle$ ); if  $P_m(\sigma_m') = 4/5$ ,  $\sigma_m' = \sigma_m 4/5$  is called the 80% or fourth quintile.

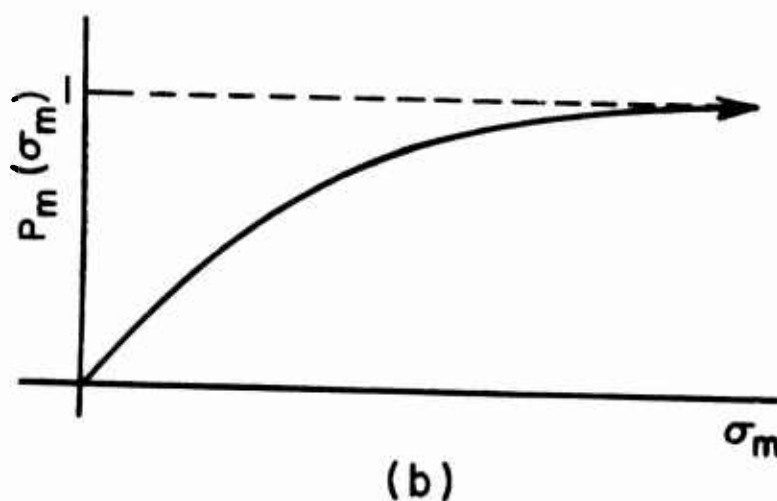
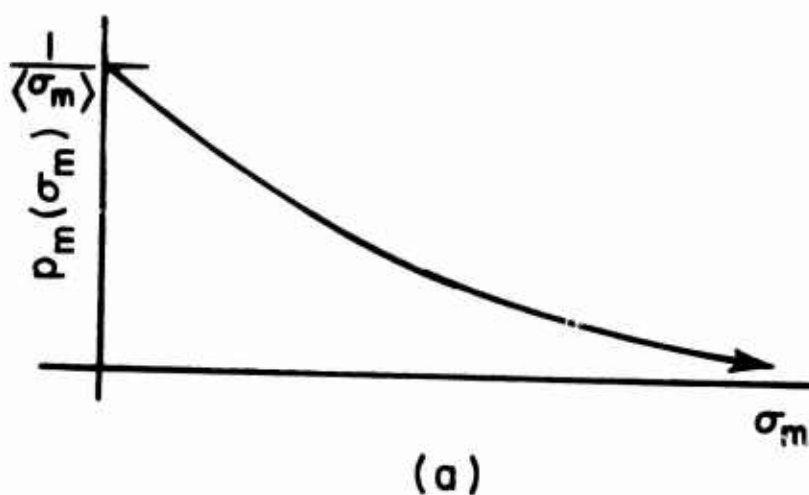


Figure I-1. Sketches of the exponential probability density function and corresponding cumulative probability function for the backscattering cross section of a chaff cloud.

In the frozen cloud model, many different sample clouds are generated (each one, of course, with the same number of dipoles spaced on the average the same). If the number of such clouds is  $M \gg 1$ , we obtain  $M$  sample functions  $\sigma_m(\theta)$ , each one representing the backscattering cross section as a function of look angle  $\theta$  of the  $m$ th cloud in the ensemble, where  $1 \leq m \leq M$ . Since the spatial average cross section  $\langle \sigma_m \rangle$  will in general differ for each  $m$  we obtain a distribution of  $M$  values of  $\langle \sigma_m \rangle$ . If  $M$  is large enough, we can obtain a relative frequency histogram<sup>17</sup> of  $\langle \sigma_m \rangle$  which may be fitted to a Gaussian probability density function  $q_{\text{mean}}(\langle \sigma_m \rangle)$  since the means of the exponential process are Gaussianly distributed. If, for convenience, the symbol  $\langle \sigma \rangle$  is used in place of  $\langle \sigma_m \rangle$ , we depict the relative frequency histogram of  $\langle \sigma \rangle$  by a bar graph and the Gaussian probability density function of the sampling distribution by a smooth curve as sketched in Fig. I-2. The Gaussian density function<sup>18</sup> is

$$(I-5) \quad q_{\text{mean}}(\langle \sigma \rangle) = \frac{1}{\sqrt{2\pi} s_{\text{mean}}} e^{-\frac{(\langle \sigma \rangle - \bar{\langle \sigma \rangle})^2}{2 s_{\text{mean}}^2}}$$

where  $\bar{\langle \sigma \rangle}$  is the ensemble mean of  $\langle \sigma \rangle$  and  $s_{\text{mean}}$  is the standard deviation of  $\langle \sigma \rangle$ . On an ensemble basis they may be expressed as

$$(I-6) \quad \bar{\langle \sigma \rangle} \equiv \int_{-\infty}^{\infty} \langle \sigma \rangle q_{\text{mean}}(\langle \sigma \rangle) d\langle \sigma \rangle,$$

and

$$(I-7) \quad s_{\text{mean}}^2 = \overline{(\langle \sigma \rangle - \bar{\langle \sigma \rangle})^2} \equiv \int_{-\infty}^{\infty} (\langle \sigma \rangle - \bar{\langle \sigma \rangle})^2 q_{\text{mean}}(\langle \sigma \rangle) d\langle \sigma \rangle.$$

The mean value  $\bar{\langle \sigma \rangle}$  is the arithmetic average of all the values of  $\langle \sigma \rangle$  (i.e.,  $\langle \sigma_m \rangle$ ) and the standard deviation (since  $q(\langle \sigma \rangle)$  is Gaussian) determines the range of values,  $(\bar{\langle \sigma \rangle} - s_{\text{mean}}) < (\langle \sigma \rangle) < (\bar{\langle \sigma \rangle} + s_{\text{mean}})$ , between which lie 68.27% of all the possible values of  $\langle \sigma \rangle$  (i.e.,  $\langle \sigma_m \rangle$ ). The two curves in Fig. I-2 both are normalized to unit area and the one may be fitted to the other by, for example, a chi-square test.<sup>19</sup> Of course, since  $\langle \sigma \rangle$  cannot be negative, the fit of a Gaussian distribution (which admits negative values) can be accomplished only in the region of  $\langle \sigma \rangle$  values about the  $\bar{\langle \sigma \rangle}$  value.

In a manner very similar to that for treating  $\langle \sigma \rangle$ , we may fit Gaussian curves to histograms of  $\sigma_m$  1/5,  $\sigma_m$  1/2,  $\sigma_m$  4/5 (using the simplified symbols,  $\sigma_{1/5}$ ,  $\sigma_{1/2}$ ,  $\sigma_{4/5}$ ).

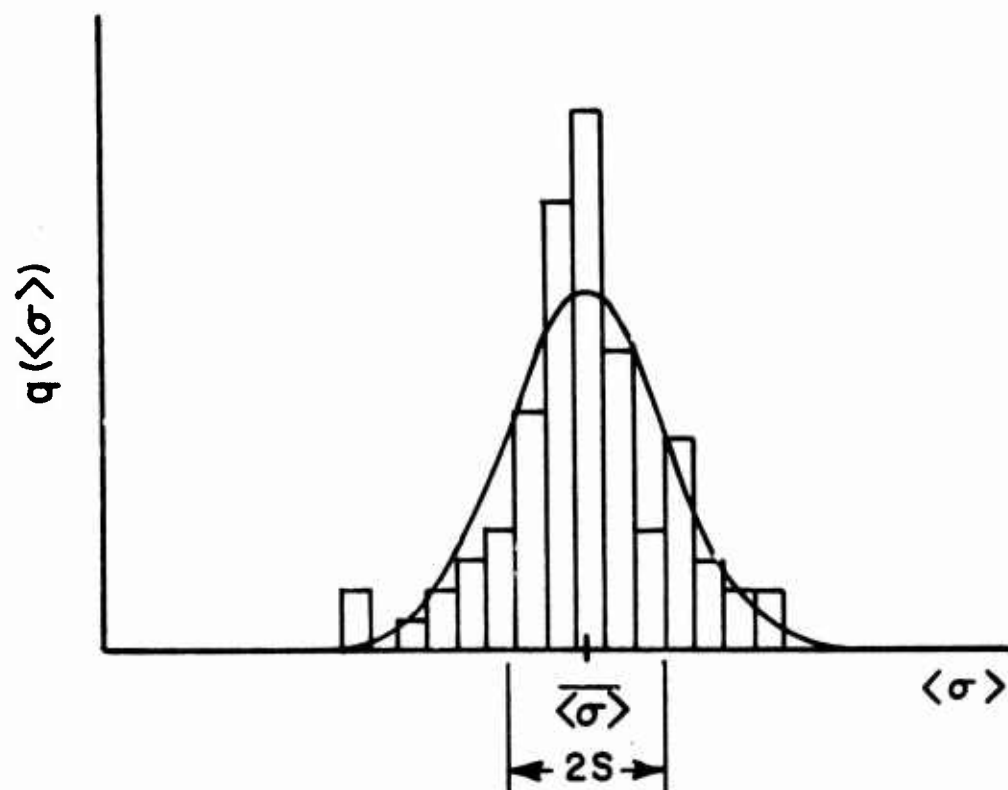


Figure I-2. Sketches of a histogram and associated Gaussian probability distribution of spatial average cross sections of frozen chaff clouds.

$$(I-8) \quad q_{1/5}(\sigma_{1/5}) = \frac{1}{\sqrt{2\pi} s_{1/5}} e^{-\frac{(\sigma_{1/5} - \bar{\sigma}_{1/5})^2}{2 s_{1/5}^2}},$$

$$(I-9) \quad q_{1/2}(\sigma_{1/2}) = \frac{1}{\sqrt{2\pi} s_{1/2}} e^{-\frac{(\sigma_{1/2} - \bar{\sigma}_{1/2})^2}{2 s_{1/2}^2}},$$

$$(I-10) \quad q_{4/5}(\sigma_{4/5}) = \frac{1}{\sqrt{2\pi} s_{4/5}} e^{-\frac{(\sigma_{4/5} - \bar{\sigma}_{4/5})^2}{2 s_{4/5}^2}},$$

where the mean and standard deviation of  $\sigma_{1/5}$ , for example, taken on an ensemble basis, are

$$(I-11) \quad \overline{\sigma_{1/5}} \equiv \int_{-\infty}^{\infty} \sigma_{1/5} q_{1/5}(\sigma_{1/5}) d\sigma_{1/5}.$$

$$(I-12) \quad s_{1/5}^2 = \overline{(\sigma_{1/5} - \overline{\sigma_{1/5}})^2} \equiv \int_{-\infty}^{\infty} (\sigma_{1/5} - \overline{\sigma_{1/5}})^2 q_{1/5}(\sigma_{1/5}) d\sigma_{1/5}.$$

Similar expressions may be used for  $\overline{\sigma_{1/2}}$ ,  $s_{1/2}$ ,  $\overline{\sigma_{4/5}}$ , and  $s_{4/5}$ .

Once a value for  $\langle \sigma \rangle$  has been obtained, we hypothesize that this value may be used in Eqs. (I-1) and (I-2) to obtain the probability density function and cumulative probability of the backscattering cross section  $\sigma$  of the frozen model, even in the presence of coupling,

$$(I-13) \quad p(\sigma) = \begin{cases} \frac{1}{\langle \sigma \rangle} e^{-\frac{\sigma}{\langle \sigma \rangle}}, & \sigma \geq 0 \\ 0, & \sigma < 0 \end{cases}$$

$$(I-14) \quad P(\sigma) = \begin{cases} 1 - e^{-\frac{\sigma}{\langle \sigma \rangle}}, & \sigma \geq 0 \\ 0, & \sigma < 0 \end{cases}$$

If these functions indeed do characterize the frozen model then it should be true that

$$(I-15a) \quad P(\overline{\sigma_{1/5}}) = 0.2,$$

$$(I-15b) \quad P(\overline{\sigma_{1/2}}) = 0.5,$$

$$(I-15c) \quad P(\overline{\sigma_{4/5}}) = 0.8.$$

One can test the data to see if equalities (I-15) are approximately true, in which case we have some assurance that Eq. (I-13) is valid for coupled clouds.

We considered the following reasoning to obtain one other indicator that Eq. (I-13) is valid. The standard deviation of  $\sigma$  is found from Eq. (I-13) to be

$$(I-16) \quad s = \left[ \int_{-\infty}^{\infty} (\sigma - \langle \sigma \rangle)^2 p(\sigma) d\sigma \right]^{1/2} = \langle \sigma^2 \rangle^{1/2}$$

This standard deviation of  $\sigma$  should be related to the standard deviation  $s_{\text{mean}}$  of the sampling distribution of means by the relationship<sup>20</sup>

$$(I-17) \quad s = s_{\text{mean}} \sqrt{N_s} \sqrt{\frac{N_p - 1}{N_p - N_s}}$$

where the numbers  $N_p$  and  $N_s$  are defined as the population and sample size, respectively, and may be obtained in our case as follows.

If, in the frozen model, there are  $M$  clouds, each viewed at 512 angles with two polarizations, then the number of pieces of backscattering data, called the population, is  $N_p = 1024M$ . By sampling each cloud at 512 look angles with two polarizations and considering these data as independent, we form  $2M$  samples of size  $N_s = 512$  data points each. However, the 512 look angles are probably not independent, i.e., we have oversampled  $\sigma_m(\theta)$ . To obtain an estimate of the number of independent samples, we observe the highest frequency in the spectrum  $W(N, d/\lambda)$  (discussed below) and consider the sample size to be  $N_s = 2W(N, d/\lambda)$ . Using these values for  $N_p$  and  $N_s$  and  $s_{\text{mean}}$  as obtained from  $q_{\text{mean}}(\langle \sigma \rangle)$ , Eq. (I-17) gives a value  $s \approx s_{\text{mean}} 2W$  which may be compared with the value  $s = \langle \sigma^2 \rangle^{1/2}$  of Eq. (I-16). We applied the above numbers to Eq. (I-17) and did not arrive at relations between  $s$  and  $s_{\text{mean}}$  which were consistent with Eq. (I-16). We can only conclude that the above method for estimating sample size is invalid probably due to the inhomogeneity of the population data from cloud to cloud.

Another parameter which may be of use in characterizing the frozen cloud model is the spatial frequency spectrum of the backscattering cross section. If  $\sigma_m(\theta)$  is the backscattering cross section of the  $m$ th cloud in the frozen model, then we define  $F_m(\omega)$  as the Fourier transform of one period of  $\sigma_m(\theta)$ ,  $0 \leq \theta \leq 360^\circ$ , where  $\omega$  is the spatial spectral variable (in say, Hz/degrees of  $\theta$ ).

A typical  $F_m(\omega)$  might appear as sketched in Fig. I-3, where  $W_m$  is the highest frequency in the spectrum. One finds that  $W_m$  varies with  $N$ , the number of dipoles in a cloud, and  $d/\lambda$ , the average spacing between dipoles, so we signify this dependence by writing  $W_m(N, d/\lambda)$ . In addition, one finds that for a fixed  $(N, d/\lambda)$  pair, different members of the ensemble of clouds, i.e.,



different values for  $1 \leq m \leq M$ , yield slightly different  $W_m(N, d/\lambda)$ . If we denote by  $W(N, d/\lambda)$  the average of these values over 22 different clouds, we can derive Table I. In this table,  $W(N, d/\lambda)$  appear in the upper triangles, while in the lower triangles appear the values of  $4\delta(N, d/\lambda)/\lambda$ ; i.e., diameters (in wavelengths) of spheres encompassing 95% of the dipoles in a typical cloud associated with the pair  $(N, d/\lambda)$ . If the parallel dipole scatterers are assumed to exist at the extremities of these diameters, then frequency  $W'(N, d/\lambda)$  can be calculated on the basis of the beamwidth of the broadside lobe according to

$$W'(N, \frac{d}{\lambda}) = \frac{180}{\sin^{-1} \frac{1}{2} \cdot \frac{\lambda}{4\delta}}.$$

Both  $W(N, d/\lambda)$  and  $W'(N, d/\lambda)$  are plotted in Fig. I-4. The 2-dipole model appears to predict values for  $W(N, d/\lambda)$  which are too low and do not decrease rapidly enough with decrease in  $N$ , but considering the simplicity of the model, the comparisons are not bad.

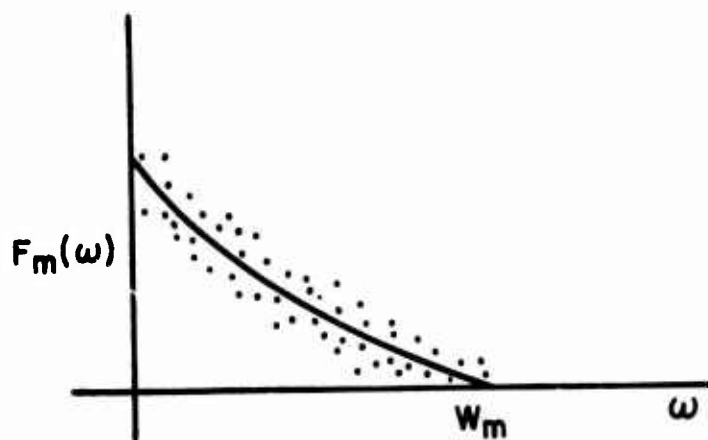


Figure I-3. Sketch of a typical spatial frequency spectrum of a frozen chaff cloud.

#### B. Statistical Analysis of Backscattering Data

A large amount of calculated backscattering data, based on the frozen model, have been obtained for several cases. To examine the properties of these data, statistical methods must be employed. The usual procedures for dealing with this kind of statistical problem are as follows:

1. Data are first classified into small intervals and by counting the relative frequencies of occurrence in each interval, a histogram can be drawn. By inspecting the histogram, it is then possible to select a suitable mathematical model, namely, the frequency distribution function. The unknown parameters are then estimated by the Maximum Likelihood Method.

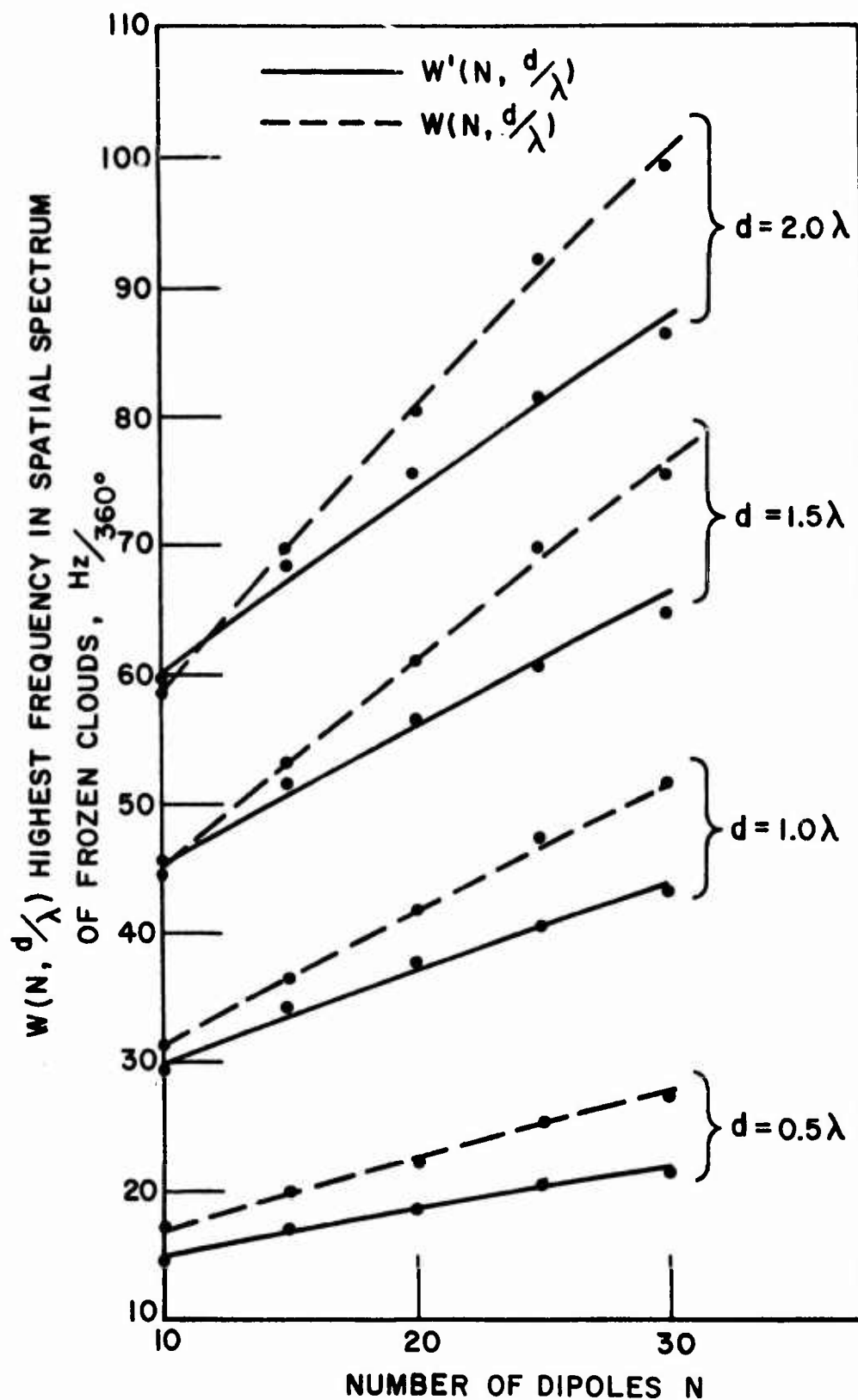


Figure I-4. The highest spatial frequency  $W_n$  in the spectrum of a frozen chaff cloud, as function of  $N$  and  $d/\lambda$ . The approximant  $W'_n$  is derived as discussed in the text.

2. The reasonableness of the mathematical model can be checked by the Chi-Square Test.<sup>19</sup> Basically, the quantity

$$\sum_{i=1}^k \frac{(o_i - e_i)^2}{e_i},$$

where  $o_i$ ,  $e_i$  are the observed and expected frequencies respectively, is compared to a  $\chi^2$  variable with  $\nu$  degree of freedom. This serves as the criterion for the goodness of fit.

3. Once the assumption of the model is justified, our interest is in the confidence limits of the parameters. This gives some idea of the expected variation of the parameters of interest. Given the size of the confidence interval, it is then possible to determine the number of data points sufficient to describe the statistical behavior of the cloud.

To illustrate the technique, we analyze the data obtained for the case  $N=30$  dipoles,  $d=2.0\lambda$  in detail here.

Table II shows the spatial average backscattering cross-section  $\langle \sigma_m(\theta) \rangle$  for  $m=1, 2, \dots, 80$  clouds. These data are then classified into 24 classes, from class mark 2.0 to 6.8 with interval size 0.2. The resultant histogram is shown in Fig. I-5. The symmetry and skewness of the histogram suggests that the data are likely to be Gaussian-distributed. We therefore assume that  $\langle \sigma_m(\theta) \rangle$  has a Gaussian distribution with mean  $\mu$  and variance  $\sigma^2$ . Since these are not known a priori, they must be estimated from the data. It can be shown<sup>19</sup> that the maximum likelihood estimators of  $\mu$  and  $\sigma^2$  are given by the sample mean  $\overline{\langle \sigma_m(\theta) \rangle}$  and sample variance  $s_{\text{mean}}^2$ . Thus,

$$(I-18) \quad q_{\text{mean}}(\langle \sigma_m(\theta) \rangle) = \frac{A}{\sqrt{2\pi} s_{\text{mean}}} e^{-\frac{(\langle \sigma_m(\theta) \rangle - \overline{\langle \sigma_m(\theta) \rangle})^2}{2 s_{\text{mean}}^2}},$$

$$\text{where the sample mean } \overline{\langle \sigma_m(\theta) \rangle} = \sum_{m=1}^{80} \frac{\langle \sigma_m(\theta) \rangle}{80} = 4.2798,$$

$$\text{sample variance } s_{\text{mean}}^2 = \sum_{m=1}^{80} \frac{(\langle \sigma_m(\theta) \rangle - \overline{\langle \sigma_m(\theta) \rangle})^2}{79} = 0.288$$

and total area of the histogram  $A = 16.0$ .

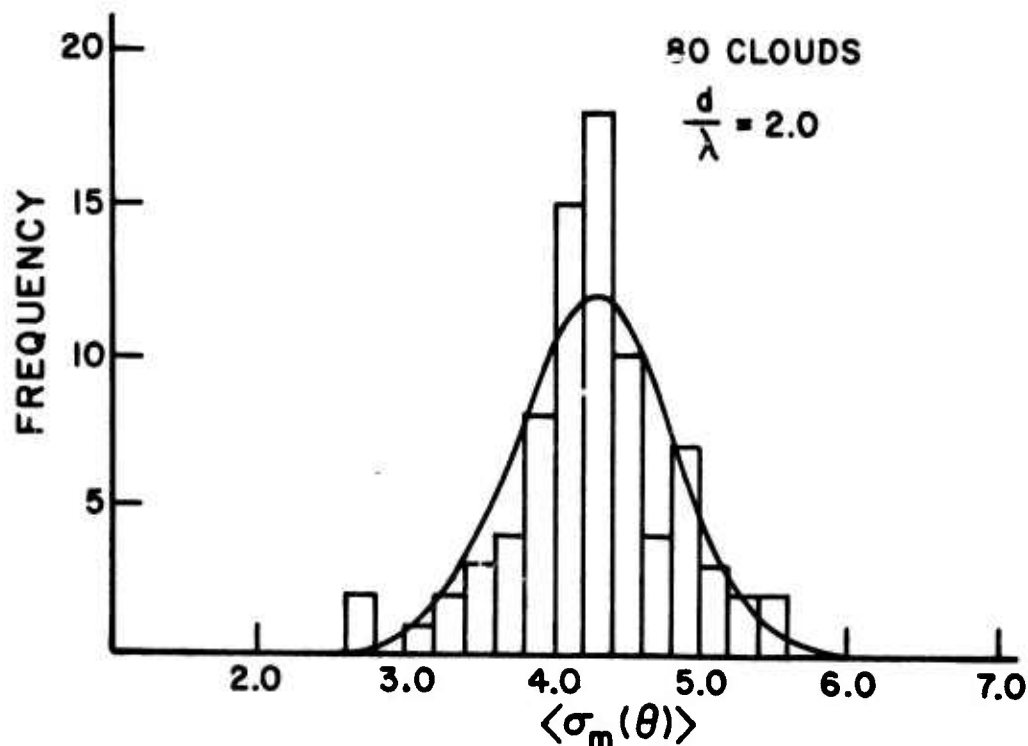


Figure I-5. The histogram and associated Gaussian probability distribution of the spatial averages of 80 frozen chaff clouds containing 30 dipoles each.

Equation (I-18) is also plotted in Fig. I-5. Here we have fit the histogram of the backscattering data to a Gaussian curve. One measure of fit is the Chi-square test which evaluates the deviation  $\chi^2$

$$\chi^2 = \sum_{i=1}^k \frac{(o_i - e_i)^2}{e_i}$$

between the observed frequencies  $o_i$  and the expected frequencies  $e_i$  in  $i=1,2,\dots,k$  intervals. The expected frequency  $e_i$  is obtained by integrating the area under the curve and the observed frequency  $o_i$  is obtained by counting the number of occurrences of the backscattering data in the  $i$ th interval. The results are shown in Table III.

In computing the deviation  $\chi^2$ , it is necessary that  $e_i \geq 5$  and  $k \geq 5$ .<sup>19</sup> Several intervals can be combined until the above condition is satisfied. This is indicated in the left column of Table III.

Calculations show that

$$\begin{aligned} \chi^2 &= \sum_{i=1}^9 \frac{(o_i - e_i)^2}{e_i} = \frac{(7-5.87)^2}{5.87} + \frac{(4-5.35)^2}{5.35} + \frac{(8-7.96)^2}{7.96} \\ &\quad + \frac{(15-10.33)^2}{10.33} + \frac{(18-11.68)^2}{11.68} + \frac{(10-11.52)^2}{11.52} \\ &\quad + \frac{(4-9.91)^2}{9.91} + \frac{(7-7.43)^2}{7.43} + \frac{(7-9.94)^2}{9.94} \\ &= 10.7088 \end{aligned}$$

This value is compared with a  $\chi_0^2$  variable with  $=K-1-l$  degrees of freedom, where  $l$  is the number of parameters that the interval probability depends upon; since  $q_{\text{mean}}(\langle \sigma_m(\theta) \rangle)$  depends on two unknown parameters, we have  $l=2$  in this case.

It is found that  $\chi_0^2=12.592$  with  $v=6$  for a 5% significant level, and since  $\chi^2 < \chi_0^2$ , we conclude that the model is satisfactory.

The 95% confidence interval for the mean is given by:

$$(\langle \sigma_m(\theta) \rangle) - \frac{bS}{m-1}, \langle \sigma_m(\theta) \rangle + \frac{bS}{\sqrt{m-1}} = (4.1613, 4.3983)$$

where  $b$  can be obtained from the Student-t[19] distribution table. For example,  $b=1.96$  for  $m > 30$ . The confidence interval of the mean is then given by  $L = 2bS/\sqrt{m-1}$ , or solving for  $m$ , we obtain:

$$(I-19) \quad m = 1 + \left( \frac{2bS}{L} \right)^2.$$

For  $L=0.1$   $\langle \sigma_m(\theta) \rangle = 0.42798$ , Eq. (I-19) can be used to obtain the value of  $m$  by trial and error. Assume  $m=26$ ,  $b=2.056$ , Eqs. (I-19) gives  $m = 26$ . We summarize the results as follows:

1. Evidence is shown that the spatial averages are Gaussian distributed.
2. The mean value will lie inside the interval (4.1613, 4.3983).
3. We predict that 95% of the data will fall in the interval (3.2050, 5.3546) in the long run.
4. Only 26 clouds are needed to determine the statistical behavior of the spatial variation of the Chaff cloud if the size of the confidence interval is allowed to be 10% of its mean value.



The backscattering data obtained for the cases  $N=30$  dipoles,  $d=0.5\lambda$  and  $N=10$  dipoles,  $d=0.5\lambda, 2.0\lambda$  were treated in the same manner as above. 80 clouds for each of these cases were used in the analysis. It turns out that in all cases, the spatial averages are Gaussian distributed to a good approximation. The results of the analysis are shown in Table IV and in Figs. I-6 and I-7.

It was mentioned in Section A that the backscattering cross-section  $\langle \sigma_m(\theta) \rangle$  under the assumption of no coupling among dipoles, follows the exponential probability density function of Eq. (I-13). If the exponential density function also holds for coupled elements, then Eq. (I-15a), (15b), (15c) should be approximately true even for small spacings  $d/\lambda$ . We now want to show that this is indeed the case.

Backscattering data were obtained for 4 cases, namely,  $N=30$  dipoles,  $d=0.5\lambda, 2.0\lambda$  and  $N=10$  dipoles,  $d=0.5\lambda, 2.0\lambda$  at 20%, 50%, 80% levels. Again, 80 clouds of each case were used in the statistical analysis. The assumption that the data were obtained from sampling a Gaussian population is good except for the case of 20% level. However, it is found that the variance in these cases are so small that even if more clouds are included in the analysis, the sample mean will not change significantly. We thus include them for comparison.

The 20%, 50% and 80% levels are obtained by substituting into Eq. (I-14) with the appropriate value of  $\langle \sigma \rangle$  used and in Table IV they are compared with the value obtained for forming histograms and approximating these with Gaussian distributions. The same results are shown in Fig. I-8, where the curves are calculated using Eq. (I-14) and dots are values calculated using histograms. In Fig. I-8 our additional curve for  $N=50$  dipoles  $d/\lambda = 2.0$  is given. The good comparison leads us to conclude that the backscattering cross section, even with severe coupling effects, appears to obey the exponential distribution when the associated value of mean cross section  $\langle \sigma \rangle$  is incorporated.



Again, 80 clouds of each case were used in the statistical analysis. The assumption that the data were obtained from sampling a Gaussian population is good except for the case of 20% level. However, it is found that the variance in these cases are so small that even if more clouds are included in the analysis, the sample mean will not change significantly. We thus include them for comparison.

The 20%, 50% and 80% levels are obtained by substituting into Eq. (I-14) with the appropriate value of  $\langle \sigma \rangle$  used and in Table IV they are compared with the value obtained by forming histograms and approximating these with Gaussian distributions. The same results are shown in Fig. I-8, where the curves are calculated using Eq. (I-14) and dots are values calculated using histograms. The good comparison leads us to conclude that the backscattering cross section, even with severe coupling effects, appears to obey the exponential distribution when the associated value of mean cross section  $\langle \sigma \rangle$  is incorporated.

TABLE I - HIGHEST SPECTRAL FREQUENCIES

$\frac{N}{d/\lambda}$	10	15	20	25	30
2.0	58.7 / 4.76	69.4 / 5.45	80.3 / 6.00	92.0 / 6.46	99.0 / 6.86
1.5	45.2 / 3.57	53.0 / 4.08	61.0 / 4.50	69.7 / 4.84	75.2 / 5.15
1.0	31.2 / 2.38	36.3 / 2.72	41.5 / 3.00	47.3 / 3.23	51.4 / 3.43
0.5	17.3 / 1.19	20.0 / 1.36	22.7 / 1.50	25.6 / 1.61	27.7 / 1.71

TABLE II - SPATIAL AVERAGES OF 80 CLOUDS

4.3842	4.4985	4.49505	5.50184
4.40	4.8349	4.17054	3.9871
4.5801	4.0279	4.64392	4.09925
4.63293	4.3948	4.18171	3.63187
4.67246	4.0599	4.34841	4.89497
3.52468	5.4608	3.31524	5.15151
3.94084	4.3303	3.90761	4.11126
5.07415	3.7248	2.62660	4.90393
3.77322	3.4994	4.45712	4.34125
3.23141	4.38457	4.12578	4.08328
2.6788	4.52723	4.38605	4.81494
4.03150	4.26477	4.02188	4.03012
4.2399	3.74232	4.22126	3.83469
5.2056	4.29156	4.18910	4.28673
4.2795	3.45858	4.30804	4.47537
4.1598	5.11655	3.9152	3.91778
4.2642	4.30620	4.93505	4.56063
4.5817	4.60128	3.84363	4.84562
4.1245	4.90631	5.36615	4.16605
4.4971	4.45655	3.95543	4.26969

TABLE III - THE DATA OF TABLE II CLASSIFIED INTO RELATIVE FREQUENCIES OF OCCURRENCE

k	Level	Freq Dist $o_i$	Theo Freq $e_i$
1	2.100	0	.00
	2.300	0	.01
	2.500	0	.03
	2.700	2	.09
	2.900	0	.28
	3.100	0	.72
	3.300	2	1.61
	3.500	3	3.14
	3.700	4	5.35
2	3.900	8	7.96
3	4.100	15	10.33
4	4.300	18	11.68
5	4.500	10	11.22
6	4.700	4	9.91
7	4.900	7	7.43
8	5.100	3	4.86
	5.300	2	2.77
	5.500	2	1.38
	5.700	0	.60
	5.900	0	.23
	6.100	0	.07
	6.300	0	.02
	6.500	0	.00
	6.700	0	.00

TABLE IV - CUMULATIVE PROBABILITY VALUES

N $d/\lambda$		30 2.0	30 0.5	10 2.0	10 0.5
$\langle \sigma_m(\theta) \rangle$		4.2798	2.6513	1.42440	1.0219
20%	$\langle \sigma_m(\theta) \rangle$ 20%	0.9484	0.5749	0.3127	0.2220
	$P(\sigma)$	0.9550	0.5916	0.3177	0.2280
50%	$\langle \sigma_m(\theta) \rangle$ 50%	3.0555	1.8215	0.9634	0.6932
	$P(\sigma)$	2.9665	1.8377	0.9870	0.7083
80%	$\langle \sigma_m(\theta) \rangle$ 80%	7.1347	4.2469	2.2597	1.6384
	$P(\sigma)$	6.8881	4.2671	2.2918	1.6447

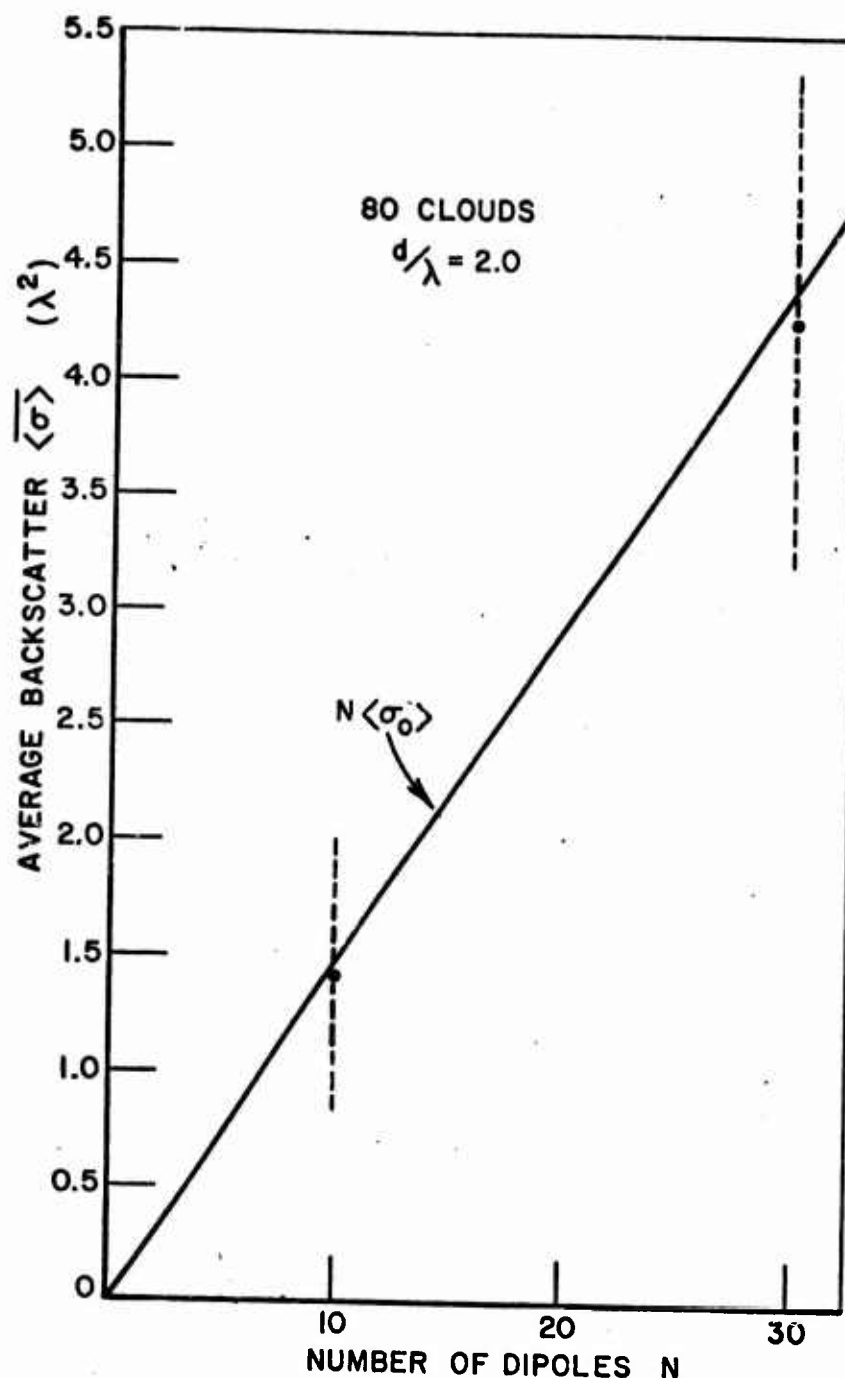


Figure I-6. Ensemble average backscatter  $\overline{\langle \sigma \rangle}$  over 80 frozen chaff clouds with average spacing  $d/\lambda = 2$ . Two cases are considered,  $N = 10$  dipoles and  $N = 30$  dipoles as indicated by the heavy dots. The heavy dashes indicate the range containing 68% of the individual spatial averages (within one standard deviation either side of  $\overline{\langle \sigma \rangle}$ ) and the light dashes indicate the range containing 95% of the individual spatial averages (within two standard deviations either side of  $\overline{\langle \sigma \rangle}$ ). The straight line represents uncoupled dipoles.

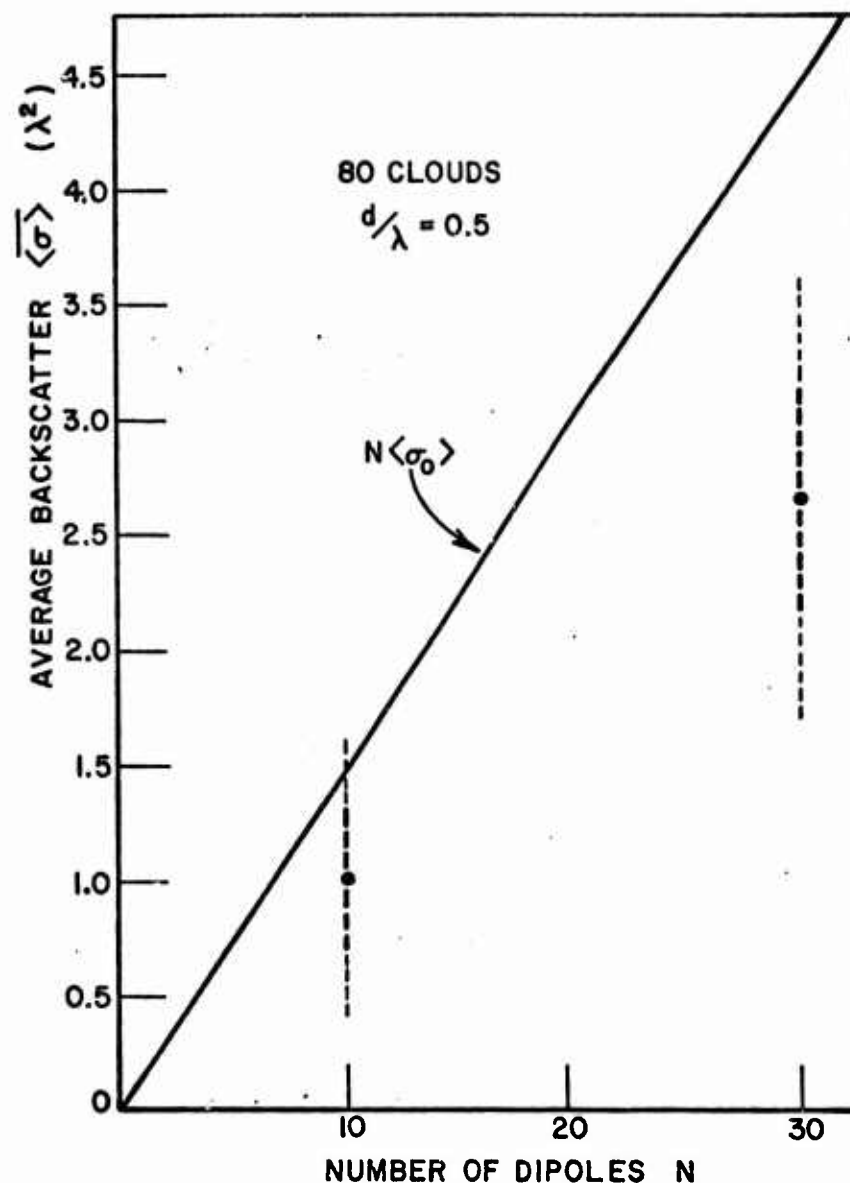


Figure I-7. Ensemble average backscatter  $\overline{\langle \sigma \rangle}$  over 80 frozen chaff clouds with average spacing  $d/\lambda = 0.5$ . Two cases are considered,  $N = 10$  dipoles and  $N = 30$  dipoles as indicated by the heavy dots. The heavy dashes indicate the range containing 68% of the individual spatial averages (within one standard deviation either side of  $\overline{\langle \sigma \rangle}$ ) and the light dashes indicate the range containing 95% of the individual spatial averages (within two standard deviations either side of  $\overline{\langle \sigma \rangle}$ ). The straight line represents uncoupled dipoles.

## APPENDIX B

### REACTION MATCHING IN ELECTROMAGNETIC PROBLEMS

The objective of this work is to determine the electromagnetic scattering properties of large (random) clouds of perfectly conducting wires (dipoles) illuminated by a monochromatic plane wave. The emphasis is on applying an integral equation solution to this problem for those cases where the number of volume density of dipoles is large (1000 dipoles, 8 dipoles/ $\lambda^3$ ) and the mutual couplings among all dipoles must be taken into account. The purpose of this appendix is to review the reaction [21] technique for developing an integral equation for the currents induced on these dipoles and to consider the transformation of this integral formulation via Moment Methods [22] to a system of algebraic equations more suitable for numerical solution by digital computer.

#### A. Scattering Properties of Obstacles

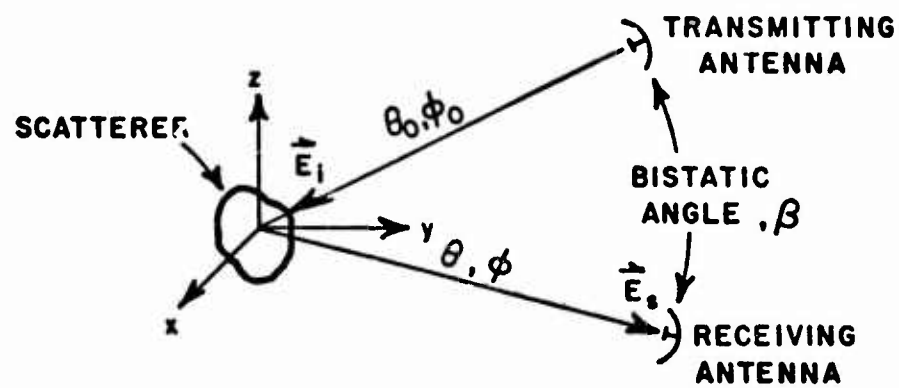
One measure often used to characterize scattering properties is radar cross section or echo area  $\sigma$  defined by

$$(II-1) \quad \sigma = \lim_{R \rightarrow \infty} 4\pi R^2 \frac{|\vec{E}_s \cdot \hat{h}_r|^2}{|\vec{E}_i|^2}$$

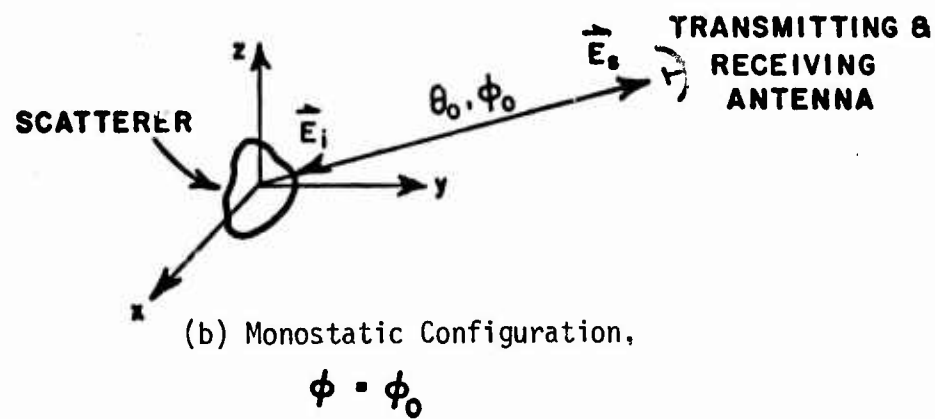
where  $\vec{E}_i$  is the electric field intensity of an incident plane wave of fixed polarization arriving from a particular direction (say  $\theta_0, \phi_0$ ) and  $\vec{E}_s$  is the electric field intensity of the scattered field a large distance  $R$  from the obstacle in an arbitrary direction  $(\theta, \phi)$ . The quantity  $\hat{h}_r$  is a unit vector specifying the direction of the vector effective height of the receiving antenna which fixes the polarization component of the scattered field intercepted by this antenna. The reader is referred to the work by Kennaugh [23] for a complete discussion of the characterization of polarization properties for arbitrary scatterers.

The units for  $\sigma$  in the MKS system are meters<sup>2</sup> and radar cross section obviously represents an area. More specifically,  $\sigma$  is the area normal to the incoming plane wave which would intercept enough power from the incident fields so that if this power were reradiated isotropically the power intercepted by the receiving antenna would be identical to that caused by the obstacle itself. Figure II-1 illustrates the two basic types of radar





(a) Bistatic Configuration.



(b) Monostatic Configuration,

$$\phi = \phi_0$$

Figure II-1. Scattering cross-section configurations.

cross section measurements; bistatic cross section where transmitter and receiver are separated by angle  $\beta \neq 0$ , and monostatic cross section where transmitter and receiver are coincident,  $\beta = 0$ . Monostatic cross section is commonly referred to as backscatter cross section and this terminology will be adhered to in all following discussions.

## B. Scattering by Perfectly Conducting Bodies

Calculation of the scattered electric field appearing in Eq. (II-1) normally requires knowledge of the "secondary sources" induced in or on the scattering obstacle. A perfectly conducting obstacle will obviously have only a secondary source of the electric type induced on its surface and an integral equation for this surface distribution can be derived by applying the usual boundary conditions and the "zero reaction" theorem of Rumsey [21]. A detailed treatment of this approach is given by Richmond [24] and is summarized here.

Consider the basic geometry for the problem shown in Fig. II-2. The arbitrary metallic scatterer is located about the origin 0 in a right hand coordinate system and the primary electric and magnetic source distributions  $\bar{J}_i, \bar{M}_i$ , of finite extent and with  $e^{j\omega t}$  time dependence, are located by position vector  $\bar{R}$ .  $R$  here is assumed large ( $R \rightarrow \infty$ ), thus assuring that the free space fields of  $\bar{J}_i, \bar{M}_i$ , in the absence of the scatterer, produce a plane wave in the vicinity of 0. For convenience consider these plane wave fields to be  $\theta$  polarized with components given by

$$(II-2) \quad \bar{E}_i = e^{jk_0 R} \hat{\theta}$$

$$(II-3) \quad \bar{H}_i = -\frac{1}{\eta_0} e^{jk_0 R} \hat{\phi}$$

where  $\eta_0 = 120\pi$  is the free space wave impedance and  $k_0 = \sqrt{\mu_0 \epsilon_0}$  is the free space propagation constant.

The surface of the perfectly conducting obstacle, defined by  $S$  in Fig. II-2, separates the interior source free region  $V$  from the exterior region containing  $\bar{J}_i, \bar{M}_i$ . Consider the total fields in the presence of the scattering obstacle. These fields are  $(\bar{E}, \bar{H})$  outside  $V$  and  $(0,0)$  inside  $V$  and are the superposition of the free space fields of  $\bar{J}_i, \bar{M}_i$  and the free space field of new secondary source  $\bar{J}_s$  on  $S$ .  $\bar{J}_s$  here is precisely the surface conduction current distribution induced on  $S$  by  $(\bar{E}_i, \bar{H}_i)$ . It is convenient at this point to define the scattered fields  $\bar{E}_s, \bar{H}_s$  in terms of the difference fields given by

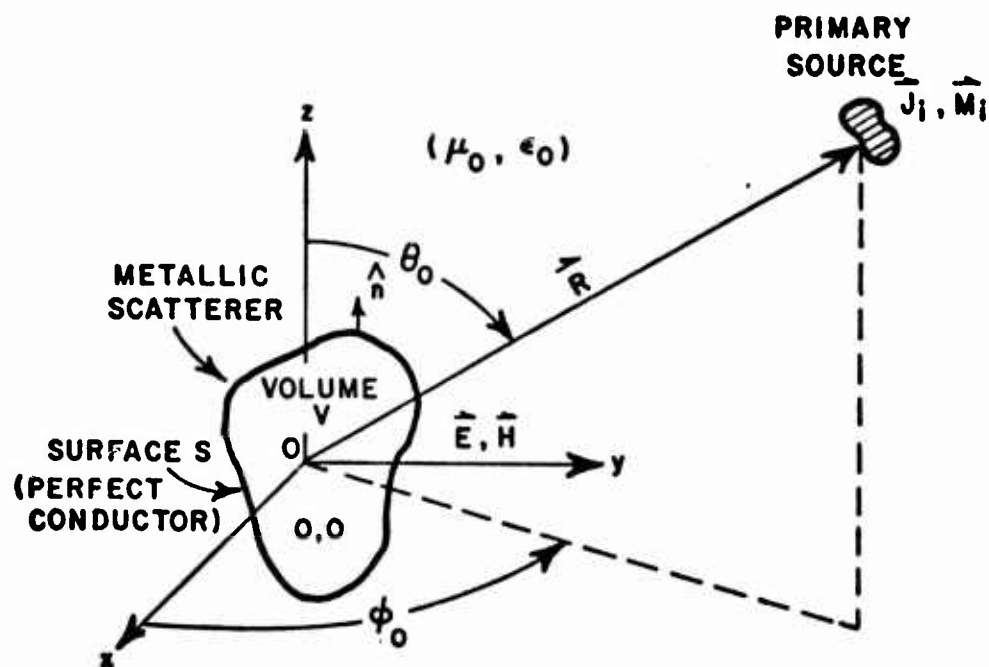


Figure II-2. Arbitrary metallic scatterer in presence of primary sources.

$$(II-4) \quad \bar{E}_S \equiv \bar{E} - \bar{E}_i$$

$$(II-5) \quad \bar{H}_S \equiv \bar{H} - \bar{H}_i$$

From this definition of fields, the surface distribution  $\bar{J}_S$ , radiating in free space, must generate  $(\bar{E}_S, \bar{H}_S)$  outside  $V$  and  $(-\bar{E}_i, -\bar{H}_i)$  inside  $V$ .  $\bar{J}_S$  can be written in terms of the boundary conditions on  $S$  (a perfect conductor) as

$$(II-6) \quad \bar{J}_S = \hat{n} \times \bar{H},$$

where  $\mathbf{n}$  is taken to be the unit outward normal. The equivalent problem stated in terms of  $(\bar{\mathbf{J}}_i, \bar{\mathbf{M}}_i)$  and  $\bar{\mathbf{J}}_s$  radiating in free space is illustrated in Fig. II-3.

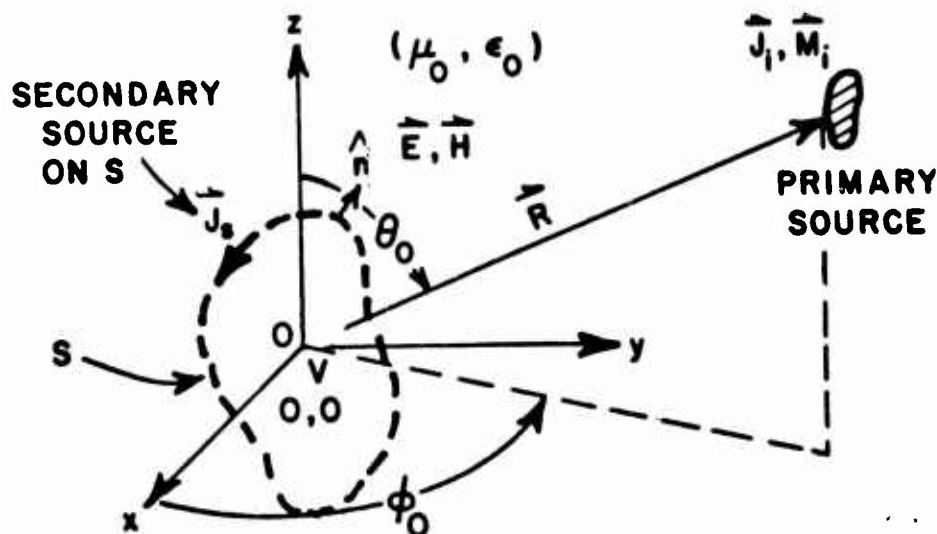


Figure II-3. Equivalent problem.

The term "reaction" was first introduced by Rumsey to describe certain measurable effects between sources and their fields. Consider two sources  $(\bar{\mathbf{J}}_a, \bar{\mathbf{M}}_a)$  and  $(\bar{\mathbf{J}}_b, \bar{\mathbf{M}}_b)$  of finite extent and radiating fields  $(\bar{\mathbf{E}}_a, \bar{\mathbf{H}}_a)$  and  $(\bar{\mathbf{E}}_b, \bar{\mathbf{H}}_b)$ , respectively. Also consider the region of space containing these sources and their fields to be isotropic but not necessarily homogeneous. The reaction of source  $b$  on source  $a$ , denoted by  $\langle a, b \rangle$  (mutual reaction), is defined by the scalar quantity

$$(II-7) \quad \langle a, b \rangle = \iiint_a (\bar{\mathbf{J}}_a \cdot \bar{\mathbf{E}}_b - \bar{\mathbf{M}}_a \cdot \bar{\mathbf{H}}_b) da'$$

where the region of integration in this case, is over the "a" sources (e.g., volumetric, surface, or filamentary). In reciprocity media the reciprocity theorem of Carson [25] can be applied to Eq. (II-7) to show equality of mutual reactions; i.e.,

$$(II-8) \quad \langle a, b \rangle = \langle b, a \rangle .$$

Sources can also be reacted with themselves to yield "self-reactions" denoted  $\langle a,a \rangle$  or  $\langle b,b \rangle$ .

Application of the reaction concept to the present scattering problem leads readily to the required integral equation formulation for the unknown surface current  $\bar{J}_s$  and to a variational solution for this current. Consider placing an arbitrary but known "test" distribution of electric current  $\bar{J}'$  ("b" source) inside  $V$  and let this source radiate free space fields  $(\bar{E}', \bar{H}')$ . These fields of the "b" source can be reacted with the superposition of sources  $\bar{J}_i$  and  $\bar{J}_s$  ("a" sources) to yield

$$(II-9) \quad \langle a,b \rangle = \iiint_{\substack{\text{primary} \\ \text{sources}}} \bar{J}_i \cdot \bar{E}' dv + \iint_S \bar{J}_s \cdot \bar{E}' ds.$$

Similarly, the fields of  $\bar{J}_i, \bar{J}_s$  can be reacted with the test source  $\bar{J}'$  and because the resulting reaction integral is taken over the  $\bar{J}'$  source located in the null field region  $V$ , this reaction is identically zero; i.e.,

$$(II-10) \quad \langle b,a \rangle = \iiint_{\substack{\text{test} \\ \text{source}}} \bar{J}' \cdot (\bar{E}_i - \bar{E}_i) dv' \equiv 0.$$

However, by way of the reciprocity between mutual reactions (Eq. II-8), Eq. (II-9) is also identically zero and can be rearranged to give

$$(II-11) \quad -\iint_S \bar{J}_s \cdot \bar{E}' ds = \iiint_{\substack{\text{primary} \\ \text{source}}} \bar{J}_i \cdot \bar{E}' dv,$$

and by applying Carson's reciprocity theorem to the right hand side of Eq. (II-11), the final form for the integral equation becomes

$$(II-12) \quad -\iint_S \bar{J}_s \cdot \bar{E}' ds = \iiint_{\substack{\text{test} \\ \text{source}}} \bar{J}' \cdot \bar{E}_i dv'.$$

This is now in a convenient form where  $\bar{E}_i$  is well defined (Eq. II-2) and  $\bar{J}'$  can be specified so that  $\bar{E}'$  can be calculated. That leaves  $\bar{J}_s$  as the only unknown quantity in this expression. Integral equation Eq. (II-12) is a special case of a more general Reaction Integral Equation (RIE) formulation discussed by Richmond [26]. Furthermore the "zero reaction" test was applied with an electric test source  $\bar{J}'$  only and the result

was the electric field integral of Eq.(II-1); however, if a magnetic test source  $M'$  had been used, the result would have been a magnetic field integral form. This use of a zero reaction test appears to have first been used by Kouyoumjian [27] and later developed by Rumsey and Richmond.

### C. Numerical Solutions

Solutions of the electromagnetic integral equation, Eq. (II-12), have in the past been obtained via a number of classic procedures, e.g., modal (eigenfunction) expansions, low frequency expansions (powers of  $k_0$ ), high frequency expansions (powers of  $1/k_0$ ), variational methods, physical and geometrical optics, etc. However, with the advent of the numerical computer, the most common method of solution, especially for complicated resonant sized obstacles, has become the method of moments [22]. This is the technique alluded to earlier by which the integral equation is converted to a system of simultaneous algebraic equations; the computer being admirably suited to compute the "inversion" type solution to this system of equations.

Consider a generalized set of vector functions  $\phi_n$ ,  $n=1,2,\dots$  defined on  $S$  to be suitable for expanding the induced surface currents on  $S$ ; i.e.,

$$(II-13) \quad \bar{J}_S = \sum_{n=1}^{\infty} J_n \bar{\phi}_n,$$

where  $J_n$  are unknown (complex) coefficients to be determined. Also assume the  $n$ th expansion "mode"  $\phi_n$  of this set radiates fields  $(\bar{E}_n, \bar{H}_n)$  in free space.

Consider another set of normalized vector modes,  $\bar{\theta}_m$ ,  $m=1,2,\dots$  as a set of arbitrary test sources  $J'$ ; i.e.,

$$(II-14) \quad \bar{J}' = \bar{\theta}_m, \quad m=1,2,\dots$$

Let mode  $m$  of this set,  $\theta_m$ , radiate  $(\bar{E}_m, \bar{H}_m)$  in free space. Equation (II-12), rewritten in terms of these expansions, becomes the doubly infinite set of algebraic equations given by

$$(II-15) \quad - \sum_{n=1}^{\infty} J_n \iint_S \bar{\phi}_n \cdot \bar{E}_m \, ds = \iiint_V \bar{\theta}_m \cdot \bar{E}_i \, dv',$$

$$m = 1, 2, \dots,$$



where the orders of integration and summation has been interchanged and the regions of integration are over the respective domains for each mode function. The practical choice of mode functions which will be used here leads to more manageable finite systems of equations than implied by Eq. (II-15).

Recall, the reaction test sources  $\bar{J}'$  have not yet been specified. Consider now the particular choice for the  $J'$  distributions  $\bar{\phi}_m = \bar{\phi}_m$ , which is known as Galerkin's method and let this mode set consist of a finite number of functions  $\bar{\phi}_n$ ,  $n=1,2,\dots,N$  where each function is nonzero only over a specific interval in space (e.g., volume region, surface area, or section of a contour); the  $\bar{\phi}_n$ 's in this case constitute an incomplete subsectional basis set. Figure II-4 illustrates one method of subsectionalizing the surface domain of  $J_s$  where  $J'$  is defined to flow on surface  $S'$ . Surface  $S'$ , in the case of a general scatterer, recall, must be located "inside"  $S$  as shown in the figure. However, for the perfectly conducting obstacles,  $S'$  may coincide with  $S$  and the zero reaction test will remain a valid test. The system of algebraic equations defined in terms of this finite subsectional mode expansion now takes the form

$$(II-16) \quad - \sum_{n=1}^N J_n \iint_n \bar{\phi}_n \cdot \bar{E}_m ds = \iint_m \bar{\phi}_m \cdot \bar{E}_i ds', \quad m=1,2,\dots,N,$$

where  $\bar{E}_m$  denotes the electric field of test source  $\bar{\phi}_m$  located on  $S'$ . This algebraic system of  $N$  equations with  $N$  unknowns  $J_n$  is commonly represented in the electromagnetics literature by the matrix formulation

$$(II-17) \quad ZI = V,$$

where  $Z = [Z_{mn}]$  represents the  $N \times N$  matrix of generalized mode impedances with elements  $Z_{mn}$  given by

$$(II-18) \quad Z_{mn} = - \iint_n \bar{\phi}_n \cdot \bar{E}_m ds; \quad m,n=1,2,\dots,N,$$

$I = (J_n)$  is the  $N \times 1$  vector of unknown mode currents and  $V = (V_m)$  is the  $N \times 1$  vector of known generalized mode voltages given by

$$(II-19) \quad V_m = \iint_m \bar{\phi}_m \cdot \bar{E}_i ds', \quad m=1,2,\dots,N.$$

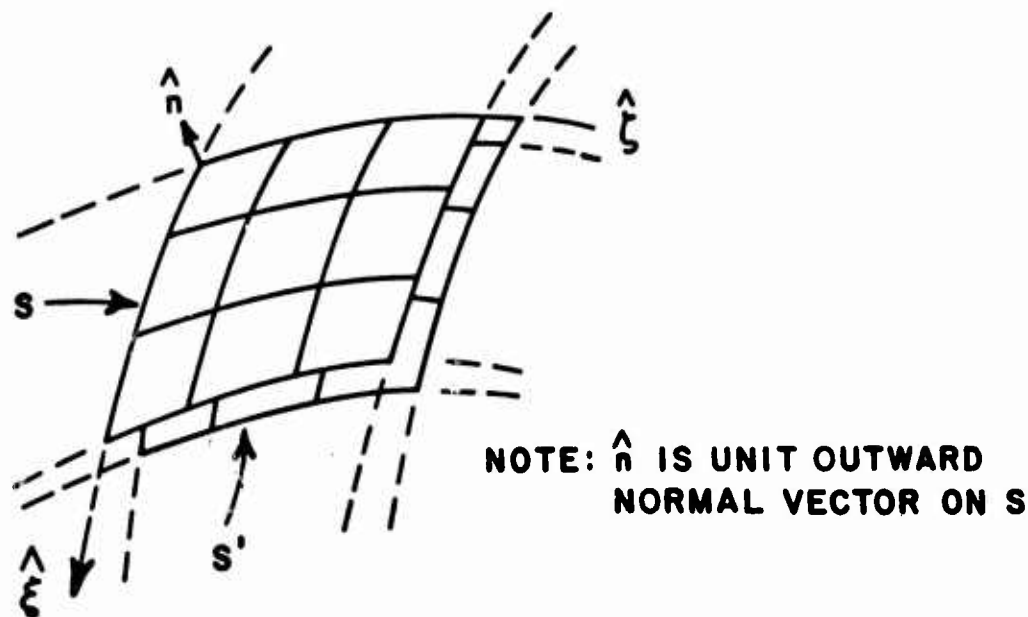


Figure II-4. Subsectionalization of S and S' and convenient surface coordinate system ( $\xi, \zeta$ ).

The expansion which defines  $\bar{J}_S$  is given by

$$(II-20) \quad \bar{J}_S \approx \sum_{n=1}^N J_n \bar{\phi}_n \text{ on } S$$

and the test sources are given by

$$(II-2) \quad \bar{J}' = \bar{\phi}_m, m=1,2,\dots,N \text{ on } S'.$$

The indicated approximation of  $\bar{J}_S$  in Eq. (II-20), under suitable conditions, will approach the true distribution when, in the limit, the subsectioning becomes infinitely "fine" and  $N \rightarrow \infty$ . This of course defeats the purpose of numerical modeling and the assumption here is that a reasonable number of samples (4-10 per  $\lambda^2$ ) will give enough information to successfully interpolate  $\bar{J}_S$ . The use of testing functions on S' instead of S when S and S' are separated, also has the particular advantage of avoiding the singular nature of the self-reaction of a source with its own field. Normal separations between S and S' should be less than  $0.01\lambda$  to give good numerical results for the types of EM problems discussed here.

#### D. Examples of Bases for Surface-Patch and Wire-Grid Modeling

The order  $N$  of the system of equations represented in Eq. (II-16) is obviously dependent on the geometry and electrical size of the scatterer, the choice of basis set and the degree and type of subsectioning required to achieve a desired numerical accuracy. The purpose of this section will be to present certain examples of basis sets for the continuous conducting obstacle and to discuss some advantages and disadvantages of each.

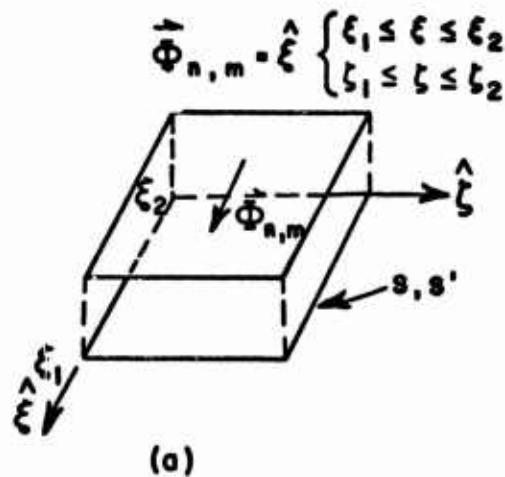
##### 1. Surface-Patch Bases (Patch subsectioning)

Figure II-5 shows examples of two basis functions suitable for the surface-patch model. Basis functions of this type were first considered by Wang, Richmond, et al. [28]. A specific example of the use of the cosine modes on a flat plate scatterer is shown in Fig. II-6 where only  $\hat{x}$  directed modes are considered; however, for more accurate results and/or the case of an arbitrarily polarized incident wave,  $\hat{z}$  directed modes would also be included. The approximation to  $J_s$  is then computed as a linear combination of modes in the two vector directions  $\hat{x}$  and  $\hat{z}$ .

##### 2. Wire-Grid Subsectional Modeling and the Piecewise Sinusoidal Basis Functions

One particular geometry of considerable interest in EM theory is the thin cylindrical antenna or scatterer and its applications to the modeling of arbitrarily shaped conducting obstacles. First developments in the use of wires for numerical modeling of continuous conducting shapes were advanced by Richmond [29] and this approach was later used extensively by Lin and Richmond [30] and Thiele [31]. The basic technique of wire-grid modeling is to define a suitable number of points on the surface of the obstacle and then interconnect these points with straight wire segments. These segments serve as approximate paths for the induced surface currents and the integral equation of Eq. (II-16) now becomes one for solving for the unknown surface currents on these wires.

One possible set of basis modes which are amenable to the wire-grid structure are the overlapping piecewise sinusoidal dipole modes introduced by Richmond [32]. Other types of subsectional bases often appear in the literature [33]; e.g., pulse bases, piecewise linear bases, etc. The literature also refers to trigonometric whole bases [34] from time to time. However, the piecewise sinusoidal basis functions have been shown [35] to have certain superior properties, making them well suited to numerical solution of wire structure problems.



$$\vec{\Phi}_{n,m} = \left\{ \begin{array}{ll} \text{UNIFORM, } \hat{\xi} & \zeta_1 \leq \zeta \leq \zeta_2 \\ \cos \left[ \frac{\pi}{2} \left( \frac{\xi_2 - \xi}{\xi_2 - \xi_1} \right) \right] \hat{\xi}, & \xi_1 \leq \xi \leq \xi_2 \\ \cos \left[ \frac{\pi}{2} \left( \frac{\xi - \xi_2}{\xi_3 - \xi_2} \right) \right] \hat{\xi}, & \xi_2 \leq \xi \leq \xi_3 \end{array} \right.$$

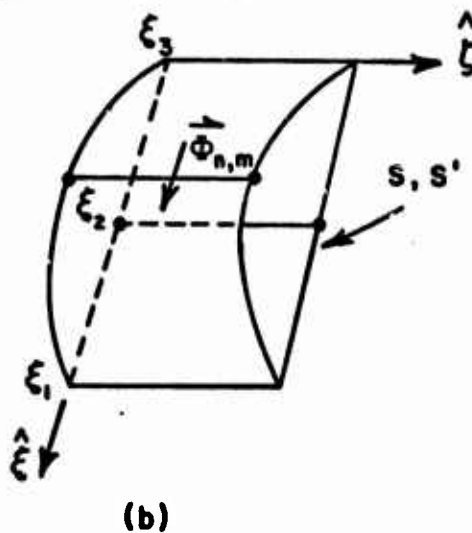


Figure II-5. Examples of subsectional basis functions for surface scatterer. (a) Uniform rectangular pulse basis functions, one pulse per subsectional region; (b) Overlapping cosinusoidal basis functions, one cosine mode per two subsections in  $\xi$ , uniform in  $\zeta$ .

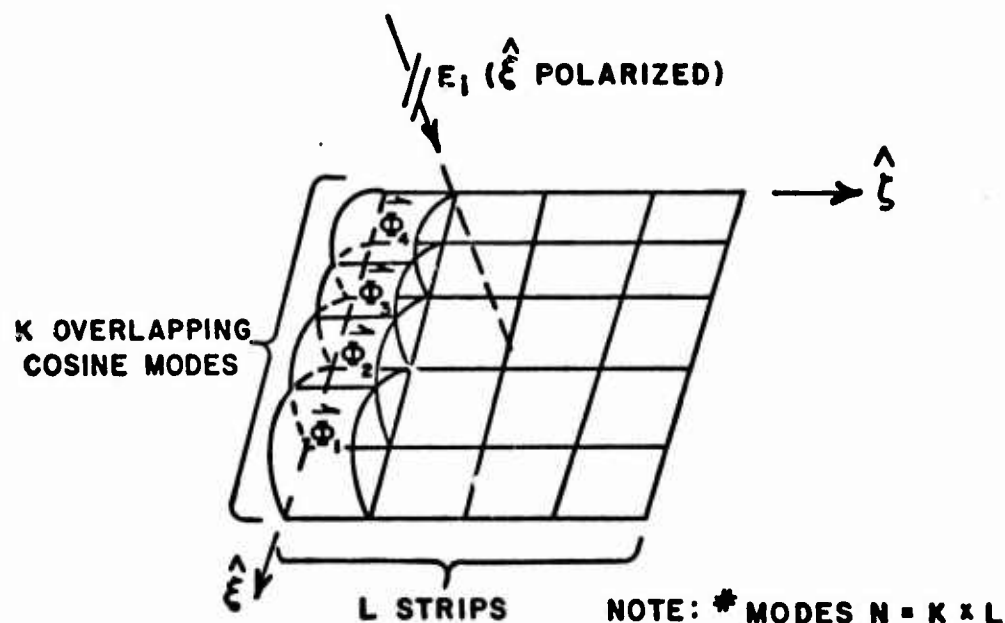


Figure II-6. Mode structure for computing backscatter cross section from thin square flat plate (perfect conductor) using overlapping cosine modes (see Fig. II-5).

Figure II-7 shows two examples of pairs of interconnecting segments - separated pairs and overlapping pairs. Consider the  $n$ th dipole mode  $\bar{\phi}_n$  given by

$$(II-22) \quad \bar{\phi}_n = \begin{cases} \frac{\sin k_0(r_2-r)}{\sin k_0(r_2-r_1)} \hat{r}, & r_1 \leq r \leq r_2 \\ \frac{\sin k_0(s_2-s)}{\sin k_0(s_2-s_1)} \hat{s}, & s_1 \leq s \leq s_2. \end{cases}$$

This mode flows as a tubular surface current density on the  $n$ th pair of intersecting segments (v-dipole) with arms in the  $r$  and  $s$  directions. Now consider the test source  $J'$  (Eq. (II-21)) to be a filamentary source on the axes of these segments. It can be shown that the reaction of this axial test source with any colinear tubular surface current mode is identical to the reaction between this same axial test source and a filamentary current mode  $2\pi a \bar{\phi}_n$  located one radius " $a$ " away from the segment axis. Figure II-8 illustrates the

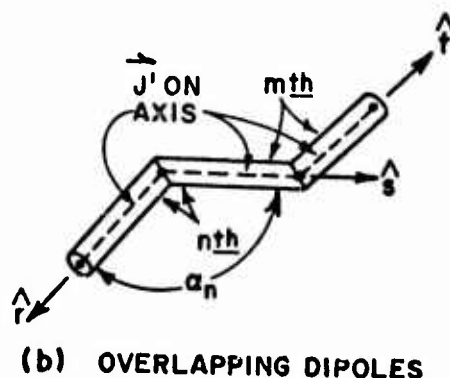
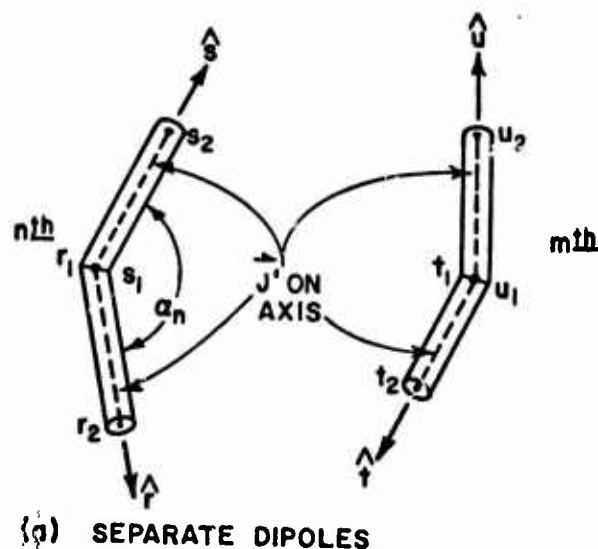
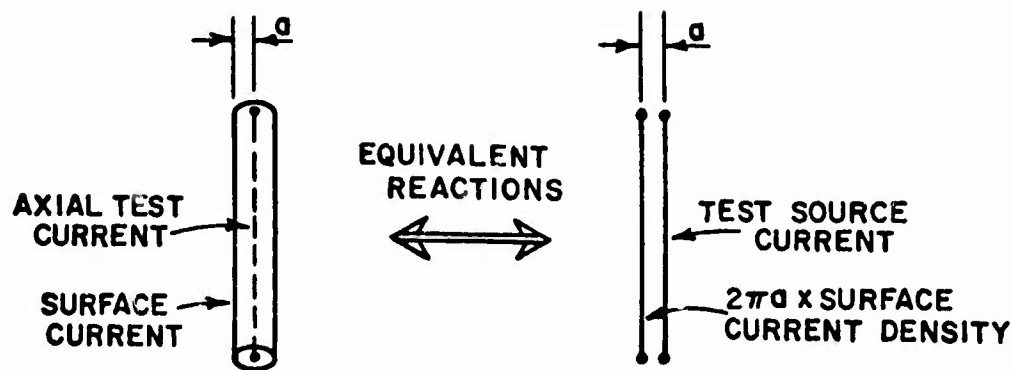


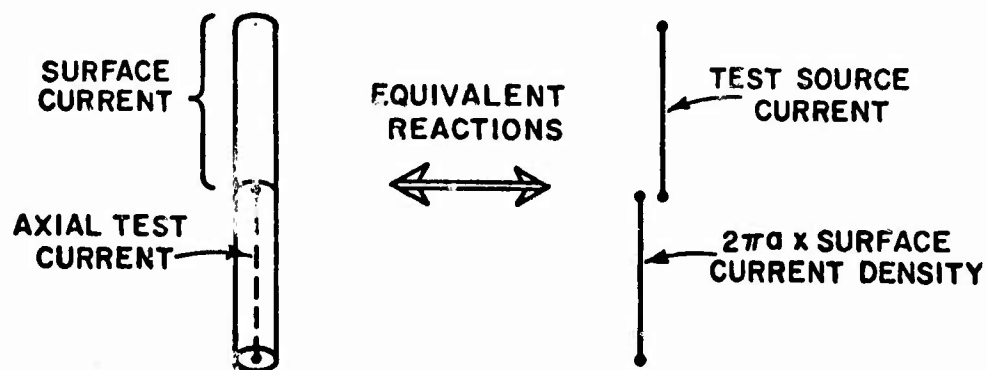
Figure II-7. Nonoverlapping dipole segments and overlapping dipole segments.

equivalent cases. Numerical calculations have indicated [36] that for the non-colinear cases (Fig. II-7), the errors introduced into the self and mutual reactions, by using the axial test sources and filamentary approximations for the surface modes, can be neglected when segment lengths exceed 20 radii and spacings between separate dipoles exceed  $a/\lambda$  or the angle  $\alpha_n$  between two intersecting (overlapping) segments exceeds  $\sim 30^\circ$ . Figure II-9 illustrates a section of wire-grid modeling for an arbitrarily shaped conducting obstacle and shows a portion of an overlapping piecewise sinusoidal mode structure. Only a few  $\hat{\xi}$  directed modes are shown; however, for an arbitrarily directed surface current, modes must be included in the  $\hat{\xi}$  direction and enforcement of continuity of the currents at each junction of multiple segments assures that a junction having  $k$  intersecting segments will have only  $k-1$  independent dipole modes passing through it.





(a) SAME SEGMENT



(b) COLINEAR SEGMENTS

Figure II-8. Equivalence of reactions between colinear axial test source and tubular surface current and equivalent parallel filamentary cases.

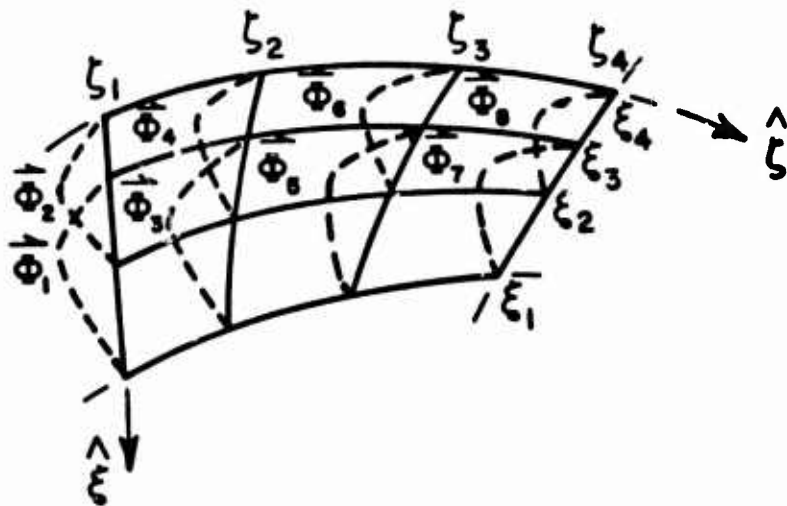


Figure II-9. Sample mode structure on wire-grid model of conducting surface. Sample of  $\xi$  basis functions shown; however, both  $\xi$  and  $\zeta$  function required in general.

The integrals in Eq. (II-16) become line integrals for this type of modeling and successful application of the piecewise sinusoidal expansion modes normally requires wire segment lengths not to exceed  $0.25\lambda$ .

### 3. Advantages and Disadvantages

Both surface patch and wire-grid modeling are generally considered suitable for continuous conducting obstacles. However, if the obstacle includes a protruding section; e.g., antenna (monopole), then the wire-grid type structure is usually more convenient. The surface patch technique, on the other hand, will model the same size surface with fewer modes but computations of the wire-grid mutual impedances are performed much faster than for the patches. If computing time is critical, then the wire-grid model might be considered to have the advantage, even though it may require a larger number of modes.

### E. Chaff Clouds

The discussion so far has emphasized the more general cases of arbitrarily shaped conducting scatterers; however, it also serves as the basic background needed for the problem at hand, namely, scattering by random clouds of thin conducting wires. Here, the wires are assumed to be of resonant length  $\sim 0.5\lambda$  and the piecewise sinusoidal modes are used. Each wire can then be modeled as a  $p=2$  segment dipole requiring only one mode per wire.

Possible exceptions to this will occur for those cases where the wire lengths are significantly greater than resonant length, a situation briefly treated in this study.

Figure II-10 shows two typical 2-segment wires and also illustrates the approximate filamentary models used; test expansion mode  $m$  on the axis of dipole  $s$  and unknown expansion mode  $I_n$  on the surface of dipole  $t$ . The actual random array will consist of many of these resonant wires with the centers of all wires chosen with uniform or nonuniform probability in a spherical volume of space and each randomly oriented according to a uniform spherical probability density function. The technique used to generate the array is discussed in detail in Appendix III.

#### F. A Convenient Change in Notation

A rather more convenient form for the matrix equation presented in Eq. (II-17) can be expressed using slightly different matrix and vector notation. The following definitions, while perhaps unconventional from the standpoint of electromagnetic theory, are in standard usage in numerical analysis and will be used throughout the remaining chapters of this study. The self and mutual reactions or generalized model impedances previously defined in Eq. (II-18) will be denoted here by the  $N \times N$  matrix  $A = [a_{mn}]$  with the elements  $a_{mn}$  given by

$$(II-23) \quad a_{mn} = - \iint_n \bar{\Phi}_n \cdot \bar{E}_m \, ds; \quad m, n = 1, 2, \dots, N,$$

and the generalized mode voltages previously defined in Eq. (II-19) are now denoted by the  $N \times 1$  vector  $b = (b_m)$  with elements  $b_m$  given by

$$(II-24) \quad b_m = \iint_m \bar{\Phi}_m \cdot \bar{E}_i \, ds', \quad m = 1, 2, \dots, N.$$

The unknown mode coefficients  $J_n$ , representing samples of the distribution  $J_s$ , will be denoted by the  $N \times 1$  vector  $x = (x_n)$ ,  $n = 1, 2, \dots, N$ . This whole system of equations is now expressed in the new notation as

$$(II-25) \quad Ax = b.$$

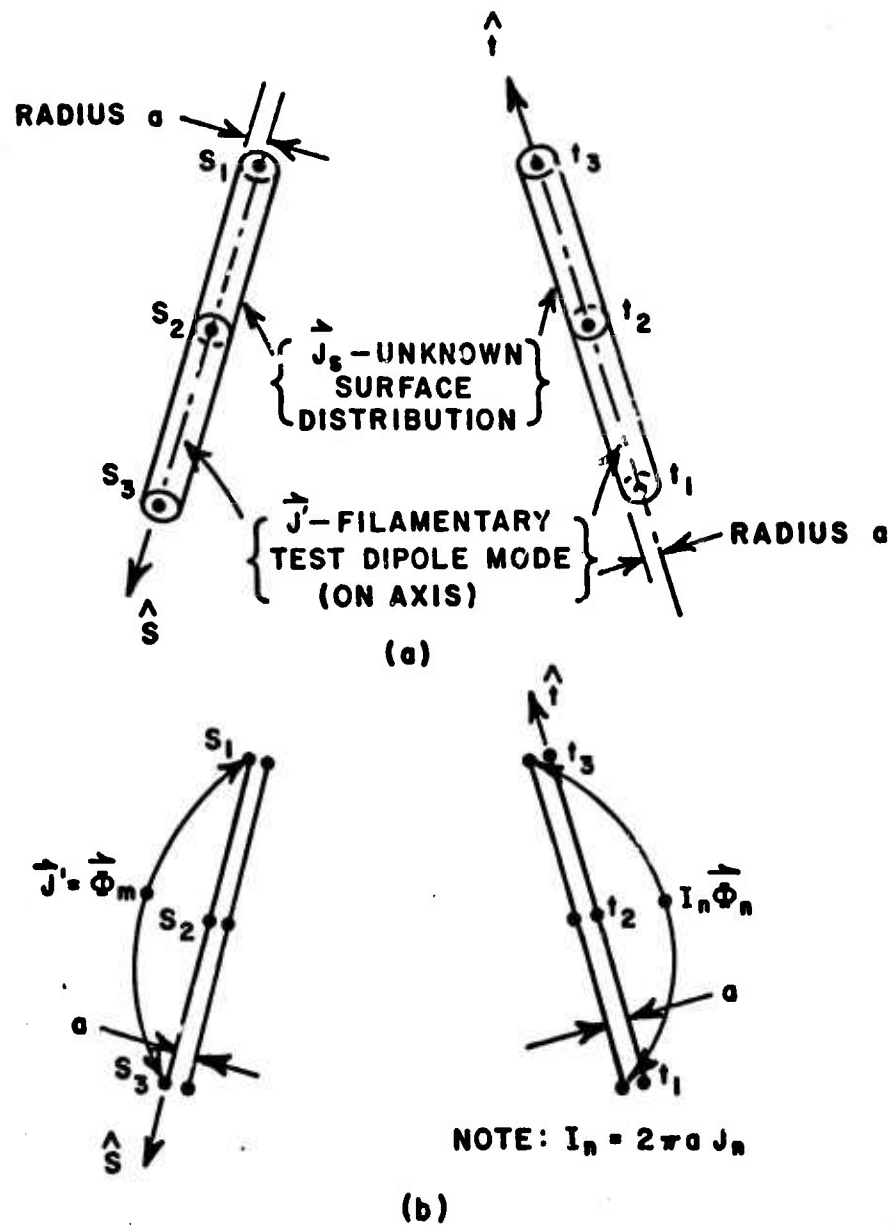


Figure II-10. a) Thin cylindrical wires, b) Approximate filamentary model using piecewise sinusoidal expansions  $\vec{\Phi}_n$  on surface and  $\vec{\Phi}_m$  on axis.

The  $N \times N$  impedance matrix  $A$  in the case of these random arrays of thin wires will contain all possible interactions among  $N$  wires and will not be a "thin" or sparse matrix. Also, the number of wires considered will be as large as  $N = 1000$  and hence, the equation to be solved, Eq. (II-25), will be a "full" matrix equation of up to order 1000. All elements of Eq. (II-25) will be complex numbers and the impedances given by Eq. (II-23) will be complex symmetric, i.e.,  $a_{mn} = a_{nm}$  for all  $m$  and  $n$ . This last condition results from the reciprocity relation of Eq. (II-8) and the use of Galerkin's method.

## APPENDIX C CLOUD GEOMETRY

### A. The Radially Inhomogeneous Cloud

To create a chaff cloud,  $N$  dipoles are randomly positioned in space and oriented according to certain statistical rules. Their orientations are specified so that all possible orientations are equally likely, i.e., a spherical probability density function for orientation is implied. Their positions are specified by the Cartesian coordinates  $(x, y, z)$  of their centers according to the following rules:

1. The probability of finding the  $x$ -coordinate of a dipole center in a small increment  $\Delta x$  about  $x$  is

$$(III-1) \quad g(x)\Delta x = \frac{\Delta x}{\sqrt{2\pi\delta^2}} e^{-\frac{1}{2}\left(\frac{x}{\delta}\right)^2}$$

2. The probability of finding the  $y$  coordinate of a dipole center in a small increment  $\Delta y$  about  $y$  is

$$(III-2) \quad g(y)\Delta y = \frac{\Delta y}{\sqrt{2\pi\delta^2}} e^{-\frac{1}{2}\left(\frac{y}{\delta}\right)^2}$$

3. The probability of finding the  $z$  coordinate of a dipole center in a small increment  $\Delta z$  about  $z$  is

$$(III-3) \quad g(z)\Delta z = \frac{\Delta z}{\sqrt{2\pi\delta^2}} e^{-\frac{1}{2}\left(\frac{z}{\delta}\right)^2}$$

4. The process by which the coordinates  $(x, y, z)$  of a dipole center are selected are statistically independent.

Note that the three probability density functions are Gaussian with zero mean and identical standard deviation  $\delta$ , implying that the cloud is most dense in the center and spherically symmetric.

Because of the statistical independence property, the probability of finding a dipole center in a small cube of volume  $v = \Delta x \Delta y \Delta z$  about the point  $(x_1, y_1, z_1)$  is

$$(III-4) \quad P(x_1, y_1, z_1; \Delta v) = \int_{z_1 - \frac{\Delta z}{2}}^{z_1 + \frac{\Delta z}{2}} \int_{y_1 - \frac{\Delta y}{2}}^{y_1 + \frac{\Delta y}{2}} \int_{x_1 - \frac{\Delta x}{2}}^{x_1 + \frac{\Delta x}{2}} g(x)g(y)g(z) dx dy dz$$



If there are a total of  $N$  dipoles in the cloud, the number of dipoles expected to lie in the small cube  $v$  about the point  $(x_1, y_1, z_1)$  is on the average,

$$(III-5) \quad \Delta N(x_1, y_1, z_1; v) = N \Delta P(x_1, y_1, z_1; \Delta v)$$

so the fraction of the total number of dipoles lying in  $v$  about  $(x_1, y_1, z_1)$  is on the average,

$$(III-6) \quad \frac{\Delta N(x_1, y_1, z_1; \Delta v)}{N} = g(x_1)g(y_1)g(z_1)\Delta v$$

If  $N$  is very large, or a large ensemble of clouds with the same  $N$  and standard deviation  $\delta$  is assumed, and if the sample volume  $\Delta v$  is made very small, we can define in the limit the relative density of dipoles at a point  $(x_1, y_1, z_1)$  by

$$(III-7) \quad n(x_1, y_1, z_1) = \lim_{\substack{N \rightarrow \infty \\ \Delta v \rightarrow 0}} \frac{\Delta N(x_1, y_1, z_1; \Delta v)}{N \Delta v} = g(x_1)g(y_1)g(z_1) \\ = n(r_1) = \frac{1}{2\pi\delta^2} \left[ \frac{1}{\sqrt{2\pi\delta^2}} e^{-\frac{1}{2}\left(\frac{r_1}{\delta}\right)^2} \right]$$

or

$$(III-8) \quad n(r) = \frac{1}{2\pi\delta^2} g(r)$$

where  $r = (x^2 + y^2 + z^2)^{1/2}$  is the radial distance from the center of the cloud. (From (III-8), we see that the dipole density is independent of  $(\theta, \phi)$  (a spherical symmetric cloud) and is proportional to a Gaussian function in the radial direction.

In our work, we chose to characterize a cloud by a constant which we call "the average spacing between dipoles,"  $d/\lambda$ , defined as follows.

1. For a given spherical volume  $V = (4/3)\pi R^3$  over which the average is desired, calculate the expected number of dipoles in  $V$ ; call this number  $kN$  where  $N$  is the total number of dipoles in the cloud and  $0 \leq k \leq 1$  is the fraction of the total number of dipoles contained in  $V$ .

2. Consider  $V$  to be divided into  $kN$  equal cubes, and call the edge dimension of each cube  $d$ . In this manner we obtain the relationship

$$(III-9a) \quad \frac{3}{4} \pi R^3 = kN d^3,$$

or

$$(III-9b) \quad \frac{d}{\lambda} = \left( \frac{4\pi}{3} \right)^{1/3} \frac{1}{k^{1/3}} \frac{1}{N^{1/3}} \frac{R}{\lambda}$$

In our case,

$$(III-10) \quad kN = N \int_0^{2\pi} \int_0^\pi \int_0^R n(r) r^2 \sin \theta \, dr \, d\theta \, d\phi$$

$$= N \int_{-R}^R \frac{r^2 e^{-\frac{1}{2} \left( \frac{r}{\delta} \right)^2}}{\delta^3 \sqrt{2\pi}} \, dr,$$

so

$$(III-11) \quad k = \frac{1}{\delta^2 \sqrt{2\pi} \delta^2} \int_{-R}^R r^2 e^{-\frac{1}{2} \left( \frac{r}{\delta} \right)^2} \, dr$$

which, evaluated by integration by parts, is

$$(III-12) \quad k = \frac{1}{\sqrt{2\pi}} \int_{-R/\delta}^{R/\delta} e^{-\frac{1}{2} t^2} \, dt - \sqrt{\frac{2}{\pi}} \frac{R}{\delta} e^{-\frac{1}{2} \left( \frac{R}{\delta} \right)^2}$$

The first term in Eq. (III-12) is the integral of the normalized Gaussian function and can be evaluated from tables. Values of  $k$  are plotted vs  $R/\delta$  in Fig. III-1.

If Eq. (III-9b) is written in the form,

$$(III-13) \quad N^{1/3} \frac{d}{\delta} = \left( \frac{4\pi}{3k} \right)^{1/3} \frac{R}{\delta}$$

the quantity  $N^{1/3}d/\delta$  may be plotted vs  $R/\delta$ , using the values of  $k$  corresponding to values of  $R/\delta$  according to Eq. (III-12). This plot is also shown in Fig. III-1. In this report, a value of  $R = 2.05\delta$ , corresponding to  $k = 0.76$ , has been chosen as the radius of the sphere over which an average is taken to obtain the relationship between  $d/\lambda$  and  $\delta/\lambda$ . For this choice Eq. (III-9b) is

$$\begin{aligned} \text{(III-14)} \quad \frac{d}{\lambda} &= \left(\frac{4\pi}{3}\right)^{1/3} \frac{1}{(0.76)^{1/3}} \frac{1}{N^{1/3}} 2.05 \frac{\delta}{\lambda} \\ &= \frac{3.62}{N^{1/3}} \frac{\delta}{\lambda} \end{aligned}$$

It was by selecting convenient values of  $d/\lambda$ , such as 2.0, 1.5, 1.0, 0.5 in this report, that corresponding values of  $\delta/\lambda$  were obtained for use in Eqs. (III-1), (III-2), (III-3).

Note that the choice  $R/\delta = 2.05$  is rather arbitrary. If, for example we chose to average over smaller and smaller spheres, in the limit as  $R/\delta \rightarrow 0$  and  $k \rightarrow 0$ , we obtain the relationship between a new average spacing  $d'/\lambda$  and  $\delta/\lambda$ ,

$$\begin{aligned} \text{(III-15)} \quad \frac{d'}{\lambda} &= \frac{\sqrt{2\pi}}{N^{1/3}} \frac{\delta}{\lambda} \\ &= \frac{2.51}{N^{1/3}} \frac{\delta}{\lambda} \end{aligned}$$

Assuming that the  $\delta/\lambda$  values calculated from Eq. (III-14) are used in (III-15), we see that  $d'/\lambda$  is about  $0.69d/\lambda$ , yielding the corresponding table

$d/\lambda$	$d'/\lambda$
2.00	1.38
1.50	1.04
1.00	0.69
0.50	0.35
0.25	0.173

$\frac{\delta}{\lambda}$  same for the two cases

Thus, the values of  $d/\lambda$  presented in this report are conservatively large, i.e., substantially smaller average spacings are encountered in the center of each cloud.

The quantity  $(1/d')^3$  is equal to the density of dipoles in the center of the cloud expressed in dipoles per cubic wavelength if  $d'$  is in wavelengths. Similarly, the quantity  $(1/d)^3$  is the density of dipoles averaged over the sphere containing 76% of the dipoles. Some typical plots of dipole density versus radius for selected values of  $N$  and  $d/\lambda$  are shown in Figs. III-2,3. The dashed lines represent the values of  $\delta/\lambda$  as related to  $d/\lambda$  by Eq. (III-14).

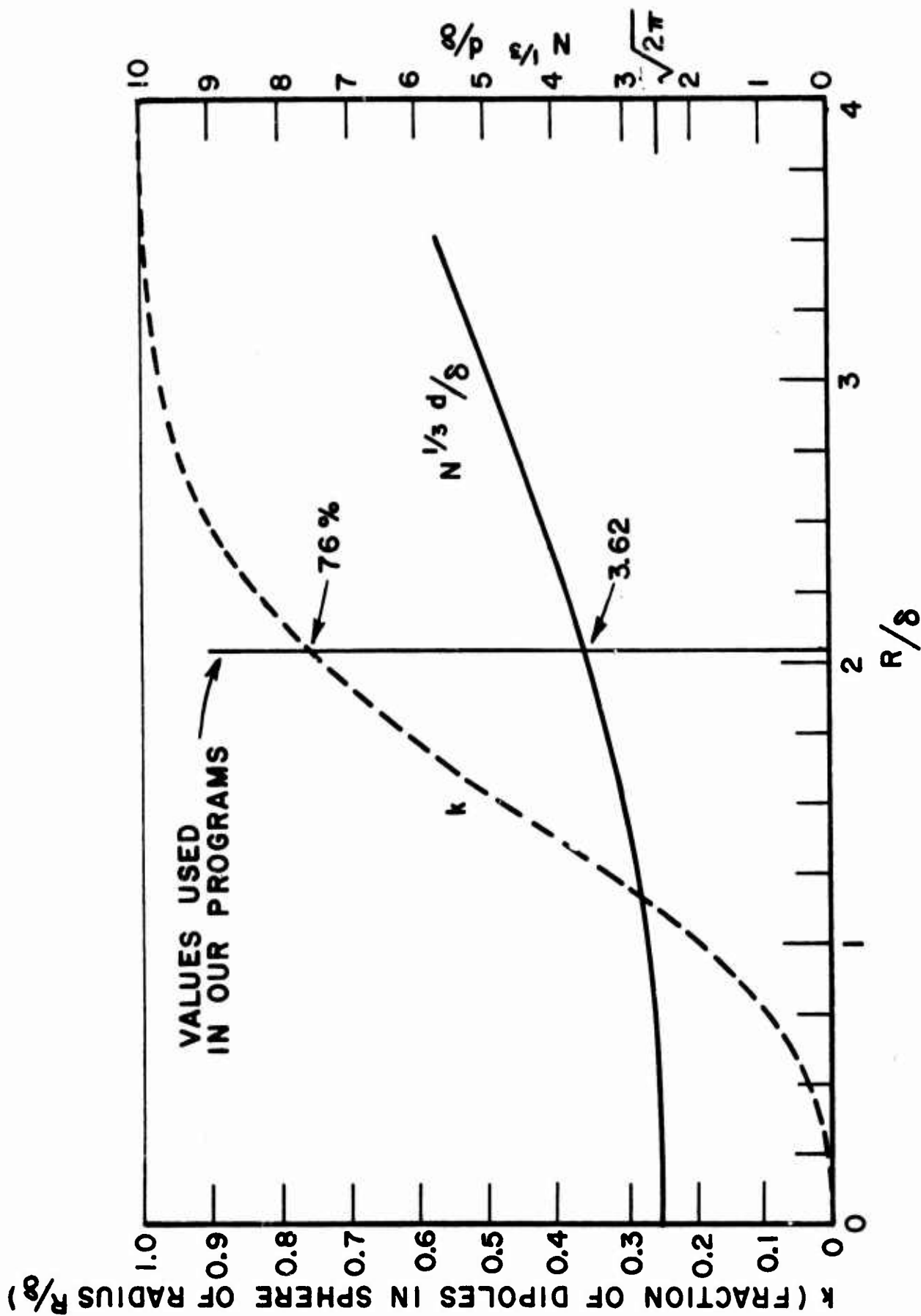


Figure III-1.

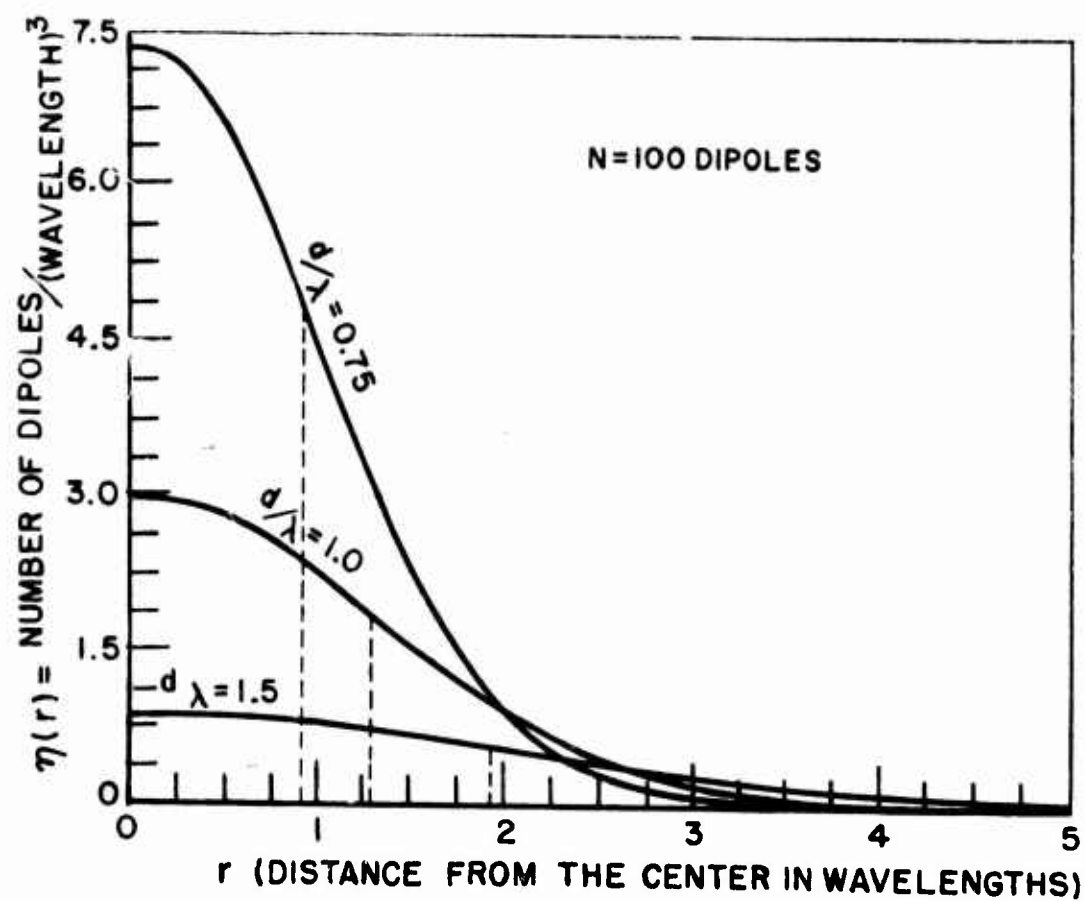


Figure III-2.

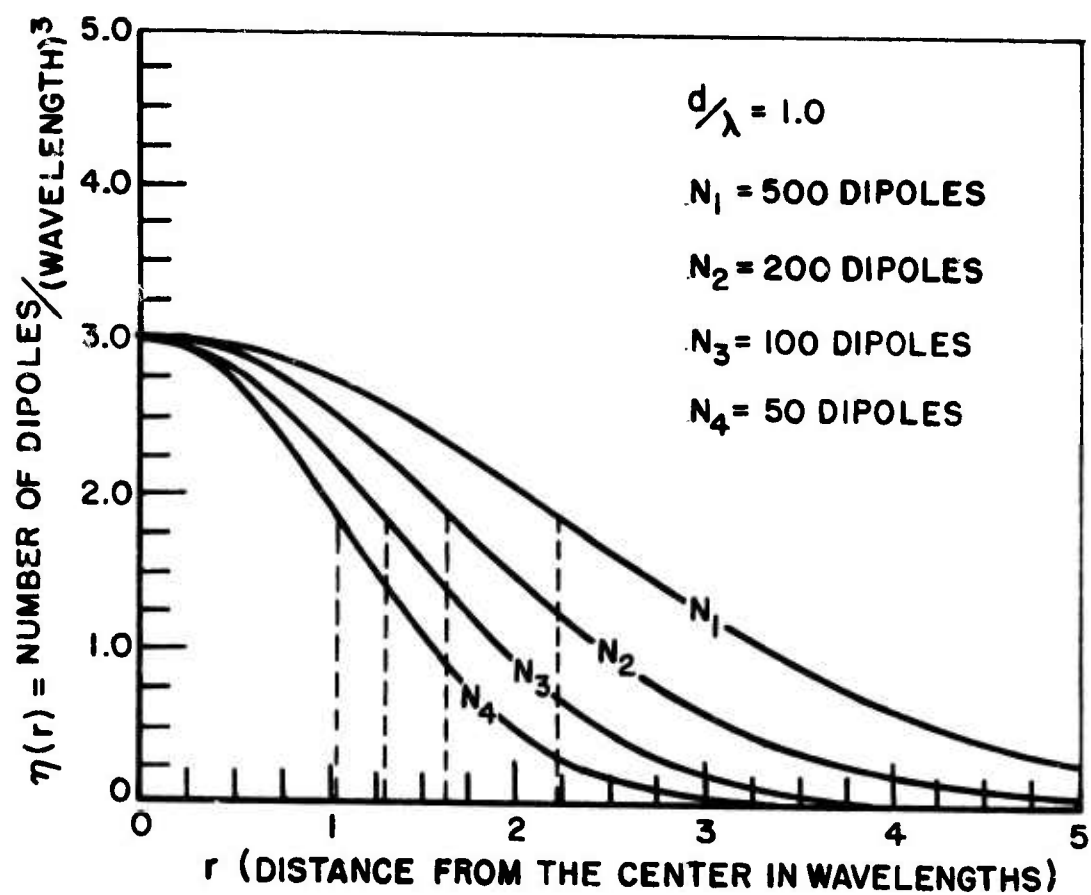


Figure III-3.



## B. The Homogeneous Cloud

Consider the generation of  $N$  randomly distributed points representing center coordinates of  $N$  dipoles. If these  $N$  points are distributed according to a uniform probability density function and are confined to a spherical volume region  $V$  around the origin with an average volume density  $D$ , then the radius of  $V$  is given by

$$(III-16) \quad R_0 = \left( \frac{3N}{4\pi D} \right)^{1/3}.$$

Consider these points to be defined in terms of statistically independent random variables  $\tilde{r}, \tilde{\theta}, \tilde{\phi}$  in the usual spherical coordinate systems. The probability of finding one of these points inside the incremental volume element  $dv$  must be given by

$$(III-17) \quad p(\tilde{r}, \tilde{\theta}, \tilde{\phi}) \, dr \, d\theta \, d\phi = \begin{cases} \frac{3}{4\pi R_0^3} \tilde{r}^2 \sin \tilde{\theta} \, dr \, d\theta \, d\phi, & 0 \leq \tilde{r} \leq R_0 \\ 0, & R_0 < \tilde{r} \end{cases}$$

to insure these points will be uniformly distributed throughout  $V$ . Since the random variables  $\tilde{r}, \tilde{\theta}, \tilde{\phi}$  are statistically independent, the independent probability density functions become

$$(III-18) \quad p(\tilde{r}) = \frac{3}{R_0^3} \tilde{r}^2,$$

$$(III-19) \quad p(\tilde{\theta}) = \frac{1}{2} \sin \tilde{\theta}$$

and

$$(III-20) \quad p(\tilde{\phi}) = \frac{1}{2\pi}.$$

The two angular density functions above can be computed in terms of direction cosines  $\cos \alpha$ ,  $\cos \beta$  and  $\cos \gamma$  as follows:

$$(III-21) \quad \cos \tilde{\theta} = 2\tilde{A}(1) - 1$$

$$(III-22) \quad \sin \tilde{\theta} = (1 - \cos^2 \tilde{\theta})^{1/2}$$

$$(III-23) \quad \tilde{\phi} = 2\pi \tilde{A}(2)$$

$$(III-24) \quad \cos \alpha = \sin \tilde{\theta} \cos \tilde{\phi}$$

$$(III-25) \quad \cos \beta = \sin \tilde{\theta} \sin \tilde{\phi}$$

$$(III-26) \quad \cos \gamma = \cos \tilde{\theta}$$

where the  $\tilde{A}(i)$ 's are obtained by independent calls to IBM-SSP subroutine RANDU:  $\tilde{A}(i)$ ,  $i=1,2,\dots$  forms a sequence of uniformly distributed pseudo random numbers in the range  $0 \leq \tilde{A}(i) \leq 1$ . The properly distributed radial variable is given by

$$(III-27) \quad \tilde{r} = R_0 (\tilde{A}(3))^{1/3}$$

where  $\tilde{A}(3)$  corresponds to another call to RANDU. Finally, orientations of the  $N$  dipoles are each chosen independently according to the same sequence of Eqs. (III-21) to (III-26), again using independent calls to RANDU. Once the midpoints and orientations are specified, this fully specifies the modeled chaff cloud used here.

APPENDIX D  
FULL MATRIX COMPUTER PROGRAM FOR MULTIPLE LENGTHS

In Reference 12, Appendix II is presented a computer program for full matrix solution (scrout) of chaff clouds with single length elements. This appendix presents a program (still using scrout) extended in two ways: it permits the analysis of clouds containing three different element lengths in any combination of numbers and lengths; and it utilizes improved algorithms for obtaining the elements  $z_{mn}$  of the impedance matrix.

The computer program in this appendix is used to calculate the random backscattering cross section of "ND" randomly distributed dipoles. These dipoles form three groups and each group has a different dipole length.

Since the dipoles are randomly distributed, one can assume that dipole No. 1 through No. N1 are in group 1 with length DL1, dipole No. N1+1 through N2 are in group 2 with length DL2, and dipole No. N2+1 through ND are in group 3 with length DL3. Dipoles within each group are further divided into segments according to the accuracy desired. Segmentation for dipoles in each group are denoted by NOS1, NOS2, and NOS3. Set NOS1 equal to 3 means all the dipoles in group 1 are divided into 3 segments, etc. If DL1=DL2=DL3 and N1=N/3, N2/3, the cloud is made up of N identical dipoles.

All the input parameters for this program are specified as follows:

1. N1: last dipole number in group 1.
2. N2: last dipole number in group 2.
3. ND: last dipole number (which is identical to the total number of dipoles) in group 3.
4. DL1: dipole length (in wavelengths) for group 1.
5. DL2: dipole length (in wavelengths) for group 2.
6. DL3: dipole length (in wavelengths) for group 3.
7. NOS1: segmentation used for dipoles in group 1.
8. NOS2: segmentation used for dipoles in group 2.
9. NOS3: segmentation used for dipoles in group 3.
10. INT: integration sampling constant (usually 10)
11. AL: wire radius for all the dipoles.
12. NSETS: number of clouds to be studied.
13. Spc: average spacing between dipoles.
14. IZ: starting point of the random generator.

This program is set up to plot the echo (in dB) for DBPP, DBTT, and DBTP. One can easily obtain the following quantities as defined in previous Report 3401-1: AVTT, AVPP, AVTP, AV11, VARTT, VARTP, VARPP and VAR11 using the outputs (from SUBROUTINE BKCD) ECTT, ECTP and FCPP.

```

1  OPTIONS 32K
2  COMPLEX C(5050),ETT(100),EPP(100),S(100)
3  DIMENSION DBTT(360),DBPP(360),DBTP(360)
4  DIMENSION CA(30),CB(30),CG(30),X(30),Y(30),Z(30)
5  DIMENSION XX(100),YY(100),ZZ(100),CCA(100),CCB(100),CCG(100)
6  DIMENSION HL123(3),HK(100)
7  DATA PI/3.141592/
8  DATA IDM,MAXND/100,30/
9  ION=(IDM*IDM-IDM)/2+IDM
10 TP=2.*PI
11 DR=0.01745329
12 ALMDA2=((1.8/.475)*0.0254)**2
13 ALMDA2=1.0
14 READ(8,*) DL1,DL2,DL3,NOS1,NOS2,NOS3,N1,N2,ND,INT,AL,NSETS
15 MODE1=(NOS1-1)*N1
16 MODE2=(NOS2-1)*(N2-N1)
17 MODE3=(NOS3-1)*(ND-N2)
18 NMODE=MODE1+MODE2+MODE3
19 INC=(NMODE*NMODE-NMODE)/2+NMODE
20 READ(8,*) SPC,I7
21 STDX=SPC/2.05/(4.*3.141592/(3.*.76*ND))**(.1/3.)
22 STDY=STDX
23 STDZ=STDX
24 DO 80 NSET=1,NSETS
25 IX=IZ
26 CALL CLDGE0(ND,STDX,STDY,STDZ,IX,X,Y,Z,CA,CB,CG)
27 CALL CLDMOD(DL1,DL2,DL3,NOS1,NOS2,NOS3,N1,N2,ND,IDM
28 2,X,Y,Z,CA,CB,CG,XX,YY,ZZ,CCA,CCB,CCG,HK,HL123)
29 C WRITE(6,2) ((I,XX(I),YY(I),ZZ(I)),I=1,NMODE)
30 2 FORMAT(5X,15,3E15.4)
31 CALL ZIJ(NMODE,XX,YY,ZZ,CCA,CCB,CCG,HK,HL123,AL,INT,
32 1IDM,MODE1,MODE2,C,ION)
33 C WRITE(8,3) ((I,C(I)),I=1,INC)
34 3 FORMAT(5X,15,2E15.4)
35 CALL SQROT1(C,NMODE,ION)
36 PH=0.0
37 CPH=1.0
38 SPH=0.0
39 NPHI=360
40 DPH=1.0
41 XNTT=-1000.0
42 XNTP=-1000.0
43 XNPP=-1000.0
44 AVTT=0.0
45 AVPP=0.0
46 DO 66 NPH=1,NPHI
47 CALL BKCU(CPH,SPH,0.0,ECTT,ECTP,ECPP,
48 2XX,YY,ZZ,CCA,CCB,CCG,HK,NMODE,IDM,C,ETT,EPP,S,ION)
49 GO TO 77
50 IF(ECTT.LT.0.000000001) ECTT=0.000000001
51 IF(ECTP.LT.0.000000001) ECTP=0.000000001
52 IF(ECPP.LT.0.000000001) ECPP=0.000000001
53 DBTT(NPH)=10.*ALOG10(ECTT*ALMDA2)
54 DBTP(NPH)=10.*ALOG10(ECTP*ALMDA2)
55 DBPP(NPH)=10.*ALOG10(ECPP*ALMDA2)

```

```

56      IF(XNTT.LT.DBTT(NPH)) XNTT=DBTT(NPH)
57      IF(XNTP.LT.DBTP(NPH)) XNTP=DBTP(NPH)
58      IF(XNPP.LT.DBPP(NPH)) XNPP=DBPP(NPH)
59  77  CONTINUE
60      AVTI=AVTI+ECTT
61      AVPP=AVPP+ECPP
62      PH=PH+DPH
63      PHR=PH*DK
64      CPH=COS(PHR)
65      SPH=SIN(PHR)
66  66  CONTINUE
67      AV11=(AVTI+AVPP)/FLOAT(NPHI)/2.
68      WRITE(8,-) SPC,AV11
69      GO TO 2000
70      DO 999 NPH=1,NPHI
71      DBTT(NPH)=DBTT(NPH)-XNTT
72      DBTP(NPH)=DBTP(NPH)-XNTP
73      DBPP(NPH)=DBPP(NPH)-XNPP
74  999  CONTINUE
75      WRITE(8,1000)
76      READ(8,-) ICC
77      CALL PLOT1(N1,N2,NO,DL1,DL2,DL3,NOS1,NOS2,NOS3,
78      2INT,ICC,DBPP,I7,XNPP,STDX)
79      WRITE(8,1000)
80      READ(8,-) ICC
81      CALL PLOT1(N1,N2,NO,DL1,DL2,DL3,NOS1,NOS2,NOS3,
82      2INT,ICC,DBTT,I7,XNTT,STDX)
83      WRITE(8,1000)
84      READ(8,-) ICC
85      CALL PLOT1(N1,N2,NO,DL1,DL2,DL3,NOS1,NOS2,NOS3,
86      2INT,ICC,DBTP,I7,XNTP,STDX)
87  1000 FORMAT(5X,'READY TO PLOT?',1,3,2')
88  2000 CONTINUE
89      IZ=IZ*8709
90      IF(IZ) 76,80,80
91  76  CONTINUE
92      IZ=IZ*8388607+1
93  80  CONTINUE
94      CALL EXIT
95      END
96      SUBROUTINE CLDMOD(DL1,DL2,DL3,NOS1,NOS2,NOS3,N1,N2,ND,IDM
97      2,X,Y,Z,CA,CB,CG,XX,YY,ZZ,CCA,CCB,CCG,HK,HL123)
98      DIMENSION X(1),Y(1),Z(1),CA(1),CB(1),CG(1),XX(1),YY(1),ZZ(1)
99      DIMENSION CCA(1),CCB(1),CCG(1),HK(1)
100     DIMENSION NM123(3),IL123(3),IU123(3),OL123(3),HL123(3)
101     TP=2.*3.141592
102     OL123(1)=DL1
103     OL123(2)=DL2
104     OL123(3)=DL3
105     HL123(1)=DL1/NOS1
106     HL123(2)=DL2/NOS2
107     HL123(3)=DL3/NOS3
108     NM123(1)=NOS1-1
109     NM123(2)=NOS2-1
110     NM123(3)=NOS3-1

```

```

111      IL123(1)=1
112      IL123(2)=1+N1
113      IL123(3)=1+N2
114      IU123(1)=N1
115      IU123(2)=N2
116      IU123(3)=ND
117      KK=3
118      TF(ND,LT,3) KK=ND
119      DO 2 K=1, KK
120      IA=IL123(K)
121      IB=IU123(K)
122      DO 1 I=1, IB
123      NM=NM123(K)
124      DO 1 II=1, NM
125      L=II+(I-IA)*NM
126      IF(K.GT.1) L=L+IR
127      XX(L)=X(1)-(DL123(K)*0.5-FLOAT(II)*HL123(K))*TP*CA(I)
128      YY(L)=Y(1)-(DL123(K)*0.5-FLOAT(II)*HL123(K))*TP*CB(I)
129      ZZ(L)=Z(1)-(DL123(K)*0.5-FLOAT(II)*HL123(K))*TP*CG(I)
130      CCA(L)=CA(I)
131      CCB(L)=CB(I)
132      CCG(L)=CG(I)
133      HK(L)=HL123(K)*TP
134      1 CONTINUE
135      IR=L
136      2 CONTINUE
137      RETURN
138      END
139      SUBROUTINE CLDGED(N,STDX ,STDY ,STDZ ,IZ,X,Y,Z,CA,CB,CG)
140      DIMENSION X(1),Y(1),Z(1),CA(1),CB(1),CG(1)
141      DATA PI/3.141592/
142      TP=2.*PI
143      IX=IZ
144      STDXK=STDX*IP
145      STDYK=STDY*TP
146      STDZK=STDZ*IP
147      DO 30 I=1,N
148      CALL GAUSS(IX,STDXK,0.0,X(I))
149      CALL GAUSS(IX,STDYK,0.0,Y(I))
150      CALL GAUSS(IX,STDZK,0.0,Z(I))
151      CALL RANDU(IX,IY,A1)
152      IX=IY
153      PHI=TP*A1
154      CALL RANDU(IX,IY,A2)
155      IX=IY
156      COSTH=2.*A2-1.0
157      SINTH=SQRT(1.-COSTH*COSTH)
158      CA(I)=SINTH*COS(PHI)
159      CB(I)=SINTH*SIN(PHI)
160      CG(I)=COSTH
161      30 CONTINUE
162      RETURN
163      END
164      SUBROUTINE GAUSS(IX,S,AM,V)
165      A=0.0

```



```

166      DO 50 I=1,12
167      CALL RANDU(IX,IY,Y)
168      IX=IY
169      50 A=A+Y
170      V=(A-6.0)*S+AM
171      RETURN
172      END
173      SUBROUTINE RANDU(IX,IY,YFL)
174      IY=IX*16645
175      IF(IY)5,6,6
176      5 IY=IY+8388607+1
177      6 YFL=IY
178      YFL=YFL*.1192093E-6
179      RETURN
180      END
181      SUBROUTINE ZIJ(N,XX,YY,ZZ,CCA,CCB,CCG,HK,HL123,AL,INT,
182      1 IDUM,MODE1,MODE2,C,IDN)
183      COMPLEX CAA,CBB,CCC
184      COMPLEX P11,P12,P21,P22,ZMN,CIJ,C(1)
185      DIMENSION XX(1),YY(1),ZZ(1),CCA(1),CCB(1),CCG(1),HK(1)
186      DIMENSION HL123(3)
187      DATA PI/3.141592/
188      TP=2.*PI
189      AK=AL*TP
190      CAA=ZMN(AL,HL123(1),0,0)
191      CBB=ZMN(AL,HL123(2),0,0)
192      CCC=ZMN(AL,HL123(3),0,0)
193      DO 40 I=1,N
194      II=(I-1)*N-(I*I-I)/2+1
195      IF(I.LE.MODE1) C(II)=CAA
196      IF(I.GT.MODE1.AND.I.LE.(MODE1+MODE2)) C(II)=CBB
197      IF(I.GT.(MODE1+MODE2)) C(II)=CCC
198      40 CONTINUE
199      N1=N-1
200      IF(N1.LT.1) N1=1
201      DO 45 I=1,N1
202      DS=HK(I)
203      COS=COS(DS)
204      SCS=SIN(DS)
205      X1=XX(I)-DS*CCA(I)
206      Y1=YY(I)-DS*CCB(I)
207      Z1=ZZ(I)-DS*CCG(I)
208      X2=XX(I)
209      Y2=YY(I)
210      Z2=ZZ(I)
211      X3=XX(I)+DS*CCA(I)
212      Y3=YY(I)+DS*CCB(I)
213      Z3=ZZ(I)+DS*CCG(I)
214      ID=(I-1)*N-(I*I-I)/2
215      IP=I+1
216      IF(IP.GT.N) RETURN
217      DO 45 J=IP,N
218      DT=HK(J)
219      SOT=SIN(DT)
220      IJ=ID+J

```

```

221      XA=XX(J)-DT*CCA(J)
222      YA=YY(J)-DT*CCB(J)
223      ZA=ZZ(J)-DT*CCG(J)
224      XB=XX(J)
225      YB=YY(J)
226      ZB=ZZ(J)
227      XC=XX(J)+DT*CCA(J)
228      YC=YY(J)+DT*CCB(J)
229      ZC=ZZ(J)+DT*CCG(J)
230      CIJ=(0.0,0.0)
231      CALL ZGS(X1,Y1,Z1,X2,Y2,Z2,XA,YA,ZA,XB,YB,ZB,
232      1AK,DS,CUS,SDS,DT,SDI,INT,P11,P12,P21,P22)
233      CIJ=CIJ+P22
234      CALL ZGS(X1,Y1,Z1,X2,Y2,Z2,XB,YB,ZB,XC,YC,ZC,
235      1AK,DS,CUS,SDS,DT,SDI,INT,P11,P12,P21,P22)
236      CIJ=CIJ+P21
237      CALL ZGS(X2,Y2,Z2,X3,Y3,Z3,XA,YA,ZA,XB,YB,ZB,
238      1AK,DS,CUS,SDS,DT,SDI,INT,P11,P12,P21,P22)
239      CIJ=CIJ+P12
240      CALL ZGS(X2,Y2,Z2,X3,Y3,Z3,XB,YB,ZB,XC,YC,ZC,
241      1AK,DS,CUS,SDS,DT,SDI,INT,P11,P12,P21,P22)
242      C(IJ)=CIJ+P11
243      45 CONTINUE
244      RETURN
245      END
246      SUBROUTINE ZFFD(X,Y,Z,CA,CB,CG,CTH,STH,CPH,SPH,
247      2SDK,CDK,HK,FT,EP)
248      COMPLEX ET,FP,EJB,ES
249      G=(CA*CPH+CB*SPH)*STH+CG*CTH
250      GK=1.-G*G
251      ET=(0.0,0.0)
252      EP=(0.0,0.0)
253      IF(GK.LT.0.001) GO TO 200
254      H=(X*CPH+Y*SPH)*STH+Z*CTH
255      EJB=CMPLX(COS(H),SIN(H))
256      FS=(0.0,60.0)*EJB*(CDK-COS(G*HK))/GK/SDK
257      T=(CA*CPH+CB*SPH)*CTH-CG*STH
258      P=-CA*SPH+CB*CPH
259      ET=T*ES
260      FP=P*ES
261      200 CONTINUE
262      RETURN
263      END
264      SUBROUTINE BKCD(CPH,SPH,CTH,ECTT,ECTP,ECPP,
265      2X,Y,Z,CA,CB,CG,HK,N,IDM,C,ETT,EPP,S,IDN)
266      DIMENSION X(1),Y(1),Z(1),CA(1),CB(1),CG(1),HK(1)
267      COMPLEX C(1),ETT(1),EPP(1),S(1),ETH,EPH
268      DATA PI/3.141592/
269      TP=2.*PI
270      STH=SQRT(1.-CTH*CTH)
271      DO 70 I=1,N
272      SDK=SIN(HK(I))
273      CDK=COS(HK(I))
274      CALL ZFFD(X(I),Y(I),Z(I),CA(I),CB(I),CG(I),CTH,STH,CPH,SPH,
275      2SDK,CDK,HK(I),ETT(I),EPP(I))

```

```

276      S(I)=ETT(I)*(0.0,1.0)/TP/30.0
277  70 CONTINUE
278      CALL SQROT2(C,S,N,10M,10N)
279      ETH=(0.0,0.0)
280      EPH=(0.0,0.0)
281      DO 80 I=1,N
282          ETH=ETH+S(I)*ETT(I)
283          EPH=EPH+S(I)*EPP(I)
284  80 CONTINUE
285      CETH=CABS(ETH)
286      CEPH=CABS(EPH)
287      ECTT=2.0*TP*CETH*CETH
288      ECTP=2.0*TP*CEPH*CEPH
289      DO 90 I=1,N
290          S(I)=EPP(I)*(0.0,1.0)/TP/30.0
291  90 CONTINUE
292      CALL SQROT2(C,S,N,10M,10N)
293      EPH=(0.0,0.0)
294      DO 100 I=1,N
295          EPH=EPH+S(I)*EPP(I)
296  100 CONTINUE
297      CEPH=CABS(EPH)
298      ECPP=2.0*TP*CEPH*CEPH
299      RETURN
300      END
301      SUBROUTINE PLOT1(NA,NB,NC,DL1,DL2,DL3,NOS1,NOS2,NOS3,
302  2INT,ICASE,F,IX,XNORM,STDY)
303          DIMENSION LX(9)
304          DIMENSION IBUF(100),L1(4),L2(5),L3(6),LD(1),LINT(2),
305  2LNOS(2),LN(7),LPHI(5),LL(2),LLAMDA(3),F(360),X(360)
306          DATA L1,L2,L3/12H PHI-PHI RCS,15H THETA-PHI RCS,
307  218H THETA-THETA RCS/
308          DATA LLAMDA,LINT,LNOS/9H LAMDA, 6H INT=,6H NOS=/
309          DATA LN,LPHI/21H DIPOLE RANDOM CLOUD,,15H PHI(DEGREES)/
310          DATA LI,LD/6H OBSW,3H L=/
311          DATA LX/25H NORM FACTOR= DB/
312          CALL PLOTS(IBUF, 100, 3)
313          CALL PLOT(0.0,0.0,-3)
314          CALL AXIS(0.0,1.5,LPHI,-15,15,0.0,0.0,0.0,24.0,1.25,-1)
315          CALL AXIS(0.0,1.5,LL,+6,6.25,90.0,-40.0,8.0,1.25,-1)
316          CALL PLOT(0.0,7.75,3)
317          CALL PLOT(15.0,7.75,2)
318          CALL PLOT(15.0,1.5,2)
319          YH=8.25
320          W=0.2
321          CALL NUMBER(0.1,7.50,0.15,FLOAT(IX),0.0,-1)
322          CALL SYMBOL(4.75,7.0,.15,LX,0.0,25)
323          CALL NUMBER(7.00,7.0,.15,XNORM,0.0,+2)
324          SPC=STDY*2.05*(4.*3.141592/(3.*.76*NC))**(1./3.)
325          CALL NUMBER(13.6,7.50,0.15,STDY,0.0,+4)
326          CALL NUMBER(13.6,7.20,0.15,SPC,0.0,+4)
327          CALL NUMBER(0.8,8.55,.15,FLOAT(NA),0.0,-1)
328          CALL NUMBER(0.8,8.25,.15,FLOAT(NB),0.0,-1)
329          CALL NUMBER(0.8,7.95,.15,FLOAT(NC),0.0,-1)
330          CALL SYMBOL(1.50,YH,W,LN,0.0,21)

```

```

331 CALL SYMBOL(5.75,YH,W,LD,0.0,3)
332 CALL NUMBER(6.35,8.55,.15,DL1,0.0,+3)
333 CALL NUMBER(6.35,8.25,.15,DL2,0.0,+3)
334 CALL NUMBER(6.35,7.95,.15,DL3,0.0,+3)
335 CALL SYMBOL(7.20,YH,W,LLAMUA,0.0,9)
336 CALL SYMBOL(8.5,YH,W,LINT,0.0,6)
337 CALL NUMBER(9.78,YH,W,FLOAT(TNT),0.0,-1)
338 CALL SYMBOL(10.4,YH,W,LNOS,0.0,6)
339 CALL NUMBER(11.6,8.55,.15,FLOAT(NOS1),0.0,-1)
340 CALL NUMBER(11.6,8.25,.15,FLOAT(NOS2),0.0,-1)
341 CALL NUMBER(11.6,7.95,.15,FLOAT(NOS3),0.0,-1)
342 IF(ICASE.EQ.1) CALL SYMBOL(11.8,YH,W,L1,0.0,12)
343 IF(ICASE.EQ.2) CALL SYMBOL(11.8,YH,W,L2,0.0,15)
344 IF(ICASE.EQ.3) CALL SYMBOL(11.8,YH,W,L3,0.0,18)
345 CALL PLOT(0.0,1.5,-3)
346 DO 20 I=1,360
347 IF(F(I).LT.-40.) F(I)=-40.
348 20 X(I)=I
349 CALL LINE(X,0.0,24.0,F,-40.,-8.0,360,0.52)
350 CALL PLOT(17.0,-1.5, 999)
351 RETURN
352 END
353 SUBROUTINE SGROT1(C,N,IDN)
354 C*****
355 C*
356 C* PURPOSE
357 C* TO TRANSFORM A SYMMETRIC MATRIX INTO AN AUXILIARY
358 C* MATRIX (IMPLICIT INVERSE)
359 C*
360 C* USAGE
361 C* CALL SGROT1(C,N,IDN)
362 C*
363 C* DESCRIPTION OF PARAMETERS
364 C* C - THE ARRAY CONTAINING THE MATRIX IN COMPRESSED
365 C* FORM ON ENTRY AND ITS AUXILIARY IN COMPRESSED
366 C* FORM ON EXIT
367 C* N - THE NUMBER OF ROWS OR COLUMNS IN THE MATRIX
368 C* IDN - THE DIMENSION OF THE ARRAY C
369 C*
370 C* REMARKS
371 C* THE UPPER TRIANGLE OF THE MATRIX IS STORED BY ROWS IN THE
372 C* ARRAY C. ONE DIMENSIONAL SUBSCRIPTS ARE RELATED TO
373 C* CORRESPONDING TWO DIMENSIONAL SUBSCRIPTS BY
374 C*  $IJ=(I-1)*N-(I*I-I)/2+J$ 
375 C* WHERE IJ IS THE ONE DIMENSIONAL SUBSCRIPT AND I AND J
376 C* ARE THE TWO DIMENSIONAL SUBSCRIPTS
377 C*
378 C* METHOD
379 C* "SQUARE ROOT" METHOD FOR SOLUTION OF A SYMMETRIC MATRIX
380 C* EQUATION. THE ORIGINAL SYMMETRIC MATRIX M AND THE UPPER
381 C* TRIANGULAR AUXILIARY MATRIX A ARE RELATED BY
382 C*  $M=TRANSPOSE(A)*A$ 
383 C*
384 C* REFERENCES
385 C* FADDEEV, D. K. AND FADDEEVA, V. N., COMPUTATIONAL

```

388 C\*  
 389 C\*\*\*\*\*

```

390     COMPLEX C(IDN)
391     C(1)=CSQRT(C(1))
392     DO 1 K=2,N
393     1 C(K)=C(K)/C(1)
394     DO 2 I=2,N
395     IPO=I-1
396     IPO=I+1
397     ID=(I-1)*N-(I*I-1)/2
398     II=ID+I
399     DO 3 L=1,IMU
400     LI=(L-1)*N-(L*L-L)/2+I
401     3 C(LI)=C(LI)-C(LI)*C(LI)
402     C(LI)=CSQRT(C(LI))
403     IF(IPO.GT.N)GO TO 2
404     DO 5 J=IPO,N
405     IU=ID+J
406     DO 6 M=1,IMO
407     MU=(M-1)*N-(M*M-M)/2
408     MI=MD+I
409     MJ=MD+J
410     6 C(IU)=C(IU)-C(MJ)*C(MI)
411     5 C(IU)=C(IU)/C(LI)
412     2 CONTINUE
413     RETURN
414     END
415     SUBROUTINE SQROT2(C,S,N>IDM>IDN)

```

416 C\*\*\*\*\*

417 C\*  
 418 C\* PURPOSE  
 419 C\* TO OBTAIN A SOLUTION TO THE SYMMETRIC MATRIX EQUATION  
 420 C\* MX=Y USING THE AUXILIARY OF M CALCULATED BY SQROT1

421 C\*  
 422 C\* USAGE  
 423 C\* CALL SQROT2(C,S,N>IDM>IDN)

424 C\*  
 425 C\* DESCRIPTION OF PARAMETERS  
 426 C\* C - AN ARRAY CONTAINING THE UPPER TRIANGULAR  
 427 C\* AUXILIARY MATRIX IN COMPRESSED FORM  
 428 C\* S - AN ARRAY CONTAINING THE RIGHT HAND SIDE VECTOR  
 429 C\* OF THE EQUATION ON ENTRY AND THE SOLUTION  
 430 C\* VECTOR ON EXIT  
 431 C\* N - THE NUMBER OF SIMULTANEOUS EQUATIONS  
 432 C\* IDM - THE DIMENSION OF THE ARRAY S  
 433 C\* IDN - THE DIMENSION OF THE ARRAY C

434 C\*  
 435 C\* REMARKS  
 436 C\* THE UPPER TRIANGLE OF THE AUXILIARY MATRIX IS STORED BY  
 437 C\* ROWS IN THE ARRAY C. ONE DIMENSIONAL SUBSCRIPTS ARE  
 438 C\* RELATED TO CORRESPONDING TWO DIMENSIONAL SUBSCRIPTS BY  
 439 C\*  $IJ=(I-1)*N-(I*I-I)/2+J$   
 440 C\* WHERE IJ IS THE ONE DIMENSIONAL SUBSCRIPT AND I AND J

```

441 C* ARE THE TWO DIMENSIONAL SUBSCRIPTS
442 C*
443 C* SQROT1 MUST BE CALLED BEFORE THE FIRST ENTRY TO SQROT2
444 C*
445 C* METHOD
446 C* "SQUARE ROOT" METHOD FOR SOLUTION OF A SYMMETRIC MATRIX
447 C* EQUATION. THE ORIGINAL SYMMETRIC MATRIX M AND THE UPPER
448 C* TRIANGULAR AUXILIARY MATRIX A ARE RELATED BY
449 C* M=TRANPOSE(A)*A
450 C*
451 C* REFERENCES
452 C* FADDEEV, D. K. AND FADDEEVA, V. N., COMPUTATIONAL
453 C* METHODS OF LINEAR ALGEBRA, W. H. FREEMAN AND CO., SAN
454 C* FRANCISCO, 1963, P. 144-147
455 C*
456 C*** *****
457 COMPLEX S(10N),C(10N)
458 S(1)=S(1)/C(1)
459 DO 10 I=2,N
460 IM0=I-1
461 DO 11 L=1,IM0
462 LI=(L-1)*N-(L+L-L)/2+I
463 1) S(I)=S(I)-C(LI)*S(L)
464 LI=(I-1)*N-(I+I-I)/2+I
465 1) S(I)=S(I)/C(I)
466 NN=((N+1)*I)/2
467 S(N)=S(N)/C(NN)
468 NN0=N-1
469 DO 25 I=1,NN0
470 KK=N-I
471 KK0=K+1
472 KU=(K-1)*N-(K*K-K)/2
473 DO 26 L=KK0,N
474 KL=K0+L
475 2) S(K)=S(K)-C(KL)*S(L)
476 KK=KK+K
477 S(K)=S(K)/C(KK)
478 2) CONTINUE
479 RETURN
480 END
481 SUBROUTINE SICI(SI,CI,X)
482 C*** *****
483 C*
484 C* PURPOSE
485 C* COMPUTES THE SINE AND COSINE INTEGRALS
486 C*
487 C* USAGE
488 C* CALL SICI(SI,CI,X)
489 C*
490 C* DESCRIPTION OF PARAMETERS
491 C* SI - THE RESULTANT VALUE SI(X)
492 C* CI - THE RESULTANT VALUE CI(X)
493 C* X - THE ARGUMENT OF SI(X) AND CI(X)
494 C*
495 C* REMARKS

```

```

SICI000
SICI001
* SICI002
* SICI003
* SICI004
* SICI005
* SICI006
* SICI007
* SICI008
* SICI009
* SICI010
* SICI011
* SICI012
* SICI013
* SICI014

```



```

496 C*      THE ARGUMENT VALUE REMAINS UNCHANGED
497 C*
498 C*      SUBROUTINES AND FUNCTION SUBPROGRAMS REQUIRED
499 C*      NONE
500 C*
501 C*      METHOD
502 C*      DEFINITION
503 C*      SI(X)=INTEGRAL(SIN(T)/T)
504 C*      CI(X)=INTEGRAL(COS(T)/T)
505 C*      EVALUATION
506 C*      REDUCTION OF RANGE USING SYMMETRY
507 C*      DIFFERENT APPROXIMATIONS ARE USED FOR ABS(X) GREATER
508 C*      THAN 4 AND FOR ABS(X) LESS THAN 4.
509 C*
510 C*      REFERENCES
511 C*      IBM SCIENTIFIC SUBROUTINE PACKAGE P. 370
512 C*      LUKE AND WIMP, "POLYNOMIAL APPROXIMATIONS TO INTEGRAL
513 C*      TRANSFORMS", MATHEMATICAL TABLES AND OTHER AIDS TO
514 C*      COMPUTATION, VOL. 15, 1961, ISSUE 74, P. 174-178
515 C*
516 C* *****
517       Z=ABS(X)
518       IF(Z-4.0)1,1,4
519       ) Y=(4-Z-2)*(4.0+Z)
520       S1=-1.670797E0
521       IF(Z)3,2,3
522       ) C1=-1.0E00
523       RETURN
524       3 SI=X*(((((1.753141E-9*Y+1.568988E-7)*Y+1.374168E-5)*Y+6.939689E-4)
525       2*Y+1.964882E-2)*Y+4.595509E-1+SI/Y)
526       C1=((15.77213E-1+LOG(Z))/Z-7*(((((1.580985E-10*Y+1.584956E-8)*Y
527       2+1.725754E-6)*Y+1.185999E-4)*Y+4.590920E-3)*Y+1.515308E-1))*Z
528       RETURN
529       4 S1=SIN(Z)
530       Y=COS(Z)
531       Z=4.0/Z
532       U=(((((1.440069E-3*Z-2.270143E-2)*Z+5.515070E-2)*Z-7.261642E-2)
533       2+Z+4.907716E-2)*Z-3.532519E-3)*Z-2.314617E-2)*Z-1.134950E-5)*Z
534       3+0.250011E-2)*Z+2.500909E-10
535       V=(((((1.510869E-3*Z+2.819175E-2)*Z-6.537285E-2)*Z
536       2+7.902034E-2)*Z-4.000416E-2)*Z-7.945556E-3)*Z+2.661293E-2)*Z
537       3-3.764000E-4)*Z-6.122410E-2)*Z-6.646441E-7)*Z+2.500000E-1
538       C1=Z*(S1*V-Y*U)
539       S1=-Z*(S1*U+Y*V)
540       IF(X)5,6,6
541       5 S1=-3.141593E0-S1
542       6 RETURN
543       END
544       SUBROUTINE ZGS(XA,YA,ZA,XB,YB,ZB,X1,Y1,Z1,X2,Y2,Z2,AK,
545       2ES,CDS,SUB,DT,SUI,IMI,P11,P12,P21,P22)
546       COMPLEX CBT,EJ1,EJ2,EJA,EJB,FR1,FR2,EI1,ET2,P11,P12,P21,P22,GAM
547       COMPLEX SGUS,SGOT
548       DATA ETA,GAP,PT/576.727,(.0,1.),3.14159/
549       CA=(X2-X1)/DT
550       CB=(Y2-Y1)/DT

```

```

* SICI015
* SICI016
* SICI017
* SICI018
* SICI019
* SICI020
* SICI021
* SICI022
* SICI023
* SICI024
* SICI025
* SICI026
* SICI027
* SICI028
* SICI029
* SICI030
* SICI031
* SICI032
* SICI033
* SICI034
* SICI035
* SICI036
* SICI037
* SICI038
* SICI039
* SICI040
* SICI041
* SICI042
* SICI043
* SICI044
* SICI045
* SICI046
* SICI047
* SICI048
* SICI049
* SICI050
* SICI051
* SICI052
* SICI053
* SICI054
* SICI055
* SICI056
* SICI057
* SICI058
* SICI059
* SICI060
* SICI061
* SICI062

```

```

551      CG=(Z2-Z1)/DT
552      CAS=(XB-XA)/DS
553      CBS=(YB-YA)/DS
554      CGS=(ZB-ZA)/DS
555      CC=CA*CAS+CB*CBS+CG*CGS
556      IF (ABS(CC).GT.0.997) GO TO 200
557      SZ=(X1-XA)*CAS+(Y1-YA)*CBS+(Z1-ZA)*CGS
558      IF (INT.EQ.0) GO TO 300
559      CGDS=CDS
560      SGDS=CMPLX(.0,SDS)
561      SGBT=CMPLX(.0,SDT)
562      INS=2*(INT/2)
563      IF (INS.LT.2) INS=2
564      IP=INS+1
565      DELT=DT/INS
566      T=.0
567      DSZ=CC*DELT
568      P11=(.0,.0)
569      P12=(.0,.0)
570      P21=(.0,.0)
571      P22=(.0,.0)
572      AKS=AK*AK
573      SGN=-1.
574      DO 100 IN=1,IP
575      ZZ1=SZ
576      ZZ2=SZ-DS
577      XXZ=X1+T*CA-XA-SZ*CAS
578      YYZ=Y1+T*CB-YA-SZ*CBS
579      ZZZ=Z1+T*CG-ZA-SZ*CGS
580      RS=XXZ**2+YYZ**2+ZZZ**2
581      R1=SQRT(RS+ZZ1**2)
582      EJA=CMPLX(COS(R1),-SIN(R1))
583      EJ1=EJA/R1
584      R2=SQRT(RS+ZZ2**2)
585      EJB=CMPLX(COS(R2),-SIN(R2))
586      EJ2=EJB/R2
587      ER1=EJA*SGDS+ZZ1*EJ1*CGDS-ZZ2*EJ2
588      ER2=-EJB*SGDS+ZZ2*EJ2*CGDS-ZZ1*EJ1
589      FAC=.0
590      IF (RS.GT.AKS) FAC=(CA*XXZ+CB*YYZ+CG*ZZZ)/RS
591      ET1=CC*(EJ2-EJ1*CGDS)+FAC*ER1
592      ET2=CC*(EJ1-EJ2*CGDS)+FAC*ER2
593      C=3.+SGN
594      IF (IN.EQ.1 .OR. IN.EQ.IP) C=1.
595      C1=C*SIN(UT-T)
596      C2=C*SIN(T)
597      P11=P11+ET1*C1
598      P12=P12+ET1*C2
599      P21=P21+ET2*C1
600      P22=P22+ET2*C2
601      T=T+DELT
602      SZ=SZ+DSZ
603      100 SGN=-SGN
604      CST=-(.0+1.)*ETA*DELT/(12.*PI*SGDS*SGDT)
605      P11=CST*P11

```

```

606 P12=CST*P12
607 P21=CST*P21
608 P22=CST*P22
609 RETURN
610 200 S21=(X1-XA)*CAS+(Y1-YA)*CBS+(Z1-ZA)*CGS
611 RH1=SQRT((X1-XA-SZ1*CAS)**2+(Y1-YA-SZ1*CBS)**2+(Z1-ZA-SZ1*CGS)**2)
612 SZ2=SZ1+DT*CC
613 RH2=SQRT((X2-XA-SZ2*CAS)**2+(Y2-YA-SZ2*CBS)**2+(Z2-ZA-SZ2*CGS)**2)
614 DDK=(RH1+RH2)/2.
615 IF(DDK.LT.AK)DDK=AK
616 CALL ZGMM(.0,DS,SZ1,SZ2,DDK,CDS,SDS,SDT,1.,P11,P12,P21,P22)
617 RETURN
618 300 SS=SQRT(1.-CC*CC)
619 CAD=(CGS*CB-CBS*CG)/SS
620 CBD=(CAS*CG-CGS*CA)/SS
621 CGD=(CBS*CA-CAS*CB)/SS
622 DK=(X1-XA)*CAD+(Y1-YA)*CBD+(Z1-ZA)*CGD
623 DK=ABS(DK)
624 IF(DK.LT.AK)DK=AK
625 XZ=XA+SZ*CAS
626 YZ=YA+SZ*CBS
627 ZZ=ZA+SZ*CGS
628 XP1=X1-DK*CAD
629 YP1=Y1-DK*CBD
630 ZP1=Z1-DK*CGD
631 CAP=CBS*CGD-CGS*CBD
632 CBP=CGS*CAD-CAS*CGD
633 C6P=CAS*CBU-CBS*CAD
634 P1=CAP*(XP1-XZ)+CBP*(YP1-YZ)+C6P*(ZP1-Z7)
635 T1=P1/SS
636 S1=T1*CC-SZ
637 CALL ZGMM(S1,S1+DS,T1,T1+DT,DK,CDS,SDS,SDT,CC,P11,P12,P21,P22)
638 RETURN
639 END
640 SUBROUTINE ZGMM(S1,S2,T1,T2,D,CGDS,SGD1,SGD2,CPSI,P11,P12,P21,P22)
641 COMPLEX E(2,2),F(2,2),GAM,P11,P12,P21,P22
642 COMPLEX EB,EC,EK,FL,EKL,EGZ1,ES1,ES2,ET1,ET2,EXPA,EXPB
643 COMPLEX EGZ(2,2),GM(2),GP(2)
644 COMPLEX EXA(2),EXB(2)
645 DATA ETA,GAM,PI/376.727,(.0,1.),3.14159/
646 DSQ=D*D
647 SGDS=SGD1
648 IF(S2.LT.S1)SGDS=-SGD1
649 SGDT=SGD2
650 IF(T2.LT.T1)SGDT=-SGD2
651 IF(ABS(CPSI).GT.0.997)GO TO 110
652 ES1=CEXP(GAM*S1)
653 ES2=CEXP(GAM*S2)
654 ET1=CEXP(GAM*T1)
655 ET2=CEXP(GAM*T2)
656 C=0/SQRT(1.-CPSI*CPSI)
657 P=C*CPSI
658 EB=CEXP(GAM*CMPLX(.0,B))
659 EC=CEXP(GAM*CMPLX(.0,C))
660 DO 10 K=1,2

```

```

661      DO 10 L=1,2
662 10    F(K,L)=(.0,.0)
663      EK=EB
664      DO 50 K=1,2
665      FK=(-1)**K
666      EL=EC
667      DO 40 L=1,2
668      FL=(-1)**L
669      EKL=EK*EL
670      XX=FK*R+FL*C
671      S1=S1
672      DO 30 I=1,2
673      R1=SQRT(DSQ+S1*S1+T1*T1-2.*S1*T1*CPSI)
674      P2=SQRT(DSQ+S1*S1+T2*T2-2.*S1*T2*CPSI)
675      CALL EXPJ(GAM*CMPLX(R1+FK*S1+FL*T1,-XX),
676 2        GAM*CMPLX(R2+FK*S1+FL*T2,-XX),EXA(I))
677      CALL EXPJ(GAM*CMPLX(R1+FK*S1+FL*T1,XX),
678 2        GAM*CMPLX(R2+FK*S1+FL*T2,XX),EXB(I))
679      IF(K.EQ.2 .OR. L.EQ.2)GO TO 30
680      ZC=S1*CPSI
681      EGZI=CEXP(GAM*ZC)
682      CALL EXPJ(GAM*(R1+ZC-T1),GAM*(R2+ZC-T2),EXPB)
683      CALL EXPJ(GAM*(R1-ZC+T1),GAM*(R2-ZC+T2),EXPA)
684      F(I,1)=2.*SGDS*(.0,1.)*EXPA/EGZI
685      F(I,2)=2.*SGDS*(.0,1.)*EXPB*EGZI
686 30    S1=S2
687      F(K,L)=F(K,L)+(EXA(2)-EXA(1))*EKL+(EXB(2)-EXB(1))/EKL
688 40    EL=1./EC
689 50    FK=1./EB
690      CST=-ETA/(16.*PI*SGDS*SGDT)
691      P11=CST*(( F(1,1)+E(2,2)*ES2-E(1,2)/ES2)*ET2
692 A      +(-F(1,2)-E(2,1)*ES2+E(1,1)/ES2)/ET2)
693      P12=CST*((-F(1,1)-E(2,2)*ES2+E(1,2)/ES2)*ET1
694 B      +( F(1,2)+E(2,1)*ES2-E(1,1)/ES2)/ET1)
695      P21=CST*((-F(2,1)-E(2,2)*ES1+E(1,2)/ES1)*ET2
696 C      +( F(2,2)+E(2,1)*ES1-E(1,1)/ES1)/ET2)
697      P22=CST*(( F(2,1)+E(2,2)*ES1-E(1,2)/ES1)*ET1
698 D      +(-F(2,2)-E(2,1)*ES1+E(1,1)/ES1)/ET1)
699      RETURN
700 110 IF(CPSI.LT.0.)GO TO 120
701      TA=T1
702      TB=T2
703      GO TO 130
704 120 TA=-T1
705      TB=-T2
706      SGDT=-SGDT
707 130 S1=S1
708      DO 150 I=1,2
709      TJ=TA
710      DO 140 J=1,2
711      ZIJ=TJ-S1
712      R=SQRT(DSQ+ZIJ*ZIJ)
713      W=R+ZIJ
714      IF(ZIJ.LT.0.)W=DSQ/(R-ZIJ)
715      V=R-ZIJ

```

```

716      IF (ZIJ.GT.0.)V=DSQ/(R+ZIJ)
717      IF (J.EQ.1)V1=V
718      IF (J.EQ.1)W1=W
719      FGZ(I,J)=CEXP(GAM*ZIJ)
720 140 TJ=TB
721      CALL EXPJ(GAM*V1,GAM*V,GP(I))
722      CALL EXPJ(GAM*W1,GAM*W,GM(1))
723 150 S1=S2
724      CST=ETA/(8.*PI*SGDS*SGDT)
725      P11=CST*(GM(2)*EGZ(2,2)+GP(2)/EGZ(2,2)
726      2-CGDS*(GM(1)*EGZ(1,2)+GP(1)/EGZ(1,2)))
727      P12=CST*(-GM(2)*EGZ(2,1)-GP(2)/EGZ(2,1)
728      2+CGDS*(GM(1)*EGZ(1,1)+GP(1)/EGZ(1,1)))
729      P21=CST*(GM(1)*EGZ(1,2)+GP(1)/EGZ(1,2)
730      2-CGDS*(GM(2)*EGZ(2,2)+GP(2)/EGZ(2,2)))
731      P22=CST*(-GM(1)*EGZ(1,1)-GP(1)/EGZ(1,1)
732      2+CGDS*(GM(2)*EGZ(2,1)+GP(2)/EGZ(2,1)))
733      RETURN
734      END
735      SUBROUTINE EXPJ(V1,V2,W12)
736      COMPLEX EC,E15,S,T,UC,VC,V1,V2,W12,Z
737      DIMENSION V(21),W(21),D(16),E(16)
738      DATA V/ 0.22284667E 00,
739      20.11889321E 01,0.29927363E 01,0.57751436E 01,0.98374674E 01,
740      20.15982874E 02,0.93307812E-01,0.49269174E 00,0.12155954E 01,
741      20.22699495E 01,0.36676227E 01,0.54253366E 01,0.75659162E 01,
742      20.10120228E 02,0.13130282E 02,0.16654408E 02,0.20776479E 02,
743      20.25623894E 02,0.31407519E 02,0.38530683E 02,0.48026086E 02/
744      DATA W/ 0.45896460E 00,
745      20.41700083E 00,0.11337338E 00,0.10399197E-01,0.26101720E-03,
746      20.89854791E-06,0.21823487E 00,0.34221017E 00,0.26302758E 00,
747      20.12642582E 00,0.40206865E-01,0.85638778E-02,0.12124361E-02,
748      20.11167440E-03,0.64599267E-05,0.22263169E-06,0.42274304E-08,
749      20.39218973E-10,0.14565152E-12,0.14830270E-15,0.16005949E-19/
750      DATA U/ 0.22495942E 02,
751      2 0.74411568E 02,-0.41431576E 03,-0.78754339E 02, 0.11254744E 02,
752      2 0.16021761E 03,-0.23862195E 03,-0.50094687E 03,-0.68487854E 02,
753      2 0.12254778E 02,-0.10161976E 02,-0.47219591E 01, 0.79729681E 01,
754      2-0.21069574E 02, 0.22046490E 01, 0.89728244E 01/
755      DATA E/ 0.21103107E 02,
756      2-0.37959787E 03,-0.97489220E 02, 0.12900672E 03, 0.17949226E 02,
757      2-0.12910931E 03,-0.55705574E 03, 0.13524801E 02, 0.14696721E 03,
758      2 0.17949528E 02,-0.32981014E 00, 0.31028936E 02, 0.81657657E 01,
759      2 0.22236961E 02, 0.39124892E 02, 0.81636799E 01/
760      Z=V1
761      DO 100 JIM=1,2
762      X=REAL(Z)
763      Y=AIMAG(Z)
764      E15=(.0,.0)
765      AB=CABS(Z)
766      IF (AB.EQ.0.)GO TO 90
767      IF (X.GE.0. .AND. AB.GT.10.)GO TO 80
768      YA=ABS(Y)
769      IF (X.LE.0. .AND. YA.GT.10.)GO TO 80
770      IF (YA-X.GE.17.5.OR.YA.GE.6.5.OR.X+YA.GE.5.5.OR.X.GE.3.)GO TO 20

```

```

771      IF(X.LE.-9.)GO TO 40 /
772      IF(YA-X.GE.2.5)GO TO 50
773      IF(X+YA.GE.1.5)GO TO 30
774      10  N=6.+3.*AB
775          E15=1./(N-1.)-Z/N**2
776      15  N=N-1
777          E15=1./(N-1.)-Z*E15/N
778      IF(N.GE.3)GO TO 15
779      E15=Z*E15-CMPLX(.577216+ALOG(AB),ATAN2(Y,X))
780      GO TO 90
781      20  J1=1
782          J2=6
783          GO TO 31
784      30  J1=7
785          J2=21
786      31  S=(.0,.0)
787          YS=Y*Y
788          DO 32 I=J1,J2
789              XI=V(I)+X
790              CF=W(I)/(XI*XJ+YS)
791      32  S=S+CMPLX(XI*CF,-YA*CF)
792          GO TO 54
793      40  T3=X*X-Y*Y
794          T4=2.*X*YA
795          T5=X*T3-YA*T4
796          T6=X*T4+YA*T3
797          UC=CMPLX(D(11)+D(12)*X+D(13)*T3+T5-E(12)*YA-E(13)*T4,
798      2      E(11)+E(12)*X+E(13)*T3+T6+D(12)*YA+D(13)*T4)
799          VC=CMPLX(D(14)+D(15)*X+D(16)*T3+T5-E(15)*YA-E(16)*T4,
800      2      E(14)+E(15)*X+E(16)*T3+T6+D(15)*YA+D(16)*T4)
801          GO TO 52
802      50  T3=X*X-Y*Y
803          T4=2.*X*YA
804          T5=X*T3-YA*T4
805          T6=X*T4+YA*T3
806          T7=X*T5-YA*T6
807          T8=X*T6+YA*T5
808          T9=X*T7-YA*T8
809          T10=X*T8+YA*T7
810          UC=CMPLX(D(1)+D(2)*X+D(3)*T3+D(4)*T5+D(5)*T7+T9-(E(2)*YA+E(3)*T4
811      2+E(4)*T6+E(5)*T8),E(1)+E(2)*X+E(3)*T3+E(4)*T5+E(5)*T7+T10+
812      3(D(2)*YA+D(3)*T4+D(4)*T6+D(5)*T8))
813          VC=CMPLX(D(6)+D(7)*X+D(8)*T3+D(9)*T5+D(10)*T7+T9-(E(7)*YA+E(8)*T4
814      2+E(9)*T6+E(10)*T8),E(6)+E(7)*X+E(8)*T3+E(9)*T5+E(10)*T7+T10+
815      3(D(7)*YA+D(8)*T4+D(9)*T6+D(10)*T8))
816      52  EC=UC/VC
817          S=EC/CMPLX(X,YA)
818      54  EX=EXP(-X)
819          T=EX*CMPLX(COS(YA),-SIN(YA))
820          E15=S*T
821      56  IF(Y.LT.0.)E15=CONJG(E15)
822          GO TO 90
823      80  E15=.409319/(Z+.193044)+.421831/(Z+1.02666)+.147126/(Z+2.56788)+
824      2.206335E-1/(Z+.90035)+.107401E-2/(Z+8.18215)+.158654E-4/(Z+
825      312.7342)+.317031E-7/(Z+19.3957)

```



826	E15=E15*CLX*(-7)	
827	90 IF (JIM.E.G.1)W12=F15	
828	100 Z=V2	
829	Z=V2/V1	
830	TH=ATAN2(A1*AG(Z),REAL(Z))-ATAN2(A1*AG(V2),REAL(V2))	
831	Z=ATAN2(A1*AG(V1),REAL(V1))	
832	AG=ABS(TH)	
833	IF (AG.LT.1.)TH=.0	
834	IF (TH.GT.1.)TH=6.2831853	
835	IF (TH.LT.-1.)TH=-6.2831853	
836	W12=W12-E15+CMPLX(1.0,TH)	
837	RETURN	
838	END	0150
839	COMPLEX FUNCTION ZMN(DL,PL,SL)	
840	REAL L,LL,LL	ZMN030
841	P=6.2831853	ZMN031
842	P=PL	
843	L=HL	
844	LL=HL	
845	HC=SL	
846	RL=3+LL	ZMN032
847	H=ABS(HC)-L	ZMN033
848	LL=LL	ZMN034
849	HPL=H+LL	ZMN035
850	HP2L=H+2.0*LL	ZMN036
851	HP3L=H+3.0*LL	ZMN037
852	HP4L=H+4.0*LL	ZMN038
853	SBL=SIN(BLE)	ZMN039
854	CBL=COS(BLE)	ZMN040
855	SBL=SIN(B*P)	ZMN041
856	CBL=COS(B*P)	ZMN042
857	S3HML=SIN(B*HML)	ZMN043
858	C3HML=COS(B*HML)	ZMN044
859	S4HPL=SIN(B*HPL)	ZMN045
860	C4HPL=COS(B*HPL)	ZMN046
861	S4HP2L=SIN(B*HP2L)	ZMN047
862	C4HP2L=COS(B*HP2L)	ZMN048
863	S4HP3L=SIN(B*HP3L)	ZMN049
864	C4HP3L=COS(B*HP3L)	ZMN050
865	TEMP=SQRT(L*(1+H*H))+H	ZMN051
866	V1=B*0/D/TEMP	ZMN052
867	U1=B*TEMP	ZMN053
868	TEMP=SQRT(L*(1+HML*HML))+HML	ZMN054
869	U3=B*TEMP	ZMN055
870	V3=B*0/D/TEMP	ZMN056
871	TEMP=SQRT(L*(1+HPL*HPL))+HPL	ZMN057
872	U5=B*TEMP	ZMN058
873	V5=B*0/D/TEMP	ZMN059
874	TEMP=SQRT(L*(1+HP2L*HP2L))+HP2L	ZMN060
875	U2=B*0/D/TEMP	ZMN061
876	V2=B*TEMP	ZMN062
877	TEMP=SQRT(L*(1+HP3L*HP3L))+HP3L	ZMN063
878	U4=B*0/D/TEMP	ZMN064
879	V4=B*TEMP	ZMN065
880	CALL SICI (SI00,CI00,U0)	ZMN066

861	CALL STC1 (SIU1,CIU1,U1)	ZMN101
862	CALL STC1 (SIV2,CIV2,V2)	ZMN102
863	CALL STC1 (SIV4,CIV4,V4)	ZMN103
864	CALL STC1 (SIU3,CIU3,U3)	ZMN104
865	IF (U,LE,0.0) GO TO 20	ZMN105
866	CALL STC1 (SIV1,CIV1,V1)	ZMN076
867	CALL STC1 (SIV0,CIV0,V0)	ZMN079
868	CALL STC1 (SIV3,CIV3,V3)	ZMN081
869	CALL STC1 (SIU2,CIU2,U2)	ZMN082
890	CALL STC1 (SIU0,CIU0,U0)	ZMN084
891	R=15.0*(CBHPL*(CIU0+CIV0-CIU1-CIV1)-SBHPL*(-SIU0+SIV0+SIU1-SIV1)+C	ZMN086
892	2BHPL*(2.*CIV3+2.*CIU3-CIV2-CIU2-CIU1-CIV1)+SBHPL*(-SIV3+SIU3+SIU2-	ZMN087
893	3SIV2-SIU1+SIV1+SIU3-SIV3)+CBHP3L*(-CIU2-CIV2+CIU4+CIV4)+SBHP3L*(SI	ZMN088
894	4U2-SIV2-SIU4+SIV4)+2.*CPL*CPH*(-CIV1-CIU1+CIV3+CIU3)+2.*CBL*SBH*(	ZMN089
895	5SIV1-SIU1-SIV3+SIU3)+2.*CBL*CBHP2L*(CIV4+CIU3-CIU2-CIV2)+2.*CBL*SB	ZMN090
896	6HP2L*(-SIV3+SIU3+SIU2-SIV2))	ZMN091
897	Y=15.0*(CBHPL*(-SIU0-SIV0+SIU1+SIV1)-SBHPL*(-CIU0+CIV0+CIU1-CIV1)+	ZMN092
898	2CBHPL*(-2.*SIV3-2.*SIU3+SIU2+SIV2+SIU1+SIV1)+SBHPL*(-2.*CIV3+2.*C	ZMN093
899	3IU3+CIU2-CIV2-CIU1+CIV1)+CBHP3L*(SIU2+SIV2-SIU4-SIV4)+SBHP3L*(CIU2	ZMN094
900	4-CIV2-CIU4+CIV4)+2.*CBL*CPH*(SIV1+SIU1-SIV3-SIU3)+2.*CBL*CPH*(CIV	ZMN095
901	51-CIU1-CIV3+CIU3)+2.*CBL*CBHP2L*(-SIV3-SIU3+SIU2+SIV2)+2.*CBL*SBHP	ZMN096
902	6PL*(-CIV3+CIU3+CIU2-CIV2))	ZMN097
903	GO TO 10	ZMN098
904	GO CONTINUE	ZMN099
905	R=15.0*(CBHPL*(CIU0-CIU1+ALOG(H/HML))+SBHPL*(SIU0-SIU1)+SBHPL*	ZMN105
906	2(2.*SIU3-SIV2-SIU1)+CBHPL*(2.*CIU3-CIV2-CIU1+ALOG(HP2L/HPL))+	ZMN106
907	3ALOG(H/HPL))+CBHP3L*(CIV4-CIV2+ALOG(HP2L/HP3L))+SBHP3L*(SIV4-SIV2	ZMN107
908	4)+2.*CBL*CPH*(CIU3-CIU1+ALOG(H/HPL))+2.*CPL*SBH*(SIU3-SIU1)+	ZMN108
909	52.*CBL*CBHP2L*(CIU3-CIV2+ALOG(HP2L/HPL))+2.*CBL*SBHP2L*(SIU3-	ZMN109
910	6SIV2))	ZMN110
911	Y=15.0*(CBHPL*(SIU1-SIU0)+SBHPL*(CIU0-CIU1+ALOG(HML/H))+CBHPL*	ZMN111
912	2(SIV2+SIU1-2.*SIU3)+SBHPL*(2.*CIU3-CIV2-CIU1+ALOG(HPL/HP2L))+	ZMN112
913	3ALOG(HPL/H))+CBHP3L*(SIV2-SIV4)+SBHP3L*(CIV4-CIV2+ALOG(HP3L/HP2L)	ZMN113
914	4)+2.*CBL*CPH*(SIU1-SIU3)+2.*CBL*SBH*(CIU3-CIU1+ALOG(HPL/H))+2.*CB	ZMN114
915	5L*CBHP2L*(SIV2-SIU3)+2.*CBL*SBHP2L*(CIU3-CIV2+ALOG(HPL/HP2L)))	ZMN115
916	50. ZMN=CMPLX(R,X)/(SBL*SBL)	Z45116
917	RETURN	ZMN117
918	END	

## APPENDIX E

### SPARSE MATRIX COMPUTER PROGRAM

The advantage of reducing the computer storage requirement can be achieved in solving a sparse matrix equation using high-speed computers if only the non-zero terms are stored. Computation time can also be reduced if only those operations (associated with solution techniques) involving nonzero terms are performed. However, most direct methods of solving systems of linear equations (e.g., square-root, Crout, Gaussian elimination, etc.) operate on the original matrix to produce an auxiliary matrix which in general is not sparse even though the original matrix was sparse.

Sparse matrix techniques require that this new auxiliary matrix be sparse as well. To accomplish this goal, special schemes are used to renumber the original matrix in order to ensure that the number of generated non-zero elements is minimum and to index the stored elements which include not only the original but also the newly-generated non-zero elements. Consequently, the advantages of reducing computer storage and computation time mentioned previously are only relative, since additional time must be devoted to the renumbering part and more storage space has to be allocated for the newly-generated non-zero elements. With these facts in mind, we proceed to describe, in general terms, one sparse-matrix method given by Berry [44].

For efficient utilization of high-speed memory and to allow for practical solution of a very large matrix equation, storage is allocated for only the non-zero elements of the original matrix. These terms are collapsed into two columnar arrays. The diagonal elements are stored by rows in a linear array  $D$  with dimensions  $N$  where  $N$  is the number of linear equations. The off-diagonal, non-zero elements of the upper triangular portion of the matrix are stored by rows in a linear array  $U$  with dimensions less or equal to  $N(N+1)/2$ . An efficient set of pointers for locating these terms in the array  $U$  is an absolute necessity. For a symmetric matrix, only the pointers associated with the upper triangular array of the matrix are retained. Two pointer arrays  $II$  and  $J$  are used to index the array  $U$ . It has dimension equal to  $N$ . The number stored in position  $k$  of this array represents the starting location in the pointer array  $J$  of terms associated with row  $k$  of the original matrix.  $J$  has dimensions equal to  $N(N-1)/2$ . This is a column identifier. The number stored in position  $k$  of this array represents the column index of the element  $U(k)$ . Using the information contained in  $II$  and  $J$ , two additional pointer arrays,  $IUR$  and  $IUC$ , are set up. They record the same information contained in  $II$  and  $J$ , but this time the full matrix is being considered. Note that  $IUR$  has dimension  $N+1$  and  $IUC$  has dimension

less or equal to  $N(N-1)$ . An example should help clarify this scheme. For the original Z matrix given below, the arrays would be as follows:

$$Z = \begin{bmatrix} Z_{11} & 0 & Z_{13} & 0 & Z_{15} \\ 0 & Z_{22} & Z_{23} & Z_{24} & 0 \\ Z_{31} & Z_{32} & Z_{33} & Z_{34} & 0 \\ 0 & Z_{42} & Z_{43} & Z_{44} & 0 \\ Z_{51} & 0 & 0 & 0 & Z_{55} \end{bmatrix}$$

II(1) = 1	J(1) = 3	NUMOFF(1) = 2
II(2) = 3	J(2) = 5	NUMOFF(2) = 2
II(3) = 5	J(3) = 3	NUMOFF(3) = 3
II(4) = 6	J(4) = 4	NUMOFF(4) = 2
II(5) = 6	J(5) = 4	NUMOFF(5) = 1

N=5

Row Locator	Column Identifier	Term Identified
IUR(1)=1	IUC(1)=3	$Z_{13}$
IUR(2)=3	IUC(2)=5	$Z_{15}$
IUR(3)=5	IUC(3)=3	$Z_{23}$
IUR(4)=8	IUC(4)=4	$Z_{24}$
IUR(5)=10	IUC(5)=1	$Z_{31}$
IUR(6)=11	IUC(6)=2	$Z_{32}$
	IUC(7)=4	$Z_{34}$
	IUC(8)=2	$Z_{47}$
	IUC(9)=3	$Z_{43}$
	IUC(10)=1	$Z_{51}$

A specialized matrix decomposition known as the "square-root method" is used to solve the system of equations. Before decomposition, the algorithm given by Berry is used to renumber the unknowns such that the number of non-zero elements in the auxiliary matrix produced by the decomposition is minimum.

There are three basic parts to the renumbering algorithm. All parts search the non-zero structure recorded by the pointer arrays IUR and IUC. An array NUMOFF with dimension  $N+1$  is set up to record the total number of non-zero off-diagonal terms associated with each equation. NUMOFF( $k$ ) equals the total number of these terms that would appear in the  $Z$  matrix in row  $k$ .

Part I of the algorithm searches the array NUMOFF once to see if there are any equations with only one non-zero off-diagonal term. If one is found, it is number 1 and the array NUMOFF is altered. A single sweep through the array NUMOFF will rapidly pick off every equation that has only one or fewer effective off-diagonal terms. Decomposition of these single off-diagonal term equations will cause no new non-zero terms in the matrix.

Part II of the algorithm searches the remaining equations (those not renumbered in Part I) for equations which can be decomposed without increasing the number of non-zero terms. As each equation is checked, an array IFILL with dimension  $N+1$  is set up which records the number of new positions that would become non-zero if that particular equation were renumbered next. If any equations were renumbered in this part, the algorithm is repeated because now the effective number of non-zero off-diagonal terms is different from the time Part II is first entered. When a complete Part II search is made without finding any equations for renumbering, then Part III is entered.

Part III finds the equation that would cause the fewest new non-zero terms by searching the array IFILL. After the choice is made and that equation renumbered, the new non-zero topology caused by decomposition of that equation is recorded in the system of pointers. After bookkeeping operations have been completed for renumbering an equation from Part III, Part II is again entered at the beginning.

After all of the equations are renumbered into the order in which the linear equations finally will appear in the matrix, the  $I$  and  $J$  pointer arrays are reorganized. For the reorganization all of the pointers are changed to correspond to the new system of equation numbers and include all non-zero terms that will ultimately be found in the upper triangular matrix  $U$ .

Finally, the solution of the matrix equation is readily obtained via the square-root method. This essentially is the very same program presented in Appendix II in Reference 12. The format sheet presented there is repeated here.

There are six input cards which are specified as follows:

Data card	Variables	Format	Descriptions
1	NSETS	I5	Number of clouds requested to be calculated
2	N	I5	Number of dipoles in a cloud
3	TL	F10.5	Length of a dipole in wavelengths
4	STDY,STDY,STD2,CF	4F10.5	Standard deviation of a Gaussian random generator for x,y,z coordinates respectively. CF is a coupling factor which weights the off-diagonal z-matrix elements. Usually set to unity.
5	IZ	I14	Starting point of the random generator
6	L2NPHI,ANGMIN,ANGMAX	I5,2F10.6	(2) is the number of look angles taken in the angle range (ANGMIN, ANGMAX)

The computer output consists of two parts: first print out of the input data with proper headings; second the average backscattering radar cross section calculations as described below.



Variables	Descriptions
AVTT	Average echo in $\theta$ - $\theta$ polarization
VARTT	Variance of the echo in $\theta$ - $\theta$ polarization
AVTP	Average echo in $\theta$ - $\phi$ polarization
VARTP	Variance of the echo in $\theta$ - $\phi$ polarization
AVPP	Average echo in $\phi$ - $\phi$ polarization
VARPP	Variance of the echo in $\phi$ - $\phi$ polarization
AV11	Average echo in both $\theta$ - $\theta$ and $\phi$ - $\phi$ polarizations
VAR11	Variance of the echo in both $\theta$ - $\theta$ and $\phi$ - $\phi$ polarizations
$S_{11}(20\%)$	The level under which 20% of the return signals belong
$S_{11}(50\%)$	The level under which 50% of the return signals belong
$S_{11}(80\%)$	The level under which 80% of the return signals belong

Finally the starting number of the random generator for the next computer run is indicated.

```

1 C*****
2 C*
3 C*      CHAXS - MAIN PROGRAM
4 C*
5 C*      PURPOSE
6 C*      CALCULATION OF SOME STATISTICAL PARAMETERS OF THE
7 C*      BACKSCATTER FROM A "RANDOM" CHAFF CLOUD. THE AVERAGE
8 C*      VALUES AND VARIANCES OF THETA-THETA, THETA-PHI, AND
9 C*      PHI-PHI POLARIZATIONS ARE OBTAINED. AN AVERAGE AND
10 C*      VARIANCE FOR LINEAR-SAME SENSE LINEAR POLARIZATION
11 C*      ARE ALSO ESTIMATED. THREE POINTS ON THE CUMULATIVE
12 C*      PROBABILITY CURVE ARE ALSO CALCULATED.
13 C*
14 C*      INPUT DATA
15 C*
16 C*      NSETS      - THE NUMBER OF DATA SETS (CLOUDS) TO BE
17 C*                  RUN.
18 C*      N          - THE NUMBER OF DIPOLES IN THE CLOUD
19 C*      TL         - THE LENGTH OF THE DIPOLES IN WAVELENGTHS
20 C*      STDX,STDY,STDZ - STANDARD DEVIATIONS OF THE DIPOLE
21 C*                  COORDINATES ALONG THE THREE PRINCIPAL
22 C*                  AXES IN WAVELENGTHS
23 C*      CF         - A SCALING FACTOR FOR THE COUPLING
24 C*                  BETWEEN DIPOLES; USUALLY SET EQUAL TO 1.0
25 C*      IZ         - A STARTING NUMBER FOR THE RANDOM
26 C*                  NUMBER GENERATORS USED TO SET UP THE
27 C*                  CLOUDS. THIS ALLOWS A GIVEN "RANDOM"
28 C*                  CLOUD TO BE REGENERATED AT ANY TIME.
29 C*      L2NPHI     - LOG BASE 2 OF THE NUMBER OF "LOOK
30 C*                  ANGLES" TO BE USED.
31 C*      ANGMIN,ANGMAX - RANGE OVER WHICH THESE LOOK ANGLES
32 C*                  WILL BE SPACED; USUALLY 0.0-360.0
33 C*      OTHER PARAMETERS
34 C*
35 C*      D,U        - COMPLEX ARRAYS CONTAINING THE COUPLING
36 C*                  MATRIX IN SPARSE MATRIX FORM
37 C*      X,Y,Z      - ARRAYS CONTAINING THE COORDINATES OF
38 C*                  THE CENTERS OF THE DIPOLES
39 C*      CA,CB,CG   - ARRAYS CONTAINING THE DIRECTION COSINES
40 C*                  OF THE DIPOLE ORIENTATIONS
41 C*      II,J       - POINTER ARRAYS FOR THE SPARSE MATRIX
42 C*      AVIT,AVTP,AVPP - CALCULATED AVERAGE BACKSCATTER FOR
43 C*      AV11        THETA-THETA, THETA-PHI, PHI-PHI, AND
44 C*                  LINEAR-SAME SENSE LINEAR POLARIZATIONS
45 C*      VARTT,VARTP - CALCULATED VARIANCES ABOUT THE ABOVE
46 C*      VARPP,VAR11 AVERAGES
47 C*      PARAMETERS IN /SORT/ ARE USED BY THE REORDERING ROUTINES
48 C*
49 C*      REMARKS
50 C*      DATA IS ONLY CALCULATED IN THE THETA EQUALS 90 DEGREES

```

```

51 C*          PLANE. THE UPPER TRIANGLE OF THE MATRIX C IS STORED BY *
52 C*          ROWS IN SPARSE MATRIX FORM. SEE SUBROUTINES EXPAND, ORDER. *
53 C*          SPSG1 & SPSG2 FOR DETAILS ON THIS STORAGE MODE. *
54 C*          *
55 C*****
56          INCLUDE FERRB.LIB
57          COMPLEX C(201),D(1613),ETI(201),FPP(201),CAA,ZMN,S(201),ZIJ
58          DIMENSION X(201),Y(201),Z(201),CA(201),CB(201),CG(201),II(201),J(1
59          2013),FREQ(120),SIG(120)
60          DIMENSION II(6),CC(6)
61          COMMON /K,SUK,CBK/FFZD,U,X,Y,Z,CA,CB,CG,II,J,F/SOFT/10RDUM(201),RO
62          ZIE(201),ICR(201),IUC(1613),NUMOFF(201),ITA(201)
63          3 FORMAT(1415)
64          CALL FERR(1)
65          4 FORMAT(7F10.5)
66 C*****
67 C*
68 C*          READ INPUT DATA AND INITIALIZE PARAMETERS
69 C*
70 C*****
71          PK=0.01745329
72          PI=3.1415927
73          TF=0.2F5115
74          READ(5,3)AS,TS
75          READ(5,3)
76          READ(5,4)TL
77          HL=TL/2.0
78          AL=HL/100.0
79          HK=PI*TL
80          AK=HK/100.0
81          READ(5,4)STIX,STIY,STIZ,CF
82          WRITE(6,10)AL,TL,STIX,STIY,STIZ,CF
83          10 FORMAT(3H0H=,F5.8H LENGTH=,F10.5,30H POSITION STANDARD DEVIATIONS=
84          2,1P3F15.4/1H ,16HCOUPLING FACTOR=,E15.8)
85          STIXK=IP*STIX
86          STIYK=IP*STIY
87          STIZK=IP*STIZ
88          READ(5,20)IZ
89          20 FORMAT(17)
90          READ(5,22)L2NPHI,ANGMIN,ANGMAX
91          22 FORMAT(15,2F10.6)
92          ANGDI=ANGMAX-ANGMIN
93          NPHI=2**L2NPHI
94          DPH=ANGDI/(FLOAT(NPHI))
95          WRITE(6,25)NPHI,L2NPHI,ANGMIN,ANGMAX
96          25 FORMAT(25HNUMBER OF LOOK ANGLES=,F5.4H=2**L2,13H ANGLE RANGE=,F6
97          2,1,3H - ,F6,17)
98          CALL GITA(6,IT,CC)
99 C*****
100 C*

```

CHAX0005

CHAX0006

CHAX0007

CHAX0008

CHAX0009

CHAX0010

CHAX0012

CHAX0013

CHAX0014

CHAX0015

CHAX0047

```

101 C*      CALCULATE SELF IMPEDANCE AND SET THRESHOLD FOR MUTUALS      *
102 C*      *
103 C*****
104      CAA=ZMM(AL,0.0,HL,HL)
105      THRSID=CABS(CAA)*0.1
106      CCF=CCS(HK)
107      SCK=SSN(HK)
108      DO 80 NSET=1,NSETS
109      IX=IZ
110      WRITE(6,26)IX
111 26  FORMAT(32HURANDOM GENERATOR INITIALIZED AT,I15//)
112      SIG(1)=0.0
113      NSIG=0.000*FLOAT(N)
114      DO 29 NSIG=1,100
115      FREQ(NSIG)=0.0
116 29  SIG(NSIG+1)=SIG(NSIG)+SIG
117      FREQ(101)=0.0
118 C*****
119 C*
120 C*      SET UP CLOUD (GENERATE X,Y,Z,CA,CB,CF)
121 C*
122 C*****
123      DO 30 I=1,N
124      CALL GAUSS(IX,STDX,0.0,Y(I))
125      CALL GAUSS(IX,STDY,0.0,Y(I))
126      CALL GAUSS(IX,STOZ,0.0,Z(I))
127      CALL RANDU(IX,IY,A1)
128      IX=IY
129      PHI=TP*A1
130      CALL RANDU(IX,IY,A2)
131      IX=IY
132      COSTH=2.0*A2-1.0
133      SINTH=SQRT(1.0-COSTH*COSTH)
134      CA(I)=SINTH*COS(PHI)
135      CB(I)=SINTH*SIN(PHI)
136 30  CF(I)=COSTH
137      DO 40 I=1,N
138      I(I)=CAA
139 C*****
140 C*
141 C*      SET UP INITIAL VALUES FOR POINTER ARRAYS AND PARAMETERS
142 C*      NEEDED FOR THE REORDERING
143 C*
144 C*****
145      DO 41 I=1,N
146      IORDER(I)=1
147      PORE(I)=1
148 41  PUMOFF(I)=0
149      IC=1
150      I1(1)=1

```

CHAX0045  
CHAX0046

CHAX0026

CHAX0034

CHAX0036

CHAX0037

CHAX0038

CHAX0039

CHAX0040

CHAX0042

```

151      NM1=N-1
152      DO 45 I=1,NM1
153      IP1=I+1
154      DO 43 JC=IP1,N
155      CALL ZGAUS(X(I),Y(I),Z(I),X(JC),Y(JC),Z(JC),CA(I),CB(I),CG(I),CA(J
156      2C),CB(JC),CG(JC),ZIJ,6,TT,CC)
157      IF(CABS(ZIJ).LT.THRSHD)GO TO 43
158      J(IC)=JC
159      IC=IC+1
160      NUMOFF(I)=NUMOFF(I)+1
161      NUMOFF(JC)=NUMOFF(JC)+1
162      43 CONTINUE
163      45 II(I+1)=IC
164      IF(IC.GT.1500)WRITE(0,46)IC
165      46 FORMAT(39H0ARRAY J OVERRUN DURING INITIALIZATION/1X,I5,15H CELLS R
166      2EQUIRED)
167      CALL EXPAND(II,J,N)
168 C*****
169 C*
170 C*      GENERATE POINTER ARRAYS FOR THE REORDERED SYSTEM
171 C*
172 C*****
173      CALL ORDER(II,J,N)
174 C*****
175 C*
176 C*      CALCULATE MUTUAL IMPEDANCES AND STORE IN D AND U
177 C*
178 C*****
179      DO 49 I=1,NM1
180      JFST=II(I)
181      JLST=II(I+1)-1
182      ISUB=IORDER(I)
183      IF(JFST.GT.JLST)GO TO 49
184      DO 47 JC=JFST,JLST
185      JJC=J(JC)
186      JSUB=IORDER(JJC)
187      47 CALL ZGAUS(X(ISUB),Y(ISUB),Z(ISUB),X(JSUB),Y(JSUB),Z(JSUB),CA(ISUB
188      2),CB(ISUB),CG(ISUB),CA(JSUB),CB(JSUB),CG(JSUB),U(JC),6,TT,CC)
189      49 CONTINUE
190 C*****
191 C*
192 C*      GENERATE "SQUARE ROOT" METHOD AUXILIARY MATRIX OF C
193 C*
194 C*****
195      CALL SPSWT1(D,U,II,J,N)
196 C*****
197 C*
198 C*      ACCUMULATE SUMS FOR AVERAGES AND VARIANCES
199 C*
200 C*****

```

```

201      PH=0.0
202      CPH=1.0
203      SPH=0.0
204      AVTT=0.0
205      AVTP=0.0
206      AVPP=0.0
207      VARTT=0.0
208      VARTP=0.0
209      VARPP=0.0
210      DO 66 NPH=1,NPHI
211      CALL FPT(CPH,SPH,0.0,ECTT,ECTP,ECPP,IORDER)
212      AVTT=AVTT+ECTT
213      AVTP=AVTP+ECTP
214      AVPP=AVPP+ECPP
215      VARTT=VARTT+ECTT*ECTT
216      VARTP=VARTP+ECTP*ECTP
217      VARPP=VARPP+ECPP*ECPP
218      C*****
219      C*
220      C*      CONSTRUCT HISTOGRAM OF THE BACKSCATTER FOR THE CUMULATIVE
221      C*      DISTRIBUTION CALCULATION
222      C*
223      C*****
224      DO 50 NSIG=1,101
225      TEMP=SIG(NSIG)
226      IF(ECTT-TEMP)60,50,50
227      50 CONTINUE
228      GO TO 62
229      60 FREQ(NSIG)=FREQ(NSIG)+1.0
230      62 CONTINUE
231      DO 63 NSIG=1,101
232      TEMP=SIG(NSIG)
233      IF(ECPP-TEMP)64,63,63
234      63 CONTINUE
235      GO TO 65
236      64 FREQ(NSIG)=FREQ(NSIG)+1.0
237      65 CONTINUE
238      PH=PH+DPH
239      PHR=PH*DK
240      CPH=COS(PHR)
241      66 SPH=SIN(PHR)
242      C*****
243      C*
244      C*      CALCULATE BACKSCATTER AVERAGES AND VARIANCES
245      C*
246      C*****
247      NPH2=2*NPHI
248      AV11=AVTT+AVPP
249      VAR11=(VARTT+VARPP-AV11*AV11/FLOAT(NPH2))/FLOAT(NPH2-1)
250      AV11=AV11/FLOAT(NPH2)

```



```

251      VARTI=(VARTI-AV11*AVIT/FLOAT(NPH))/FLOAT(NPH-1)
252      AVTI=AVTI/FLOAT(NPH)
253      VARTP=(VARTP-AVTP*AVIP/FLOAT(NPH))/FLOAT(NPH-1)
254      AVTP=AVTP/FLOAT(NPH)
255      VARPP=(VARPP-AVPP*AVPP/FLOAT(NPH))/FLOAT(NPH-1)
256      AVPP=AVPP/FLOAT(NPH)
257      FREQ(1)=FREQ(1)/FLOAT(NPH)/2.0
258      FX=FREQ(1)
259      (*****
260      C*
261      C*      CALCULATE THREE POINTS ON THE CUMULATIVE DISTRIBUTION CURVE
262      C*
263      (*****
264      DO 70 NSIG=2,101
265      FREQ(NSIG)=FREQ(NSIG)/FLOAT(NPH)/2.0
266      FX=FX+FREQ(NSIG)
267      IF(FX.LE.0.2) SIG20=SIG(NSIG)
268      IF(FX.LE.0.5) SIG50=SIG(NSIG)
269      IF(FX.LE.0.7) SIG80=SIG(NSIG)
270      70 FREQ(NSIG)=FX
271      WRITE(6,7) AVIT,VARTI,AVTP,VARTP,AVPP,VARPP,AV11,VAR11,SIG20,SIG50
272      70 SIG80
273      75 FORMAT(6H)AVIT=.E15.8,7H VARTI=.E15.8,6H AVTP=.E15.8,7H VARTP=.E
274      25.8,6H AVPP=.E15.8,7H VARPP=.E15.8,6H AV11=.E15.8,7H VAR11=.E15.8
275      3/11H SIG20 BELOW .E15.8,19H 20% OF THE SAMPLES/11H SIG50 BELOW .E15.8,
276      41H 50% OF THE SAMPLES/11H SIG80 BELOW .E15.8,19H 80% OF THE SAMPLES
277      5//)
278      IZ=12*3709
279      IF(IZ/76.E0.80
280      76 IZ=IZ+6366207+1
281      80 CONTINUE
282      WRITE(6,8) IZ
283      85 FORMAT(75H)A GOOD NUMBER TO USE FOR INITIALIZING THE RANDOM GENERA
284      2TOR ON THE TEXT RUN IS .I7)
285      CALL EXIT
286      END
287      SUBROUTINE GITAB(M,T,C)
288      (*****
289      C*
290      C*      PURPOSE
291      C*      SETS UP COEFFICIENT TABLES FOR ZGAUS
292      C*
293      C*      USAGE
294      C*      CALL GITAB(M,T,C)
295      C*
296      C*      DESCRIPTION OF PARAMETERS
297      C*      M - THE NUMBER OF POINTS ZGAUS IS TO USE IN
298      C*      INTEGRATION
299      C*      T - THE ABSCISSA VALUES FOR ZGAUS
300      C*      (MUST BE DIMENSIONED IN MAIN PROGRAM)

```

```

GTAB0000
*GTAB0001
*GTAB0002
*GTAB0003
*GTAB0004
*GTAB0005
*GTAB0006
*GTAB0007
*GTAB0008
*GTAB0009
*GTAB0010
*GTAB0011
*GTAB0012
*GTAB0013

```

```

301 C*      C      - THE WEIGHTING COEFFICIENTS FOR ZGAUS
302 C*      (MUST BE DIMENSIONED IN MAIN PROGRAM)
303 C*      HK      - THE HALF LENGTH OF THE DIPOLES IN ELECTRIC/L
304 C*      RADIANS
305 C*      CDK      - COS(HK)
306 C*      SDK      - SIN(HK)
307 C*
308 C*****
309      DIMENSION T(N),C(N),V(40),Z(40)
310      COMMON HK,SDK,CDK
311      DATA V/.33998104,.66115031,.23361919,.66120939,.93246951,
312      2.18343464,.52556241,.79666400,.90028965,.14827433,.43339139,
313      3.67990757,.76505557,.97490153,.12523340,.36733150,.50731795,
314      4.76990267,.90411726,.98156063,.09501201,.23110354,.45801778,
315      5.81797825,.75500441,.86563120,.94457502,.98940093,.06435039,
316      6.19111867,.81504267,.93379351,.54542147,.64609365,.74012419,
317      7.62000199,.86641553,.93827455,.97472006,.99511722/
318      DATA W/.5214515,.34705495,.46791383,.38076157,.17132448,
319      2.36260370,.1370666,.22201103,.10122624,.29552822,.26926872,
320      3.21906530,.14905130,.06667133,.24914704,.23346254,.20316742,
321      4.16037832,.10604932,.04717527,.18245001,.16206340,.16915151,
322      5.14959599,.12442097,.09515551,.06226383,.02715244,.12795720,
323      6.12583740,.12167047,.11551367,.10744426,.0971865,.08615116,
324      7.07334647,.15929857,.04427744,.02653159,.01234122/
325      MU=(N*N-N)/2
326      IF(N.EQ.0)MU=21
327      IF(N.EQ.12)MU=29
328      I1=MU+N-1
329      J=1
330      DO 100 I=MU,NI
331      T(I)=HK*V(I)
332      C(I)=SIN(HK-T(I))*W(I)
333      100 J=J+1
334      RETURN
335      END
336      SUBROUTINE ZGAUS(XA,YA,ZA,XP,YB,ZB,CAS,CBS,CGS,CA,CB,CG,SM12,N,T,CZGUS0000
337      Z)
338      C*****
339      C*
340      C*      PURPOSE
341      C*      CALCULATES THE MUTUAL IMPEDANCE BETWEEN TWO DIPOLES
342      C*
343      C*      USAGE
344      C*      CALL ZGAUS(XA,YA,ZA,XP,YB,ZB,CAS,CBS,CGS,CA,CB,CG,SM12,
345      C*      N,T,C)
346      C*
347      C*      DESCRIPTION OF PARAMETERS
348      C*      XA,YA,ZA      - COORDINATES OF THE POSITION OF THE CENTER
349      C*      OF THE FIRST DIPOLE IN ELECTRICAL RADIAN
350      C*      YB,YB,ZB      - COORDINATES OF THE POSITION OF THE CENTER

```

353 C*		OF THE SECOND DIPOLE IN ELECTRICAL RADIIANS	*ZGUS0015
352 C*	CAS,COS,COS	- DIRECTION COSINES OF THE ORIENTATION OF THE	*ZGUS0016
353 C*		FIRST DIPOLE	*ZGUS0017
354 C*	CA,CE,CG	- DIRECTION COSINES OF THE ORIENTATION OF THE	*ZGUS0018
355 C*		SECOND DIPOLE	*ZGUS0019
356 C*	SM12	- THE RESULTANT MUTUAL IMPEDANCE	*ZGUS0020
357 C*	N	- THE NUMBER OF POINTS USED IN THE GAUSSIAN	*ZGUS0021
358 C*		INTEGRATION	*ZGUS0022
359 C*	T	- THE ABSCTSSA VALUES GENERATED BY GITAB	*ZGUS0023
360 C*	C	- THE WEIGHTING COEFFICIENTS GENERATED BY	*ZGUS0024
361 C*		GITAB	*ZGUS0025
362 C*	HK	- THE HALF LENGTH OF THE DIPOLES IN	*ZGUS0026
363 C*		ELECTRICAL RADIIANS	*ZGUS0027
364 C*	COS	- COS(HK)	*ZGUS0028
365 C*	SIN	- SIN(HK)	*ZGUS0029
366 C*			*ZGUS0030
367 C*	REMARKS		*ZGUS0031
368 C*		GITAB MUST BE CALLED WITH THE APPROPRIATE VALUE OF N	*ZGUS0032
369 C*		BEFORE ZGABS MAY BE CALLED. ONE CALL TO GITAB IS ALL THAT	*ZGUS0033
370 C*		IS REQUIRED FOR ANY NUMBER OF CALLS TO ZGABS AS LONG AS	*ZGUS0034
371 C*		N REMAINS UNCHANGED	*ZGUS0035
372 C*			*ZGUS0036
373 C*	SUBROUTINES AND FUNCTION SUBPROGRAMS REQUIRED		*ZGUS0037
374 C*	GITAB		*ZGUS0038
375 C*			*ZGUS0039
376 C*	METHOD		*ZGUS0040
377 C*		INDUCED EMF EVALUATED BY GAUSSIAN INTEGRATION. PIECEWISE	*ZGUS0041
378 C*		SINUSOIDAL CURRENTS (TWO SEGMENTS PER DIPOLE) ARE	*ZGUS0042
379 C*		ASSUMED	*ZGUS0043
380 C*			*ZGUS0044
381 C*	*****		*ZGUS0045
382 C*	COMPLEX SM12,FJR1,FJR2,FJR3,FT1,FR1		*ZGUS0046
383 C*	DIRECTION T(N),C(N)		*ZGUS0047
384 C*	COMMON HK,SMK,COS		*ZGUS0048
385 C*	CE=CA*CA+CG*CG+CG*CG		*ZGUS0049
386 C*	SM12=(0.0,0.0)		*ZGUS0050
387 C*	DO 90 I=1,N		*ZGUS0051
388 C*	T1=T(I)		*ZGUS0052
389 C*	DO 90 J=1,2		*ZGUS0053
390 C*	X=XH+T1*CA		*ZGUS0054
391 C*	Y=YH+T1*CE		*ZGUS0055
392 C*	Z=ZH+T1*CG		*ZGUS0056
393 C*	ZZ2=(X-XH)*(CA+(Y-YH)*COS+(Z-ZH)*CG		*ZGUS0057
394 C*	ZZ1=ZZ2+FR		*ZGUS0058
395 C*	ZZ3=ZZ2-HK		*ZGUS0059
396 C*	XZ=XH+ZZ2*CA		*ZGUS0060
397 C*	YZ=YH+ZZ2*COS		*ZGUS0061
398 C*	ZZ=ZH+ZZ2*CG		*ZGUS0062
399 C*	XXZ=X-YZ		*ZGUS0063
400 C*	YYZ=Y-ZZ		*ZGUS0064

401	ZZ=Z-ZZ	ZGUS0065
402	RS=XXZ+XXZ+YYZ+YYZ+ZZZ+ZZZ	ZGUS0066
403	R1=SQRT(RS+ZZ1+ZZ1)	ZGUS0067
404	FJR1=CMPLX(COS(R1),-SIN(R1))/R1	ZGUS0068
405	R2=SQRT(RS+ZZ2+ZZ2)	ZGUS0069
406	FJR2=CMPLX(COS(R2),-SIN(R2))/R2	ZGUS0070
407	R3=SQRT(RS+ZZ3+ZZ3)	ZGUS0071
408	FJR3=CMPLX(COS(R3),-SIN(R3))/R3	ZGUS0072
409	E11=CL*(2.0*EJR2*CHK-EJR1-EJR3)/SDK	ZGUS0073
410	IF(RS.LT.1.0E-4*HK)GO TO 40	ZGUS0074
411	SKY=(CA*XXZ+CP*YYZ+CG*ZZZ)/RS	ZGUS0075
412	ER1=(EJR1+ZZ1+FJR3*ZZ3-2.0*CHK*EJR2+ZZ2)/SDK	ZGUS0076
413	ET1=E11+L*1*SKY	ZGUS0077
414	SM12=CM12-E11*CL	ZGUS0078
415	IF T1=-T1	ZGUS0079
416	SM12=SM12*(0.0,50.0)*HK/SLK	ZGUS0080
417	RETURN	ZGUS0081
418	END	ZGUS0082
419	SUBROUTINE FAREF(X,Y,Z,CA,CP,CG,CTH,STH,CPH,SPH,ET,EP)	FRF00000
420	C*****	FRF00001
421	C*	FRF00002
422	C* PURPOSE	FRF00003
423	C* CALCULATES THE FAR ELECTRIC FIELDS OF A TWO SEGMENT	FRF00004
424	C* PIECEWISE SINUSOIDAL DIPOLE CURRENT	FRF00005
425	C*	FRF00006
426	C* USAGE	FRF00007
427	C* CALL FAREF(X,Y,Z,CA,CP,CG,CTH,STH,CPH,SPH,ET,EP)	FRF00008
428	C*	FRF00009
429	C* DESCRIPTION OF PARAMETERS	FRF00010
430	C* X,Y,Z - COORDINATES OF THE CENTER OF THE DIPOLE	FRF00011
431	C* CA,CP,CG - DIRECTION COSINES OF THE ORIENTATION OF	FRF00012
432	C* THE DIPOLE	FRF00013
433	C* CTH - COS(THETA)	FRF00014
434	C* STH - SIN(THETA)	FRF00015
435	C* CPH - COS(PHI)	FRF00016
436	C* SPH - SIN(PHI)	FRF00017
437	C* ET - THETA COMPONENT OF THE CALCULATED E-FIELD	FRF00018
438	C* EP - PHI COMPONENT OF THE CALCULATED E-FIELD	FRF00019
439	C* HK - HALF LENGTH OF THE DIPOLE IN ELECTRICAL	FRF00020
440	C* RADIANS	FRF00021
441	C* SDK - SIN(HK)	FRF00022
442	C* CHK - COS(HK)	FRF00023
443	C*	FRF00024
444	C* REMARKS	FRF00025
445	C* THETA AND PHI ARE THE LOOK ANGLES FOR WHICH THE FIELDS ARE	FRF00026
446	C* CALCULATED	FRF00027
447	C*	FRF00028
448	C*****	FRF00029
449	C* COMPLEX ET,EP,FJR1,2,3	FRF00030
450	C* COMMON HK,SDK,CHK	FRF00031

451	G=(CA*CPH+CB*SPH)*STH+CG*CTH	FRFD0032
452	GK=1.0-G*G	FRFD0033
453	F1=(0.0,0.0)	FRFD0034
454	F2=(0.0,0.0)	FRFD0035
455	IF (GK.LT..001) GO TO 200	FRFD0036
456	P=(X*CPH+Y*SPH)*STH+Z*CTH	FRFD0037
457	FJR=CMPLX(COS(P),SIN(P))	FRFD0038
458	ES=(J.0,0.0)*FJR*(CDK-COS(G*HK))/GK/SPH	FRFD0039
459	T=(CA*CPH+CB*SPH)*CTH-CG*STH	FRFD0040
460	F=-CA*SPH+(P*CPH	FRFD0041
461	FT=T*ES	FRFD0042
462	FP=P*ES	FRFD0043
463	200 CONTINUE	FRFD0044
464	RETURN	FRFD0045
465	END	FRFD0046
466	SUBROUTINE FPT(CPH,SPH,CTH,ECT1,ECIP,ECPP,IONIER)	FPT0000
467	*****	FPT0001
468	C*	* FPT0002
469	C* PURPOSE	* FPT0003
470	C* CALCULATES THE BACKSCATTER FROM A CLOUD OF DIPOLES AT A	* FPT0004
471	C* GIVEN LOOK ANGLE	* FPT0005
472	C*	* FPT0006
473	C* USAGE	* FPT0007
474	C* CALL FPT(CPH,SPH,CTH,ECT1,ECIP,ECPP)	* FPT0008
475	C*	* FPT0009
476	C* DESCRIPTION OF PARAMETERS	* FPT0010
477	C* CPH - COS(PHI)	* FPT0011
478	C* SPH - SIN(PHI)	* FPT0012
479	C* CTH - COS(THETA)	* FPT0013
480	C* ECT1 - THETA-THETA BACKSCATTER	* FPT0014
481	C* ECIP - THETA-PHI BACKSCATTER	* FPT0015
482	C* ECPP - PHI-PHI BACKSCATTER	* FPT0016
483	C* HK - HALF LENGTH OF THE DIPOLES IN ELECTRICAL	* FPT0017
484	C* RADIANS	* FPT0018
485	C* SGK - SIN(HK)	* FPT0019
486	C* CDK - COS(HK)	* FPT0020
487	C* D,U - ARRAYS CONTAINING THE DIAGONAL TERMS AND THE	*
488	C* OFF-DIAGONAL TERMS RESPECTIVELY OF THE	*
489	C* AUXILIARY MATRIX CALCULATED FROM THE ACTUAL	*
490	C* IMPEDANCE MATRIX BY SPSP11. THE MATRIX IS IN	*
491	C* THE SPARSE MATRIX STORAGE MODE.	*
492	C* X,Y,Z - ARRAYS CONTAINING THE COORDINATES OF THE	* FPT0023
493	C* CENTERS OF THE DIPOLES	* FPT0024
494	C* CA,CB,CG - ARRAYS CONTAINING THE DIRECTION COSINES OF THE	* FPT0025
495	C* ORIENTATIONS OF THE DIPOLES	* FPT0026
496	C* IONIER - INDEXING ARRAYS FOR THE SPARSE MATRIX	*
497	C* II,U - STORAGE MODE	*
498	C* N - THE NUMBER OF DIPOLES	* FPT0027
499	C* NC - NOT USED	* FPT0028
500	C*	* FPT0029

256



551 C*	DESCRIPTION OF PARAMETERS	* Z4N010
552 C*	Z - THE RESULTANT VALUE OF THE MUTUAL IMPEDANCE	* Z4N011
553 C*	D - THE HORIZONTAL DISTANCE BETWEEN THE DIPOLES IN	* Z4N012
554 C*	WAVELENGTHS.	* Z4N013
555 C*	HC - THE VERTICAL DISTANCE BETWEEN THE DIPOLES IN	* Z4N014
556 C*	WAVELENGTHS.	* Z4N015
557 C*	LE - THE "EFFECTIVE HALF LENGTH" OF THE DIPOLES IN	* Z4N016
558 C*	WAVELENGTHS (SEE FOR INSTANCE SCHELMKOFF & FRITS	* Z4N017
559 C*	ANTENNAS THEORY AND PRACTICE P. 244-246 & P. 420)	* Z4N018
560 C*	L - THE PHYSICAL HALF LENGTH OF THE DIPOLES	* Z4N019
561 C*		* Z4N020
562 C*	SUBROUTINES AND FUNCTION SUBPROGRAMS REQUIRED	* Z4N021
563 C*	SICI - SSP ROUTINE FOR SINE AND COSINE INTEGRALS	* Z4N022
564 C*		* Z4N023
565 C*	REFERENCES	* Z4N024
566 C*	HOWARD E. KING, "MUTUAL IMPEDANCE OF UNEQUAL LENGTH	* Z4N025
567 C*	ANTENNAS IN ECHELON", THE TRANS. ANTENNAS & PROPAGATION	* Z4N026
568 C*	VOL AP-5, JULY 1957 P. 306-313	* Z4N027
569 C*		* Z4N028
570 C*	*****	* Z4N029
571	REAL L,LE,LL	* Z4N030
572	DEG,28.5)253	* Z4N031
573	BLF=B*LE	* Z4N032
574	H=ABS(HC)-L	* Z4N033
575	LL=LE	* Z4N034
576	HP2L=H+LL	* Z4N035
577	HP3L=H+2.0*LL	* Z4N036
578	HP3L=H+3.0*LL	* Z4N037
579	HPL=H-LL	* Z4N038
580	SBL=SIN(LE)	* Z4N039
581	CLL=COS(LE)	* Z4N040
582	SBL=SIN(LE)	* Z4N041
583	CLL=COS(LE)	* Z4N042
584	SCHML=SIN(B*HML)	* Z4N043
585	CHML=COS(B*HML)	* Z4N044
586	SCHPL=SIN(B*HPL)	* Z4N045
587	CHPL=COS(B*HPL)	* Z4N046
588	SCHP2L=SIN(B*HP2L)	* Z4N047
589	CHP2L=COS(B*HP2L)	* Z4N048
590	SCHP3L=SIN(B*HP3L)	* Z4N049
591	CHP3L=COS(B*HP3L)	* Z4N050
592	TEMP=SQRT(L*(D+H*H)+H)	* Z4N051
593	V1=R*D*D/TEMP	* Z4N052
594 C*	*****	* Z4N053
595 C*		* Z4N054
596 C*	NOTE: SQRT(D*D+H*H)-H = D*D/(SQRT(D*D+H*H)+H)	* Z4N055
597 C*		* Z4N056
598 C*	THE FORM ON THE RIGHT HAND SIDE OF THIS EQUATION HAS	* Z4N057
599 C*	SUPERIOR ROUND OFF CHARACTERISTICS AND WAS USED FOR THIS	* Z4N058
600 C*	REASON.	* Z4N059

```

601 C*
602 C*****
603     U1=B*TEMP
604     TEMP=SQRT(D*D+HML*HML)+HML
605     U0=B*TEMP
606     V0=B*U0/D/TEMP
607     TEMP=SQRT(D*D+HPL*HPL)+HPL
608     U3=B*TEMP
609     V3=B*U3/D/TEMP
610     TEMP=SQRT(D*D+HP2L*HP2L)+HP2L
611     U2=B*U0/D/TEMP
612     V2=B*U2/HPL
613     TEMP=SQRT(D*D+HPAL*HPAL)+HPAL
614     U4=B*U0/D/TEMP
615     V4=B*U4/TEMP
616     IF (U1E+U0E) GO TO 80
617     CALL STC1 (SIV1,CIV1,V1)
618     CALL STC1 (SIU1,CIU1,U1)
619     CALL STC1 (SIU0,CIU0,U0)
620     CALL STC1 (SIV0,CIV0,V0)
621     CALL STC1 (SIU3,CIU3,U3)
622     CALL STC1 (SIV3,CIV3,V3)
623     CALL STC1 (SIU2,CIU2,U2)
624     CALL STC1 (SIV2,CIV2,V2)
625     CALL STC1 (SIU4,CIU4,U4)
626     CALL STC1 (SIV4,CIV4,V4)
627     P=15.0*(C*HPL*(CIU0+CIV0-(CIU1-CIV1))-SHHPL*(-SIU0+SIV0+SIU1-SIV1)+C
628     2*HPL*(2.*CIV3+2.*CIU3-CIU2-CIV2-CIU1-CIV1)+SHHPL*(-SIV3+SIU3+SIU2-
629     3SIV2-SIU1+SIV1+SIU3-SIV3)+CHHP3L*(-CIU2-CIV2+CIU4+CIV4)+SHHP3L*(SI
630     4U2-SIV2-SIU3+SIU4)+2.*CBL*CBH*(-CIV3-CIU1+CIV3+CIU3)+2.*CBL*SBH*(
631     5SIV1-SIU1-SIV3+SIU3)+2.*CBL*CBHP2L*(CIV3+CIU3-CIU2-CIV2)+2.*CBL*SB
632     6HP2L*(-SIV3+SIU3+SIU2-SIV2))
633     X=15.0*(C*HPL*(-SIU0-SIV0+SIU1+SIV1)-SHHPL*(-CIU0+CIV0+CIU1-CIV1)+
634     2CHHP2L*(-2.*SIV2-2.*SIU3+SIU2+SIV2+SIU1+SIV1)+SHHPL*(-2.*CIV3+2.*C
635     3IU3+CIU2-CIV2-CIU1+CIV1)+CHHPAL*(SIU2+SIV2-SIU4-SIV4)+SBHP3L*(CIU2
636     4-CIV2-CIU4+CIV0)+2.*CBL*CBH*(SIV1+SIU1-SIV3-SIU3)+2.*CBL*SBH*(CIV
637     5I-CIU1-CIV3+CIU3)+2.*CBL*CHHP2L*(-SIV3-SIU3+SIU2+SIV2)+2.*CBL*SBHP
638     62L*(-CIV3+CIU3+CIU2-CIV2))
639     GO TO 90
640 or CONTINUE
641     CALL STC1 (SIU0,CIU0,U0)
642     CALL STC1 (SIU1,CIU1,U1)
643     CALL STC1 (SIV2,CIV2,V2)
644     CALL STC1 (SIV4,CIV4,V4)
645     CALL STC1 (SIU3,CIU3,U3)
646     P=15.0*(CBHPL*(CIU0-CIU1+ALOG(H/HML))+SHHPL*(SIU0-SIU1)+SHHPL*
647     2 (2.*SIU3-SIV2-SIU1)+CHHP2L*(2.*CIU3-CIV2-CIU1+ALOG(HP2L/HPL))+
648     3ALOG(H/HML))+CHHPAL*(CIV4-CIV2+ALOG(HP2L/HPAL))+SHHP3L*(SIV4-SIV2
649     4)+2.*CBL*CBH*(CIU2-CIU1+ALOG(H/HPL))+2.*CBL*SBH*(SIU3-SIU1)+
650     5 2.*CBL*CBHP2L*(CIU3-CIV2+ALOG(HP2L/HPL))+2.*CBL*SBHP2L*(SIU3-

```

```

ZMN000
ZMN001
ZMN002
ZMN003
ZMN004
ZMN005
ZMN006
ZMN007
ZMN008
ZMN009
ZMN010
ZMN011
ZMN012
ZMN013
ZMN014
ZMN015
ZMN016
ZMN017
ZMN018
ZMN019
ZMN020
ZMN021
ZMN022
ZMN023
ZMN024
ZMN025
ZMN026
ZMN027
ZMN028
ZMN029
ZMN030
ZMN031
ZMN032
ZMN033
ZMN034
ZMN035
ZMN036
ZMN037
ZMN038
ZMN039
ZMN040
ZMN041
ZMN042
ZMN043
ZMN044
ZMN045
ZMN046
ZMN047
ZMN048
ZMN049
ZMN050
ZMN051
ZMN052
ZMN053
ZMN054
ZMN055
ZMN056
ZMN057
ZMN058
ZMN059
ZMN060
ZMN061
ZMN062
ZMN063
ZMN064
ZMN065
ZMN066
ZMN067
ZMN068
ZMN069
ZMN070
ZMN071
ZMN072
ZMN073
ZMN074
ZMN075
ZMN076
ZMN077
ZMN078
ZMN079
ZMN080
ZMN081
ZMN082
ZMN083
ZMN084
ZMN085
ZMN086
ZMN087
ZMN088
ZMN089
ZMN090
ZMN091
ZMN092
ZMN093
ZMN094
ZMN095
ZMN096
ZMN097
ZMN098
ZMN099
ZMN100
ZMN101
ZMN102
ZMN103
ZMN104
ZMN105
ZMN106
ZMN107
ZMN108
ZMN109
ZMN110

```

651	6 SIV2))	ZMN110
652	Y=15.0*(CML*(SI0-SJ00)+SBHML*(CI00-CI01+ALOG(HPL/H )+CBIPL*	ZMN111
653	2 (SIV2+SI01-2.*SI03)+SBHPL*(2.*CI03-CIV2-CI11+ALOG(HPL/HP2L)+	ZMN112
654	3ALOG(HPL/H )+CBHPL*(SIV2-SIV4)+SBHPL*(CIV0-CIV2+ALOG(HPL/HP2L)	ZMN113
655	4)+2.*CBL*CB*(SI01-SJ03)+2.*CBL*SBH*(CI03-CI01+ALOG(HPL/H )+2.*CB	ZMN114
656	5L*CBHP2L*(SIV2-SI02)+2.*CBL*SBHP2L*(CI04-CIV2+ALOG(HPL/HP2L)))	ZMN115
657	90 ZMN=CMPLX(F,X)/(SPL*SBL)	Z45116
658	RETURN	ZMN117
659	END	ZMN116
660	SUBROUTINE SICT(SI,CI,X)	SIC1000
661	*****	SIC1001
662	C*	* SIC1002
663	C* PURPOSE	* SIC1003
664	C* COMPUTES THE SINE AND COSINE INTEGRALS	* SIC1004
665	C*	* SIC1005
666	C* USAGE	* SIC1006
667	C* CALL SICT(SI,CI,X)	* SIC1007
668	C*	* SIC1008
669	C* DESCRIPTION OF PARAMETERS	* SIC1009
670	C* SI - THE RESULTANT VALUE SI(X)	* SIC1010
671	C* CI - THE RESULTANT VALUE CI(X)	* SIC1011
672	C* X - THE ARGUMENT OF SI(X) AND CI(X)	* SIC1012
673	C*	* SIC1013
674	C* REMARKS	* SIC1014
675	C* THE ARGUMENT VALUE REMAINS UNCHANGED	* SIC1015
676	C*	* SIC1016
677	C* SUBROUTINES AND FUNCTION SUBPROGRAMS REQUIRED	* SIC1017
678	C* NONE	* SIC1018
679	C*	* SIC1019
680	C* METHOD	* SIC1020
681	C* DEFINITION	* SIC1021
682	C* SI(X)=INTEGRAL(SIN(T)/T)	* SIC1022
683	C* CI(X)=INTEGRAL(COS(T)/T)	* SIC1023
684	C* EVALUATION	* SIC1024
685	C* REDUCTION OF RANGE USING SYMMETRY	* SIC1025
686	C* DIFFERENT APPROXIMATIONS ARE USED FOR ABS(X) GREATER	* SIC1026
687	C* THAN 4 AND FOR ABS(X) LESS THAN 4.	* SIC1027
688	C*	* SIC1028
689	C* REFERENCES	* SIC1029
690	C* IBM SCIENTIFIC SUBROUTINE PACKAGE P. 370	* SIC1030
691	C* LUKE AND WIMP, 'POLYNOMIAL APPROXIMATIONS TO INTEGRAL	* SIC1031
692	C* TRANSFORMS', MATHEMATICAL TABLES AND OTHER AIDS TO	* SIC1032
693	C* COMPUTATION, VOL. 15, 1961, ISSUE 74, P. 174-178	* SIC1033
694	C*	* SIC1034
695	C*****	SIC1035
696	Z=2dS(X)	SIC1036
697	IF(Z=4.0)1,1,4	SIC1037
698	1 Y=(4.0-Z)*(4.0+Z)	SIC1038
699	S1=-1.57079780	SIC1039
700	TF(Z)5.2+5	SIC1040

701	2 C1=-1.0E30	SIC1041
702	RETURN	SIC1042
703	3 S1=X*(((1.753141E-5*Y+1.56A988E-7)*Y+1.374168E-5)*Y+6.939889E-4)	SIC1043
704	2*Y+1.964882E-2)*Y+4.395509E-1+SI/X)	SIC1044
705	C1=((5.772156E-1+ALOG(Z))/Z-7*(((1.38E-30E-10*Y+1.584926E-2)*Y	SIC1045
706	2+1.725754E-6)*Y+1.185999E-4)*Y+4.990920E-3)*Y+1.315306E-1))*Z	SIC1046
707	RETURN	SIC1047
708	4 S1=SIN(Z)	SIC1048
709	Y=COS(Z)	SIC1049
710	Z=4.0/Z	SIC1050
711	U=(((((((4.044068E-3*Z-2.270143E-2)*Z+5.515170E-2)*Z-7.261642E-2)	SIC1051
712	2*Z+4.967716E-2)*Z-3.532519E-3)*Z-2.314617E-2)*Z-1.134956E-5)*Z	SIC1052
713	3+5.250011E-2)*Z+2.536899E-10	SIC1053
714	V=(((((((5.108509E-3*Z+2.019175E-2)*Z-5.527285E-2)*Z	SIC1054
715	2+7.902034E-2)*Z-4.400416E-2)*Z-7.945556E-3)*Z+2.601293E-1)*Z	SIC1055
716	3-5.764000E-4)*Z-5.122418E-2)*Z-6.646441E-7)*Z+2.500000E-1	SIC1056
717	C1=Z*(S1*V-Y*U)	SIC1057
718	S1=-Z*(S1*U+Y*V)	SIC1058
719	IF(X)5,6,6	SIC1059
720	5 S1=-3.1415926E-0-SI	SIC1060
721	6 RETURN	SIC1061
722	END	SIC1062
723	SUBROUTINE EXPAND(II,J,N)	
724	*****	
725	C*	*
726	C* PURPOSE	*
727	C* GENERATES POINTER ARRAYS FOR THE FULL MATRIX GIVEN POINTER	*
728	C* ARRAYS FOR THE UPPER TRIANGLE OF A SYMMETRIC SPARSE MATRIX	*
729	C*	*
730	C* USAGE	*
731	C* CALL EXPAND(II,J,N)	*
732	C*	*
733	C* DESCRIPTION OF PARAMETERS	*
734	C* II - ARRAY CONTAINING THE STARTING LOCATIONS OF	*
735	C* TERMS IN J ASSOCIATED WITH THE ROWS OF THE	*
736	C* UPPER TRIANGULAR MATRIX	*
737	C* J - ARRAY CONTAINING THE COLUMN INDICES OF THE	*
738	C* NON-ZERO ELEMENTS IN THE UPPER TRIANGULAR	*
739	C* MATRIX	*
740	C* N - THE NUMBER OF EQUATIONS IN THE SYSTEM (MUST	*
741	C* BE LESS THAN OR EQUAL TO THE DIMENSION OF	*
742	C* II IN THE CALLING PROGRAM)	*
743	C* IORDER - NOT USED	*
744	C* NOOE - NOT USED	*
745	C* IUC - ARRAY CONTAINING THE STARTING LOCATIONS OF	*
746	C* TERMS IN IUC ASSOCIATED WITH THE ROWS OF THE	*
747	C* FULL MATRIX ON OUTPUT	*
748	C* IUC - ARRAY CONTAINING THE COLUMN INDICES OF THE	*
749	C* NON-ZERO ELEMENTS OF THE FULL MATRIX ON OUTPUT	*
750	C* NUMOFF - ARRAY CONTAINING THE NUMBER OF NON-ZERO OFF	*



```

751 C*          DIAGONAL TERMS IN EACH ROW OF THE FULL MATRIX *
752 C*          MUST BE SET BY THE CALLING PROGRAM! *
753 C*          ITA      - NOT USED *
754 C* *
755 C* REFERENCES *
756 C*   HERRY, R. D. "AN OPTIMAL ORDERING OF ELECTRONIC CIRCUIT *
757 C*   EQUATIONS FOR A SPARSE MATRIX SOLUTION" IEEE TRANSACTIONS *
758 C*   ON CIRCUIT THEORY VOL CT-18 NO. 1 JANUARY 1971 P. 40-50 *
759 C* *
760 C*****
761 COMMON /SORT/IORDER(201),NODE(201),IUR(201),IUC(1613),NUMOFF(201),
762 2ITA(201)
763 DIMENSION II(1),J(1)
764 IUR(1)=1
765 ITA(1)=1
766 DO 10 I=1,N
767 IP1=I+1
768 IUR(IP1)=IUR(I)+NUMOFF(I)
769 10 ITA(IP1)=IUR(IP1)
770 IF(IUR(N+1).GT.1613)WRITE(0,12)IUR(N+1)
771 12 FORMAT(20H0ARRAY IUC OVERRUN IN EXPAND/1X,I5,1X,14HCELLS REQUIRED)
772 NM1=N-1
773 DO 30 I=1,NM1
774 JFST=II(I)
775 JLST=II(I+1)-1
776 IF(JFST.GT.JLST)GO TO 30
777 ISUB=ITA(I)
778 DO 20 JC=JFST,JLST
779 JJC=J(JC)
780 IUC(ISUB)=JJC
781 JSUB=ITA(JJC)
782 IUC(JSUB)=I
783 JSUB=JSUB+1
784 20 ITA(JJC)=ITA(JJC)+1
785 30 CONTINUE
786 RETURN
787 END
788 SUBROUTINE ORDER(II,JJ,N)
789 C*****
790 C*
791 C* PURPOSE *
792 C* DETERMINES A REORDERING OF THE UNKNOWN IN A SPARSE *
793 C* MATRIX EQUATION SUCH THAT THE NUMBER OF NON-ZERO TERMS *
794 C* CREATED BY AN L-U TYPE DECOMPOSITION IS REDUCED. THE *
795 C* SPARSE MATRIX MUST HAVE A SYMMETRIC STRUCTURE, I.E. IF *
796 C* C(I,J) .NE. 0 THEN C(J,I) .NE. 0 IT IS NOT NECESSARY *
797 C* THAT C(I,J)=C(J,I) *
798 C*
799 C* USAGE *
800 C* CALL ORDER(II,J,N)

```

```

801 C*
802 C*      DESCRIPTION OF PAKAMETERS
803 C*      II      -
804 C*      II      - - ARRAY CONTAINING THE STARTING INDICES FOR THE
805 C*                      ROWS OF THE UPPER TRIANGLE OF THE REORDERED
806 C*                      MATRIX ON EXIT. II(J)=K IMPLIES THAT J(K)
807 C*                      AND U(K) CONTAIN THE COLUMN INDEX AND VALUE
808 C*                      RESPECTIVELY OF THE FIRST OFF DIAGONAL TERM
809 C*                      IN ROW J OF THE UPPER TRIANGLE
810 C*      J      - ARRAY CONTAINING THE COLUMN INDICES OF THE
811 C*                      UPPER TRIANGLE OF THE REORDERED MATRIX ON
812 C*                      EXIT
813 C*      N      - THE NUMBER OF ROWS (COLUMNS) IN THE MATRIX
814 C*      IORDER  - ARRAY CONTAINING THE ORIGINAL INDICES OF THE
815 C*                      UNKNOWN IN THE REORDERED SEQUENCE. IORDER(I)
816 C*                      MUST EQUAL I ON ENTRY
817 C*      NODE    - ARRAY COMPLIMENTARY TO IORDER; IF IORDER(J)=K
818 C*                      THEN NODE(K)=J NODE(I) MUST EQUAL I ON ENTRY
819 C*      IUR      - SAME AS II BUT FOR THE FULL MATRIX, NOT JUST
820 C*                      THE UPPER TRIANGLE (DESTROYED)
821 C*      IUC      - SAME AS J BUT FOR THE FULL MATRIX (DESTROYED)
822 C*      NUMOFF   - ARRAY CONTAINING THE NUMBER OF OFF DIAGONAL
823 C*                      TERMS IN EACH ROW OF THE ORIGINAL FULL MATRIX
824 C*                      ON ENTRY (DESTROYED)
825 C*      ITA      - WORK ARRAY USED BY THE ROUTINE
826 C*
827 C*      REMARKS
828 C*      ALL ARRAYS IN COMMON EXCEPT ITA MUST BE INITIALIZED
829 C*      BEFORE ENTRY. THE ACTUAL VALUES OF THE MATRIX ELEMENTS ARE
830 C*      NOT USED BY THIS ROUTINE. THE DIAGONAL ELEMENTS AND THE
831 C*      OFF DIAGONAL ELEMENTS ARE STORED IN SEPARATE ARRAYS WITH
832 C*      THE OFF DIAGONAL ELEMENTS INDEXED BY II AND J. IUR(N+1)
833 C*      MUST BE DEFINED BEFORE ENTRY
834 C*
835 C*      SUBROUTINES AND FUNCTION SUBPROGRAMS REQUIRED
836 C*      RENMBR, INSERT
837 C*
838 C*      REFERENCES
839 C*      BERRY, R. D. "AN OPTIMAL ORDERING OF ELECTRONIC CIRCUIT
840 C*      EQUATIONS FOR A SPARSE MATRIX SOLUTION" IEEE TRANSACTIONS
841 C*      ON CIRCUIT THEORY VOL CT-18 NO. 1 JANUARY 1971 P. 40-50
842 C*
843 C*****
844 C      COMMON /SORT/IORDER(201),NODE(201),IUR(201),IUC(1613),NUMOFF(201),
845 C      2ITA(201)
846 C      DIMENSION IFILL(201),II(1),JJ(1)
847 C      ASSIGN 150 TO IRTN
848 C*****
849 C*
850 C*      BEGIN PART I

```



```

851 C*      PICK UP ROWS WITH ZERO OR ONE OFF DIAGONAL TERM      *
852 C*      *
853 C*****
854      LOAD=1
855      DO 10 I=1,N
856      IR=IORDER(I)
857      IF (NUMOFF(IR).LE.1)CALL RENMBR(IR,LOAD,N,IRTN)
858      10 CONTINUE
859 C*****
860 C*
861 C*      END OF PART I BEGIN PART II
862 C*      PICK UP ROWS WHICH WILL NOT INCREASE THE NUMBER OF
863 C*      OFF DIAGONAL TERMS
864 C*
865 C*****
866      INSRTS=0
867      11 LOADED=0
868      IRO=LOAD
869      12 IR=IORDER(IRO)
870      IFILL(IRO)=0
871      ICS=IUR(IR+1)-1
872      ICT=IUR(IR)
873      NUM=0
874      15 IC=IUC(ICT)
875      IF (NODE(IC).LT.LOAD)GO TO 20
876      NUM=NUM+1
877      ITA(NUM)=IC
878      20 ICT=ICT+1
879      IF (ICT.LE.ICS)GO TO 15
880      I=1
881      25 J=I+1
882      IF (J.GT.NUM)GO TO 65
883      30 IRT=ITA(J)
884      IC=ITA(J)
885      ICS=IUR(IR+1)-1
886      ICT=IUR(IR)
887      40 IF (IC.EQ.IUC(ICT))GO TO 50
888      ICT=ICT+1
889      IF (ICT.LE.ICS)GO TO 40
890      IFILL(IRO)=IFILL(IRO)+1
891      IF (INSRTS.EQ.1)CALL INSERT(IRT,IC,N)
892      50 IF (J.EQ.NUM)GO TO 60
893      J=J+1
894      GO TO 30
895      60 I=I+1
896      GO TO 25
897      65 IF (INSRTS.NE.1)GO TO 70
898      CALL RENMBR(IR,LOAD,N,IRTN)
899      INSRTS=0
900      GO TO 11

```

```

901      70 IF(IFILL(IRO).NE.0)GO TO 75
902      LOADED=1
903      CALL RENMBR(IR,LOAD,N,IRTN)
904      75 IRO=IRO+1
905      IF(IRO.LE.N)GO TO 12
906      IF(LOADED.NE.0)GO TO 11
907 C*****
908 C*
909 C*      END PART II BEGIN PART III
910 C*      PICK UP ROW WHICH WILL ADD THE FEWEST NON-ZERO OFF DIAGONAL
911 C*      TERMS
912 C*
913 C*****
914      J=LOAD
915      80 ITEST=IORDER(J)
916      K=J+1
917      90 IF(IFILL(K).GE.IFILL(J))GO TO 100
918      IR=IORDER(K)
919      IORDER(K)=ITEST
920      IORDER(J)=IR
921      NODE(IR)=J
922      NODE(ITEST)=K
923      ITEST=IR
924      IR=IFILL(K)
925      IFILL(K)=IFILL(J)
926      IFILL(J)=IR
927      100 K=K+1
928      IF(K.LE.N)GO TO 90
929      IF(IFILL(LOAD).NE.IFILL(J))GO TO 110
930      J=J+1
931      IF(J.LT.N)GO TO 80
932      110 KE=J-1
933      ITEST=IORDER(LOAD)
934      K=LOAD+1
935      120 IF(K.LE.KE)GO TO 130
936      INSRTS=1
937      GO TO 11
938      130 IK=IORDER(K)
939      IF(NUMOFF(IR).LE.NUMOFF(ITEST))GO TO 140
940      IORDER(K)=ITEST
941      IORDER(LOAD)=IR
942      NODE(IR)=LOAD
943      NODE(ITEST)=K
944      ITEST=IR
945      140 K=K+1
946      GO TO 120
947 C*****
948 C*
949 C*      END PART III
950 C*      REORGANIZE POINTER ARRAYS

```

```

951 C*
952 C*****
953   150 I=1
954     IF(IUR(N+1).GT.1613)WRITE(0,152)IUR(N+1)
955   152 FORMAT(27HLCARRAY IUC OVERRUN IN ORDER/1X,15,15H CELLS REQUIRED)
956     DO 170 LOAD=1,N
957       II(LOAD)=I
958       IR=IORDER(LOAD)
959       ICS=IUR(IR+1)-1
960       ICT=IUR(IR)
961       IF(ICT.GT.ICS)GO TO 170
962       DO 165 IC=ICT,ICS
963         IUCIC=IUC(IC)
964         IF(IC.EQ.ICS)GO TO 162
965         ICP1=IC+1
966         DO 160 JC=ICP1,ICS
967           IUCJC=IUC(JC)
968           IF(NODE(IUCIC).LE.NODE(IUCJC))GO TO 160
969           IUC(IC)=IUCJC
970           IUC(JC)=IUCIC
971           IUCIC=IUCJC
972   160 CONTINUE
973   162 IF(NODE(IUCIC).LT.LOAD)GO TO 165
974       JU(I)=NODE(IUCIC)
975       I=I+1
976   165 CONTINUE
977   170 CONTINUE
978     RETURN
979     END
980     SUBROUTINE RENMBR(IR,LOAD,N,IRIN)
981 C*****
982 C*
983 C*   PURPOSE
984 C*     TO RENUMBER ONE UNKNOWN AND UPDATE THE INDEXING ARRAYS
985 C*     IUR AND IUC ACCORDINGLY. CALLED FROM SUBROUTINE ORDER
986 C*
987 C*   USAGE
988 C*     CALL RENMBR(IR,LOAD,N,IRIN)
989 C*
990 C*   DESCRIPTION OF PARAMETERS
991 C*     IR      - ORIGINAL INDEX OF THE UNKNOWN
992 C*     LOAD    - THE NEW INDEX TO BE ASSIGNED TO THE UNKNOWN
993 C*     N       - THE NUMBER OF UNKNOWN IN THE SYSTEM OF
994 C*               EQUATIONS
995 C*     IRIN    - ALTERNATE RETURN ADDRESS
996 C*
997 C*   REMARKS
998 C*     ALL ARRAYS IN COMMON ARE THE SAME AS IN SUBROUTINE ORDER
999 C*
1000 C*   REFERENCES

```

```

1001 C*          PERRY, R. D. "AN OPTIMAL ORDERING OF ELECTRONIC CIRCUIT
1002 C*          EQUATIONS FOR A SPARSE MATRIX SOLUTION" IEEE TRANSACTIONS
1003 C*          ON CIRCUIT THEORY VOL CT-18 NO. 1 JANUARY 1971 P. 40-50
1004 C*
1005 C*****
1006          COMMON /SOPT/IORDER(201),NODE(201),IUP(201),IUC(1613),NUMOFF(201),
1007          ZITA(201)
1008          LOADIR=0
1009          NUMFIL=0
1010          10 IF (NODE(IR).LT.LOAD)GO TO 40
1011             ITEMP=IORDER(LOAD)
1012             IROT=NODE(I-1)
1013             IORDER(LOAD)=I
1014             NODE(I)=LOAD
1015             IORDER(IROT)=ITEMP
1016             NODE(ITEMP)=IROT
1017             LOAD=LOAD+1
1018             IF (LOAD.GT.4)RETURN IRTM
1019             ICS=IUP(IR+1)-1
1020             ICT=IUP(IR)
1021             IF (ICT.GT.ICS)GO TO 40
1022             20 IR=IUC(ICT)
1023             IF (NODE(IR).LT.LOAD)GO TO 30
1024             NUMOFF(IR)=NUMOFF(IR)-1
1025             IF (NUMOFF(IR).GT.1)GO TO 30
1026             NUMFIL=NUMFIL+1
1027             ITA(NUMFIL)=IR
1028             30 ICT=ICT+1
1029             IF (ICT.LE.ICS)GO TO 20
1030             40 LOADIR=LOADIR+1
1031             IF (LOADIR.GT.NUMFIL)RETURN
1032             IR=ITA(LOADIR)
1033             GO TO 10
1034          END
1035          SUBROUTINE INSERT(IRT,IC,N)
1036 C*****
1037 C*
1038 C*          PURPOSE
1039 C*          TO INSERT TERMS INTO THE INDEXING ARRAYS IUP AND IUC
1040 C*          WHICH REFER TO NON-ZERO OFF DIAGONAL TERMS WHICH WILL BE
1041 C*          CREATED BY AN L-U DECOMPOSITION.
1042 C*          CALLED FROM SUBROUTINE UNDER
1043 C*
1044 C*          USAGE
1045 C*          CALL INSERT(IRT,IC,N)
1046 C*
1047 C*          DESCRIPTION OF PARAMETERS
1048 C*          IRT      - THE INDEX OF THE ROW INTO WHICH THE TERMS ARE
1049 C*                   TO BE INSERTED
1050 C*          IC       - THE COLUMN INDEX WHICH IS TO BE INSERTED

```

```

1051 C*          N          - THE NUMBER OF UNKNOWN IN THE SYSTEM OF
1052 C*                      EQUATIONS
1053 C*
1054 C*          REMARKS
1055 C*          ALL ARRAYS IN COMMON ARE THE SAME AS IN SUBROUTINE ORDER
1056 C*
1057 C*          REFERENCES
1058 C*          HERRY, R. D. "AN OPTIMAL ORDERING OF ELECTRONIC CIRCUIT
1059 C*          EQUATIONS FOR A SPARSE MATRIX SOLUTION" IEEE TRANSACTIONS
1060 C*          ON CIRCUIT THEORY VOL CT-18 NO. 1 JANUARY 1971 P. 40-50
1061 C*
1062 C*****
1063 C*          COMMON /SOL1/ IORDER(201), ILOFF(201), IUR(201), IUC(1613), NUMOFF(201),
1064 C*          ZIFA(201)
1065 C*          IDOWN=IUR(N+1)-IUR(IRT+1)
1066 C*          I=0
1067 C*          10 L=L+1
1068 C*             K=IUR(N+1)-L
1069 C*             IUC(K+1)=IUC(K)
1070 C*             IF(L.LT.IDOWN)GO TO 10
1071 C*             NUMOFF(IRT)=NUMOFF(IRT)+1
1072 C*             IUC(K)=IC
1073 C*             I=IRT
1074 C*             20 L=L+1
1075 C*                IUR(L)=IUR(L)+1
1076 C*                IF(L.LE.N)GO TO 20
1077 C*                IDOWN=IUR(N+1)-IUR(IC+1)
1078 C*                I=0
1079 C*                30 L=L+1
1080 C*                   K=IUR(N+1)-L
1081 C*                   IUC(K+1)=IUC(K)
1082 C*                   IF(L.LT.IDOWN)GO TO 30
1083 C*                   NUMOFF(IC)=NUMOFF(IC)+1
1084 C*                   IUC(K)=IRT
1085 C*                   L=IC
1086 C*                   40 L=L+1
1087 C*                      IUR(L)=IUR(L)+1
1088 C*                      IF(L.LE.N)GO TO 40
1089 C*                      RETURN
1090 C*                      END
1091 C*          SUBROUTINE SPSOT1(I,U,II,J,N)
1092 C*****
1093 C*
1094 C*          PURPOSE
1095 C*          TO TRANSFORM A SYMMETRIC SPARSE MATRIX INTO A SPARSE
1096 C*          AUXILIARY MATRIX (IMPLICIT INVERSE)
1097 C*
1098 C*          USAGE
1099 C*          CALL SPSOT1(I,U,II,J,N)
1100 C*

```

```

1101 C*      DESCRIPTION OF PARAMETERS
1102 C*      U      - ARRAY CONTAINING THE DIAGONAL OF THE ORIGINAL
1103 C*                MATRIX ON ENTRY AND THE DIAGONAL OF THE
1104 C*                AUXILIARY MATRIX ON EXIT
1105 C*      U      - ARRAY CONTAINING THE NON-ZERO OFF DIAGONAL
1106 C*                TERMS OF THE UPPER TRIANGLE OF THE ORIGINAL
1107 C*                MATRIX PLUS SPACE FOR NON-ZERO OFF DIAGONAL
1108 C*                TERMS CREATED BY THIS ROUTINE ON ENTRY AND THE
1109 C*                NON-ZERO OFF DIAGONAL TERMS OF THE UPPER
1110 C*                TRIANGLE OF THE AUXILIARY MATRIX ON EXIT
1111 C*      II     - ARRAY CONTAINING THE STARTING INDICES IN U AND
1112 C*                U OF TERMS ASSOCIATED WITH EACH ROW OF BOTH
1113 C*                MATRICES
1114 C*      J      - ARRAY CONTAINING THE COLUMN INDICES OF
1115 C*                CORRESPONDING TERMS IN U
1116 C*      N      - THE NUMBER OF ROWS (COLUMNS) IN THE MATRIX
1117 C*
1118 C*      REMARKS
1119 C*      THE NON-ZERO OFF DIAGONAL ELEMENTS OF THE UPPER TRIANGLE
1120 C*      ARE STORED BY ROWS. SUBROUTINE ORDER SHOULD BE CALLED
1121 C*      BEFORE ENTRY TO IMPROVE THE ORDERING OF THE ELEMENTS
1122 C*      AND TO RESERVE SPACE FOR ELEMENTS CREATED BY THIS ROUTINE
1123 C*
1124 C*      METHOD
1125 C*      "SQUARE ROOT" DECOMPOSITION OF A SYMMETRIC MATRIX
1126 C*
1127 C*      REFERENCES
1128 C*      BEKRY, R. D. "AN OPTIMAL ORDERING OF ELECTRONIC CIRCUIT
1129 C*      EQUATIONS FOR A SPARSE MATRIX SOLUTION" IEEE TRANSACTIONS
1130 C*      ON CIRCUIT THEORY VOL CT-18 NO. 1 JANUARY 1971 P. 40-50
1131 C*      FADDEEV, D. K. AND FADDEEVA, V. N., COMPUTATIONAL
1132 C*      METHODS OF LINEAR ALGEBRA, W. H. FREEMAN AND CO., SAN
1133 C*      FRANCISCO, 1963, P. 144-147
1134 C*
1135 C*****
1136 C      COMPLEX U(1),U(1)
1137 C      DIMENSION II(1),J(1)
1138 C      N=1=N-1
1139 C      DO 100 I=1,NM1
1140 C      JMIN=II(1)
1141 C      JMAX=II(1+1)-1
1142 C      C(1)=CSORT(U(1))
1143 C      IF(JMIN.GT.JMAX)GO TO 100
1144 C      DO 10 K=JMIN,JMAX
1145 C 10  U(K)=U(K)/C(1)
1146 C      DO 30 K=JMIN,JMAX
1147 C      JJ=J(K)
1148 C      C(JJ)=C(JJ)-U(K)*U(K)
1149 C      LMIN=K+1
1150 C      IF(LMIN.GT.JMAX)GO TO 100

```



```

1151      M=II(JJ)-1
1152      PLST=II(JJ+1)-1
1153      DO 30 L=PLST,JMAX
1154      20 M=M+1
1155      IF (M.GT.PLST)WRITE(0,15)
1156      15 FORMAT(16H0ERROR IN SPSOT1//)
1157      IF (J(N).NE.U(L))GO TO 20
1158      30 U(M)=U(N)-U(L)+U(L)
1159      100 CONTINUE
1160      C(N)=CSQR1(C(N))
1161      RETURN
1162      END
1163      SUBROUTINE SPSOT2(D,U,S,II,J,N)
1164      C*****
1165      C*
1166      C*      PURPOSE
1167      C*      TO OBTAIN A SOLUTION TO THE SYMMETRIC SPARSE MATRIX
1168      C*      EQUATION MAYE USING THE AUXILIARY MATRIX CALCULATED BY
1169      C*      SPSM11
1170      C*
1171      C*      USAGE
1172      C*      CALL SPSOT2(D,U,S,II,J,N)
1173      C*
1174      C*      DESCRIPTION OF PARAMETERS
1175      C*      D      - ARRAY CONTAINING THE DIAGONAL OF THE
1176      C*      AUXILIARY MATRIX
1177      C*      U      - ARRAY CONTAINING THE NON-ZERO OFF DIAGONAL
1178      C*      TERMS OF THE UPPER TRIANGLE OF THE AUXILIARY
1179      C*      MATRIX STORED BY ROWS
1180      C*      S      - ARRAY CONTAINING THE RIGHT HAND SIDE VECTOR
1181      C*      Y ON ENTRY AND THE SOLUTION VECTOR X ON EXIT
1182      C*      II     - ARRAY CONTAINING THE STARTING INDICES IN J AND
1183      C*      U OF TERMS ASSOCIATED WITH EACH ROW OF THE
1184      C*      AUXILIARY MATRIX
1185      C*      J      - ARRAY CONTAINING THE COLUMN INDICES OF
1186      C*      CORRESPONDING TERMS IN U
1187      C*
1188      C*      METHOD
1189      C*      "SQUARE ROOT" DECOMPOSITION OF A SYMMETRIC MATRIX
1190      C*
1191      C*      REFERENCES
1192      C*      BERRY, R. D. "AN OPTIMAL ORDERING OF ELECTRONIC CIRCUIT
1193      C*      EQUATIONS FOR A SPARSE MATRIX SOLUTION" IEEE TRANSACTIONS
1194      C*      ON CIRCUIT THEORY VOL CT-18 NO. 1 JANUARY 1971 P. 40-50
1195      C*      FADDEEV, D. K. AND FADDEEVA, V. N., COMPUTATIONAL
1196      C*      METHODS OF LINEAR ALGEBRA, W. H. FREEMAN AND CO., SAN
1197      C*      FRANCISCO, 1963, P. 144-147
1198      C*
1199      C*****
1200      COMPLEX D(1),U(1),S(1)

```

```

1201      DIMENSION I(1),J(1)
1202      NM1=N-1
1203      DO 35 I=1,NM1
1204          JMIN=I(1)
1205          JMAX=I(I+1)-1
1206          S(I)=S(I)/I(1)
1207          IF (JMIN.GT.JMAX)GO TO 35
1208          DO 30 K=JMIN,JMAX
1209              JJ=J(K)
1210          30 S(JJ)=S(JJ)-S(I)*U(K)
1211          35 CONTINUE
1212          S(N)=S(N)/(L(N)*D(N))
1213          DO 45 K=1,NM1
1214              L=N-K
1215              JMIN=I(L)
1216              JMAX=I(L+1)-1
1217              IF (JMIN.GT.JMAX)GO TO 45
1218              DO 40 M=JMIN,JMAX
1219                  IC=J(M)
1220          40 S(L)=S(L)-U(M)*S(IC)
1221          45 S(L)=S(L)/D(L)
1222      RETURN
1223      END
1224      SUBROUTINE RANDU(IX,IY,YEL)
1225      C*****
1226      C*
1227      C*      PURPOSE
1228      C*      COMPUTES UNIFORMLY DISTRIBUTED RANDOM REAL NUMBERS BETWEEN
1229      C*      0.0 AND 1.0 AND RANDOM INTEGERS BETWEEN ZERO AND
1230      C*      2**23. EACH ENTRY USES AS INPUT AN INTEGER RANDOM NUMBER
1231      C*      AND PRODUCES A NEW INTEGER AND REAL RANDOM NUMBER.
1232      C*
1233      C*      USAGE
1234      C*      CALL RANDU(IX,IY,YEL)
1235      C*
1236      C*      DESCRIPTION OF PARAMETERS
1237      C*      IX - FOR THE FIRST ENTRY IT MUST CONTAIN ANY ODD INTEGER
1238      C*      NUMBER WITH SEVEN OR LESS DIGITS. AFTER THE FIRST
1239      C*      ENTRY, IX SHOULD BE THE PREVIOUS VALUE OF IY COMPUTED
1240      C*      BY THIS SUBROUTINE.
1241      C*      IY - A RESULTANT INTEGER RANDOM NUMBER REQUIRED FOR THE
1242      C*      NEXT ENTRY TO THIS SUBROUTINE. THE RANGE OF THIS
1243      C*      NUMBER IS BETWEEN ZERO AND 2**23.
1244      C*      YEL- THE RESULTANT UNIFORMLY DISTRIBUTED, FLOATING POINT,
1245      C*      RANDOM NUMBER IN THE RANGE 0.0 TO 1.0.
1246      C*
1247      C*      REMARKS
1248      C*      THIS SUBROUTINE IS SPECIFIC TO THE DATACRAFT 6024.
1249      C*      16645=2**14+2**6+2**2+1=5 MOD 8
1250      C*      4306607=2**23-1 IS THE LARGEST INTEGER THE DC 6024

```

```

1251 C*      CAN STORE
1252 C*      0.1192094E-6=1.0/8368607
1253 C*
1254 C*      REFERENCES
1255 C*      SYSTEM/360 SCIENTIFIC SUBROUTINE PACKAGE P. 77
1256 C*      MALLAREN AND MARSAGLIA, JACM 12, P. 83-89
1257 C*
1258 C*      *****
1259 C*      IY=IX*16645
1260 C*      IF(IY)5,6,6
1261 C*      5 IY=IY+8368607+1
1262 C*      6 YFL=IY
1263 C*      YFL=YFL*.1192094E-6
1264 C*      RETURN
1265 C*      END
1266 C*      SUBROUTINE GAUSS(IY,S,AM,V)
1267 C*      *****
1268 C*
1269 C*      PURPOSE
1270 C*      COMPUTES A NORMALLY DISTRIBUTED RANDOM NUMBER WITH A GIVEN
1271 C*      MEAN AND STANDARD DEVIATION.
1272 C*
1273 C*      USAGE
1274 C*      CALL GAUSS(IY,S,AM,V)
1275 C*
1276 C*      DESCRIPTION OF PARAMETERS
1277 C*      IX - IX MUST CONTAIN AN ODD INTEGER NUMBER WITH SEVEN OR
1278 C*      LESS DIGITS ON THE FIRST ENTRY TO GAUSS. THEREAFTER
1279 C*      IT WILL CONTAIN A UNIFORMLY DISTRIBUTED INTEGER RANDOM
1280 C*      NUMBER GENERATED BY THE SUBROUTINE FOR USE ON THE NEXT
1281 C*      ENTRY TO THE SUBROUTINE.
1282 C*      S - THE DESIRED STANDARD DEVIATION OF THE NORMAL
1283 C*      DISTRIBUTION
1284 C*      AM - THE DESIRED MEAN OF THE NORMAL DISTRIBUTION
1285 C*      V - THE VALUE OF THE COMPUTED NORMAL RANDOM VARIABLE
1286 C*
1287 C*      REMARKS
1288 C*      THIS SUBROUTINE USES RANDU WHICH IS MACHINE SPECIFIC
1289 C*
1290 C*      SUBROUTINES AND FUNCTION SUBPROGRAMS REQUIRED
1291 C*      RANDU
1292 C*
1293 C*      METHOD
1294 C*      USES 12 UNIFORM RANDOM NUMBERS TO COMPUTE NORMAL RANDOM
1295 C*      NUMBERS BY THE CENTRAL LIMIT THEOREM. THE RESULT IS THEN
1296 C*      ADJUSTED TO MATCH THE GIVEN MEAN AND STANDARD DEVIATION.
1297 C*      THE UNIFORM RANDOM NUMBERS COMPUTED WITHIN THE SUBROUTINE
1298 C*      ARE FOUND BY THE POKER RESIDUE METHOD.
1299 C*
1300 C*      REFERENCES

```

```

*GAUSS000
*GAUSS001
*GAUSS002
*GAUSS003
*GAUSS004
*GAUSS005
*GAUSS006
*GAUSS007
*GAUSS008
*GAUSS009
*GAUSS010
*GAUSS011
*GAUSS012
*GAUSS013
*GAUSS014
*GAUSS015
*GAUSS016
*GAUSS017
*GAUSS018
*GAUSS019
*GAUSS020
*GAUSS021
*GAUSS022
*GAUSS023
*GAUSS024
*GAUSS025
*GAUSS026
*GAUSS027
*GAUSS028
*GAUSS029
*GAUSS030
*GAUSS031
*GAUSS032
*GAUSS033
*GAUSS034

```



1301	C*	SYSTEM/360 SCIENTIFIC SUBROUTINE PACKAGE P. 77	*GAUSS0035
1302	C*****		*GAUSS0036
1303		A=0.0	GAUSS0037
1304		DO 50 I=1,12	GAUSS0038
1305		CALL RANDU(IX,JY,Y)	GAUSS0039
1306		TX=IY	GAUSS0040
1307	50	A=A+Y	GAUSS0041
1308		V=(A-5.0)*S+AM	GAUSS0042
1309		RETURN	GAUSS0043
1310		END	GAUSS0044

## APPENDIX F ITERATION COMPUTER PROGRAM (SOR)

### A. Far Zone Mutual Impedance Between Moderate and Distantly Separated Sinusoidal Dipoles

Calculation time for filling in mutual impedance elements of A has been improved considerably using a far zone approximation for mutuals between general skew dipoles for dipole spacing  $\geq 1\lambda$ . Figure VI-1 shows the complete bistatic pattern for a 100 dipole array ( $8 \text{ dip}/\lambda^3$ ) using impedance calculations with two criteria for the far zone approximation;  $\geq 1\lambda$ ,  $\geq 1.5\lambda$ . Also included is the pattern obtained without using the far zone approximations (exact). Agreement is quite good over these patterns and Table VI-1 gives additional data on backscatter,  $360^\circ$  bistatic average and computation times for this same array using the various methods including sparsed matrix solution using the 10% rule. Figure VI-2 compares bistatic patterns for the full and sparsed matrix calculations. The 10% rule resulted in approximately 90% zeroes in the A matrix. Calculations using the far zone approximation for  $N = 1000$  resulted in an order of magnitude (1/10) savings in time to compute A. The predicted time without the approximation was 10-12 hours, whereas the actual time using far zone mutuals was  $\sim 1$  hour. Any errors that occur, due to this far zone approximation, are not likely to affect the scattering and scintillation statistics.

These simplified mutual impedances are computed based on the far zone electric fields of the two sinusoidal dipoles. Consider dipole #1 located in Fig. VI-3a to have far zone electric field given by

$$(VI-1) \quad E(r, \theta, \phi) \simeq - \frac{j k_0^2 n_0}{4\pi} \left\{ \frac{e^{-jk_0 r}}{k_0 r} \left( 1 - \frac{j}{k_0 r} - \frac{1}{k_0^2 r^2} \right) \right. \\ \left. F_1(\theta_1, \phi_1) + 2j \frac{e^{-jk_0 r}}{k_0^2 r^2} \left( 1 - \frac{j}{k_0 r} \right) \right. \\ \left. G_1(\theta_1, \phi_1) \hat{r} \right\}$$

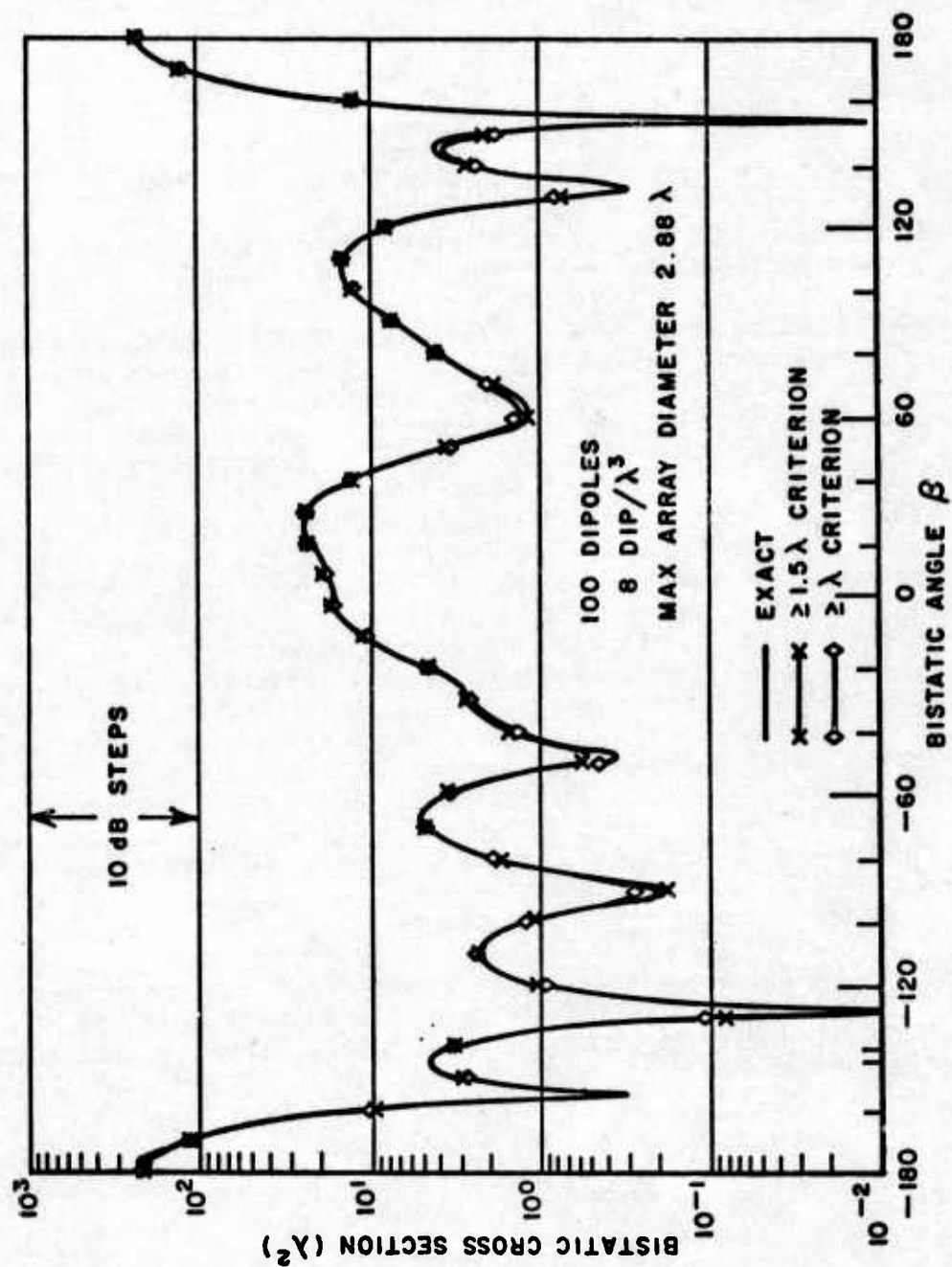


Figure VI-1. Bistatic scatter cross section for 100 dipole array ( $8 \text{ dip}/\lambda^3$ ) comparing exact and far zone A matrix calculations.



TABLE VI-1

DATA COMPARISON FOR DIFFERENT MUTUAL IMPEDANCE  
CALCULATIONS FOR 100 DIPOLE ARRAY (8 dip/ $\lambda^3$ ).

All cross section results obtained using CROUT type (SQROT) solutions.

Calculations	Backscatter $\sigma$	360° Bistatic Average	Computation Time for Z
Far Zone* $\geq 1\lambda$	$16.4\lambda^2$	$21.3\lambda^2$	88 sec
Far Zone* $\geq 1.5\lambda$	16.6	21.5	167
Exact**	16.4	21.4	607
Sparsed*** (10%)	9.07	26.4	607

\* Mutuals between dipoles spaced  $\geq 1\lambda$  ( $1.5\lambda$ ) computed using far zone approximation.

\*\* Mutuals between all dipoles computed using closed form expressions of Richmond (ESL Tech Report #2708-4, 1969).

\*\*\* Mutuals falling below 10% of diagonal ( $a_{ij}$ ) are set to zero.

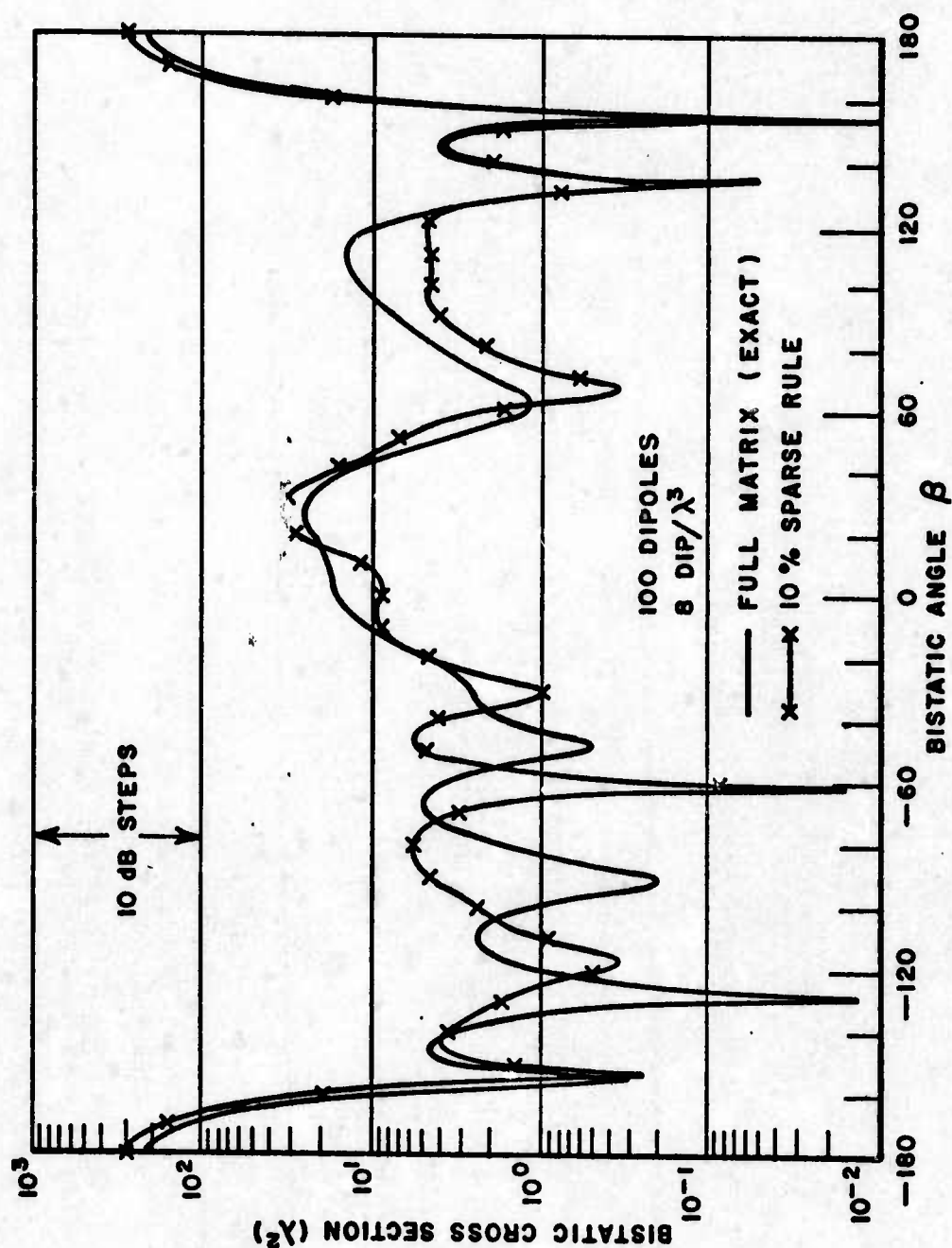


Figure VI-2. Bistatic scatter cross section for 100 dipole array ( $8 \text{ dip}/\lambda^3$ ) comparing full (exact) A matrix and sparse A matrix using 10% sparsing rule, i.e.,  $a_{ij} = 0$  if  $|a_{ij}| < .1 |a_{11}|$ ,  $i = 1, 2, \dots, N$ .

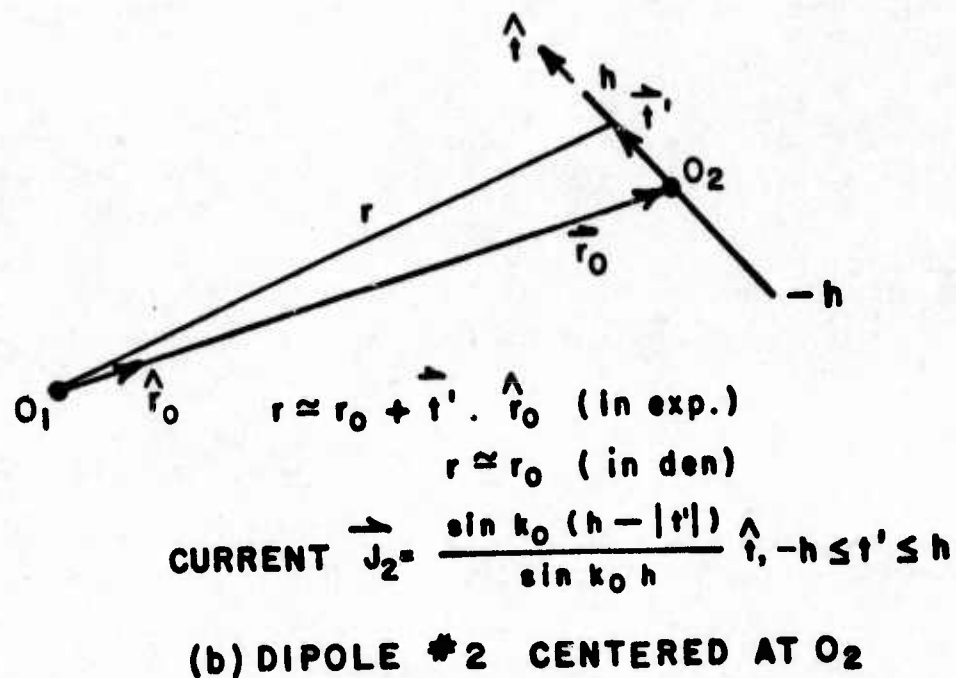
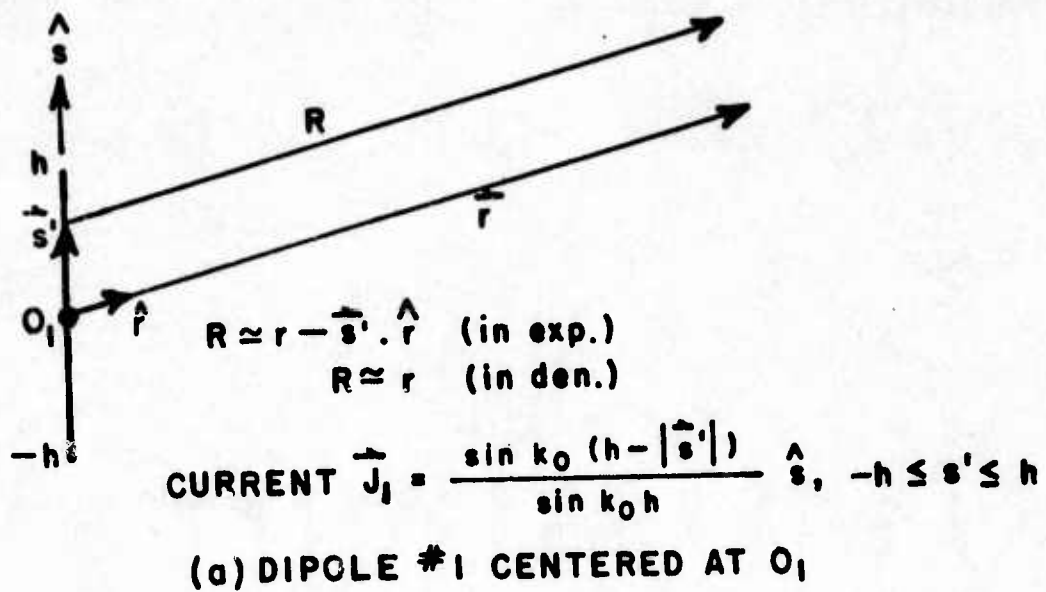


Figure VI-3. Sinusoidal dipoles and far zone approximations.

where the field pattern functions are given by the usual radiation integrals, i.e.,

$$(VI-2) \quad F_1(\theta, \phi) = \int_1 [\mathbf{J}_1 - (\hat{\mathbf{r}} \cdot \mathbf{J}_1) \hat{\mathbf{r}}] e^{jk_0 \bar{\mathbf{s}}' \cdot \hat{\mathbf{r}}} ds'$$

and

$$(VI-3) \quad G_1(\theta, \phi) = \int_1 (\hat{\mathbf{r}} \cdot \mathbf{J}_1) e^{jk_0 \bar{\mathbf{s}}' \cdot \hat{\mathbf{r}}} ds'.$$

Recall from Chapter II the mutual impedance between two dipoles is defined by the following formula,

$$(VI-4) \quad a_{12} = - \int_2 \mathbf{J}_2 \cdot \mathbf{E}_1 dt'.$$

Consider dipole #2 in Fig. VI-3(b) to be located by  $\bar{\mathbf{r}}_0$  with respect to  $O_1$ . Then, for moderate to large  $r_0$ , Eq. (H-4) simplifies to

$$(VI-5) \quad a_{12} \approx \frac{j k_0^2 \eta_0}{4\pi} \left\{ \frac{e^{-jk_0 r_0}}{k_0 r_0} \left( 1 - \frac{j}{k_0 r_0} - \frac{1}{k_0^2 r_0^2} \right) \right. \\ \left. F_1(\theta_1, \phi_1) \cdot F_2(\theta_2, \phi_2) + 2j \frac{e^{-jk_0 r_0}}{k_0^2 r_0^2} \left( 1 - \frac{j}{k_0 r_0} \right) \right. \\ \left. G_1(\theta_1, \phi_1) G_2(\theta_2, \phi_2) \right\}$$

where pattern functions of dipole #2 are

$$(VI-6) \quad F_2(\theta_2, \phi_2) = \int_2 \mathbf{J}_2 e^{-jk_0 \bar{\mathbf{r}}' \cdot \hat{\mathbf{r}}_0} dt'$$



and

$$(VI-7) \quad G_2(\theta_2, \phi_2) = \hat{r} \cdot \int_2 \bar{J}_2 e^{-jk_0 \bar{r}' \cdot \hat{r}_0} dt'$$

The  $(\theta_1, \phi_1)$  angular variations are measured with respect to origin  $O_1$  (center dipole #1) and similarly, the  $(\theta_2, \phi_2)$  angles are measured with respect to origin  $O_2$  (center dipole #2).

## B. Computer Programs

Note that the "INCLUDE" statement and "CALL ASSIGN" statement in the following computer programs are special commands implemented on the ESL computer. Their functions are explained in the following paragraphs.

Nine logical unit numbers (0-8) are available for use with Fortran. The nine logical unit numbers correspond to nine locations in the I/O device assignment table of the Fortran library I/O system. Before I/O operations can proceed each device or disk file to be used by a Fortran program must either have been assigned to a logical unit number by the user's program or have been assigned by default. The device assignment table is initialized to the default assignments according to the table. Logical unit numbers are referenced in READ and WRITE statements, to specify the device or file on which the read or write operation is to be performed.

Examples:

```
READ (8,-)x,y,z  
WRITE(0)(a(i),i=1,100)  
WRITE(6,40)a2,zL3
```

Assuming the default assignments are used the first example specifies that three variables, x,y, and z be read from the terminal keyboard in free format. When input from the terminal keyboard is specified the terminal bell is rung to indicate that the READ statement has been executed and the user is expected to supply the input data. The input data should be followed by a carriage return. In the second example the WRITE statement specifies that 100 words be written unformatted (binary format) on the magnetic tape unit 0. The WRITE statement of the third example specifies that formatted output be performed to the temporary output file named .OUT.

Any of the system I/O devices with the exception of the card reader (.CDR) and the line printer (.LPT), or any named disk file can be assigned to any logical unit number from 0 to 7 by means of an OPEN statement or a CALL ASSIGN statement. The user's terminal is permanently assigned to logical unit 8 and cannot be altered by the Fortran program. Logical unit 8 is unavailable for assignment. The format for CALL ASSIGN is:

```
CALL ASSIGN(FILE,USER,LU,$N)
```

where, FILE is a literal constant of from one to six characters (see "Literal Constants" section 2-3 of the Fortran manual) or a floating point variable name or an array name containing a one to six character file or device name. USER is a literal constant of from one to six characters in length, a floating point variable name or array name containing a one to six character user name or floating point zero (0.0). LU is a logical unit number from 0 through 7. N is an optional Fortran statement label number. FILE and USER, if less than six characters, must be filled with trailing spaces to make six characters. If the names are four or more characters in length this is done automatically. If not the names should be extended to be at least four characters in length by adding trailing spaces.



If the array or floating point variable is used for a name, data may be assigned to it using a READ statement with an A format or by means of a literal constant in a DATA statement. If floating point zero is used as the USER calling parameter the user name under which the program is being executed is assumed. If the FILE calling parameter specifies the name of a non-disk device the USER parameter is not used but must be present. A floating point zero may be used. Devices .LPT and .CDR are not available for assignment. The function of the CALL ASSIGN statement is to cause the specified name (file and user) to be placed in the Fortran library I/O device assignment table in the location corresponding to the specified logical unit number thereby assigning that name to the logical unit number. If the file or device which was previously assigned as the specified logical unit has been engaged in I/O activity and has not been closed it will be automatically closed by call assign before a new assignment is made. If the parameter \$N is present, control will be returned to the statement having the label N if an error occurs. An error will be indicated if a non-disk device has been reserved by another user (i.e., the device is busy).

Default logical unit assignments		
Logical Unit	Device Number	Description Assignment
0	.MTO	magnetic tape drive 0
1	.DSK	temporary (disk) scratch file
2	.MT1	magnetic tape drive 1
3	.LU3	temporary (disk) scratch file
4	.LU4	temporary (disk) scratch file
5	.IN	temporary disk input file
6	.OUT	temporary disk output file
7	.LU7	temporary (disk) scratch file
8	terminal only -- not reassignable	

The INCLUDE statement provides the user with a means of specifying, as part of a Fortran program, that one or more binary object files be loaded along with the program containing the include statement during thyload operation. The INCLUDE statement is used primarily to load subroutines called by Fortran programs or subprograms but not contained in either of the Fortran libraries.

Use of the INCLUDE statement provides the following benefits:

- 1) Frequently used subroutines (not contained in the Fortran libraries) need not be edited in source language form into each program which calls them. This saves both editing time and file space. File space is conserved because only one compiled binary object version of a subroutine need be kept in the file system even though several programs may call it.
- 2) Useful subprograms may be easily shared among a number of users since any file in any user's directory may be specified in an INCLUDE statement.

3) A subroutine which is used by many programs may be altered and recompiled without necessitating the recompilation of any of the calling program. (This, of course, also holds for a single calling program).

The format for the INCLUDE statement is:

INCLUDE NAME1,USER1; NAME2,USER2;...;NAMEN,USERN

(1) File Name: TESBGF, SYSAC

Main Program TESBGF computes and stores elements of impedance matrix (A) and sets up SOI submatrices. Include statements (lines 5-7) are as follows:

PAPER, SYSAC	CALL PAPER advances output paper on LU-6 with 1H1 format.
ZGS, SYSAC	subroutine used by ZSKEWF subroutine
CLDB, SYSAC	SUBROUTINE UNICLD
ADEXB, SYSAC	contains LDG load-go-execute subroutine
STGETB, SYSAC	contains SUBROUTINES STOR, CLSTOR and SUBFUNCTION GET
ZSKEWB, SYSAC	SUBROUTINE ZSKEWF

Dimensioned variables:

IJ	integer array denoting $m_i$ for N SOI submatrices
X,Y,Z	coordinates of dipole i
XX,YY,ZZ	coordinates of dipole j
ZR	one row of impedance matrix (A)
XR	one row of impedance matrix separating ZR into real and imaginary parts (See Equivalence statement, line 12.)
ZDIA	diagonal block of impedance matrix - only 1 x 1 for 2 segment model

Assigned files (lines 22-25):

ZZAT	LU 3 contains subscripts of SOI submatrices (Binary format).
ZIND	LU 5 saves iteration method code (0 = J, 1 = SOR, 2 = SOI) and OM (omega) relaxation factor if SOR is used (formatted data).
ZOUT	LU 6 contains error messages (lines 149 or 152) when TESBGF defaults to CALL EXIT or contains bistatic angle, increment and iteration start information (formatted data) for TESBG4.
DATA	LU 1 saves number of dipoles (NOD), number of segments (NOS), array density (DEN), influence coefficient (CF), aspect (TH, PHI), time (IT), max submatrix size (ICK) and max broad-side mode voltage (EBS) (binary format).

Input parameters are as follows:

HAFBIS	one-half bistatic pattern sector (degrees); if <0, bistatic pattern is not computed.
DPHZ	bistatic angle increment (degrees)
ISTART	iteration starting step (k).
NOD	number of dipoles in array
NOS	number of segments per dipole
DEN	density of array ( $\text{dip}/\lambda^3$ )
METH	iteration method code (0 = J, 1 = SOR, 2 = SOI)
OM	relaxation factor (SOR)
CF	influence coefficient (SOI)
TH, PHI	aspect angle in degrees ( $\theta_0, \phi_0$ )

Variable names used:

NOSP	number of coordinate points per dipole
------	--



NOSM	number of modes per dipole
N	total number of modes
AK	dipole radius
HK	dipole half-length
DK	segment length
RS	overall radius of array ( $R_0$ )
IP	random number generator starting number (IBM-SSP RANDU); 7 digit odd number preferable.

Lines 77 through 139 compute positions of array dipoles (UNICLD, lines 80 and 102) and mutual impedances are then computed by ZSKEWF in line 121. Note, RHO is center to center distance between  $i^{th}$  and  $j^{th}$  dipoles and lines 113 to 120 prescribe type of impedance calculation is to be used, e.g.,  $INT < 0$  specifies "far zone" calculations (see Appendix H),  $INT = 0$  requires exact "closed form" integration and  $INT = 4$  chooses Simpson's Rule 4-point integration. Lines 128 to 132 apply SOI influence criterion to generate SOI submatrices. Impedance calculations are only necessary for the upper triangular elements of the impedance matrix (A is symmetric). However, the CALL STOR (line 137) packs and stores full rows of matrix on disk storage. The symmetric lower triangular elements of the A matrix are read into the ZR array (for the  $i^{th}$  row) in lines 89 to 97. SUBFUNCTION GET (line 97) retrieves and unpacks previously stored data from the disk to fill in the  $i^{th}$  row for  $j < i$ . The CALL CLSTOR (line 142) permanently closes all "packed" storage disk files. Once this is done, files can only be read using the GET subfunction contained in binary file GETB,SYSAC found in main program TESBG4,SYSAC. Line 157 automatically executes TESBG4,SYSAC (BIGCO,SYSAC) which solves the system of equations via the prescribed iterative method.

(2) File Name: TESBG1,SYSAC

Main program TESBG1 is identical to TESBGF,SYSAC except it does not use "far zone" calculations for mutual impedances, but instead uses only closed form and Simpson's four point integration.

(3) File Name: TESBG4,SYSAC

Main program TESBG4 solves simultaneous system using either J, SOR or SOI iteration. Compiled (binary) version of TESBG4 must be under file name BIGCO,SYSAC and is executed by either TESBGF, TESBG1 or TESBG5. All input data for TESBG4 are available on disk files ZZAT, ZINP and DATA. Parameters are identical to

definitions given for TESBGF, except for ITE which corresponds to iteration method code (METH).

Assigned files (lines 21-29):

PLOT	LU $\phi$ will contain bistatic cross section pattern output data (formatted data).
ZZAT	LU 3 same as for TESBGF
ZADT	LU 4 sample of output which can be read without removing program from "background" running mode (formatted data).
ZINP	LU 5 same as for TESBGF
DATA	LU 1 same as for TESBGF
ZOUT	LU 6 contains output data from iteration (formatted data).

All iterations are performed between lines 93 to 222. CALL EZFFD sets up excitation column (b) and lines 98-129 solve N subsystems using the SOI submatrices and SUBROUTINE SQROT (Cholesky). Lines 130-156 compute the residuals for SOI (line 148) or solve system via J or SOR (lines 150-153). Lines 157-159 save "latest" solution information in the event the iteration is stopped and restarted with ISTART  $\neq$  1. Lines 160-175 compute residual 1-norm  $\|r^{(k)}\|_1$  and lines 176 to 196 compute bistatic cross section pattern SIGG ( $\lambda^2$ ). Bistatic pattern is written into file name PLOT. Line 197 computes bistatic pattern average (SIG) over sector and line 198 computes normalized average residual  $\epsilon^{(k)}$ . Lines 199-204 compute total scatter cross section  $\sigma_T$  (TSC) via Forward Scatter Theorem. Lines 205-219 write and rewrite output data in following form:

IPEP	iteration k
SIG	bistatic average $\langle \sigma \rangle$
A	$\epsilon^{(k)}$ norm
TSC	total scatter cross section $\sigma_T$
ETH	forward scattered electric field (complex)
CI(N)	dipole mode current on Nth dipole (complex)

Reading and writing into LU 4 and 5 allows the latest accumulation of output data to be observed without removing program from background. Final output is accumulated in file ZOUT and is closed by escaping (ESC) program. Note,  $\sigma$  backscatter data are available only in PLOT as the "center" data point in the bistatic pattern.

(4) File Name: TESBG5,SYSAC

Main program TESBG5 is a utility program to be used to execute TESBG4 (BIGCO) when a new impedance matrix is not required. TESBG5 has two modes of operation. Both modes request input data (same as TESBGF) in line 18, then PAUSE (line 19). A transfer directly to TESBG4 is affected at this point, by pressing ESCAPE (ESC); however, file ZINP must already have the prescribed method code written on line 1 (and relaxation factor on line 2) in any format. This mode is especially useful when changing bistatic pattern cut or restarting SOR with a different relaxation factor. The second mode is initiated by pressing RETURN after the PAUSE. The "old data" will be displayed and a request for new parameters will occur. This mode can be used to change all parameters including SOI matrices; however, it is most used for changing only the desired aspect angle.

(5) File Name: UNICLD, SYSAC

SUBROUTINE UNICLD computes position and orientation of one dipole-at-a-time. The calling parameters are as follows:

IX	random number initialization on entry and next random number in sequence on return to main program.
RS	random array max radius
HK	dipole half-length
DK	segment length
NOSP	number of coordinate points per dipole
X,Y,Z	dipole coordinates returned to main program

Subroutine call to RANDU uses following I/O parameters:

IX	random number initialization
IY	next random number
A1	uniformly distributed random variable in range $0 \leq A1 \leq 1$ .



(6) File Name: ZSKEWF,SYSAC

SUBROUTINE ZSKEWF computes mutual impedance between two general skew dipoles. Calling parameters are as follows:

XA,YA,ZA XB,YB,ZB XC,YC,ZC	three coordinate points of dipole i
X1,Y1,Z1 X2,Y2,Z2 X3,Y3,Z3	three coordinate points of dipole j
INT	type of calculation; INT < 0 = far zone approx, INT = 0 closed form integrals, INT = 4 Simpson's integration (4 pt.).
CDK	Cos (DK)
SDK	Sin (DK)
D	dipole half-length
R	center-to-center spacing between ith and jth dipoles.
Z12	mutual impedance returned to main program.

Lines 5-31 calculate far zone approximation and lines 32-50 calculate "exact" values using SUBROUTINE ZGS, a standard Richmond subroutine for calculating mutual impedances between two general skew monopoles.

(7) File Name: EZFFD,SYSAC

SUBROUTINE EZFFD computes far zone electric fields scattered from random array assuming one ampere of current flows on each dipole. Calling parameters are as follows:

X,Y,Z	array dipole coordinates (dummy variables)
ET,EP	$\hat{e}$ polarized and $\hat{p}$ polarized electric fields (dummy variables)
ETT	$\hat{e}$ polarized electric field (N dimensional) returned to main program.
NOD	same as TESBGF

NOSM	same as TESBGF
NOSP	same as TESBGF
IP	same as TESBGF
RS	same as TESBGF
HK	same as TESBGF
DK	same as TESBGF
CTH	Cos ( $\theta$ ) scattering angle
STH	Sin ( $\theta$ ) scattering angle
PHI	$\phi$ scattering angle (degrees).

Subroutine regenerates random array with UNICLD and calculates the far zone electric field of each dipole using SUBROUTINE ZFFD, a standard Richmond routine for computing the far zone electric field of a single skew dipole located near the origin.

(8) File Name: STGETS,SYSAC

SUBROUTINES STOR, CLSTOR and SUBFUNCTION GET are listed here in assembler programming language. The assembled version of this program must be included in TESBGF and TESBG1 under file name STGETB,SYSAC.

(9) File Name: GETS,SYSAC

SUBFUNCTION GET is listed here in assembler language. The assembled version of this program must be included in TESBG4 under file name GETB,SYSAC.

```

1 C THIS PROGRAM COMPUTES MUTUAL IMPEDANCE MATRIX FOR N ELEMENT
2 C RANDOM ARRAY OF RESONANT DIPOLES AND PROCESSES THE MATRIX
3 C FOR USE IN TESBOL WHICH COMPUTES THE RADAR CROSS SECTION BY
4 C JACOBI, SQR AND SQR ITERATION METHODS.....
5     INCLUDE PAPER.SYSAC, ZGS.SYSAC
6     INCLUDE CLOP.SYSAC, AUEXB.SYSAC
7     INCLUDE SIGFTN.SYSAC, ZRNEWB.SYSAC
8     INTEGER IJ(115)
9     DIMENSION X(1), XY(5), Y(5), YY(5), Z(5), ZZ(5)
10    COMPLEX ZH(1200)
11    DIMENSION XR(2400)
12    EQUIVALENCE (ZH(1), XR(1))
13    COMPLEX CJI, P11, P12, P21, P22
14    COMPLEX ECC, ZDIA(5,5)
15    DATA PI, TH, ETA/3.14159, 6.28318, 376.727/
16    DATA CJI/(0.7, -0.30686F-2)/
17    CALL ESC(10*0)
18    WRITE(6,7)
19    7 FORMAT(1X, 'HALF BISTATIC ANG. INCR & ISTART =')
20    READ(8, -) HAFRIS, NPHZ, ISTART
21    CALL FERM (0)
22    CALL ASSIGN(NHZ70T, 6MSYSVC(1,6))
23    CALL ASSIGN(NHZ10P, 6MSYSVC(1,5))
24    CALL ASSIGN(NHZOUT, 6MSYSVC(1,6))
25    CALL ASSIGN(NHDATA, 6MSYSVC(1,1))
26    IDME115
27    WRITE(6,250)
28    250 FORMAT('HEAD NOS, NOS, DEN, METH =')
29    READ(8, -) NOS, NS, DEN, METH
30    WRITE(6,2) NOS, NS, DEN
31    WRITE(6, -) METH
32    IF (METH, 1, 1160 TO 4
33    WRITE(6,5)
34    5 FORMAT(' LEAD NMEGA =')
35    READ(8, -) OM
36    WRITE(6, -) OM
37    8 FORMAT(1X, 'HELIX', 114, 2X, 'NSF6', 118, 2X, 'ELE DENSITY', 1E9, 3)
38    4 WRITE(6,9)
39    9 FORMAT('HEAD Z THRESHOLD =')
40    READ(8, -) ZCF
41    WRITE(6,3) ZCF
42    3 FORMAT(1X, 'C', 1E9, 3)
43    13 NOS=NS
44    WRITE(6,20)
45    20 FORMAT(' READ TH, PHI =')
46    READ(8, -) TH, PHI
47    WRITE(6,200) TH, PHI
48    200 FORMAT('TH, PHI =', 2E9, 3)
49    CALL OLASSN
50    THR=TH, 0.17453
51    PHR=PHI, 0.17453
52    CBI=SI(THR)*COS(PHR)
53    CBI=SI(THR)*SI(PHR)
54    CBI=COS(THR)
55    CALL GETCPIT)

```



PAGE

8

TEBDF,SYBAC

```

56      NOSP=NOS+1
57      NOS=NUS-1
58      NH=NOD+NUS
59      NP=NOD+NOSP
60      NND=NOSP-NOR/2
61      HL=.2367
62      CK=TP/10
63      NE=NOD+NUSH
64      ZOS=.600*TP*TP
65      AL=HL/100
66      AK=AL*TP
67      HK=HL*TP
68      DK=2*HK/NOS
69      COK=COS(DK)
70      SOK=SIN(DK)
71      ANTS=NLC/DEH
72      RS=.62035*ANTS*(1/3)*TP
73      TP=7*AS111
74      NI=NOS
75      ICK="
76      IX=IP
77      DO 82 I=1,N
78      IF(NI.LT.NOS)60 TO 82
79      IY=IY
80      CALL UNICLO(IX,RS,HK,DK,NOSP,X,Y,Z)
81      NI=1
82  S2 T1=NI
83      I2=NI+1
84      I3=NI+2
85      NJ=NI'S
86      IDI=(I-1)/NORM+1
87      IN=0
88      IF(I.EQ.1)60 TO 80
89      ISL=I-1
90      DO 40 INZ=1,ISL
91      KP=I+N*(INZ-1)
92      KI=KP+KP-1
93      JP=INZ+INZ-1
94      DO 40 INE=1
95      JP=JP+JP
96      KI=KI+IM
97  40 VR(JP)=GLT(KI)
98  50 NO 80 J=1,N
99      IF(J.LT.1)60 TO 84
100     IDJ=(J-1)/NORM+1
101     IF(NJ.LT.NOS)60 TO 53
102     CALL UNICLO(IY,RS,HK,DK,NOSP,XX,YY,ZZ)
103     NJ=1
104  53 J1=NJ
105     J2=NJ+1
106     J3=NJ+2
107     INT=0
108     IDIA=I-NOSP*(IDJ-1)
109     JDIA=J-NUSH*(IDJ-1)
110     IF(IDI.NE.IDJ)60 TO 51

```

```

111      IF (INT.NE.1) GO TO 76
112      GO TO 56
113      51 YUTS=1
114      RHO=SQRT((XY(NPD)-X(NMU))2+(XK(PD)-X(MU))2+(YY(NPD)-Y(NMU))2
115      +(YY(NMU)-Y(MPD))2+ZZ(NPD)-Z(MU))2+(ZZ(NMU)-Z(NPD))2)
116      IF (RHO.GT.CK) GO TO 54
117      INT=0
118      GO TO 56
119      54 YF(RHO.GT.YP) GO TO 56
120      INT=0
121      56 CALL ZSKLWF(X(1),Y(1),Z(1),X(2),Y(2),Z(2),X(3),Y(3),
122      X(7),Y(7),Z(7),X(12),Y(12),Z(12),X(13),Y(13),
123      Z(13),INT,CDK,SDK,CK,RHO,ZR(J))
124      IF (I.EQ.10) ZDIA(I,DIA,JDTA)=ZR(J)
125      ZDK=CAUS(ZDIA(I,DIA,IUTA))
126      GO TO 54
127      76 ZR(J)=ZDIA(I,DIA,JDTA)
128      80 IF (CAH*(ZK(J)),LT.CF*ZDK) GO TO 80
129      IN=IN+1
130      IF (IN.GT.ICK) ICK=IN
131      IF (ICK.GT.100) GO TO 80
132      IJ(I)=J
133      80 IJ=IN+1
134      IF (ICK.GT.100) GO TO 81
135      WRITE(8)IN,(IJ(J),J=1,IN)
136      81 ICK=2
137      CALL STOR(ZR(1),IS,IERR)
138      IF (IERR.NE.0) GO TO 14
139      82 N=IN+1
140      CLOSE 8
141      CALL CLSTOR
142      CALL GETCF(JT)
143      IT=(IT-1)/100
144      EUSE=.992674146
145      WRITE(8)AOU,MS,DEFN,CF,YH,PHI,IT,ICK,EUS
146      IF (ICK.LT.100) AND (METH.EQ.0) GO TO 15
147      GO TO 996
148      14 WRITE(4,411)
149      411 FORMAT(1X,'OVERFLOW RANGE IN SUBZ')
150      GO TO 1000
151      15 WRITE(4,412)ICK
152      412 FORMAT('MAX DIM EXCEEDED ICK=',I4)
153      GO TO 1000
154      99A CLOSE 4
155      999 CALL ASSIGN(447OUT,6MSTVCI,4)
156      WRITE(6,6)MFRIS,DPHZ,ISTART
157      CALL LOG(5H016CO,5HSTBAC)
158      1000 CALL EXIT
159      END

```

```

1 C THIS PROGRAM COMPUTES MUTUAL IMPEDANCE MATRIX FOR N ELEMENT
2 C RANDOM ARRAY OF RESONANT DIPOLES AND PROCESSES THE MATRIX
3 C FOR USE IN TSSOL WHICH COMPUTES THE RADAR CROSS SECTION BY
4 C JACOBI, SOR AND SOR ITERATION METHODS.....
5     OPTIONS 32K
6     INCLUDE PAPER.SYSAC,IZGS.SYSAC
7     INCLUDE CLOM.SYSAC,ADFX9.SYSAC
8     INCLUDE STG1TA.SYSAC
9     DIMENSION XC(11340)
10    COMMON XC
11    INTEGER IS(115),INJ(1200),IJJ(115)
12    DIMENSION X(5),XY(5),Y(5),YY(5),Z(5),ZZ(5)
13    COMPLEX ZR(1200)
14    DIMENSION XH(2400)
15    EQUIVALENCE (Z(1),XH(1))
16    COMPLEX CC(6670)
17    EQUIVALENCE (XC(1),CC(1))
18    COMPLEX CJI,P11,P12,P21,P22
19    COMPLEX ECC,ZDTA(5,5)
20    DATA P1,TP,ETA/3.14159,6.28318,376.727/
21    DATA CJI/(0.0,--53088E-2)/
22    CALL ESC(1000)
23    WRITE(*,7)
24    7 FORMAT(1X,'HALF DISTANT ANG. INCR & ISTART =')
25    READ(8,--1)HAFBIS,DPH2,ISTART
26    CALL FRRH (0)
27    CALL ASSIGN(4H7ZAT,6HSYSVCI,3)
28    CALL ASSIGN(4H7TNP,6HSYSVCI,4)
29    CALL ASSIGN(4H7OUT,6HSYSVCI,6)
30    CALL ASSIGN(4HDATA,6HSYSVCI,1)
31    IUM=115
32    WRITE(*,250)
33    250 FORMAT('READ NOO,NOS,DEN,METH =')
34    READ(8,--1)NOO,NS,DEN,METH
35    WRITE(6,2)NOO,NS,DEN
36    WRITE(5,--1)METH
37    IF(METH,NE,1)GO TO 4
38    WRITE(*,5)
39    5 FORMAT(' READ OMEGA =')
40    READ(8,--1)OM
41    WRITE(5,--1)OM
42    9 FORMAT(1X,'SELF='*.114,2X,'NSFG='*.118,2X,'ELF DENSITY='*.1E9,3)
43    4 WRITE(*,9)
44    9 FORMAT('READ 2 THRESHOLD =')
45    READ(8,--1)CF
46    WRITE(6,6)CF
47    8 FORMAT(1X,'C='*.1E9,3)
48    13 NOS=NS
49    WRITE(*,20)
50    20 FORMAT(' READ TH, PHI =')
51    READ(8,--1)TH,PHI
52    WRITE(6,88)TH,PHI
53    88 FORMAT('TH, PHI ='.2E9,3)
54    CALL DFASSN
55    THR=TH*.017453

```



PAGE 2

TC8001.GYSAC

```

56 PHR=PHI*.017453
57 PAI=SI*(THR)*COS(PHR)
58 CBI=SI*(THR)*STN(PHR)
59 C.I=COS(THR)
60 CALL GETCP(IT)
61 NOSP=NOS+1
62 NUSM=NOS-1
63 NM=NOU*NUS
64 NP=NOU*NOSP
65 MAD=NOSP-NOS/2
66 ML=.2367
67 PK=TP*TP/100
68 N=NOU*NOSM
69 ZUS=3600*TP*TP
70 AL=ML/100
71 AK=AL*TP
72 MK=ML*TP
73 CK=2*MK/NUS
74 CMK=COS(PK)
75 SK=SI*(UK)
76 ANUS=NOU/DLM
77 PS=.62035*ANUS*(1/3)*TP
78 TP=738*111
79 NI=NOS
80 TCK=0
81 IX=IP
82 DO 82 (=1,N
83 IF(NI,LT,NOS)GO TO 52
84 TY=IX
85 CALL UHICLD(IX,RS,MK,OK,NOSP,X,Y,Z)
86 NI=1
87 59 I1=NI
88 I2=NI+1
89 I3=NI+2
90 NJ=NOS
91 TUI=(I1-1)/NOSM+1
92 INJ(I1)=0
93 IF(I1,EQ,1)GO TO 50
94 ISL=I1-1
95 DO 40 INZ=1,ISI
96 KP=I+N*(INZ-1)
97 K1=KP+KP-1
98 JP=INZ+INZ-1
99 DO 40 IME0,1
100 JP=JP+IM
101 K1=K1+IM
102 40 XR(JP)=6LT(K1)
103 50 DO 80 J=1,N
104 IF(J,LT,I)GO TO 84
105 IJU=(J-1)/NOSM+1
106 IF(NJ,LT,NOS)GO TO 53
107 CALL UHICLD(IJ,RS,MK,PK,NOSP,XX,YY,ZZ)
108 NJ=1
109 53 J1=NJ
110 J2=NJ+1

```

```

111      J3=NJ+2
112      INT=0
113      IDIA=I-NOSH*(I01-1)
114      IDIA=J-NOSH*(I0J-1)
115      IF(I01.NE.IDJ)GO TO 51
116      IF(I01.NE.1)GO TO 76
117      GO TO 46
118
119      51  IN=4
120      DO 55 MI=1,13
121      DO 55 MJ=1,J3
122      RHOS=(XX(MJ)-X(MI))*(XX(MJ)-Y(MI))*(YY(MJ)-Y(MI))*(YY(MJ)-
123      Z(MI))*(ZZ(MJ)-Z(MI))*(ZZ(MJ)-Z(P1))
124      T1(RHOS,GT,CK)GO TO 55
125      INT=0
126      GO TO 46
127
128      54  CONTINUE
129      56  ZR(J)=(0.0,0.0)
130      CALL ZGS(X(I1),Y(I1),Z(I1),Y(I2),Y(I2),7,I2),XX(J1),YY(J1)
131      &ZZ(J1),XX(J2),YY(J2),ZZ(J2),AK,OK,CDK,SDK,DK,SDK,INT,P11,P12,
132      &P21,P22)
133      ZK(J)=ZR(J)+P22
134      CALL ZGS(X(I1),Y(I1),Z(I1),X(I2),Y(I2),Z(I2),XX(J2),YY(J2)
135      &ZZ(J2),XX(J3),YY(J3),ZZ(J3),AK,OK,CDK,SDK,DK,SDK,INT,P11,P12,
136      &P21,P22)
137      ZK(J)=ZR(J)+P21
138      CALL ZGS(X(I2),Y(I2),Z(I2),X(I3),Y(I3),Z(I3),XX(J1),YY(J1)
139      &ZZ(J1),XX(J2),YY(J2),ZZ(J2),AK,OK,CDK,SDK,DK,SDK,INT,P11,P12,
140      &P21,P22)
141      ZK(J)=ZR(J)+P11
142      IF(I01.EQ.I0J)ZDIA(IDIA,J0IA)=ZK(J)
143      ZDM=CARS(ZDIA(IDIA,I0IA))
144      GO TO 46
145
146      76  ZK(J)=ZDIA(IDIA,J0IA)
147      84  IF(CABS(ZK(J)).LT.CF*ZDM)GO TO 80
148      INJ(I)=INJ(I)+1
149      IN=INJ(I)
150      IF(IN.GT.IDM)GO TO 15
151      IF(IN.GT.ICK)ICK=IN
152      T1(IN)=J
153
154      80  NJ=NJ+1
155      WRITE(5)IN,(IJ(JK),JK=1,IN)
156      IS=N2
157      CALL STOK(ZK(1),IS,IERR)
158      IF(IERR.NE.0)GO TO 14
159      82  NI=NI+1
160      CLOSE 3
161      CALL CLTOR
162      CALL GETCP(JT)
163      IT=(JT-IT)/100
164      EDS=2*2674156
165      WRITE(1)MOD,NS,DEN,CF,TH,PH,IT,ICK,EOS

```

PAGE 4

TESB01.SYSAC

```
166      GO TO 990
167      14 WRITE(4,411)
168      411 FORMAT(1X,'OVERFLOW RANGE IN SUFZ')
169      GO TO 1000
170      15 WRITE(4,412)ICK
171      412 FORMAT('MAX DIM EXCEEDED ICK=',I14)
172      GO TO 1000
173      990 CLOSE *
174      999 CALL ASSIGNINWOUT,SHSYSVC1,61
175      WRITE(4,*)HAFRTS,OPHZ,ISTART
176      CALL LOGISHUIGOU,SHSYSAC)
177      1000 CALL EXIT
178      END
```

```

1 C THIS PROGRAM COMPUTES SCATTER CROSS SECTION OF N ELEMENT RANDOM
2 C ARRAY USING JACOBY, FOR 3 SOI ITERATION. MUTUAL IMPEDANCE
3 C MATRIX MUST BE PREPROCESSED BY TESB01, TESB01 or TESB05.....
4     OPTIONS 32K
5     INCLUDE EZFF0.SYSAC,ISOPUTR.SYSAC
6     INCLUDE CLUH.SYSAC,IZFF0.SYSAC
7     INCLUDE PAFF0.SYSAC,IZFF0.SYSAC
8     DIMENSION XC(1340)
9     COMPLEX CC(6470),CCI(115)
10    INTEGER IJ(115)
11    DIMENSION X(5),YX(5),Y(5),YY(5),Z(5),ZZ(5)
12    COMPLEX CI(1200),CJ(1200),FTT(1200),ZH(1200)
13    DIMENSION XR(2400)
14    EQUIVALENCE (ZH(1),XR(1)),ICC(1),XC(1)
15    COMMON CC
16    COMPLEX CJI,FTI,FTF,FPI,FPT,LTH,LPH,ET,EP
17    DATA PI,TP,ETA/3.14159,6.28318,376.727/
18    DATA CJI/(0.0,-.55088E-7)/
19    CALL ESC(1998)
20    CALL FERR (0)
21    CALL ASSIGN(4HZOUT,6HSYSVC1,6)
22    READ(6,-)HAFBIS,CPH2,ISTART
23    RISTATE=HAFBIS*2
24    CLOSE 6
25    CALL ASSIGN(4HPL0T,6HSYSVC1,0)
26    CALL ASSIGN(4HZAT,6HSYSVC1,3)
27    CALL ASSIGN(4HZAT,6HSYSVC1,4)
28    CALL ASSIGN(4HZIMP,6HSYSVC1,5)
29    CALL ASSIGN(4HDATA,6HSYSVC1,1)
30    READ(1)H00,H01,H02,CF,TH,PMT,IT,ICK,CBS
31    IF(ISTART.EQ.1)CLOSE 1
32    WRITE(6,5)H00,H01,H02
33    5 FORMAT(1X,'H00=' ,1I4,2X,'H01=' ,1I4,2X,'H02=' ,1I4,2X,'ELE DENSITY=' ,1E9,3)
34    WRITE(6,10)
35    10 FORMAT(' J=0, FOR=1, SFI=2 , ')
36    READ(5,-)ITE
37    IF(ITE.EQ.0)WRITE(6,2)
38    2 FORMAT(1X,'JACOBI')
39    IF(ITE.NE.2)GO TO 12
40    WRITE(6,3)
41    3 FORMAT(1X,'SOI')
42    12 IF(ITE.NE.1)GO TO 13
43    WRITE(6,14)
44    14 FORMAT(' OMEGA= ')
45    READ(5,-)OMEGA
46    WRITE(6,4)OMEGA
47    4 FORMAT(1X,'SOI',2X,'OMEGA=' ,1E9,3)
48    13 NOS=NS
49    REWIND 5
50    WRITE(6,884)TH,PMT
51    884 FORMAT('TH, PMT =',2E9,3)
52    WRITE(6,6)IT
53    6 FORMAT(' TIME TO COMP Z =',1I12,'SEC')
54    WRITE(6,11)CF,ICK
55    11 FORMAT(1X,'C=' ,1E9,3,2X,'MAX DIM=' ,1I5)

```

PAGE 9

TEB664.SYSAC

```

86      CALL CLASSN
87      THR=THA.017493
88      CALL GLTCP(ITF)
89      NOSP=NUS+1
90      NOSH=NUS-1
91      NM=NOD+NUS
92      NP=NOD+NOSP
93      NMO=NOSP-105/2
94      HL=.2367
95      CK=TP*TP/100
96      N=NOD+NOSH
97      AL=HL/100
98      AK=AL*TP
99      HK=HL*TP
100     PK=2*HK/NOS
101     COK=COS(PK)
102     SOK=SIN(PK)
103     ANOS=NOD/DEM
104     RS=.2045*ANOS**((1/3.)*TP
105     EHS=.2026741*6
106     EHS=
107     RANDOM ARRAY N1
108     IP=2165413
109     RANDOM ARRAY N2
110     IP=7559111
111     NI=NUS
112     102 T12=1
113     CTH=COS(THR)
114     STH=SIN(THR)
115     IF(ISTART.EQ.1)GO TO 121
116     REAU(1)ISTART.(CJ(JK).CI(JK).JK=1,N)
117     ISTART=ISTART+1
118     CLOSE 1
119     GO TO 125
120     121 DO 124 IFK=1,N
121     124 CI(IFK)=(0.0,0.0)
122     125 IAK=1
123     DO 943 IFEP=ISTART.1000
124     A=0
125     PHZ=PH1
126     CALL EZFFO(Y.Y.Z.ET.EP.ETT.NOD.NOSH.NOSP.IP.RS.HK.CK.CTH*STH*PHZ)
127     IF(ITF.NE.2)GO TO 131
128     IF(IPEP.NE.1)GO TO 123
129     DO 122 I=1,N
130     122 CJ(I)=-ETT(I)*CJ1
131     123 DO 130 L=1,N
132     REAU(3)IN.(IJ(JK).JK=1,IN)
133     DO 640 I=1,IN
134     IDI=IJ(I)
135     CCI(I)=CJ(IDI)
136     DO 630 J=1,IN
137     IDJ=IJ(J)
138     IOF=IOJ+N*(INI-1)
139     KIE=(1-1)*IN-(I+J-1)/2+J
140     IOF=10F+IOF-1

```



PAGE 3

TE0000, SYSAC

```

111      KI=KI+KI-1
112      DO 600 IM=0,1
113      IOF=IOF+IM
114      KI=KI+IM
115      600 YC(KI)=GLT(IOF)
116      CALL SGROT(CC,CCI,0,1,IM)
117      IF(IM.EQ.N)GO TO 12A
118      DO 605 I=1,IM
119      IF(IJ(I).NE.1)GO TO 605
120      ET=CCI(I)
121      GO TO 606
122      605 CONTINUE
123      606 CI(L)=CI(L)+ET
124      130 CONTINUE
125      REWIND 4
126      GO TO 161
127      12A DO 129 I=1,N
128      129 CI(I)=CI(I)
129      131 CONTINUE
130      DO 138 I=1,N
131      I=I
132      IF((IM.LT.0)YMN=I)+1
133      EP=(0,0,0,0)
134      DO 136 J=1,N
135      KI=J+N*(I-1)
136      JP=J+J-1
137      KI=KI+KI-1
138      DO 139 IM=0,1
139      JP=JP+IM
140      KI=KI+IM
141      135 YK(JP)=GLT(KI)
142      IF((ITE.NE.2.AND.1.EQ.J)GO TO 136
143      139 FP=EP+7R(J)+CI(J)
144      136 CONTINUE
145      ET=ET*(I)+CJ
146      ETM=CABS(ET)
147      IF(ETM.GT.FAS)EBS=ETM
148      177 CJ(I)=-EP-ET
149      IF(ITE.EQ.2)GO TO 138
150      CJ(I)=CJ(I)/7R(I)
151      IF(ITE.NE.1)GO TO 13A
152      CI(I)=CI(I)+OMEGA*(CJ(I)-ET(I))
153      13A CONTINUE
154      IF(ITE.NE.0)GO TO 141
155      DO 142 I=1,N
156      142 CI(I)=CJ(I)
157      141 WRITE(1)MOD,NS,DEM,CF,TH,PHI,IT,ICK,EBS
158      WRITE(1)IPEP,(CJ(JK),CI(JK),JK=1,N)
159      CLOSE 1
160      ISK=-ISK
161      DO 160 I=1,N
162      EP=(0,0,0,0)
163      ET=ET*(I)+CJ
164      DO 156 J=1,N
165      KI=J+N*(I-1)

```



PAGE 4

YCR964,SY8AC

```
166 JP=J+J-1
167 K1=K1+K1-1
168 NO 155 IM=0.1
169 JP=JP+IM
170 K1=K1+IM
171 155 YH(JP)=GRT(K1)
172 156 EP=EP+ZH(J)*CI(J)
173 R=CAHS(EP+ET)
174 A=A+R
175 160 CONTINUE
176 IF(HAFBIS)162,164,164
177 162 PHZ=PHI
178 DPHZ=0
179 INUM=1
180 GO TO 166
181 164 INUM=HAFBIS/DPHZ
182 PHZ=PHI-OPHZ*INUM
183 INUM=INUM+2+1
184 164 SIG=0
185 DO 158 ITH=1,INUM
186 IF(HAFBIS)16A,167,167
187 167 CALL E7FFD(X,Y,Z,ET,EP,ETT,NOD,NOSH,NOSP,IP,RS,HK,DK,CTH,BTH,PHZ)
188 16A FTH=(0.0,0.0)
189 DO 150 I=1,N
190 150 ETH=ETH+CI(I)*FT(I)
191 ETH=CAHS(ETH)
192 SIGG=4*PI*ETH*FTH
193 SIG=SIG+SIGG
194 WRITE(10,1)IPEP,PHZ,SIGG
195 1 FORMAT(1X,114.2X,1F8.2,2X,1E9.4)
196 15A PHZ=PHZ+DPHZ
197 SIG=SIG/INUM
198 A=A/R/ENS
199 PHZ=PHI+180
200 CALL E4FFD(X,Y,Z,ET,EP,ETT,NOD,NOSH,NOSP,IP,RS,HK,DK,CTH,BTH,PHZ)
201 ETH=(0.0,0.0)
202 DO 170 I=1,N
203 170 FTH=ETH+CI(I)*FT(I)
204 TSC=-2*AIMAG(ETH)
205 IF(IPEP.EQ.1)GO TO 248
206 IOUT=IPEP-1
207 DO 247 ISU=1,IOUT
208 READ(4,300)IFC,SIGP,AA,TS,FT,EP
209 247 WRITE(5)IFC,SIGP,AA,TS,ET,EP
210 REWIND 4
211 24A WRITE(4,300)IPEP,SIG,A,TSC,ETH,CI(N)
212 WRITE(5)IPEP,SIG,A,TSC,ETH,CI(N)
213 WRITE(6,300)IPEP,SIG,A,TSC,ETH,CI(N)
214 REWIND 5
215 DO 249 IOS=1,IPEP
216 READ(5)IFC,SIGP,AA,TS,FT,EP
217 249 WRITE(4,300)IFC,SIGP,AA,TS,ET,EP
218 REWIND 5
219 REWIND 4
220 300 FORMAT(1X,114.1X,1E10.4,1X,1F10.4,1X,1E10.4,1X,4E10.4)
```

PAGE 5

TESB64.SYSAC

```
221 IF(IN.EQ.N)GO TO 998
222 999 CONTINUE
223 99A CALL GUTCP(JT)
224 JT=(JT-ITT)/100
225 WRITE(6,7)JT
226 7 FORMAT(2,'ITER TIME E',1112,'SEC')
227 IF(MFPTS100*.802*.002
228 802 WRITE(6,9)HISTAT,DPH2
229 9 FORMAT(1A,'HISTATIC AVE OVER',1F8.2,'DER IN',1F8.2,'DEG INCR')
230 804 CALL PAPER
231 CALL EXIT
232 END
```

```

1 C THIS PROGRAM COMPUTES NEW S01 FOR A GIVEN Z MATRIX AND/OR
2 C SETS UP NEW INCIDENCE ASPECT ANGLE...
3 C
4     INCLUDE PAPER.SYSAC,GETR.SYSAC
5     INCLUDE AUXYR.SYSAC
6     INTEGER IJ(115)
7     DIMENSION X(5),YX(5),Y(5),YY(5),Z(5),ZZ(4)
8     COMPLEX ZH(1200)
9     DIMENSION XM(2000)
10    EQUIVALENCE (Z(1),XM(1))
11    COMPLEX C01,P11,P12,P21,P22
12    COMPLEX ECC,ZNTA(5,5)
13    DATA PI,TP,ETA/3.14159,6.28318,376.727/
14    DATA C01/0.0,--.5300E-2/
15    CALL ERC(1979)
16    WRITE(7)
17    7 FORMAT(1X,'HALF HISTATIC ANG. INCR & ISTART =')
18    READ(8,--INAFRTS,UPHZ,ISTART)
19    PAUSE
20    CALL FRRH (0)
21    CALL ASSIGN(447ZAT,6HSYSVCI,3)
22    CALL ASSIGN(447INP,6HSYSVCI,5)
23    CALL ASSIGN(447OUT,6HSYSVCI,4)
24    CALL ASSIGN(447DATA,6HSYSVCI,1)
25    IOM=117
26    WRITE(7,6)
27    6 FORMAT(1X,'OLD DATA')
28    READ(11,NOO,NS,DEN,CF,TH,PHI,IT,ICK)
29    WRITE(4,2)NOO,NS,DEN
30    WRITE(5,3)CF
31    WRITE(6,68)TH,PHI
32    WRITE(4,14)IT,ICK
33    14 FORMAT(1X,'TIME=',116.2X,'MAX OIME',113)
34    REWIND 1
35    WRITE(5,36)
36    16 FORMAT(1X,'NEW ASPECT ONLY? 0=YES 1=NO')
37    READ(8,--INASP)
38    WRITE(4,250)
39    250 FORMAT(1X,'READ NOO,NOS,DEN,METH =')
40    READ(8,--INGO,NS,DEN,METH)
41    WRITE(4,2)NOO,NS,DEN
42    WRITE(4,--IPETH)
43    IF(METH,NE,1)GO TO 4
44    WRITE(3,5)
45    5 FORMAT(' READ OMEGA =')
46    READ(8,--IOM)
47    WRITE(5,--IOM)
48    2 FORMAT(1X,'HELF=',114.2X,'NSFG=',112.2X,'ELF DENSITY=',1E9.3)
49    4 WRITE(4,9)
50    9 FORMAT('HEAD Z THRESHOLD =')
51    READ(8,--ICF)
52    WRITE(4,5)CF
53    3 FORMAT(1X,'C=',1E9.3)
54    13 NOS=NS
55    WRITE(4,20)

```

PAGE 9

TESSAS.GVSAC

```

56 20 FORMAT(' HEAD TH, PHI =')
57 READ(8,*)TH,PHI
58 WRITE(6,8F4)TH,PHI
59 884 FORMAT('TH, PHI =',2E9.3)
60 CALL ESC(13000)
61 IF(NASP,10.0)GO TO 90
62 CALL OFASN
63 NOSH=NUS-1
64 N=NOO+NOSH
65 ICK=0
66 DO 82 I=1,N
67   IN=0
68   DO 65 J=1,N
69     K=J+N*(I-1)
70     J=J+J-1
71     K=K+I-1
72     DO 63 IM=0,1
73       J=J+IM
74       K=K+IM
75     63 XH(JP)=GLT(YI)
76     70M=CAH'SIZ(I))*CF
77     DO 80 J=1,N
78       IF(CAH'(ZP(J)).LT.70M)GO TO 80
79       IN=IN+1
80       IF(IN.GT.ICK)ICK=IN
81       IF(ICK.GT.10M)GO TO 80
82       TJ(IN)=J
83     80 NJ=NJ+1
84     IF(ICK.GT.10M)GO TO 82
85     WRITE(5)IN,(TJ(JM),JM=1,IN)
86     82 NI=NI+1
87     CLOSE 4
88     95 WRITE(1)POD,NS,DEV,CF,TH,PHI,IT,ICK,ERS
89     IF(ICK.GT.10M.AND).ETH.EQ.2)GO TO 15
90     GO TO 790
91     15 WRITE(6,412)ICK
92     412 FORMAT('AX 01M EXCEEDED ICK=',114)
93     GO TO 1000
94     998 CLOSE 4
95     999 CALL ASSIGN(4M7OUT,6MSYSVC(6)
96     WRITE(4,*)HAFRTS,DPHZ,ISTANT
97     CALL LOG(SHRTGCO,6MSYSAC)
98     1000 CALL EXIT
99     FNO

```



1 C THIS PROGRAM COMPUTES UNIFORM DENSITY SPHERICAL CLOUD DISTRIBUTION...

```

2 C
3 SUBROUTINE UNICLU(IK,NS,HK,NW,NOSP,X,Y,Z)
4 DIMENSION X(1),Y(1),Z(1)
5 TP=2*3.14159
6 CALL RANDU(IK,TY,A1)
7 IX=IY
8 PPH=A1*TP
9 CALL RANDU(IK,TY,A1)
10 IX=IY
11 COST=2*A1-1
12 SINT=SQRT(1-COST*COST)
13 CA=SINT*COS(PPH)
14 CB=SINT*SIN(PPH)
15 CG=COST
16 CALL RANDU(IK,TY,A1)
17 IX=IY
18 PC=A1+SQRT(SOSP*RE)
19 RC=RC*(1/B.)
20 XX=RC*CA
21 YY=RC*CB
22 ZZ=RC*CG
23 CALL RANDU(IK,TY,A1)
24 IX=IY
25 PPH=A1*TP
26 CALL RANDU(IK,TY,A1)
27 IX=IY
28 COST=2*A1-1
29 SINT=SQRT(1-COST*COST)
30 CA=SINT*COS(PPH)
31 CB=SINT*SIN(PPH)
32 CG=COST
33 S=HK
34 DO 45 I=1,NOSP
35 Y(I)=XY+S*CA
36 Y(I)=YY+S*CB
37 Z(I)=ZZ+S*CG
38 45 S=S+UK
39 RETURN
40 END

```

```

41 C
42 C
43 SUBROUTINE RANNU(IK,IY,A1)
44 IY=IK*16645
45 IF(IY)5,6,6
46 4 IY=IY+4308607+1
47 6 A1=IY
48 A1=A1*.1192093E-6
49 RETURN
50 END

```

PAGE 1

ZSKWF.BYBAC

```

1  SUBROUTINE ZSKWF(YA,YA,ZA,XR,YB,ZB,XC,YC,ZC,X1,Y1,Z1,X2,Y2,
2  179,X3,Y3,Z3,INT,CDK,SUK,n,P,P12)
3  COMPLE (LJNR,Z12,P11,P12,P21,P22)
4  IF (INT.GE.0160 TO 50
5  CAT=(X2-X1)/D
6  CHT=(Y2-Y1)/D
7  CGT=(Z2-Z1)/D
8  CAS=(Y4-X4)/D
9  CBS=(Y4-Y4)/D
10 CCS=(Z4-Z4)/D
11 CAR=(X2-AR)/R
12 CBR=(Y2-AR)/R
13 CCR=(Z2-ZB)/R
14 SCT=CAS+CAT+CBS+CGT+CCS+CGT
15 CTH1=CAS+CAR+CBS+CCR+CCS+CCR
16 CTH2=-(CAT+CAR+CBT+CBR+CGT+CCR)
17 SS1=1.-CTH1*CTH1
18 SS2=1.-CTH2*CTH2
19 SUKS=SUK+SUK
20 F1=COS(D*CTH1)
21 F2=COK-C1
22 F2=COK-CUS(D*CTH2)
23 R2=R*R
24 FUJR=C*PLX(COS(P),-SIN(R))
25 ON2=D*1/N2
26 FND=(1.+(K2*SS1)*SIN(D*CTH1)+2.*DNR*CTH1
27 AR=ARS(SS1+SS2)
28 IF (AR.GT..001) GO TO 30
29 FND=60.*CTH2*FR*7/(R2+SUK)
30 Z12=FN+EJNR
31 GO TO 60
32 30 FND=CTH2*FR/R
33 FT=F1* (SDT+CTH1*CTH2)/SS1
34 CST=120.*F2/(R+SUK+SS2)
35 Z12=FR+F1*CPPLV(1./N,1.-1./R2)
36 Z12=CST+EJNR+Z12
37 GO TO 60
38 50 AK=D/50
39 CALL ZGSIXA,YA,ZA,XR,YB,ZB,X1,Y1,Z1,X2,Y2,Z2
40 2.AK,D,CDK,SUK,n,SOK,INT,P11,P12,P21,P22)
41 Z12=P22
42 CALL ZGSIXA,YA,ZA,XR,YB,ZB,X2,Y2,Z2,X3,Y3,Z3
43 2.AK,D,CDK,SUK,n,SOK,INT,P11,P12,P21,P22)
44 Z12=Z12+P21
45 CALL ZGSIXB,YB,ZB,XC,YC,ZC,X1,Y1,Z1,X2,Y2,Z2
46 2.AK,D,CDK,SUK,n,SOK,INT,P11,P12,P21,P22)
47 Z12=Z12+P12
48 CALL ZGSIXB,YB,ZB,XC,YC,ZC,X2,Y2,Z2,X3,Y3,Z3
49 2.AK,D,CDK,SUK,n,SOK,INT,P11,P12,P21,P22)
50 Z12=Z12+P11
51 60 RETURN
52 END

```



PAGE 1

EZFED.3401V

```

1  SUBROUTINE EZFED(X,Y,Z,ET,EP,ETT,NOD,NOS,NOSP,IP,RS,HK,NK,
2  ACTH,STH,PHI)
3  DIMENSION X(1),Y(1),Z(1)
4  COMPLEX ET,EP,ETT(1)
5  PH=PHI*.017453
6  CPH=COS(PH)
7  SPH=SIN(PH)
8  TX=IP
9  L=1
10  INET=0
11  DO 125 JFL=1,NOD
12  CALL UICLO(IY,RS,HK,NK,NOSP,X,Y,Z)
13  IN=1
14  DO 120 I=1,NOS
15  J=ISD
16  JFF=J+1
17  CALL ZIFD(X(J),Y(J),Z(J),X(JFF),Y(JFF),Z(JFF),DK,CIH,STH,
18  XCPH,SPH,ET,EP)
19  FT(L)=ET
20  L=L+1
21  120 ISD=ISD+1
22  125 CONTINUE
23  RETURN
24  END

```

PAGE 1

STGETS.SYSAC

```

1 * CALL STOR(Y,NX,NOVPFL)
2 * CALL CLSTON
3 * YEGFY(N)
4     XDEF STOR,STOR
5     XDEF CLSTON,CLS
6     XDEF GET,GET
7 STOR  TFM  LFN
8     PNZ  ST1
9     TLO  WBUF1
10    TKM  PNTR
11    AOK  1024
12    TKM  PMAX
13    TMA  LS
14    TAM  FILE+1
15    TMA  VC
16    TAM  FILE+3
17    TZM  NBLKW1
18    TOA  1
19    TAM  NBLKW2
20 ST1   GAP  1
21    TIM  SRCEAD
22    GAP  1
23    TMK  DACH/I
24    GAP  1
25    TJM  SAVJ
26    TIM  OVHAD
27    TZM  OVHAD
28    MKK
29    RNN  KETN
30 STLOOP TZM  KOUNO
31    TMO  SRCEAD
32    RAD  5
33    REE
34    LAD  5
35    RNO  SQ1
36    AUM  KOUNO
37    AME  2*2000*U00
38 SQ1   AUM  SKCFAD
39    TMA  SKCFAD
40    AMB  ROUNO
41    R00  OVERFL
42    COB  17
43    BOP  OVERFL
44    COB  1A60
45    BON  UNDERFL
46    RRD  5
47 SQSTR TCM  PNTR
48    AUM  PNTR
49    AUM  SRCEAD
50    TMA  PMAX
51    CMA  PNTR
52    ROP  ST2
53    RSL  ULKOUT
54 ST2   BWK  STLOOP
55 PETN  BUC  SAVJ

```

PAGE 2

STGETS,SYAC

56	OVERFL	AUM*	OVRAU	
57		CZE		
58		HON	**3	
59		TME	=*66777777	
60		BUC	SUSTR	
61		TME	=*27000000	
62		RUC	SUSTR	
63	UNDRFL	TZE		
64		RUC	SGSTR	
65	.....			
66	CLS	TJM	SAVJ	
67		TLO	WBUF1	
68		CMK	PNTK	BUF EMPTY?
69		ROZ	**2	YES
70		BSL	BLKOUT	DIITPUT LAST BLOCK
71		TZM	UPN	
72		RUC*	SAVJ	
73	.....			
74	GET	GAP	1	
75		TJM	SAVJ	
76		TMA*	UACU/I	
77		SOA	1	
78		BON	ERR	
79		ESA		
80		DVM	=512	
81		CMA	NBLKW1	
82		RNZ	GET2	
83		TLO	WBUF1	
84		AEK		
85		RUC	GET1	
86	GET2	CMA	NBLKW2	
87		RNZ	GET3	
88		TLO	WBUF2	
89		AEK		
90		BUC	GET1	
91	GET3	TLO	BUF	
92		AEK		
93		CMA	NBLK	
94		BOZ	GET1	
95		TAM	NBLK	
96		DMA	=UC	
97		TAM	BLOCK	
98		TMA	NBLK	
99		RLA	1	
100		ESA		
101		DVM	=79	
102		AME	LS	
103		TEM	FILFGT+1	
104		AMA	VC	
105		COB	"1"	
106		HON	**5	
107		AOA	1	
108		COB	"1"	
109		HON	**2	
110		AOA	1	

PAGE 3

STGTS.SYNAC

```

111 TAM FILEGT+3
112 BLU SCOPEN
113 DAC ID
114 DAC FILEGT
115 BNZ ENR
116 HLU SSETCM
117 DAC ID
118 DAC BLOCK
119 BNZ ENR
120 BLU SIN
121 DAC ID
122 DAC BUF
123 BNZ ENR
124 BLU SWAIT
125 DAC ID
126 BLU SCLOSE
127 DAC ID
128 RET1 TMC+ UAC0/K
129 BNZ +3
130 TOA *201
131 BUC UNS01
132 TZA
133 LRD S
134 QBB M4
135 ROZ UNS01
136 OMA #B7P6R4
137 UNS01 TDZ
138 BUC+ SAVJ
139 *****
140 RLKOUT ***
141 TKM SAVK
142 BLU SCOPEN
143 DAC ID
144 DAC FILE
145 BNZ ENR
146 BLU SDELETE
147 DAC ID
148 BNZ NPU
149 BLU SCOPEN
150 DAC ID
151 DAC FILE
152 BNZ ENR
153 BLU SOUT
154 DAC ID
155 DAC WBUF1
156 BNZ ENR
157 BLU SWAIT
158 DAC ID
159 BLU SOUT
160 DAC ID
161 DAC WBUF2
162 BNZ ENR
163 BLU SWAIT
164 DAC ID
165 BLU SCLOSE

```

OUTPUT 2-BLOCK FILE

```

166      DAC      IO
167      AUM      FILE+1
168      TMA      ES
169      AOA      79
170      CMA      FILE+1
171      ROP      BLKOUT1
172      TMA      ES
173      TAM      FILE+1
174      AUM      FILE+3
175      TOB      "0"
176      CMB      FILE+3
177      ROZ      SKIP
178      TOR      "1"
179      CMB      FILE+3
180      RNZ      *+2
181      SKIP      AUM      FILE+3
182      BLKOUT1  AUM      2
183      DAC      NBLKW1
184      AOM      2
185      DAC      NBLKW2
186      TLO      NBLF1
187      TKM      NMTF
188      TMK      SAVK
189      BUC*      BLKOUT
190      *****
191      MMU      RLU      SCRLF
192      BLU      SWPK
193      DAC      218
194      DAC      "NO MORE USER NAMES"
195      BUC      ERRCL
196      *****
197      FRR      RLU      SCRLF
198      BLU      SWPK
199      DAC      217
200      DAC      "STOR OR GET ERROR"
201      FRRCL    BLU      SCLOSE
202      DAC      IO
203      TZM      UPN
204      PLL      SEX17
205      *****
206      NYRAN    ***
207      ROUNN    ***
208      RAVJ     ***
209      NPN      ***
210      NMTF     ***
211      SAVK     ***
212      PMAX     ***
213      RUF      EQIV    '177000
214      TO      DATA    7
215      FILE     DATA    "FILES SYS"  " (CHANGE SYS TO SYS)"
216      FILERT   DATA    "FILES SYS"  " (CHANGE SYS TO SYS)"
217      SHCEAII  ***
218      NACO/T   DAC      0.1
219      NACO/K   DAC      0.1
220      NBLK     DATA    -1

```



PAGE 4

BTGETS.SYNAC

```
221 PLOCK ***  
222 VC DATA '25441442 SVC* (CHANGE TO '25441442 SVC*)  
223 FS DATA '21251442 =FS*  
224 PHLKW1 ***  
225 NBLKW2 ***  
226 WRUF1 ROAT 512(0)  
227 WRUF2 ROAT 512(0)  
228 END
```



PAGE 1

SETS.SYSAC

```

1 * Y=GET(N)
2 XDEF GET,GET
3 GET GAP 1
4 TJM SAVJ
5 TMA= DACC/I
6 SOA 1
7 RON LRR
8 ESA
9 OVM =512
10 TEK
11 CMA NBLK
12 ROZ GET1
13 TAM NBLK
14 OMA =80
15 TAM BLOCK
16 TMA NBLK
17 RLA 1
18 ESA
19 OVM =79
20 AME ES
21 TEM FILE+1
22 AMA VC
23 COH ","
24 RON **5
25 AOA 1
26 COH "1"
27 RON **2
28 AOA 1
29 TAM FILE+3
30 ALU $OPEN
31 DAC IO
32 DAC FILE
33 BNZ LRR
34 ALU $SETCON
35 DAC IO
36 DAC BLOCK
37 BNZ LRR
38 BLU $IN
39 DAC IO
40 DAC BUF
41 BNZ LRR
42 ALU $WAIT
43 DAC IO
44 BLU $CLCSF
45 DAC IO
46 GET1 TME= HUF/K
47 BNZ **3
48 TOA '201
49 BUC UNSQ1
50 TZA
51 LRD 5
52 QBB B4
53 ROZ UNSC1
54 OMA =B7R6B5
55 UNSQ1 TOX

```

PAGE 2

SETS, SYSAC

```

56          RUC* SAVJ
57 .....
58 FRR      ALU $CRLF
59          BLU $WPK
60          DAC $?
61          DAC $"GET FRROR"
62          ALU $CLOSE
63          DAC ID
64          RLL $EXIT
65 .....
66 SAVJ     ***
67 RUF      EQIV '177000
68 TD       DATA 7
69 FILE     DATA "FILE SYS " (CHANGE SYS TO SYS)
70 PACO/I   DAC U.I
71 RUF/K    UAC RUF.K
72 APLK     DATA -1
73 RLOCK    ***
74 VC       DATA '25441442 EVC" (CHANGE TO '25441442 EVC")
75 FS       DATA '21251442 EES"
76          END

```

APPENDIX G  
SPLIT-GATE AND LEADING EDGE TRACKER PERFORMANCE ON SHORT PULSE ECHOES

A. INTRODUCTION

This report considers the tracking behavior of split-gate and leading edge range trackers against short pulse target returns with several peaks. The objective is to learn where these trackers tend to track on such waveforms.

Section II of this report discusses the characteristics of split-gate and leading edge trackers, and explains the effects of lockup. Section III of the report describes a computer simulation used to observe tracker behavior in typical missile attack situations. Section IV shows some typical curves of tracking performance.

B. DISCUSSION OF TRACKER PERFORMANCE

The performance of a range tracker with an extended target echo depends on several factors, the two most important being the shape of the waveform and the design of the tracker. In this report, we consider two types of range trackers, a split-gate tracker and a leading edge tracker.

A split-gate tracker multiplies the received echo pulse by a pair of gates. The video waveform during each gate is integrated and the two integrator outputs are subtracted. The resulting difference voltage is proportional to the gate offset from the center of the pulse. This difference voltage is used to correct the gate position for the next pulse.

A leading edge tracker first differentiates the received waveform and then tracks the result with a split gate tracker. Only the positive side of the differentiated waveform is used by the split gate tracker. Negative values of the derivative are excluded.

In the absence of thermal noise, a split gate tracker may track at any point in the echo waveform where there is equal area under each gate. In a waveform with multiple peaks, there may be several such points, depending on the gate width and the specific waveform. For example, if the echo waveform is as shown in Figure 1, and the gate width is as indicated,

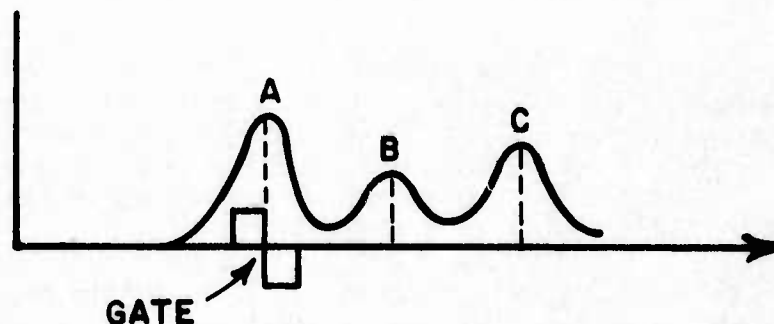


Figure G-1. An extended target echo.

there will be at least three points where the gate can track, points A, B and C. Which point is actually tracked in a given situation depends on the method used to lock up the tracker, as discussed below.

Similarly, a leading edge tracker will track at any point where the differentiated video waveform has equal area under each gate. Figure G-2 shows a possible video waveform  $v(t)$  and its derivative  $v'(t)$ . (The regions where  $v'(t)$  is negative are not included in the differentiated version).

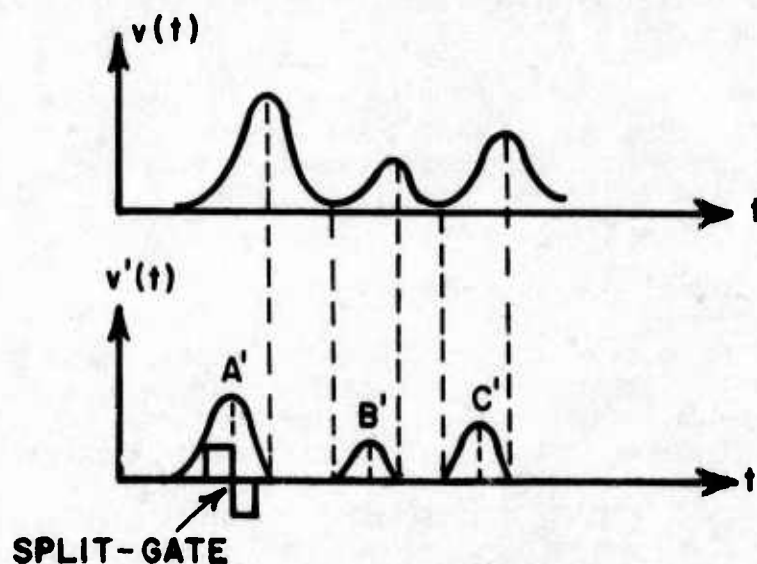


Figure G-2. A differential target echo.

When  $v'(t)$  is tracked by a split gate tracker, the waveform in Figure G-2 will have three points where the tracker can track, A', B' and C'. Again, the actual point chosen by the tracker depends on how the tracker locks up.

The most common method for locking up a split gate tracker uses two different gates, a wide gate and a narrow gate. The wide gate is much wider than the target echo width and is used for locking up the tracker. The narrow gate is matched to the target echo width and is used for tracking. In the search mode, the range is tracked with the wide gate until successive samples of the error voltage indicate that the wide gate is centered on the echo pulse. When this happens, the tracker switches to the narrow gate, which tracks with greater accuracy because it admits less noise than the wide gate.

With this method of lockup, the wide gate tends to align itself with the point which divides the area under the entire echo pulse in half. When the tracker switches to the narrow gate, the tracker then moves to the local peak in the waveform nearest this point. In an echo waveform with several peaks, the particular peak chosen by the tracker depends on the relative strengths and locations of the peaks.

A second method of locking up a split gate tracker is to slew the gate position across the range interval where the target is located. The two gate outputs are summed and compared with a threshold. When the gate enters the echo pulse, the sum output will rise and cross the threshold.



At this point, the loop is changed to a tracking mode, and the difference output is used to time the gate.

With this method of lockup, the tracker locks on the first part of the waveform it encounters where the early and late gates have equal output. Normally, one slews from short range out towards longer range. In this case, the tracker locks on the earliest part of the waveform where the gate outputs are equal, i.e., on the first pulse of the extended echo.

Thermal noise in the tracking loop complicates the situation because it produces tracking jitter. If the tracker is tracking a low amplitude peak, the tracking jitter may be large enough to make the loop drop out of lock. If this happens, the loop will then try to relock. Where it winds up depends on the lockup procedure used. A wide gate technique will return the tracker to the point which divides the area of the total echo waveform in half. A slewing technique moves the gate to the next peak of the waveform in the direction slewed.

Typically, the short pulse return from an aircraft contains several peaks with different amplitudes. The shape of the waveform is highly dependent on viewing angle. The number of peaks, their locations, widths and amplitudes all change with viewing angle. During a missile attack against an aircraft, the echo waveform seen by the missile radar changes continuously.

It is obvious that the part of the echo tracked by the split gate or leading edge tracker depends on the shape of the waveform. With wide gate-narrow gate lockup technique, some waveforms will cause the tracker to track the earliest peak and other waveforms will cause it to track a later peak. Since the shape of the echo from an aircraft target changes rapidly with aspect angle, and since thermal noise also causes the loop to unlock at random times and then relock, it is impossible to generalize about where a tracker will track.

For a missile attacking an aircraft, the evolution of the echo waveform with time during the track is difficult to predict unless all parameters of the attack situation are taken into account. For example, the performance of the range tracker depends on the angle tracker, because the angle tracker affects the trajectory of the missile and hence the target look angle. Range tracker performance is also dependent on aircraft and missile dynamics (acceleration rates, turning rates, etc.), since these also affect the trajectories and hence the look angle. Of course, the signal-to-noise ratio is dependent on target range, so tracking loop jitter changes as the missile closes on the aircraft.

For these reasons, the most realistic way to determine how a tracker behaves is to simulate a missile attack with the important dynamic variables included and observe the tracker performance. Such a simulation was developed and is described in the next section.

### C. THE SIMULATION

A Fortran program has been written to simulate the important aspects of the missile attack situation. The missile is fired from the ground at the

aircraft; the aircraft trajectory is controlled by the computer operator. Realistic velocities, turning rates, etc., are programmed for both the aircraft and missile (see details below). The missile has a monopulse angle tracker, and homes on a predicted intercept point continuously updated during the attack. The echo waveform of the aircraft is simulated as the sum of three gaussian pulses whose relative strengths and time delays depend on the aircraft viewing angle. The aircraft can drop a chaff scatterer on command, modeled as a single scatterer contributing an additional gaussian pulse to the target echo. The chaff scatterer decelerates instantly to zero velocity when dropped from the aircraft. The Fortran program used for this simulation is given below. Some of the detailed characteristics are described below.

The simulation details can be broken down into six areas -- airplane maneuvering, missile maneuvering, range tracker characteristics, angle tracker characteristics, radar properties of the aircraft, and intercept point prediction. We briefly describe the assumptions below.

#### Airplane Maneuvering

The airplane is maneuvered by the computer operator. The program allows a maximum turning rate of  $4.5^\circ/\text{second}$  in steps of  $0.6^\circ$  per second. There is no interrelation in  $\theta$  and  $\phi$  maneuvering. The velocity of the plane can be set from 100 meters/second to 410 meters/second in steps of 10 meters/second with no acceleration restrictions. These figures give a turning radius of about 0.5 km at full speed.

#### Missile Maneuvering

The missile speed is controlled automatically. The velocity is 50 meters/second at launch and the missile accelerates at 0.1 meter/second/second. These numbers result in a typical impact velocity of about 60 meters/second, since most encounters take approximately 100 seconds. The missile has a maximum turning rate of  $11.5^\circ/\text{second}$ , controlled by the angle tracker described below.

#### Range Tracker Characteristics

Two types of range trackers are used, a split-gate and a leading edge tracker. The leading edge tracker operates by differentiating the received video waveform, excluding negative values of the derivative, and tracking the resultant waveform with a split-gate tracker, as discussed earlier.

The range tracker uses two gate widths to lock up. A wide gate is used for initial acquisition and a narrow gate for tracking. The narrow gate width is 10 meters and the wide gate width is 100 meters.

#### Angle Tracker Characteristics

The angle tracker is a conventional 4-channel monopulse tracker that derives pointing error information in both angular coordinates. The sum beamwidth is  $20^\circ$ .



## Radar Properties of the Target

The target echo waveform is modelled as a sum of three gaussian shaped pulses along the aircraft separated 10 meters apart. Short pulse radar returns from scale models under controlled conditions appear to have such a structure. From front to back, the three pulses have relative strengths of 5, 3 and 4 units of voltage.

## Intercept Point Prediction

A predicted path is computed for the target. During the track, if the target is found to deviate from the predicted path by more than 5 meters in range and  $1^\circ$  in angle, the predictor readjusts the path calculation. This window area is to allow for noise and overshoot in the gates. The prediction is based on the assumption of a straight line path.

### D. TYPICAL RESULTS

Figures G-3 through G-16 show typical plots of range tracking error for a missile attacking an aircraft in straight level flight. The curves show the range tracking error as a function of the target range, with the smallest range at the left side of the curve. Thus, time runs from right to left on the curve, since the missile starts at large range and then closes to zero range. Ten second increments are marked with x's on the graphs.

Figure G-3 shows a typical curve of tracking error for a leading edge tracker. At large range, the range tracker is using the wide gate. At the point marked "0" on the curve, the tracker converts to the narrow gate. It is seen that the sinusoidal wandering stops at this point, and the tracker performance improves.

It is seen that after the tracker switches to the narrow gate, the tracking error persists at about +12 meters. On these curves, range is measured from the center pulse in the (three pulse) echo waveform, so this residual range error means that the tracker is tracking the leading pulse in the echo waveform.

Figures G4-7 show several additional runs, all with the same leading edge tracker. Figures G-3 through G-7 are all run under the same conditions, except for aircraft velocity. In Figure G-3, the aircraft velocity is 140 meters/second, in Figure G-4 it is 180 m/s, in Figure G-5 it is 220 m/s, in Figure G-6 it is 260 m/s and in Figure G-7 it is 300 m/s. We note that at 180 m/s (Figure F-4), the steady-state error is approximately -7 meters; in this case,, the tracker is tracking the rear pulse. At 220 m/s (Figure G-5), the tracker tracks the center pulse. (The residual error is approximately +2 meters -- it is not zero because the leading edge tracker tracks the front edge of the center pulse). In Figure G-5, the tracker switches to the narrow tracking gate at a range of 4.85 km, but then goes back to the wide gate at 4.5 km, and finally returns to the narrow gate at 3.2 km. This case illustrates how the tracker returns to the wide gate if the narrow gate drops out of lock due to range jitter. Figures G-6 and G-7 (aircraft velocities of 260 m/s and 300 m/s), the range tracker again tracks the leading pulse.

Figures G-8 through G-15 show a similar set of runs using a split gate tracker instead of a leading edge tracker. All curves are run under the same conditions, except for different aircraft velocities. The velocity spans the range 100 meters/second to 410 meters/second, as labelled on the individual curves. In this set of runs, it is seen that the split-gate tracker tracked any of the three pulses, depending on the aircraft velocity.

Observe the expanded scale used in the split gate tracker results. The reason is that the split gate tracker tended to lock on to the first pulse it observed with little overshoot. It shifted to the narrower gate almost immediately. Tracking jitter is also higher for the split gate tracker. This is most likely caused by the larger width of the pulse being tracked. Compare pulses A and A' Figures G-1 and G-2. These pulse widths tend to correlate with the jitter magnitudes observed, approximately 1-1/2 meters peak to peak for the leading edge tracker and four meters peak to peak for the split gate tracker. Another factor may be the additional separation or isolation of the pulses being tracked for the leading edge tracker. This would also tend to reduce the jitter for the leading edge tracker.

#### E. CONCLUSIONS

In general, a split-gate tracker may track on any peak in a waveform where there is equal area under each gate. In a waveform with several peaks, the particular peak chosen depends on the lockup method used and the evolution of the waveform shape during the lockup procedure. Moreover, the lockup has a statistical behavior because of the thermal noise in the loops. Thus, with a given echo waveform, the tracker may sometimes lock on one peak and sometimes on another peak.

A leading edge tracker operates by first differentiating the received video waveform and then tracking that waveform with a split-gate tracker. Hence the same comments apply to a leading edge tracker.

Usually, if a particular peak in an echo waveform (or its derivative) is predominant, the split-gate tracker will settle on that peak. However, during a typical missile attack trajectory, the strongest peak in an aircraft echo will sometimes be from the front of the aircraft and sometimes from the rear. Hence it is not possible to draw any general conclusions about which part of an aircraft is tracked. Moreover, the tracker does not always track the strongest peak. The examples shown in Figures G-4 and G-5 are cases where the tracker tracks the intermediate peak and the weakest peak.

In this study, we assumed the short pulse response for an aircraft in the form of three Gaussian pulses of different magnitudes. The simulation of the reflections from the scattering centers as a Gaussian pulse is probably reasonable in that the precise shape of

the individual pulses would not materially alter the results. The important feature is the pulse position and duration, their relative maximum values, the number and spacing of the received pulses. Of particular importance is the manner in which these pulse properties change as the relative orientation of the radar and the aircraft changes in flight. These parameters were not available to us at the time of this study. Any future effort of this type should be prefaced by a study that would generate this specific data.

It is observed that since the precise pulse shape is not critical, it may be practical to generate these pulse returns in a relatively simple way. It is generally conceded that present GTD capabilities are such that the scattered fields can be predicted with reasonable accuracy and costs for all parts of the aircraft except the jet intake and jet exhausts. It should be practical to obtain the appropriate pulse properties experimentally from these critical scatterers using a short pulse radar. Used in conjunction with a directional antenna to isolate the intake response from other scatterers as the radar is moved around an actual aircraft, this type of measurement would provide the additional data required to evaluate the performance of the range trackers.



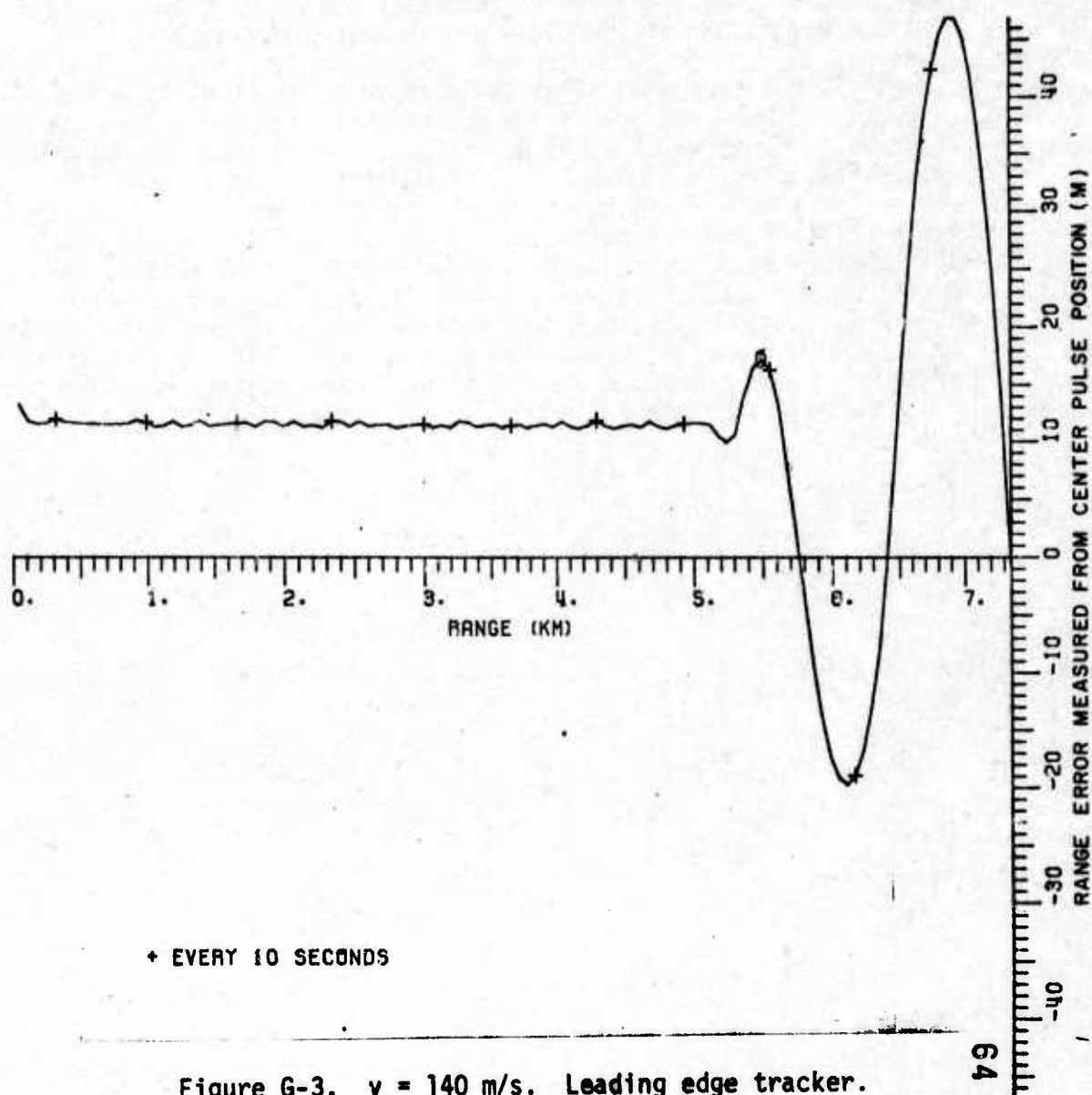
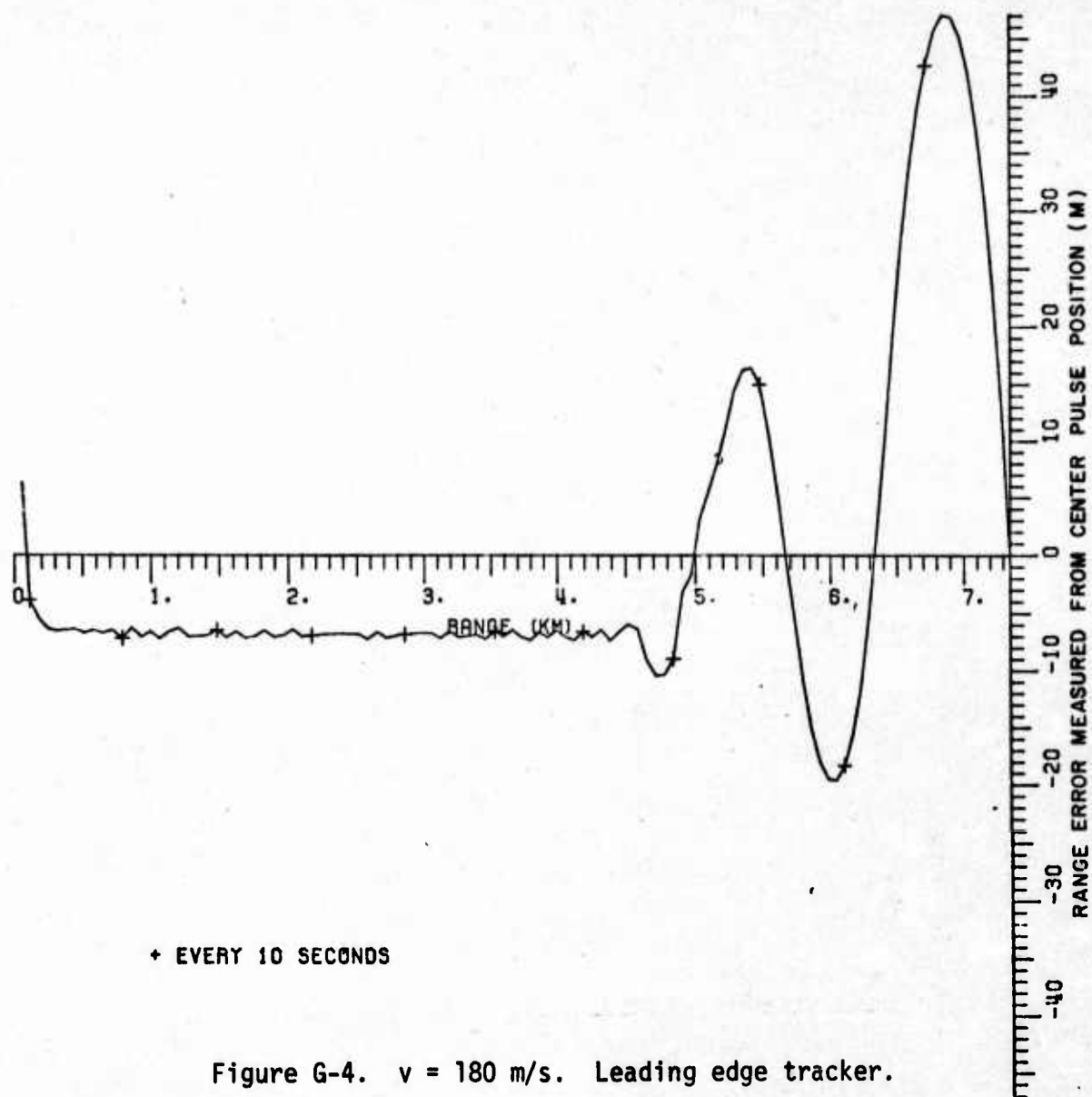
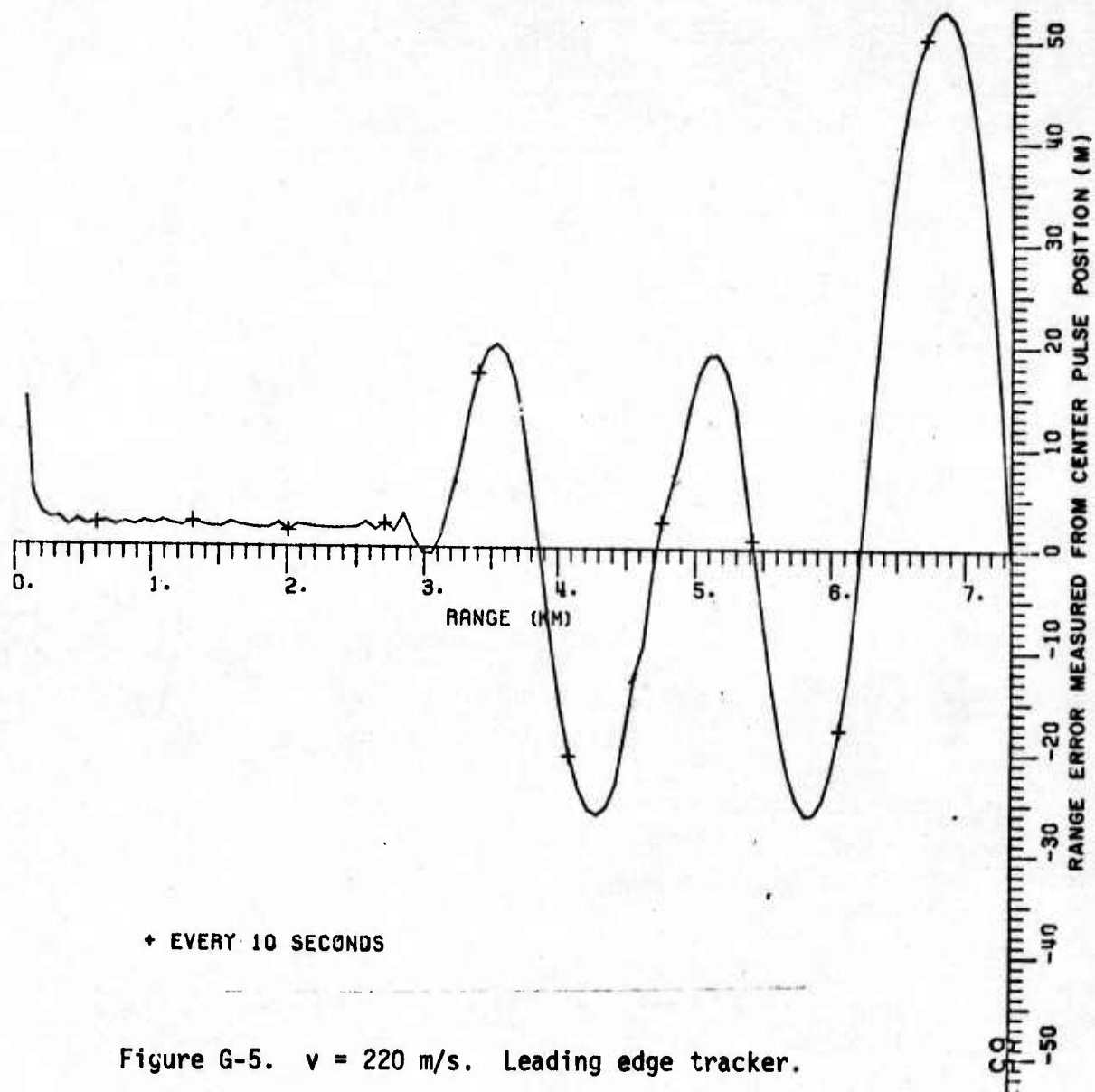


Figure G-3.  $v = 140$  m/s. Leading edge tracker.



+ EVERY 10 SECONDS

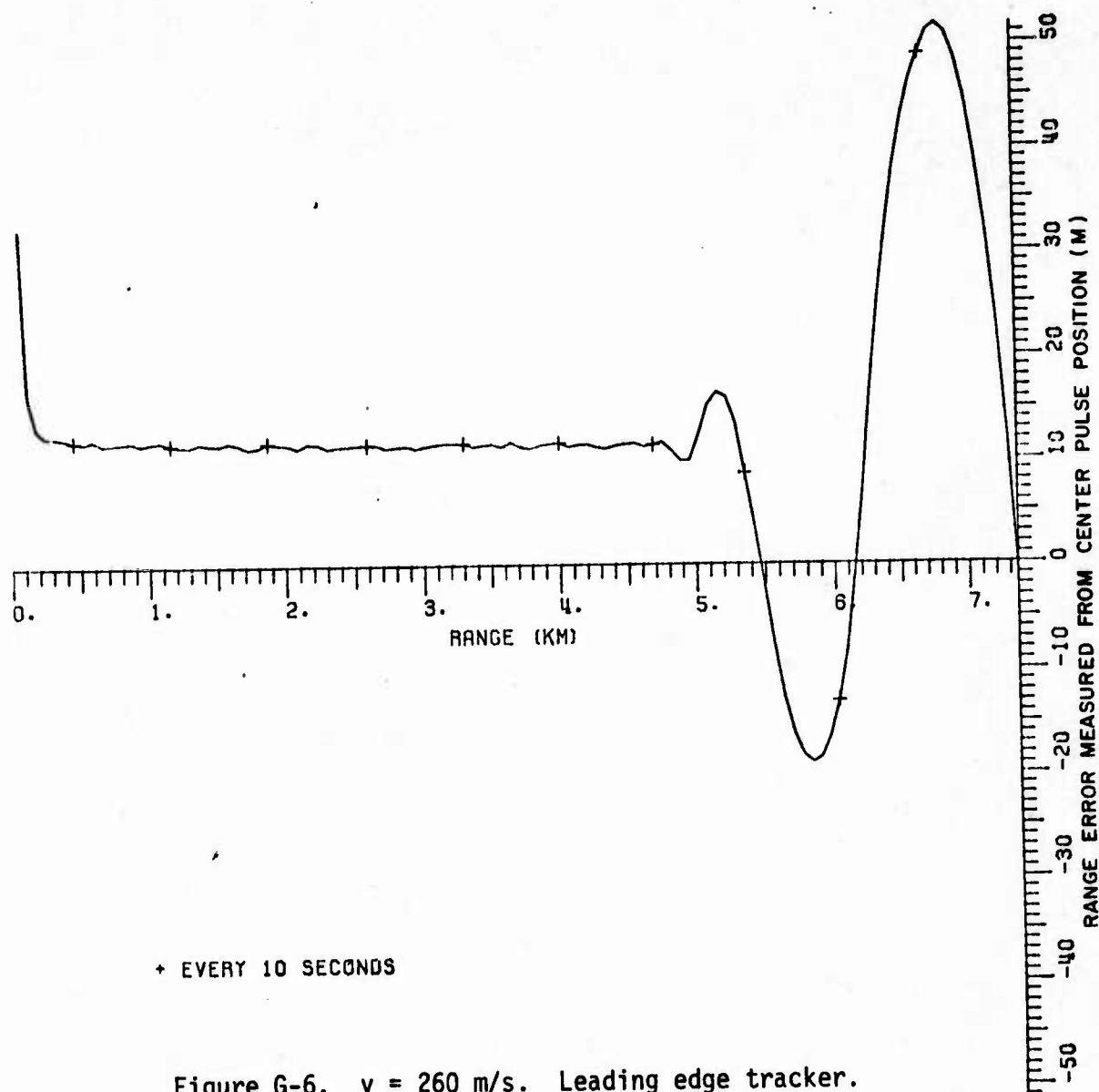
Figure G-4.  $v = 180$  m/s. Leading edge tracker.



+ EVERY 10 SECONDS

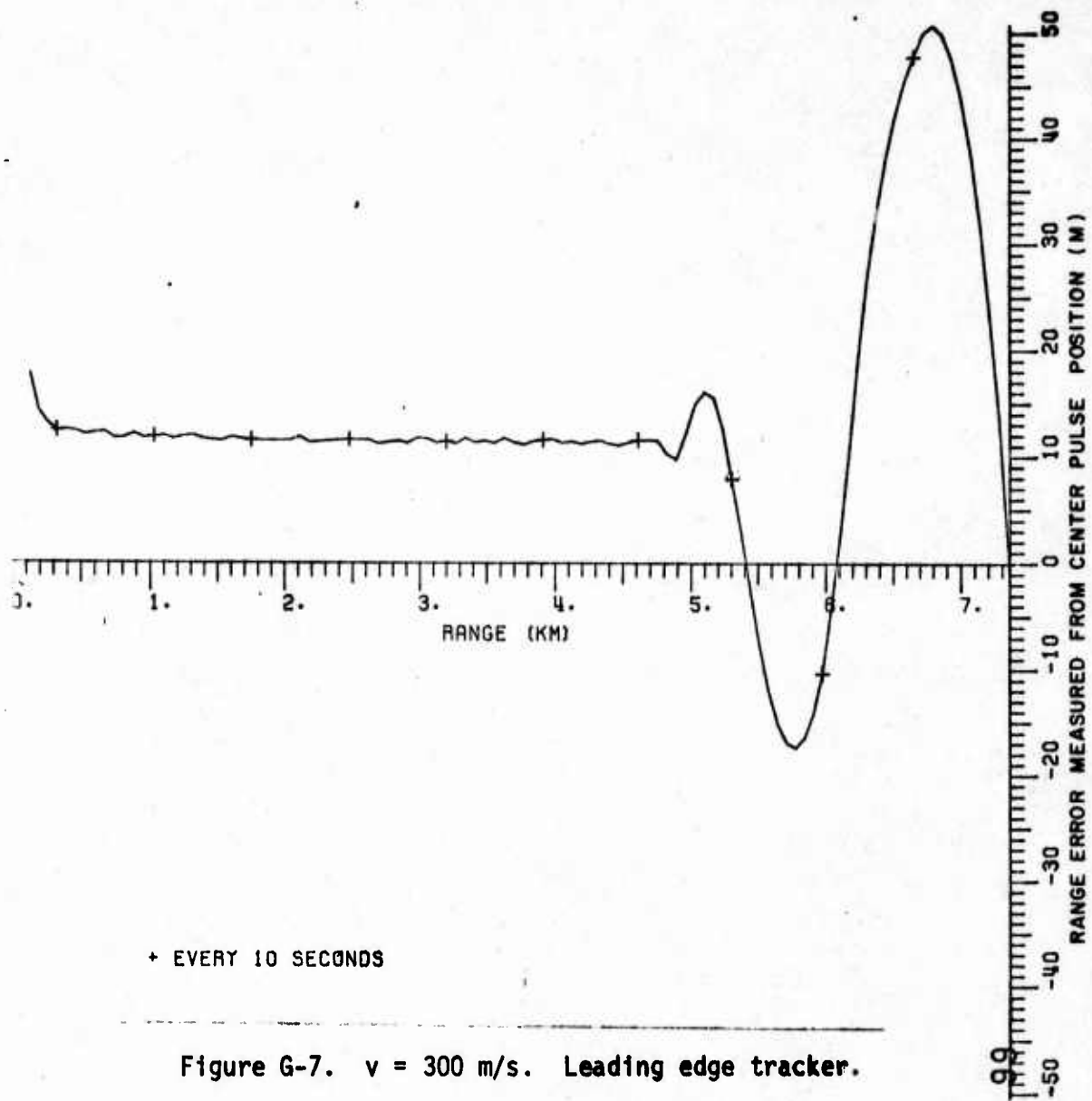
Figure G-5.  $v = 220$  m/s. Leading edge tracker.





+ EVERY 10 SECONDS

Figure G-6.  $v = 260$  m/s. Leading edge tracker.



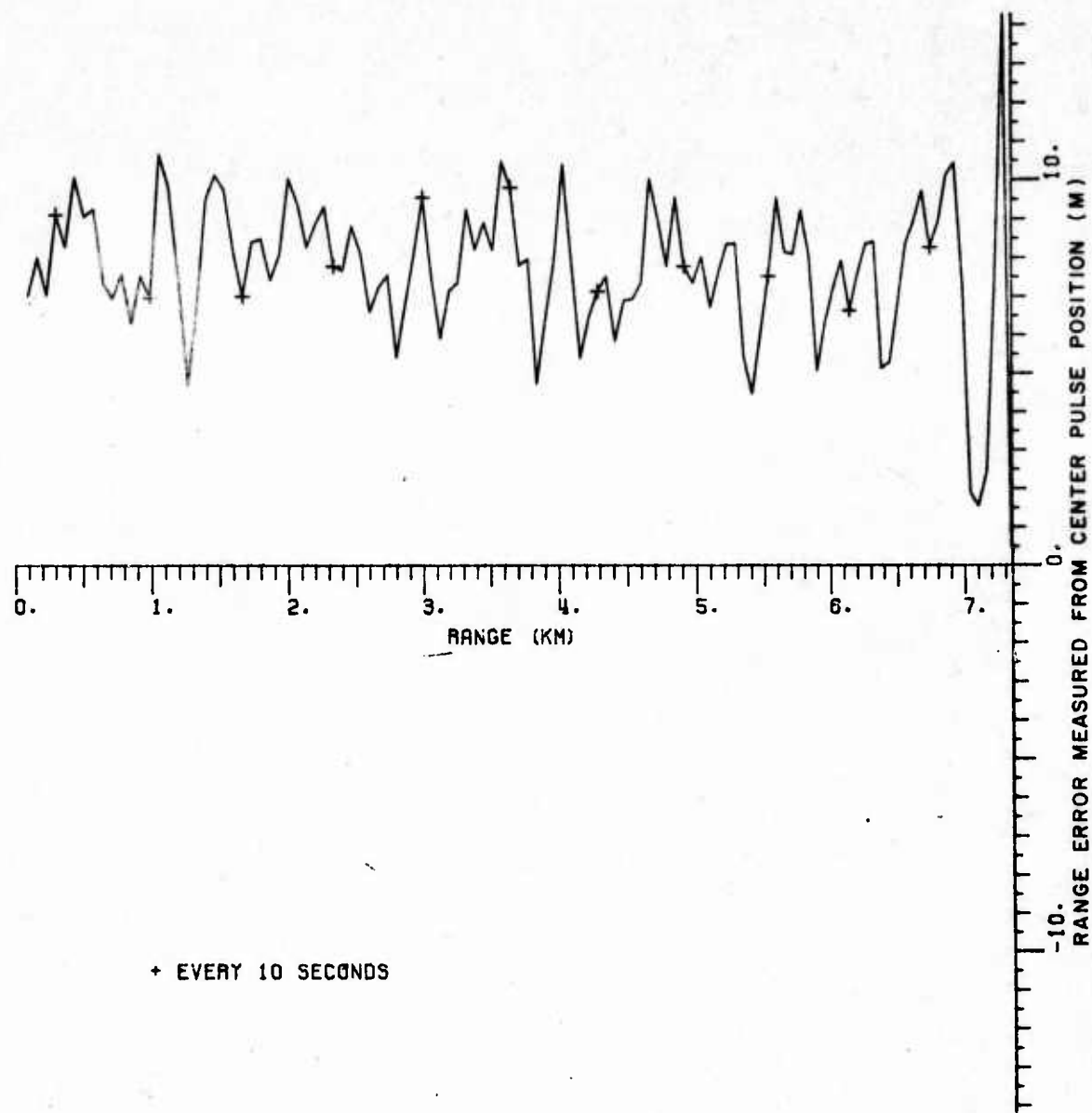


Figure G-8.  $v = 100$  m/s. Split-gate tracker.

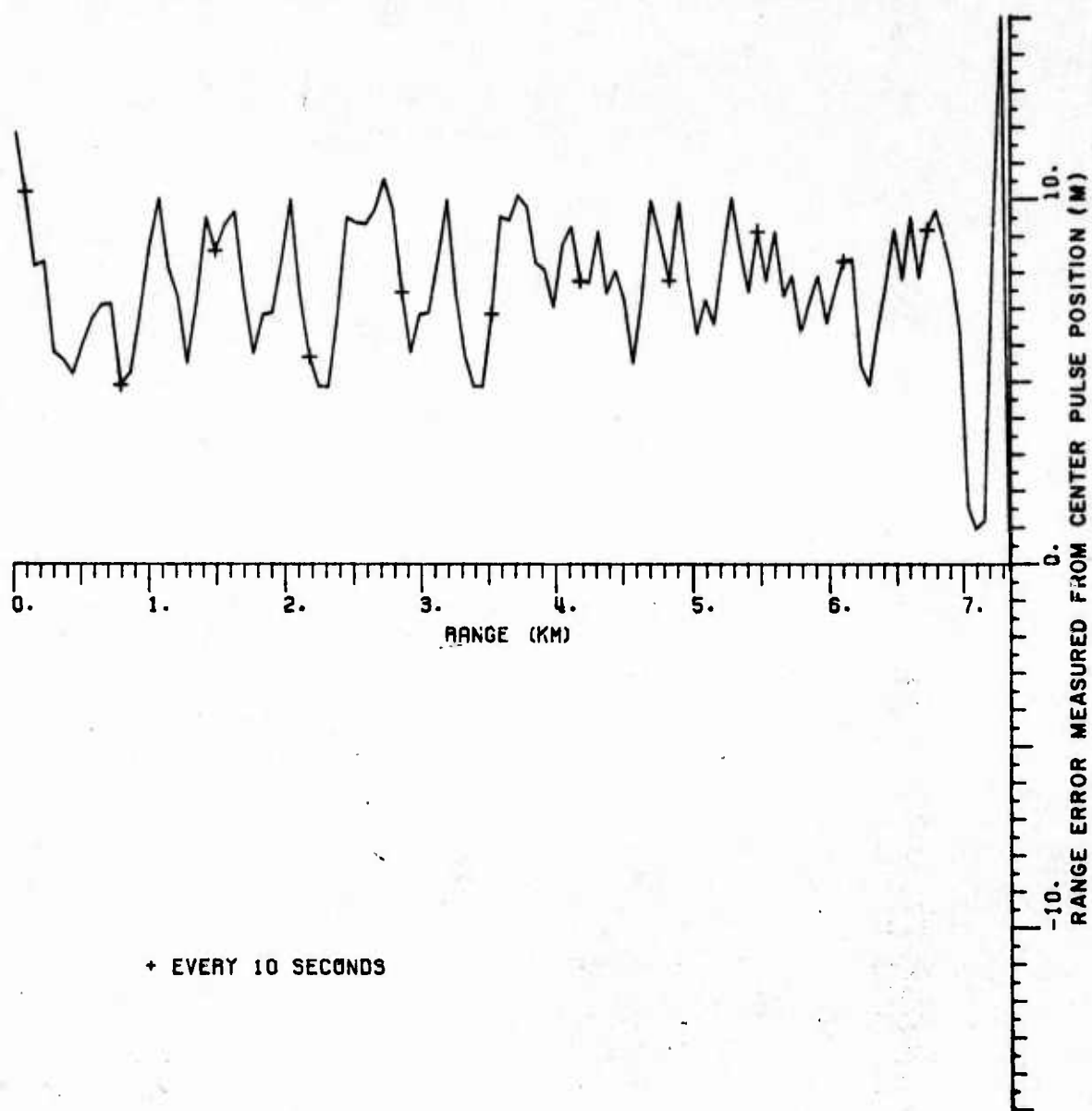
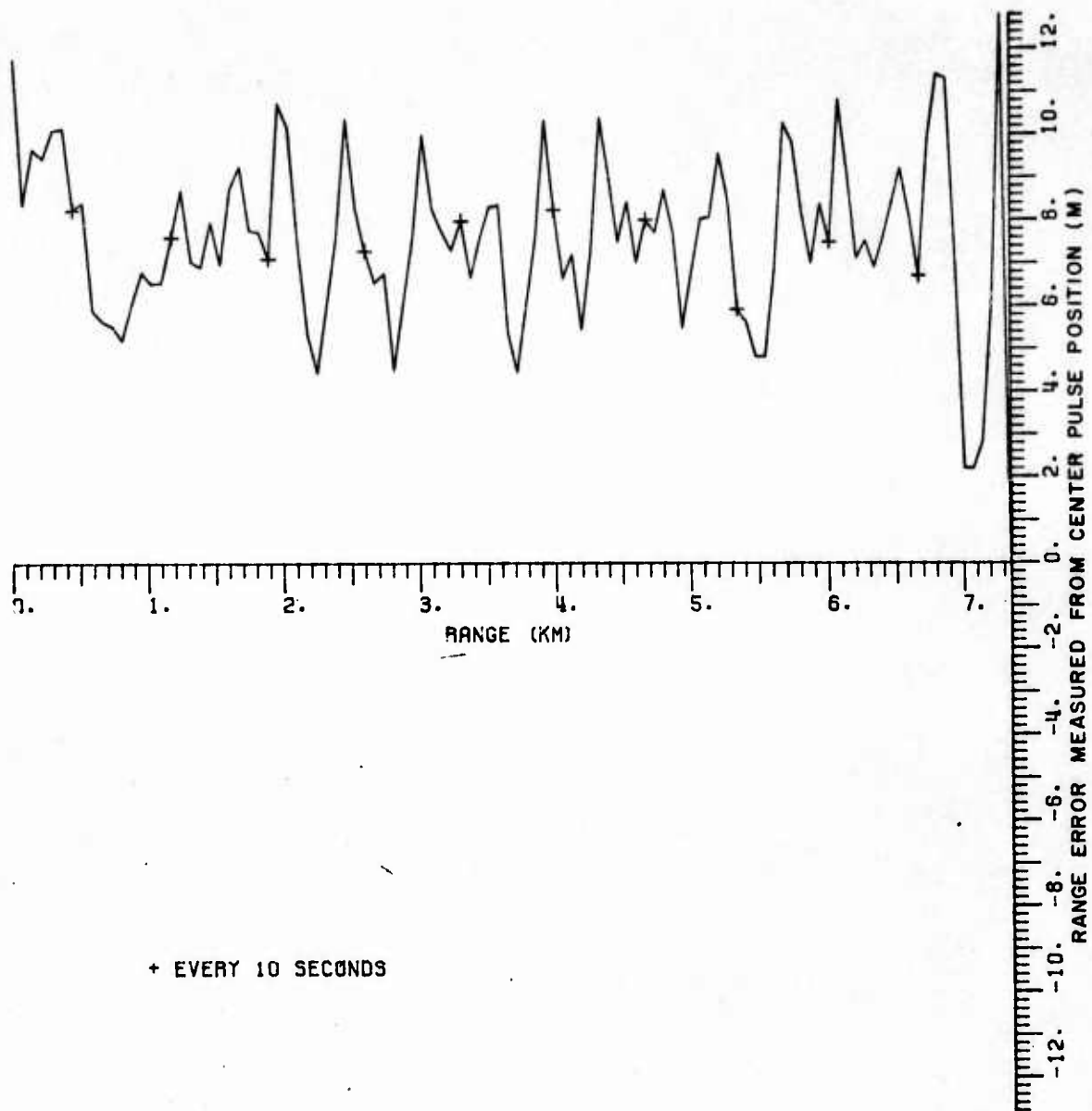


Figure G-9.  $v = 180$  m/s. Split-gate tracker.



+ EVERY 10 SECONDS

Figure G-10.  $v = 200$  m/s. Split-gate tracker.

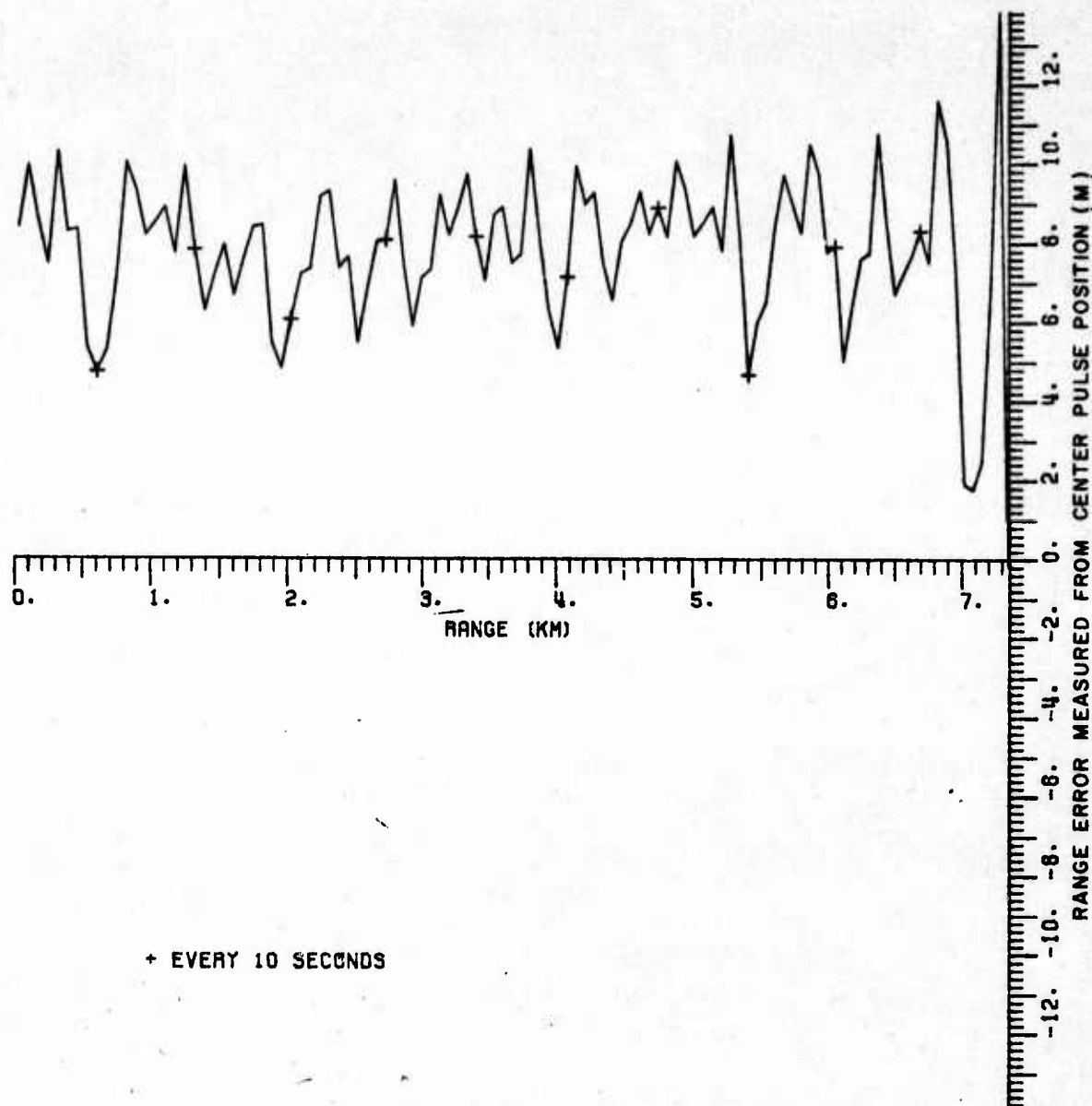


Figure G-11.  $v = 200$  m/s. Split-gate tracker.



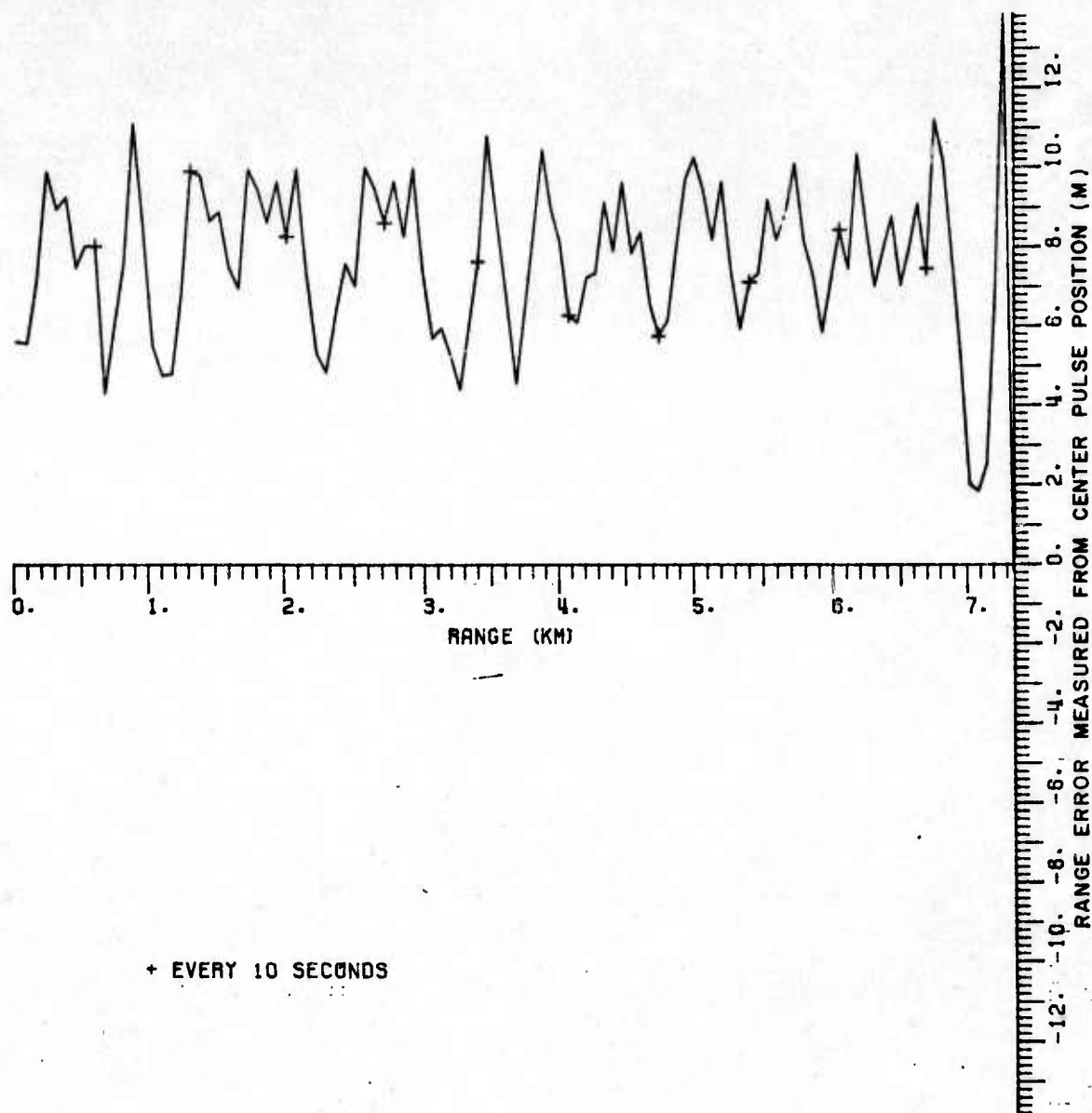


Figure G-12.  $v = 260$  m/s. Split-gate tracker.

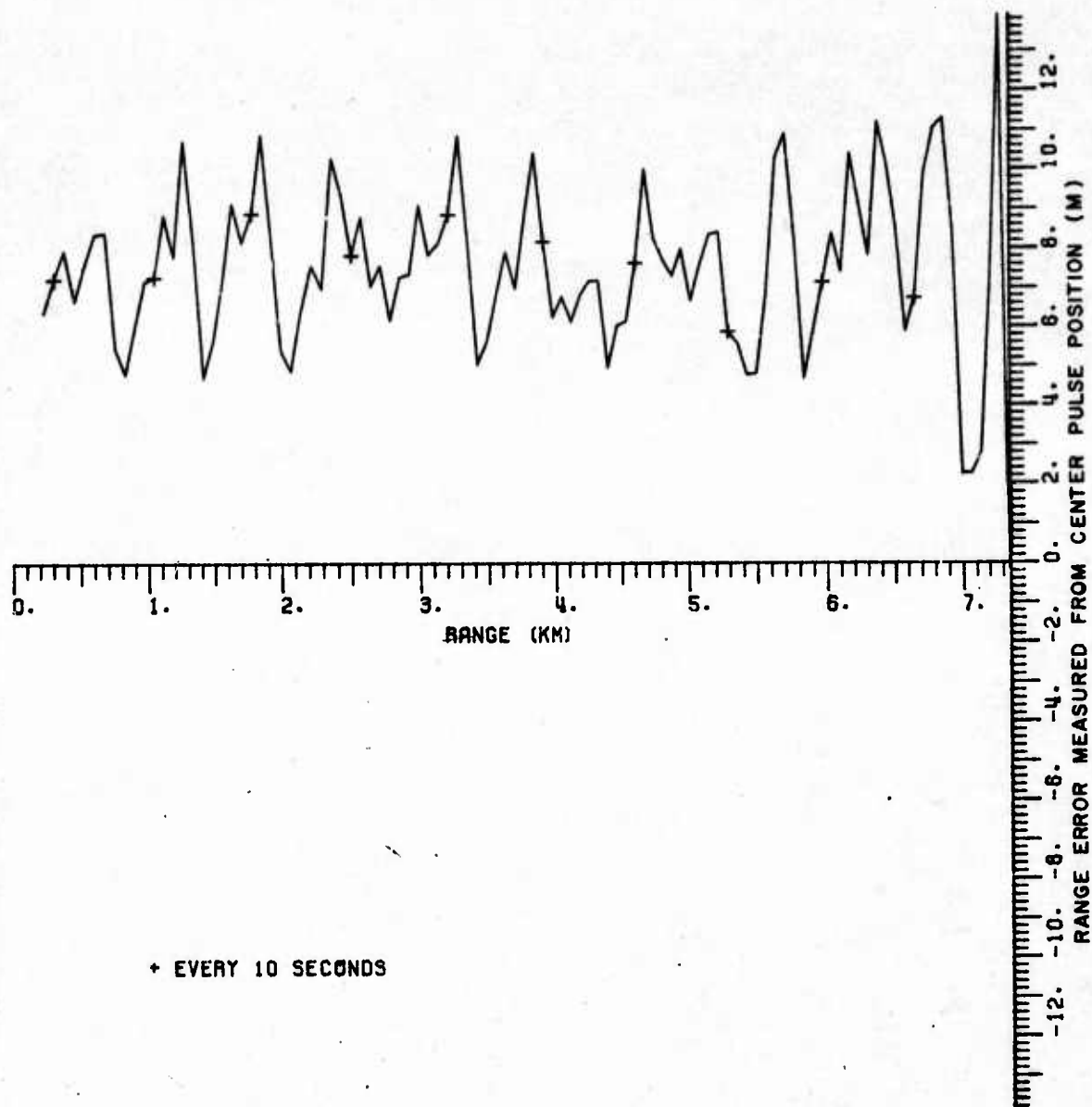


Figure G-13.  $v = 340$  m/s. Split-gate tracker.

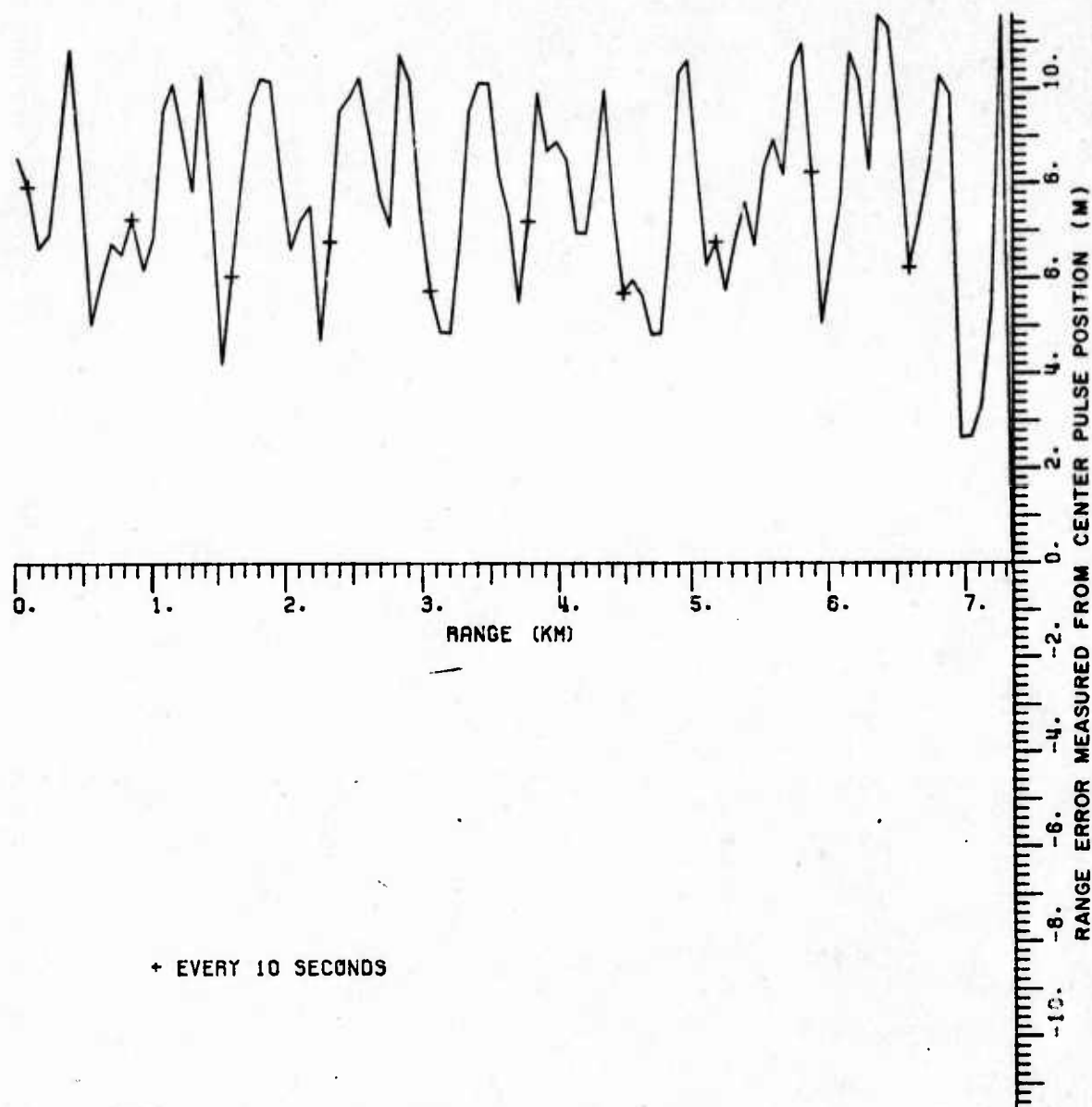


Figure G-14.  $v = 380$  m/s. Split-gate tracker.

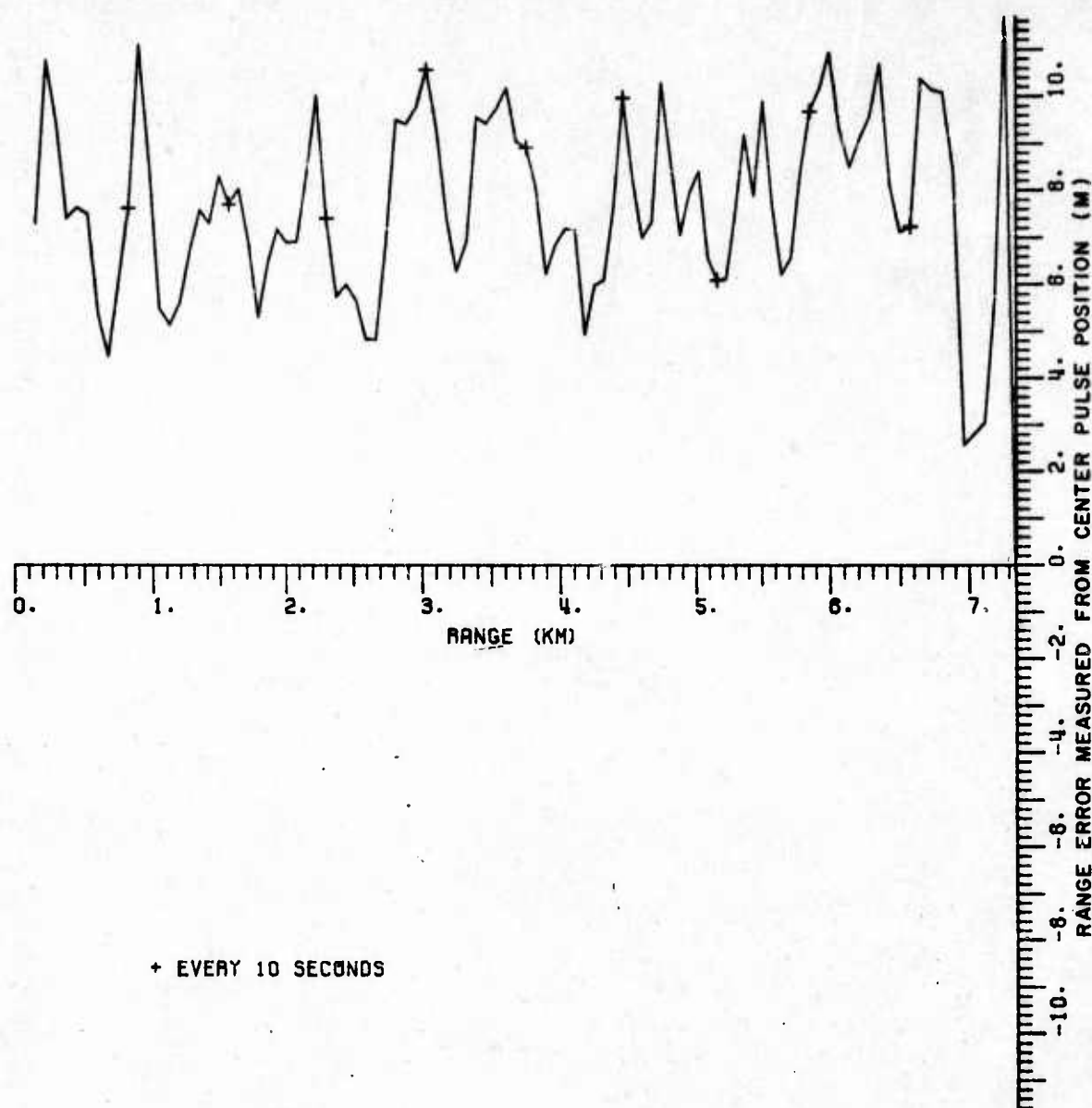


Figure G-15.  $v = 410$  m/s. Split-gate tracker.

# F. COMPUTER PROGRAM

```

1  INCLUDE DELAY.LIB1
2  INCLUDE POPSWB.LIB1
3  INCLUDE MISSB.P800
4  LOGICAL LOOT,ICHAFF,LANS
5  DIMENSION CPA(3),V(3)
6  DIMENSION PLANE(5),ROCKET(5),CHAFF(3,100),IRIFF(510)
7  DIMENSION SPLITA(3),DAMP(3),OR(3)
8  EXTERNAL CRTFLT
9  COMMON SIZE,PLANE,ROCKET,CHAFF,NCHAFF,LOOT,PANGE,THETA,PHI
10 COMMON RANGES,THETAS,PHIS,SNP,EARLY,ALATE,ADJUST,XINTER,YINTER
11 COMMON IMODE
12 DATA SPLANE,WPLANE/.01,4000./
13 DATA SCHAFF,WCHAFF/.04,150./
14 DATA KIN/.1/
15 DATA DZ1/.15/
16 DATA SPLITA/-.01,--.0015,--.01/
17 DATA TURNS,TURNS1/.01,.01/
18 DATA SIGNO/100./
19 DATA BNOISE/1./
20 DATA WFACT/.05/
21 DATA WMAX/.5/
22 DATA BASEV/.01/
23 DATA UV/.001/
24 DATA ROCKV/.05/
25 DATA ROCKV2/.05/
26 DATA ICHAFF/.FALSE./
27 DATA DR/.35,.003,7./
28 DATA THEIAN/.01/
29 DATA PHIN/.01/
30 DATA RANGEN/1./
31 DATA TSPLIT/.008/
32 DATA PSPLIT/.008/
33 DATA RANGN1/1./
34 DATA DZMP/-.01,--.0015,--.01/
35 DATA CFAMIN/.03/
36 DATA THAMP,POAMP/.007,.007/
37 DATA WNEW/.2/
38 DATA VROCK1/.0001/
39 DATA SYMODE/.3/
40 DATA PLANE1/.001/
41 DATA WNEW/.01/
42 C DDT IS THE TIME INTERVAL, ASSUMED TO BE ONE SECOND
43 CALL CRTON
44 CALL CRTPTS(IPUFF,510,4)
45 R DDT=1.
46 RANGE=0.
47 RANGES=0.
48 THETA=0.
49 THE TAS=0.
50 PHI=0.
51 PHIS=0.
52 TPP=0.
53 TMP=0.
54 XINTER=0.
55 YINTER=0.

```



```

56      CALL FERM(2)
57      *CHAFF=0
58      TANG=4
59      TANG=1
60      LOUT=.FALSE.
61      PLANE(3)=5.
62      PLANE(4)=0.
63      PLANE(5)=0.
64      ROCKET(1)=5.
65      ROCKET(2)=2.
66      ROCKET(3)=0.
67      ROCKET(4)=-160.
68      ROCKET(5)=42.
69      RANGES=-1.
70      ROCKET(4)=ROCKET(4)*3.1415926/180.
71      ROCKET(5)=ROCKET(5)*3.1415926/180.
72      PLANE(4)=PLANE(4)*3.1415926/180.
73      PLANE(5)=PLANE(5)*3.1415926/180.
74      TURNS1=ABS(TURNS1)
75      WRITE(8,9)
76  9      FORMAT('USE CANNED DATA? (Y/N)')
77      READ(8,-)LANS
78      IF(LANS) GO TO 101
79      CALL ESC($12)
80      WRITE(8,10)
81  10      FORMAT('ENTER OPTION VALUES: 1=R**2 2=SPLIT GATE 3=DELAY LINE,
82      * 4=THRESHOLD 5=1=COS**2 6=
83      *T=DUMP TO TAPE F=NO DUMP')
84  12      READ(8,-)IKNG,JANG,LOUT
85  15      WRITE(8,20)
86  20      FORMAT('ENTER PLANE ELEVATION, HEADING, DIVE ANGLE')
87      READ(8,-)PLANE(3),PLANE(4),PLANE(5)
88      PLANE(4)=PLANE(4)*3.1415926/180.
89      PLANE(5)=3.1415926*PLANE(5)/180.
90      PLANE(1)=0.
91      PLANE(2)=0.
92      WRITE(8,30)
93  30      FORMAT('ENTER MISSILE POSITION (X,Y,Z), HEADING, DIVE ANGLE')
94      READ(8,-)ROCKET
95      ROCKET(4)=ROCKET(4)*3.1415926/180.
96      ROCKET(5)=ROCKET(5)*3.1415926/180.
97      CALL CALANG(-ROCKET(1),-ROCKET(2),PLANE(3)-ROCKET(3)
98      *,RANGE,THETA,PHI)
99      RANGES=RANGE
100     CALL OUTPUT
101     WRITE(8,40)
102  40     FORMAT('OK? (Y/N)')
103     READ(8,-)LANS
104     IF(.NOT.LANS)GO TO 15
105     WRITE(8,50)
106  50     FORMAT('ENTER TRACKING INFO. (K,THETA,PHI,DR) ')
107     READ(8,-)RANGES,THETAS,PHIS,RANGEV
108  101     THETAS=THETAS*3.1415926/180.
109     PHIS=PHIS*3.1415926/180.
110     IS=0

```



```

111      DO 55 I=1,5
112      CALL PPSW(S=I,J)
113 55    TS=IS*2+2-J
114      PLANEV=BASEV+DV*IS
115      IF(RANGES.GT.0)GO TO 60
116      CALL CALANG(-ROCKET(1),-ROCKET(2),PLANE(3)-ROCKET(3),
117      * RANGES,THEIAS,PHIS)
118      RANGEV=PLANEV*COS(PLANE(4)-THEIAS)*COS(PLANE(5)-PHIS)-
119      * ROCKETV*COS(ROCKET(4)-THEIAS)*COS(ROCKET(5)-PHIS)
120      RANGES=RANGES-RANGEV
121 60    THETA=THEIAS
122      PHIP = PHIS
123      NCHAFF=0
124      TMISS=0
125      THETA=0.
126      PHIL=0.
127      THETA=0.
128      PHIV=0.
129      YR=0.
130      YB=0.
131      ADJUST=0.
132      IMODE=1
133      CALL ESC(1000)
134 C      MAIN LOOP. TRACKING SEGMENT
135 100    DO 250 II=1,250
136 C      PRIME ANGLE VALUES
137      CALL CALANG(-ROCKET(1),-ROCKET(2),PLANE(3)-ROCKET(3),
138      * RANGE,THETA,PHI)
139      DIS2=RANGE*RANGE
140      GO TO(110,120,130,140),IPNG
141 110    SIGNAL=SINGNO/AMAX1(DIS2,RMIN)
142      SIGNAL=SIGNAL*(1.+COS(THETA-ROCKET(4)))*2*(1.+COS(PHI-ROCKET(5)))*2
143      RANGES=RANGE
144      ANOISE=BNOISE+RETUR1(1,RANGE-DR1,RANGE+DR1)
145      SNR=(SIGNAL+ANOISE)/ANOISE
146      RANGES=RANGES+RANG*(RANGM1)/SNR
147      GO TO 150
148 120    RANGES=RANGES+RANGEV
149      TRNG1=TRNG/2
150      EARLY=RETURN(IPNG1,RANGES-DR(IMODE),RANGES)+
151      * RETURN1(IPNG1,RANGES-DR(IMODE),RANGES)
152      ALATE=RETURN(IPNG1,RANGES,RANGES+DR(IMODE))+
153      * RETURN1(IPNG1,RANGES,RANGES+DR(IMODE))
154      SIGNAL=RETURN(1,RANGES-DR(IMODE),RANGES+DR(IMODE))
155      ANOISE=BNOISE+RETUR1(1,RANGES-DR(IMODE),RANGES+DR(IMODE))
156 125    FORMAT(2F10.4)
157      SNR=(SIGNAL+ANOISE)/ANOISE
158      EARLY=ABS(EARLY+RANG(RANGEN)/SNR)
159      ALATE=ABS(ALATE+RANG(RANGEN)/SNR)
160      IF(SIGNAL.LE.0.)GO TO 150
161      ADJUST=(EARLY-ALATE)/(EARLY+ALATE)
162      IF(II.EQ.1)ADJSL=ADJUST
163      RANGEV=RANGEV+SPLITA(IPNG1)*ADJUST+DAMP(TRNG1)*(ADJUST-ADJSL)
164      IF(ABS(ADJUST)+ABS(ADJUST-ADJSL).GT.SWMODE)GO TO 120
165      IF(IMODE.EQ.2.OR.II.LT.5)GO TO 120

```

```

166      TMODE=2
167      WRITE(6,127)
168 127    FORMAT(' TARGET ACQUIRED')
169 128    ADJUST=ADJUST
170      GO TO 150
171 130    STOP RANGE
172 140    GO TO 120
173 150    THETA=THETA+THETA*V
174      PHIS=PHIV+ATAN(COS(THETA*V)*TAN(PHIS))
175      GO TO(155,160,170,180),IANG
176 155    CONTINUE
177      THETA=THETA+RANF(THETA)/SNR
178      PHIS=PHI+RANF(PHIS)/SNR
179      WEIGHT=SIGNAL*WFACT
180      IF(WEIGHT.GT.WMAX)WEIGHT=WMAX
181      GO TO 200
182 160    PH=0.
183      PL=0.
184      TH=0.
185      TL=0.
186      CALL ANGLE2(-ROCKET(1),-ROCKET(2),PLA E(3)-ROCKET(3),
187      *SPLANE,WPLANE,PH,PL,TH,TL)
188      IF(NCHAFF.EQ.0)GO TO 165
189      DO 162 I=1,NCHAFF
190 162    CALL ANGLE2(CHAFF(1,I)-ROCKET(1),CHAFF(2,I)-ROCKET(2),
191      *CHAFF(3,I)-ROCKET(3),SCHAFF,WCHAFF,PH,PL,TH,TL)
192 165    CONTINUE
193      TH=ABS(TH+RANF(THETA)/SNR)
194      TL=ABS(TL+RANF(THETA)/SNR)
195      PH=ABS(PH+RANF(PHIS)/SNR)
196      PL=ABS(PL+RANF(PHIS)/SNR)
197      ATHETA=(TH-TL)/(TH+TL)
198      APHI=(PH-PL)/(PH+PL)
199      IF(I.NE.1)GO TO 168
200      THETA=ATHETA
201      PHIL=APHI
202 168    ATHETA=ATHETA*TSPLIT+(ATHETA-THETA)*TDAMP
203      APHI=APHI*PSPLIT+(APHI-PHIL)*PDAMP
204      THETA=THETA+ATHETA/RANGES
205      PHIV=PHIV+APHI/RANGES
206      IF(ABS(PHIS).LT.1.5707969)GO TO 200
207      THETA=THETA+3.1415926
208      IF(PHIS)166,166,167
209 166    PHIS=-3.1415926-PHIS
210      GO TO 200
211 167    PHIS=3.1415926-PHIS
212      GO TO 200
213 170    PH=0.
214      PL=0.
215      TH=0.
216      TL=0.
217      CALL ANGLE2(-ROCKET(1),-ROCKET(2),PLANE(3)-ROCKET(3),SPLANE
218      *WPLANE,PH,PL,TH,TL)
219      GO TO 165
220 180    STOP ANGLE

```

```

221 200 CONTINUE
222 2200 X2=XB+ROCKET(1)+RANGES*COS(THETAS)*COS(PHIS)
223      Y2=YB+ROCKET(2)+RANGES*SIN(THETAS)*COS(PHIS)
224      T=(II-1)/2201,2202,2203
225 2201 XU=X2
226      YU=Y2
227      GO TO 2220
228 2202 X1=X0
229      Y1=Y0
230      VX=(X2-X1)/DOTT
231      VY=(Y2-Y1)/DOTT
232      VJ=SQRT(VX*VX+VY*VY)
233      TINTER=RANGES/ROCKV
234      TMP=TINTER
235      TMP=TINTER
236      GO TO 2204
237 2203 XP=X1+VX*DOTT
238      YP=Y1+VY*DOTT
239 2209 W=NEW/ANAX1(RANGES,1.)
240      X2=(XP+W*X2)/(1+W)
241      Y2=(YP+W*Y2)/(1+W)
242      VX=(X2-XU)/DOTT/2.
243      VY=(Y2-YU)/DOTT/2.
244      VJ=SQRT(VX*VX+VY*VY)
245 2210 TINTER=(TINTER+TMP)/2.-DOTT
246 2204 XINTER=(XINTER+VX*TINTER+X2)/2.
247      YINTER=(YINTER+VY*TINTER+Y2)/2.
248      RPH=SQRT((XB+ROCKET(1)-XINTER)**2+(YB+ROCKET(2)-YINTER)**2)
249      COS5=COS(ROCKET(5))
250      IF(COS5.EQ. 0.)COS5=1.
251      TMP=TMP/(ROCKV+(1*P-DOTT)*VROCKI*.5)/COS5
252      XU=X1
253      YU=Y1
254      X1=X2
255      Y1=Y2
256 C1 WRITE(6,2303)XP,YB,X2,Y2,XP,YP,VX,VY,XINTER,YINTER,VROCK.
257 C1 * TMP,TINTER,THETAP,PHIP,PTHETA,PPHI
258 2303 FORMAT(5('(',F8.5,',',F8.5,',',F8.5,',',F8.5,')'),F8.5/
259      *5('(',F8.5,',',F8.5,')'))
260 C SINCE WE NOW HAVE X,Y INTERCEPT THEN, FIND
261 C RELATIVE ANGLE FROM ROCKET TO PLANE
262 RELIX=YINTER-ROCKET(1)-X2
263 RELIY=YINTER-ROCKET(2)-Y2
264 RELIZ=RANGES*SIN(PHIS)
265 CALL CALANG(RELIX,RELIY,RELIZ,RNG,PTHETA,
266      *PPHI)
267 C1 IF(RNG.GT..1) GO TO 2212
268 C1 WRITE(6,2304) TINTER,RNG,ROCKV,PLANE(3),ROCKET(1),
269 C1 *ROCKET(2),ROCKET(3)
270 2304 FORMAT('INTERCEPT '7F10.5)
271 2212 IF((SUR.LE.1.5).OR.(TINTER.LT.4).OR.(TMP.LT.3)) GO TO 2219
272 2213 IF(II-10) 2220,2230,2231
273 C INITIALLY SET TO CALCULATED VALUES
274 2230 THETAP=THETAS
275      PHIP=PHIS

```

```

276      GO TO 2220
277 C    TEST TO SEE IF GOING TOO FAST
278 2231 TCOR = .0*PRIME(PTHETA-THETAP)
279      IF (ABS(TCOR).LT..2) GO TO 2234
280      IF(TCOR) 2232,2233,2233
281 2232 TCOR = -.2
282      GO TO 2234
283 2233 TCOR = .2
284 2234 THETAP = THETAP+TCOR
285      PHIP=PHIP+.3*PRIME(PPHI-PHIP)
286 C1    WRITE(6,2305) YP,YP,VX,VY,VJ
287 C1    WRITE(6,2307) TINTER,XINTER,YINTER,RNG,PTHETA,PPHI,THETAP
288 C1    *,PHIP
289 2307 FORMAT('TINTER,XINTER,YINTER,RNG,PTHETA,PPHI,THETAP',
290            *,AP,PHIP'/BF10.5)
291 2206 CONTINUE
292      GO TO 2216
293 C    TURN ROCKET TOWARDS PREDICTED TARGET IF COURSE PREDICTED
294 C    IF NEAR TARGET COMPUTE CPA AND CHECK IF TIME TO EXPLODE
295 2219 V(1)=ROCKV*COS(THETAP)*COS(PHIP)-PLANEX
296      V(2)=ROCKV*SIN(THETAP)*COS(PHIP)-PLANEY
297      V(3)=ROCKV*SIN(PHIP)*PLANEZ
298 C1    WRITE(6,2321)SNR,TINTER,TMP
299 2321 FORMAT('CHECKING CPA ',3F10.5)
300 C    CALCULATE TIME TO CPA
301      S1=0.
302      S2=0.
303      DO 2218 I=1,3
304          S1=S1+V(I)*(ROCKET(I)-PLANE(I))
305 2218 S2=S2+V(I)*V(I)
306          TIMCPA=-S1/S2
307 C1    WRITE(6,2323)V,S1,S2,TIMCPA,PLANEX,PLANEY,PLANEZ
308 2323 FORMAT('TERMS',12F10.5)
309 C    CHECK IF MISSILE HAS LOST TRACK
310      IF(SNR.LT.1.5)GO TO 2229
311 C    CHECK IF CPA COMING UP
312      IF(TIMCPA.GT.1.0)GO TO 2213
313      IF(TIMCPA.LT.0.)GOTO2215
314 C    CALCULATE POSITION OF CPA
315 2214 S1=0
316      DO 2217 I=1,3
317          CPA(I)=ROCKET(I)-PLANE(I)+V(I)*TIMCPA
318 2217 S1=S1+CPA(I)*CPA(I)
319      S1=SQRT(S1)
320 C    IS CPA CLOSE ENOUGH TO COUNT
321 C1    WRITE(6,2324)S1
322 2324 FORMAT('DIS',F10.5)
323      TINTER=TINTER-TIMCPA
324      WRITE(6,2320)CPA,TIMCPA,S1,TINTER,ROCKV
325 2320 FORMAT('INTERCEPT',7F10.5)
326      CALL LPTTR(3.,7.5,3,4,12H INTERCEPT ,10,10,12)
327      CALL LPTTR(2.,7.,1,4,6H CPA ,10,10,6)
328      CALL NUMBER(2,7,7.,.15,1000.,*CPA(1),0.,1)
329      CALL NUMBER(3,7,7.,.15,1000.,*CPA(2),0.,1)
330      CALL NUMBER(4,7,7.,.15,1000.,*CPA(3),0.,1)

```

```

331 CALL LETTER(5.5.7.1.4.3H ) ,ID,ID.3)
332 CALL LETTER(2.6.5.1.4.6H RANGE,ID,ID.6)
333 CALL NUMBER(3.6.5.15.1000*S1.0.1)
334 CALL CRTPLT(0.0.999)
335 GO TO 1000
336 C HERE IF SNR SMALL
337 2229 IF (IMODE.EQ.2)GO TO 2228
338 IF (TIMCPA .GT. 4.)GO TO 2215
339 IF (TIMCPA.LT.1.)GO TO 2214
340 GO TO 2216
341 2215 TMISS=TMIS-1
342 C1 WRITE(6,2322)TMIS,TIMCPA
343 2322 FORMAT('NO GOOD*2F10.5)
344 TIMCPA=0.
345 IF (TMIS)2214,2214,2216
346 2229 IMODE=1
347 WRITE(6,2227)
348 2227 FORMAT('SWITCHING TO ACQUISITION MODE')
349 2216 POCKET(4)=THETAP
350 RCKET(5)=PRIP
351 C OUTPUT INFO TO OPERATOR
352 C PUT FIRST INTERCEPT MUST BE CONVERTED TO PLANES REF
353 C FROM ABSOLUTE REF
354 C SWITCH TO ACQUIRE MODE IF MISSILE LOSSES TRACK
355 2220 YINTER=XINTER-Y2
356 YINTER=YINTER-Y2
357 CALL OUTPUT
358 XINTER=XINTER+Y2
359 YINTER=YINTER+Y2
360 IS=0
361 DO 205 I=1,5
362 CALL POPSW(5-I,J)
363 IS=IS*2+2-J
364 205 CONTINUE
365 PLANV1=BASEV+OV*IS
366 IF (ABS(PLANV1-PLANEV).GT.PLANEA)GO TO 2051
367 PLANEV=PLANV1
368 GO TO 2053
369 2051 IF (PLANV1.LT.PLANEV)GO TO 2052
370 PLANEV=PLANV1+PLANEV
371 GO TO 2053
372 2052 PLANEV=PLANEV-PLANEV
373 2053 CUSP=COS(PLANE(5))
374 PLANEX=PLANEV*COS(PLANE(4))*COSP
375 PLANEY=PLANEV*SIN(PLANE(4))*COSP
376 PLANEZ=PLANEV*SIN(PLANE(5))
377 PLANE(3)=PLANE(3)+PLANEZ
378 C GET PLANE TURNINGS
379 C HEADING CHANGE IN 6-9
380 C RISE ANGLE CHANGE IN 10-13
381 IS=0
382 DO 206 I=1,4
383 CALL POPSW(10-I,J)
384 206 IS=IS*2+2-J
385 PLANE(4)=PLANE(4)+(IS-8)*TURNS

```



```

386      IS=0
387      DO 207 I=1,4
388      CALL POPSW(14-Y,J)
389 207   IS=IS*2+2-J
390      PLANE(5)=PLANE(5)+(IS-0)*TURNS1
391 C     PROCESS PLANE LOOPINGS
392      IF(ABS(PLANE(5)).LT.1.57079)GO TO 209
393      PLANE(4)=PLANE(4)+3.14159
394      TURNS1=-TURNS1
395      IF(PLANE(5).LT.0)GO TO 208
396      PLANE(5)=3.1415926-PLANE(5)
397      GO TO 209
398 208   PLANE(5)=-3.1415926-PLANE(5)
399 209   CONTINUE
400 C     MOVE THE PLANE (PLANE IS MOVED BY MOVING EVERYTHING ELSE
401 C     IN THE OPPOSITE DIRECTION)
402      ROCKET(1)=ROCKET(1)-PLANEX
403      ROCKET(2)=ROCKET(2)-PLANEY
404      XB=XB+PLANEY
405      YB=YB+PLANEX
406      DO 210 I=1,NCHAFF
407      CHAFF(1,I)=CHAFF(1,I)-PLANEX
408 210   CHAFF(2,I)=CHAFF(2,I)-PLANEY
409      COSP=COS(ROCKET(5))
410 C     MOVE THE MISSILE IN ITS STRAIGHT LINE PATH
411 C     INCREASE SPEED VS TIME
412      ROCKV=ROCKV2+I1*VROCK1
413      ROCKET(1)=ROCKET(1)+ROCKV*COS(ROCKET(4))*COSP
414      ROCKET(2)=ROCKET(2)+ROCKV*SIN(ROCKET(4))*COSP
415      ROCKET(3)=ROCKET(3)+ROCKV*SIN(ROCKET(5))
416 C     DROP A CHAFF CLOUD IF SWITCH 17 IS UP AND WAS DOWN BEFORE
417 C     (ICHAFF INDICATES PREVIOUS STATE OF CHAFF SWITCH)
418      CALL POPSW(17,1)
419      GO TO (220,230),I
420 220   IF(ICHAFF)GO TO 240
421      NCHAFF=NCHAFF+1
422      DO 225 I=1,3
423      CHAFF(1,NCHAFF)=PLANE(I)
424 225   CONTINUE
425      ICHAFF=.TRUE.
426      GO TO 240
427 230   ICHAFF=.FALSE.
428 240   CONTINUE
429 C     CHECK IF MISSILE HAS LOST TRACK
430 250   CONTINUE
431 C     THIS IS THE SECTION TO DECIDE WHAT TO DO WHEN THE PROGRAM
432 C     HAS BEEN TERMINATED
433 1000  II=II-1
434      WRITE(6,1010)IT
435 1010  FORMAT(14,'CONTINUE.CODE(EXIT,CONT,RESTART)')
436      READ(6,*)I
437      IF(I)1020,100,=
438 1020  CALL EXIT
439      END

```



## REFERENCES

1. Van de Hulst, H. C., Light Scattering by Small Particles, John Wiley and Sons, Inc., 1957.
2. Glock, F., M. Hammermesh, and M. Phillips, "Return Cross Section from Randomly Oriented Resonant Half-Wavelength Chaff," Radio Research Laboratory, Harvard University, Cambridge, Massachusetts, Tech. Memo 411-TM-427, June 1944.
3. Fink, B., "Radar Countermeasures," Electronics, Vol. 19, pp. 92-97, January 1946.
4. Hessenrer, R. A., Jr., "Scatter Communications with Radar Chaff," Proc. IRE, Vol. 49, No. 3, March 1961, pp. 211-217.
5. Kaiper, G. P., "A Study of Chaff Echoes at 515 MHz," Radio Research Lab., Harvard University, Cambridge, Massachusetts, Rept. 411-73, December 1943.
6. Kelly, E. J., and E. C. Lerner, "A Mathematical Model for the Radar Echo from a Random Collection of Scatterers," Tech. Rept. No. 123, M.I.T. Lincoln Laboratory, 15 June 1956, AD 48613.
7. Wong, J. L., I. S. Reed, and Z. A. Kaprielian, "A Model for Radar Echo from a Collection of Rotating Dipole Scatterers," IEEE Trans. on Aero. and Elect. Syst., Vol. AES-3, No. 2, March 1967.
8. Wong, J. L., I. S. Reed, and Z. A. Kaprielian, "Scattering by Randomly Varying Media with Application to Radar Detection and Communications," Report USCEE 247, University of S. California, L.A., January 1968, AD 835 645.
9. Richmond, J. H., "Computer Analysis of Three Dimensional Wire Antennas," Report 2708-4, 22 December 1969, The Ohio State University ElectroScience Laboratory, Department of Electrical Engineering; prepared under Contract DAAD05-69-C-0031 for Department of the Army, Aberdeen Proving Ground, Maryland.
10. Richmond, J. H., L. Schwab and R. Wickliff, "Scattering Characteristics of Some Thin Wire Chaff Elements," Report 2584-8, 19 February 1970, The Ohio State University ElectroScience Laboratory, Department of Electrical Engineering; prepared under Contract F33615-68-C-1252 for Air Force Avionics Laboratory, Wright-Patterson Air Force Base, Ohio. (AD 865 406)

11. Wickliff, R. G., "Scattering from Some Finite Arrays of Randomly Oriented Coupled Dipole Elements," Report 2584-12, June 1971, The Ohio State University ElectroScience Laboratory, Department of Electrical Engineering; prepared under Contract F33615-68-C-1252 for Air Force Avionics Laboratory, Wright-Patterson Air Force Base, Ohio. (AD 885 859)
12. Garbacz, R. J., R. Wickliff, V. Cable, R. Caldecott and D. Lam, "Advanced Radar Reflector Studies," Report 3401-1, June 1974, The Ohio State University ElectroScience Laboratory, Department of Electrical Engineering; prepared under Contract F33615-72-C-1435 for Wright-Patterson Air Force Base.
13. Rayleigh, Lord (J. W. Strutt), The Theory of Sound, 1877, Dover Publications, pp. 35-42.
14. Borison, S. L., "Probability Density for the Radar Cross Section of One or More Randomly Oriented Dipoles," Group Rept. 1964-33, M.I.T. Lincoln Laboratory, 22 June 1964. AD 442 679.
15. Stantar, R., "Chaff Cloud Signature I Measurement Program," Rept. AFAL-TR-73-57, Hycor, Inc., Woburn, Mass., under USAF Avionics Laboratory Contract F33615-72-C-1606.
16. Spiegel, M. R., Theory of Problems of Statistics, Schaum Publishing Co., New York, 1961, p. 70.
17. Spiegel, M. R., op. cit., p. 29.
18. Spiegel, M. R., op. cit., p. 123.
19. Hoel, P. G., Introduction to Mathematical Statistics, 3rd Ed., John Wiley and Sons.
20. Spiegel, M. R., op. cit., pp. 142-144.
21. Richmond, J. H., "Reaction Theorems and Plane Surface Waves," Engineering Experiment Station, College of Engineering, The Ohio State University, Vol. 28, No. 4, July 1959, Part I.
22. Harrington, R. F., Field Computation by Moment Methods MacMillan Company, New York, 1968.

23. Kennaugh, E. M., "Polarization Properties of Radar Reflections," Report 389-12, The Ohio State University ElectroScience Laboratory, Department of Electrical Engineering; prepared under Contract AF 28(099)-90 for Rome Air Development Center, March 1952.
24. Richmond, J. H., "Radiation and Scattering by Thin-Wire Structures in the Complex Frequency Domain," Report 2902-10, The Ohio State University ElectroScience Laboratory, Department of Electrical Engineering; prepared under Grant NGL 36-008-138 for National Aeronautics and Space Administration, July 1973.
25. Carson, J. R., "Reciprocal Theorems in Radio Communication," Proc. of the IRE, Vol. 17, June 1929, pp. 952-956.
26. Richmond, J. H., "Radiation and Scattering by Thin-Wire Structures in the Complex Frequency Domain," Report 2902-10, July 1973, The Ohio State University ElectroScience Laboratory, Department of Electrical Engineering; prepared under Grant No. NGL 36-008-138 for National Aeronautics and Space Administration.
27. Kouyoumjian, R. G., "The Calculation of the Echo Areas of Perfectly Conducting Objects by the Variational Method," Doctoral Thesis, The Ohio State University, Columbus, Ohio, 1953.
28. Wang, N. N., J. H. Richmond, et al., "Sinusoidal Reaction Formulation for Radiation and Scattering from Conducting Surfaces," IEEE Trans. on Antennas and Propagation, Vol. AP-23, No. 3, May 1975, pp. 376-382.
29. Richmond, J. H., "A Wire-Grid Model for Scattering by Conducting Bodies," IEEE Trans. on Antennas and Propagation, Vol. AP-14, No. 4, November 1966, pp. 782-786.
30. Lin, Y. T. and J. H. Richmond, "EM Modeling of Aircraft at Low Frequencies," IEEE Trans. on Antennas and Propagation, Vol. AP-23, No. 1, January 1975, pp. 53-56.
31. Thiele, G. A., "Wire Antennas," in Computer Techniques for Electromagnetics, ed. by R. Mittra, Pergamon Press, New York, 1973, Chapter 2.
32. Richmond, J. H., "Computer Analysis of Three-Dimensional Wire Antennas," Report 2708-4, The Ohio State University ElectroScience Laboratory, Department of Electrical Engineering; prepared under Contract DAAD05-69-C-0031 for Ballistic Research Laboratory, Aberdeen Proving Ground, December 1969.



33. Miller, E. K. and F. J. Deadrick, "Some Computational Aspects of Thin Wire Modeling," Interaction Notes, Note 153, Lawrence Livermore Laboratory, University of California, Livermore, June 19, 1973.
34. Tai, C. T., "Electromagnetic Back-Scattering from Cylindrical Wires," Journal of Applied Physics, Vol. 23, No. 8, August 1952, pp. 909-916.
35. Miller, E. K. and F. J. Deadrick, "Thin Wire Modeling."
36. Richmond, J. H., "Computer Analysis."
37. Ibid, pp. 10-15.
38. Cable, V.P., "Application of Linear Iteration to Electromagnetic Scattering by Random Arrays of Wires," Report 3401-2, August 1975, The Ohio State University ElectroScience Laboratory, Department of Electrical Engineering; prepared under Contract F33615-72-C-1435 for Wright-Patterson Air Force Base, Ohio.
39. Ibid, pp. 10-15.
40. Rose, D. J. and R.A. Willoughly (Ed.), Sparse Matrices and Their Applications, Plenum Press, New York - London, 1972.
41. Tinney, W. F. and J. W. Walker, "Direct Solutions of Sparse Network Equations by Optimally Ordered Triangular Factorization," IRRE Proceedings, Vol. 55, No. 11, November 1967, pp. 1801-1809.
42. Sato, N. And W. F. Tinney, "Techniques for Exploiting the Sparsity of the Network Admittance Matrix," IEEE Trans. on Power Apparatus and Systems, Vol. 82, December 1963, pp. 944-950.
43. Gustavson, F. G. W. Liniger, and R. Willoughby, "Symbolic Generation of an Optical Crout Algorithm for Sparse Systems of Linear Equations," Journal of the Association for Computing Machinery, vol. 17, no. 1, January 1970, pp. 87-109.
44. Berry, R.D., "An optimal Ordering of Electronic Circuit Equations for a Sparse Matrix Solution," IEEE Trans. on Circuit Theory, vol. CT-18, no. 1, January 1971, pp. 40-50.
45. Tewarson, R. P., Sparse Matrices, Academic Press, New York-London, 1973.
46. Fedeev, D. K. and V. N. Faddeeva, Computational Methods of Linear Algebra, W. H. Freeman and Co., San Francisco, 1963, pp. 144-147.

47. Westlake, J. R., A Handbook of Numerical Matrix Inversion and Solution of Linear Equations, John Wiley and Sons, Inc., New York, London, Sydney, pp. 4-15.
48. Varga, R. S., Matrix Iterative Analysis, Prentice-Hall, Inc., Englewood Cliffs, New Jersey, 1962, pp. 56-57.
49. Varga, Matrix Iterative Analysis pp. 56-57.
50. Ibid, p. 58.
51. Young, D. M., Iterative Solution of Large Linear Systems, Academic Press, New York, 1975, Chapter 11.
53. Ibid.
54. Ibid.
55. Varga, Matrix Iterative Analysis, Chapter 3.
56. Ibid,
57. Young, Iterative Solution, p. 41.
58. Fair, G., "ALLMAT: ATSS-360 FORTRAN IV Subroutine for Eigenvalues and Eigenvectors of a General Complex Matrix," Lewis Research Center, NASA TN O-7032, N71-15833, January 1971.
59. Tai, C. T., "An Iterative Method."
60. Castello, D. and B.A. Munk, "Table of Mutual Impedance of Identical Dipoles in Echelon," Report 2382-1, The Ohio State University ElectroScience Laboratory, Department of Electrical Engineering; prepared under Contract F 33615-67-C-1507 for Air Force Avionics Laboratory, Wright-Patterson Air Force Base, October 1967.
61. Garbacz, R. J., "Introduction of Characteristic Modes for Chaff Applications," Report 2584-6, April 1970, The Ohio State University ElectroScience Laboratory, Department of Electrical Engineering; prepared under Contract F33615-68-C-1252 for Air Force Avionics Laboratory, Wright-Patterson Air Force Base, Ohio. (AD 869 208) p. 38.
62. Potter, E. A. and R. T. Compton, Jr., "Computer Simulation of Aircraft Tracker Problems in the Presence of Chaff," Report 3401-3, September 1975, The Ohio State University ElectroScience Laboratory, Department of Electrical Engineering; prepared under Contract F33615-73-C-1173 for Aeronautical Systems Division/PPMEB, Wright-Patterson Air Force Base, Ohio.

**SUPPLEMENTARY**

**INFORMATION**



Errata

AD-B013 005

Page 112 is not available.

DTIC-DDAC  
14 Dec 84